NASA Technical Memorandum 108802

Final Reports of the U.S. Experiments Flown on the Soviet Biosatellite Cosmos 2044

Volume II: Experiments K-7-16 – K-7-41

September 1994

National Aeronautics and
Space Administration

NASA Technical Memorandum 108802

Final Reports of the U.S. Experiments Flown on the Soviet Biosatellite Cosmos 2044

Volume II: Experiments K-7-16 – K-7-41

James P. Connolly, Richard E. Grindeland, and Rodney W. Ballard, Editors
Ames Research Center, Moffett Field, California

September 1994

National Aeronautics and
Space Administration

Ames Research Center
Moffett Field, California 94035-1000

PREFACE

On September 15, 1989, the Soviet Union launched Cosmos 2044, an unmanned spacecraft carrying biological and radiation physics experiments from several countries. Those participating included countries from the InterCosmos Council (U.S.S.R., Czechoslovakia, etc.), along with the United States, France, Great Britain, Canada, and the European Space Agency. This mission included 29 U.S./U.S.S.R. joint experiments and involved more than 80 American scientists.

Cosmos 2044 represents the seventh consecutive Soviet biosatellite mission involving U.S./U.S.S.R. joint experiments. Earlier flights included Cosmos 782 in November 1975, Cosmos 936 in August 1977, Cosmos 1129 in September 1979, Cosmos 1514 in December 1983, Cosmos 1667 in July 1985, and Cosmos 1887 in September 1987. These Cosmos Biosatellite missions, involving experiments with monkeys, rats, plants, and insects, have provided scientists with valuable information on how the basic biology of living organisms is affected by the space environment.

The Cosmos 1887 mission had two problems which complicated interpretation of some experiment results. First, a feeder failure within one of the primate capsules on day 5 resulted in reduced food intake by the monkey, requiring termination of the mission at 12.5 days. Second, the biosatellite landed significantly off-course, delaying post-landing processing of the biospecimens by more than 40 hours. For these reasons, Soviet specialists recommended a reflight of the Cosmos 1887 experiments on Cosmos 2044. In addition to these experiments, several new experiments were added for Cosmos 2044, some involving extensive preflight and postflight testing of the flight pool of rhesus monkeys. The Cosmos 2044 mission was conducted according to plan and produced a significant body of scientific and technical results which are described in this report.

Cosmos 2044 was a very successful mission. It was a complex mission, requiring the utmost dedication and cooperation by all participants to achieve this success. Throughout the preparations for this mission, there was a great deal of trust displayed between the Soviet and American teams; the outstanding results of the Cosmos 2044 mission serve as a tribute to this mutual trust.

On behalf of all American participants, I wish to thank the Institute of Biomedical Problems, SKTB Biophyspribor, and the many fine Soviet scientists, engineers and other specialists who supported these joint experiments.

James P. Connolly
Cosmos Project Manager
NASA Ames Research Center

Page intentionally left blank

Technical Memorandum 108802 consists of two volumes.

Volume I contains:

- The Mission Description
- U.S. Flight and Ground-Support Hardware
- Rat Studies, Science Reports K-7-01 through K-7-15. (Rat Studies are continued in Volume II).

Volume II contains:

- Rat Studies, Science Reports K-7-16 through K-7-29
- A Comparison of The Physiology of the Spaceflight and the Suspended Rat
- Primate Studies, Science Reports K-7-30 through K-7-35
- Radiation Studies, Science Report K-7-41

Page intentionally left blank

TABLE OF CONTENTS—VOLUME 2

PREFACE iii

EDITORIAL NOTE v

TABLE OF CONTENTS vii

SUMMARY 1

K-7-16 3
Effects of Microgravity or Simulated Launch on Testicular Functions in Rats
R.P. Amann, et al.

K-7-17 25
Effects of Spaceflight on the Proliferation of Jejunal Mucosal Cells
R.W. Phillips, et al.

K-7-18 33
Effects of Spaceflight in the Muscle Adductor Longus of Rats Flown in the Soviet Biosatellite Cosmos 2044

I. A Study Employing Neural Cell Adhesion Molecules (N-CAM) Immunocytochemistry and Conventional Morphological Techniques (Light and Electron Microscopy) 35
N.G. Daunton, et al.

II. Quantitative Autoradiographic Analysis of GABA (Benzodiasephine) and Muscarinic Cholinergic Receptors in the Forebrain of Rats Flown on Cosmos 2044 73
L.-Wu, et al.

K-7-19 83
Pineal Physiology after Spaceflight: Relation to Rat Gonadal Function
D.C. Holley, et al.

K-7-20 101
Pituitary Oxytocin and Vasopressin Content of Rats Flown on Cosmos 2044
L. Keil, et al..

K-7-21 109
Effect of Microgravity

I. Metabolic Enzymes of Type 1 and Type 2 Muscle Fibers 111
O.H. Lowry, et al.

II. The Distribution of Selected Enzymes and Amino Acids in the Hippocampal Formation 137
O.H. Lowry, et al.

K-7-22 155
Growth Hormone Regulation Synthesis and Secretion in Microgravity

I. Growth Hormone Regulation Synthesis and Secretion in Microgravity 157
R. Grindeland, et al.

II. Hypothalamic Growth Hormone-Releasing Factor, Somatostatinimmunoreactivity and Messenger RNA Levels in Microgravity 173
P. Sawchenko, et al.

III. Plasma Analysis Hormone Measurements 183
R. Grindeland, et al.

IV. Muscle Hormone Receptors .....
(Not available at time of publication)

K-7-23 193
Effect of Spaceflight on Level and Function of Immune Cells

I. Immunology Studies 195
G. Sonnenfeld, et al.

II. Proliferation and Cytokines 207
A. Mastro, et al.

K-7-28 221
Lung Morphology Study
J.B. West, et al.

K-7-29 233
Connective Tissue Studies

I. Rat Skin, Normal and Repair 235
A.C. Vailas, et al.

II. Changes in Muscle Serine Proteases, Serpins and Matrix Molecules 239
B. Festoff, et al.

III. Rodent Tissue Repair: Skeletal Muscle 255
W. Stauber, et al.

B. COMPARISON OF THE PHYSIOLOGY OF THE SPACEFLIGHT AND THE HINDLIMB SUSPENDED RAT 271
F.W. Booth and R.E. Grindeland

C. PRIMATE STUDIES 283

K-7-30 285
Effects of Spaceflight in the Cosmos Biosatellite 2044 on the Vestibular-Ocular Reflex (VOR) of Rhesus Monkeys
B. Cohen, et al.

K-7-31 303
Studies of Vestibular Primary Afferents and Eye Movements in Normal, Hypergravity and Hypogravity - AXON
M.J. Correia, et al.

K-7-33 333
Functional Neuromuscular Adaptation to Spaceflight
V.R. Edgerton, et al.

K-7-35 353
Circadian Rhythms and Temperature Regulation

I. Circadian Rhythms and Temperature Regulation 355
C. Fuller, et al.

II. Metabolism 361
C. Fuller, et al.

D. RADIATION STUDIES 385

K-7-41 387
Radiation Experiments on Cosmos 2044
E.V. Benton, et al.

Page intentionally left blank

TABLE OF CONTENTS—VOLUME 1

PREFACE.. iii

EDITORIAL NOTE v

TABLE OF CONTENTS vii

SUMMARY 1

I. COSMOS 2044 MISSION DESCRIPTION 2

A. INTRODUCTION 2

B. MISSION OVERVIEW (V. I. Korolkov, Ye. A. Ilyin) 3

U.S.S.R. Experiments 3
1. Introduction 3
2. Rodent Experiments 4
3. Primate Experiments 5
4. General Biology Experiments 7
5. Radiation Dosimetry 10
6. Radiation Biology Studies 10

C. U.S.S.R. HARDWARE SUPPORT OF EXPERIMENTS
(V. K. Golov, V.S. Magedov, V.I. Korolkov) 11

D. HABITATION CONDITIONS IN THE PRESSURIZED MODULE OF THE BIOSATELLITE
(N.N. Lizko, L.N. Petrova, A.K. Burets, I.N. Kornyushenkova, R.D. Rokhlenko, T.I. Kuznetsova, V.P. Savina, V.I. Korolkov, V.K. Golov) 14

E. PREPARING THE PRIMATES FOR SPACE FLIGHT
(V.I. Korolkov, B.A. Lapin, A.N. Truzhennikov, T.G. Urmancheyeva, A.N. Nazin) 15

F. U.S. MISSION MANAGEMENT 17

U.S. Experiments 17
1. Primate Experiments 17
2. Rodent Experiments 18
3. Radiation Dosimetry and Spectrometry Experiment 18
Spacecraft Description 18
1. Primate-Bios 18
2. Bios-Vivaria (Rodent-Bios) 19
Mission Management Plan 19
1. Hardware Development 19
2. Training 19
3. Hardware and Experiment Verification Tests 19
4. Data/Specimen/Hardware Transfer for Postflight Analysis 20
5. Documentation 20

G. MISSION OPERATIONS 20

General Mission Design for Rat Experiments 20
1. Basal Control Group 20
2. Vivarium Control Group 20
3. Synchronous Control Group 21
4. Tail-Suspension Group 21
Preflight Events 21
1. Rat Experiments 21
2. Primate Experiments 21
3. Radiation Dosimetry and Spectrometry Experiment 21
Launch, On-Orbit and Reentry Events 22
1. Rat Experiments 22
2. Primate Experiments 22
3. Radiation Dosimetry and Spectrometry Experiment 22
Postflight Experiments 22
1. Rat Experiments 22
2. Primate Experiments 22
3. Radiation Dosimetry and Spectrometry Experiment 23

TABLES AND FIGURES FOR SECTION I 24

II. U.S. FLIGHT AND GROUND-SUPPORT HARDWARE 47

A. HARDWARE OVERVIEW 47
1. Flight Hardware Description and Test Plan 47
2. Ground-Support Hardware and Test Plan 47
3. Hardware/Software Documentation and Data Transfer 48

B. EXPERIMENT-SPECIFIC HARDWARE (M. Skidmore, J. Connolly) 48
1. Circadian Rhythm/Temperature Regulation Experiment 48
Flight Hardware 48
Ground-Support Hardware 49
2. Radiation Dosimetry Experiment 49
Flight Hardware 49
Ground-Support Hardware 49
3. Neurovestibular Experiments 49
Ground-Support Hardware 49

C. BIOTRANSPORTER DEVELOPMENT (M. Skidmore) 50
+23°C Active Biotransporter 50
1. Development and Operation 50
2. Test Plan 51
3. Test Procedure 51
+4°C Active Biotransporter 51
1. Development and Operation 51
2. Test Plan 52
3. Test Procedure 52
+4°C Passive Biotransporter 52
1. Development and Operation 52
2. Test Plan 53
3. Test Procedure 53
-70°C Passive Biotransporter (Dry Ice) 53
1. Development and Operation 53
2. Test Plan 53
3. Test Procedure 54
Biomailers 54

TABLES AND FIGURES FOR SECTION II 55

III. SCIENCE REPORTS 67

A. RAT STUDIES 67

K-7-01 69
Bone Biochemistry, Mineral Distribution and Calcium Regulating Hormones in Rats After the Cosmos 2044 Biosatellite Flight
S. Arnaud, et al.

K-7-02 103
Biomechanical, Biochemical and Morphological Alterations of Intramuscular and Dense Fibrous Connective Tissues After 14 Days in Spaceflight

I. Connective Tissue Studies 105
A. Vailas, et al.

II. The Effects of Microgravity on the Composition of the Intervertebral Disc 153
A. Pedrini-Mille, J. Maynard, et al.

K-7-03 187
Gravity and Skeletal Growth

I. Gravity and Skeletal Growth 189
E.R. Holton, et al.

II. Morphological Studies of Bone and Tendon 193
S. Doty, et al.

III. Preosteoblast Production in Cosmos 2044 Rats: Short-Term Recovery of Osteoblast Potential 201
L. Garetto, et al.

IV. Immunohistochemistry of Collagenase in Calvaria of Rats Flown on Cosmos 2044 213
N. Partridge, et al.

V. Biomechanical Properties of Rat Tarsus Bones .....
(Not available at time of publication)

K-7-04 225
Mineral Distribution and Balance in Rats During Spaceflight
C. Cann, et al.

K-7-06 235
Morphometric and EM Analyses of Tibial Epiphyseal Plates from Cosmos 2044 Rats
P.J. Duke, et al.

K-7-07 253
Metabolic and Morphologic Properties of Muscle Fibers after Spaceflight, Cosmos 2044

I. Metabolic and Morphologic Properties of muscle fibers after spaceflight, Cosmos 2044 255
V. R. Edgerton, et al.

II. Ventral Horn Cell Responses to Spaceflight and Hindlimb Suspension 261
B. Jiang, et al.

K-7-08 271
Skeletal Muscle Atrophy in Response to 14 Days of Weightlessness
X.J. Musacchia, et al.

K-7- 09 289
Morphological, Histochemical, Immunocytochemical, and Biochemical Investigation of Microgravity-Induced Nerve and Muscle Breakdown
I. Muscle Biochemistry 291
D.A. Riley, et al.
II. Muscle Studies 327
S. Ellis, et al.
K-7-10 339
Effects of Zero Gravity on Contractile Protein Content and Isomyosin Distributions in Fast and Slow Quadriceps Muscles of Rodents Flown on Cosmos 2044
K.M. Baldwin, et al.

K-7-11 357
mRNA Levels in Skeletal and Smooth Muscle
I. mRNA Decrease in Skeletal Muscle 359
F.W. Booth, et al.
II. mRNA Levels in Smooth Muscle 363
N. Weisbrodt, et al.

K-7-12 373
Natriuretic Peptide Content of Atria from Rats Exposed to 14 Days of Spaceflight
L. Keil, et al.

K-7-13 381
Morphological and Biochemical Examination of Heart Tissue
I. Ultrastructural Alteration in Rat Hearts after Cosmos 2044 Compared to Cosmos 1887 383
D. Philpott, et al.
II. Cardiac Morphology after Microgravity Conditions 401
M. Goldstein, et al.
III. Cyclic AMP Receptor Protein Distribution in Rat Heart Muscle Exposed to Microgravity 433
M. Mednieks, et al.
IV. Altered Myosin Expression in Rat Ventricular Muscle During Exposure to Microgravity 453
D. Thomason, et al.

K-7-14 461
Hepatic Function in Rats after Spaceflight
I. Analyses of Selected Parameters, Carbohydrate, Amino Acid, Lipid, and Xenobiotic Metabolism in Liver and Serum 463
A. H. Merrill, et al.
II. Hepatic Function (Histology) in Rats After Spaceflight 471
S. Cormier, et al.

K-7-15 491
Hematology Studies in Rats Flown on the Soviet Biosatellite Cosmos 2044
R.D. Lange, et al.

LIST OF TABLES

SECTION I

1. Cosmos biosatellite missions with U.S. participation 24

2. Summary list of all experiments flown on Cosmos 2044 25

3. Electrodes and sensors implanted in primates for recording of physiological parameters 33

4. Primate cardiovascular data before and after flight 34

5. Summary of rodent experiment design 35

SECTION II

1. Summary list of all hardware by experiment 55

Page intentionally left blank

LIST OF FIGURES

SECTION I

1. Food consumption by Zabiyaka inflight. 36
2. Food consumption by Zhakonya inflight 37
3. Juice consumption by Zabiyaka inflight. 38
4. Juice consumption by Zhakonya inflight. 39
5. Data flow schematic for Cosmos 2044 spacecraft 40
6. Cosmos spacecraft 41
7. Primate-Bios. 42
8. Primate in Bios restraint chair. 43
9. Flight Monkeys 44
10. Response System (hand level & command portion) 45
11. Tail Suspension Study Equipment 46

SECTION II

1. CR/T flight signal processor/recorder with ground-based signal simulator 59
2. CR/T flight hardware (battery pack, disassembled showing 16 lithium batteries) ... 60
3. CR/T flight hardware (signal processor, interconnection unit, 6 U.S. sensors) 61
4. 4-Channel Temperature Recorder 62
5. Optokinetic rotator 63
6. Three-axis stimulator 64
7. +4°C biotransporter. 65
8. Passive +4°C Biotransporter test configuration 66

SUMMARY

Cosmos 2044 was launched on September 15, 1989, containing radiation dosimetry experiments and a biological payload including two young male rhesus monkeys, ten adult male Wistar rats, insects, amphibians, protozoa, cell cultures, worms, plants and fish.

The biosatellite was launched from the Plesetsk Cosmodrome in the Soviet Union for a mission duration of 14 days, as planned. The major research objectives were:

- Study adaptive response mechanisms of mammals during flight
- Study physiological mechanisms underlying vestibular, motor system and brain function in primates during early and later adaptation phases
- Study the tissue regeneration processes of mammals
- Study the development of single-celled organisms, cell cultures and embryos in microgravity
- Study radiation characteristics during the mission and investigate doses, fluxes and spectra of cosmic radiation for various types of shielding

American and Soviet specialists jointly conducted 29 experiments on this mission including extensive preflight and postflight studies with rhesus monkeys, and tissue processing and cell culturing postflight. Biosamples and data were subsequently transferred to the United States. The U.S. responsibilities for this flight included development of flight and ground-based hardware, the preparation of rat tissue sample procedures, the verification testing of hardware and experiment procedures, and the postflight analysis of biospecimens and data for the joint experiments. The U.S. investigations included four primate experiments, 24 rat experiments, and one radiation dosimetry experiment. Three scientists investigated tissue repair during flight for a subgroup of rats injured preflight by surgical intervention.

A description of the Cosmos 2044 mission is presented in this report including preflight, on-orbit and postflight activities. The flight and ground-based bioinstrumentation which was developed by the U.S. and U.S.S.R. is also described, along with the associated preflight testing of the U.S. hardware. The major hardware components for this mission (Bios systems and major instrumentation systems) were developed by SKTB Biophyspribor in St. Petersburg, Russia. Final Science Reports for each of the U.S./U.S.S.R. joint experiments are also included.

Richard Mains, Gretchen Gold and the staff of Mains Associates expended a great deal of effort on the compilation and organization of materials for this Cosmos 2044 report. Their assistance in the preparation of this document is greatly appreciated.

Page intentionally left blank

51-51

51346

EXPERIMENT K-7-16

EFFECTS OF MICROGRAVITY OR SIMULATED LAUNCH ON TESTICULAR FUNCTION IN RATS

Principal Investigator:

R.P.Amann
Animal Reproduction and Biotechnology Laboratory
Colorado State University
Fort Collins, Colorado 80523

Co-Investigators:

J.W. Clemens
D. Deaver
Department of Dairy and Animal Sciences
Pennsylvania State University
University Park, Pennsylvania 16802
S.D. Banerjee

J. Folmer
B. Zirkin
Department of Population Dynamics
The John Hopkins University
Baltimore, Maryland 21205

D.N.R. Veeramachaneni
Animal Reproduction and Biotechnology Laboratory
Colorado State University
Fort Collins, Colorado 80523

G.S. Grills
C.M. Gruppi
D. Wolgemuth
Department of Genetics and Development
Center for Reproductive Sciences
Columbia University College of Physicians and Surgeons
New York, New York 10032

L.V. Serova
Institute for Biomedical Problems
Moscow, USSR 123007

W.J. Sapp
C.S. Williams
Department of Biology
Tuskegee University
Tuskegee, Alabama 36088

Page intentionally left blank

EXPERIMENT K-7-16

EFFECTS OF MICROGRAVITY OR SIMULATED LAUNCH ON TESTICULAR FUNCTION IN RATS

R. P. Amann, D. R. Deaver, B. R. Zirkin, G. S. Grills, W. J. Sapp, D. N. R. Veeramachaneni, J. W. Clemens, S. D. Banerjee, J. Folmer, C. M. Gruppi, D. J. Wolgemuth, C. S. Williams, and L. V. Serova

SUMMARY

Fixed or frozen testicular tissues from five rats per group were analyzed by: subjective and quantitative evaluations of spermatogenesis; Northern-blot analysis for expression of selected genes; quantification of testosterone and receptors for LH; and morphometric analysis of Leydig cells. Based on observations of fixed tissue, it was evident that some rats in the flight and vivarium groups had testicular abnormalities unassociated with treatment, and probably existing when they were assigned randomly to the four treatment groups; the simulated-launch group contained no abnormal rat. Lesions induced in testes of caudal-elevation rats precluded discernment of any pre-existing abnormality. Considering rats without pre-existing abnormalities, diameter of seminiferous tubules and numbers of germ cells per tubule cross section were lower ($P < 0.05$) in flight rats than in simulated-launch or vivarium rats. However, ratios of germ cells to each other, or to Sertoli cells, and number of homogenization-resistant spermatids did not differ from values for simulated-launch or vivarium controls. There was no effect of flight on normal expression of testis-specific *hsp* gene products, or evidence for production of stress-inducible transcripts of the *hsp70* or *hsp90* genes. Concentration of receptors for rLH in testicular tissue, and surface densities of smooth endoplasmic reticulum and peroxisomes in Leydig cells, were similar in flight and simulated-launch rats. However, concentrations of testosterone in testicular tissue or peripheral blood plasma were reduced ($P < 0.05$) in flight rats to <20% of values for simulated-launch or vivarium controls. Thus, spermatogenesis was essentially normal in flight rats, but production of testosterone was severely depressed. Sequela of reduced androgen production on turnover of muscle and bone should be considered when interpreting data from mammals exposed to microgravity.

INTRODUCTION

There is seemingly contradictory evidence on effects of space flight or microgravity on testicular function in mammals. Although a slight decrease in number of spermatogonia per cross section of seminiferous tubule in testes from rats flown for 7 days on Space Lab-3 or 13 days on Cosmos-1887 were reported (Philpott et al., 1985; Sapp et al., 1990), Serova et al. (1989) concluded that spermatogenesis was not affected in rats flown 7 or 13 days on Cosmos-1667 or Cosmos-1887. Serum concentrations of testosterone were low in rats after return from space flight (Grindeland et al., 1990), indicating that endocrine function of the testes might be altered by stress factors associated with space flight or effects of microgravity. The reasons for abnormalities of the endocrine and possibly the exocrine (spermatogenic) functions of the testes associated with space flight, at least in rats, are unknown, but could be related to altered function of the hypothalamus or adenohypophysis (Grindeland, 1990), altered fluid distribution in the body (Moore and Thornton, 1987), and/or restricted blood and lymph flow within the testis.

Starting with the assumption that stress factors associated with space flight, or effects of microgravity *per se*, represent simply a unique set of environmental toxins, we used approaches of reproductive toxicology and cellular and molecular biology to evaluate testicular function in rats

from Cosmos-2044. Sensitive methods for quantification of alterations of testicular function by enumeration of germ cells, morphometric analyses, and techniques of cellular endocrinology have proven to be invaluable in identifying reproductive toxins (Amann, 1982, 1986; Amann and Berndtson, 1986; Berndtson et al., 1989; Lamb and Foster, 1988; Thomas et al., 1985; Working, 1989). As understanding of the genetic regulation of testicular function evolved, it became evident that eukaryotic organisms synthesize a subset of gene products in response to environmental stress; these have been termed cellular-stress or heat-shock proteins. Some members of this gene family also are expressed at specific points during spermatogenesis in mammals (Wolgemuth et al., 1990) and their expression is associated with specific germ cell types (Zakeri and Wolgemuth, 1987; Zakeri et al., 1988). Thus, expression of these genes provides molecular markers which can indicate normal spermatogenesis or can reveal if a testis is responding to an altered environment.

MATERIALS AND METHODS

Animals and Tissue Collection

Details of the history, age and body weight of the rats; assignment to four treatment groups (flight, simulated launch, vivarium, and caudal elevation); animal care before and during the experiment; conditions of simulated or actual launch, flight and reentry; and timing of tissue sampling relative to reentry are presented by Grindeland et al. (1991). For each of five rats (those numbered 6-10) in the four groups, each testis was separated from its epididymis; both organs were trimmed free of extraneous tissue and weighed. The right testis was cut into three pieces: a central portion was placed into a container and immersed in liquid nitrogen (-196°C), and the two poles (each representing about 0.25 of the testicular length) were immersed into fixative at 4°C. The epididymis also was immersed in fixative. The fixative was "Triple Fix" (Philpott et al., 1980) which contained 1% (w/v) paraformaldehyde, 3% (v/v) glutaraldehyde, 88 mM sucrose, and 2.5mM difluorodinitrobenzene in 0.1 M sodium cacodylate buffer.

Frozen tissues remained in liquid nitrogen or on solid CO_2, and fixed tissues in 4°C fixative, until receipt at Colorado State University. There, frozen tissue was aliquoted, while at -79°C, for shipment at -79°C to Dr. Deaver for enumeration of homogenization-resistant spermatids and quantification of testosterone and LH receptors, and to Dr. Wolgemuth for measurement of expression of cellular-stress genes. Fixed tissue also was divided: the poles of a testis were randomly designated as A or B, and the outer portion of each pole was sliced off and shipped to Dr. Zirkin in 0.1 M cacodylate buffer, at 4°C, for morphometric analysis of Leydig cells. The inner portion of each testicular pole was retained by Dr. Amann for subjective and objective evaluations of spermatogenesis and measurement of seminiferous tubule diameter; this tissue later was shared with Dr. Sapp. Epididymal tissue was examined microscopically to estimate the number of sloughed immature germ cells present among the spermatozoa, to enable deductions concerning onset of alterations in the seminiferous epithelium.

Spermatogenesis

Histological Evaluations

Thin slices of fixed tissue were rinsed in 0.1 M cacodylate buffer, immersed 1 hr in OsO_4 (1% (w/v) in 0.1 M cacodylate buffer), rinsed in buffer, dehydrated through graded ethanols, and embedded in a mixture of Araldite and PolyBed-812 (1:1.64 by wt). For 2-4 blocks per testis pole, 4 x 6 mm sections were cut at 0.8μm, collected on glass slides and stained with toluidine blue. Each slide was coded with a number which precluded identification of treatment or end of the testis by observers making subjective or morphometric evaluations. Epididymal tissue was similarly processed. Using light microscopy, testicular tissue was subjectively evaluated, independently, by two individuals (RPA and DNRV) expert in spermatogenesis and pathophysiology, for normalcy of both the seminiferous epithelium and the interstitial tissue.

Diameters of 25 essentially round, cross sections through seminiferous tubules, and their lumina, were measured for each of 2-4 loci (blocks) representing each testicular pole. For each Stage VII cross section (Leblond and Clermont, 1952; Berndtson, 1977), the number of Sertoli cells with a discernible nucleolus, and numbers of nuclei of A-spermatogonia, preleptotene spermatocytes, pachytene spermatocytes or step-7 spermatids were recorded. Diameters of two nucleoli of Sertoli cells and of two nuclei of each type of germ cell also were measured. Concurrently, for each tissue section, appearance of the seminiferous epithelium was classified as normal or having minor, moderate, or severe degenerative changes. Counts of germ cells were corrected for differences in nuclear diameter and section thickness using a modification of Abercrombie's formula (Curtis and Amann, 1981), and the resulting data were used to calculate numbers of germ cells per Sertoli cell or ratios among germ cell types (Berndtson, 1977; Amann and Berndtson, 1986).

In addition, 2-μm sections were cut from selected blocks (abnormal rats were excluded) and stained with toluidine blue for enumeration of nuclei of spermatogonia (type A- or B-spermatogonia) and Sertoli cells in essentially round cross sections of Stage VI seminiferous tubules. Tubules were staged on the basis of spermatogonial configuration (Oakberg and Huckins, 1976) with verification of staging based on morphologic features of spermatids (Leblond and Clermont, 1952). Nuclei in every other section through one, or occasionally two, stage VI tubule were counted until 50 cross sections had been scored. Counts were corrected for nuclear diameter and section thickness, after which the mean value was divided by 2.5 to make the data comparable to those for stage VII tubules (sections were 2.0 rather than 0.8μm thick).

Efficiency of Sperm Production

The number of homogenization-resistant spermatids per gram of testicular tissue, a measure of the efficiency of sperm production (Amann, 1982, 1986) was determined by modifying the procedure of Robb et al. (1978). Briefly, frozen tissue was thawed, weighed (131-253 mg), and minced using two razor blades. The tissue was transferred quantitatively using 2.0 ml buffer (0.5 M Tris-HCl, 0.23 M sucrose, 5 mM $MgCl_2$, and 4 mM NaN_3) into a 7-ml Dounce homogenizer and subjected to 10 strokes with pestle-B followed by 10 strokes with pestle-A. The homogenate was centrifuged (800 x g for 10 min) at 4°C. The supernatant was saved (see Leydig Cell Function), and the pellet was resuspended in 2 ml buffer and homogenized a second time. After centrifugation, the supernatant was added to the previous one, and the pellet was resuspended in 5-10 ml of 0.145 M NaCl containing 4 mM NaN_3 and 0.05% (v/v) Triton X-100 (Robb et al., 1978). The number of homogenization-resistant (elongated) spermatid nuclei in each suspension was determined by cytometer counts; data were expressed on a tissue wet-weight basis. The resulting values should provide a sensitive measure of the efficiency of spermatogenesis, but because the homogenization procedure is different from that pioneered by Robb et al. (1978), the absolute values are not comparable with those of Robb et al. (1978), Amann and Berndtson (1986), or others.

Gene Expression

Molecular Probes

Expression of *hsp70* and *hsp90* was examined. The *hsp70* probe is a 1.3 kb *Hind* III-*Eco*RI cDNA insert from plasmid pHMS213 (a gift from Dr. L. Moran; Lowe and Moran, 1986). This mouse cDNA recognizes high levels of a novel 2.7 kb transcript in spherical and elongating spermatids in normal mice (Zakeri and Wolgemuth, 1987, Zakeri et al., 1988) and also heat-inducible 2.5 and 3.5 kb transcripts in heat-shocked L mouse cells. The *hsp90* probe is a 1.1 kb *Pst* I cDNA insert from the plasmid pHS801 (a gift of Drs. E. Hickey and L. Weber; Hickey et al., 1986, 1989). This human cDNA recognizes a 3.2 kb transcript in mouse testis, expressed most abundantly in primary spermatocytes in prophase of the first division of meiosis (Gruppi et al.,

1990), and also recognizes a 2.95 kb transcript present in heat-shocked or non-heat-shocked HeLa cells (Hickey et al., 1986).
*
Analytical Methods

Control testis and liver tissues were obtained from male rodents: Sprague-Dawley rats (Camm Research Industries), Swiss Webster mice (Camm Research Industries), and B6D2F1/J mice (Jackson Laboratory). Tissues were quickly plunged into liquid nitrogen, and stored at -70°C. Total RNA was extracted from tissues by lithium chloride precipitation (Cathala et al., 1983). Samples were processed in sets, with each set containing tissue from one rat in each of the four treatment groups from Cosmos-2044, plus samples of testis and liver from a normal rat and mouse as controls. Similar amounts of RNA from each sample were loaded onto denaturing gels (0.8% Agarose, 2.2 M formaldehyde), electrophoresed, semi-dry electroblotted to Nytran membrane, and linked to the membrane by exposure to UV light for 5 min. Probes (see above) were labeled by random priming with [^{32}P]deoxynucleotide triphosphates (Feinberg and Vogelstein, 1984). [^{32}P]probes were hybridized to mRNA on the filters at high stringency in the presence of dextran sulphate (Wahl et al., 1979), washed sequentially for 20 min each in 2X SSC plus 1% (v/v) sodium dodecylsulfate (SDS) at room temperature, twice in 2X SSC plus 0.1% SDS at 65°C, once in SSC plus 0.1% SDS at 65°C, once in 0.1X SSC plus 0.1% SDS at 65C, and once in 0.1X SSC at 65°C (SSC = 0.15 M NaCl and 0.015 M sodium citrate). The integrity and relative abundance of RNA on the membranes was assessed by UV visualization of ethidium bromide incorporated by rRNA, and recorded on Polaroid Type-55 film. Molecular weight of each mRNA transcript was estimated, using the 28S and 18S bands of rRNA as internal size standards. The 28S rRNA is 4.729 kb in rats and 4.712 kb in mice (Hassouna et al., 1984) and the 18S rRNA is 1.869 kb in both rats and mice (Raynal et al., 1984).

Hybridization was detected by exposure of a Northern blot to Kodak X-ray film, with an intensifying screen, at -70°C for 1-14 d. Both autoradiograms of Northern blots and negatives of gels were digitized (256-point grey scale) and relative amounts of RNA estimated by video image analysis with a JAVA system (Jandel Scientific). An arbitrary standard scale was used to calibrate intensity, with a randomly selected area of background set at 0 and a randomly selected area of high density assigned a value of 100. Densitometry values represented the average intensity over the entire area of a band. To provide a correction factor for unequal sample loading within a gel, the value for the most intense rRNA band in a gel was divided by the value for the corresponding rRNA in each sample. This correction factor for relative amount of total RNA loaded for each sample was used to adjust intensity values for the amount of mRNA or mRNA hybridization signal for that sample. Thus, comparisons could be made among bands within a gel or Northern blot.

Leydig Cell Ultrastructure

For each testicular pole (A or B), 3-5 blocks of tissue were examined for each rat; thus 30-50 blocks of tissue were examined for the five rats in each treatment group. Thin sections from each block were mounted on formvar-coated, 200-mesh grids and stained with uranyl acetate and lead citrate. Grids were examined in a Hitachi HU-12A electron microscope. To minimize sampling bias, Leydig cells were identified at 1,000X magnification; cytoplasmic organelles could not be visualized. Usually three micrographs, prepared at 20,000X original magnification, were necessary to encompass each Leydig cell, and three Leydig cells on each grid were photographed. Thus, 18-30 Leydig cells were examined per rat.

Prints were prepared (at 2.75X) so that all stereological determinations were made on micrographs at a final magnification of 55,000X. Surface density was determined for: smooth endoplasmic reticulum (SER), rough endoplasmic reticulum (RER), outer mitochondrial membrane (OMM), inner mitochondrial membrane (IMM), peroxisomes (PER), and lysosomes (LYS). The 20 x 25 cm stereologic overlay was of a multipurpose test-system, containing 112 short test-lines (each

terminating as a line-end point) arrayed as 14 rows of 8 test-lines each. The overlay was placed over a micrograph and used to determine surface density of each organelle (Weibel and Bolender, 1973) by counting intersections of test-lines on the overlay with membranes of the organelles. Surface density (S_v) was calculated using the formula $S_v = 4(I)/(P_T)(d)$, in which "I" is the number of intersections between test-lines and organelle membrane, "P_T" is the number of line-end points over cytoplasm of Leydig cells, and "d" is the length of the test-line corrected for magnification.

Leydig Cell Function

The pooled low-speed supernatants prepared from thawed testicular tissue (see last paragraph under spermatogenesis) were centrifuged at 20,000 x g for 15 min at 4°C. The supernatant was removed and testosterone concentration determined by radioimmunoassay. Reagents for the liquid-phase assay, using [^{125}I]testosterone-TME as the ligand, were from ICN (Costa Mesa, CA). All samples were quantified in a single assay and the intraassay coefficient of variation was 11%. The assay was validated for rat testicular tissue by demonstrating: (a) increasing amounts of tissue extract displaced [^{125}I]testosterone-TME in a dose-dependent manner parallel to the standard curve, (b) tissue extracts did not bind detectable amounts of [^{125}I]testosterone-TME in the range of dilutions used to assay testicular testosterone, and (c) testosterone added to extracts was recovered in an amount essentially equal to that added.

The capacity of membrane fragments in the 20,000 x g pellet to bind human chorionic gonadotropin (hCG) was used to estimate the number of unoccupied receptors for rLH per gram of testicular tissue; presumably rLH receptors all were on Leydig cells. A "standard curve" technique was used, since there was insufficient tissue for a Scatchard analysis of each sample. A standard testicular membrane preparation was prepared, as above, using testes from 10 Sprague-Dawley rats 90-120 days old; it must be assumed that affinity of the rLH receptor is similar in American and Soviet rats. In developing the assay, the amount of hCG necessary to saturate rLH receptors in an aliquot of standard preparation of testicular membranes was determined. Duplicate aliquots representing 20 mg testicular tissue were incubated in 12x75 mm tubes with 1.2, 2.4, 3.6, 4.8, or 6.0 ng [^{125}I]hCG, prepared from NIDDK hCG CR-127 by the chloramine-T procedure, in a total of 350 µl buffer for 18 hr at 25°C. Tubes were centrifuged 30 min at 9,000 x g and the supernatant decanted; radioactivity of the pellet was determined. It was found (Fig. 1) that 4.8 ng [^{125}I]hCG was sufficient to saturate rLH receptors in extract representing 20 mg testicular tissue. To further validate the assay, aliquots of 0, 5, 10, 15 or 20 mg of standard membrane preparation (in 100 µl buffer),100 µl of [^{125}I]hCG solution containing 6.0 ng hCG, and 150 µl of buffer containing 0 or a 100 IU (about a 1000-fold excess of hCG; Sigma #CG-10) were mixed and incubated for 18 hr at 25°C. Tubes were centrifuged and radioactivity was measured as above; the amount of [^{125}I]hCG specifically bound was calculated as binding without excess ligand minus binding with excess ligand. Specific binding was directly proportional to the mass of testicular tissue present and increased in a linear manner from 0 to 20 mg (Fig. 2). For analysis of the Cosmos-2044 samples, a series of duplicate aliquots of the standard membrane preparation representing 5-20 mg of tissue, or 20-mg aliquots representing each sample, were incubated with 6.0 ng [^{125}I]hCG plus 0 or 100 IU hCG, and specific binding quantified as above. All samples were included in one assay, and the intraassay coefficient of variation was 4.8%.

Statistical Analyses

Data for organ weights, number of spermatogonia in Stage VI seminiferous tubules, surface density of organelles in Leydig cells, concentration of testosterone in blood plasma (data provided by R. E. Grindeland), and concentrations of testosterone or LH receptors were analyzed using the SAS General Linear Model (GLM) procedure and a 1-way analysis of variance. Quantitative data for characteristics of seminiferous tubules and numbers or ratios of germ cells were analyzed using a 2-way analysis of variance considering pole of the testis (2, random) and treatment group (3 or 4, fixed). All four treatment groups were included in analyses of diameters of seminiferous tubules

and their lumina, but for other attributes the caudal-elevated rats were excluded since their seminiferous tubules contained virtually no germ cells. There was no significant difference between the A and B poles for any characteristic, except for corrected numbers of preleptotene spermatocytes (considered to be a Type-I error). If the F-value associated with treatment was significant ($P < 0.05$), Duncan's multiple range test was used to establish which groups differed ($P < 0.05$).

RESULTS AND DISCUSSION

General Testicular Function

Mean testicular weight for rats in the vivarium group did not differ from those for either the flight or simulated-launch groups, but testis weight was greater ($P<0.05$) for rats in the simulated-launch group than those in the flight or caudal-elevation groups (Table 1). However, some rats in the flight and vivarium groups had small testes, and all rats in the cauda-elevation group had very small testes. The probable causes of these differences were revealed by subjective histological evaluations of each testis and attached epididymis (Fig. 3), and confirmed by quantitative data.

One must assume that vivarium rats had not been exposed to stress factors associated with launch or flight, and were the best representation of the population of rats shortly before launch. However, in three vivarium rats one or both testes weighed ≤900 mg, and histological examinations of three of these four testes (only right testes were available) revealed that they were abnormal (see below). Similarly, right testes from two flight rats weighed ≤650 mg and had histological abnormalities similar to those in abnormal vivarium rats, but different from those characteristic of caudal-elevation rats. Thus, the cause of lesions in the testes of these two abnormal flight rats probably was the same as that inducing lesions found in three vivarium rats, and was not flight. By this reasoning, three flight rats (#7, 9 and 10), five simulated-launch rats (#6-10), and two vivarium rats (#7 and 10) did not have marked pre-existing abnormalities; weights of their right testes ranged from 1200 to 1500 mg, whereas the right testes for the other five rats in these three groups weighed 450 to 900 mg. Thus, we concluded that testes of some rats in the flight and vivarium, and possibly the caudal-elevation, groups had been abnormal when they were assigned to treatment groups. By random chance, all rats in the simulated-launch group had normal testes.

Lesions in testes of rats with a pre-existing abnormality were different from those in caudal-elevation rats. Based on testicular weight, the lesion was unilateral in some rats with pre-existing abnormalities, but for caudal-elevation rats the lesion inevitably was bilateral. For caudal-elevation rats, the entire testis was uniformly affected (based on histologic examinations of both poles and data for efficiency of sperm production in the central portion of the testis). Seminiferous tubules contained only Sertoli cells plus a complement of spermatogonia, a few primary spermatocytes and occasional spermatids (Figs. 3A and 3B). In contrast, in an abnormal testis from a flight or vivarium rat, there was a mixture of normal and abnormal seminiferous tubules (Figs. 3D and 3E), and the extent of involvement was not uniform throughout the entire testis. Based on histological evaluations, these testes should have been producing spermatozoa, although in reduced numbers. These subjective observations were confirmed by data for efficiency of sperm production in the central portion of each testis (<0.5 vs 22 x 10^6 spermatids/gram testis). Other quantitative differences ($P < 0.05$) were evident. Caudal-elevation rats had a smaller right testis than rats with pre-existing abnormalities, with smaller seminiferous tubules, and lower intratesticular and plasma concentrations of testosterone (492 vs 690 mg; 185 vs 228 μm diameter; 23.4 vs 60.9 ng/g; and 0.51 vs 2.85 ng/ml), but a similar concentration of receptors for rLH in testicular tissue (63.7 vs 78.8 ng/g). Morphometric characteristics of Leydig cells were similar for both groups (data not presented). In caudal-elevation rats, the epididymis contained numerous germ cells sloughed from the seminiferous epithelium (Fig. 3C), which were indicative of recent destruction of the seminiferous epithelium. Undoubtedly the testes of caudal-elevation rats fell into the abdominal

cavity (Serova et al. 1989; Deaver et al., 1991), through the inguinal canal which remains patent in rats (in contrast to humans), and were damaged by exposure to body temperature. Epididymides of rats with pre-existing abnormalities had few immature germ cells among the spermatozoa (Fig. 3F), which precluded extensive destruction of the seminiferous epithelium within 2 wk prior to tissue fixation. In flight rats without pre-existing abnormalities, spermatogenesis was normal (Figs. 3G and 3H) and the cauda epididymidis was filled with spermatozoa (Fig. 3I).

The high values for intratesticular concentrations of testosterone and receptors for rLH in caudal-elevation rats, and rats with pre-existing testicular abnormalities, probably reflect atrophy of the seminiferous tubules so that Leydig cells constitute a larger proportion of the testis. However, it is possible that these rats had more Leydig cells or Leydig cells that secreted more testosterone.

Only tissues from rats 6-10 in each of the four treatment groups were available to us for detailed examination. However, it is likely that at least two of the other rats (F-3 and V-1) had abnormal testes prior to assignment to the project, based on testicular weight (≤850 vs 1200-1650 mg). Thus, at least 7 of 30 rats (23%) in the flight, simulated-launch and vivarium rats probably were abnormal before imposition of treatments involved in the Cosmos-2044 study.

Spermatogenesis

Considering the facts that testes of several rats probably were abnormal before assignment to treatment, and that groups of five rats/group are of marginal size to detect subtle treatment effects (Berndtson et al., 1989), dogmatic conclusions concerning effects on spermatogenesis of exposure to the stress factors of simulated or actual launch and reentry, or exposure to microgravity *per se*, are impossible. Data for all rats, including those with pre-existing testicular abnormalities, are presented in Table 1, because minor sequelae on spermatogenesis of the unknown agent or genetic factor causing pre-existing abnormalities in some rats may have been undetected in others. Considering all rats, based on subjective histologic evaluations (Fig. 3) and quantitative data (Table 1), spermatogenesis in flight rats generally was similar to that in vivarium rats, but inferior to that in simulated-launch rats. This probably reflects the variable impact of pre-existing abnormalities in certain rats. If there had been a profound treatment effect, the corrected numbers of germ cells per Stage VII seminiferous tubule cross section, or one or more of the ratios between a specific type of germ cell and Sertoli cells, would have been reduced. Although such differences were detected between the flight and simulated-launch groups for preleptotene spermatocytes and step-7 spermatids, there was no difference for the ratios. Since the ratio of preleptotene spermatocytes to A-spermatogonia was not reduced, spermatogonia were completing mitosis. Ratios of pachytene spermatocytes to preleptotene spermatocytes and step-7 spermatids to pachytene spermatocytes were similar, so primary spermatocytes were completing meiosis. Thus, the differences detected may not reflect a treatment effect.

At the penalty of reducing the number of available animals, data also were summarized after excluding the two flight and three vivarium rats with obvious pre-existing abnormalities in the right testis (Table 2). This summary is considered to provide the best basis for conclusions concerning effects of flight. The reductions ($P<0.05$) in weight of the right testis and seminiferous tubule diameter persisted in flight rats, as did differences in numbers of Sertoli cells or germ cells per seminiferous tubule cross section. However, as for the complete data set, the ratios of germ cells to Sertoli cells or among types of germ cells were not affected by treatment. The number of homogenization-resistant spermatids per gram of testis was not affected by treatment and was independent of testicular weight ($r = -0.34$; $P>0.05$).

TABLE 1

CHARACTERISTICS OF THE RIGHT TESTIS FOR ALL RATS OF THE COSMOS 2044 STUDY

	Flight	Simulated Launch	Vivarium	Caudal Elevation
Right Testis wt. (mg)	960[a]	1416[b]	1048[a b]	492[c]
Right Epid. wt. (mg)	317[a]	401[a]	314[a]	242[a]
Seminiferous Tubule Diameter (μm)	222[a]	266[b]	247[a b]	185[c]
Tubule Lumen Diameter (μm)	90[a b]	109[c]	101[b c]	85[a]
Normal (%)	49[a]	88[b]	65[a b]	nd
Early Degeneration (%)	7[a]	5[a]	5[a]	nd
Mod. Degeneration (%)	5[a]	5[a]	5[a]	nd
Severe Degeneration (%)	39[a]	3[b]	21[a b]	nd
Stage VII Seminiferous Tubules				
Nuclei / Tubule X-Sect.				
Sertoli Cells	1.26[a]	2.15[b]	1.41[a]	nd
A-Spermatogonia	1.57[a]	0.88[a]	0.84[a]	nd
Preleptotene Spematocytes	4.40[a]	6.65[b]	5.25[a b]	nd
Pachytene Spermatocytes	4.24[a]	7.15[a]	6.00[a]	nd
Spermatids	13.67[a]	21.09[b]	16.64[a b]	nd
Ratio (# / Sertoli Cell)				
A-Spermatogonia	1.08[a]	0.42[a]	0.63[a]	nd
Preteptotene Spermatocytes	3.46[a]	3.14[a]	3.85[a]	nd
Pachytene Spermatocytes	3.40[a]	3.38[a]	4.23[a]	nd
Spermatids	10.82[a]	9.96[a]	12.14[a]	nd
Ratio				
Preleptotene: A	9.13[a]	7.71[a]	6.44[a]	nd
Pachytene: Preleptotene	0.98[a]	1.08[a]	1.10[a]	nd
Spermatid: Pachytene	3.22[a]	2.95[a]	3.08[a]	nd
Spermatids / g Testis (10^6)	28.9[a]	37.8[a]	33.2[a]	<0.5[b]
LH Receptors (ng hCG bound / g testis)	65.8[a]	56.8[a]	63.1[a]	63.7[a]
Testosterone (ng / g testis)	7.0[a]	15.1[a]	64.5[b]	23.4[a]
(ng / ml blood plasma)[d]	0.27[a]	1.91[b]	3.50[c]	0.51[a]
Leydig Cells ($\mu m^2 / \mu m^3$)				
Smooth Endoplasmic Reticulum	7.75[a]	7.23[a]	6.07[b]	7.85[b]
Rough Endoplasmic Reticulum	0.59[a]	0.66[a]	1.06[b]	0.87[b c]
Outer Mitochondrial Membrane	1.43[a]	1.47[a]	1.71[b]	1.48[b]
Inner Mitochondrial Membrane	3.85[a]	3.76[a]	4.26[a]	3.94[b]
Peroxisomes	0.22[a]	0.36[a]	0.29[a]	0.17[b]
Lysosomes	0.14[a]	0.09[a]	0.10[a]	0.08[b]

nd = Not determined.

[a,b,c] Means with the same superscript do not differ ($P > 0.05$).

[d] Data for testosterone in blood plasma from Merrill et al. (1991).

TABLE 2

CHARACTERISTICS OF THE RIGHT TESTIS IN RATS WITH PRE-EXISTING ABNORMALITIES IN THE FLIGHT, SIMULATED-LAUNCH, AND VIVARIUM GROUPS OF THE COSMOS 2044 STUDY[a]

	Flight	Simulated Launch	Vivarium
Right Testis wt. (mg)	1230[b]	1420[c]	1450[c]
Seminiferous Tubule Diameter (μm)	229[b]	266[c]	267[c]
Tubule Lumen Diameter (μm)	98[b]	108[b]	106[b]
Stage VI Seminiferous Tubules			
Total Spermatogonia	5.26[b]	5.57[b c]	5.79[c]
Stage VII Seminiferous Tubules			
Nuclei / Tubule X-Sect.			
Sertoli Cells	1.04[b]	2.15[c]	1.70[b c]
A-Spermatogonia	0.38[b]	0.88[c]	0.89[c]
Preleptotene Spematocytes	3.65[b]	6.65[c]	6.10[c]
Pachytene Spermatocytes	3.92[b]	7.15[c]	7.20[c]
Spematids	11.93[b]	21.09[c]	20.57[c]
Ratio (# / Sertoli Cell)			
A-Spermatogonia	0.35[b]	0.42[b]	0.51[b]
Preteptotene Spermatocytes	3.44[b]	3.14[b]	3.69[b]
Pachytene Spermatocytes	3.67[b]	3.38[b]	4.24[b]
Spermatids	11.18[b]	9.96[b]	12.42[b]
Ratio			
Preleptotene: A	10.98[b]	7.71[b]	7.43[b]
Pachytene: Preleptotene	1.06[b]	1.07[b]	1.17[b]
Spermatid: Pachytene	3.08[b]	2.95[b]	2.92[b]
Spermatids / g Testis (10^6)	42.3[b]	37.8[b]	38.2[b]
LH Receptors (ng hCG bound / g testis)	55.8[b]	56.8[b]	44.0[b]
Testosterone (ng / g testis)	3.81[b]	15.06[c]	20.82[c]
(ng / ml blood plasma)[d]	0.23[b]	1.91[c]	1.96[c]
Leydig Cells ($\mu m^2 / um^3$)			
Smooth Endoplasmic Reticulum	7.93[b]	7.23[b]	5.51[c]
Rough Endoplasmic Reticulum	0.53[b]	0.66[b]	1.05[b]
Outer Mitochondrial Membrane	1.46[b]	1.47[b]	1.64[b]
Inner Mitochondrial Membrane	3.98[b]	3.76[b]	4.08[b]
Peroxisomes	0.22[b]	0.36[b]	0.29[b]
Lysosomes	1.60[b]	0.09[b]	0.10[b]

[a] Rats with a testis ≤ 0.90g and abnormal histologic appearance were considered to have a pre-existing abnormality. Data for corrected number of spermatogonia in 2.0-μm sections for Stage VI were divided by 2.5 to make them comparable to those for 0.8 μm sections for Stage VII.

[b,c] Means with the same superscript do not differ (P> 0.05).

[d] Data for testosterone in blood plasma are from Merrill et al. (1991).

Counts of all spermatogonia in cross sections of Stage VI tubules (by CSW) were consistent with those for A-spermatogonia in Stage VII (by DNRV). In Stage VI cross sections, there were fewer ($P<0.05$) spermatogonia in testes from normal flight rats than in testes of simulated-launch or normal vivarium rats (Table 2), although number of Sertoli cell nuclei was not significantly different (data not shown). The 5.3% reduction in number of total spermatogonia per cross section of Stage VI seminiferous tubule for flight rats, relative to simulated-launch rats, was similar to results of Sapp et al. (1990) for rats flown on Space Lab-3 or Cosmos-1887.

Diameter of seminiferous tubules in normal flight rats was less than in normal simulated-launch or vivarium animals (Table 2), despite apparent normalcy of spermatogenesis. This might reflect a distortion of the seminiferous tubules induced by microgravity, that persisted through the 11 hr between landing and fixation of tissue. Although there is no known precedent, it is possible that there was a decrease in diameter and an offsetting increase in length of seminiferous tubules, so that internal surface area of the basement membrane and space available for each Sertoli cell were essentially unaltered. Such a change would explain the decreases in numbers of Sertoli cells and germ cells per seminiferous tubule cross section, while the ratios of germ cells were normal and number of homogenization-resistant spermatids per gram of testis was unaffected.

Given the totality of the qualitative and quantitative findings (Tables 1 and 2), it is unlikely that exposure to microgravity for ≤2 wk had an immediate deleterious effect on mitosis of spermatogonia, survival of spermatocytes through meiosis, or maturation of spermatids. If the Sertoli cells or germ cells were affected directly by microgravity, or indirectly by reduced secretion of testosterone, other hormones, or regulatory factors, the lesion(s) must be either subtle or not discernible after 14 days of flight.

Gene Expression

Yield of total RNA ranged from 39 to 600 mg, and probably was a function of the mass of testicular tissue available. The weight of each sample of testicular tissue was not determined, because thawing the tissue before extraction might have resulted in degradation of the RNA. Efforts were made to load similar amounts of RNA (20 μg) on each lane of the gels used for Northern analyses, and data later were normalized within each gel to minimize the effect of differences in the amount of RNA loaded. Figs. 4 and 5 show, respectively, samples of RNA from rats without (Fig. 4) or with (Fig. 5) pre-existing abnormalities of the right testis.

The expression of the *hsp* genes was given high priority in this study because several members of the *hsp70* and *hsp90* gene families are expressed in specific germ cells (see Materials and Methods). Thus, they can serve as molecular markers of the presence of these germ cells. Moreover, certain members of the *hsp70* and *hsp90* gene families respond to cellular stress and are affected by altered testicular environment, including elevated temperature. Although a stress response of the testes could be elicited by increased temperature, due to movement of the testes from the scrotum into the body cavity during exposure to microgravity or caudal elevation, it could be elicited by one or a combination of other factors associated with flight. Availability of testicular samples from caudal-elevation rats, which became cryptorchid, enabled distinction of effects induced by heat from those possibly induced by other aspects of space flight.

From the data depicted (Figs. 4 and 5), and similar data for the other four sets of tissues, two conclusions were reached. First, flight, vivarium, or simulated-launch rats without pre-existing testicular abnormalities (Fig. 4) had more of the germ-cell specific 2.7 kb *hsp70* and 3.2 kb *hsp90* transcripts (mRNA) than flight or vivarium rats with pre-existing abnormalities (Fig. 5) or caudal-elevation rats (Figs. 4 and 5). Reductions of *hsp70* and *hsp90* transcripts reflected corresponding changes in the seminiferous epithelium (Fig. 3) and a reduction in the proportion of germ cells to somatic cells within the testis. The pronounced reduction in amount of germ-cell-specific mRNA in caudal-elevation rats, in comparison to rats with pre-existing lesions, supports the morphologic

distinction (see above) between pre-existing abnormalities and those induced by caudal elevation. Second, we observed no induction of the somatic heat- or stress-inducible *hsp70* transcripts of 2.5 kb and 3.5 kb or *hsp90* transcript of 2.95 kb in any sample.

Leydig Cell Ultrastructure

Leydig cells in vivarium rats had less ($P<0.05$) surface density of smooth endoplasmic reticulum and more ($P<0.05$) surface densities of rough endoplasmic reticulum and outer mitochondrial membrane than Leydig cells in rats from the other three groups (Table 1). Surface densities of inner mitochondrial membrane, peroxisomes or lysosomes did not differ among treatment groups.

When data for the caudal-elevation rats and rats with pre-existing abnormalities were deleted, the only significant difference remaining among treatment groups was that for smooth endoplasmic reticulum (Table 2); surface density for this component was lower in vivarium rats than in flight or simulated-launch rats. Typically, the surface densities of smooth endoplasmic reticulum and peroxisomes are positively correlated, with each other as well as with testosterone production (Mendis-Handagama et al., 1988), but in the present study the correlation between surface densities of these two organelles was negative ($r = -0.63$, data for 10 normal rats as in Table 2; $P>0.05$).

Leydig Cell Function

The number of unoccupied receptors for rLH in the testis, as estimated by binding of hCG, was similar for all four treatment groups (Table 1). Nevertheless, it was evident that Leydig cells in flight and simulated-launch rats produced much less testosterone than those in vivarium rats. This was reflected in both concentration of testosterone in whole testicular tissue and in plasma from trunk blood (Table 1). However, these conclusions probably were influenced by inclusion of rats with pre-existing abnormal testes. Considering only the normal rats, mean concentrations of testosterone in testicular tissue or blood plasma both were lower in flight rats than in either simulated-launch or vivarium rats (Table 2). Thus, it appears that testosterone production was reduced in flight rats which had been normal before the experiment, but was similar in simulated-launch and vivarium rats without pre-existing testicular abnormalities. Values for concentration of receptors for rLH were similar for all three of these groups (Table 2).

Based on data for 10 normal rats in the flight, simulated-launch and vivarium groups, the correlation between intratesticular concentrations of testosterone and receptors for rLH ($r = 0.19$) was nonsignificant, although that between concentrations of testosterone in testicular tissue and in blood plasma was significant ($r = 0.66$). Surprisingly, the correlation between intratesticular concentration of testosterone and surface density of smooth endoplasmic reticulum was negative ($r = -0.62$; $P = 0.055$) and that between intratesticular concentration of testosterone and surface density of peroxisomes was nonsignificant ($r = 0.30$), although typically the surface area of smooth endoplasmic reticulum or peroxisomes is highly and positively correlated with testosterone secreting capacity (Zirkin et al., 1980, 1982; Ewing et al., 1983). The negative correlation between surface density of smooth endoplasmic reticulum and intratesticular testosterone concentration probably is not a consequence of the fact that we measured surface area per unit volume of Leydig cell, rather than total surface area of smooth endoplasmic reticulum per Leydig cell or testis as had Ewing et al. (1983). This was necessary because differential shrinkage of tissue, and other artifacts associated with imperfectly fixed tissue, precluded enumeration of Leydig cells per testis. Other data (Zirkin et al., 1980, 1982) show that surface density is highly correlated with testosterone production under carefully controlled conditions. More plausible, are the concepts that (a) intratesticular concentration at any instant need not necessarily reflect the capacity of a testis to secrete testosterone, and (b) testosterone production in flight rats was considerably less than would be expected given the concentration of rLH receptors in the tissue and the surface density of smooth endoplasmic reticulum. Although data for concentration of LH in

blood plasma from these rats are not available, we speculate that the problem probably is one of intratesticular fluid hydrodynamics or changes in availability of oxygen and substrates to Leydig cells. Alternatively, Leydig cells rather than reduced concentrations of LH in the blood might have undergone death or dedifferentiation.

GENERAL DISCUSSION

Utility of the Caudal-Elevation Model

The caudal-elevation (tail suspension or hind limbs unweighted) model frequently is used to simulate effects of microgravity to study atrophy of muscle or loss of calcium from bone after elimination of their need to support the animal, but also results in tissue fluid shifts (Hargens et al., 1984). The present data confirm those of Serova et al. (1989) and Deaver et al. (1991), in that both spermatogenesis and testosterone secretion are abnormal in caudal-elevation rats. Two separate problems exist in caudal-elevation rats: (a) the testes descend into and remain in the abdominal cavity, and the resulting rise in intratesticular temperature causes destruction of the germinal epithelium, and (b) positioning the testes at a level equal to or above the heart alters blood flow to the testis and intratesticular fluid hydrodynamics (probably affecting balance among blood, interstitial fluid, lymph, and seminiferous tubule fluid), and reduces secretion of testosterone.

Separation of these two sources of damage, by studying caudal-elevation rats in which the testes were retained in the scrotum by a loose ligature around the inguinal canal (Deaver et al., 1991), revealed that concentrations of testosterone in testicular interstitial fluid and in blood serum were abnormally low even in caudal-elevation rats with intrascrotal testes and normal spermatogenesis. Maintenance of normal spermatogenesis in caudal-elevation rats with intrascrotal testes, despite low testosterone concentrations in interstitial fluid of about 125 ng/ml (as compared to 350 ng/ml for control rats; Deaver et al., 1991), is possible because spermatogenesis proceeds normally if testosterone is present in testicular tissue at 20-25% of the normal intratesticular concentration (Zirkin et al., 1989). Thus, in caudal-elevation rats from the Cosmos-2044 project, collapse of spermatogenesis was primarily a consequence of elevated temperature, whereas the decreased blood plasma concentration of testosterone (0.5 vs 1.9 ng/ml for normal rats) was a consequence of altered fluid flow to and within the testis. As noted above, the measured intratesticular concentration of testosterone probably remained near normal because the proportion of the testis occupied by seminiferous tubules was greatly reduced.

Regardless of whether a whole-body harness or a tail sling was used to provide caudal-elevation, testosterone production was decreased (Deaver et al., 1991). However, the reduction of testosterone concentration in peripheral blood plasma of caudal-elevation rats was less than that for normal flight rats in the Cosmos-2044 study (0.51 vs 0.23 ng/ml; 1.93 ng/ml in normal simulated-launch or vivarium rats). Thus, the caudal-elevation model should not be rejected because testosterone production is reduced. Although the suppression of testosterone in caudal-elevation rats imperfectly mimics what may happen in microgravity, testosterone production is reduced in flight, so some sequelae of androgen deprivation might be detected using the caudal-elevation model.

Effects of Microgravity on the Testis

In flight rats from Cosmos-2044 without pre-existing lesions, spermatogenesis was normal, based on subjective evaluations and most quantitative data, but testosterone concentrations in testicular tissue and blood plasma were low. However, in the normal flight rats, the testicular testosterone concentration of 3.8 ng/g whole tissue was about 2X that in peripheral blood plasma for normal rats in the simulated-launch and vivarium groups (1.92 ng/ml; n=7). It is likely that testosterone production in normal flight rats was very close to the minimal amount obligatory for normal spermatogenesis (20-25% of the normal intratesticular concentration; Zirkin et al., 1989). If fluid

redistribution in the body or among the testicular compartments was further altered in flights of >13 days, further suppression of testosterone production probably would occur and abnormalities or cessation of spermatogenesis would follow. We speculate that testosterone production in rats exposed to microgravity for <14 days, in Cosmos or similar flights, is barely sufficient to maintain spermatogenesis.

Decreased secretion of testosterone (and probably other gonadal steroids including estradiol) is reflected in lower concentrations in peripheral blood from flight rats (Grindeland et al., 1990; Tables 1 and 2). This would affect not only the hypothalamus and adenohypophysis, but also anabolism and catabolism of protein in muscle and deposition and retention of calcium in bone. It would seem prudent for individuals interested in non-reproductive aspects of exposure of mammals to microgravity to consider altered hormonal concentrations as a contributory proximate cause of any change detected in muscle, bone or other body systems. Beneficial effects of prophylactic steroid therapy on maintenance of muscle mass or bone density of mammals exposed to microgravity should be considered, since such therapy is beneficial in reducing muscle changes in caudal-elevated rats (Tiska et al., 1987).

CONCLUSIONS

1. Some but not all aspects of testicular function were altered in rats subjected to space flight.

2. Spermatogenesis probably continued without major change during this space flight of <14 days.

3. Space flight for <14 days did not result in transcription of the stress-inducible *hsp70* or *hsp90* members of the cellular-stress gene family

4. Leydig cell function was altered in terms of ability to secrete testosterone about 9-11 hr after reentry despite normalcy of the number of rLH receptors per gram of testicular tissue. This may be a consequence of insufficient LH, because of alterations of the hypothalamic-adenohypophyseal axis, conversion of testosterone to other metabolites prior to secretion from Leydig cells, or altered fluid distribution and blood flow within the animal, especially in the testes. There was no evidence that this inability of Leydig cells to secrete testosterone was a consequence of reduced surface area of smooth endoplasmic reticulum or peroxisomes, or similar changes.

5. Spermatogenesis probably proceeded normally in flight rats, despite decreased availability of testosterone to the seminiferous tubules, because the concentration of testosterone in interstitial tissue fluid remained just above the critical concentration necessary for spermatogenesis.

6. Sequelae of low concentrations of testosterone in peripheral blood in flight animals should be considered in studies of bone or muscle loss. Delivery of exogenous androgens or estrogens to animals or humans in space may be desirable to compensate for reduced gonadal production of steroid hormones.

7. It is imperative that appropriate samples be obtained from animals or humans while they are in space, as well as before launch and after landing, to enable deductions concerning the underlying cause of abnormal Leydig cell function and sequelae of reduced testosterone production on loss of muscle and bone mass.

ACKNOWLEDGMENTS

This research would have been impossible without the skilled assistance of the Soviet dissection team, headed by Dr. A. S. Kaplansky of the Institute for Biomedical Problems, Moscow, USSR. The skilled technical assistance of C. Marshall, J. S. Palmer, J. Peters, Dr. S. M. L. C. Mendis-

Handagama, and K. Stav is gratefully acknowledged. This research was sponsored by contracts and cooperative agreements NAG-2-597, NAG-2-612, NAG-2-613, NAGW-1579, NCC2-12, NCC2-455 and NGT-50315 from the National Aeronautics and Space Administration, and grants G12RR03059-01A1 and HD-07,313 from the National Institutes of Health.

REFERENCES

1. Amann, R. P. Use of Animal Models for Detecting Specific Alterations in Reproduction. Fund. Appl. Toxicol. 2:13-26, 1982.

2. Amann, R. P. Detection of Alterations in Testicular and Epididymal Function in Laboratory Animals. Envir. Health Perspect. 70:149-158, 1986.

3. Amann, R. P., and W. E. Berndtson. Assessment of Procedures for Screening Agents for Effects on Male Reproductive Function: Effects of Dibromochloropropane (DBCP) on the Rat. Fund. Appl. Toxicol. 7:244-255, 1986.

4. Berndtson, W. E. Methods for Quantifying Mammalian Spermatogenesis: A Review. J. Anim. Sci. 44:818-833, 1977.

5. Berndtson, W. E., C. Neefus, R. H. Foote, and R. P. Amann. Optimal Replication for Histometric Analyses of Testicular Function in Rats or Rabbits. Fund. Appl. Toxicol. 12:291-302, 1989.

6. Cathala, G., J.-F. Savouret, B. Mendez, B. L. West, M. Karin, J. A. Martial, and J. D. Baxter. Laboratory Methods: A Method of Isolation of Intact Translationally Active Ribonucleic Acid. DNA. 2:329-335, 1983.

7. Curtis, S. K., and R. P. Amann. Testicular Development and Establishment of Spermatogenesis in Holstein Bulls. J. Anim. Sci. 53:1645-1657, 1981.

8. Deaver, D. R., R. P. Amann, R. H. Hammerstedt, R. Ball, D. N. R. Veeramachaneni, X.J. Musacchia. Effects of Caudal Elevation on Testicular Function in Rats; Separation of Effects on Spermatogenesis and Steroidogenesis. J. Appl. Physiol. (submitted), 1991.

9. Ewing, L. L., T.-Y. Wing, R. C. Cochran, N. Kormann, and B. R. Zirkin. Effect of Luteinizing Hormone on Leydig Cell Structure and Testosterone Secretion. Endocrinology. 112:1763-1769, 1983.

10. Feinberg, A. P., and B. Vogelstein. A Technique for Radiolabeling DNA Restriction Endonuclease Fragments to High Specific Activity. Addendum. Anal. Biochem. 137:266-267, 1984.

11. Grindeland, R. E. Cosmos 1887: Science Overview. FASEB J. 4:10-15, 1990.

12. Grindeland, R. E., I. A. Popova, M. Vasques, and S. P. Arnaud. Cosmos 1887 Mission Overview: Effects of Microgravity on Rat Body and Adrenal Weights and Plasma Constituents. FASEB J. 4: 105-109, 1990.

13. Grindeland, R. E., R. W. Ballard, J. C. Connolly. Cosmos 2044 Mission Overview. J. Appl. Physiol. in press 1991.

14. Gruppi, C. M., Z. F. Zakeri, and D. J. Wolgemuth. Stage and Lineage-Regulated Expression of Two sp 90 Transcripts During Mouse Germ Cell Differentiation and Embryogenesis. Mol. Reprod. Dev. (submitted), 1990.

15. Hargens, A. R., J. Steskal, C. Johansson, and C. M. Tipton. Tissue Fluid shift, forelimb loading, and tail tension in tail-suspended rats. Physiologist. 27 (Suppl.):S37-S38, 1984.

16. Hassouna, N., B. Michot, and J. P. Bachellerie. The Complete Nucleotide Sequence of Mouse 28 rRNA Gene, Implications for the Process of Size Increase of the Large Subunit rRNA in Higher Eukaryotes. Nucleic Acids Res. 12:3563-3583, 1984.

17. Hickey, E., S. E. Brandon, S. Sadis, G. Smale, and L. A. Weber. Molecular Cloning of Sequences Encoding the Human Heat-Shock Proteins and Their Expression During Hyperthermia. Gene. 43:147-154, 1986.

18. Hickey, E., S. E. Brandon, G. Smale, D. Lloyd, and L. A. Weber. Sequence and Regulation of a Gene Encoding a Human 89-Kilodalton Heat Shock Protein. Mol. Cell Biol. 9:2615-2626, 1989.

19. Lamb, J. C., Jr., and P. M. D. Foster. In: Physiology and Toxicology of Male Reproduction. Academic Press, New York. 1988.

20. Leblond, C. P., and Y. Clermont. Definition of the Stages of the Cycle of the Seminiferous Epithelium in the Rat. Ann. N.Y. Acad. Sci. 55:548-573, 1952.

21. Lowe, D. G., and L. A. Moran. Molecular Cloning and Analysis of DNA Complementary to Three Mouse M_r=68,000 Heat Shock Protein mRNAs. J. Biol. Chem. 261:2102-2110, 1986.

22. Mendis-Handagama, S. M. L. C., B. R. Zirkin, and L. L. Ewing. Comparison of Components of the Testis Interstitium with Testosterone Secretion in Hamster, Rat, and Guinea-Pig Testes Perfused *In Vitro*. Amer. J. Anat. 181:12-22, 1988.

23. Merrill, A., R. E. Mullens, R. E. Grindeland, and I. A. Popova. Analysis of Plasma from Cosmos 2044 Rats. J. Appl. Physio. (In press), 1991.

24. Moore, T. P., and W. E. Thornton. Space Shuttle Inflight and Postflight Fluid Shifts Measured by Leg Volume Changes. Aviat. Space Environ. Med. 58(Suppl.):A91-A96, 1987.

25. Oakberd, E.F. and C. Huckins. Spermatogonial Stem-Cell Renewal in the Mouse as Revealed by H^3-Thymidine Labeling and Irradiation. In: Stem Cells of Renewing Populations. Eds: A.B. Cairnie, P Lala, and D.G. Osmond. Academic Press, New York. 287-302, 1976.

26. Philpott, D.E., R. Corbett, C. Turnbill, S. Black, D. Dayhoff, J. McGourty, R. Lee, G. Harrison, and L. Savick. Retinal Changes in Rats Flown on Cosmos 936: A Cosmic Ray Experiment. Aviat. Space Environ. Med. 51:556-562, 1980.

27. Philpott, D. E., W. Sapp, C. Williams, J. Stevenson, S. Black, and R. Corbett. Reduction of the Spermatogonial Population in Rat Testes Flown on Space Lab-3. Physiologist. 28(Suppl.):S211-S212, 1985.

28. Raynal, F., B. Michot, and J.-P. Bachellerie. Complete Nucleotide Sequence of Mouse 18 S rRNA Gene; Comparisons With Other Available Homologs. FEBS Lett. 167:263-268, 1984.

29. Robb G. W., R. P. Amann, and G. W. Killian. Daily Sperm Production and Epididymal Sperm Reserves of Pubertal and Adult Rats. J. Reprod. Fertil. 54:103-1-7, 1978.

30. Sapp, W. J., D. E. Philpott, C. W. Williams, K. Kato, J. Stevenson, M. Vasques, and L. V. Serova. Effects of Spaceflight on the Spermatogonial Population of Rat Seminiferous Epithelium. FASEB J. 4:102-104, 1990.

31. Serova, L. V., L. A. Denisova, and O. V. Baikova. The Effect of Microgravity on the Reproductive Function of Male-Rats. Physiologist 32(Suppl.):S29-S30, 1989.

32. Thomas, J. A., K. J. Korach, and J. A. McLachlan. In: Endocrine Toxicology. Raven Press, New York. 1985.

33. Tiska, R. W., R. E. Herrick, and K. M. Baldwin. Effect of Anabolic Steroids on Skeletal Muscle Mass During Hindlimb Suspension. J. Appl. Physiol. 63:2122-2127, 1987.

34. Wahl, G. M., M. Stern, and G. R. Stark. Efficient Transfer of Large DNA Fragments from Agarose Gels to Diazobenzyloxymethyl Paper and Rapid Hybridization by Using Dextran Sulfate. Proc. Natl. Acad. Sci. USA. 76:3683-3687, 1979.

35. Weibel, E. R., and R. P. Bolender. Stereological Techniques for Electron Microscopic Morphometry. In: Principles and Techniques of Electron Microscopy. Ed: M. A. Nyas. Van Nostrand Reinhold, New York. 237-296, 1973.

36. Wolgemuth, D. J., C. M. Gruppi, V. Vambutas, and A. G. Wadewitz. Patterns of Expression and Potential Functions of Cellular Oncogenes and Heat Shock Protein Genes During Germ Cell Development. In: Cell and Molecular Biology of the Testis. Eds: C. Desjardins and L. Ewing. Oxford University Press. (In press), 1990.

37. Working, P.K. In: Toxicology of the Male and Female Reproductive Systems. Hemisphere Publ. Corp, New York. 1989.

38. Zakeri, Z.F., and D.J. Wolgemuth. Developmental-Stage-Specific Expression of the *hsp 70* Gene Family During Differentiation of the Mammalian Male Germ Line. Mol. Cell Biol. 87:1791-1796, 1987.

39. Zakeri, Z. F., D. J. Wolgemuth, and C. R. Hunt. Identification and Sequence Analysis of a New Member of the Mouse *hsp70* Gene Family and Characterization of Its Unique Cellular and Developmental Pattern of Expression in the Male Germ Line. Mol. Cell Biol. 8:2925-2932, 1988.

40. Zirkin, B. R., L. L. Ewing, N. Kormann, and R. C. Cochran. Testosterone Secretion by Rat, Rabbit, Guinea-Pig, Dog, and Hamster Testes Perfused *In Vitro* : Correlation with Leydig Cell Ultrastructure. Endocrinology. 107:1867-1874, 1980.

41. Zirkin, B. R., D. D. Dykman, N. Kormann, R. C. Cochran, and L. L. Ewing. Inhibition and Recovery of Testosterone Secretion in Rats are Tightly Coupled to Quantitative Changes in Leydig Cell Smooth Endoplasmic Reticulum. Ann. N.Y. Acad. Sci. 38:17-28, 1982.

42. Zirkin, B. R., R. Samfulli, C. A. Awoniyi, and L. L. Ewing. Maintenance of Advanced Spermatogenic Cells in the Adult Rat Testis: Quantitative Relationship to Testosterone Concentrations within the Testis. Endocrinology. 124:3043-3049, 1989.

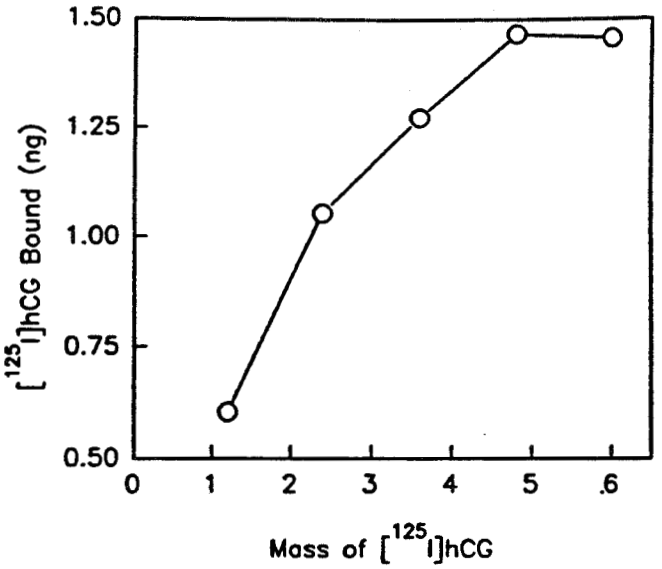

Figure 1. Mass of hCG required to saturate receptors for rLH in 20 mg rat testicular tissue in a total volume of 350 l; incubated 18 hr at 25°C. Data were corrected for non-specific binding. See text for details.

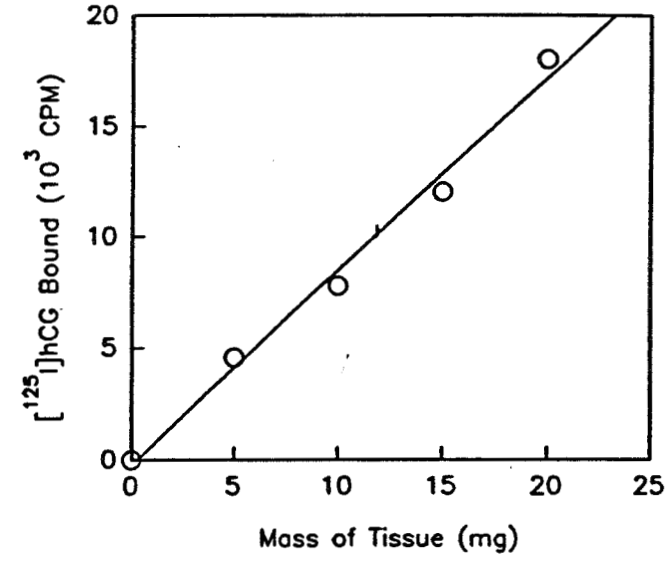

Figure 2. Binding of [^{125}I]hCG to receptors for rLH as a function of mass of testicular tissue (0-20 mg/tube); incubated in 350 l for 18 hr at 25°C. Data were corrected for non-specific binding. See text for details.

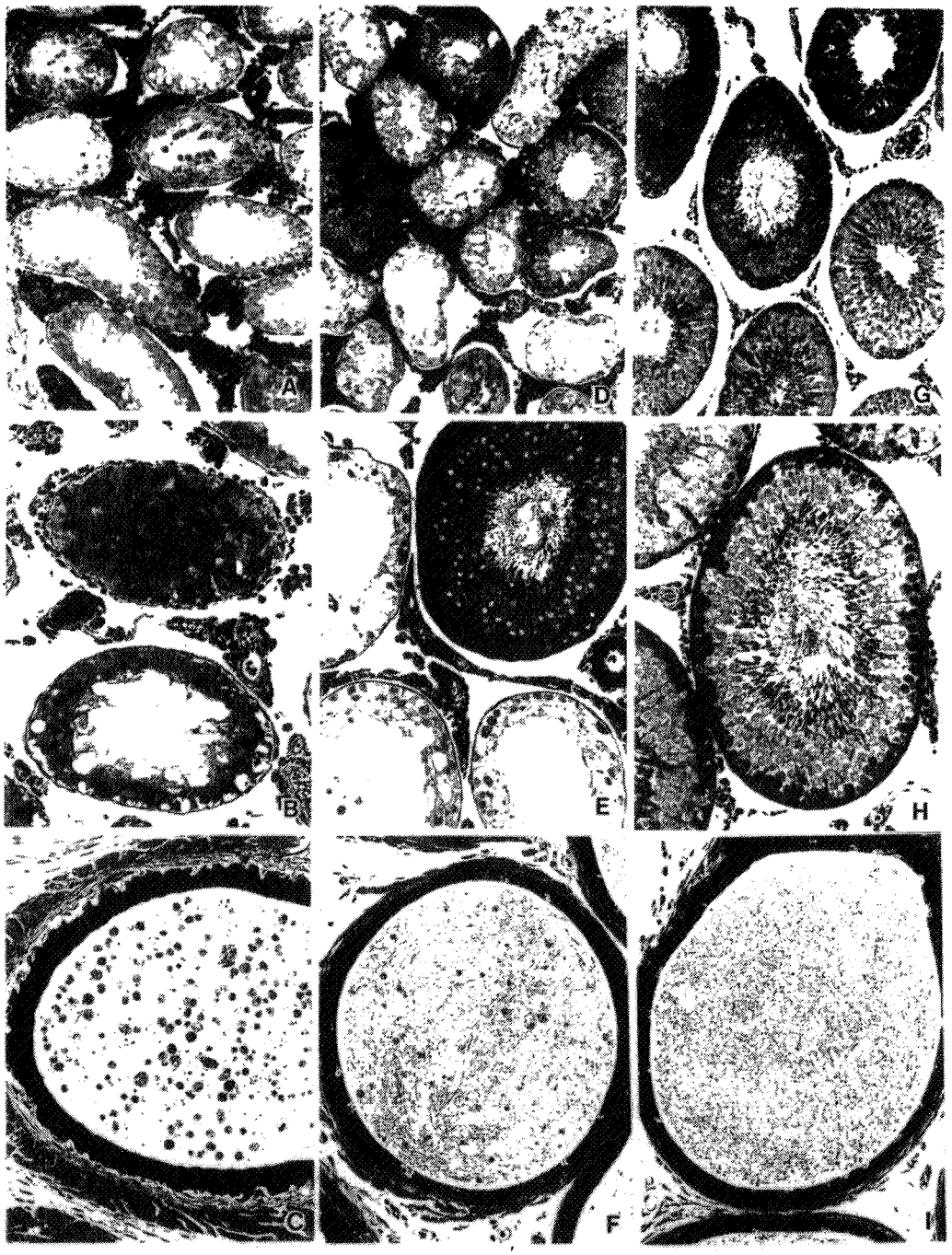

Figure 3.(A–I) Micrographs of testicular (figs. 3A, 3B, 3D, 3E, 3G, 3H) and epididymal tissue (figs. 3C, 3F and 3I). Testicular tissue from a caudal-elevation rat (3A, 3B) contained only grossly abnormal seminiferous tubules, but a few germ cells were present in some tubules. These lesions were induced by the treatment. Testicular tissue from a vivarium rat with a pre-existing abnormality (3D, 3E) contained both normal and abnormal seminiferous tubules; the abnormal ones contained few germ cells and Sertoli cells predominated. Distinction of pre-existing testicular abnormalities from those induced by caudal elevation also was evident from content of the cauda epididymidis; in caudal-elevation rats sloughed germ cells rather than spermatozoa predominated (3C), whereas in rats with pre-existing lesions there were few sloughed germ cells among the spermatozoa in the cauda epididymidis (3F). Testicular tissue from flight rats without a preexisting testicular abnormality was normal in appearance (3G) and Stage-VII seminiferous tubules (fig. 3H) had normal ratios of germ cells to Sertoli cells (see text and Table 2); the luminal content of the cauda epididymidis also was normal (3I). Figures 3A, 3D and 3G are at 62X and 3B, 3C, 3E, 3F, 3H, and 3I are at 125X magnification; toluidine blue staining.

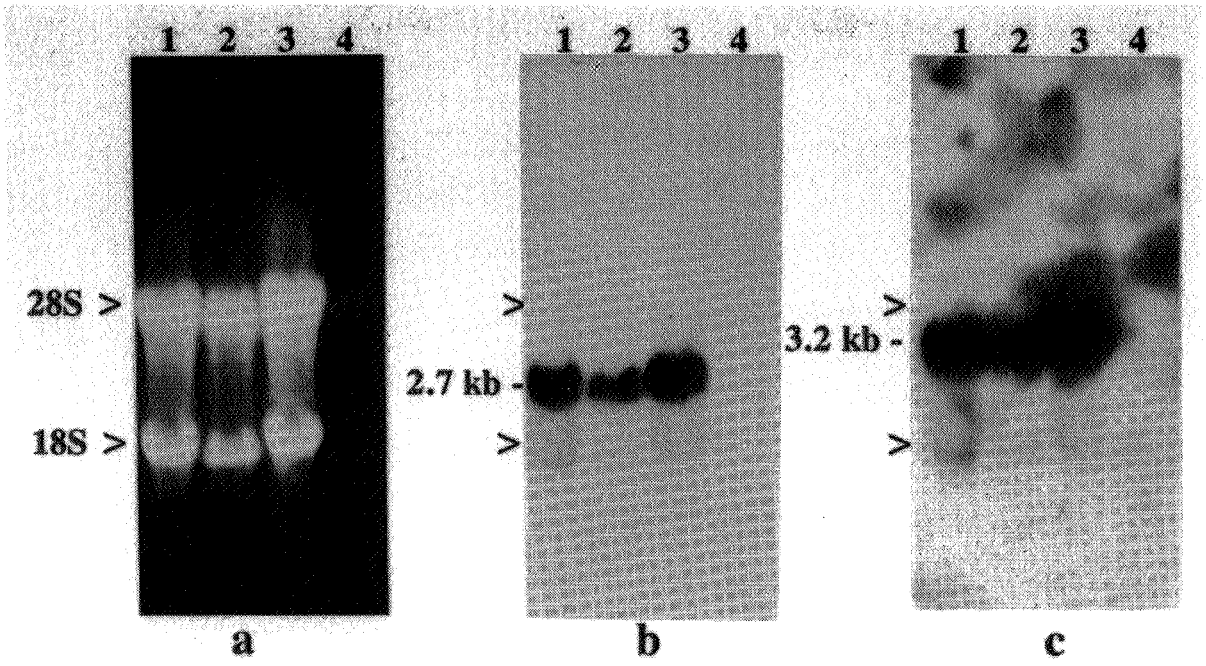

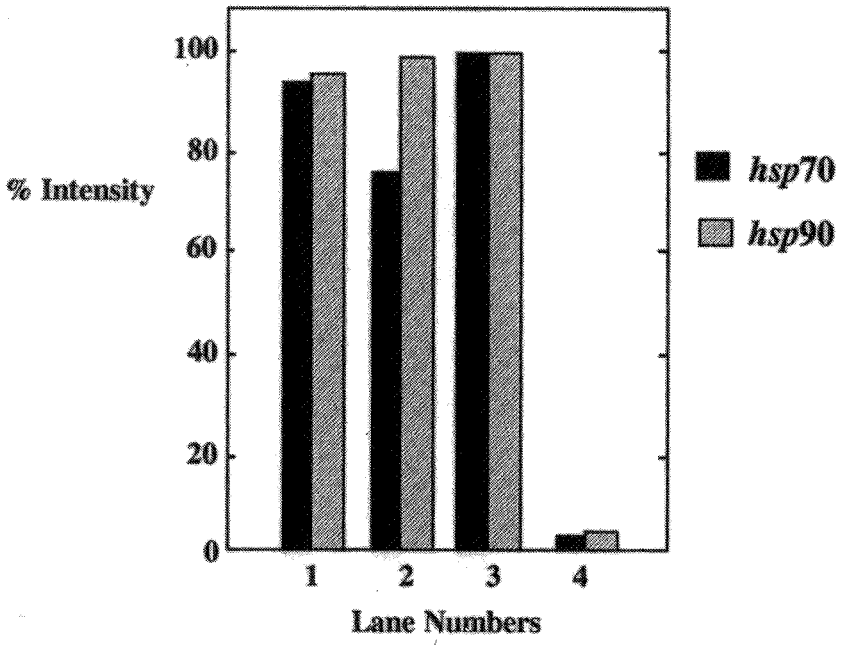

d

Figure 4. mRNAs isolated from testes of rats without pre-existing testicular abnormalities (F-7, S-7, V-7); it is not known if the caudal-elevation rat (T-7) was normal or abnormal when treatment was started. Total RNA was isolated from the testes of rats designated #7 which had been subjected to flight (lane 1), vivarium (lane 2), simulated launch (lane 3), or caudal-elevation (lane 4). Total RNA was size fractionated by gel electrophoresis with ethidium bromide, and photographed under UV light (fig. 4A). The 28S and 18S rRNAs are designated. Hybridization of the [P^{32}]labeled hsp70 (fig. 4B) and hsp90 (fig. 4C) probes to mRNA after transfer to membranes was detected by autoradiography. Relative amount of hybridization (fig. 4D) was determined by densitometric analysis.

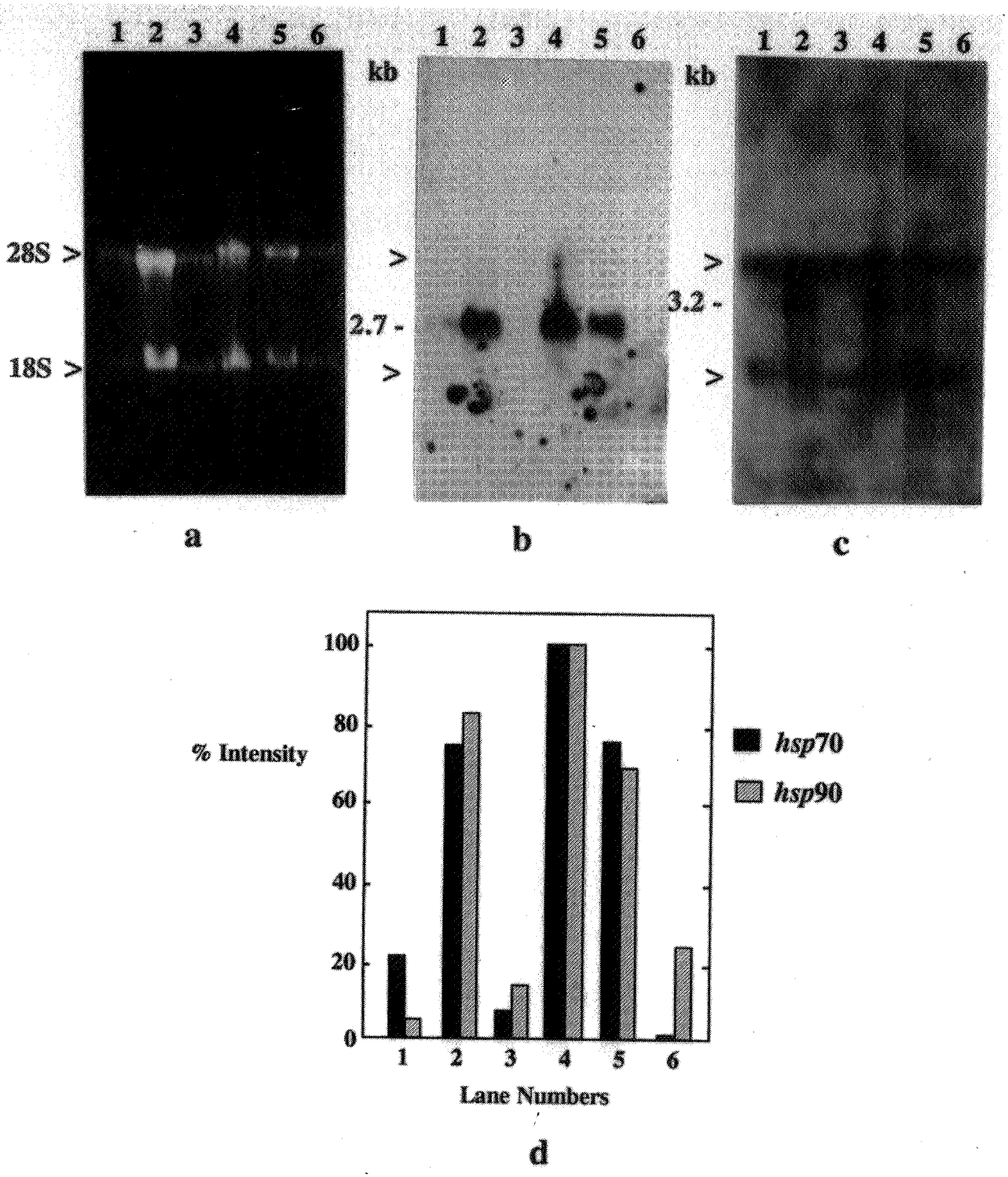

Figure 5. mRNAs isolated from testes of rats with pre-existing testicular abnormalities (F-6, V-6), and one rat without a pre-existing abnormality (S-6); it is not known if the caudal-elevation rat (T-6) was normal or abnormal when treatment was started. Total RNA was isolated from the testes of rats designated #6, which had been subjected to flight (lane 1), vivarium (lane 2), caudal-elevation (lane 3), or simulated launch (lane 4); control RNA was from normal mouse testis (lane 5; positive control) and mouse liver (lane 6; negative control). Total RNA was size fractionated by gel electrophoresis with ethidium bromide, and photographed under UV light (fig. 5A). The 28S and 18S rRNAs are designated. Hybridization of the [P^{32}]labeled hsp70 (fig. 5B) and hsp90 *(fig. 5C) probes to mRNA after transfer to membranes was detected by autoradiography. The* hsp90 *probe cross-hybridized with the 28S and 18S rRNA. Relative amount of hybridization (fig. 5D) was determined by densitometric analysis.*

S2-51

51347

EXPERIMENT K-7-17

EFFECTS OF SPACEFLIGHT ON THE PROLIFERATION OF JEJUNAL MUCOSAL CELLS

Principal Investigator:

R.W. Phillips
Department of Physiology
College of Veterinary Medicine and Biomedical Science
Colorado State University
Fort Collins, Colorado

Co-Investigators:

C.L. Moeller
H.R. Sawyer
Department of Physiology
College of Veterinary Medicine and Biomedical Science
Colorado State University
Fort Collins, Colorado

K.L. Smirnov
Institue of Biomedical Problems
Moscow, USSR

Page intentionally left blank

EXPERIMENT K-7-17

EFFECTS OF SPACEFLIGHT ON THE PROLIFERATION OF JEJUNAL MUCOSAL CELLS

R.W. Phillips, C.L. Moeller, H.R. Sawyer, and K.L Smirnov

SUMMARY

The purpose of this project was to test the hypothesis that the generalized, whole body decrease in synthetic activity due to microgravity conditions encountered during spaceflight would be demonstrable in cells and tissues characterized by a rapid rate of turnover. Jejunal mucosal cells were chosen as a model since these cells are among the most rapidly proliferating in the body. Accordingly, the percentage of mitotic cells present in the crypts of Lieberkuhn in each of 5 rats flown on the COSMOS 2044 mission were compared to the percentage of mitotic cells present in the crypts in rats included in each of 3 ground control groups (i.e., vivarium, synchronous and caudal-elevated). No significant difference ($p>.05$) was detected in mitotic indices between the flight and vivarium group. Although the ability of jejunal mucosal cells to divide by mitosis was not impaired in flight group, there was, however, a reduction in the length of villi and depth of crypts. The concommitant reduction in villus length and crypth depth in the flight group probably reflects changes in connective tissue components within the core of villi.

INTRODUCTION

Although the observed negative nitrogen balance (1,2), muscle atrophy (1-3), loss in bone mass (2) and decreased proliferation of lymphocytes (4) in astronauts exposed to microgravity conditions is thought to reflect a generalized, whole body decrease in synthetic activity (1), the effects of microgravity on rapidly proliferating cells and tissues have not been thoroughly examined. Thus, the purpose of this study was to test the hypothesis that the generalized, whole body decrease in synthetic activity due to microgravity conditions that accompany spaceflight would also be manifested in cells and tissues characterized by a rapid rate of turnover. Accordingly we chose to examine the effects of microgravity on jejunal mucosal cells that line the small intestine. Jejunal mucosal cells are among the most rapidly proliferating in the body and are derived from stem cells present in the crypts of Lieberkühn (5,6). Once formed they migrate out of the crypts onto intestinal villi; are progressively "pushed up" villi as new cells are formed; and, ultimately reach the tips of villi where they are then desquamated. In rats the entire process, from initial formation in crypts to desquamation, normally takes approximately 2 days (5,6). .

To determine the effects of spaceflight on the proliferation of jejunal cells the percentage of mitotic cells present in the crypts of Lieberkühn in each of five rats aboard the COSMOS 2044 flight were compared to the percentage of mitotic cells present in the crypts of Lieberkühn in each of three ground control groups (i.e. vivarium, synchronous and caudal-elevated). In addition, the depth of crypts and length of jejunal villi in each of five rats per group were measured.

MATERIALS AND METHODS

Tissue Samples

Tissue samples (each 1 cm in length) from the proximal, middle and distal regions of the jejunum from each of 5 rats from the vivarium, synchronous, caudal-elevated and flight groups were processed and shipped to Colorado State University per pre- and post-flight protocols described

for the COSMOS 2044 mission. Briefly, jejunal regions of interest were removed and flushed with 1 to 2 ml of physiological saline. Immediately thereafter each sample was flushed with 2 ml of a solution of 4% glutaraldehyde-0.1M cacodylate (pH 7.4) containing 5% sucrose and placed into 25 ml screw-top vials containing approximately 20 mls of the same fixative. After 6 - 24 hours of fixation, the samples were rinsed 3 times in 0.1 M cacodylate buffer and shipped to Colorado State University. Upon arrival, each sample was cut into 5 equal segments, post-fixed in 1% osmium tetroxide for 90 min, washed in cacodylate buffer, dehydrated in a graded series of ethanols and embedded in Polybed 812.

Mitotic Index

Sections 1 μm-thick were cut from each of the 5 segments from each of the 3 jejunal regions per animal and stained with toluidine blue. To accurately determine the mitotic index for each respective region, at least 2000 cells per region per animal were examined. Since mitosis is restricted to the crypts of Lieberkühn (5), cells outside the crypts proper were not considered in determining mitotic indices. Prior to evaluation all slides were coded so that the technician reading the slides did not know the region or treatment group being examined. All tissue sections used to determine mitotic index were also evaluated for the presence of microscopic lesions by a pathophysiologist.

Villus Length and Crypt Depth

To determine villus length and crypt depth at least 20 villi and crypts were measured per region per animal. Measurements were obtained using a computerized image analysis system (Bioquant System IV) coupled to a Olympus bright field microscope equipped with a 4X objective and a video camera. Special care was taken to ensure that measurements were taken only on villi and crypts that had been cut in cross-section.

Statistics

All data were statistically analyzed by analysis of variance and differences between means were detected using the Student-Newman-Keuls procedure.

RESULTS

General Observations

With only one exception no microscopic lesions of pathological significance were observed. The exception was limited to the distal region of the jejunum in one rat included in the vivarium group. The lesion observed consisted of a localized fibrotic patch indicative of a previous ulceration that had subsequently healed.

Mitotic Index

The percentage (mean±sem) of mitotic cells present in the crypts of Lieberkühn in the proximal, middle and distal regions of the jejunum for rats included in each of the respective treatment groups is summarized in Table 1. The only significant difference ($p < .05$) detected was that the percentage of mitotic cells present in the middle region of the jejunum of rats included in the synchronous group was slightly higher than in any of the other treatment groups. Similarly, the only statistically significant difference in mitotic index among regions within group was apparent only in the synchronous group where the mitotic index in the proximal region was lower than in either the middle or distal regions.

Villus Length and Crypt Depth

The length of jejunal villi and depth of crypts of Lieberkühn in the proximal, middle and distal regions of the jejunum are summarized in Tables 2 and 3, respectively. Regardless of region examined jejunal villi in rats included in the vivarium group were greater in length than in rats included in the synchronous and flight groups (Table 2). The length of villi in the middle and distal regions in rats included in the caudal-elevated group was similar ($p>.05$) to that measured in rats in the vivarium group. However, the length of villi in the proximal region differed (vivarium = 738.2 μm vs. caudal-elevated = 643.6μm). Differences among jejunal regions within group were restricted to the caudal-elevated group where villi were longer in the middle and distal jejunum than in the proximal jejunum.

Treatment effects on the depth of the crypts of Lieberkühn were primarily restricted to the proximal and distal jejunal regions: no significant difference among groups was detected with respect to the depth of crypts in the middle region of the jejunum (Table 3). Thus, with the exception of the distal region in the flight group rats, the depth of crypts in the proximal and distal regions was greater in the vivarium group than in the synchronous, caudal-elevated and flight groups. As evident from the data presented in Table 3, there was no significant variation in the depth of crypts among regions within treatment groups.

DISCUSSION

The percentages of mitotic cells present in the crypts of Lieberkühn in the proximal, middle and distal regions of the jejunum in rats included in the flight group did not significantly differ from the percentage of mitotic cells present in identical regions in rats included in the ground control vivarium group. Thus, while there may be a generalized, whole body decrease in synthetic activity associated with microgravity conditions during spaceflight, the proliferation of jejunal mucosal cells does not appear to be affected. These data also support our previous conclusions from the Cosmos 1887 mission that the effects, if any, of spaceflight on the proliferation of jejunal mucosal cells are minimal and short-lived (7). However, it should be noted that while the ability of cells in the crypts of Lieberkühn to divide by mitosis was not found to be impaired in the present study, the length of villi was significantly reduced in all jejunal regions in flight rats as compared to vivarium rats. Since villi in flight rats were lined by normal mucosal cells, the concomitant reduction in villus height and crypt depth probably reflects changes (e.g, shrinkage) in the connective tissue core of villi and is not due to an impairment in the migration of newly proliferated cells needed to replace those desquamated. At present, the physiological basis and potential significance of this observation is not clear.

SUMMARY AND CONCLUSIONS

To examine the effects of spaceflight on the proliferation and turnover of jejunal mucosal cells, the percentages of mitotic cells present in the crypts of Lieberkuhn in the proximal, middle and distal jejunum in each of 5 rats flown on the COSMOS 2044 mission were compared to percentages in the identical regions in rats included in the vivarium, synchronous and caudal-elevated groups. Based on the data obtained, there was no difference in mitotic indices between animals in the flight and vivarium (ground control) groups. Thus, it appears that the ability of jejunal mucosal cells to proliferate is not affected by microgravity conditions associated with spaceflight. Although the length of villi and depth of crypts were reduced in flight animals as compared to those in the vivarium group, the observed reduction is probably attributable to changes in the connective tissue core of villi, and is not likely due to an impairment of the proliferation and migration of jejunal mucosal cells.

ACKNOWLEDGEMENTS

We gratefully acknowledge the assistance of Dr. Rao Veeramachaneni in evaluating tissue sections for microscopic lesions of potential pathological significance.

REFERENCES

1. Nicogossian, A. E. and J.F. Parker, Jr. Space Physiology and Medicine. NASA SP-447. National Aeronautics and Space Administration, Washington, D.C. 324, 1982

2. Rambaut, P. C. and P.C. Johnson. Nutrition. In: Space Physiology and Medicine. Eds: A.E. Nicogossian, C.L. Huntoon, and S.L. Lea & Febiger, Philadelphia, PA. 1989.

3. Oganov, V.S. Results of Biosatellite Studies of Gravity-Dependent Changes in the Musculo-Skeletal System of Mammals. Physiologist. 24(Suppl.):S55-S58, 1981

4.Bechler, B. and A. Cogoli, A. Lymphozyten Sind Schwerkraftempfindlich. Naturwissenschaften. 73:40-403, 1986

5. Cairnie, A.B., L.F. Lamerton, and G.G. Steele. Cell Proliferation Studies in the Intestinal Epithelium of the Rat: I. Determination of the Kinetic Parameters. Exp. Cell Res. 39:528-538, 1965.

6. Lipkin, M. Proliferation and Differentiation of Gastrointestinal Cells. Physiol. Rev. 53:891-915, 1973.

7. Sawyer, H. R., C.L. Moeller, R.W. Phillips, and K.L. Smirnov. Effects of Spaceflight on Proliferation of Jejunal Mucosal Cells. FASAB J. 4:92-94, 1990.

TABLE 1

MIOTIC INDEX FOR JEJUNAL MUCOSL CELLS

	Treatment Groups[a]			
Region	Vivarium	Synchronous	Caudal-Elevated	Flight
Proximal	3.1 ± .2	3.3 ± .2[b]	3.3 ± .3	4.0 ± .4
Middle	3.6 ± .4[AB]	3.9 ± .1[Aa]	3.3 ± .2[B]	3.4 ± .1[B]
Distal	3.3 ± .2	3.9 ± .2[a]	4.0 ± .1	3.9 ± .2

[a] Means (± SEM) with different uppercase letter superscript within rows are different ($P < 0.05$). Means (± SEM) with different lowercase letter superscript within columns are different ($P < 0.05$).

TABLE 2

LENGTH (μm) OF JEJUNAL VILLI

	Treatment Groups[a]			
Region	Vivarium	Synchronous	Caudal-Elevated	Flight
Proximal	738.2 ± 23.7[A]	634.0 ± 13.0[B]	643.6 ± 10.9[Bb]	608.5 ± 19.0[B]
Middle	730.2 ± 47.0[A]	632.0 ± 17.9[B]	689.5 ± 7.5[ABa]	622.1 ± 10.5[B]
Distal	717.1 ± 27.1[A]	623.2 ± 16.0[B]	672.5 ± 8.1[ABa]	628.2 ± 20.0[B]

[a] Means (± SEM) with different uppercase letter superscript within rows are different ($P < 0.05$). Means (± SEM) with different lowercase letter superscript within columns are different ($P < 0.05$).

TABLE 3

JEJUNAL CRYPT (μm)

Region	Treatment Groups[a]			
	Vivarium	Synchronous	Caudal-Elevated	Flight
Proximal	164.2 ± 1.2^{A}	133.3 ± 2.4^{B}	139.5 ± 4.5^{B}	134.6 ± 3.5^{B}
Middle	143.4 ± 7.5	133.4 ± 3.0	131.8 ± 2.4	135.0 ± 5.1
Distal	161.6 ± 11.3^{A}	129.6 ± 2.9^{B}	129.1 ± 3.5^{B}	152.0 ± 7.3^{AB}

[a] Means (± SEM) with different uppercase letter superscript within rows are different ($P < 0.05$).

53-51
5134B

EXPERIMENT K-7-18

EFFECTS OF SPACEFLIGHT IN THE MUSCLE ADDUCTOR LONGUS OF RATS FLOWN IN THE SOVIET BIOSATELLITE COSMOS 2044:

PART I: A STUDY EMPLOYING NEURAL CELL ADHESION MOLECULES (N-CAM) IMMUNOCYTOCHEMISTRY AND CONVENTIONAL MORPHOLOGICAL TECHNIQUES (LIGHT AND ELECTRON MICROSCOPY)

PART II: QUANTITATIVE AUTORADIOGRAPHIC ANALYSIS OF GABA (BENZODIAZEPINE) AND MUSCARINIC (CHOLINERGIC) RECEPTORS IN THE FOREBRAIN OF RATS FLOWN ON COSMOS 2044

Principal Investigator:

N.G. Daunton
NASA-Ames Research Center
Moffett Field, CA.

Co-Investigators:

F. D'Amelio
L. Wu
San Jose State University Foundation
NASA-Ames Research Center
Moffett Field, CA

E.I. Ilyina-Kakueva
I.B. Krasnov
Institute of Biomedical Problems
Moscow, USSR

T.M. Hyde
S.K. Sigworth
Clinical Brain Disorders Branch
National Institute of Mental Health
Bethseda, MD

Page intentionally left blank

EXPERIMENT K-7-18

PART I: A STUDY EMPLOYING NEURAL CELL ADHESION MOLECULES (N-CAM) IMMUNOCYTOCHEMISTRY AND CONVENTIONAL MORPHOLOGICAL TECHNIQUES (LIGHT AND ELECTRON MICROSCOPY)

F. D'Amelio, N.G. Daunton, and E.I. Ilyna-Kakueva

Technical Assistance:
R. Binnard, E. Harris, and A. Russell

The present report includes studies performed in the muscle adductor longus of rats flown in the Soviet Biosatellite COSMOS 2044 and of synchronous, vivarium and basal controls. Studies of the muscle tibialis anterior and of the muscle adductor longus of tail suspended rats will be the subject of a forthcoming report.

ABSTRACT

The effects of spaceflight upon the "slow" muscle adductor longus was examined in rats flown in the Soviet Biosatellite COSMOS 2044. Three groups -synchronous, vivarium and basal- served as controls. The techniques employed included standard methods for light microscopy, N-CAM immunocytochemistry and electron microscopy.

Light microscopic observations revealed myofiber atrophy, contraction bands and segmental necrosis accompanied by cellular infiltrates composed of macrophages, leucocytes and mononuclear cells.

N-CAM immunoreactivity was seen (N-CAM-IR) on the myofiber surface, satellite cells and in regenerating myofibers reminiscent of myotubes.

Ultrastructural alterations included Z band streaming, disorganization of myofibrillar architecture, sarcoplasmic degradation, extensive segmental necrosis with preservation of the basement membrane, degenerative phenomena of the capillary endothelium and cellular invasion of necrotic areas. Regenerating myofibers were identified by the presence of increased amounts of ribosomal aggregates and chains of polyribosomes associated with myofilaments that displayed varied distributive patterns.

The principal electron microscopic changes of the neuromuscular junctions consisted of a decrease or absence of synaptic vesicles, degeneration of axon terminals, increased number of microtubules, vacant axonal spaces and axonal sprouting.

The present observations indicate that major alterations such as myofibrillar disruption and necrosis, muscle regeneration and denervation and synaptic remodeling at the level of the neuromuscular junction may take place during spaceflight.

INTRODUCTION

The effects of spaceflight upon muscle tissue are far from being understood. Although progress has been made in understanding the differences in response to weightlessness of fiber types, some aspects of the dynamics of these responses remain elusive. Both flight and ground-based (mostly hind-limb suspension) experiments have provided useful information on the effects of microgravity and simulated microgravity upon the morphology, metabolic properties, histochemistry and electrophysiology of various muscles (Oganov and Potapov, 1976; Oganov *et al.*, 1980; Simard *et al.*, 1982; Hoh and Chow, 1983; Musacchia *et al.*, 1983; Jaspers and Tischler, 1984; Templeton et al., 1984a,b; Fell et al., 1985; Riley *et al.*, 1985; Fitts *et al.*, 1986; Loughna *et al.*, 1986; Steffen and Musacchia, 1986; Alford *et al.*, 1987; Haushka *et al.*, 1987; Oomura and Katafuchi, 1987; Roy *et al.*, 1987; Thomason *et al.*, 1987a,b; Winiarski *et al.*, 1987; Herbert *et al.*, 1988; Martin, 1988; Martin *et al.*, 1988; Thomason *et al.*, 1988; Graham *et al.*, 1989; Riley *et al.*, 1990a). Through these investigations we have learned that -as was expected- "slow" muscles, mostly composed of type I fibers (e.g., soleus, adductor longus), carry the burden of the changes.

This report will place emphasis upon some particular responses to weightlessness observed by us in the adductor longus muscle of rats flown in the Soviet COSMOS flight 2044, namely, 1) muscle fiber injury, 2) regenerative phenomena, 3) alterations of the neuromuscular junctions.

We chose to perform N-CAM immunocytochemistry in view of the fact that, among other functions, N-CAM is a glycoprotein of heavy molecular weight that seems to mediate surface interactions of nerves with muscle. Data obtained mostly in rats by means of biochemical or immunocytochemical methods have shown that N-CAM: 1) is abundant on the surface of myoblasts, embryonic myotubes and intramuscular nerves, 2) declines in level as muscle development proceeds, disappears during the first two postnatal weeks and is undetectable on the surface of adult muscle fibers, 3) is present in postynaptic and perisynaptic areas of the neuromuscular junctions of adult muscle fibers, in the surface of the motor nerve terminals and in the Schwann cells that cap nerve terminals, 4) is detectable in sensory and sympathetic innervation in adult muscle, 5) is not detectable on myelinated portions of axons, on myelinating Schwann cells and on nonsynaptic portions of muscle fibers (Rieger *et al.*, 1985; Covault and Sanes, 1986; Covault *et al.*, 1986; Sanes *et al.*,1986). The application of N-CAM immunocytochemistry (to our knowledge never applied before on muscle tissue of animals subjected to weightlessness) together with more conventional techniques, might assist in the interpretation of some of the changes observed in muscle when gravitational conditions are altered.

MATERIAL AND METHODS

1) Animals

Male Czechoslovakian Wistar rats born 5-29-89 were used in this experiment. The animals were received in Moscow 7-11-89 with an average weight of approximately 100 grams. Five animals per group (1 flight group and 3 control groups) were employed. Muscles from rats number 6-10 were employed in this study.

2) Relevant flight information

The animals were launched in the Biosatellite COSMOS 2044 on 9-15-89 at 10:30 A.M. and recovered 9-29-89 at 6 A:M. Euthanasia took place the same day between 2:22 P.M. and 5:05 P.M.

Generic data used in the Soviet Union to represent a typical Cosmos Biosatellite Mission as to acceleration and vibration profiles are the following: *Launch*: acceleration, 4 g for 10 minutes (plateau, 7 minutes); vibration frequency, 50-70 Hz; vibration amplitude, 0.4 mm; vibration duration, 10 minutes; noise, 110 db. *Reentry:* deceleration, 6 g for 5 minutes (constant level, 3 minutes).

3) Control groups

Three control groups composed of 5 animals each were employed. *Basal controls* were euthanized at the time of launch; *vivarium controls* were euthanized 5 days after the flight animals; *synchronous controls* were euthanized 3 days after the flight animals. The latter group received treatment similar to the flight animals (except actual flight) which included simulation of conditions during acceleration and reentry.

4) Muscles

Five adductor longus muscles of each group were dissected by Soviet scientists at the landing place and divided longitudinally in 2 halves. One half was frozen in Freon 12 cooled in liquid nitrogen, stored and sent to the U.S. in biotransporters at -70°C. The other half was fixed in a mixture of 1.5% glutaraldehyde and 1 % paraformaldehyde in 0.12M phosphate buffer, pH 7.2-7.4.

5) Conventional light microscopy

One slide of all groups (flight and controls, frozen half) with 3 sections each were stained with hematoxylin and eosin.

6) N-CAM immunocytochemistry

a) Antibodies

Polyclonal anti-N-CAM antibodies raised in rabbits were generously provided by Dr. Stanley Hoffman (Rockefeller University).

b) Immunocytochemical procedure

The frozen half of the sample was cut on a cryostat set at- 20°C. Sections (25μm) were mounted on gelled slides on a drop of EDTA to prevent retraction (Pearson and Sabarra, 1974). The sections were fixed for 1 h in 4% paraformaldehyde in 0.1M phosphate buffer, pH 7.2-7.4., and then treated in the following sequence: 1) 5-10 minutes at room temperature (RT) with 3% hydrogen peroxide (30% solution) in 10% methanol in phosphate buffer saline (PBS), 2) 4 rinses in PBS x 30 min (RT), 3) incubation for 60 min (RT) in normal swine serum (1:20 in PBS with 1% powdered milk), 4) incubation in anti-N-CAM (1:500 to1:1000 in PBS with 1% powdered milk) overnight at 4°C, 5) 4 rinses in PBS x 30 min (RT), 6) incubation for 60 min (RT) in swine anti-rabbit IgG diluted 1:100 in PBS containing 1% powdered milk, 7) 4 rinses in PBS x 30 min (RT), 8) incubation for 60 min (RT) with peroxydase antiperoxydase complex diluted 1:200 in PBS containing 1% powdered milk, 9) 4 rinses in PBS x 30 min (RT), 10) reaction at RT, with 12.5 mg diaminobenzidine tetrahydrochloride in 50 ml TBS (0.05M Tris

buffer-0.9% saline, pH 7.6) + 5 µl 30% hydrogen peroxyde, 5-10 min to develop reaction product, 11) rinse of the sections in PBS, 2 changes x 10 min (RT), 12) sections were dehydrated in graded alcohols and xylenes and coverslipped with Permount.

Control sections were treated in a similar fashion except that PBS was substituted for the primary antibody.

7) Electron microscopy

For the localization of motor endplates the whole half of the muscle fixed in glutaraldehyde-paraformaldehyde was incubated in a mixture of hexazotized pararosaniline and indoxyl acetate in citrate buffer according to a protocol developed by Strum and Hall-Craggs (1982). The motor endplate region was in this way identified by the acethylcholinesterase activity under the stereomicroscope and dissected. Tissue fragments containing the endplates and pieces of nonsynaptic regions were postfixed in 2% osmium tetroxyde in 0.12M phosphate buffer (pH 7.2-7.4), dehydrated in graded alcohols and embedded in Quetol 651 epoxy resin. Silver-gold ultrathin sections were obtained, stained with uranyl acetate-lead citrate, mounted in copper grids (100 mesh), and observed in a Philips 300 electron microscope.

RESULTS

1) Conventional light microscopy

Primary pathological changes observed in the flight animals and not present in any of the control groups were: myofiber atrophy (Fig. 1C,D), muscle fiber disarray (Fig. 2C), contraction bands (Fig. 2B) and segmental necrosis frequently accompanied by extensive cellular infiltration composed of macrophages, polymorphonuclear leucocytes and mononuclear cells (Figs. 1A,B)

2) N-CAM immunocytochemistry

N-CAM immunoreactivity (N-CAM-IR) was observed in segments of the surface of muscle fibers and in interstitial structures of all flight animals. On the myofiber surface, the N-CAM-IR regions frequently contained collections of large, prominent nuclei (Fig. 3A) that most likely corresponded to rows of myonuclei. Satellite cells also expressed N-CAM-IR (Fig. 3B). N-CAM-IR structures of cylindrical shape with straight or undulatory outlines interpreted as regenerating myofibers, were seen within the interstitial spaces between muscle fibers. When observed at high power some of them contained rows of large nuclei reminiscent of myotubes (Fig. 4). These N-CAM-IR structures were concentrated in the middle region of the muscle close to the area occupied by the neuromuscular junctions. Control sections appeared completely devoid of staining (Fig. 3) and in all control groups N-CAM-IR was present only in nerve fibers running along vessel walls, in unmyelinated fibers and in synaptic regions (Fig. 5).

3) Electron microscopy

a) Muscle fibers

Ultrastructural abnormalities were present in all flight animals. They ranged from minor changes to myofiber necrosis. The observation of 15-20 grids (100 mesh) per animal allowed us to estimate that up to 60% of the myofibers were affected by some of the described changes. The alterations were expressed by the presence of Z band streaming (Figs.6A, 7B), disruption and disorganization of the myofibrillar architecture (Figs. 6B, 7A), sarcoplasmic degradation manifested by the existence of myelin bodies, autophagic vacuoles and granular and membranous

material (Fig.8). Some partially injured myofibers revealed subsarcolemmal accumulation of nuclei that showed dispersed chromatin and membrane indentations (Fig.9). The necrotic areas frequently contained shrunken sarcolemmal nuclei that exhibited chromatin clumping and membrane breakdown (Fig. 10). In these areas mitochondria population was decreased or non-existent and revealed loss of ultrastructural detail. Although the plasma membrane of the necrotic myofibers was often ill-defined, the basement membrane remained intact. Cellular infiltration mainly composed of macrophages, polimorphonuclear leucocytes and occasional mononuclear cells of lymphoid appearance was a common finding of the most injured (necrotic) areas (Figs. 11,12,13). Mural alterations of the capillaries were spatially related to the cellular infiltration. The lumen of the capillaries was frequently occupied by platelets in unusual number. Control animals did not reveal any of these changes except for the occasional finding of circumscribed Z band streaming or the presence of quiescent macrophages.

Changes interpreted as evidence of regenerative activity of muscle fibers were found in all flight animals. Mononucleated cells were seen in interstitial position surrounded by a basement membrane. Some of these cells, apparently originated in satellite cells, contained a nucleus with dispersed chromatin, abundant clusters of ribosomes and occasional filamentous material (Fig.14). Other cells containing one or more nuclei displayed myofilaments that exhibited varied distributive patterns. In some cells the myofilaments were present in small number and showed developing Z bands (Fig.15), in others the myofilaments were aligned parallel to the main axis of the fiber and displayed shortened and immature Z bands (Figs. 16,17). An occasional fiber in advanced stage of regeneration showed a prominent nucleus peripherally located in subsarcolemmal position protruding toward the insterstitium and partially organized sarcomeres. The nucleus displayed dispersed chromatin and membrane indentations (Fig.18). Another sign of regenerative activity was provided by the presence of ribosomes in increased amounts in all regenerating myofibers. They were seen as ribosomal aggregates or in the form of polyribosomes associated with the myofilaments. In addition, some of these regenerating myofibers showed multiple innervation (Fig. 15) or neuromuscular junctions with fairly normal appearance (Fig.17). In spite of careful search for regenerating myofibers in the control animals, none was found.

b) Neuromuscular junctions

It is important to point out that the sampling of the neuromuscular junctions was done without the benefit of composite microphotographs to encompass the entire structure (see Cardasis, 1983). Hence, in several cases, part of the neuromuscular junction was missed in the section.

The most salient changes in the neuromuscular junctions of the flight animals (n=40) were: absence of synaptic vesicles with replacement by microtubules and neurofilaments, found in 4 neuromuscular junctions; interposition of Schwann cell processes between pre- and postsynaptic membranes, in 5; "unemployed" axonal spaces with shallow primary clefts, in 4; complete degeneration of axon terminals, in 6; axon terminals with dense core vesicles in 5; and axonal sprouting, in 5 (Figs.19,20,21,22,24). The criteria employed to suggest axonal regeneration (sprouting) is based on Cardasis' study (1983) of the aging neuromuscular junction. Motor endplates were also seen contacting the esterase-positive basement membrane of myofibers undergoing necrosis (Figs.23,24). Control groups did not reveal substantial differences among them. In 38 neuromuscular junctions, vacant axonal spaces were found in 2 neuromuscular junctions and interposition of Schwann cell cytoplasm in one. In all control groups the population of synaptic vesicles of axon terminals was preserved and no signs of sprouting was detected.

DISCUSSION

The present study provides evidence of a complex and dynamic process of muscle injury and regeneration taking place in the "slow" muscle adductor longus as a consequence of spaceflight-related conditions. Since in the present experiment the animals were sacrificed within 8-11 hours after landing, the alterations that have been described must have occurred during spaceflight and not as a consequence of post-flight exercise. Concerning myofiber regeneration for example, previous studies, although performed under different experimental conditions, indicate that typical mononucleated myoblasts appear 2-3 days after muscle injury (see Snow, 1977; Nichols and Shafiq, 1979). Therefore, it is necessary to place emphasis upon the difference between the present flight and a previous COSMOS mission (COSMOS 1887) in which the animals were euthanized 48 hours after landing. Due to this delay it was suggested that the postflight exercise might have contributed to the pathological modifications observed in antigravity muscles (Riley *et al.*, 1990).

Everything we know at present indicates that several factors acting in unison might be involved in triggering the process of muscle atrophy and subsequent deterioration of the myofibrillar structure in conditions of microgravity. The structural and metabolic foundations underlying these changes have been reviewed by Ilyn and Oganov (1989).

The results obtained by the application of N-CAM immunocytochemistry suggest that an active process of regeneration occurs during weightless conditions and support our interpretations at the ultrastructural level. It has been reported that embryonic muscle accumulate N-CAM in myoblasts and myotubes before myosin is expressed. In addition, the time of appearance of N-CAM during embryogenesis has favored the view of its role in processes such as synaptogenesis, early interactions between axons and myotubes, synaptic maintenance, and nerve injury and regeneration (Daniloff *et al.*, 1986; Covault and Sanes, 1986; Rieger *et al.*, 1988). Reappearance of N-CAM-IR in adult muscle has been previously reported after experimental denervation and paralysis (Covault and Sanes, 1985; Covault *et al.*, 1986)) In our case, the presence of N-CAM-IR in the surface of the myofibers, in satellite cells and regenerating myofibers speak in favor of a regenerative process that follows a pattern similar to that observed during muscle development.

We believe that the extensive necrosis with the overlapping effects of the denervation-reinnervation process are the triggering factors for myofiber regeneration. In this regenerative phase of the process the survival of the basement membrane shown in the electron microscopic images plays a critical role that parallels conditions observed in human muscle pathology. A "selective" type of necrosis, i.e., with intact basement membrane, has been reported in disorders such as muscular dystrophies and acquired metabolic and nutritional myopathies, while the "non-selective" type, i.e., with loss of the basement membrane, is observed after trauma, hemorrhage or ischemia. In the latter situation effective regeneration is compromised (see Cullen and Mastaglia, 1982, for review). Hence, although capillary lesions should be considered in part accountable for the appearance of the necrotic phenomena observed in flight animals (Ilyna-Kakueva and Portugalov, 1977, 1981; Ilyna-Kakueva *et al.*, 1976; see also Riley *et al.*, 1990b), other causes, e.g., metabolic, should not be ruled out.

The cellular infiltrates that frequently accompany the necrotic myofibers deserve careful assessment for future and more prolonged spaceflights. The presence of macrophages and occasional unclassified lymphoid cells could be related to immune responses (probably autoimmune) that might contribute to perpetuate the deterioration of muscle fibers (see Tashpulatov *et al.*, 1979).

The ultrastructural study, besides complementing and supporting the immunocytochemical findings, provides new insight as to the extent of the regenerative process. The picture that emerges is that of progressive differentiation with cells that show areas of still- unorganized thick

and thin filaments alternating with others in which bundles start to organize oriented parallel to the main axis. Z bands develop across some of the bundles and the classical striated pattern becomes more apparent. Ribosomes are always present in large amounts in all the regenerating fibers in close association to the filaments. This association is progressively lost in myofibers with advanced stages of differentiation but is visible in areas of the same myofibers that still show unorganized sarcoplasm. These ribosomes are seen close to filaments without preferential arrangement as is illustrated in Fig. 18, that reveals a striking similarity with regenerating myofibers reported in human muscle distrophy (Mastaglia *et al.*, 1970) and in hereditary muscular dystrophy in chicken (Nichols and Shafiq, 1979).

It is interesting to note that in some of our preparations subsarcolemmal myonuclei of partially injured myofibers appeared with morphological modifications evocative of proliferative activity. This picture, added to the expression of N-CAM on the surface of myofibers of all flight animals, supports previous suggestions on the possibility that the sarcolemmal myonuclei might participate in the regenerative process (Reznik, 1969; see also Aström and Adams, 1981).

Denervation-induced changes at the neuromuscular junctions have been reported in both spaceflight and ground based experiments (Il'ina-Kakuyeva and Portugalov, 1977b; Baranski *et al.*, 1979; D'Amelio *et al.*, 1987; Pozdnyakov *et al.*, 1988; Riley *et al.*, 1990b). One of our main concerns in relation to the neuromuscular junctions was to find satisfactory clues to establish patterns of synaptic remodeling. On some occasions small axon terminals were seen contacting the same primary cleft and separated from the main axon terminal by Schwann cell cytoplasm (see Cardasis, 1983). In other circumstances the presence of innervation or "multiple" innervation on regenerating myofibers speaks in favor of the existence of a process of remodeling of axon terminals. The ultrastructural preservation of the basement membrane of the necrotic fibers seen in our preparations lends support to this assumption, since it is consistent with the observations that newly formed axons innervate regenerated muscle fibers at their original synaptic sites due to the survival of the basement membrane. The basement membrane influences the accumulation of acethylcholine receptors and is known to be associated with cholinesterase activity (Marshall *et al.*, 1977; Sanes *et al.*, 1978; McMahan *et al.*, 1978; Burden *et al.*, 1979; Sanes and Chiu, 1983; McMahan and Slater, 1984). It is also interesting to note that axonal regeneration has been demonstrated upon the basement membrane of the frog neuromuscular junction even in the absence of myofibers (Sanes *et al.*, 1978; Glicksman and Sanes, 1983). A situation of somewhat similar characteristics is provided by the presence in the flight animals of myofibers undergoing necrosis supplied by apparently normal axon profiles apposing an esterase-positive basement membrane. Although there is obvious difficulty in distinguishing old from newly formed axons, the presence of regenerative axonal sprouts on these fibers seems to support the suggestion of the dependence of axonal regeneration upon an intact basement membrane. However, the possibility of a later demise of the neuromuscular junction on the necrotic myofibers can not be ruled out, since studies carried out in mice have shown that axon terminals on damaged myofibers are lost and that maintenance of the innervation is dependent upon the presence of intact myofibers (Rich and Lichtman, 1989).

A further suggestion of axonal remodeling is provided by the presence of axon terminals almost totally devoid of synaptic vesicles and with an unusual amount of microtubules. It seems reasonable to speculate that such appearance may be related to variations in the metabolism of some motoneurons reflecting a reversal from a "transmitting" (stable) to a "growing" (plastic) state (Watson, 1976; see also Gordon, 1983). It has been shown that microtubules predominate during development and that during the regenerative response of motoneurons there is an increase in the ratio of tubulin to neurofilament which expresses a recapitulation of the more plastic states that take place during development (Hoffman and Lasek, 1980; Lasek, 1981).

The observations reported in the foregoing reflect the power of self-repair of two systems -nervous system and skeletal muscle- subjected to the environmental conditions of spaceflight.

The mechanisms employed for this repair are reminiscent of developmental events that have been shown to involve mutually interacting processes (see Gordon, 1983, for review). It is obvious that after a 14-day flight a precise sequence of events in the changes observed is difficult to establish. According to these observations it seems likely that at some point during the course of the flight, muscle injury and repair and neural alterations and remodeling would alternatively share the cause-and-effect relationship reflecting the "trophic" collaboration between the two systems.

In conclusion, the present study suggests that major processes such as myofibrillar disruption and necrosis, muscle regeneration, denervation and synaptic remodeling at the level of the neuromuscular junction may take place during spaceflight. This research, however, only represents a fragmentary view of the response of the neuromuscular system to spaceflight. Proceeding from these findings a new phase of this research should develop a more "systemic" approach addressing problems such as alterations in the metabolic responses and cytoskeletal properties of motoneurons and satellite glial cells. The latter have been reported to show metabolic changes after experimental denervation (see Gordon, 1983).

Another aspect in need of study is related to the fact that, although skeletal muscle is mostly seen as an effector organ, the majority of its nerve fibers are sensory (Barker, 1974). An obvious conclusion is that they also should be compromised by the extensive lesions. In this regard, a number of morphological, immunohistochemical and physiological investigations have reported substantial reorganization of somatosensory cortical maps after the interruption (partial or total) of afferent volleys arising from the periphery of the body, e.g., deafferentation of rat hindlimb granular cortex (see Merzenich *et al.*, 1983a,b; Rasmusson and Turnbull, 1983; Merzenich *et al.*,1984; Dykes and Lamour,1988; Lamour and Dykes, 1988; Warren *et al.*, 1989). These investigations have also shown that removal of afferent input to specific regions of the cerebral cortex does not reduce neuronal activity and neuronal excitability but brings about through "plastic" changes new afferent drives that have been described as "reorganization of the somatotopy" (Dykes and Lamour,1988). From our own perspective and considering that peripheral receptive fields also include muscle receptors we have to surmise that changes in biological modalities have to be expressed, for example, by alterations in the chemical behavior of the neurons and glial cells of the projection areas of the cerebral cortex related to inputs from muscle receptors (Landgren and Silfvenius, 1969,1971; McIntyre, 1974; Wiesendanger and Miles, 1982; Matthews, 1991). We think that a natural result of this approach will be a more thorough understanding of the adaptive capabilities of the organism to altered gravitational conditions.

ACKNOWLEDGMENTS

The authors extend their deep appreciation to Soviet and US investigators whose efforts made this study possible. The authors are also specially grateful to Richard E. Grindeland, James P. Connolly and Marilyn F. Vasques for their support. This study was supported by NASA-COSMOS Parts Program.

REFERENCES

1. Alford,E.K., R.R.Roy, J.A. Hodgson and V.R.Edgerton. Electronmyography of Rat Soleus, Medial Gastrocnemius and Tibialis Anterior During Hindlimb Suspension. Exp.Neurol. 96: 635-649, 1987.

2. Aström,K.E. and R.D.Adams. Pathological Reactions of the Skeletal Muscle Fiber in Man. In: Disorders of Voluntary Muscle, Sir John Walton, Ed., Churchill Livingstone, New York. 151-208, 1981.

3. Baranski,S., W.Baranska, M.Marciniak and E.I.Ilyina-Kakueva. Ultrasonic ("ultrastructural") Investigations of the Soleus Muscle after Spaceflight on the Biosputnik 936. Aviat.Space Environ.Med. 50: 930-934, 1979.

4. Barker,D. The Morphology of Muscle Receptors. In: Muscle Receptors; D.Barker, C.C.Hunt and A.K.Mcintyre, eds., Springer, New York. 1-190, 1974.

5. Burden, S.J., P.B. Sargent and U.J.McMahan. Acetylcholine Receptors in Regenerating Muscle Accumulate at Original Synaptic Sites in the Absence of the Nerve. J.Cell Biol.. 82: 412-425, 1979.

6. Cardasis, C.A. Ultrastructural Evidence of Continued Reorganization of the Aging (11-26 months) Rat Soleus Neuromuscular Junction. Anat.Rec. 207:399-415, 1983.

7. Covault,J. and J.R.Sanes. Neural Cell Adhesion Molecules (N-CAM) Accumulates in Denervated and Paralyzed Muscle. Proc.Natl.Acad.Sci. USA. 82: 4544-4548,1985.

8. Covault, J. and J.R.Sanes. Distribution of N-CAM in Synaptic and Extrasynaptic Portions of Developing and Adult Skeletal Muscle. J.Cell Biol. 102: 716-730, 1986.

9. Covault,J., J.P.Merlie, C.Goridis and J.R.Sanes. Molecular Forms of N-CAM and its RNA in Developing and Denervated Skeletal Muscle. J. Cell Biol. 102: 731-739, 1986.

10..Cullen, M.J. and F.L.Mastaglia. Pathological Reactions of Skeletal Muscle. In: Skeletal Muscle Pathology, F.L.Mastaglia and Sir John Walton, eds., Churchill Livingstone, New York. 88-139, 1982.

11. D'Amelio,F., N.G.Daunton, T.Fast and R.Grindeland. Preliminary Findings in the Neuromuscular Junctions of the Soleus Muscle of Adult Rats Subjected to Simulated Weightlessness. Light and Electron Microscopy, Space Life Sciences Symposium: Three Decades of Life Science Research in Space, Washington, D.C. 204-205, 1987.

12. Daniloff,J.K., G.Levi, M.Grumet, F.Rieger and G.M.Edelman. Altered Expression of Neuronal Cell Adhesion Molecules Induced by Nerve Injury and Repair. J. Cell Biol. 103: 929-945, 1986.

13. Dykes,R.W. and Y.Lamour. An Electrophysiological Laminar Analysis of Single Somatosensory Neurons in Partially Deafferented Rat Hindlimb Granular Cortex Subsequent to Transection of the Sciatic Nerve, Brain Research. 449:1-17, 1988.

14. Fell,R.D., L.B.Gladden, J.M.Steffen and X.J.Musacchia. Fatigue and Contraction of Slow and Fast Muscles in Hypokinetic/Hypodynamic Rats. J.Appl.Physiol., 58:65-69, 1985.

15. Fitts,R.H., J.M.Metzger, D.A. Riley and B.R.Unsworth. Models of Disuse: a Comparison of Hindlimb Suspension and Immobilization. J.Appl.Physiol. 60: 1946-1953, 1986.

16. Glicksman,M.A. and J.R.Sanes. Differentiation of Motor Nerve Terminals Formed in the Absence of Muscle Fibers. J.Neurocytol. 12: 661-671, 1983.

17. Gordon,T. Dependence of Peripheral Nerves on Their Target Organs. In: G. Burnstock, R.O'Brien and G. Vrbová, eds., Somatic and Autonomic Nerve-Muscle Interaction, Elsevier. 289-325, 1983.

18. Graham,S.C., R.R.Roy, S.P.West, D.Thomason and K.M.Baldwin. Exercise Effects on the Size and Metabolic Properties of Soleus Fibers in Hindlimb-Suspended Rats. Aviat.Space Environ.Med. 60: 226-234, 1989.

19. Hauschka, E.O., R.R.Roy and V.R.Edgerton. Size and Metabolic Properties of Single Muscle Fibers in Rat Soleus After Hindlimb Suspension. J.Appl.Physiol. 62: 2338-2347, 1987.

20. Herbert,M.E., R.R.Roy and V.R.Edgerton. Influence of One Week Hindlimb Suspension and Intermittent High Load Exercise on Rat Muscles. Exp.Neurol. 102: 190-198, 1988.

21. Hoffman, P.N. and R.J.Lasek. Axonal Transport of the Cytoskeleton in Regenerating Motor Neurons: Constancy and Change. Brain Research. 202: 317-333, 1980.

22. Hoh, J.F.Y. and C.J.Chow. The Effect of the Loss of Weight- bearing on the Isomyosin Profile and Contractile Properties of Rat Skeletal Muscles. In: Molecular Pathology of Nerve and Muscle. A.D. Kidman, J.K. Tomkins, C.A. Morris and N.A. Cooper, eds., Humana Press, New Jersey. 371-384, 1983.

23. Ilyin, E.A. and V.S.Oganov. Microgravity and Musculoskeletal System of Mammals. Adv.Space Res. 9: 11-19, 1989.

24. Ilina-Kakueva, E.I. and V.V. Portugalov. Combined Effect of Spaceflight and Radiation on Skeletal Muscles of Rats. Aviat.Space Environ.Med. 48:115-119, 1977a.

25. Il'ina-Kakuyeva, Ye.I. and V.V. Portugalov. State of Rat Muscle Motoneuron System in the Case of Restricted Mobility. Kosmicheskaya Biologiya i Aviakomicheskaya Meditsina. 6:31-35, 1977b.

26. Ilina-Kakueva, E.I. and V.V. Portugalov. Structural Changes in the Coleus Muscles of Rats Flown Aboard the Cosmos Series of Biosatellites and Submitted to Hypokinesia. Kosm.Biol.Aviakosm.Med. 15:37-40, 1981.

27. Ilina-Kakueva, E.I., V.V. Portugalov and N.P.Kirvenkova. Space-light Effects on Skeletal Muscle of Rats. Aviat.Space Environ.Med. 47:700-703, 1976.

28. Jaspers, S.R. and M.E. Tischler. Atrophy and Growth Failure of Rat Hindlimb Muscles in Tail-cast Suspension. J.Appl.Physiol: Respirat.Environ.Exercise Physiol. 57:1472-1479, 1984.

29. Lamour,Y. and R.W.Dykes. Somatosensory Neurons in Partially Deafferented Rat Hindlimb Granular Cortex Subsequent to Transection of the Sciatic Nerve: Effects of Glutamate and Acetylcholine. Brain Research. 449:18-33, 1988.

30. Landgren, S. and H. Silfvenius. Projection to Cerebral Cortex of Group I Muscle Afferents from the Cat's Hind Limb. J.Physiol. (London). 200:353-372, 1969.

31. Landgren, S. and H. Silfvenius. Nucleus Z, the Medullary Relay in the Projection Path to the Cerebral Cortex of Group I Muscle Afferents from the Cat's HindLimb. J.Physiol. (London). 218:551-571, 1971.

31. Lasek,R.J. The Dynamic Ordering of Neuronal Cytoskeletons. Neurosciences Res.Prog.Bull. 19: 7-32, 1981.

32. Loughna,P., G. Goldspink and D.F.Goldspink. Effect of Inactivity and Passive Stretch on Protein Turnover in Phasic and Postural Rat Muscles. J.Appl.Physiol. 61:173-179, 1986.

33. Marshall, L.M., J.R. Sanes and U.J.McMahan. Reinnervation of Original Synaptic Sites on Muscle Fiber Basement Membrane after Disruption of the Muscle Cells. Proc.Natl.Acad.Sci. USA. 74: 3073-3077, 1977.

34. Martin,T.P. Protein and Collagen Content of Rat Skeletal Muscle Following Spaceflight. Cell Tissue Res. 254: 251-253, 1988.

35. Martin,T.P., V.R.Edgerton and R.E.Grindeland. The Influence of Spaceflight on Rat Skeletal Muscle. J.Appl.Physiol. 65: 2318-2325, 1988.

36. Mastaglia,F.L., J.M. Papadimitriou and B.A.Kakulas. Regeneration of Muscle in Duchenne Muscular Distrophy: an Electron Microscope Study. J.Neurol.Sci. 11: 425-444, 1970.

37. Matthews, P.B. The Human Stretch Reflex and the Motor Cortex. TINS. 14: 87-91, 1991.

38. Merzenich,M.M., J.H.Kaas, J.Wall, R.J.Nelson, M.Sur D.Felleman. Topographical Reorganization of Somatosensory Cortical Areas 3B and 1 in Adult Monkeys Following Restricted Deafferentation, Neuroscience. 8:33-55, 1983a.

39. Merzenich,M.M., J.H.Kaas, J.T.Wall., M.Sur, R.J.Nelson, D.J.Felleman. Progression of Change Following Median Nerve Section in the Cortical Representation of the Hand in Areas 3b and 1 in Adult Owl and Squirrel Monkeys. Neuroscience. 10:639-665, 1983b.

40. Merzenich,M.M., R.J.Nelson, M.P.Stryker, M.S. Cynader, A.Schoppmann, J.M. Zook. Somatosensory Cortical Map Changes Following Digit Amputation in Adult Monkeys, J.Comp.Neurol. 224:591-605, 1984.

41. McIntyre,A.K. Central Actions of Impulses in Muscle Afferent Fibers. In: Muscle Receptors; D.Barker, C.C.Hunt and A.K.Mcintyre, eds., Springer, New York. 235-288, 1974.

42. McMahan, U.J., J.R. Sanes and L.M.Marshall. Cholinesterase is Associated with the Basal Lamina at the Neuromuscular Junction. Nature. 271: 172-174, 1978.

43. McMahan, U.J. and C.R. Slater. The Influence of Basal Lamina on the Accumulation of Acetylcholine Receptors at Synaptic Sites in Regenerating Muscle. J.Cell Biol. 98: 1453-1473, 1984.

44. Musacchia, X.J., J.M.Steffen and D.R. Deavers. Rat Hindlimb Muscle Responses to Suspension Hypokinesia/Hypodynamia. Aviat.Space Environ.Med. 54: 1015-1020, 1983.

45. Nichols, J.R. and S.A Shafiq. Muscular Regeneration in the Muscular Dystrophies. Ann.N.Y.Acad.Sci. 317: 478-493, 1979.

46. Oganov, V.S. and A.N.Potapov. On the Mechanisms of Changes in Skeletal Muscles in the Weightless Environment. In: Life Science and Space Research, Vol. 14. F.Guba, G.Marechal and O.Takacs, eds. Akademic-Verlag, Berlin. 137-143, 1976.

47. Oganov, V.S., S.A.Skuratova, A.N.Potapov and M.A.Shirvinskaya. Physiological Mechanisms of Adaptation of Rat Skeletal Muscles to Weightlessness and Similar Functional Requirements. Physiologist. 23: S16-S21, 1980.

48. Oomura, Y. and T.Katafuchi. Neurophysiological Responses in Suspended Animal Models. Physiologist. 30: S106-S108, 1987.

49. Pearson, J. and A. Sabarra. A Method for Obtaining Longitudinal Cryostat Sections of Living Muscle Without Contraction Artifacts. Stain Technol. 49: 143-146, 1974.

50. Pozdnyakov,O.M., L.L.Babakova, M.S.Demorzhi and E.I.Ilyina-Kakueva. Changes in Rat Neuro-Muscular Synapse Ultrastructure During Space-flights. Bull.Exp.Biol.Med. 6:752-755, 1988.

51. Rasmusson,D.D. and B.G.Turnbull. Immediate Effects of Digit Amputation on SI Cortex in the Raccoon: Unmasking of Inhibitory Fields. Brain Research. 288:368-370, 1983.

52. Reznik,M. Origin of Myoblasts During Skeletal Muscle Regeneration. Laborat.Investigat. 20: 353-363, 1969.

53. Rich, M. and J.W.Lichtman. Motor Nerve Terminal Loss from Degenerating Muscle Fibers. Neuron. 3:677-688, 1989.

54. Rieger,F., M.Grumet and G.M.Edelman. N-CAM at the Vertebrate Neuromuscular Junction. J.Cell Biol. 101: 285-293, 1985.

55. Rieger,F., M.Nicolet, M.Pinçon-Raymond, M.Murawsky, G.Levi and G.M.Edelman. Distribution and Role in Regeneration of N-CAM in the Basal Laminae of Muscle and Schwann cells. J.Cell Biol. 107: 707-719, 1988.

56. Riley,D.A., S.Ellis, G.R.Slocum, T.Satyanarayana, J.L.W.Bain and F.R.Sedlak. Hypogravity-Induced Atrophy of Rat Soleus and Extensor Digitorum Longus Muscles. Muscle and Nerve. 10: 560-568, 1985.

57. Riley, D.A., G.R. Slocum, J.L.W.Bain, F.R.Sedlak, T.E.Sowa and J.W.Mellender. Rat Hindlimb Unloading: Soleus Histochemistry, Ultrastructure and Electromyography. J.Appl.Physiol. 69: 58-66, 1990a.

58. Riley,D.A., E.I. Ilyina-Kakueva, S.Ellis, J.L.W.Bain, G.R.Slocum and F.R. Sedlak. Skeletal Muscle Fiber, Nerve, and Blood Vessel Breakdown in Space-flown Rats. FASEB Journal. 4: 84-91, 1990b.

59. Roy,R.R., M.A.Bello, P.Bouissou and V.R. Edgerton. Size and Metabolic Properties of Fibers in Fast-Twitch Muscles After Hindlimb Suspension. J.Appl.Physiol. 62: 2348-2357, 1987.

60. Sanes, J.R. and A.Y. Chiu. The Basal Lamina of the Neuro-muscular Junction. Cold Spring Harbor Symp.Quant.Biol. 48: 667-678, 1983.

61. Sanes,J.R., L.M.Marshall and U.J.McMahan. Reinnervation of Muscle Fiber Basal Lamina After Removal of Myofibers. J.Cell.Biol. 78: 176-198, 1978.

62. Sanes, J.R., M.Schachner and J. Covault. Expression of Several Adhesive Macromolecules (N-CAM, L1, J1, NILE, Uvomorulin, Laminin, Fibronectin, and a Heparan Sulfate Proteoglycan) in Embryonic, Adult, and Denervated Adult Skeletal Muscle. J. Cell Biol. 102: 420-431, 1986.

63. Simard, C.P., S.A.Spector and V.R.Edgerton. Contractile Properties of Rat Hindlimb Muscles Immobilized at Different Lengths. Exp. Neurol. 77: 467-482, 1982.

64. Snow, M.H. Myogenic Cell Formation in Regenerating Rat Skeletal Muscle Injured by Mincing: I. A Fine Structural Study. Anat.Rec. 188: 181-200, 1977.

65. Steffen,J.M. and X.J.Musacchia. Spaceflight Effects on Adult Rat Muscle Protein, Nucleic Acids and Aminoacids. Am.J.Physiol. 251: R1059-R1063, 1986.

66. Strum, J.M and E.C.B. Hall-Craggs. A Method Demonstrating Motor Endplates for Light and Electron Microscopy. J.Neurosc.Methods. 6: 305-309, 1982.

67. Tashpulatov, R.Y., T.A.Danilova, A.T.Lesnyak, V.I.Legenykov, V.S.Znamenskii and I.I.Dedyuyeva. Antibodies to Myofibril Antigens in Cosmonauts After Spaceflight. Zh.Mikrobiol.Epidemiol.Immunobiol. 12:36-39, 1979.

68. Templeton, G.H., M.Paladino,J.Manton,M.Glasberg, C.J.Silver, P. Silver, G.Demartino, T.Leconey, G.Klug, H. Hagler and J.L.Sutko. Influence of Suspension Hypokinesia on Rat Soleus Muscle. J.Appl.Physiol. 56: 278-286, 1984a.

69. Templeton, G.H., M.Paladino, J.Manton, T.Leconey, H.Hagler and M. Glasberg. The Influence of Rat Suspension-Hypokinesia on the Gastrocnemius Muscle. Aviat.Space Environ.Med. 55: 381-386, 1984b.

70. Thomason, D.B., R.B.Briggs and F.W.Booth. Rapid Protein Synthesis Decrease andTransient Protein Degradation Increase in Atrophying Soleus Muscle. FASEB Journal. 2:A959, 1988.

71. Thomason,D.B., R.E.Herrick and K.M.Baldwin. Activity Influences on Soleus Muscle Myosin During Rodent Hindlimb Suspension. J.Appl.Physiol. 63: 138-144, 1987b.

72. Thomason, D.B., R.E.Herrick, D.Surdyka and K.M.Baldwin. Time Course of Soleus Muscle Myosin Expression During Hindlimb Suspension and Recovery. J.Appl.Physiol. 63:130-137, 1987a.

73. Warren, R., N. Tremblay and R.W. Dykes. Quantitative Study of Glutamic Acid Secarboxylase-Immunoreactive Neurons and Cytochrome Oxydase Activity in Normal and Partially Deafferented Rat Hindlimb Somatosensory Cortex. J.Comp.Neurol. 288: 583-592, 1989.

74. Watson,W.E. Cell Biology of Brain, John Wiley, New York. 1976.

75. Wiesendanger, M. and T.S.Miles. Ascending Pathways of Low-Threshold Muscle Afferents to the Cerebral Cortex and its Possible Role in Motor Control. Physiol.Rev. 62:1234-1270, 1982.

76. Winiarski, A.M., R.R.Roy, E.K.Alford, P.C.Chiang and V.R.Edgerton. Mechanical Properties of Rat Skeletal Muscle after Hindlimb Suspension. Exp.Neurol. 96:650-660, 1987.

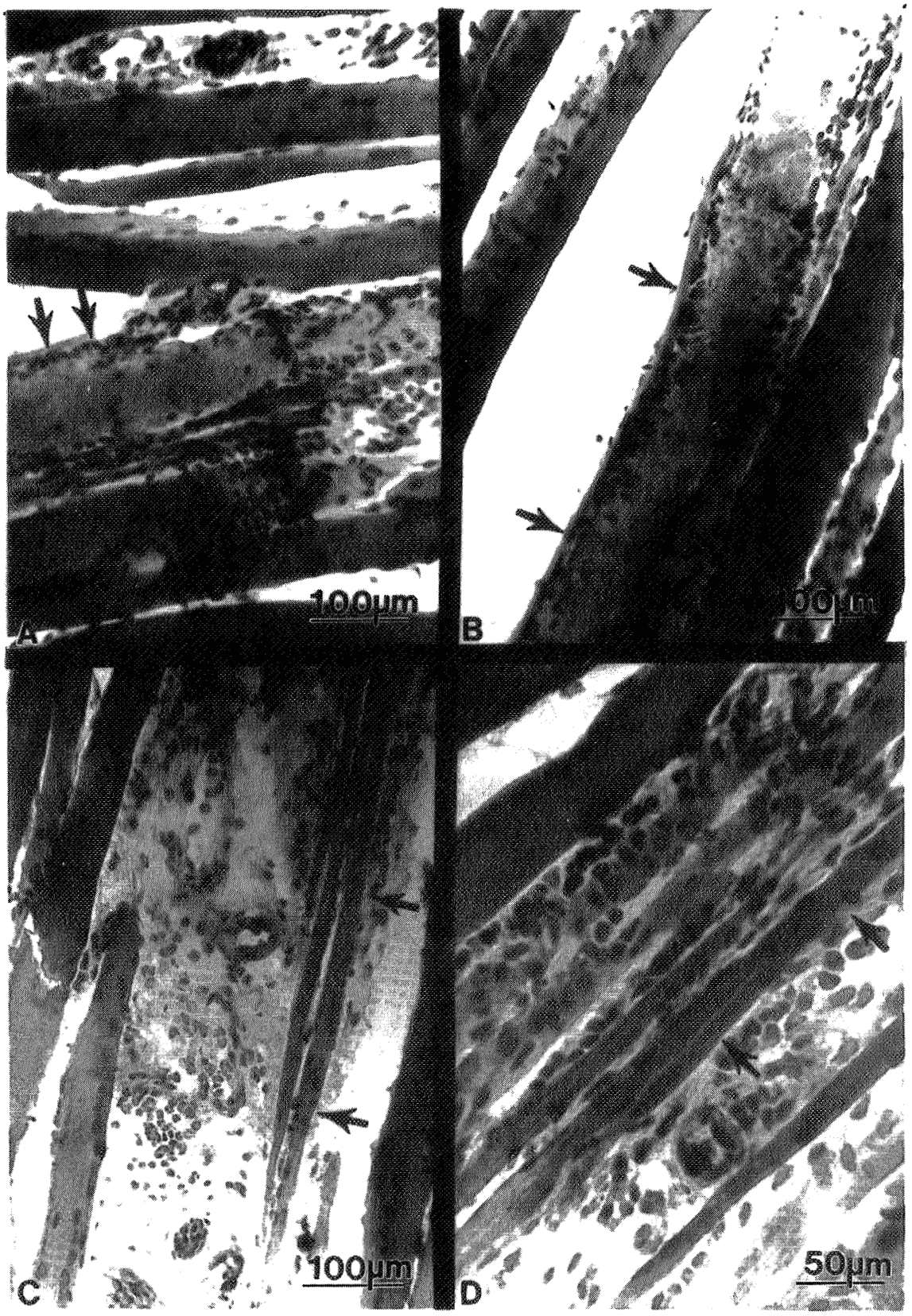

Figure 1. Flight animals. (A) and (B) Longitudinal sections show segmental necrosis of myofibers (arrows) accompanied by inflammatory cellular infiltration. (C) and (D). Atrophic fibers (arrows), edema and cellular infiltrates mainly composed of histiocytes and polymorfonuclear leucocytes. In (C) the grouping of the fibers is suggestive of denervation. Hematoxilin and eosin.

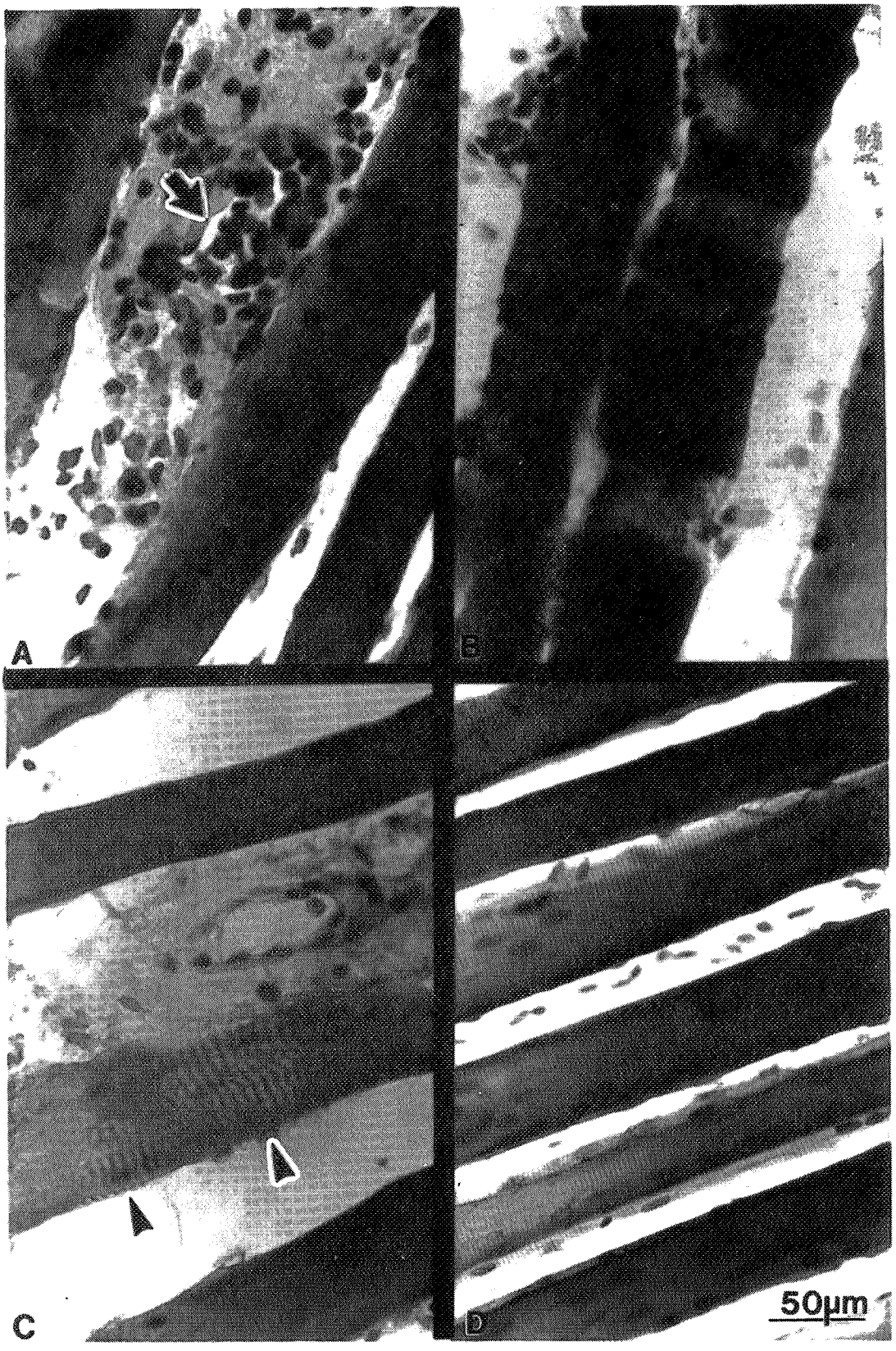

Figure 2. (A) Flight animal. A disrupted blood vessel (arrow) is surrounded by inflammatory infiltrates. (B) Flight animal. Contraction bands and disruption of the sarcoplasm. (C) Flight animal. Disarray of sarcoplasmic architecture very commonly observed in all flight animals. (D) Vivarium control. Normal striation of fibers. Hematoxilin and eosin.

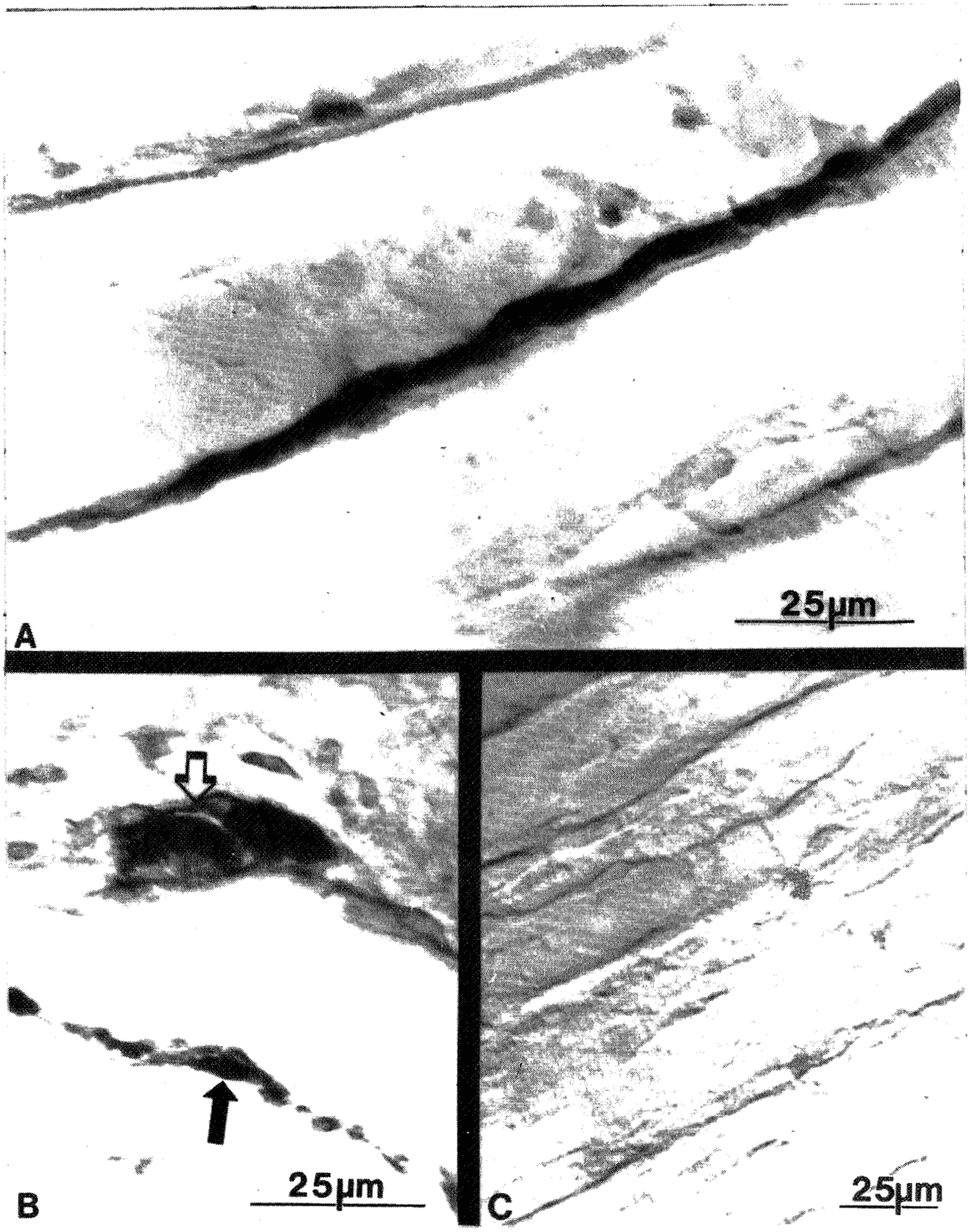

Figure 3. Flight animals. (A) N-CAM immunoreactivity is present in the surface of muscle fibers. Sarcolemmal nuclei are apparent. (B) N-CAM immunoreactive cell suggestive of a satellite element (arrow) opposite to a motor end plate (open arrow). (C) Control section. Staining is abolished by omission of the primary antibody. All photographs taken with Nomarski optics.

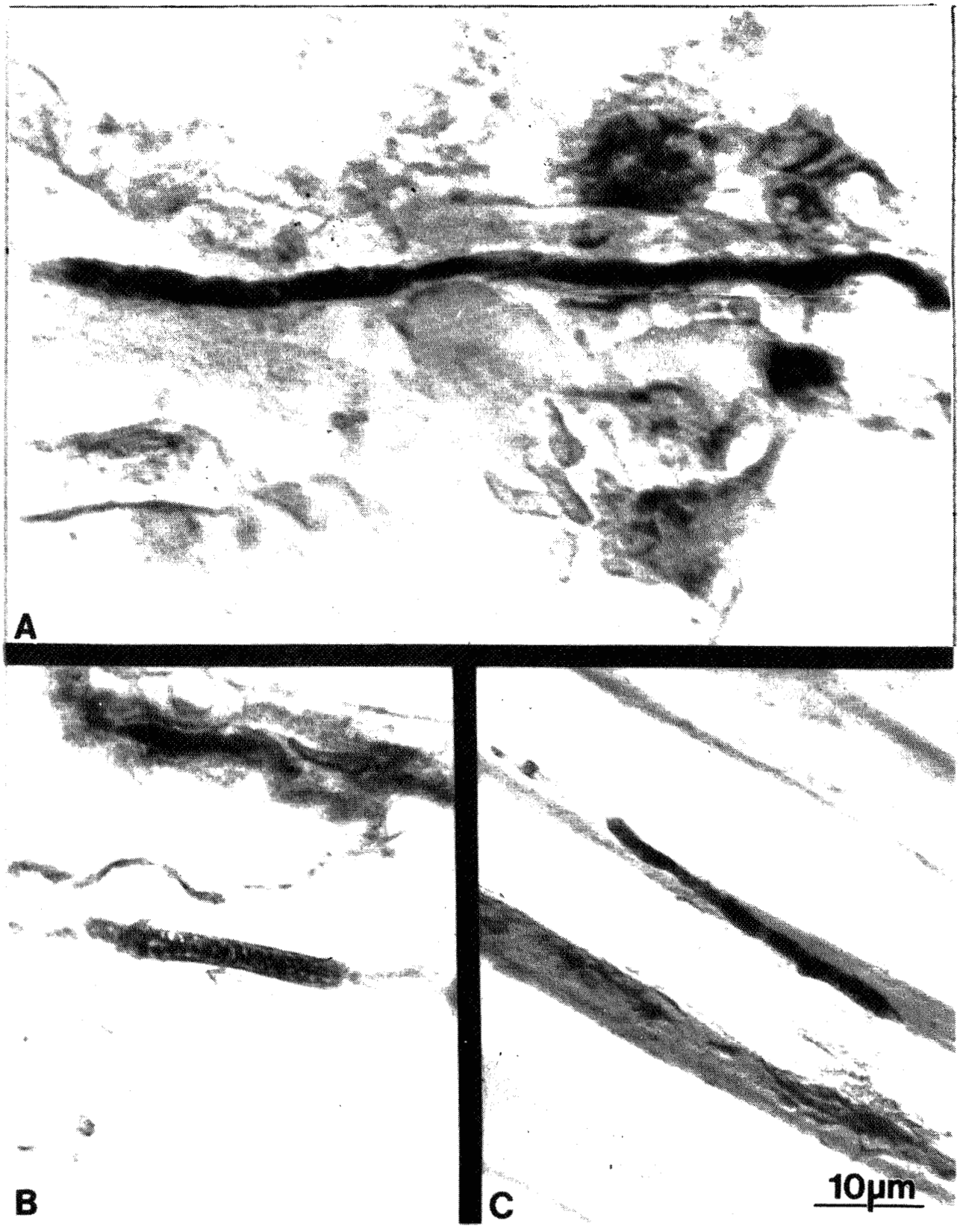

Figure 4. Flight animals. (A), (B) and (C) depict N-CAM immunoreactive regenerating myofibers in three different flight animals. In (A) and (B) the row of nuclei with prominent nucleoli are visible. Photographs taken with Nomarski optics.

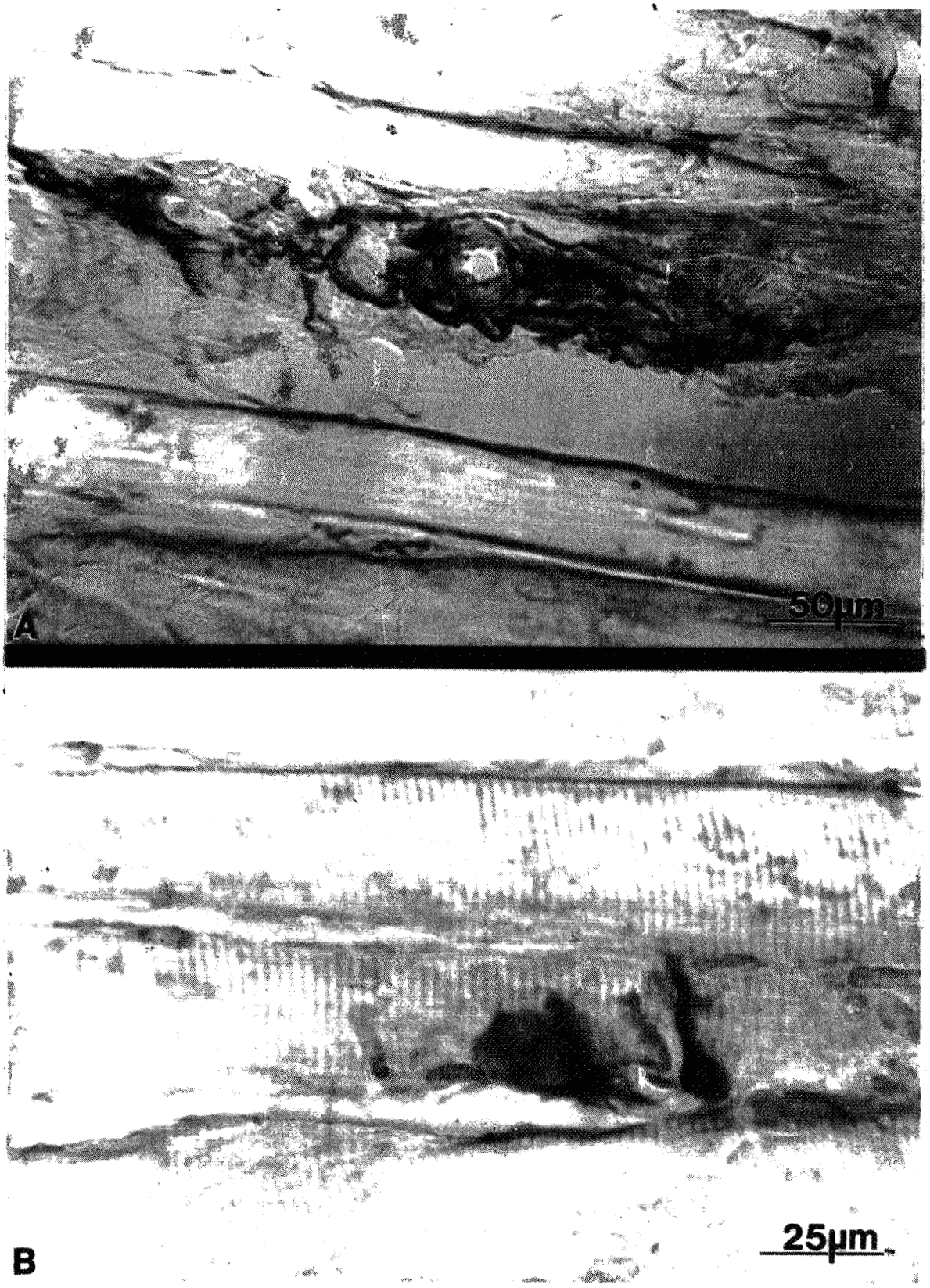

Figure 5. (A) Synchronous control. N-CAM immunoreactivity is absent from the muscle fibers but present in the innervation around a blood vessel. (B) Basal control. N-CAM staining is present on the surface of motor nerve terminals. Photographs taken with Nomarski optics.

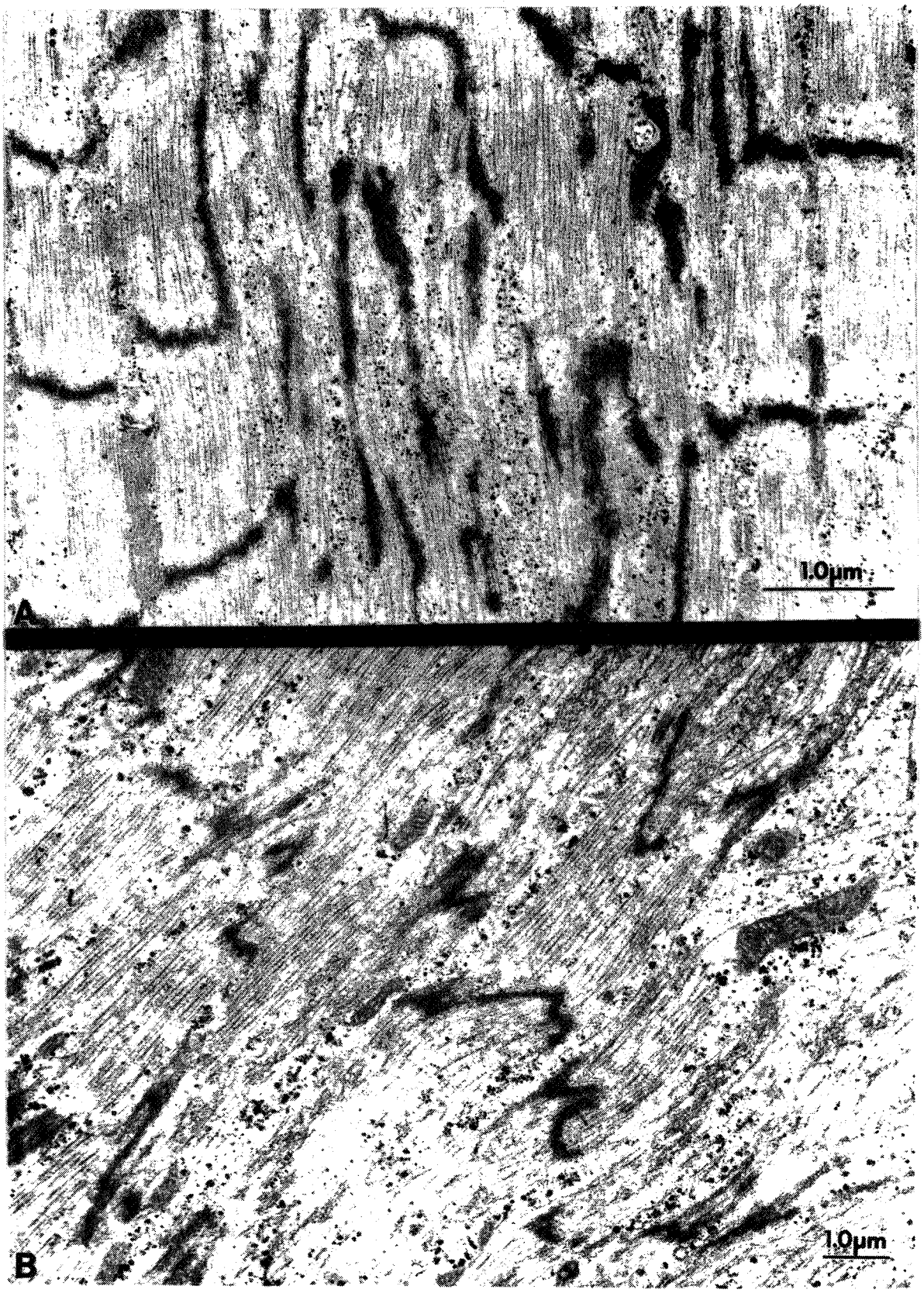

Figure 6. Flight animals. (A) Segment of a muscle fiber with Z band streaming. (B) Advanced disorganization of the myofibrillary structure. Both were very common findings in all flight animals.

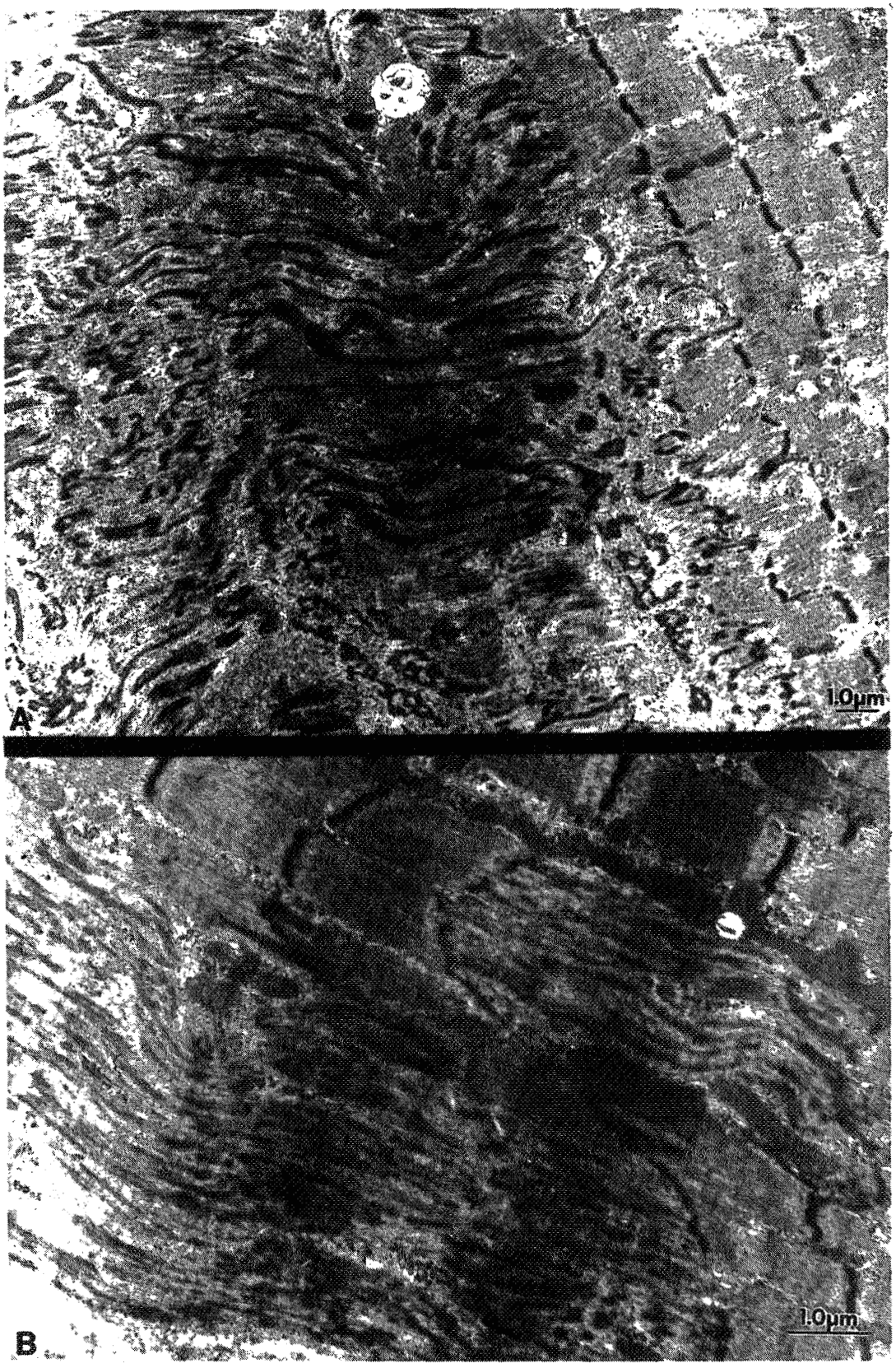

Figure 7. Flight animals. (A) Marked disruption of sarcomeres somewhat reminiscent of unstructured core (very frequent finding). (B) Segmental streaming of Z bands.

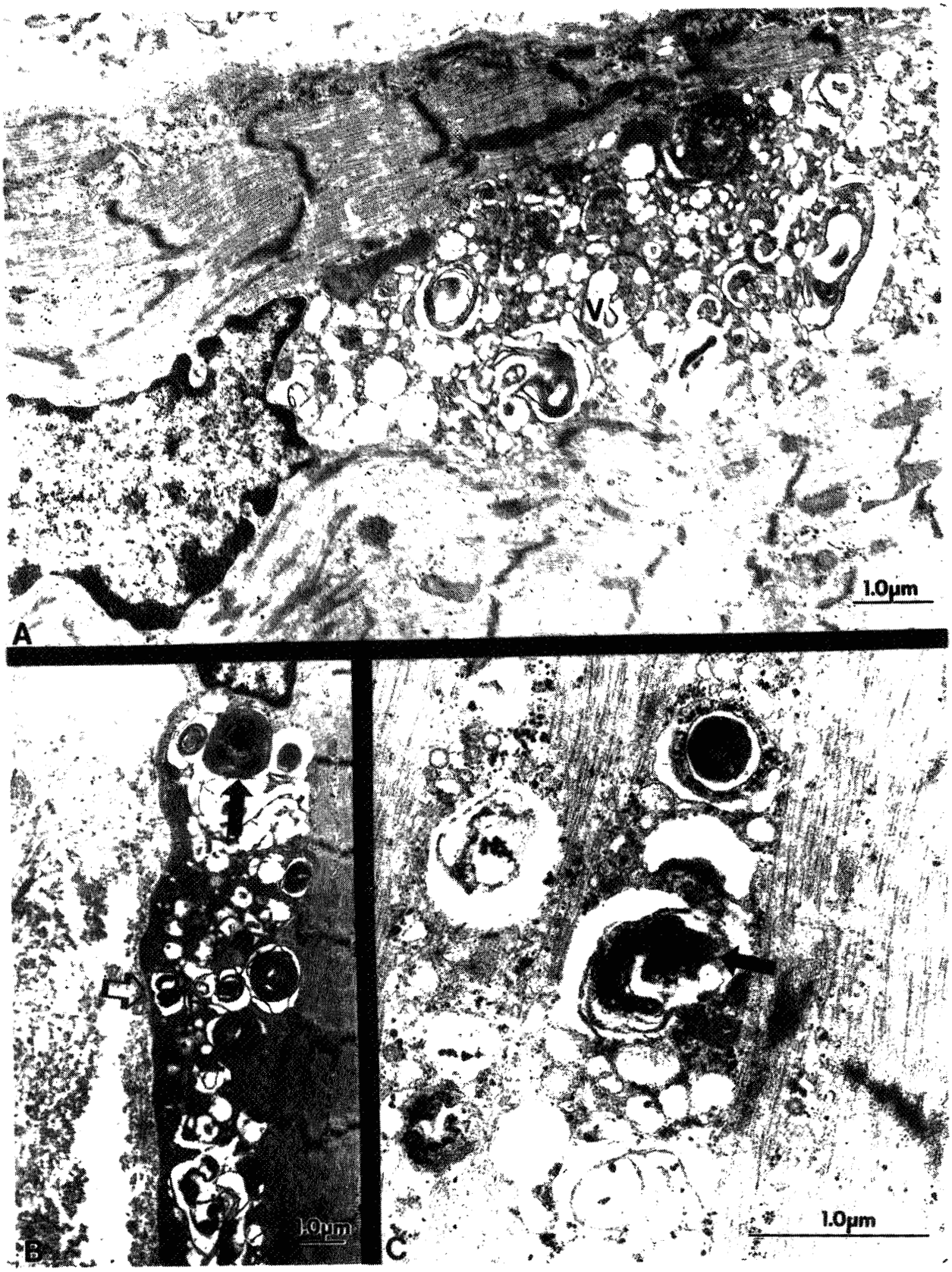

Figure 8. Flight animals. (A) Muscle fiber displaying so-called autophagic vacuoles (V) and membranous material. Part of a nucleus in central position is also visible and the rest of the myofiber shows Z band streaming and myofibrillar disorganization. (B) The periphery of a myofiber shows numerous myelin bodies (open arrow) and concentric lamellated bodies (arrow). (C) Myelin bodies (arrow) and autophagic vacuoles. The pictures correspond to three different animals.

Figure 9. Flight animal. Several sarcolemmal nuclei overlying a portion of a myofiber with sarcomeric disruption. The nuclei exhibit peripheral clumping and dispersion of the chromatin and membrane infolding.

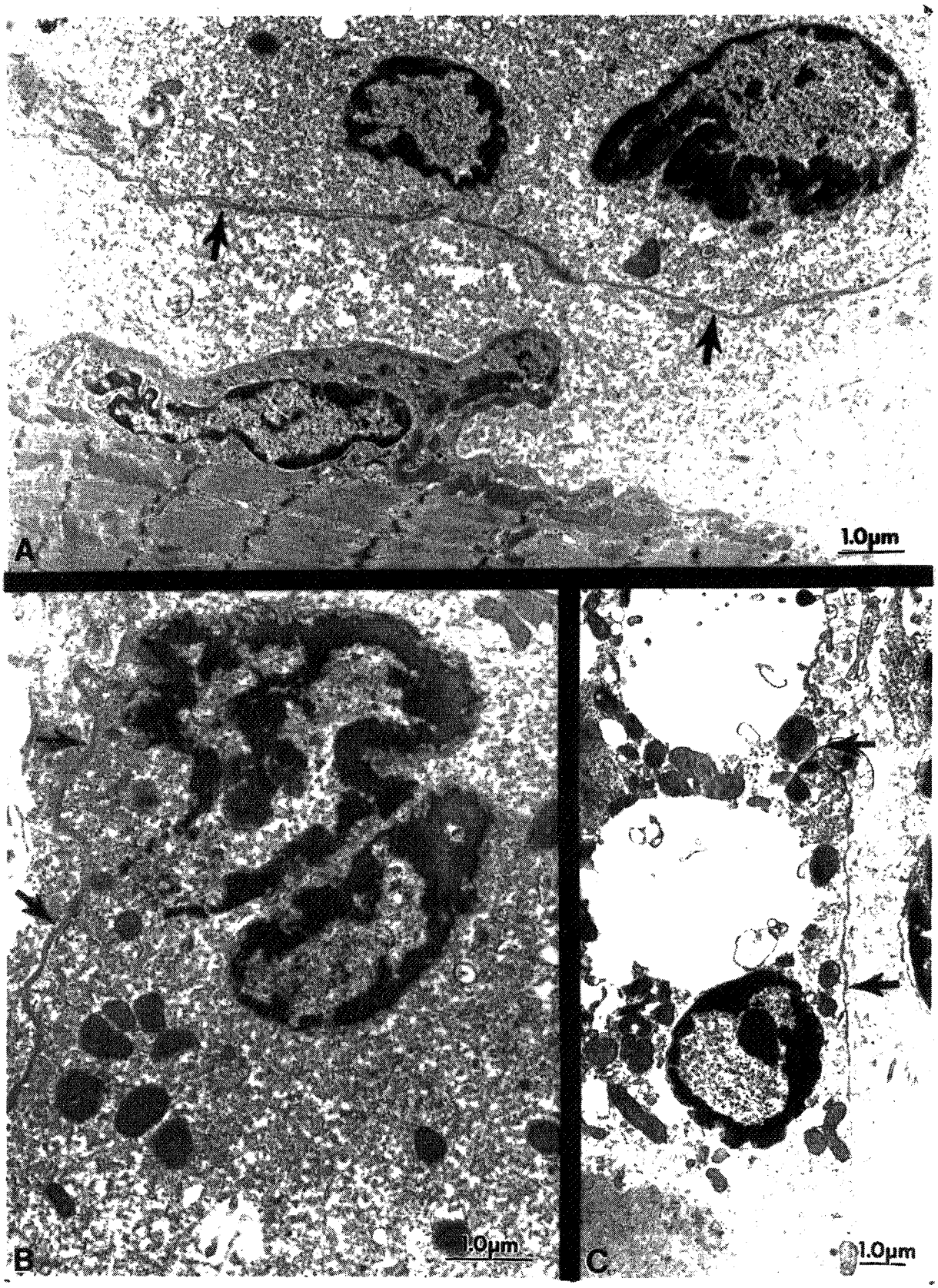

Figure 10. Flight animals. (A), (B) and (C) show myofiber necrosis in three different animals. There is dissolution of the sarcomeric organization, rounding off of mitochondria and different stages of nuclear disruption (chromatin clumping, lysis). In all three myofibers the basement membrane (arrows) is preserved.

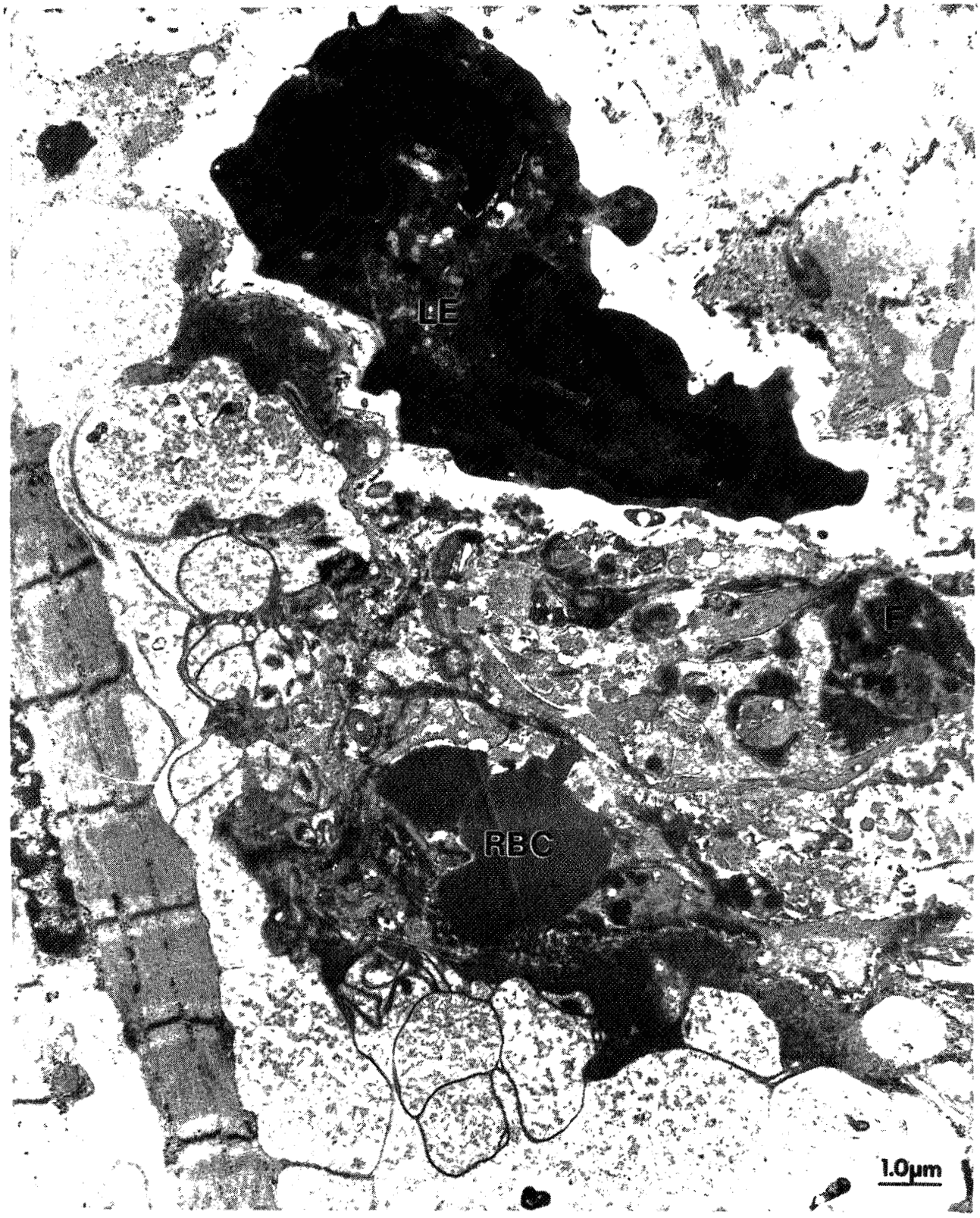

Figure 11. Flight animal. A necrotic area showing a disrupted capillary containing a red blood cell (RBC), remains of myofilaments (F) and a polymorphonuclear leucocyte (LE).

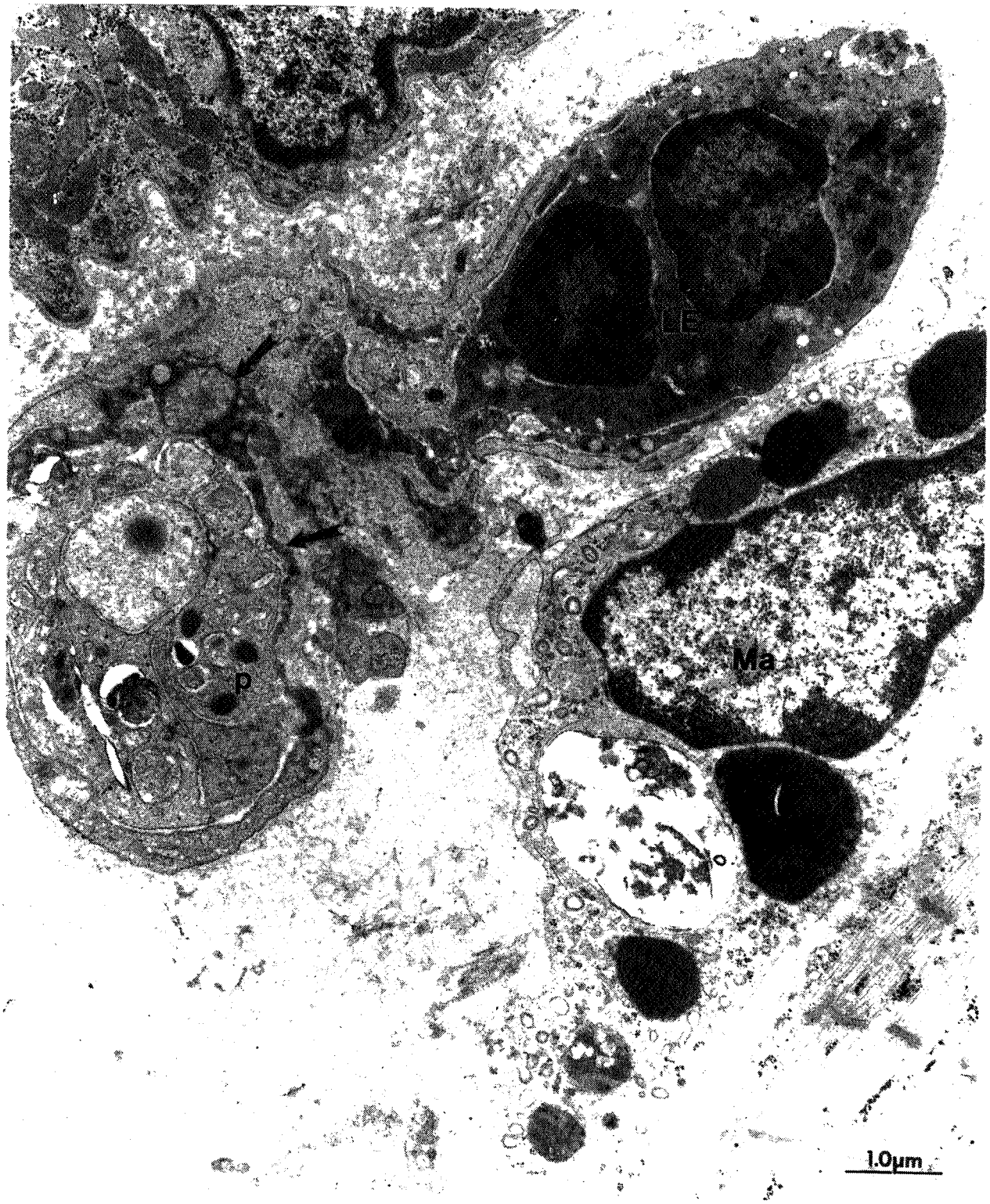

Figure 12. Flight animal. Area of cellular invasion showing a macrophage (Ma), a leucocyte (LE) and a capillary with vacuolation and advanced degenerative phenomena of the endothelium (arrows). (p), platelet.

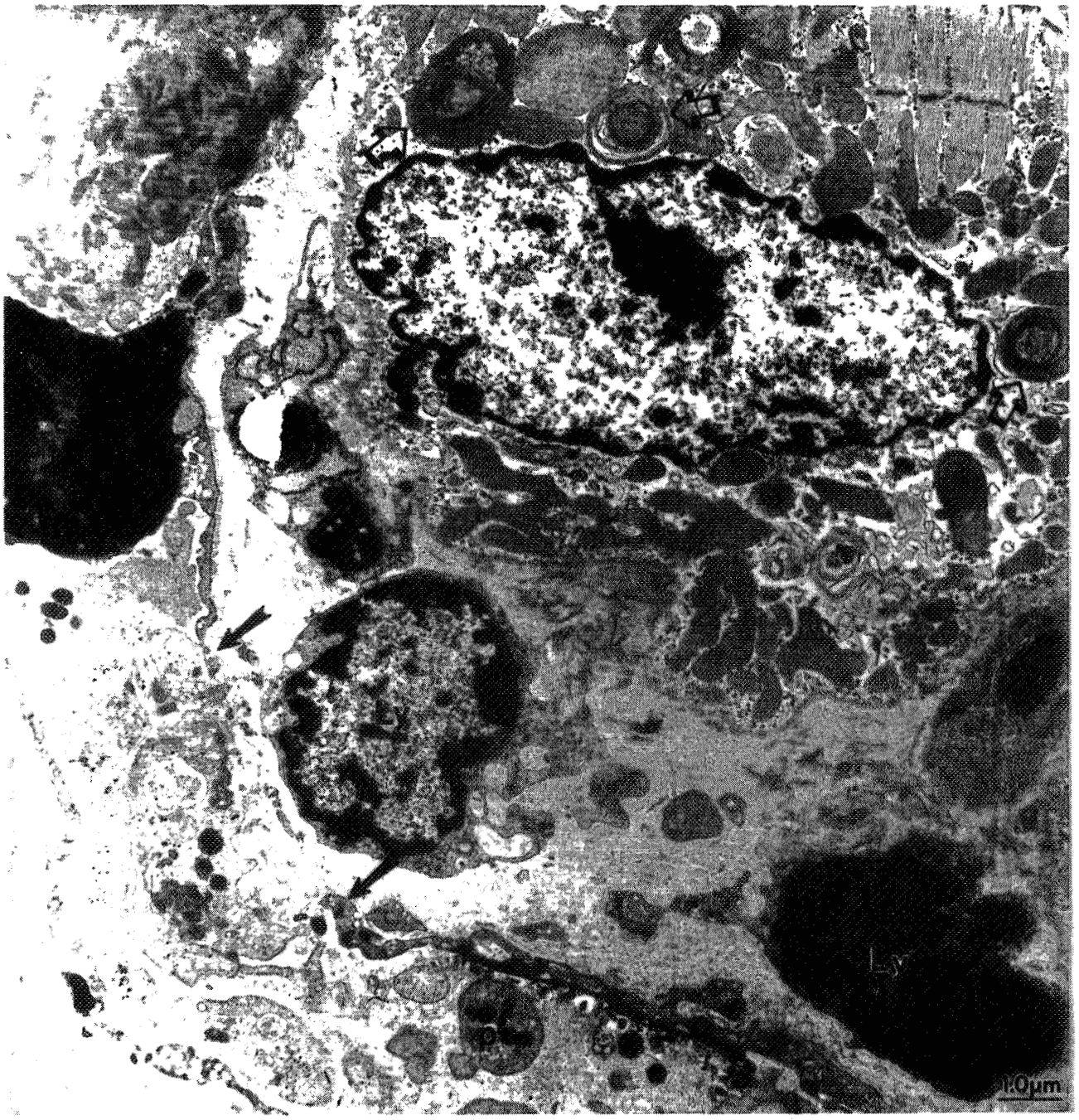

Figure 13. Flight animal. The picture shows a capillary oriented longitudinally with endothelial degeneration and a ruptured area (arrows). Unclassified lymphoid cells (Ly) are also present. In the upper right, a portion of a degenerating myofiber displays numerous concentric lamellated bodies, probably the product of mitochondrial alterations (open arrows). (p), platelet.

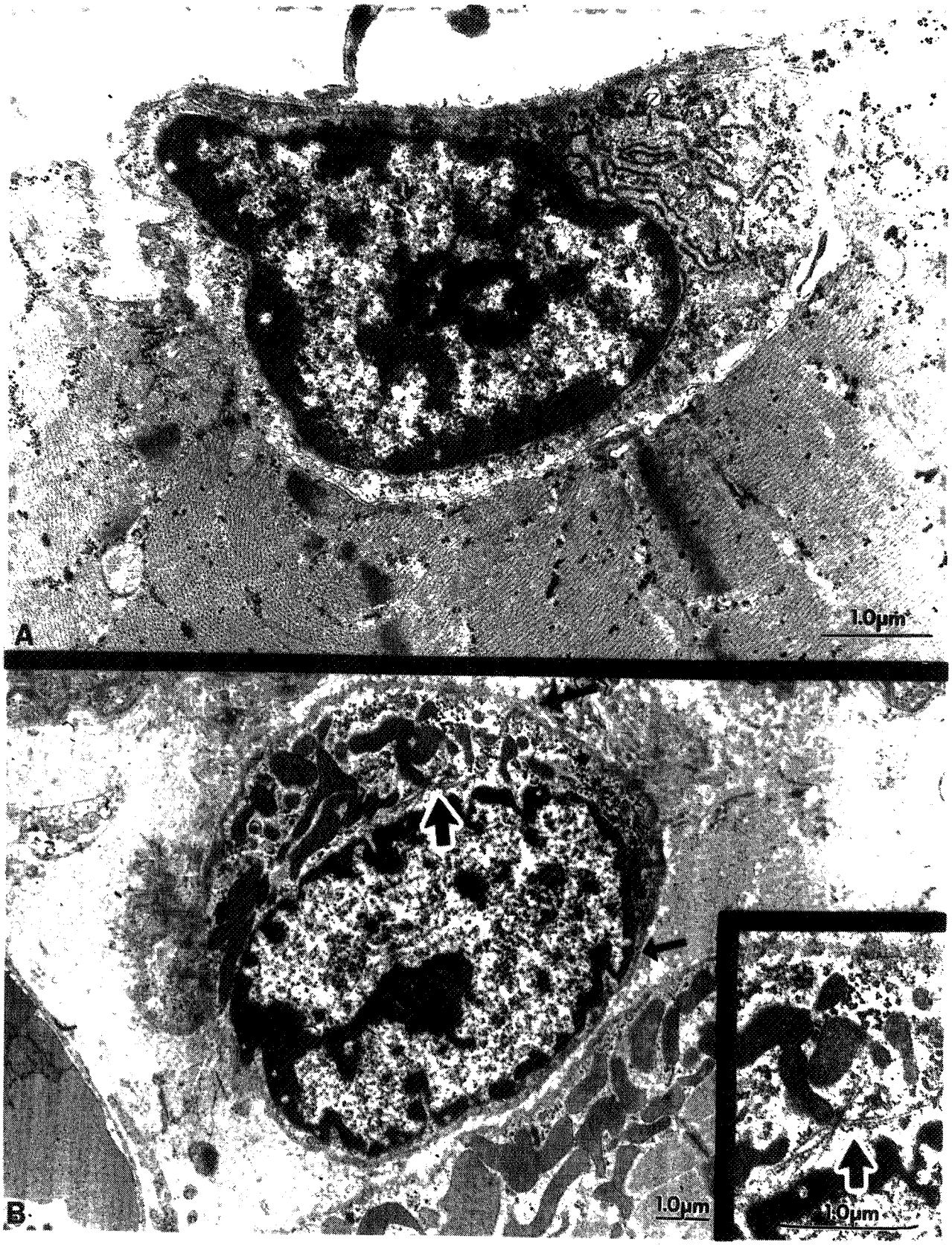

Figure 14. (A) Synchronous control. A morphologically normal satellite cell clearly separated from the underlying muscle fiber by a basement membrane. (B) Flight animal. A cell suggestive of an early regenerating muscle cell lying close to a muscle fiber, shows a nucleus with dispersed chromatin and some peripheral clumping surrounded by abundant free ribosomes and mitochondria. A few filaments (arrow and inset) are present at the periphery of the nucleus. The cell is surrounded by its own basement membrane (arrows).

Figure 15. Flight animal. A regenerating muscle fiber that shows incipient myofibrillary development (arrowhead) and ribosomal aggregates is completely surrounded by axon profiles (Ax), some of them containing numerous synaptic vesicles. They lie apposed to a postsynaptic membrane that shows short and rudimentary junctional folds (open arrows). The juxtaposition of the two axons at the lower left of the picture covered by a common Schwann cell process suggests axonal sprouting such as is seen during neuromuscular junction development.

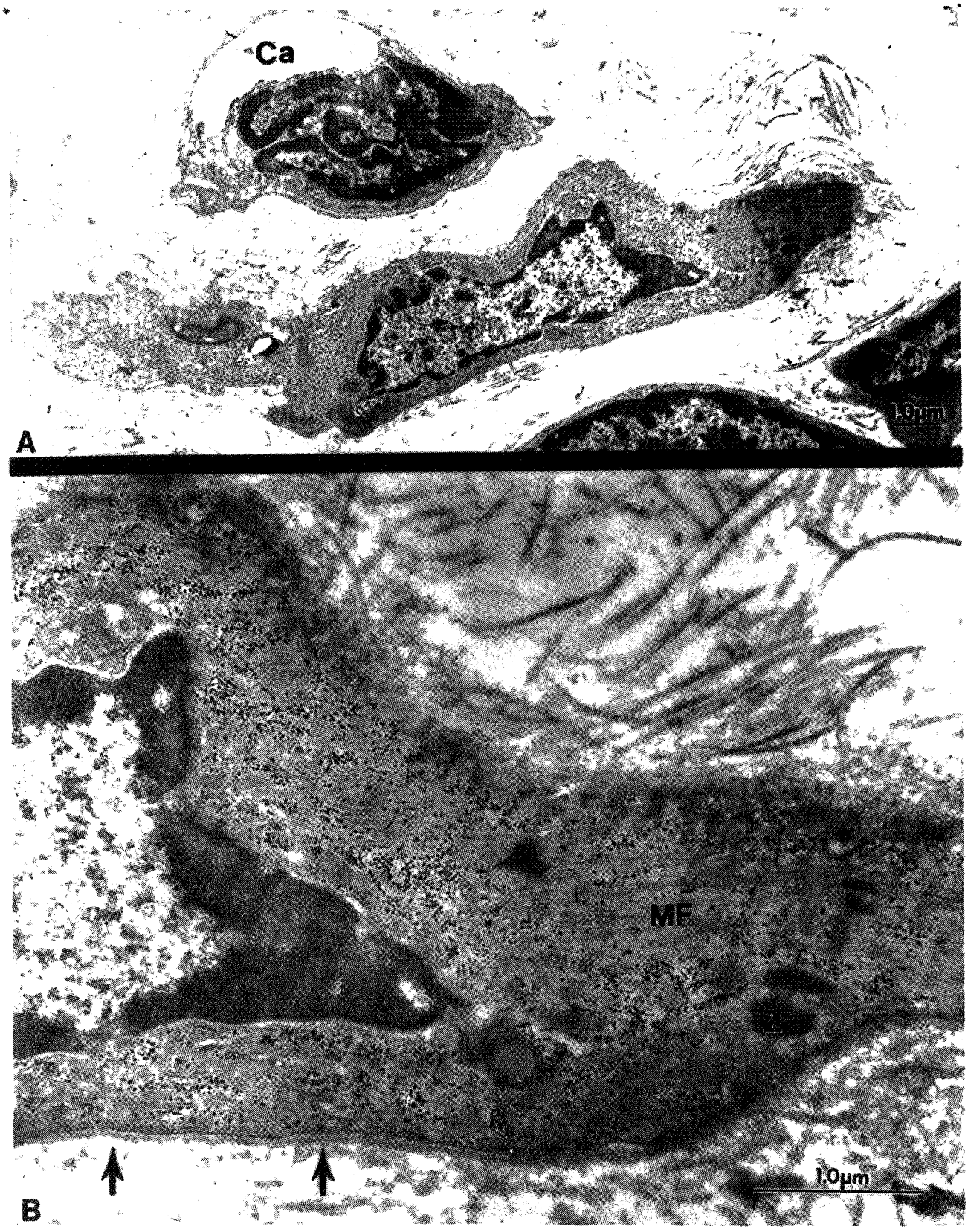

Figure 16. Flight animals. (A) An elongated regenerating myofiber lying freely within the interstitial space is seen surrounded by collagen fibers and close to a capillary (Ca). The nucleus shows dispersed chromatin. (B) Higher magnification of (A) reveals a cytoplasm containing abundant ribosomal aggregates associated to bundles of still disorganized myofilaments (MF). Immature Z bands (Z) are also conspicuous. A clearly visible basement membrane (arrows) surrounds the cell.

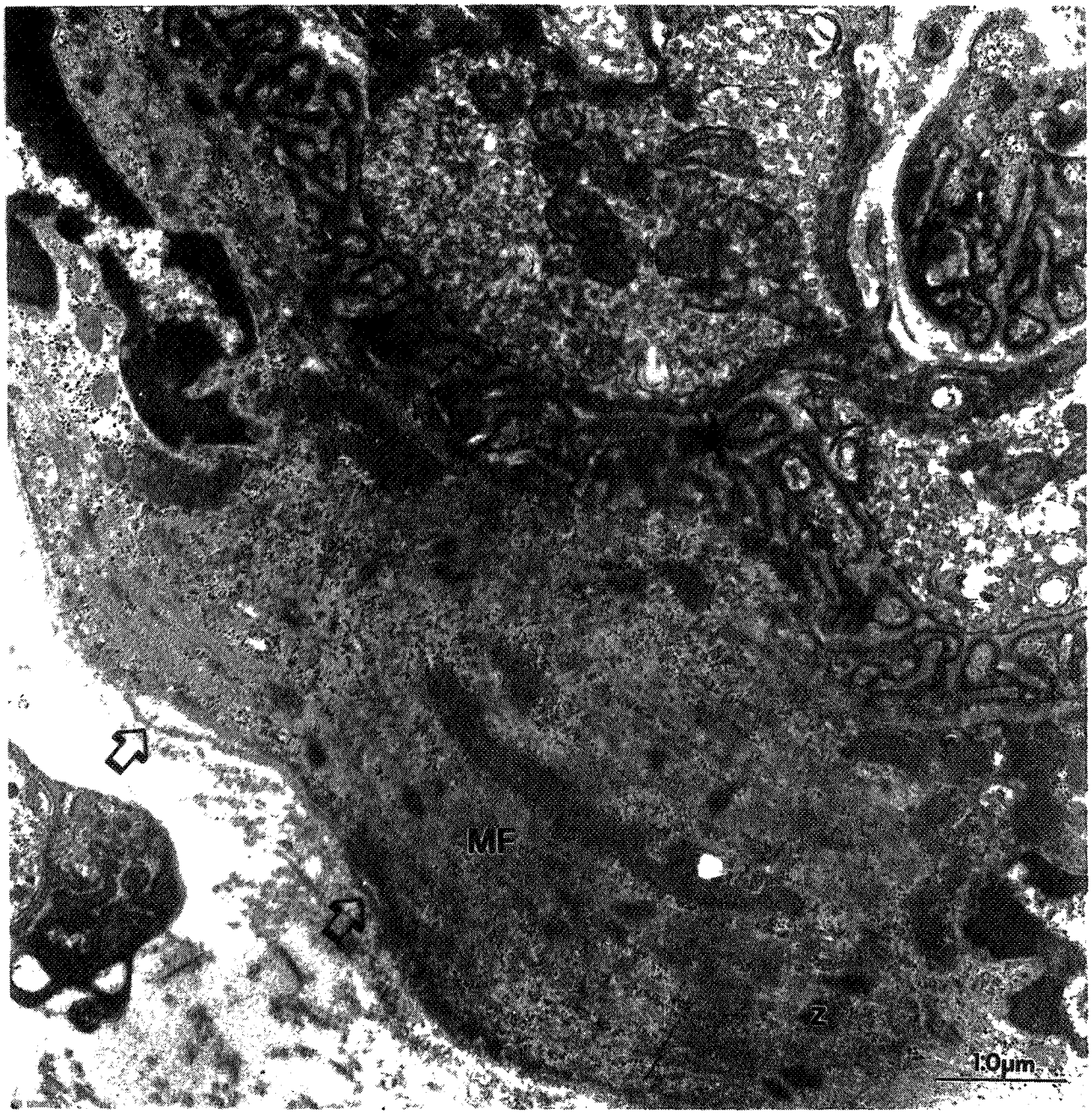

Figure 17. Flight animal. A regenerating muscle fiber encased in its basement membrane (open arrows) shows large amount of ribosomal aggregates associated with rudimentary myofibrils (MF) oriented parallel to the main axis and immature Z bands (Z). Part of the nuclei of the myofiber are seen at the upper left and lower right of the picture. A neuromuscular junction shows axon terminals and junctional folds of normal appearance except for the interposition of Schwann cell cytoplasm (arrow) between the pre- and postsynaptic membranes.

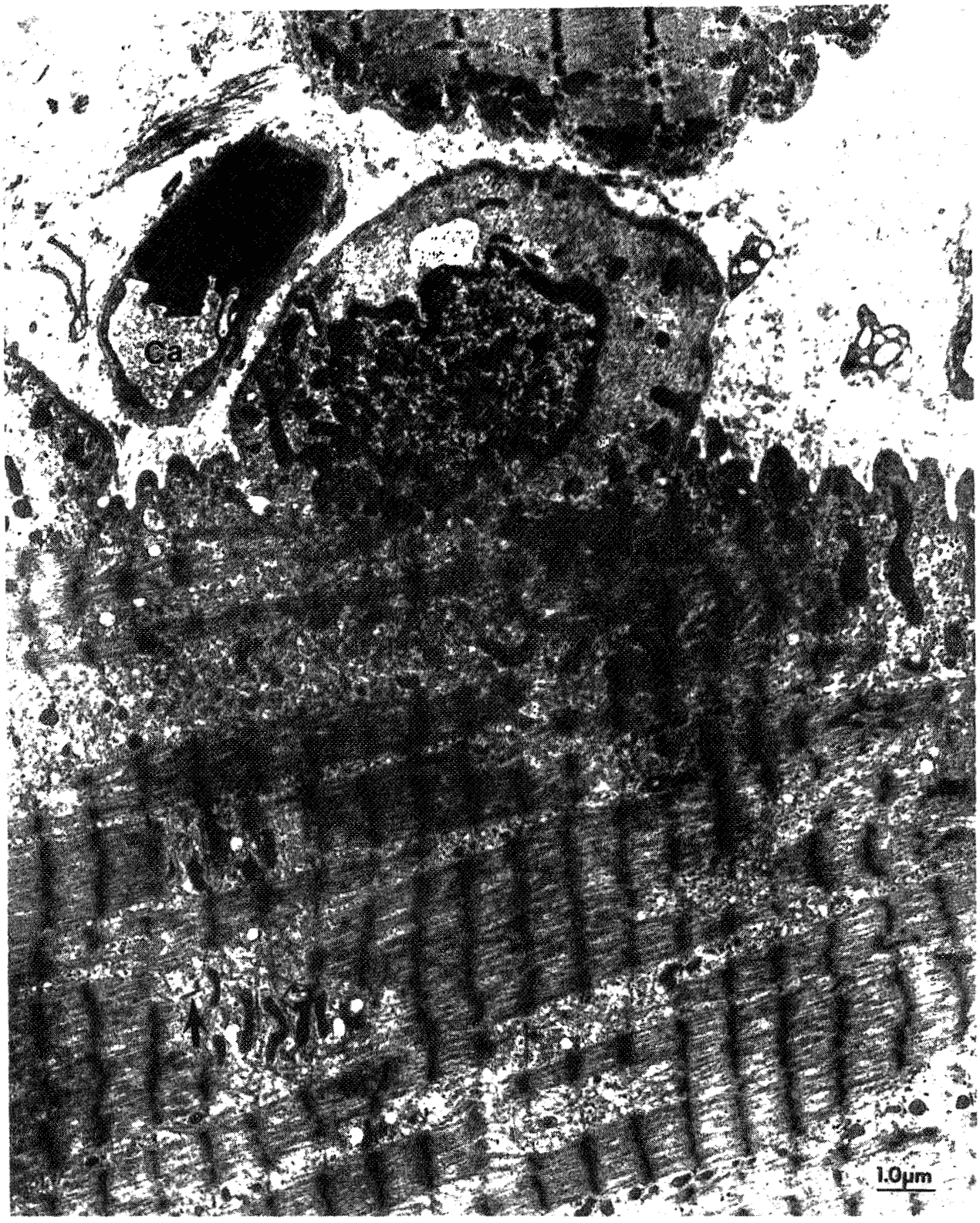

Figure 18. Flight animal. Regenerating myofiber at an advanced stage with a peripheral and protruding nucleus. The myofibrils are aligned, they are still immature, but the sarcomeric organization is already apparent. Ribosomal aggregates are present in the sarcoplasm in association to the myofibers and polyribosomes (arrow) can be seen close to loose thick filaments (open arrow) with no preferential orientation.

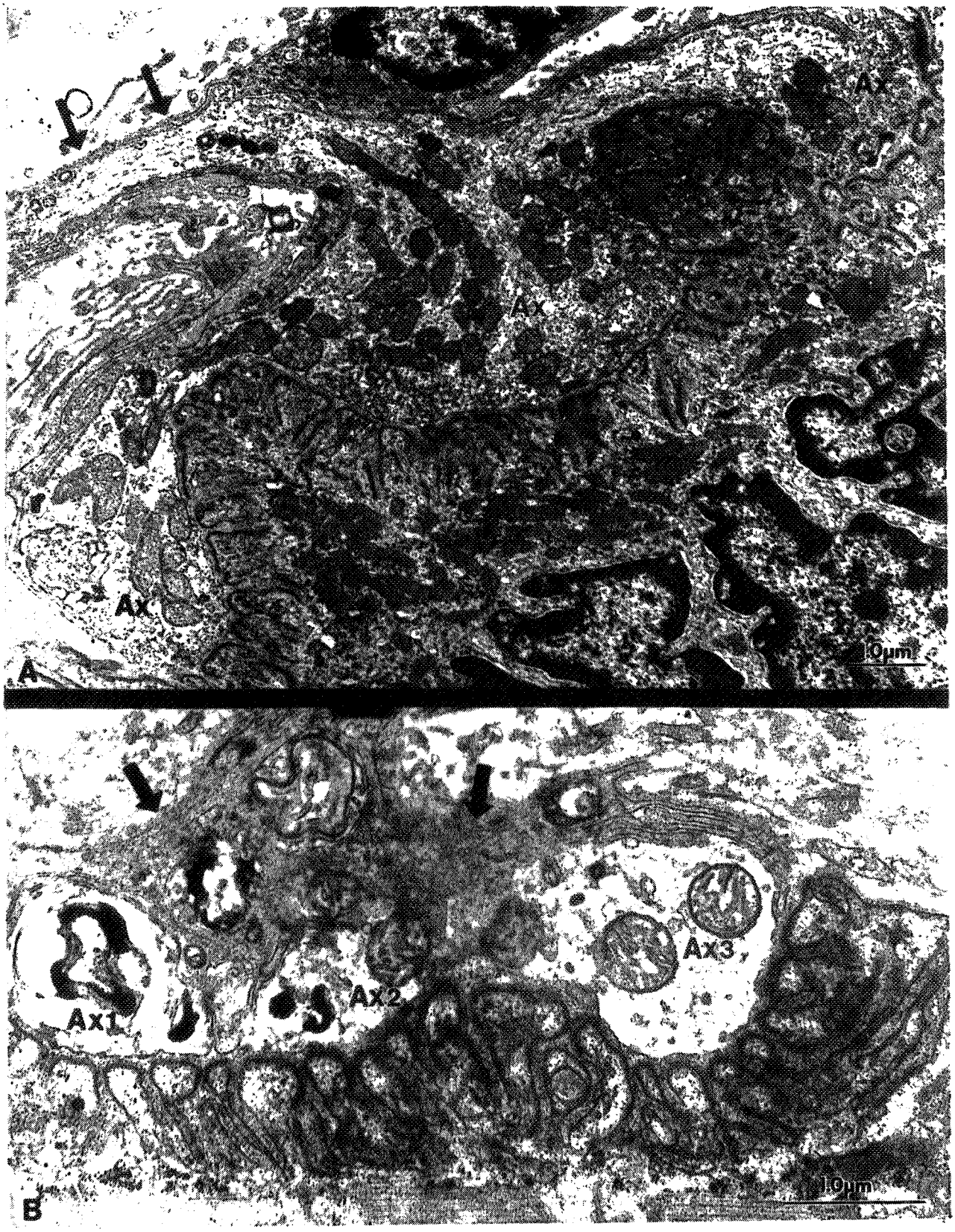

Figure 19. (A) Synchronous control. Neuromuscular junction showing a preterminal axon (arrows) that gives rise to three axon terminals (Ax) apposing normal junctional folds. (B) Flight animal. Neuromuscular junction displaying shrunken axon profiles (Ax1 and Ax2) occupied by myelin figures. Ax3 is completely devoid of synaptic vesicles. Schwann cell processes with degenerative alterations surround Ax1 and Ax2 (arrows) while Ax3 is covered by identifiable Schwann cell processes.

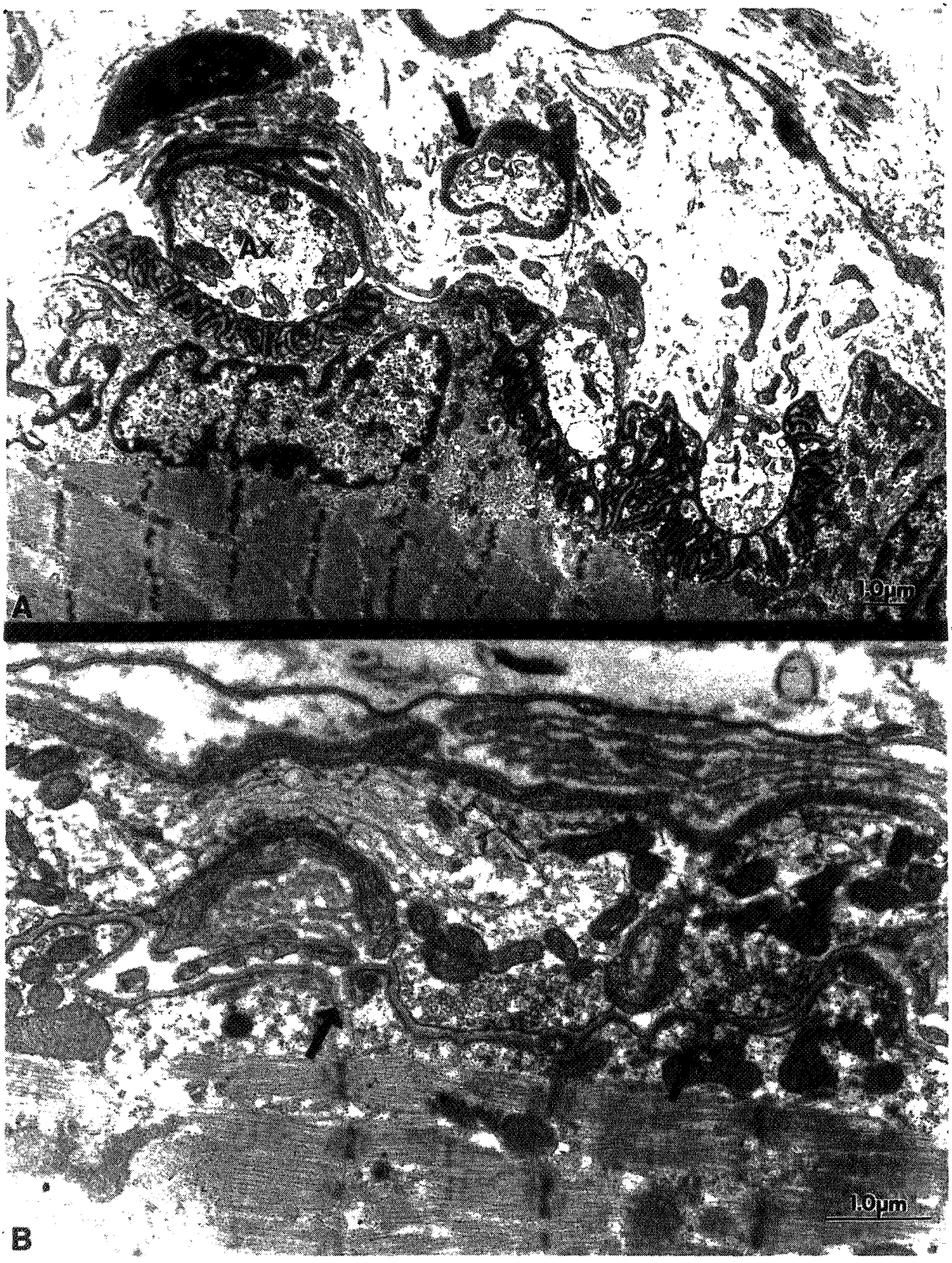

Figure 20. Flight animals. (A) Neuromuscular junction showing an axon profile (Ax) devoid of synaptic vesicles and occupied by microtubular structures (see figure 21 for details). An axon terminal completely surrounded by Schwann cell cytoplasm (arrow) lies far from the junctional region. Collagen fibers are conspicuous in the vicinity of the terminals. (B) Neuromuscular junction with marked decrease of postsynaptic profiles (arrows).

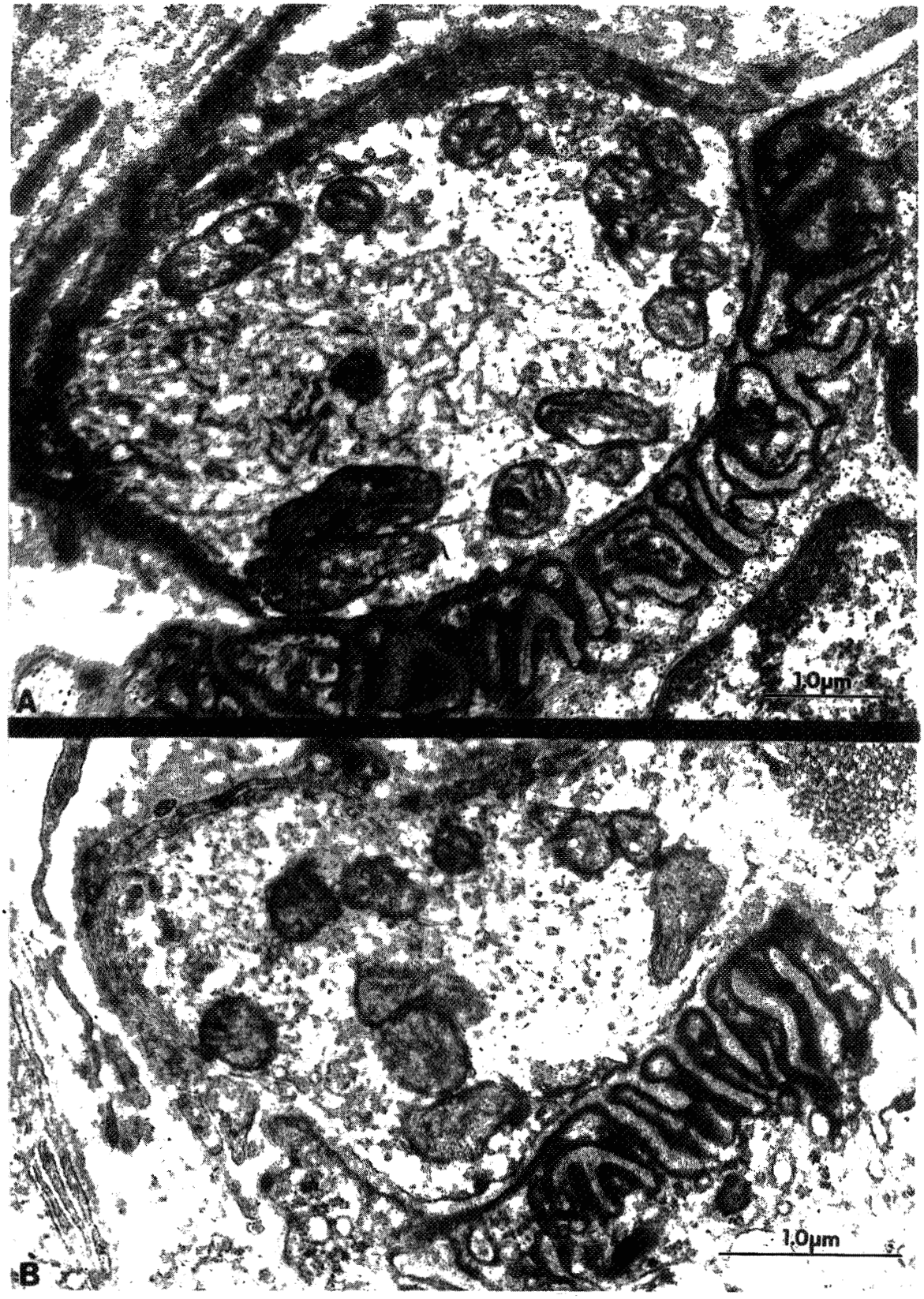

Figure 21. Flight animals. Figures (A) (detail of figure 20A) and (B) show two axon profiles devoid of synaptic vesicles and containing microtubular structures and few neurofilaments.

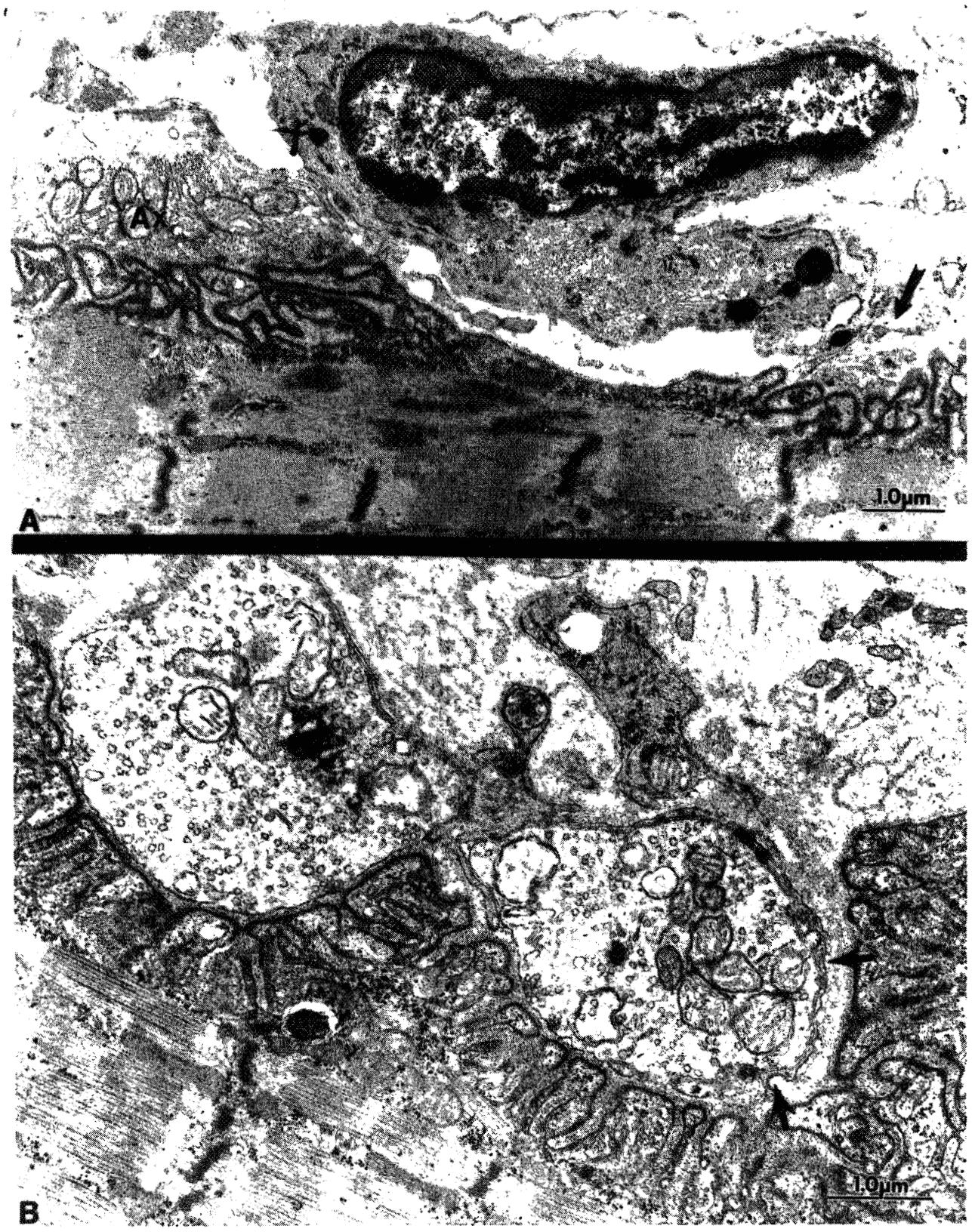

Figure 22. Flight animals. (A) Neuromuscular junction showing an apparently normal axon profile (Ax) to the left and a vacated axonal space occupied by Schwann cell cytoplasm, to the right (arrow). The junctional folds are widened and simplified. The underlying myofiber shows sarcomeric disorganization. (B) Neuromuscular junction showing a wide primary synaptic cleft (right of the figure) and a Schwann cell process (arrows) interposed between pre- and postsynaptic membranes and partially surrounding the axon profile.

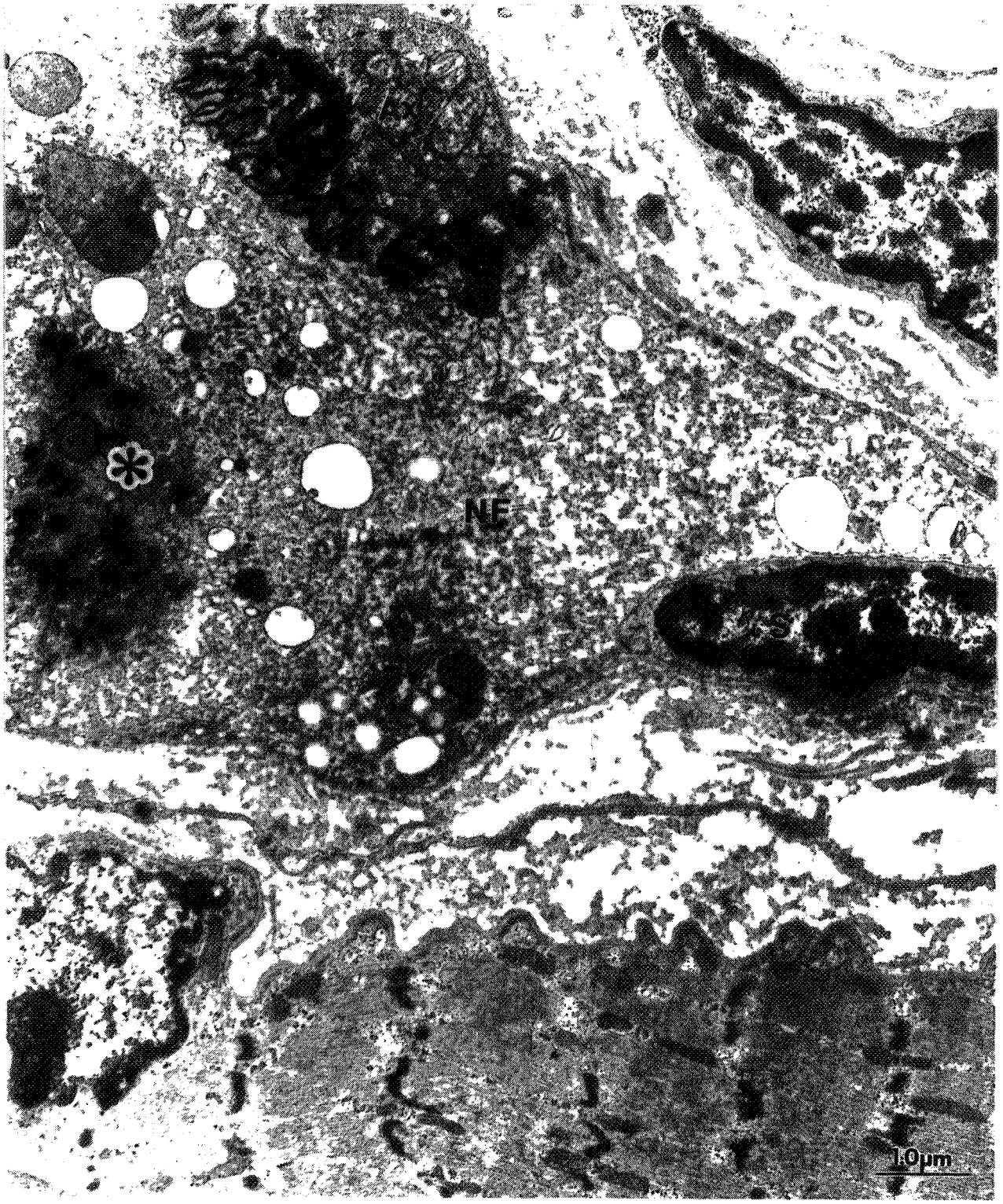

Figure 23. Flight animal. A myofiber undergoing necrosis (NF) shows dissolution of myofibrillar architecture and remains of altered myofibrils (*). A neuromuscular junction displays an axon profile (Ax) and junctional folds of apparently normal morphological characteristics. The osmiophilic reaction of the synaptic cleft and junctional folds corresponds to esterase activity revealed by the staining procedure used to localize motor endplates. At the center-right of the picture, part of a satellite cell (S) is visible.

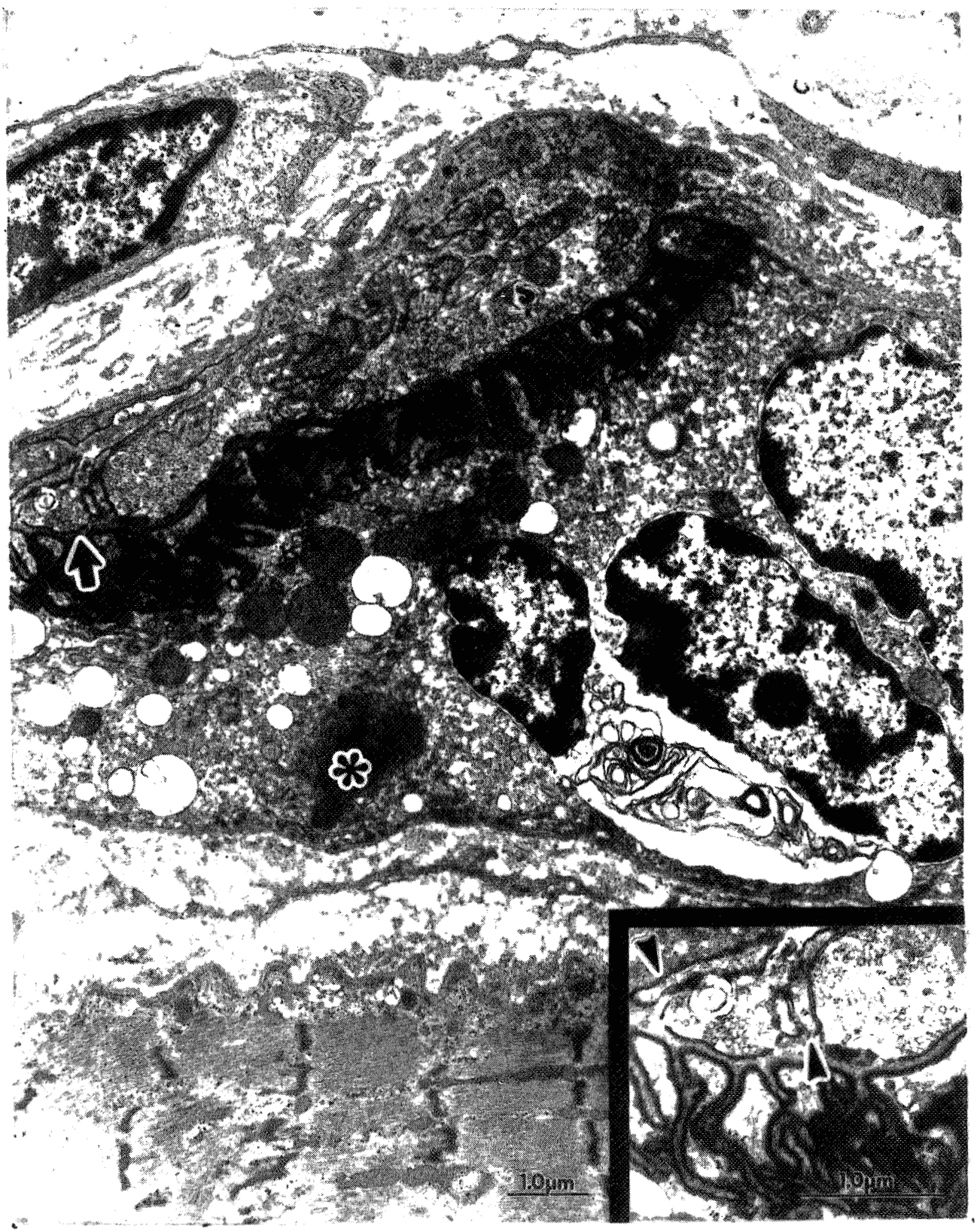

Figure 24. Flight animal. A myofiber undergoing necrosis with similar characteristics to that of the previous picture. Additional features include chromatin clumping and lysis of nuclei, and the presence of an axonal sprout (arrow and inset) that is separated from a single elliptical main axon terminal by Schwann cell processes that also covers the sprout (arrowheads in inset). Notice again the esterase activity of the synaptic cleft and junctional folds. (*), myofibril remains.

Page intentionally left blank

54-51
57349

EXPERIMENT K-7-18

PART II: QUANTITATIVE AUTORADIOGRAPHIC ANALYSIS OF GABA (BENZODIAZEPINE) AND MUSCARINIC (CHOLINERGIC) RECEPTORS IN THE FOREBRAIN OF RATS FLOWN ON COSMOS 2044

L. Wu, N.G. Daunton, I.B. Krasnov, F. D'Amelio, T.M. Hyde, S.K. Sigworth

INTRODUCTION

Quantitative autoradiographic analysis of receptors for GABA and acetylcholine in the forebrain of rats flown on COSMOS 2044 was undertaken as part of a joint US -Soviet study to determine the effects of microgravity on the central nervous system, and in particular on the sensory and motor portions of the forebrain. Changes in binding of these receptors in tissue from animals exposed to microgravity would provide evidence for possible changes in neural processing as a result of exposure to microgravity. Tritium-labelled diazepam and Quinuclidinyl-benzilate (QNB) were used to visualize GABA (benzodiazepine) and muscarinic (cholinergic) receptors, respectively. The density of tritium-labelled radioligands bound to various regions in the forebrain of both flight and control animals were measured from autoradiograms. Data from rats flown in space and from ground-based control animals that were not exposed to microgravity were compared.

MATERIAL AND METHODS

Samples of the left hemisphere of the brain from rats flown in space for 14 days on COSMOS 2044 in September, 1989, and from three ground-based control groups (synchronous, vivarium, and tail suspended) were provided by Soviet scientists. The samples were frozen in Freon cooled in liquid nitrogen, stored at -70° C and sent in biotransporters to the U.S.

Coronal sections (20 μm) were cut in a cryostat held at -20° C. The sections were mounted on microscope slides that had been previously cleaned with 95% ethyl alcohol and subbed with 1% gelatin solution. The slide-mounted tissues were dried in a refrigerator (0°) overnight and then stored at -70° C. Adjacent sections were used for assessment of total binding, non-specific binding and for anatomical location by means of Nissl staining. The atlas of the rat brain by Paxinos and Watson (1986) was used as reference.

It is important to point out that many samples were fractured (most likely due to the freezing procedure). Although the anatomical orientation of the samples proved easy to determine, difficulties were encountered trying to establish precise boundaries of the regions under examination because of differences in sampling among the groups, e.g., some of them contained only rostral portions of the basal ganglia.

GABA (Benzodiazepine) Receptor Binding

The incubation solution used to assess total binding of GABA (benzodiazepine) receptors consisted of 1nM [^{3}H] Diazepam (New England Nuclear, Massachusetts, specific activity 85.2 Ci/mmol) added to 0.17M Tris buffer (pH 7.6). For assessment of non-specific binding 1mM Valium(Rouche, 1M/ml) was added to a different aliquot of the same solution. The slide-mounted tissues were incubated for 40 minutes in ice-cold buffer containing the radiolabelled ligands, and then washed for 10 minutes in ice-cold buffer, followed by a brief rinse in distilled water.

Muscarinic (Cholinergic) Receptor Binding

The Wamsley [Wamsley, 1981] procedure was used to visualize muscarinic cholinergic receptors. The incubation solution for assessment of total binding consisted of 1nM [^{3}H]-QNB (New England Nuclear, Massachusetts, specific activity 45.7 Ci/mmol) added to 0.4M PBS buffer (pH 7.4). The slide-mounted tissues were incubated for 2 hours at room temperature and washed. For assessment of non-specific binding 1mM unlabeled atropine was used to compete for the receptors, following the same procedure used for total binding.

Dried radiolabeled slides were apposed to [^{3}H] Hyperfilm (Amersheim) X-ray film and then placed into a stainless steel X-ray cassette. The film was exposed to the tritiated slides for five weeks in a refrigerator located in a darkroom. A radiolabeled polymer standard {[^{3}H]microscales strip (Amersheim)}, with activities ranging from 1.3 to 33.0 nCi/mg tissue equivalent, was exposed with each film. At the end of the five-week period the film was developed.

Image Analysis

A video camera-based image analysis system (Loats Image Analysis System, Winchester, MD) was used to quantify the densities of the autoradiograms. The system included a DAGE-MTI Series 68 Newvicon tube camera, fitted with a Nikon Nikor 55mm f/2.8 lens, that was mounted on a calibrated copy stand. A RS170 cable connected the camera with the frame-grabber board in the IBM PC/AT. This system digitized images up to 752x480 pixels, with 8 bit resolution. Thus, 256 levels of gray scale or pseudocolor mapping could be displayed. The system was located in a light-tight room and operated with room lights turned off. The software used was Receptor Autoradiography Analysis System, RAS1001P.EXE., v 2.04, 1986.

Ten forebrain regions were selected for quantitative analysis of receptor binding. These regions included: the superficial and deep layers of the cingulate gyrus, frontal motor cortex, frontal sensory cortex, and olfactory cortex, as well as the dorsal and ventral regions of the striatum (caudate nucleus and putamen). For each region investigated the size of the area sampled, mean optical density and equivalent density per minute values were computed. In addition, a measure of fentomoles (fmoles) per milligram of tissue was obtained based on the specific activity of the radioligands. The final results reflect the amount of tritium bound to the tissue, and thus the amount of the receptor present.

Statistical Analysis

The fmole values computed by the RAS software were entered into a spreadsheet (Excel, v. 2.2a, Microsoft) on a Macintosh II computer, and then exported to Statview II (Abacus, v. 1.03) for statistical analysis (ANOVA, Dunnett's t) to determine significance of differences in receptor binding densities between flight and the various control animals. Statistical significance was taken to be $p < .05$. Within each brain area, the two different regions (superficial vs deep or dorsal vs ventral) were analyzed separately to determine differences among the conditions. In addition, because variations in the blocking of individual brains made it difficult to measure densities in exactly the same subdivisions of each brain region, each brain region was analyzed further using the combined data from the two subdivisions.

RESULTS

GABA (Benzodiazepine) Receptors

Table 1 shows the mean density of receptors in animals from the flight group as compared with those from the three control groups for each of the areas investigated, with data provided for the two regions within an area as well as for the combined data from the whole area. Figure 1 shows

graphically the mean density of the GABA receptors in the different areas, with both regions combined, for the flight and various control groups. Figure 2 shows a comparison of mean receptor densities in the different areas for the flight and synchronous control animals (the most appropriate control group for assessment of effects of spaceflight). It can be seen from these tables and figures that there were no significant differences in densities of benzodiazepine receptors among flight and the various control animals in any of the brain regions evaluated.

Muscarinic Cholinergic Receptors

Table 2 shows the mean density of muscarinic receptors in the various forebrain areas in flight animals and in animals from the control groups. No significant differences were seen between flight and various control animals when receptor densities within subdivisions of given brain regions were compared, partially due to small numbers of observations and large variation of values. However, when data from the two subdivisions were combined, a significant difference was found between the density of receptors in the striatum (caudate nucleus and putamen of the basal ganglia) of the flight animals as compared with those in the striatum of animals in the synchronous control group. Thus, for the striatum muscarinic receptor density was lower in the flight animals than in the synchronous control animals (316.0 vs 454.9). The data for each brain region, with subdivisions combined, for the flight and control groups are shown graphically in Figure 1. Figure 2 shows a comparison of data from the flight and the synchronous control group for all brain areas (subdivisions combined).

DISCUSSION

This research was conducted after a preliminary study in 1987 demonstrated the feasibility of investigating receptor binding on brain tissue of spaceflight rats. GABA (benzodiazepine) and muscarinic receptors were chosen because their prominent distribution within the forebrain. GABA receptors mediate the effect of gamma-aminobutyric acid (GABA), the best known of all the inhibitory neurotransmitters. Muscarinic (cholinergic) receptors mediate the effect of acetylcholine, a predominantly excitatory neurotransmitter.

GABA (Benzodiazepine) Receptors

GABA is the main inhibitory neurotransmitter in the vertebrate brain. Both tritium labeled diazepam and benzodiazepine are commonly used to label GABA receptors [Möhler, Okada,1977; Unnerstall et al.,1981]. Several subtypes of GABA receptors have been identified and characterized. [Costa, 1988, Lambert et al , 1988].

For this study the total GABA receptor binding was quantified using [^{3}H]diazepam [Briley, Langer, 1978]. The absence of significant differences between flight and three groups of control animals in the regions under study is not in itself conclusive due to the small number of samples and the anatomical variations among the samples. These results, however, suggest that for future studies other procedures should be implemented to establish variations or similarities among GABA receptors subtypes, e.g., Type I and II benzodiazepine receptors .

Muscarinic (Cholinergic) Receptors

The most significant finding in this study is the decrease in muscarinic cholinergic receptors in the striatum of flight rats. Once again, however, the differences in sampling among the various groups and the fracture of many of the specimens, added to the known structural complexity of the basal ganglia, allow only some reasonable speculation about the implications of this finding.

The caudate putamen is a part of the basal ganglia that modulates the delicate balance of motor function [Pansky, Allen, & Budd, 1988]. Decrease of receptor binding sites may reflect a disruption in motor responses.

It is conceivable that the down-regulation of striatal muscarinic cholinergic receptors might be a compensatory response to increased release of acetylcholine. Striatal acetylcholine release is mainly regulated by dopamine. It has been shown that increased striatal dopaminergic transmission reduces striatal acetylcholine release (Parker and Cubeddu, 1986). Since dopamine regulates motor behavior, and taking into account that spontaneous motor behavior may be reduced during weightlessness, it is reasonable to assume that the decrease in striatal muscarinic receptors observed in the flight animals is the result of decreased dopaminergic transmission.

GABA also plays a role in the regulation of striatal muscarinic receptor density. It has been suggested that endogenous GABA release potentiates striatal acetylcholine release (Lim et al., 1988). Hence, increased GABA release might have contributed to the decrease in muscarinic receptor binding density.

While striatal muscarinic receptors were decreased in this study, no changes were observed in the cerebral cortex. It is known that most of the cholinergic innervation of the striatum is derived from interneurons, whereas the cortex receives its cholinergic input from the nucleus basalis of Meynert (see Fibiger,1982, for review). Whether these differences in cholinergic systems within the striatum and cerebral cortex may account for differences in the regulation of muscarinic receptors can not be assessed in this study.

The observations that have been described seem to indicate that microgravity-induced alterations in motor activity may result in a decrease of muscarinic receptor binding density in the striatum. Additional study needs to be performed to confirm and expand upon these results. For example, future manned spaceflights should address the importance of in-depth observations of the motor behavior of rats in space to correlate with the changes in receptor binding sites.

ACKNOWLEDGEMENTS

The authors want to express their appreciation to the Soviet and U.S. scientists for providing the samples used in this study. Funding for this research was provided by the NASA-COSMOS parts program and by the Intramural Research Program to the Clinical Brain Disorders Branch of the National Institute of Mental Health.

Special thanks to Richard E. Grindeland, James P. Connolly and Marilyn F. Vasques for their constant support.

REFERENCES

1. Briley, M.S. and S.Z. Langer. Influence of GABA Receptor Agonists and Antagonists on the Binding of [^{3}H] Diazepam to the Benzodiazepine Receptor. European J. Pharmacol. 52:129-132, 1978.

2. Costa, E. "Polytypic Signaling at GABAergic Synapses." The Pennsylvania State University College of Medicine, 1987 B.B. Brodie Lecture. Life Sci. 42:1407-1417, 1987.

3. Fibiger, H.C. The Organization and Some Projections of Cholinergic Neurons of the Mammalian Forebrain. Brain Res. Rev. 4:327-388, 1982.

4. Lambert, J.D.C., E.N. Petersen, M.S. Jensen, and L.H. Jensen. Chap 13: Modulatory Sites of New, Potentially Specific Therapeutic Agents. In: Neurotransmitter and Cortical Function From Molecules to Mind. Eds: M. Avoli and T.A. Reader. Plenum Press, New York. 207-226, 1988.

5. Lim, D.K., Y. Ito, B. Hoskins, and I.K. Ho. Effects of Acute and Subacute Administration of Bicuculline on Dopamine and Muscarinic Receptors in Rat Brain. Brain Res. Bull. 21:21-24, 1988.

6. Möhler, H. and T. Okada. Properties of [^{3}H] Diazepam Binding to Benzodiazepine Receptors in Rat Cerebral Cortex. Life Sci. 20:2101-2110, 1977.

7. Pansky, B, D.J. Allen, and G.C. Budd. Review of Neuroscience, 2nd Edition. Macmillan Publishing Company, New York. 192, 1988.

8. Parker, E.M. and L.X. Cubeddu. Effects of D-Amphetamine and Dopamine Synthesis Inhibitors on Dopamine and Acetylcholine Neurotransmission in the Striatum: II. Release in the Presence of Vesicular Transmitter Stores. J. Pharm. Exp. Ther. 1237:193-203, 1986.

9. Paxinos, G. and C. Watson. The Rat Brain in Stereotaxic Coordinates, Second Edition. Academic Press, New York. 1986

10. Unnerstall, J.R., M.J. Kuhar, D.L. Neihoff, and J.M. Palacios. Benzodiazepine Receptors are Coupled to a Subpopulation of Gamma-Aminobutyric Acid (GABA) Receptor: Evidence from a Quantitative Autoradiography Study. J. Pharmacol. Exp.Ther. 218:797-804, 1981.

11. Wamsley, J.K., M.S. Lewis, and W.S. Young. Autoradiographic Localization of Muscarinic Cholinergic Receptors in Rat Brainstem. J. Neurosci. 1:176, 1981.

TABLE 1.

GABA (BENZODIAZEPINE) RECEPTORS

	Flight			Vivarium			Synchronous			Tail Suspended		
	X	(SE)	N	X	(SE)	N	X	(SE)	N	X	(SE)	N
A.Cingulate												
Superficial	44.0	(8.5)	3	35.0	-	1	48.8	(4.7)	5	44.8	(7.2)	4
Deep	65.5	(13.5)	2	28.0	-	1	50.3	(6.5)	6	41.8	(8.7)	4
Combined	52.6	(8.2)	5	31.5	(3.5)	2	49.6	(4.0)	11	43.2	(5.2)	8
B.Motor												
Superficial	50.0	(6.5)	8	51.8	(4.9)	6	58.2	(5.0)	8	58.8	(5.8)	5
Deep	62.6	(6.3)	8	63.8	(4.2)	6	57.4	(3.6)	8	61.8	(6.3)	5
Combined	56.3	(4.7)	16	57.8	(3.6)	12	57.8	(3.0)	16	60.3	(4.1)	10
C.Sensory												
Superficial	53.4	(5.3)	8	69.2	(7.4)	4	62.0	(5.2)	8	51.2	(3.1)	5
Deep	62.8	(6.9)	8	69.0	(3.6)	4	56.8	(6.7)	8	55.0	(5.1)	5
Combined	58.1	(4.4)	16	69.1	(3.8)	8	59.4	(4.2)	16	53.1	(2.9)	10
D.Olfactory												
Superficial	28.0	(2.6)	7	29.7	(6.2)	3	29.7	(5.0)	6	41.4	(4.5)	5
Deep	39.6	(4.8)	8	37.0	(6.2)	4	34.8	(4.2)	6	44.8	(6.3)	5
Combined	34.2	(3.1)	15	33.8	(4.3)	7	32.2	(3.2)	12	43.1	(3.7)	10
E.Striatum												
Dorsal	31.0	(4.7)	6	28.7	(6.4)	3	30.4	(3.0)	7	24.7	(5.8)	3
Ventral	29.3	(3.0)	6	32.7	(8.4)	3	29.8	(2.8)	8	24.0	(5.1)	3
Combined	30.2	(2.6)	12	30.7	(4.8)	6	30.1	(2.0)	15	24.3	(3.5)	6

Mean density, standard error and number of observations in different brain regions in flight and control animals: A. Cingulate gyrus; B. Motor cortex; C. Sensory cortex; D. Olfactory cortex; E. Striatum (caudate and putamen). Underlined means indicate significant difference between mean of flight and of underlined control group.

TABLE 2.

MUSCARINIC RECEPTORS

	Flight			Vivarium			Synchronous			Tail Suspended		
	X	(SE)	N	X	(SE)	N	X	(SE)	N	X	(SE)	N
A.Cingulate												
Superficial	309.5	(0.5)	2	-	-	-	449	-	1	555	-	1
Deep	312.6	(31.3)	5	259	-	1	309.2	(48.8)	6	375.7	(108.9)	3
Combined	311.7	(21.6)	7	259	-	1	329.1	(45.8)	7	420.5	(89.1)	4
B.Motor												
Superficial	354.8	(36.9)	5	301.0	(15.0)	3	328.0	(20.9)	5	314.0	(41.3)	4
Deep	348.0	(28.6)	7	302.3	(22.2)	3	355.8	(13.3)	6	395.0	(50.2)	4
Combined	350.8	(21.6)	12	301.7	(12.0)	6	343.2	(12.1)	11	354.5	(33.8)	8
C.Sensory												
Superficial	301.6	(36.0)	7	354.0	(33.0)	2	309.7	(35.7)	6	361.8	(31.9)	4
Deep	325.1	(11.7)	7	331.3	(34.5)	3	343.1	(12.4)	7	382.2	(25.3)	4
Combined	313.4	(18.5)	14	340.4	(22.3)	5	327.7	(17.6)	13	372.0	(19.2)	8
D.Olfactory												
Superficial	40.0	(22.0)	2	-	-	-	107.0	(70.8)	3	-	-	-
Deep	232.2	(34.6)	4	-	-	-	256.5	(24.2)	4	-	-	-
Combined	168.2	(46.4)	6	-	-	-	192.4	(42.8)	7	-	-	-
E.Striatum												
Dorsal	320.8	(30.6)	5	292.5	(24.5)	2	467.5	(33.0)	6	387.8	(102.7)	4
Ventral	311.2	(33.8)	5	205.5	(49.5)	2	442.3	(36.8)	6	386.0	(92.0)	4
Combined	316.0	(21.5)	10	249.0	(33.8)	4	454.9	(23.9)	12	386.9	(63.8)	8

Mean density, standard error and number of observations in different brain regions in flight and control animals. A. Cingulate gyrus; B. Motor cortex; C. Sensory cortex; D. Olfactory cortex; E. Striatum (caudate and putamen). Underlined means indicate significant difference between mean of flight and of underlined control group.

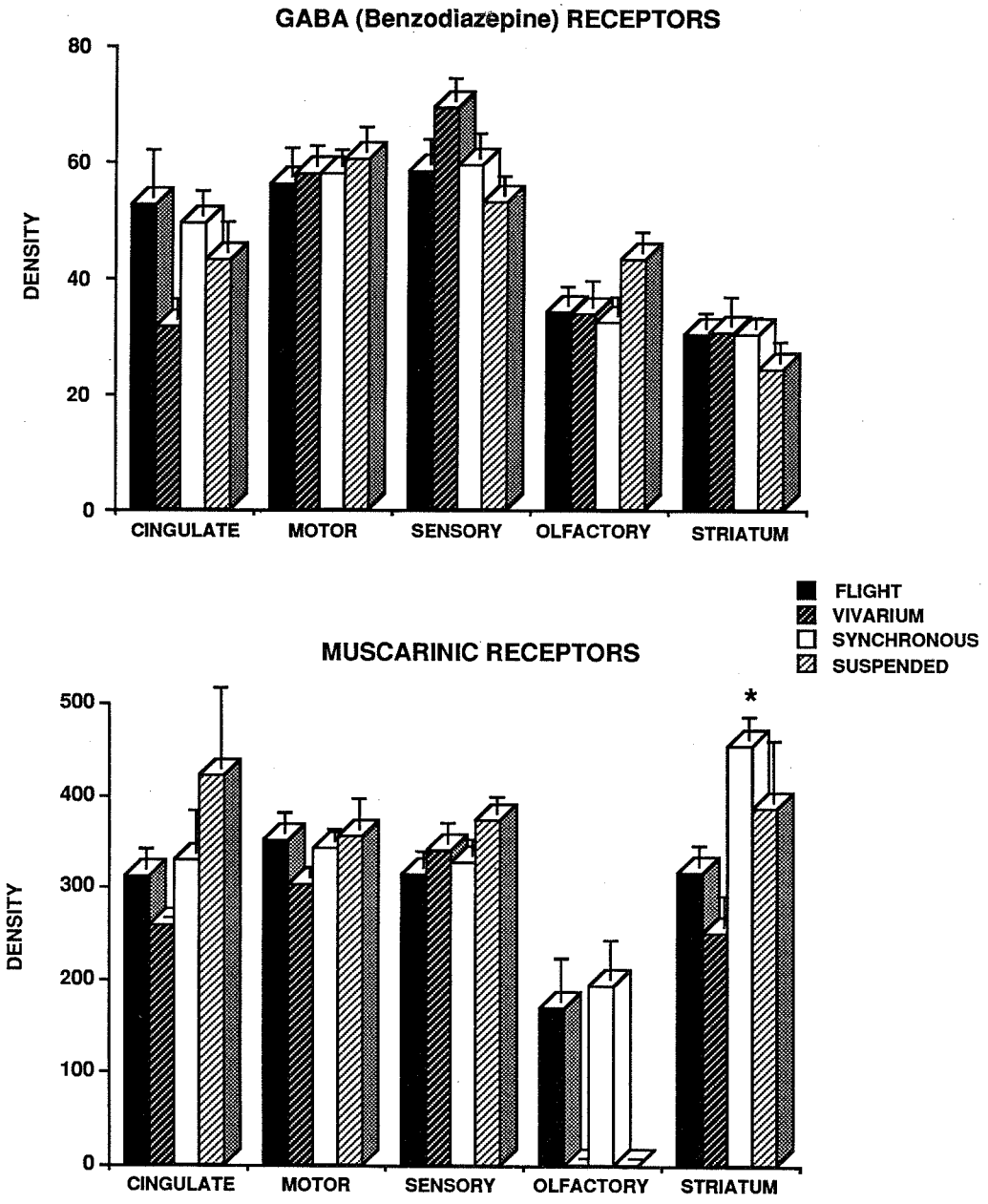

Figure 1. Mean densities of GABA (benzodiazepine) and Muscarinic receptors in each brain region for Flight, Vivarium, Synchronous, and Suspended groups. Error bars indicate standard error of the mean. Asterisk indicates significant ($p<.05$) difference between Flight and marked control group.

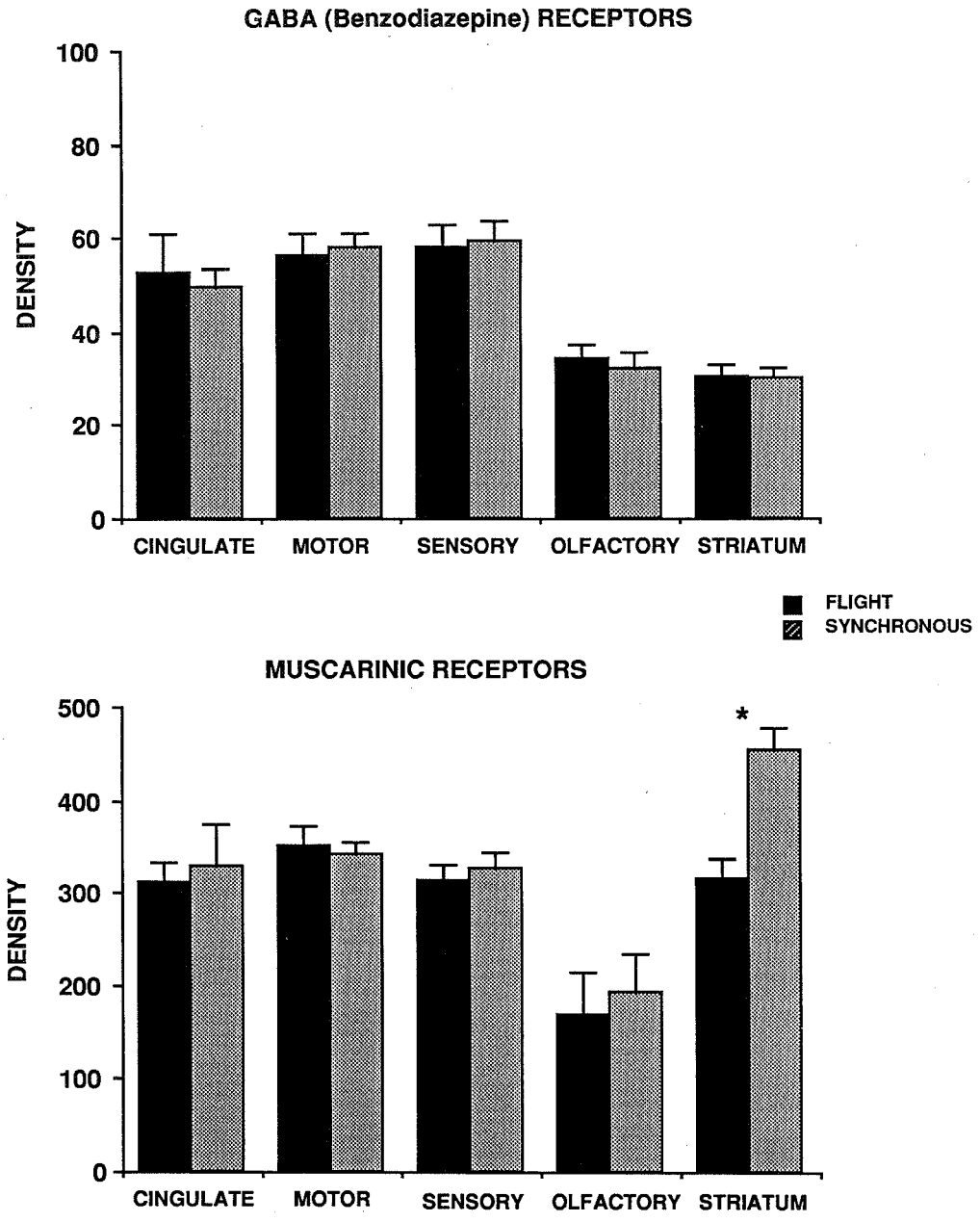

Figure 2. Comparison of mean densities of GABA (benzodiazepine) and Muscarinic receptors from Flight and Synchronous groups for each brain area. Error bars indicate standard error of the mean. Asterisk indicates significant ($p<.05$) difference between Flight and Synchronous control group.

Page intentionally left blank

S5-57
51350

EXPERIMENT K-7-19

PINEAL PHYSIOLOGY AFTER SPACEFLIGHT: RELATION TO RAT GONADAL FUNCTION

Principal Investigator:

D.C. Holley
Department of Biological Sciences
San Jose State University
San Jose, CA

Co-Investigators:

M.R.I. Soliman
College of Pharmacy and Pharmaceutical Sciences
Florida A&M University
Tallahassee, FL

I. Krasnov
Institute of Biomedical Problems
Moscow, USSR

H. Asadi
Department of Biological Sciences
San Jose State University
San Jose, CA

107314
18P

Page intentionally left blank

EXPERIMENT K-7-19

PINEAL PHYSIOLOGY IN MICROGRAVITY: RELATION TO RAT GONADAL FUNCTION

D.C. Holley, H. Asadi, I. Krasnov, and M.R.I. Soliman

INTRODUCTION

Relative to other endocrine organs, research on the physiology of the pineal has been a rather recent endeavor, and discoveries relative to pineal physiology have proceeded rather slowly. Considerable advances in this area have occurred over the past two decades and many textbooks are now espousing it as a true endocrine gland (Hadley, 1988). It is now known that the pineal organ can interact with many endocrine and nonendocrine tissues in a regulatory fashion. It is well established that an antigonadal hormone of pineal origin (most likely the indoleamine melatonin) is involved in the photoperidodic regulation of reproduction in seasonally breeding mammalian species, and some nonseasonal breeding species (possibly also humans). Recent reviews implicate the pineal in the functioning of other organs and systems besides those involved in reproduction including: temperature regulation, thyroid, growth hormone, adrenal glucocorticoid synthesis, behavior (arousal/depression), circadian system (activity/rest), and skin pigmentation (in lower animals). Several excellent journal reviews and books on pineal physiology have appeared over the past ten years (See Reiter, 1981a; Reiter, 1981b; Vollrath, 1981; Reiter, 1982; Binkley, 1983; Axelrod, et al. 1983; Preslock, 1984; Reiter, 1984; Brown and Wainwright, 1985; O'Brien and Klein, 1986). In view of the fact that the pineal is an important link to the environment (Reiter, 1986), it is conceivable that exposure to microgravity and spaceflight might alter the function of this gland and, in turn, affect various physiological functions including the circadian timing system and reproduction.

Primary control of pineal function is mediated by the photoenvironment. Light impinging upon the retina influences the pineal via the following pathway: retino-hypothalamanic tract, suprachiasmatic nuclei, median forebrain bundle, superior cervical ganglia, sympathetic efferents. Adrenergic receptor activation results in stimulation of N-Acetyltransferase (NAT) activity with resulting production of melatonin from the precursor serotonin (5-hydroxytryptamine, 5-HT). Indeed, the serotonin concentration of the pineal gland exceeds that of any other organ and is fifty times that of any other brain area (Quay, 1963). Melatonin is probably the most important pineal secretory product in terms of distant regulatory responses (e.g. antigonadal effects). However, several other non-indole hormones are reputed to be synthesized there, (e.g., arginine vasotocin, oxytocin, arginine vasopressin, an alpha-MSH like peptide, GnRh, TRH, renin, and angiotensin I). The pineal melatonin content fluctuates with a pronounced circadian rhythm (amplitude of about 20-plus orders of magnitude) and it is rapidly inhibited when the animal is exposed to light. Wurtman and Ozaki (1978) suggested that the availability of serotonin may be involved in regulating the synthesis of melatonin in the pineal. Chan and Ebadi (1980) provided evidence that under certain experimental conditions serotonin may inhibit the activity of NAT, a key enzyme in the synthesis of melatonin. Serotonin also exhibits circadian rhythmicity (amplitude of approximately 2-3 orders of magnitude) and this rhythm persists even in blinded weanling rat: Given its key role in the regulation of melatonin synthesis, its high concentration, and that its levels may persist longer than the more rapidly changing melatonin, we felt that serotonin might give a more accurate assessment of the effects of microgravity on pineal function following recovery of the animals from the flight. We also measured 5-hydroxyindole acetic acid (5-HIAA), a major metabolite of serotonin, hoping that we might be able to assess an effect on serotonin metabolism (turnover).

One of the most interesting concomitants to spaceflight and exposure to microgravity has been the disturbing alteration in calcium metabolism and resulting skeletal effects. It was recognized as early as 1895 (cited in Kitay and Altschule, 1954) that the pineal of humans calcified with age. However, little can be found in the literature relating calcification and pineal function. Given the link between exposure to microgravity and pertubation of calcium metabolism and the fact that the pineal is apparently one of the only "soft tissues" to calcify, we examined pineal calcium content following the spaceflight.

MATERIALS AND METHODS

Cosmos 2044 Animal Groups

A) Flight Animals.

Pineals were obtained from 4(#6, #8, #9 and #10) of the 10 male rats (Czechoslovakian - Western origin, Institute of Experimental Endocrinology, Bratislave, Czechoslovakia) that were flown aboard the Soviet Biosatellite Cosmos 2044. The flight launched on September 15, 1989 at 10:30 and landed at 05:45 (Moscow time) on September 29, 1989 for a flight of 13 days and 19+ hours. Except for a slight rise in cabin temperature the last two days, the mission went flawlessly. Starting on August 25, 1989, the rats were fed the flight diet (70% water). The animals were adapted to flight cages prior to the loading of the flight rats on to the vehicle at 15:00 on September 13, 1989. Fourteen gram boluses of food (total 55 g/rat/day) were provided at 2:00, 8:00, 14:00 and 20:00 hrs each day. Food consumption averaged 45 g per day. Rats had free access to water and their consumption was 203 ml per day. The lights were on from 8:00 to 24:00 hr each day. The partial pressure of oxygen was 140-160 mm Hg and 2 mm or less for carbon dioxide. Ambient temperatures varied as follows: Days 1-3, 21-25°C and days 13-14, 26-29°C (rising occasionally to 30°C). After recovery, the rats were sacrificed on September 29, 1989 starting at 11:00 hr.

B) Basal Control Animals.

They were put into flight-type cages and had a flight (paste) diet supplied in a single bolus of 55 g for 14 days before sacrifice on September 15, 1989. Temperature, humidity, and lighting were similar to in-flight conditions.

C) Synchronous Control Animals.

These rats were maintained in flight-type cages on a flight (paste) diet. They were exposed to the launch G forces and vibration and exposed to the same lighting regimen and temperature as flight rats. The feeding schedule was similar to the flight rats (food consumption averaged 50 g/rat/day). They were sacrificed on October 3, 1989, starting at 11:00 hr.

D) Vivarium Control Animals.

These animals were kept in cages of the same size as the flight cages with environmental conditions similar to those in flight. They were fed the same quantity of food per day (55 g), but in only one feeding. They were sacrificed on October 5, 1989, starting at 11:00 hr.

E) Tail Suspended.

These animals were caged individually and were given a single daily bolus of paste diet (55 g/day). They were sacrificed on October 7, 1989, starting at 11:00 hr.

Sample Collection and Initial Tissue Extraction Step

Upon dissection, the pineals were immediately placed in prechilled cryovials (10 x 55 mm), placed into liquid nitrogen for quick-freeze, and shipped to Moscow in a liquid nitrogen biotransporter. The samples were shipped to the U.S.A. and stored until analysis at -70°C. Trunk blood was collected immediately following decapitation into heparinized tubes and centrifuged at 4°C. Plasma (1.5 ml) was rapidly frozen in liquid nitrogen and shipped to the U.S.A. in a biotransporter. In the U.S.A., this volume was thawed and aliquoted (100µl) for distribution to various investigators.

The pineal glands were kept on dry ice, weighed, and individually homogenized in 200 µl of perchloric acid. 100 µl of the crude homogenate was frozen and saved for melatonin and calcium analysis. The remaining aliquots (100 µl) were immediately used for the HPLC analysis of 5-HT and 5-HIAA.

HPLC Analysis of Pineal Serotonin, 5-HIAA, and Plasma 5-HT

Aliquots (100 µl) of the crude pineal homogenate were centrifuged using Centrex brand microfilters (0.45 un pore size, Schleicher and Schuell, Inc. Keene, New Hampshire, U.S.A.). Homovanilly alcohol was added to the homogenates to act as an internal standard at a final concentration of $2x10^{-7}$M. Serotonin and 5-HIAA were analyzed in the filtered homogenates by HPLC using a modification of the method of Medfford and Barchas (1980). The filtered homogenates were injected into a u-Bondapack brand C-18 reverse phase column (100 mmx4.6 mm) of a high pressure liquid chromatograph (Bioanalytical Systems, Inc.). The mobile phase consisting of 0.1 M sodium acetate, 0.1 M citric acid and 25% v/v methanol (pH 4.1) was run through the column at a flow rate of 0.8 ml/min. The various peaks were detected using an electrochemical detector (Bioanalytical Systems, Inc.) mounted with a glassy carbon working electrode and Ag/AgC1 reference electrode set at an oxidation potential of 0.85 V and sensitivity of 10 nAmps/V. Peaks were integrated and analyzed using the Baseline 810 program (Dynamic Solutions).

For analysis of plasma 20µl of 1.0 M perchloric acid was added to 100µl of plasma. The mixture was filtered using micro-filter centrifuge tubes (Centrex brand, see above). The filtrate (10-15µl) was injected onto the HPLC column as above.

Radioimmunoassay of Pineal Melatonin Content

The melatonin content of the pineal homogenates (75 µl aliquots) were determined by radioimmunoassay using "ultraspecific" melatonin antiserum and a procedure provided by Dr. Brown (CIDtech Research, Inc., Ontario, Canada) using ^{3}H-melatonin (Amersham Corp., Arlingon Heights, IL, U.S.A.). The melatonin for standard was obtained from Sigma Chemical Co., St. Louis, MO, U.S.A. (cat, #M5250). The assay performance characteristics in our laboratory were: sensitivity (defined as three standard deviations from the counts for the zero reference standard tube), 5 pg/ml; interassay coefficient of variation, 11.5%; and intraassay coefficient of variation, 6.27%.

Atomic Absorption Analysis of Pineal Calcium Content

Total calcium content of the pineal homogenates was determined by atomic absorption spectrophotometry using an electrothermal atomizer equipped with a carbon rod. Aliquots (5 µl) of the homogenates were filtered with ultra-pure water (7 mohm resistance, Multi-Q Water System, Millipore, Corp., Bedford, MA, U.S.A.). Volume added was 200 or 250 µl to achieve absorbance values in the range 0.1-0.5 absorbance units. Calcium reference standard was obtained from VWR, Inc., San Francisco, CA, U.S.A. (cat. #EM-CX0082-1). Assay sensitivity was approximately 4 pg/µl.

Statistical Analysis

Given the experimental design, the groups were analyzed by one-way analysis of variance (ANOVA). If the ANOVA indicated a between group difference ($p<0.05$), then the data were further analyzed by one or more of the following statistical tests: Duncan's Multiple Range Test, Newman-Keul's Multiple Comparison Test, or Fisher's Least Significant Difference Test. In certain instances, Student's t-test for nonpaired samples was applied. The 95% confidence limit was considered significant in all tests.

RESULTS

The results of this study are summarized in Tables 1-3 and Figures 1-4.

A. Organ Weights

The data (Table 1) indicate that at the time of sacrifice, the flight, synchronous and tail suspended rats were smaller than the vivarium control animals ($P<0.05$). Due to this difference, pineal, testes and adrenal weights were normalized to percent of the body weight for group comparison. Although the average pineal weight of flight animals was not significantly different from that of vivarium or synchronous control animals, the relative pineal weight (weight/100 gm body weight) of the flight animals was significantly greater than that of the vivarium controls ($P<0.05$). On the other hand, both the average pineal weight and relative pineal weight of tail suspended animals were significantly greater than those of vivarium control rats ($P<0.01$) (see also Fig. 1). In addition, the average testes weight as well as the relative testes weight of flight animals were statistically lower than those of the synchronous control rats ($P<0.05$). The testes weight and the relative testes weight of tail suspended rats were statistically lower than those of vivarium and synchronous controls ($P<0.01$). The relative adrenal weight of flight and tail suspended animals were significantly higher than that of vivarium control rats. The adrenal enlargement is consistent with chronic exposure to one or more environmental stressors. It should be noted also, that although there was no significant difference between the plasma corticosterone levels of tail suspended rats and those of vivarium controls at time of sacrifice, the plasma corticosterone levels of flight animals were significantly higher than those of vivarium control rats ($P=0.016$) (data courtesy of Dr.R. Grindeland and M. Vasques, NASA - Ames Research Center).

B. Pineal Gland Analysis

Pineal melatonin content was determined for individual glands and the values normalized and reported as pg/milligram pineal tissue (See Table 2). There were no statistically significant differences among the test groups. The results are also summarized in Figure 2.

Serotonin (5-HT) and 5-HIAA content were also determined for individual glands and the values normalized and reported as ng/milligram pineal tissue (see Table 2). The pineal serotonin (5-HT) content of flight animals expressed as ng/mg tissue) and of tail suspended rats (expressed as ng/gland) were significantly higher than those of synchronous controls ($P<0.05$). In addition, the pineal 5-HIAA content of flight rats was significantly higher than that of synchronous controls ($P<0.01$), while that of tail suspended animals was significantly higher than either vivarium or synchronous controls ($P<0.01$). (See Figure 3 and 4).

Table 2 summarizes the pineal calcium determinations. The pineal calcium content of flight and tail suspended rats (expressed as µg/gld) was significantly higher than that of synchronous controls ($P<0.01$).

C. Plasma Serotonin (5-HT) and Testosterone Concentrations

The data shown in table 3 indicates that plasma testosterone concentration of the flight and tail suspended animals was significantly lower than that of synchronous, vivarium or basal rats.

As shown in table 3, plasma 5-HT concentration of flight animals was significantly lower than that of basal rats ($P<0.01$). In addition, plasma 5-HT concentration of tail suspended rats was significantly higher than that of synchronous controls ($P<0.05$). It should also be noted that plasma 5-HT concentration of synchronous controls was significantly lower than that of basal rats ($O<0.01$).

DISCUSSION

Considerable evidence supports the existence of a pineal humoral factor or factors (most likely melatonin) that can influence the hypothalamic-pituitary gonadal axis in many vertebrate species (Vollrath, 1981) including the rat (Binkley, 1983). If indeed the pineal is a major "link to the environment" (Reiter, 1986) it is, therefore, possible that gonadal function of rats flown in space might be altered via a mechanisms that includes involvement of the pineal.

Several pieces of evidence indicate that gonadal function of the rats aboard Cosmos 2044 spaceflight may have been compromised. The testes weight and relative testes weight of flight animals were statistically lower than those of synchronous control rats (Table 1). Plasma testosterone concentration of flight animals was significantly lower than that of synchronous, vivarium or basal rats (Table 3).

A similar compromise of gonadal function was observed in rats flown aboard Cosmos 1877 (Holley et al., 1989). It is also interesting to note, that tail suspended rats had lower testes weight and lower plasma testosterone concentration than synchronous, vivarium or basal rats (Table 3).

It is known that light has a dramatic and rather immediate inhibitory effect upon rat pineal N-acetylserotonin and pineal melatonin levels (Binkley, 1983). As a result we felt that to assess pineal function we would have to measure parameters that were less labile. Green, et. al. (1977) indicated that potent stressors (e.g. electroconvulsive shocks) could alter serotonin turnover for up to 6 days post exposure. Since serotonin is an important precursor to melatonin we felt that its measurement and relative inertia with respect to relative changes in concentration might be used as an indirect indicator of melatonin synthesis. To do this, however, we felt measurement of 5-HIAA, a major serotonin metabolite, would be necessary as an indication of serotonin turnover.

As suspected, the pineal melatonin levels were very low at time of sacrifice (Table 2 and Figure 1). Given that the rats were sacrificed about 3 hours after lights on, and that the major circadian drop in circulating melatonin is locked to the time of lights on (Binkley, 1983), it is not surprising that the pineal melatonin content was low in all groups. given the limited amount of plasma available to us for the analysis of 5-HT (100µl), and given the low pineal melatonin levels, we did not measure the plasma melatonin concentration.

Table 2 and Figures 3 and 4 summarize the pineal 5-HT and 5-HIAA determinations. Note that exposure to space environment resulted in a significant increase in the pineal content of these substances. A similar observation was noted in animals flown aboard Cosmos 1877 (Holley et al., 1989). The pineal gland profile was not reflected in the blood however (Table 3). It is known that the plasma 5-HT levels may reflect peripheral secretion and may not be an accurate indicator of central serotonergic mechanisms. The results indicate that exposure to the space environment had an effect on the pineal 5-HT content and its turn-over as indicated by concomitant increase in 5-HIAA. This would be consistent with increased melatonin secretion during the spaceflight which may have been involved in the antigonadal activity noted.

It has been suggested that melatonin may be a hormone of "stress" given its increased secretion during conditions such as insulin-induced hypoglycemia (Wurtman and Moskowitz, 1977). Yet the melatonin circadian rhythm is 180 degrees out of phase with the corticosterone circadian rhythm and there is evidence for a direct inhibitory role of the pineal and melatonin on adrenal glucocorticoid synthesis (Ogle and Kitay, 1978). The adrenal hypertrophy in flight animals as evidenced by a significant increase in the relative adrenal weight as compared to vivarium controls and the elevated plasma corticosterone levels of flight animals would indicate a chronic stress response.

It is interesting to note that alterations in pineal 5-HT and 5-HIAA content as well as plasma testosterone levels observed in the present study in tail suspended rats are quite similar to those observed in flight rats.

The pineal of humans and some other mammalian species contain multi-layered hydroxyapatite concentrations called corpora arenacea, or brain sand. Although the degree of radiologically detectable calcification of the human pineal gland appears to increase with age, there is no indication that increased calcification is related to loss of cellular activity. Histological and biochemical studies have shown that the appearance of the pinealocyte cell type, pineal serotonin content and HIOMT enzyme activity do not change with age (Giarman, 1960; Rodin and Overall, 1967; Smith, et al. 1977; Wurtman, 1964). Lukaszyk and Reiter (1975), suggest that the deposition of calcium may be related to polypeptide secretion by the pineal gland, suggest that the deposition of calcium may be related to polypeptide secretion by the pineal gland, and may serve as an index of previous glandular activity rather than degeneration. In the present study, the pineal calcium content of flight and tail suspended rats was significantly higher that that of synchronous controls.

In summary, we conclude that the spaceflight resulted in a stress response as indicated by adrenal hypertrophy, that gonadal function was compromised, and that the pineal may be linked as part of the mechanisms of the responses noted.

REFERENCES

1. Binkley, S.A. Circadian Rhythms of Pineal Function in Rats. Endocrine Reviews. 4: 255-270, 1983.

2. Bosin, T.R. Serotonin Metabolism. In: Serotonin Metabolism in Health and Disease. Ed: W.B. Essman. S.P. Medical and Scientific Books, New York. 181-300, 1978.

3. Brown, G.M. and S.D. Wainright, S.D.(eds.). Advances in the Biosciences Volume 53: The Pineal Gland: Endocrine Aspects. Pergamon Press, Elmsford, New York. 367, 1985

4. Chan, A. and M. Ebadi. The Kinetics of Norepinephrine-Induced Stimulation of Serotonin-N-Acetyltransferase in Bovine Pineal Glands. Neuroendocrinol. 31:244-251, 1980.

5. Giarman, N.J., D.X. Freedman, and L. Picard-Ami. Serotonin Content of the Pineal Glands of Man and Monkeys. Nature (London). 186:480, 1960.

6. Green, A.R., D.U. Heal, and D.G. Grahame-Smith. Further Observations on the Effect of Repeated Electroconvulsive Shocks on the Behavioral Responses of Rats Produced by Increases in the Functional Activity of Brain 5-Hydroxytryptamine and Dopamine. Psychopharmacology. 52:195-200, 1977.

7. Hadley, M.E. Endocrinology (2nd ed.). Prentice Hall, Englewood Cliffs, New Jersey. 549, 1988.

8. Kitay, J.I. and M.D. Atschule. The Pineal Gland: A Review of the Physiologic Literature. Harvard University Press, Cambridge, Mass. 280, 1954.

9. Lukaszyk, A. and R.J. Reiter. Histophysiological Evidence for the Secretion of Polypeptides by the Pineal Gland. Am. J. Anat. 143:451, 1975.

10. Medfford, I.N. and J.D. Barchas. Determination of Tryptophan and Metabolites in Rat Brain and Pineal Tissue by Reverse Phase High Performance Liquid Chromatography with Electrochemical Detection. J. Chrom. 181:187-193, 1980.

11. O'Brien, P.J. and D.C. Klein. (eds.) Pineal and Retinal Relationships. Academic Press, Florida. 442, 1986.

12. Ogle, T.F. and J.I. Kitay. *In Vitro* Effects of Melatonin and Serotonin on Adrenal Steroidogenesis. Proc. Soc. Exptl. Biol. Med. 157:103-105, 1978.

13. Preslock, J.P. The Pineal Gland: Basic Implications and Clinical Correlations. Endocrine Reviews. 5:282-308, 1984.

14. Quay, W.B. Circadian Rhythms in Rat Pineal Serotonin and Its Modification by Estrous Cycle and Photoperiods. Gen. Comp. Endocrinol. 3:473-47, 1963.

15. Reiter, R.J. (ed.). Comprehensive Endocrinology: The Pineal Gland. Raven Press, New York. 1984.

16. Reiter, R.J. (ed.). The Pineal Gland Volume I: Anatomy and Biochemistry. CRC Press, Boca Raton, Florida. 320, 1981.

17. Reiter, R.J. (ed.). The Pineal Gland Volume II: Reproductive Effects. CRC Press, Boca Raton, Florida. 227, 1981.

18. Reiter, R.J. (ed.). The Pineal Gland, Volume III: Extra-Reproductive Effects. CRC Press, Boca Raton, Florida. 240, 1982.

19. Reiter, R.J. The Pineal Gland: An Important Link to the Environment. NIPS. 1:202-205, 1986.

20. Rodin, A.E. and J. Overall. Statistical Relationships of Weight of the Human Pineal to Age and Malignancy. Cancer. 20:1203, 1967.

21. Smith, J.A., D. Padwick, T. Mee, K.P. Minneman, and E.D. Bird. Synchronous Nyctohemeral Rhythms in Human Blood Melatonin and in Human Post-Mortem Pineal Enzyme. Clin. Endocrinol. 6:219, 1977.

22. Vollrath, L. The Pineal Organ. Springer-Verlag, New York. 665, 1981.

23. Wurtman, R.J., J. Axelrod, and J.D. Barchas. Age and Enzyme Activity in the Human Pineal. J. Clin. Endocrinol. 24:299, 1964.

24. Wurtman, R.J. and M.A. Moskowitz. The Pineal Organ. New Engl. J. Med. 296:1329-1333, 1383-1386, 1977.

25. Wurtman, R.J. and Y. Ozaki. Physiological Control of Melatonin Synthesis and Secretion: Mechanisms Generating Rhythms in Melatonin, Methoxytryptophol and Arginine Vasotocin Levels and Effects on the Pineal of Endogenous Catecholamines, the Estrous Cycle and Environmental Lighting. J. of Neural. Transmission. 13:59-70, 1978.

TABLE 1

BODY WEIGHT, PINEAL WEIGHT, TESTES WEIGHT, AND ADRENAL WEIGHT OF RATS FLOWN ABOARD COSMOS 2044

Group-Subject #	Body Wt. (g)	Pineal Wt. (mg)	Pineal Wt. (% B.W.)	Testes Wt. (% B.W.)	Testes Wt. (% B.W.)	Adrenal Wt.(mg)	Adrenal Wt. (% B.W.)
F-6	332	1.16	0.349	0.96	0.289	42.0	12.65
F-7	334	-	-	2.60	0.778	45.0	13.47
F-8	342	1.34	0.392	1.65	0.482	41.5	12.13
F-9	338	1.29	0.382	2.30	0.385	47.0	13.91
F-10	342	1.50	0.439	2.40	0.701	43.5	12.72
Mean	337.6[a]	1.32	0.391[a]	1.98[c]	0.527[c]	43.8[c]	12.98[b]
S.E.M.	2.0	0.07	0.019	0.31	0.093	1.0	0.32
V-6	360	1.2	0.33	1.84	0.511	42.5	11.81
V-7	365	-	-	2.80	0.767	39.5	10.82
V-8	360	-	-	2.35	0.653	43.0	11.94
V-9	360	-	-	1.60	0.444	41.5	11.53
V-10	370	1.2	0.324	3.10	0.838	44.5	12.02
Mean	363	1.2	0.327	2.34	0.643	42.2	11.62
S.E.M.	2.0	0.0	0.002	0.28	0.074	0.8	0.22
S-6	355	1.22	0.343	2.30	0.648	45.0	12.68
S-7	360	1.70	0.472	2.95	0.819	50.5	14.03
S-8	340	1.38	0.410	2.65	0.779	50.0	14.71
S-9	320	1.51	0.470	2.76	0.863	57.0	17.81
S-10	340	1.16	0.340	3.05	0.897	46.0	13.53
Mean	343[a]	1.39	0.407	2.74	0.801	49.7	14.55
S.E.M.	7.0	0.09	0.029	0.13	0.043	2.1	0.88
T-6	351	1.46	0.416	0.98	0.279	55.5	15.81
T-6	365	-	-	1.02	0.279	48.5	13.29
T-6	313	1.56	0.498	0.72	0.230	47.5	15.18
T-6	322	1.46	0.453	1.08	0.335	50.0	15.53
T-6	345	1.65	0.478	1.20	0.348	53.0	15.36
Mean	339.2[a]	1.53[b]	0.461[b]	1.00[b,d]	0.294[b,d]	50.9[b]	15.03[b]
S.E.M.	9.5	0.05	0.017	0.08	0.021	1.5	0.45

F = Flight Group
S = Synchronous Control Group
V = Vivarium Control Group
Wt. = Weight
B.W.= Body Weight

a = Versus V, $P < 0.05$
b = Versus V, $P < 0.01$
c = Versus S, $P < 0.05$
d = Versus S, $P < 0.01$

TABLE 2

PINEAL CONTENT OF RATS FLOWN ABOARD COSMOS 2044: MELATONIN (Mel), SSEROTONIN (5-HT), 5-HYDROXINDOLEACETIC ACID (5-HIAA), CALCIUM (Ca)

Group Subject #	Mel (Pg / gl)	Mel (Pg / mgt)	5-HT (ng / gl)	5-HT (ng / mgt)	5-HIAA (ng / gl)	5-HIAA (ng / mgt)	Ca (µg / gl)	Ca (µg / mgt)
F-6	192.9	166.3	39.26	33.85	4.83	4.16	-	-
F-8	142.8	106.5	34.66	25.87	16.09	12.01	5.07	3.78
F-9	170.3	132.1	46.60	36.12	15.06	11.68	5.06	3.29
F-10	227.1	151.4	60.58	40.38	4.45	2.97	-	-
Mean	183.3	138.6	45.28	34.06[a]	10.11[b]	7.70	5.07[b]	3.54[a]
S.E.M.	17.8	18.7	5.66	3.05	3.17	2.40	0.005	0.25
V-6	130.2	108.5	32.56	27.14	3.33	2.77	4.83	4.02
V-10	170.3	141.9	26.37	21.98	3.55	2.96	4.08	4.00
Mean	150.3	135.7	29.47	24.56	3.44	2.86	4.46	4.01
S.E.M.	14.2	6.25	3.09	2.58	0.11	0.09	0.38	0.01
S-6	120.2	98.5	33.44	27.41	2.81	2.31	2.85	2.33
S-7	177.9	104.6	29.48	17.34	4.10	2.41	2.02	1.18
S-8	243.0	176.1	28.56	20.70	3.31	2.40	-	-
S-9	220.4	145.9	32.35	21.42	3.38	2.24	3.54	2.34
S-10	227.9	196.5	37.68	32.48	2.20	1.90	2.76	2.37
Mean	197.9	144.32	32.30	23.87	3.16	2.25	2.79	2.06
S.E.M.	22.2	19.38	1.61	2.70	0.32	0.09	0.31	0.29
T-6	205.4	140.7	53.09	36.36	18.69	12.80	-	-
T-8	177.7	75.5	41.23	26.43	16.23	10.40	4.35	2.78
T-9	185.4	126.9	40.78	27.93	7.64	5.23	4.15	2.84
T-10	250.0	151.5	35.06	21.25	13.56	8.22	4.36	2.64
Mean	189.6	123.6	42.54[a]	27.9	14.03[b, c]	9.16[b, c]	4.29[b]	2.75[c]
S.E.M.	27.5	16.8	3.79	3.13	2.37	1.61	0.07	0.06

F = Flight Group
S = Synchronous Control Group
T = Tail Suspended Group
Mel = Melatonin
5-HT = Serotonin
5-HIAA = 5-Hydroxyindoleacetic Acid
Ca = Calcium

1 gl = 1 Whole Pineal Gland
1 mgt = 1 Milligram Pineal Tissue

a = Versus S, $P < 0.05$
b = Versus S, $P < 0.01$
c = Versus V, $p < 0.01$

TABLE 3

CONCENTRATION OF PLASMA SEROTONIN (5-HT) AND TESTOSTERONE OF RATS FLOWN ABOARD COSMOS 2044

Group - Subject #	5-HT (ng / ml)	Testosterone* (ng / ml)
F-6	59.92	0.41
F-7	66.24	0.28
F-8	68.96	0.27
F-9	161.16	0.09
F-10	115.28	0.32
Mean	94.31[a]	0.27[c, d, e]
S.E.M.	19.39	0.05
V-6	117.76	4.88
V-7	92.00	1.93
V-8	71.44	4.90
V-9	86.16	3.80
V-10	96.48	1.98
Mean	92.77	3.50
S.E.M.	7.54	0.66
S-6	88.08	1.44
S-7	75.84	2.64
S-8	69.68	1.70
S-9	67.20	0.79
S-10	73.12	3.00
Mean	74.78[a]	1.91
S.E.M.	3.63	0.40
T-6	89.60	0.88
T-7	124.44	1.40
T-8	114.32	0.22
T-9	259.04	0.03
T-10	274.16	0.04
Mean	172.31[b]	0.51[b, c, e]
S.E.M.	38.98	0.27
B-6	145.52	1.28
B-7	187.84	4.96
B-8	222.16	0.70
B-9	288.88	2.46
B-10	181.20	5.68
Mean	205.12	3.02
S.E.M.	24.22	0.99

F = Flight
S = Synchronous Control Group
V = Vivarium Control Group
B = Basal Control Group
T = Tail Suspended Group

a = Versus B, $P < 0.01$
b = Versus S, $P < 0.05$
c = Versus B, $P < 0.05$
d = Versus S, $P < 0.01$
e = Versus V, $P < 0.01$

* = Determined by RIA; data provided by Dr. R. Grindeland and M. Vasques (NASA, Ames).

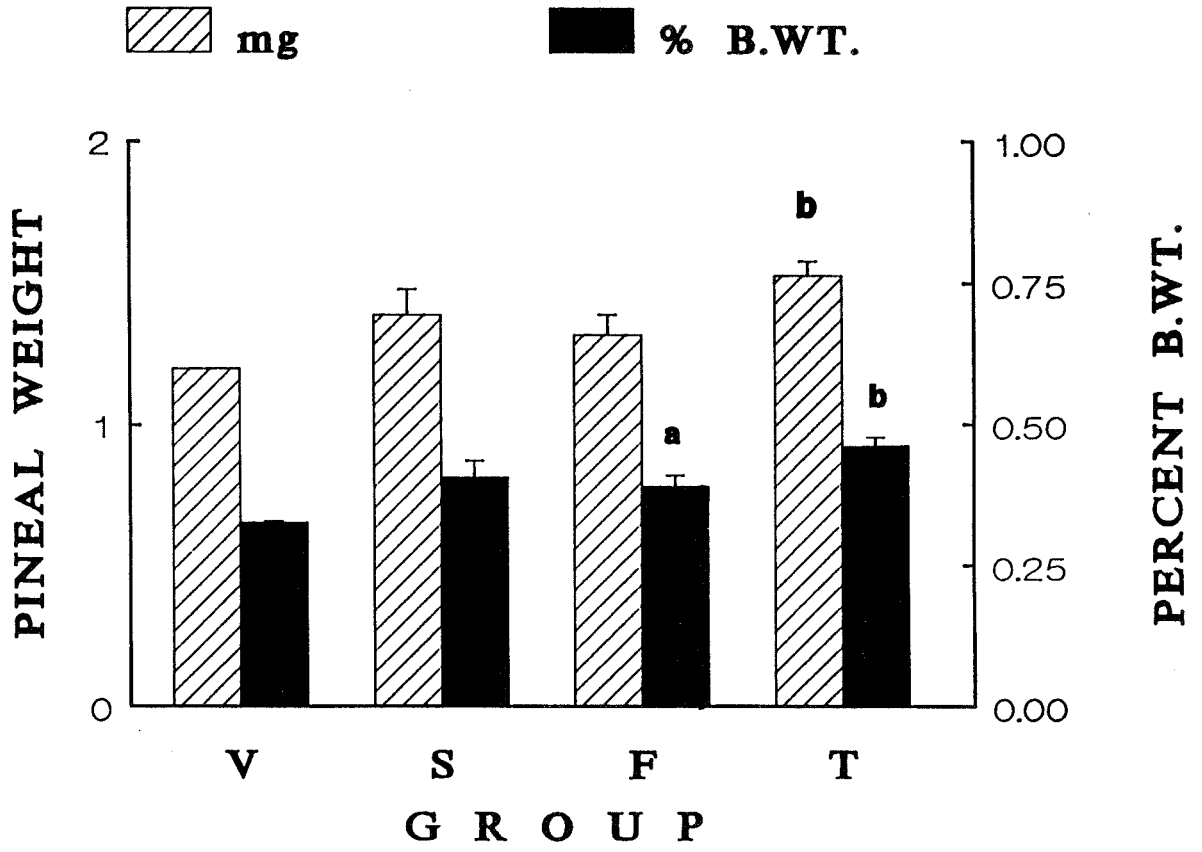

Figure 1. Pineal weight and pineal relative weight (percent body weight = mg/100 g body weight) of vivarium control (V), synchronous control (S), flight animals aboard Cosmos 2044 (F) and tail suspended rats (T). Values are means ± S.E.M. (a = versus V, P<0.05; b = versus V, P <0.01).

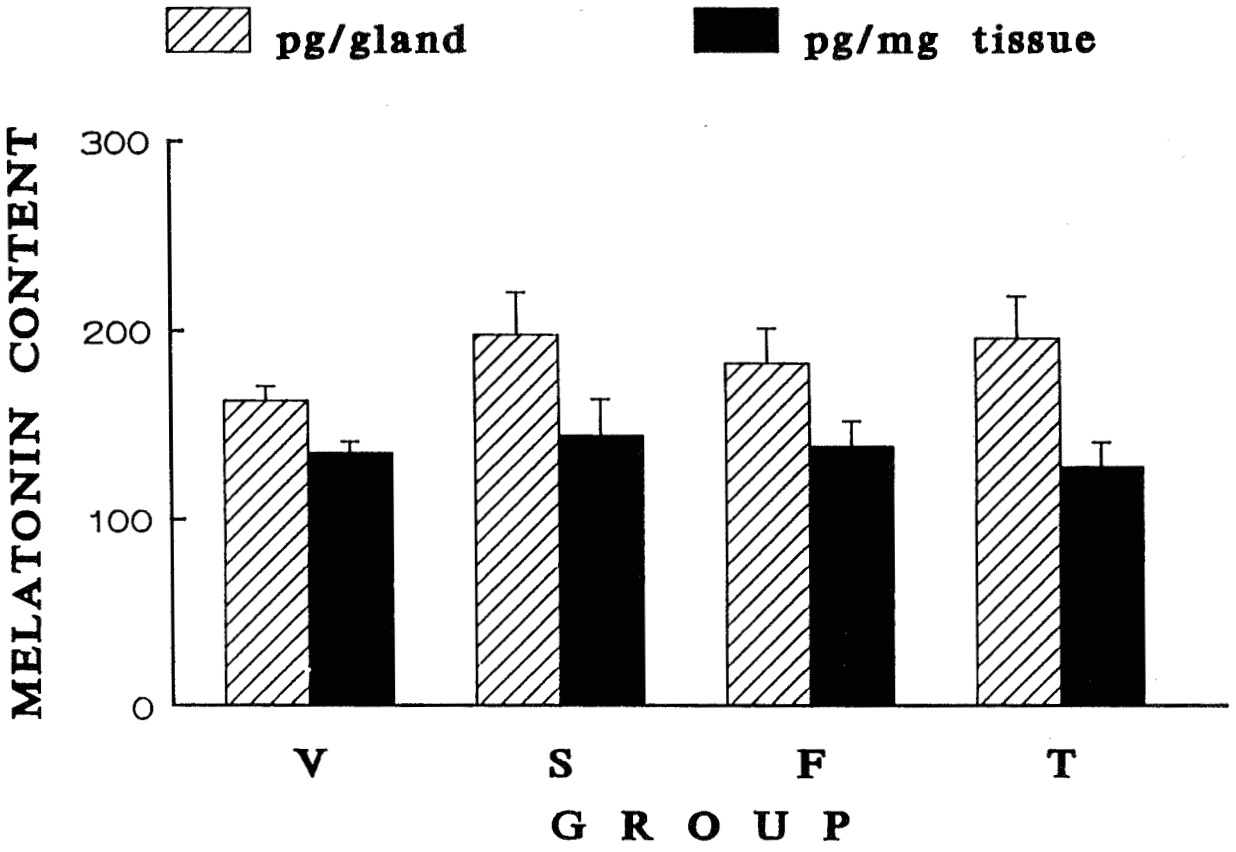

Figure 2. Pineal melatonin expressed as pg/gland and pg/mg tissue in vivarium control (V), synchronous control (S), flight animals aboard Cosmos 2044 (F) and tail suspended rats (T), values are means ± S.E.M.

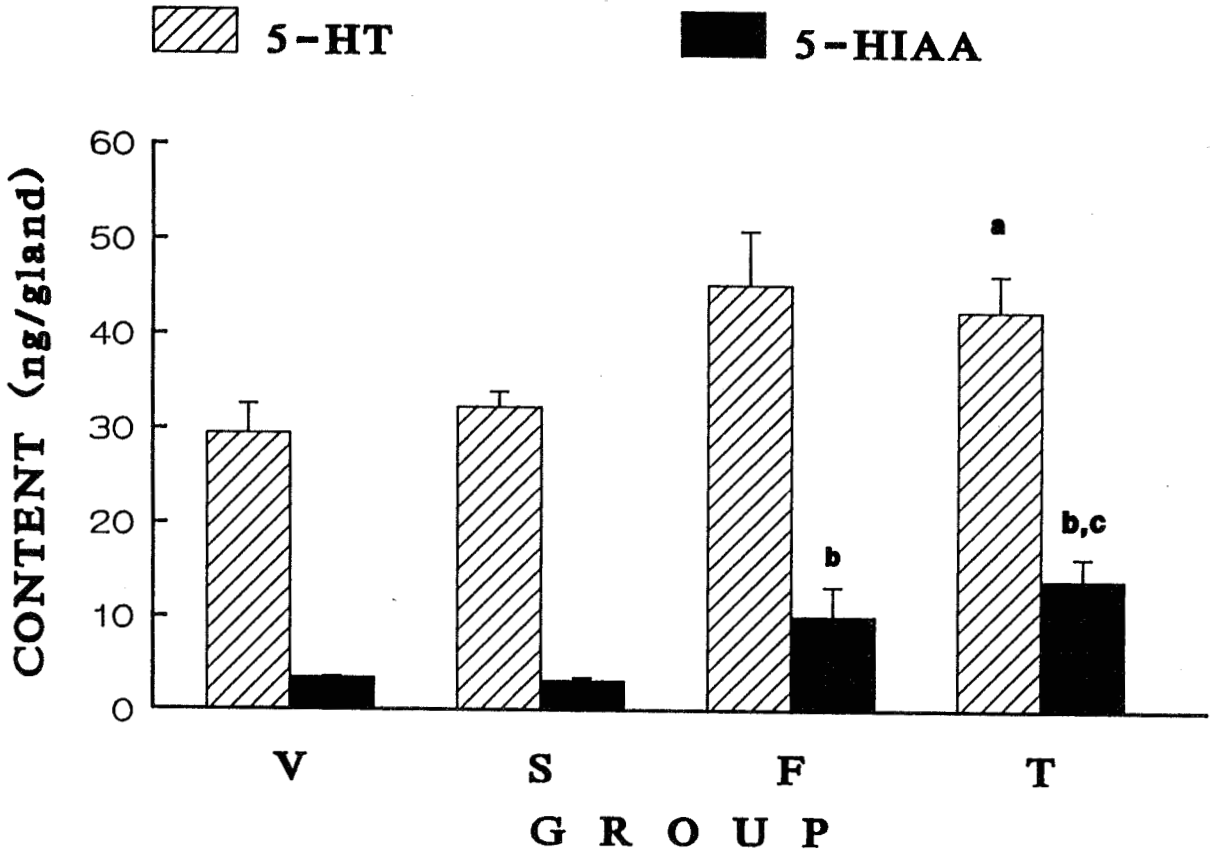

Figure 3. Pineal serotonin (5-HT) and 5-hydroxyindoleacetic acid (5-HIAA) expressed as ng/gland in vivarium control (V), synchronous control (S), flight animals aboard Cosmos 2044 (F) and tail suspended rats (T). Values are means ± S.E.M. (a = versus S, P<0.05; b = versus S, P<0.01; c = versus V, P<0.01).

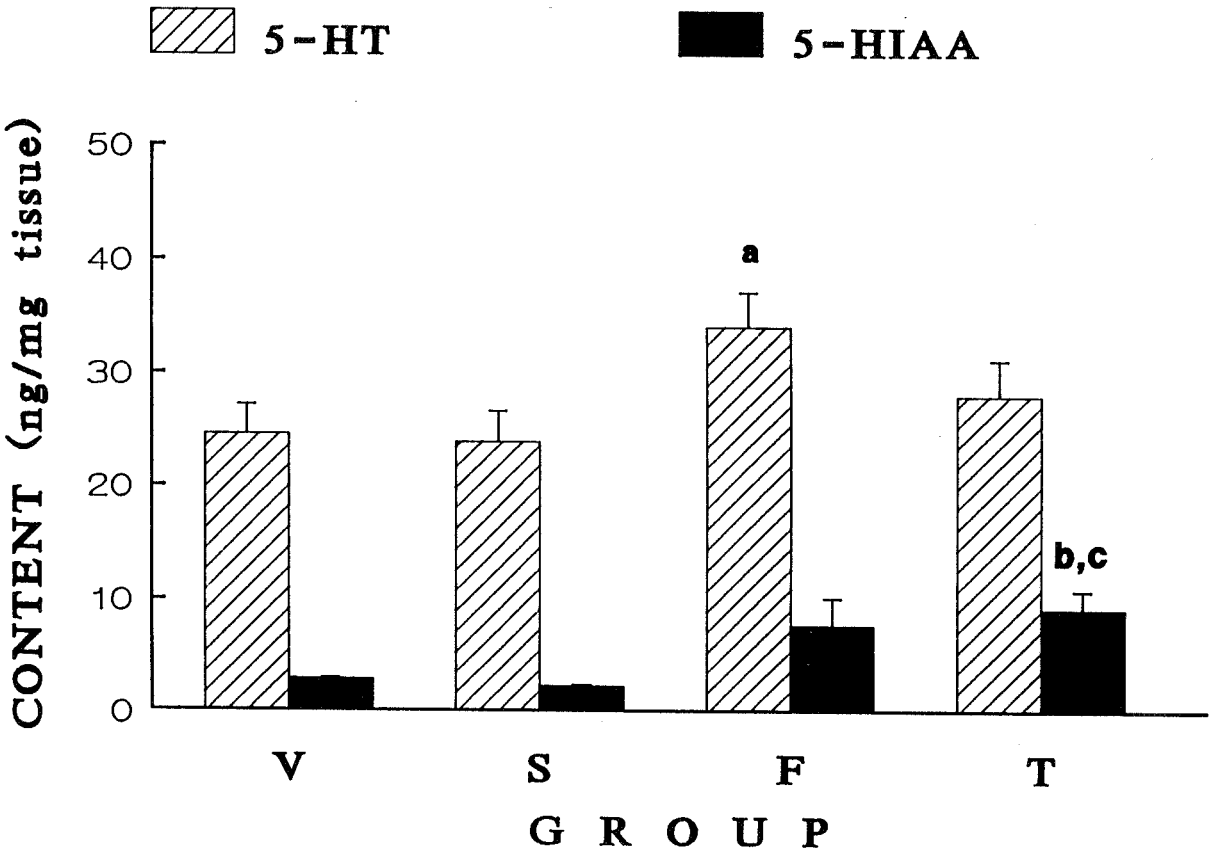

Figure 4. Pineal serotonin (5-HT) and 5-hydroxyindoleacetic acid (5-HIAA) expressed as ng/mg tissue in vivarium control V), synchronous control (S), flight animals aboard Cosmos 2044 (F) and tail suspended rats (T). Values are means ± S.E.M. (a = versus S, P<0.05; b = versus S, P<0.01; C = versus V, P<0.01).

Page intentionally left blank

56-51

51351

EXPERIMENT K-7-20

PITUITARY OXYTOCIN AND VASOPRESSIN CONTENT OF RATS FLOWN ON COSMOS 2044

Principal Investigator:

L. Keil
NASA Ames Research Center
Moffett Field, CA

Co-Investigators:

J. Evans
R. Grindeland
NASA Ames Research Center
Moffett Field, CA

I. Krasnov
Institute of Medical-Biological Problems
Moscow, USSR

Page intentionally left blank

EXPERIMENT K-7-20

PITUITARY OXYTOCIN AND VASOPRESSIN CONTENT OF RATS FLOWN ON COSMOS 2044

L. Keil, J. Evans, R. Grindeland, and I. Krasnov

SUMMARY

Pituitary levels of oxytocin (OT) and vasopressin (VP) were measured in rats exposed to 14 days of spaceflight (FLT) as well as in ground-based controls, one group synchronously maintained in flight-type cages with similar feeding schedules (SYN), one group in vivarium cages (VIV) and a group of tail suspended (SUS) animals. Flight rats had significantly less ($p < 0.05$) pituitary OT and VP (4.48 ± 0.31 and 7.48 ± 0.53 μg hormone / mg protein, n=5) than either the SYN ($6.66 \pm$ 0..59 and 10.98 ± 1.00, n=5), VIV (6.14 ± 0.40 and $10.98 \pm 0..81$, n=5) or SUS (5.73 ± 0.24, n=4) control groups, respectively. The reduced levels of pituitary OT and VP are similar to measurements made on rats from the previous 12.5 day Cosmos 1887 mission and appear to be a direct result of exposure to spaceflight.

INTRODUCTION

Disturbances in fluid and electrolyte balance have been noted in humans exposed to spaceflight (1). This was shown by a loss of plasma volume and increased excretion of sodium and potassium during flight (1). Upon return to Earth these imbalances are quickly corrected with rehydration and increased renin-angiotensin-aldosterone activity (2). Similar postflight fluid-electrolyte and hormone responses have been observed in rats exposed to microgravity (3). Microscopic examination of the hypothalamus and posterior pituitary gland of rats exposed to spaceflight shows changes indicative of increased activity, e.g., increased hormone synthesis and secretion (4). The purpose of this investigation was to measure levels of pituitary oxytocin (OT) and vasopressin (VP) as possible indicators of changes in fluid-electrolyte balance during spaceflight.

METHODS

Animals

Male, specific pathogen-free Czechoslovakian-Wister rats were divided into four groups of 10 animals each. Except for the SUS rats each group was housed in a single cage equipped with 10 paste-food dispensers and 10 water lixits. All animals were fed a special paste diet before flight (5). The flight group (FLT) was selected and transported, with a second group that was designated as the synchronous control group (SYN), to the launch site. The vivarium controls (VIV) and SUS rats remained at the Institute in Moscow. The SYN animals were exposed to centrifugation and vibration to simulate the increased gravity associated with launch. The SYN animals were fed on the same schedule as the FLT rats. The VIV and SUS rats received an equivalent amount of paste diet each day, but it was dispensed in a single bolus at a fixed time each day. Water was available to all animals ad lib except during reentry and recovery (5). Five rats from each group were available for posterior pituitary measurements of OT and VP. Further details concerning the care and treatment of the flight and control animals during flight and recovery are presented elsewhere in this issue (5).

Collection of Pituitaries

The animals were sacrificed at various times after recovery (5). Immediately after decapitation, the skull was opened, and the brain was carefully removed to expose the anterior and posterior pituitary. The posterior pituitary, along with the intermediate lobe, was teased free from the anterior lobe, placed on a small square of aluminum foil, and frozen by immersion in liquid nitrogen. The foil containing the pituitary was placed in a small cryrovial and reimmersed in liquid nitrogen. The vials were transported and maintained on dry ice until they were thawed immediately prior to homogenization. The pituitaries were thawed individually and homogenized in 1 ml of 0.1 N HCl. An aliquot of the homogenate was diluted 1:200,000 in 0.05 m phosphate assay buffer for radioimmunoassay of OT and VP (6,7). To eliminate interassay variability, aliquots from all four groups (FLT, SYN, VIV, and SUS) were measured within the same OT or VP radioimmunoassay. After the hormone levels were determined, protein concentrations were measured in aliquots from each homogenate (Pierce BCA. protein assay, Pierce Chemical Co.) with bovine serum albumin as the standard. Hormone concentrations were then calculated as a function of total protein for each posterior pituitary homogenate. Statistical comparisons were made among the various groups by one-way ANOVA and the Newman-Keul range statistic as well as the nonparametric Mann-Whitney U test.

RESULTS

Pituitary hormone content was expressed on the basis of protein content (μg hormone / mg protein) in posterior pituitary homogenate. Both neural lobe hormone levels were significantly reduced in the FLT animals when compared to either set of controls by either parametric or nonparametric tests. Oxytocin was 4.48 ± 0.31 ($p < 0.05$) in the FLT group compared to 6.66 ± 0.59 in the SYN rats, 6.14 ± 0.40 in the VIV and 5.73 ± 0.22 in the SUS controls (Fig. 1). Pituitary VP in the FLT animals (7.48 ± 0.53 μg/mg protein) was lower ($p < 0.05$) than in either of the control groups, SYN (10.98 ± 1.00); VIV (10.98 ± 0.81); and in SUS (9.40 ± 0.24, Fig. 2).

DISCUSSION

Postflight investigations of both humans and animals have indicated that fluid-electrolyte balance is altered by exposure to microgravity (1,3). Postflight reductions in sodium excretion, and urine volume, and increases in plasma renin activity are indications that changes in fluid-electrolyte homeostasis occurred during flight (2). In humans, the headward fluid shift observed during flight is thought to be the stimulus for the plasma volume reduction and other adjustments in fluid-electrolyte metabolism. Rats and other horizontal animals may not experience this headward fluid shift, and if such a shift did take place, it may be proportionally less than that of humans because of the difference in hydrostatic columns. However, results of rat postflight experiments are similar to those of humans, e.g., sodium and water excretion was reduced, and water consumption increased (3). When flight rats were challenged with a water-load on the first day of recovery, sodium and water excretion by these were significantly elevated compared to similarly treated synchronous controls (3). This response indicates possible changes had taken place during flight in either the hormonal or renal regulation fluid/electrolyte balance. These postflight results demonstrate that changes in fluid-electrolyte balance have occurred during flight. Whether the same physiological mechanisms are responsible for these changes in rodents remains to be determined.

VP content of the FLT rats was 32%, 32% and 20% lower than either SYN, VIV and SUS control groups, respectively. This reduced content indicates that the FLT animals may have been dehydrated during flight, or, alternatively, pituitary stores of the hormones may have been reduced due to decreased synthetic activity of the magnocellular neurons. Synchronous controls had access to water on the same schedule as the FLT animals; however, the pituitary OT and VP content of the these rats was significantly higher than that of the FLT group. Mean body weight of the FLT

group was not significantly less than the other groups except for the VIV. This indicates that the FLT animals had consumed adequate amounts of the paste diet and water, but were unable to maintain comparable levels of the pituitary hormones. However, increased hemotocrits in the FLT group also raises the possibility that blood volume was reduced which would also be stimulus for VP secretion (14).

Pituitary OT was also significantly lower in FLT rats (Figs. 1). Dehydration reduces pituitary OT as well as VP (8). In addition, data from recent papers indicate that OT secretion, at least in rats, is increased by stress (9). Oxytocin facilitates the action of Corticotrophin Releasing Factor (CRF) on the anterior pituitary to stimulate the release of Adrenocorticotrophic hormone (ACTH) (10). Gibbs (9) also points out that OT may be released in response to "neurogenic" stress, whereas VP, which also has been shown to increase CRF activity, is released in response to "physical" stress. Perhaps some of the decrease in pituitary OT may be attributed to the chronic neurogenic stress the animals experienced during flight in their effort to adapt to microgravity. This OT response to stress may be unique to rats since a similar response has not been observed in humans (11).

In rats, administration of nausea-producing agents such as lithium chloride and apomorphine results in learned taste aversion as well as a relatively specific release of OT rather than VP (12). Increased plasma levels of the gut hormone, cholecystokinin (CCK), are also associated with taste aversion and nausea (12). This hormone appears to be a specific stimulus for the secretion of OT in rats (13). Interestingly, lesions of the area postrema, a circumventricular organ associated with nausea and the emetic response, significantly reduced OT secretion in response to CCK injections (13). If the rats experienced motion sickness during flight, it is possible that this condition, along with stress and dehydration, would contribute to increased OT secretion and depletion of pituitary OT stores.

In summary, FLT rats showed a significant reduction in both pituitary OT and VP. This reduction cannot be totally attributed to a decrease in food and water intake and may be one of the physiological changes that result from exposure to a microgravity environment .

REFERENCES

1. Leach, C. S. and P.C. Rambaut. Biochemical Responses of the Skylab Crewmen: An Overview. In: Biomedical Results From Skylab. Washington, D.C. NASA SP-377. 204-216, 1977.

2. Leach, C. S.and P.C. Rambaut. Endocrine Response in Long Duration Manned Spaceflight. Acta Astronautiac. 2:115-127, 1975.

3. Gazenko, O. G., Y.V. Natochin, Y.A. Ilyin, N.A. Ilyushko, Y.I. Kondratiev, Y.A. Lavrova, and Y.I. Shakhmatova. Fluid-Electrolyte Metabolism and Renal Function of the White Rats in Experiments Aboard Cosmos Biosatellites. Aviat. Space Environ. Med. 55(8):685-691, 1984.

4. Savina, E. A., A.S. Pankova, E.I. Alekseyev, and V.K. Podymov. Morphological Manifestations of Functional Changes in the Hypothalamic-Pituitary Neurosecretory System and Kidneys of Rats after Spaceflight. Aviat. Space Eviron. Med. 47(8):853-855, 1976.

5. Grindeland, R. E., I.A. Popova, M. Vasques, and Arnaud. Cosmos 1887 Mission Overview; Effects of Microgravity on Rat Body and Adrenal Weights and Plasma Constituents. FASEB J. 4:105-109, 1989.

6. Keil, L. C., L.M. Rosella-Dampman, S. Emmert, O. Chee, and J.Y. Summy-Long. Enkephalin Inhibition of Angiotensin-Stimulated Release of Oxytocin and Vasopressin. Brain Res. 297:329-336, 1984.

7. Keil, L. C. and W.B. Severs. Reduction in Plasma Vasopressin Levels of Dehydrated Rats Following Acute Stress. Endocrinology. 100:30-38, 1977.

8. Summy-Long, J. Y., D.S. Miller, L.M. Rosella-Dampman, R.D. Hartman, and S.E. Emmert. A Functional Role for Opioid Peptides in the Differential Secretion of Vasopressin and Oxytocin. Brain Res. 309:362-366, 1984.

9. Gibbs, D. M. Vasopressin and Oxytocin: Hypothalamic Modulators of the Stress Response: A Review. Psychoneuroendocrinology. 11:131-140, 1986a.

10. Gibbs, D. M. Stress-Specific Modulation of ACTH Secretion by Oxytocin. Neuroendocrinology. 42:456-458, 1986b.

11. Legros, J. J., P. Chiodera, V. Geenen, and R. von Frenckell. Confirmation of the Inhibitory Influence of Exogenous Oxytocin on Cortisol and ACTH in Man: Evidence of Reproductivity. Acta Endocrinologica (Copenh). 114:345-349, 1987.

12. Verbalis, J. G., M.J. McCann, C.H. McHale, and E.M. Stricker. Oxytocin Secretion in Response to Cholecystokinin and Food: Differentiation of Nausea from Satiety. Science. 232:1417-1419, 1986.

13. Carter, D. A. and S.L. Lightman. A Role for the Area Postrema in Mediating Cholecystokinin-Stimulated Oxytocin Secretion. Brain Res. 437:327-330, 1987.

14. Grindeland, R.E., M.F. Vasques, R.W. Ballard, and J.P. Connolly. Cosmos 2044 Mission Overview. J. Appl. Physiol. (this issue), 1990.

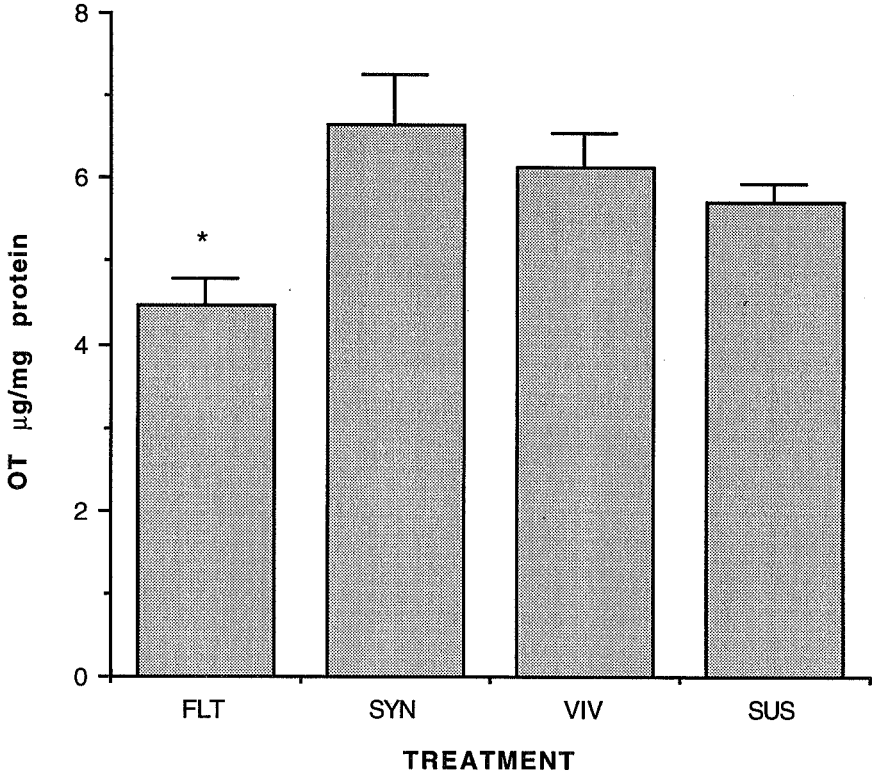

*Figure 1. Pituitary oxytocin (OT) content expressed as µg OT per mg posterior pituitary protein. * $p < 0.05$ for comparison of Flight (FLT) to either Synchronous (SYN), Vivarium (VIV) or Suspended (SUS) control by both the ANOVA or Mann-Whitney U tests. Values are means ± S.E.*

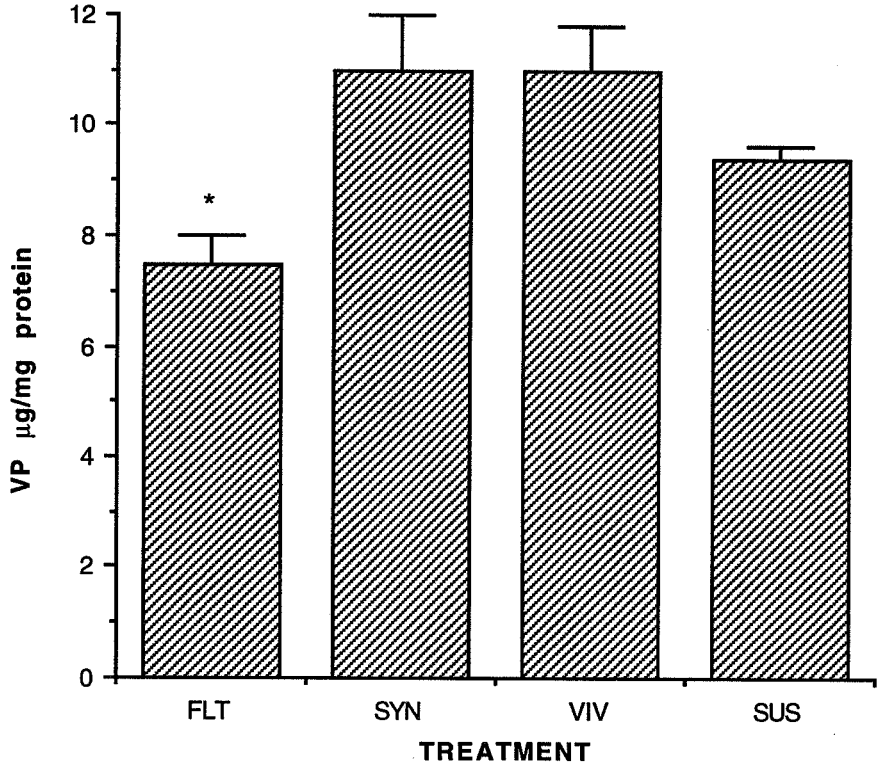

Figure 2. Pituitary vasopressin (VP) content expressed at µg VP per mg of posterior pituitary protein.

57-51
51352

EXPERIMENT K-7-21

EFFECT OF MICROGRAVITY ON I. METABOLIC ENZYMES OF TYPE 1 AND TYPE 2 MUSCLE FIBERS; AND ON II. METABOLIC ENZYMES, NEUROTRANSMITTER AMINO ACIDS, AND NEUROTRANSMITTER ASSOCIATED ENZYMES IN SELECTED REGIONS OF THE CENTRAL NERVOUS SYSTEM

PART I: METABOLIC ENZYMES OF INDIVIDUAL MUSCLE FIBERS

PART II: THE DISTRIBUTION OF SELECTED ENZYMES AND AMINO ACIDS IN THE HIPPOCAMPAL FORMATION

Principal Investigator:

O.H. Lowry
Washington University School of Medicine
St. Louis, Missouri

Co-Investigators:

E.I. Ilyina-Kakueva
I.B. Krasnov
Institute of Biomedical Problems
Moscow, USSR

J.G. Carter
M.M-Y. Chi
R. Choksi
J.K. Manchester
D.B. McDougal
P.M. Nemeth
M.E. Pusateri
Washington University School of Medicine
St. Louis, Missouri

Page intentionally left blank

EXPERIMENT K-7-21

PART I: METABOLIC ENZYMES OF INDIVIDUAL MUSCLE FIBERS

O.H. Lowry, I. Krasnov, E.I. Ilyina-Kakueva, P.M. Nemeth, D.B. McDougal, Jr., R. Choksi, J.G. Carter, M.M.Y. Chi, J.K. Manchester and M.E. Pusateri

INTRODUCTION

Individual fibers of any given muscle vary widely in enzyme composition, a fact obscured when enzyme levels of whole muscle are measured. Therefore, the purpose of this part of the study was to assess the effects of microgravity and hind limb suspension on the enzyme patterns within a slow twitch muscle (soleus) and a fast twitch muscle (tibialis anterior).

METHODS

The samples for assay were prepared in two different ways. In the first case, a 3-5 mg piece of each muscle was freeze-dried at -35°C. Portions of individual fibers, 2-3 mm long, were dissected free, weighed, the length measured, and then stored separately under vacuum at -70°C. Most of the enzymes from a given fiber were measured in a single extract prepared from a dry sample weighing about 0.5 μg (0.5 to 1 mm long). This was added to 5 μl of special detergent- containing medium known to preserve without loss all but a few of the enzymes of interest during storage at -70°C. After initial incubation for 2 hours at room temperature (to permit extraction and even distribution of the enzymes), the samples were transferred to a -70°C freezer. Since each assay required only 0.1 to 0.2 μl of extract (equivalent to 10 to 20 ng of dry fiber), the single 5 μl extract was sufficient for duplicate assays of a large number of enzymes.

In a few special cases, assays were performed on single 10 to 20 ng samples added directly to the appropriate specific reagent.

The alternate method used to prepare samples for assay was to cut frozen cross sections at -20°C from a piece of the original frozen muscle. Thinner sections (16 μm) were stained for myosin ATPase to type the individual fibers. Alternate thicker slices (32 μm) were freeze-dried at -35°C and samples were dissected from individual fibers identified as to type by the adjacent stained sections.

These studies were made on 95 soleus fibers and about 300 tibialis anterior (TA) fibers. Each of the soleus fibers was analyzed for 4 or 5 different enzymes, and 139 TA fibers were assayed for 3 to 5 different enzymes. Other single TA fibers were assayed for an additional 3 enzymes. Altogether, over 2200 individual enzyme measurements were made.

The enzymes were selected for assay in view of the results obtained in the previous Cosmos flight (1887), and the known metabolic enzyme characteristics of fast and slow muscle fibers. For example, TA fibers were first assayed for malate dehydrogenase, hexokinase, and thiolase, all of which had increased markedly in the TA flight muscles; in addition, they are highly variable among TA fibers. Similarly, soleus fibers were initially assayed for hexokinase because it was markedly increased in the 1987 Cosmos flight fibers, and for pyruvate kinase because it was consistently variable among control soleus fibers, and had increased in the fibers of at least one soleus flight muscle of the earlier Cosmos experiment.

Fibers were obtained from synchronous rats 6 and 7 (S6, S7), flight rats 6 and 7 (F6, F7) and tail suspension rats 6 and 7 (T6, T7).

RESULTS

Soleus Muscle

Average Values

Table 1 gives average values for size and activities of five enzymes in 15 or 16 fibers from soleus muscles of rats S6 and S7, F6 and F7, and T6 and T7.

Size

Average fiber size was much smaller for both flight and tail suspension muscles ($P < 0.01$) than for either S6 or S7. The average dry weight loss was 38% for T6 and T7 and 36% for F6 and F7.

The dry weights (μg per mm) are based on the assumption that all the muscles were frozen at the same fraction of their resting lengths, and are subject to error if this were not the case. With this proviso it is interesting to compare these dry weight losses with the losses in wet weight of the whole and soleus muscles: 20% and 3% respectively for F6 and F7, and 27% and 29% respectively for T6 and T7. Even if F7 is ignored because the wet weight value is so far out of line, it seems clear that the fibers lost relatively more dry weight than the loss in total mass. Thus, there must have been an increase in relative H_2O content, either in the fibers themselves or the extracellular space or both.

Soleus Enzymes That are Usually Higher in Fast-Twitch than Slow-Twitch Muscle

Pyruvate kinase was higher in fibers of both flight muscles and both tail suspension muscles than in either synchronous muscle. The increases were respectively 43% and 38% in F6 and F7, and 126% and 7% in T6 and T7. Only the increases in F7 and T6 were statistically significant.

Glycerol-3-phosphate dehydrogenase (GOPDH) was on average also higher than either S6 or S7 in fibers of both flight and tail suspension muscles with $P \leq 0.05$ in each case. The increases were equal or greater than for pyruvate kinase: 65% and 46% respectively in F6 and F7, and 126% and 44% in T6 and T7.

P-fructokinase was higher in fibers of both F7 and T7 than in S7 (the only muscles analyzed for this enzyme). The differences, however, were small (+27% and +18% respectively), and not statistically significant in either case.

Two Soleus Enzymes Usually Higher in Slow-Twitch Muscles

Hexokinase was higher in the fibers of both flight and both tail suspension muscles than in S7 (the higher of the two synchronous muscles). The differences were statistically significant ($P < 0.02$ in all cases). Relative to the average for S6 and S7, the respective increases were 35% and 60% for F6 and F7, and 31% and 108% for T6 and T7.

3-ketoacid CoA transferase was the only one of the five enzymes which was decreased in the fibers of either flight or tail suspension muscles, and the differences were not great although statistically significant (($P \leq 0.05$ in all but T7). The changes relative to the lower of the two synchronous muscle values were -10% for both F6 and F7, and respectively -21% and -2% for T6 and T7.

Individual Soleus Fiber Values

The above average values obscure the large differences among fibers in size and enzyme levels and the degree of correlation between different enzymes in individual fibers.

Figs. 1 to 3 compare *GOPDH* and *pyruvate kinase* activities in 15 or 16 fibers from each of the 6 muscles. In both S6 and S7 (Fig. 1) the two enzymes vary coordinately over a range of about 2.5-fold in each case. The correlation coefficients (r) are 0.801 for S6 and 0.77 for S7, both highly significant ($P < 0.001$). For F6 and F7 (Fig. 2), the activity ranges are both increased to about 5-fold for F6 and 3- to 4-fold for F7. The correlation coefficients are increased to 0.961 and 0.948 for fibers from the two respective muscles. Very similar effects are seen for T6 and T7 (Fig. 3) with values for half or more of the fibers rising above the control boundary zone for S6 and S7.

Correlations between *phosphofructokinase* and pyruvate kinase for S7, F7 and T7 were similar to those for GOPDH and pyruvate kinase. The r values were 0.705, 0.793, and 0.886 respectively, with $P < 0.01$ in each case (data not shown in a figure).

Hexokinase was also *positively* correlated with pyruvate kinase among fibers from S6 ($r = 0.524$, $P < 0.05$) and S7 ($r = 0.819$, $P < 0.001$) (Fig. 4). However, no significant positive or negative correlations were observed between these two enzymes among flight or tail suspension fibers. Moreover, although hexokinase on average increased significantly in all four fiber groups (Figs. 5 and 6), the range of activities did not increase above the synchronous range of less than 2. Note how few F or T fibers remained within the soleus boundary for the two enzymes. To anticipate the results with TA fibers, hexokinase levels did not correlate with *fiber size*.

Individual *KACAT* activities did not correlate positively or negatively with hexokinase or with any of the other enzymes measured.

Tibials Anterior Muscle

Average Values

Most of the soleus fibers are slow-twitch (Type 1), therefore the relatively few fibers that it is practicable to analyze individually should furnish a reasonable indication of the composition of the muscle as a whole. This is not true for TA muscles which contain two distinct fiber types that are non-uniformly distributed among different regions of the muscle. Therefore, although an attempt was made to choose fibers at random, there can be no assurance that the 20 or so fibers analyzed from each muscle were truly representative of the muscle as a whole. The average values in Table 2 should consequently be evaluated with this in mind.

It is rather clear that in contrast to the soleus fibers, there was no major change in fiber size (dry weight per unit length) related to flight or tail suspension. This fits with the lack of substantial difference in total wet weight of the muscles from which these TA fibers came.

In contrast to the results for soleus fibers there were only two statistically significant differences ($P < 0.05$) between TA enzyme activities for synchronous fibers and those of either flight or tail suspension TA fibers: *Hexokinase* activity of T7 averaged 57% higher than the average for S7, the higher of the two synchronous sets; *thiolase* activity of F7 was 27% lower than the average for S6, the lower of the two synchronous fiber sets.

Individual TA Fiber Values

Examination of the data on a fiber-by-fiber basis shows some interesting relationships between different enzymes and between size and enzyme activities, as well as some effects of flight and tail

suspension obscured by averaging all the data.

Figs. 7-9 show the rather striking negative correlation between fiber size and malate dehydrogenase (MDH) which applies as well to synchronous (Fig. 7) flight (Fig. 8) tail suspension (Fig. 9) fibers. Note that almost all of the values from F6, F7, T6 and T7 fall within the S6 plus S7 domain or close by. The correlation coefficients between size and MDH ranged from -0.603 for F7 to -0.915 for S7 ($P < 0.01$ in all cases).

Hexokinase and MDH activities were closely correlated, and in the synchronous and flight data could be almost superimposed (Fig. 10). The correlation coefficients were all very high: 0.946 (S6), 0.985 (S7), 0.890 (F6), 0.890 (F7). There was no sign of any important differences in the range of values. In contrast, among the tail suspension fibers (Fig. 11), although hexokinase and MDH were also tightly correlated for T6 and T7 ($r = 0.951$ and 0.861 respectively), the slope of the regression lines were much steeper than for S6 and S7. Consequently, the hexokinase to MDH ratios were very similar at the low end of the MDH scale and much higher at the upper end. Clearly, there had been relative increases in hexokinase among TA fibers with high MDH from both T6 and T7, but the increase in T6 was obscured in Table 2 because fibers with low MDH had predominated either in the original selection or in the muscle as a whole.

Figs. 12 and 13 bring out another aspect of the increase in hexokinase which took place in the tail suspension fibers. In the control (S6 and S7) fibers hexokinase and size were closely correlated (Fig. 12) as might have been expected ($r = -0.733$ and -0.920 for S6 and S7 respectively). However, in the case of T6 and T7, the relationship between size and hexokinase ceased with hexokinase activities greater than control (Fig. 13).

Pyruvate kinase and hexokinase activities in TA fibers proved to be negatively correlated (Figs. 4-6), in contrast to the positive correlation seen in the same figures for soleus fibers. There was little change in the distribution among the flight fibers except for one fiber from each muscle which drifted toward the soleus region in regard to pyruvate kinase. The increases in hexokinase activity among the tail suspension fibers were clearly much larger for those with lowest pyruvate kinase activity, just as they had been larger for fibers with highest MDH activity.

Thiolase was closely correlated with both MDH and hexokinase. A plot of hexokinase against thiolase (not shown) was almost indistinguishable from that against MDH (Fig. 10) with r values ranging from 0.813 to 0.980. As expected, thiolase is negatively correlated with pyruvate kinase (Fig. 14). Only the 15 out of 36 flight and tail suspension fibers which fell outside the S6 and S7 zone are indicated. There seems to be no specific trend in these deviations from S6 and S7.

Phosphoglucoisomerase correlated well with pyruvate kinase among individual fibers but there were no substantial differences between synchronous, flight, and tail suspension muscles in the interrelationships or range of values (data not shown).

Relationship of Enzyme Levels to Myosin ATPase Fiber Types

Table 3 records activities of phosphofructokinase (PFK) and GOPDH in fibers from S7, F7, and T7 identified as to fiber type by staining for myosin ATPase. PFK was significantly higher in type 1 and 2B fibers from F7 than from S7 (+58% and +31% respectively). PFK was also 27% higher in F7, 2A fibers but the difference was not statistically significant. GOPDH, however, was significantly higher in 2A and 2B fibers of both F7 and T7 fibers by significant amounts (respectively, 162% and 88% higher in 2A and 2B fibers of F7, and 88% and 47% higher in 2A and 2B fibers of T7). Fig. 15 displays the relationships between PFK and GOPDH among individual fibers analyzed for both enzymes. Note that the GOPDH levels of all 2B fibers from each muscle (S7, F7 or T7) are higher than the level in any 2A fiber from the same muscle.

MDH and glycogen phosphorylase were also measured in fibers typed for myosin ATPase (Table 4, Fig. 16). Only in one case was a statistically significant difference related to flight or tail suspension observed among the average values (Table 3). Average phosphorylase activity in T7 2B fibers was 24% higher than in S7, and 41% higher than in F7. The plot of MDH against phosphorylase (Fig. 16) shows complete separation of MDH activities of 2A and 2B fibers of all three muscles, and only a slight overlap of phosphorylase activities which was limited to F7 fibers. A few 2C fibers were identified and assayed from the F7 muscle. Their MDH activities overlapped completely with type 1 fibers and their phosphorylase levels were on the average 18% lower, but the difference was not statistically significant.

TABLE 1

SIZE AND LEVELS OF FIVE ENZYMES IN INDIVIDUAL SOLEUS FIBERS

Rat	Size (μg / mm)	Pyruvate Kinase	Hexokinase (mol	KACAT $h^{-1} kg^{-1}$ (dry)	GOPDH at 20° C)	P-Fructokinase
S6	0.705	11.7	0.388	0.478	0.43	-
S.E.	± 0.021	± 0.8	± 0.017	± 0.014	± 0.04	-
CV	12%	28%	17%	12%	35%	-
S7	0.818	11.5	0.506	0.470	0.43	3.52
S.E.	± 0.041	± 1.0	± 0.020	± 0.016	± 0.04	± 0.28
CV	20%	35%	16%	14%	37%	32%
F6	0.545*	16.6	0.602*	0.421*	0.71*	-
S.E.	± 0.033	± 2.6	± 0.013	± 0.018	± 0.10	-
CV	24%	63%	9%	17%	60%	-
F7	0.393*	16.0*	0.716*	0.423*	0.63*	4.46
S.E.	± 0.029	± 1.8	± 0.026	± 0.016	± 0.10	± 0.48
CV	30%	45%	15%	15%	57%	40%
T6	0.491*	26.2*	0.587*	0.372*	0.97*	-
S.E.	± 0.024	± 3.9	± 0.023	± 0.022	± 0.14	-
CV	19%	57%	15%	23%	52%	-
T7	0.470*	12.4	0.929*	0.463	0.62*	4.17
S.E.	± 0.018	± 0.9	± 0.024	± 0.012	± 0.06	± 0.45
CV	5%	30%	10%	10%	40%	43%

Each entry is the average for the same 16 fibers (15 for T6) analyzed in duplicate, ± S.E..
Abbreviations are KACAT, 3-ketoacid CoA transferase; GOPDH, glycerol-3-phosphate dehydrogenase; and CV, coefficient of variation.
An asterisk (*) indicates a significant difference ($P \leq 0.05$) from both S6 and S7.

TABLE 2

SIZE AND LEVELS OF FIVE ENZYMES IN INDIVIDUAL TA MUSCLE FIBERS

Rat		Size (μg / mm)	MDH	HK	Thiolase	PK	PG1
S6		0.641	12.4	0.387	1.35	81.4	69.2
(23)	S.E.	± 0.035	± 1.1	± 0.026	± 0.13	± 5.3	± 2.6
	CV	26%	43%	32%	46%	20%	11%
S7		0.790	13.9	0.543	1.53	89.2	64.2
(23)	S.E.	± 0.061	± 1.6	± 0.053	± 0.21	± 9.3	± 3.3
	CV	37%	55%	47%	66%	31%	15%
F6		0.615	14.2	0.533	1.49	90.3	73.5
(22)	S.E.	± 0.031	± 1.0	± 0.031	± 0.17	± 7.7	± 4.4
	CV	24%	33%	27%	54%	26%	18%
F7		0.634	12.7	0.499	0.98*	92.7	66.2
(21)	S.E.	± 0.035	± 1.1	± 0.038	± 0.12	± 9.7	± 5.1
	CV	25%	40%	35%	56%	31%	23%
T6		0.749	11.6	0.546	1.00	91.6	71.6
(23)	S.E.	±0.039	± 1.3	± 0.061	± 0.16	± 8.2	± 3.2
	CV	25%	54%	54%	77%	27%	13%
T7		0.624	12.1	0.850*	1.47	95.6	69.3
(24)	S.E.	± 0.042	± 1.2	± 0.120	± 0.17	± 7.1	± 3.4
	CV	33%	49%	69%	57%	22%	15%

Activities are recorded as in Table 1, ± S.E. for the number of fibers given in parentheses in the left hand column, except that pyruvate kinase (PK) and phosphoglucoisomerase (PGI) are for only 9 fibers from each muscle.
An asterisk (*) indicates a significant difference ($P < 0.05$) from both S6 and S7.

TABLE 3

PHOSPHOFRUCTOKINASE (PFK) AND GLYCERO-DEHYDROGENASE (GOPDH) IN TIBIALIS ANTERIOR FIBERS TYPED BY STAINING FOR MYOSIN ATPase

Fiber Type	Phosphofructokinase			Glycerol-P Dehydrogenase		
	S7	F7	T7	S7	F7	T7
1	1.99 (3)	3.15 (4)*	-	-	-	-
S.E.	± 0.38	± 0.27	-	-	-	-
CV	33%	17%	-	-	-	-
2A	5.08 (10)	6.43 (10)	5.24 (9)	0.85 (7)	2.23 (6)*	1.60 (6)*
S.E.	± 0.51	± 0.49	± 0.41	± 0.18	± 0.19	± 0.25
CV	31%	24%	23%	56%	21%	38%
2B	7.64 (8)	10.0 (10)*	8.6 (12)	2.03 (8)	4.52 (9)*	2.99 (12)*
S.E.	± 0.58	± 0.43	± 0.42	± 0.12	± 0.20	± 0.16
CV	21%	14%	15%	17%	13%	19%

Activities are mol h^{-1} kg^{-1} (dry wt) at 20°C ± S.E. for the number of samples in parentheses. Asterisks (*) indicate a statistically significant difference from the corresponding S7 value ($P \leq 0.05$).

TABLE 4

MALATE DEHYDROGENASE AND PHOSPHORYLASE IN TIBIALIS ANTERIOR FIBERS TYPED BY STAINING FOR MYOSIN ATPase

Fiber Type	Malate Dehydrogenase			Phosphorylase		
	S7	F7	T7	S7	F7	T7
1	12.1 (5)	12.4 (4)	13.7 (6)	1.19 (5)	0.97 (4)	1.09 (6)
S.E.	± 0.6	± 0.41	± 1.6	± 0.14	± 0.13	± 0.10
CV	11%	7%$	28%	25%	27%	23%
2C	-	14.2 (7)	-	-	0.80 (7)	-
S.E.	-	± 1.06	-	-	± 0.06	-
CV	-	20%	-	-	20%	-
2A	14.5 (8)	15.5 (7)	17.0 (6)	2.65 (8)	3.01 (7)	2.50 (6)
S.E.	± 1.3	± 1.4	± 1.0	± 0.16	± 0.25	± 0.22
CV	26%	23%	14%	18%	22%	21%
2B	4.11 (7)	4.79 (9)	4.85 (10)	4.98 (7)	4.38 (9)	6.17 (10)*
S.E.	± 0.35	± 0.39	± 0.21	± 0.24	± 0.27	± 0.39
CV	23%	24%	14%	13%	16%	20%

Activities recorded as in Table 1 for the number of fibers given in parentheses.
An asterisk (*) indicates a significant difference from the corresponding S7 value.

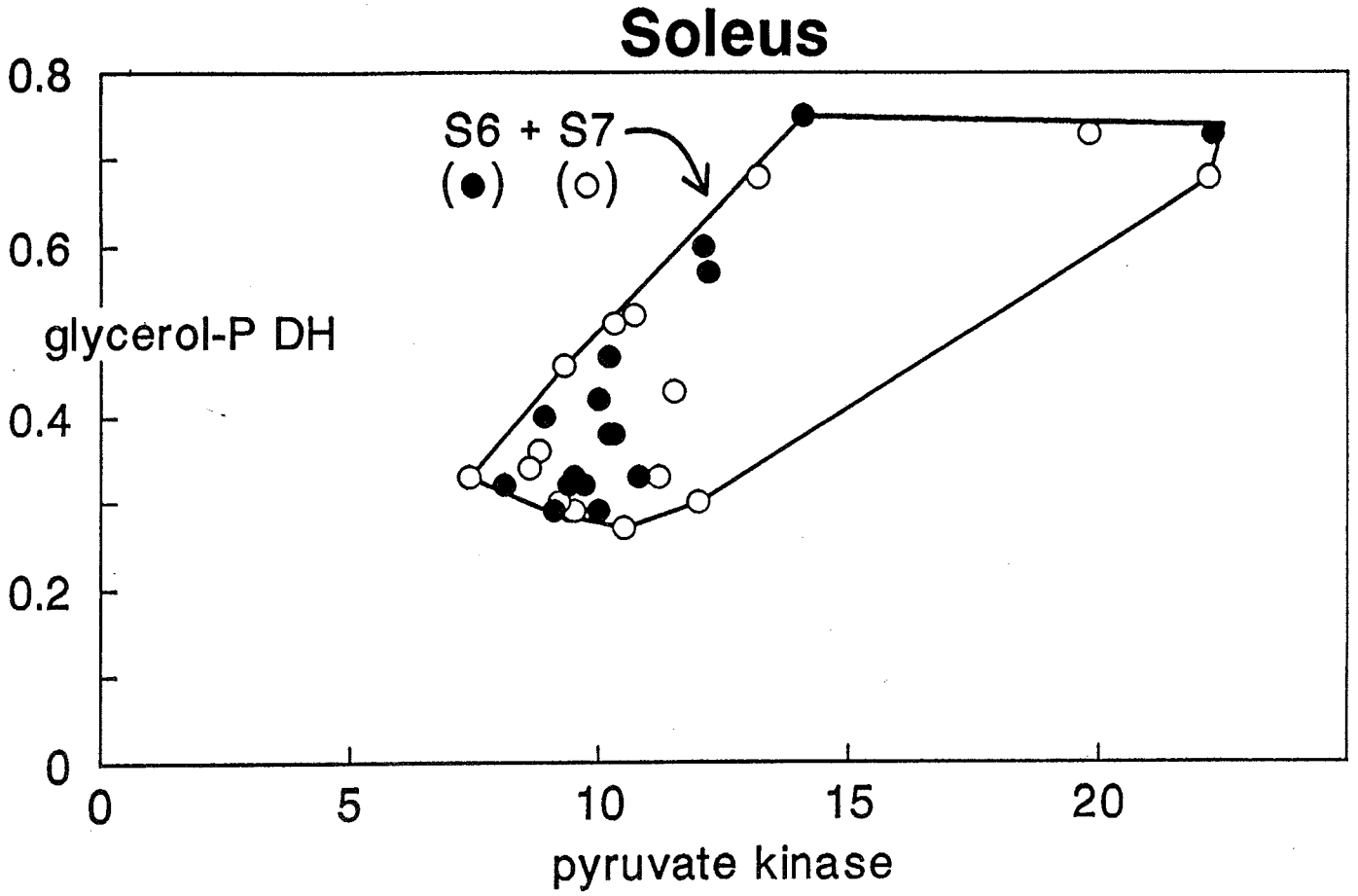

Figure 1. Glycerol-P dehydrogenase and pyruvate kinase levels in the same individual S6 and S7 soleus fibers. Activities are recorded as mol h^{-1} kg^{-1} (dry weight) at 20°C.

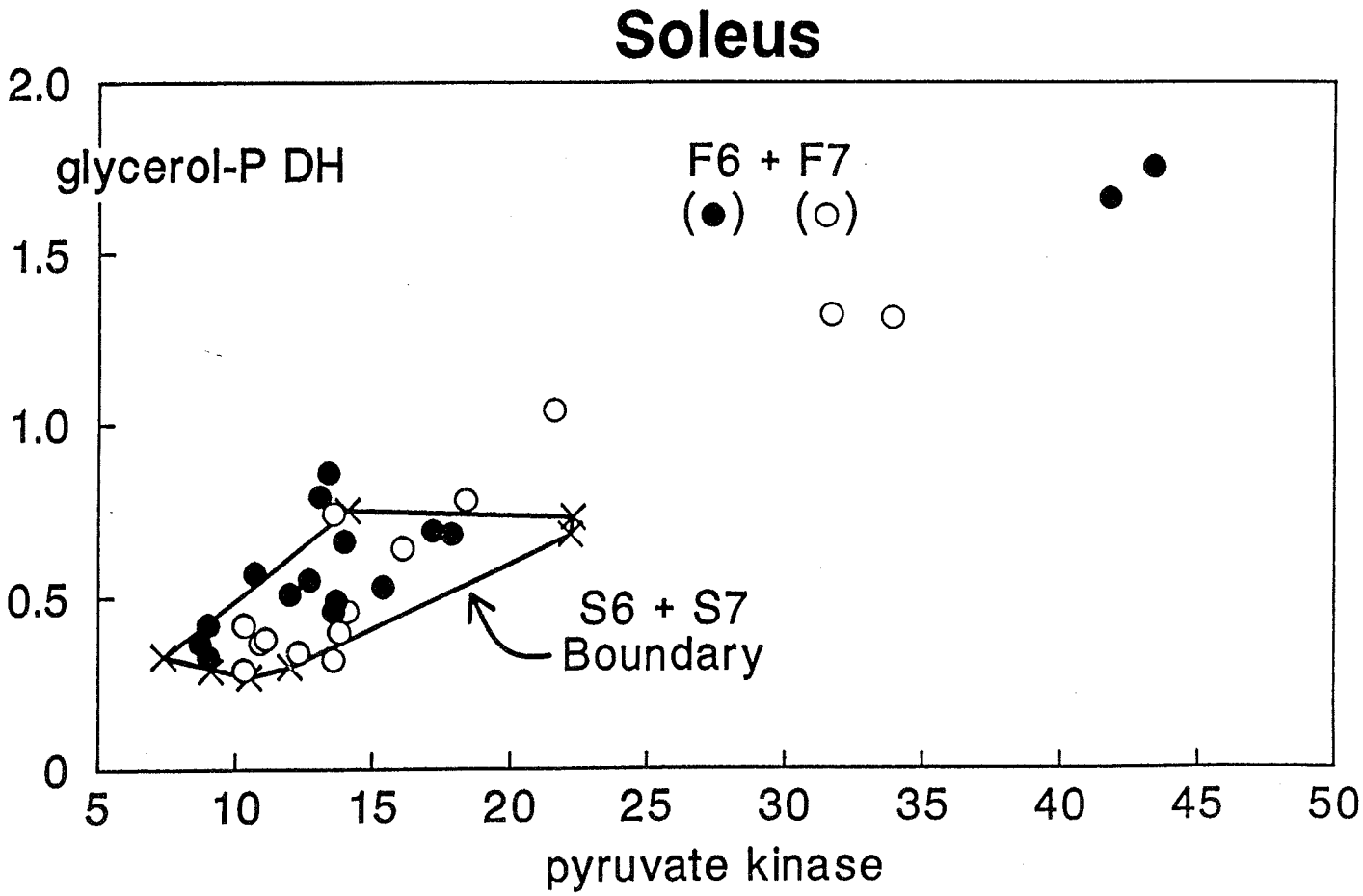

Figure 2. The same as figure 1 but for F6 + F7 fibers. The boundary for S6 + S7 fibers is shown in this case.

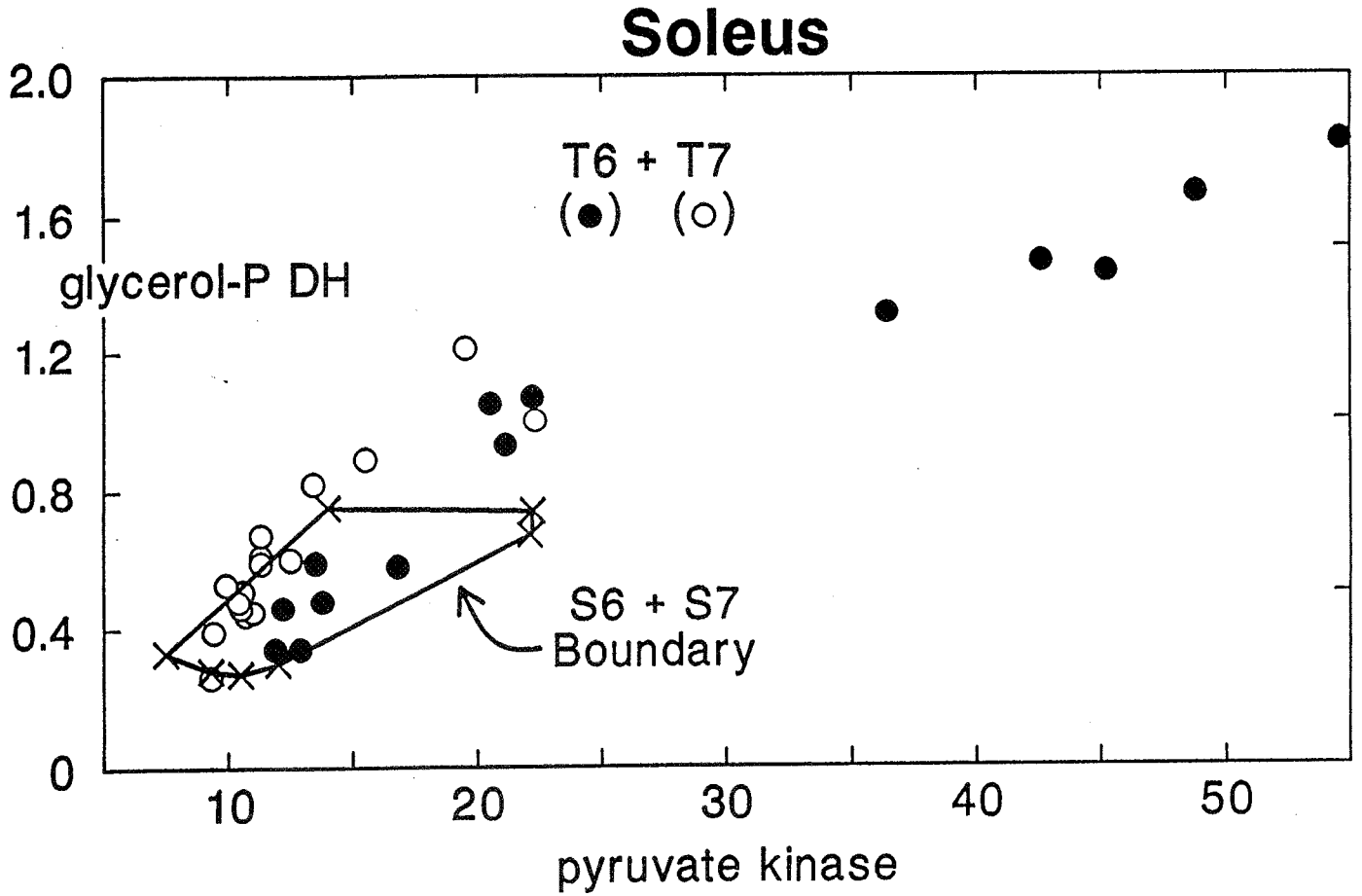

Figure 3. The same as figure 1 but for T6 + T7 fibers. The boundary for S6 + S7 fibers is shown in this case.

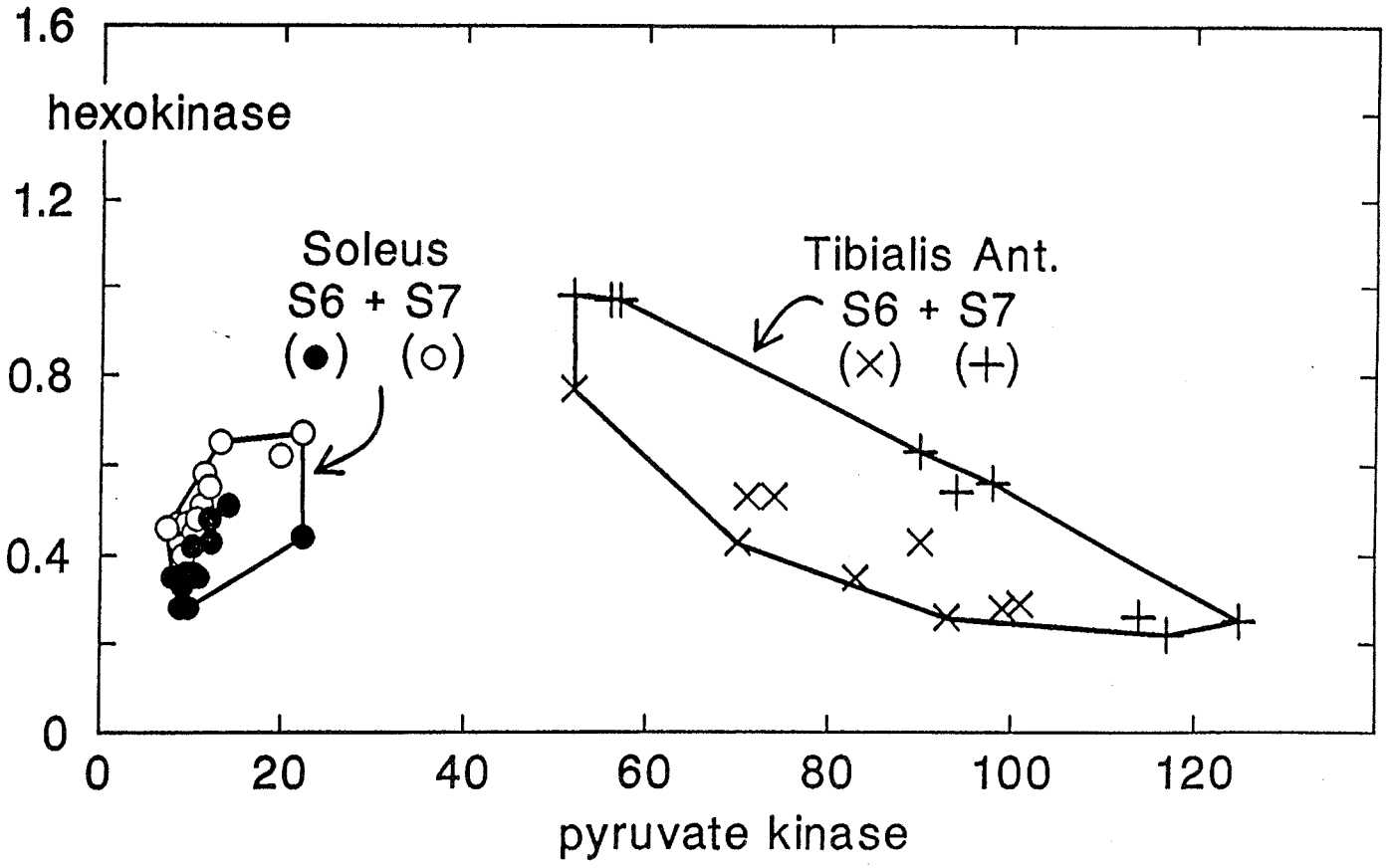

Figure 4. Hexokinase and pyruvate kinase levels in the same individual S6 and S7 soleus and S6 and S7 TA fibers. Activities are recorded as in figure 1.

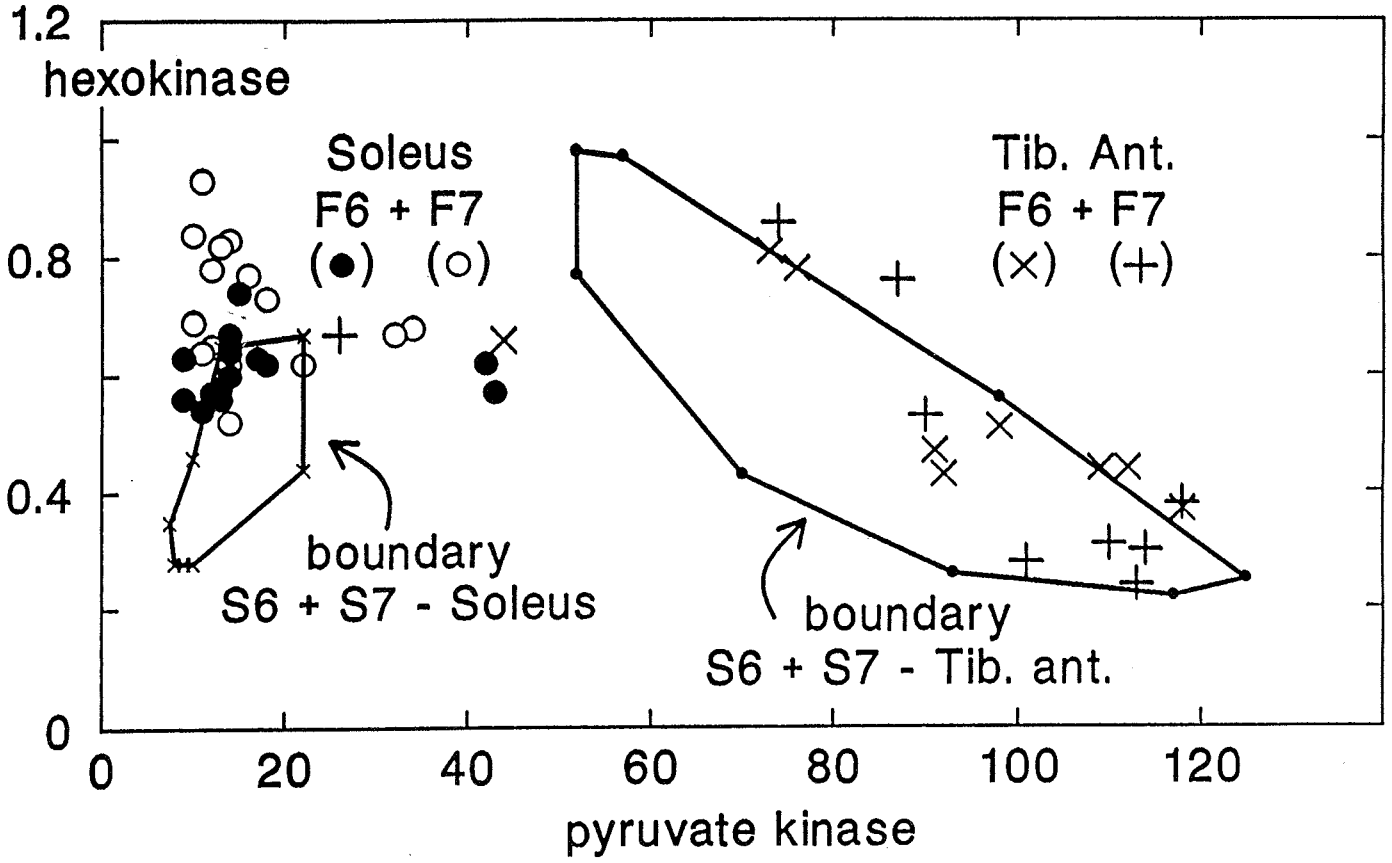

Figures 5. The same as figure 4 but for F6 + F7 fibers. The boundary for S6 + S7 fibers is shown.

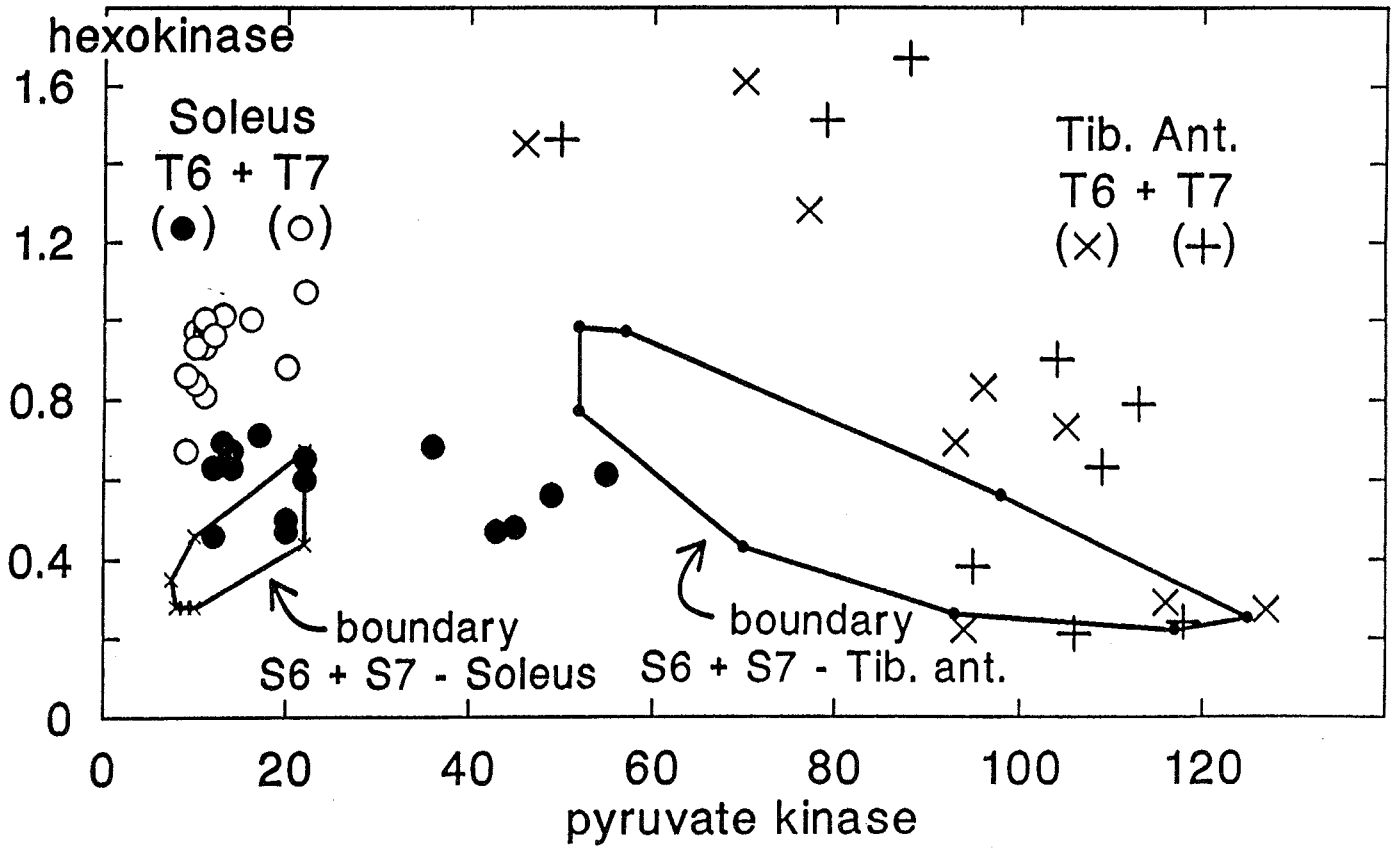

Figure 6. The same as figure 4 but for T6 + T7 fibers. The boundary for S6 + S7 fibers is shown.

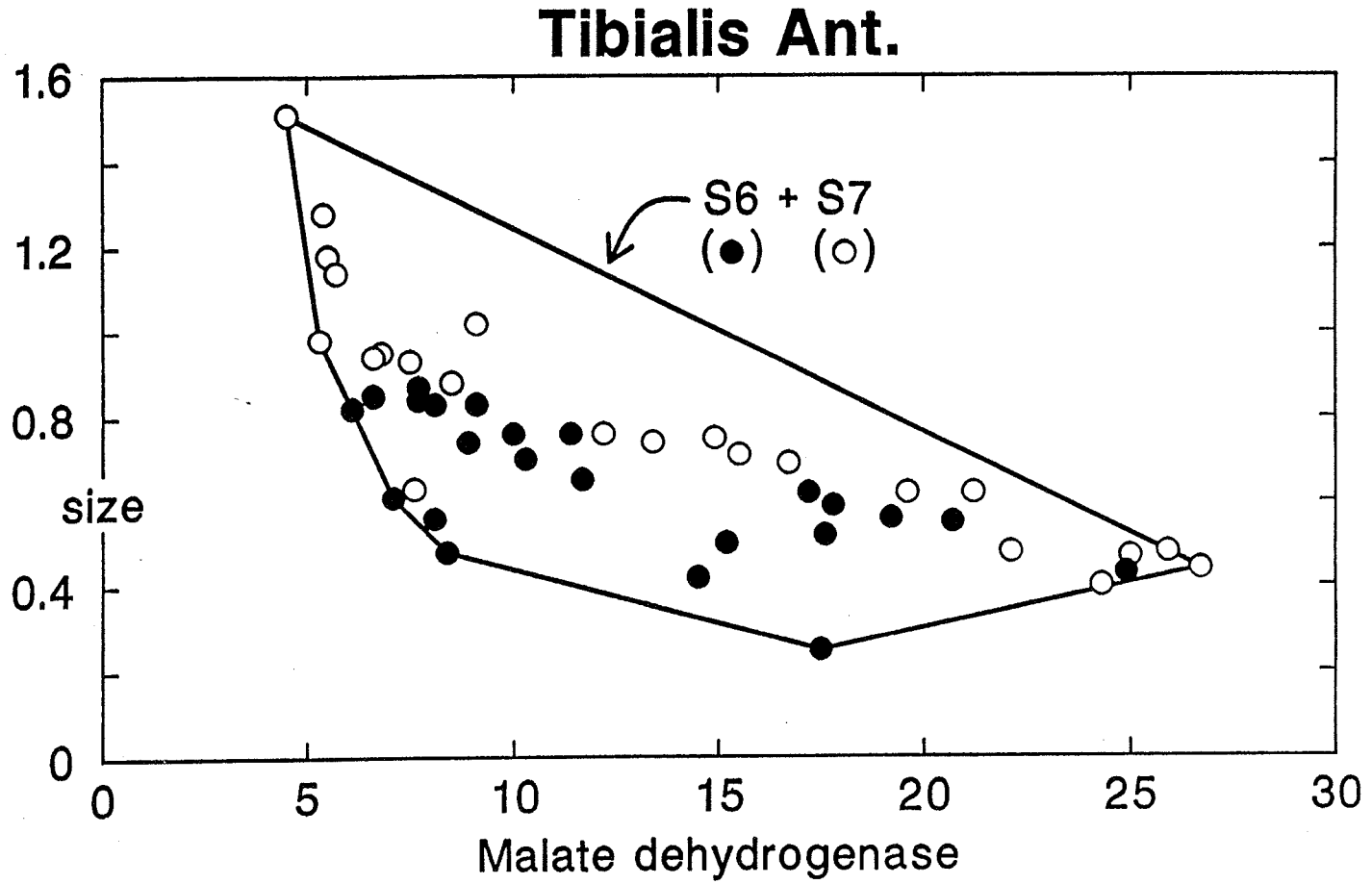

Figure 7. Fiber size (µg/mm) and MDH levels in the same individual soleus S6 and S7 fibers. MDH activity is recorded as for the enzymes of figure 1.

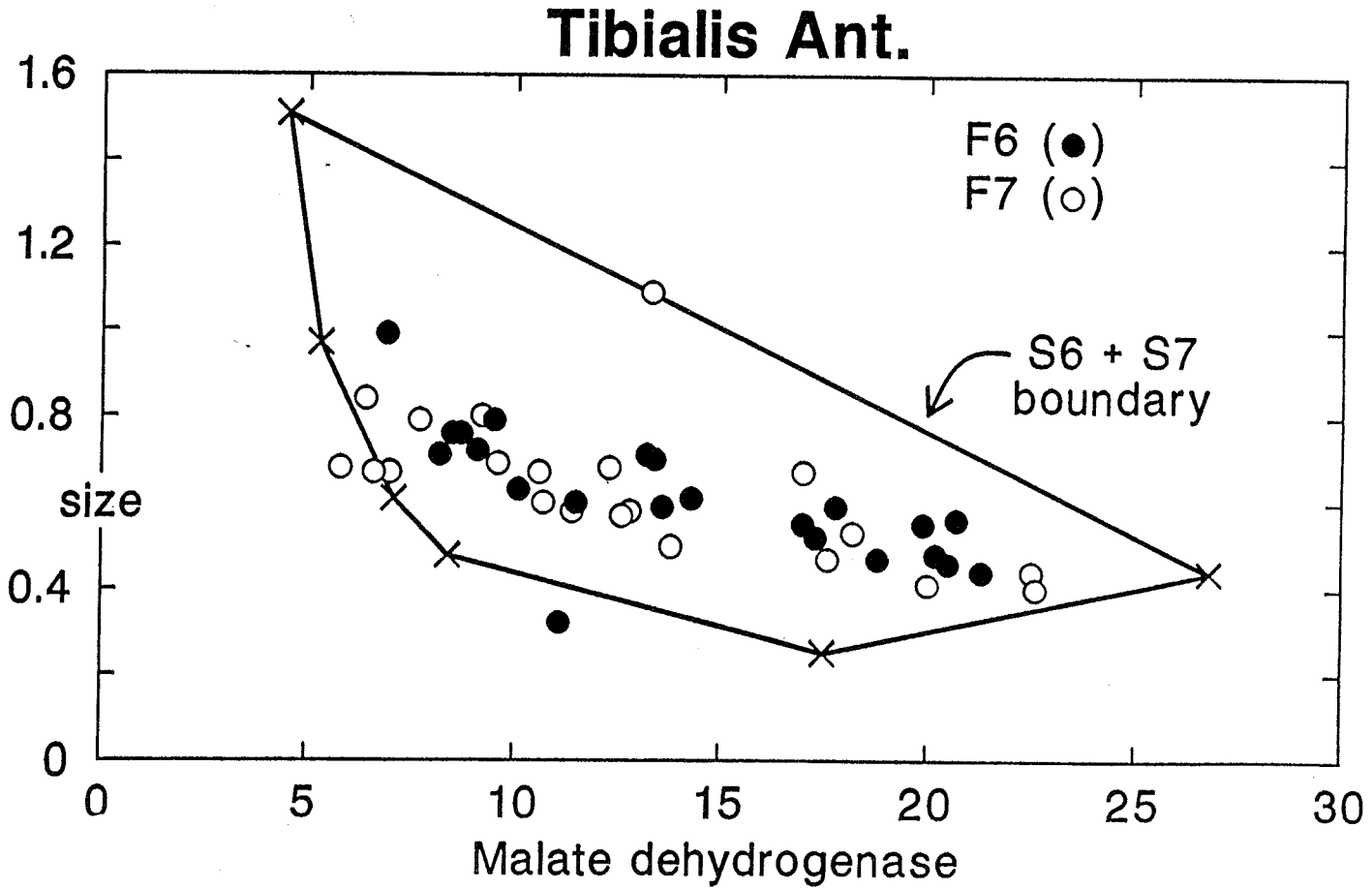

Figure 8. The same as figure 7 but for F6 + F7 fibers. The boundary for S6 and S7 fibers is shown.

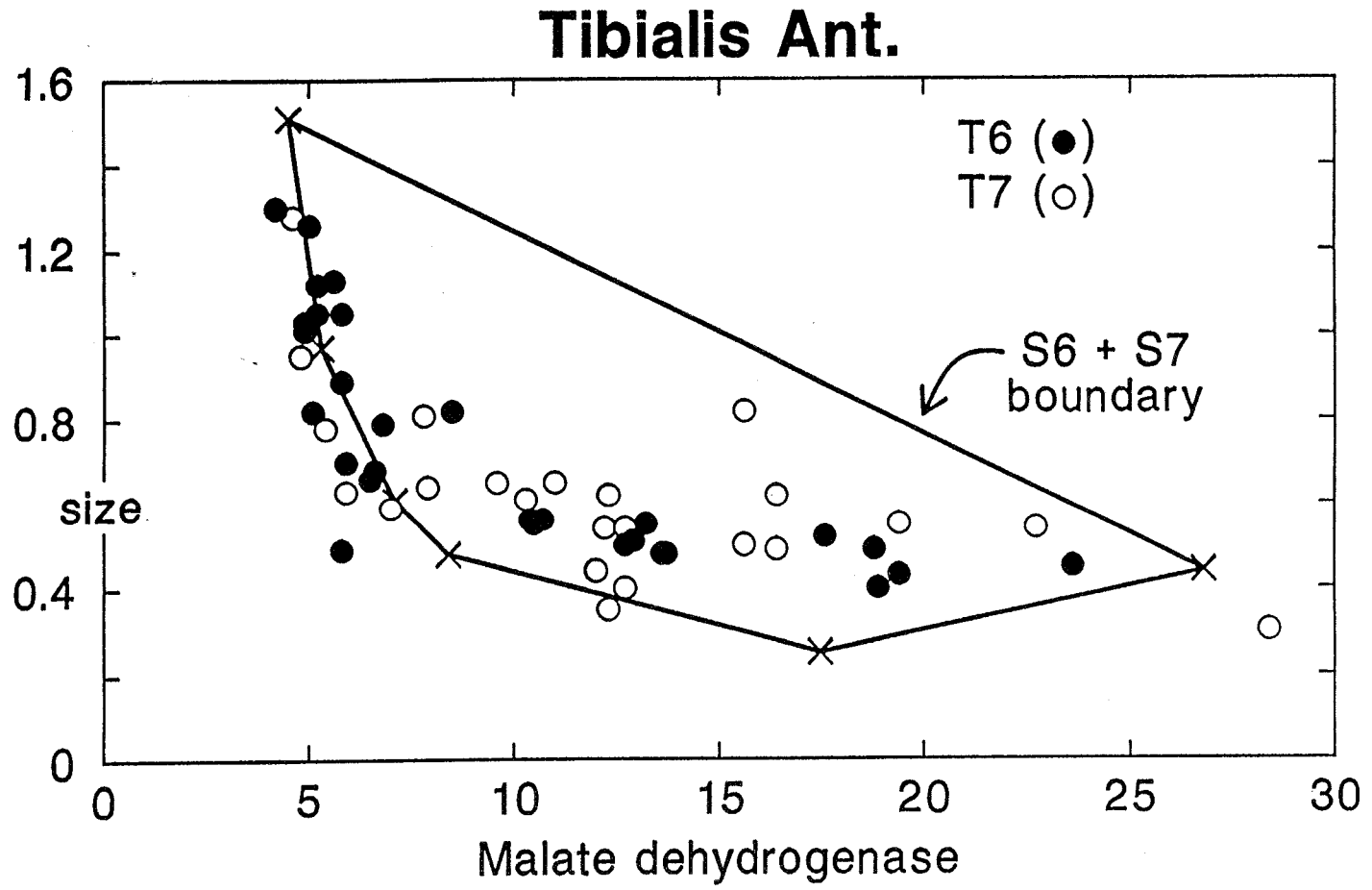

Figure 9. The same as figure 7 but for T6 + T7 fibers. The boundary for S6 and S7 fibers is shown.

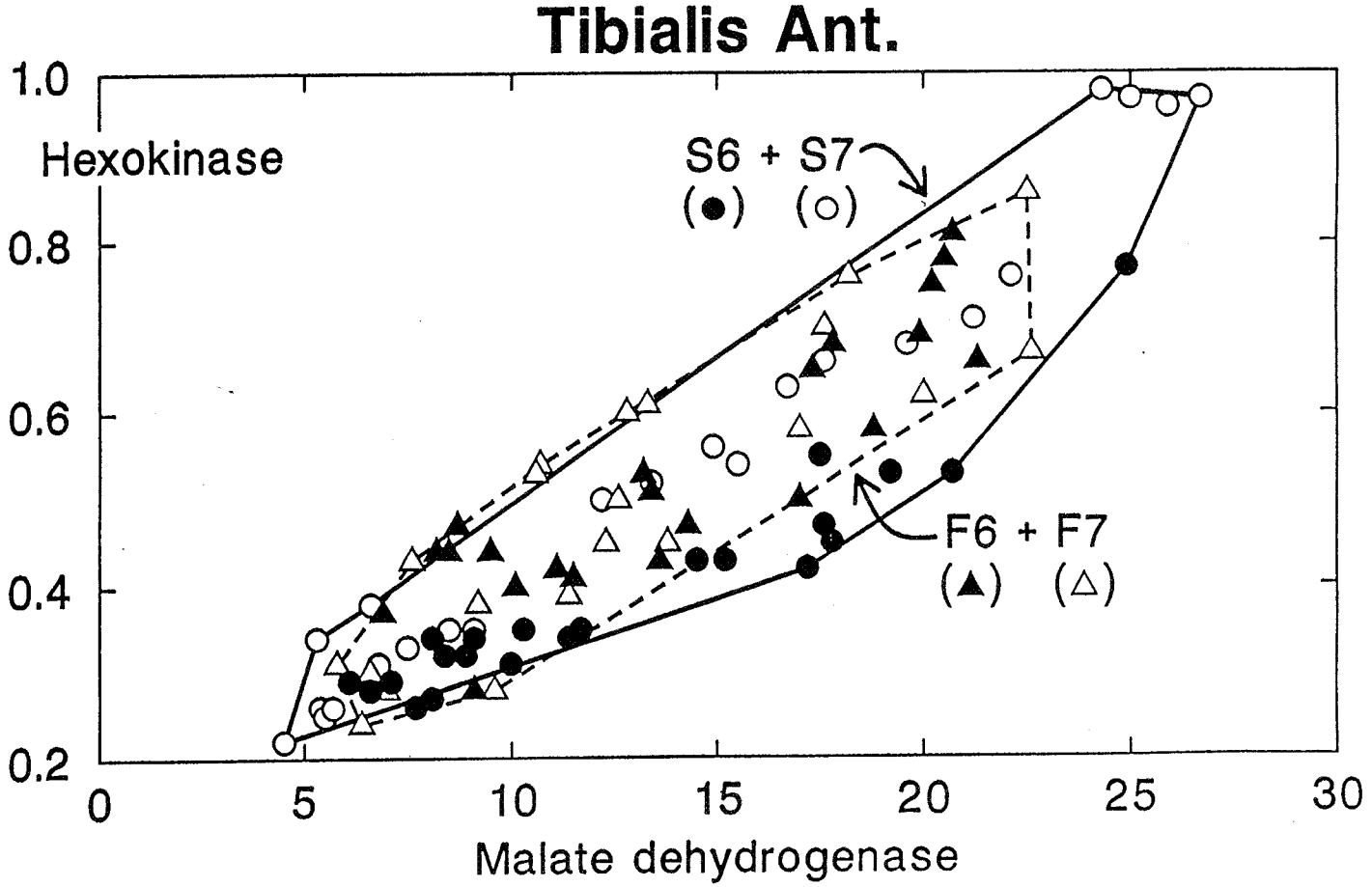

Figure 10. Hexokinase and MDH levels in the same individual TA, S6 + S7 and F6 + F7 fibers. Activities are recorded as in figure 1.

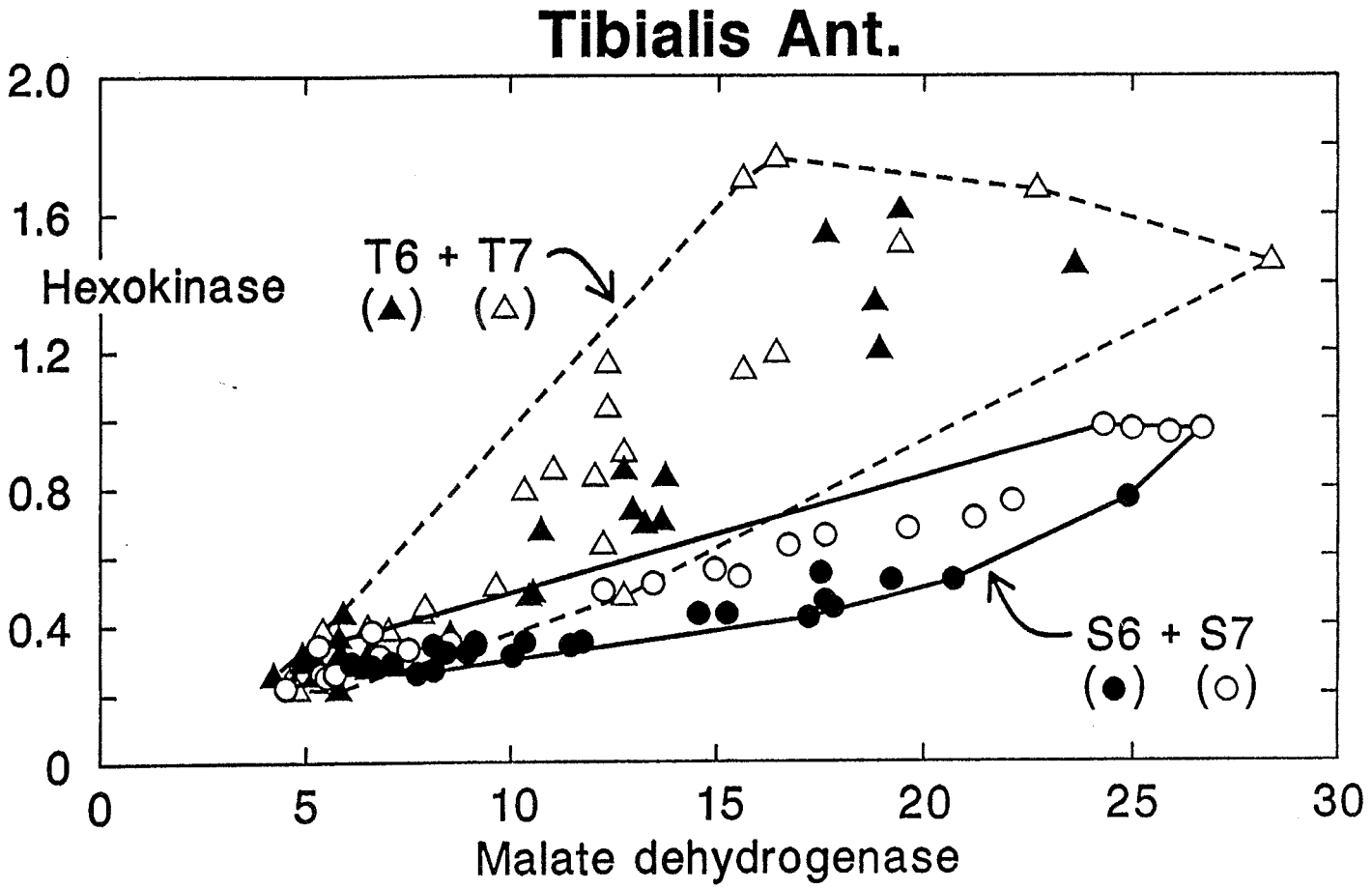

Figure 11. The same as figure 10 but for S6 + S7 and T6 + T7.

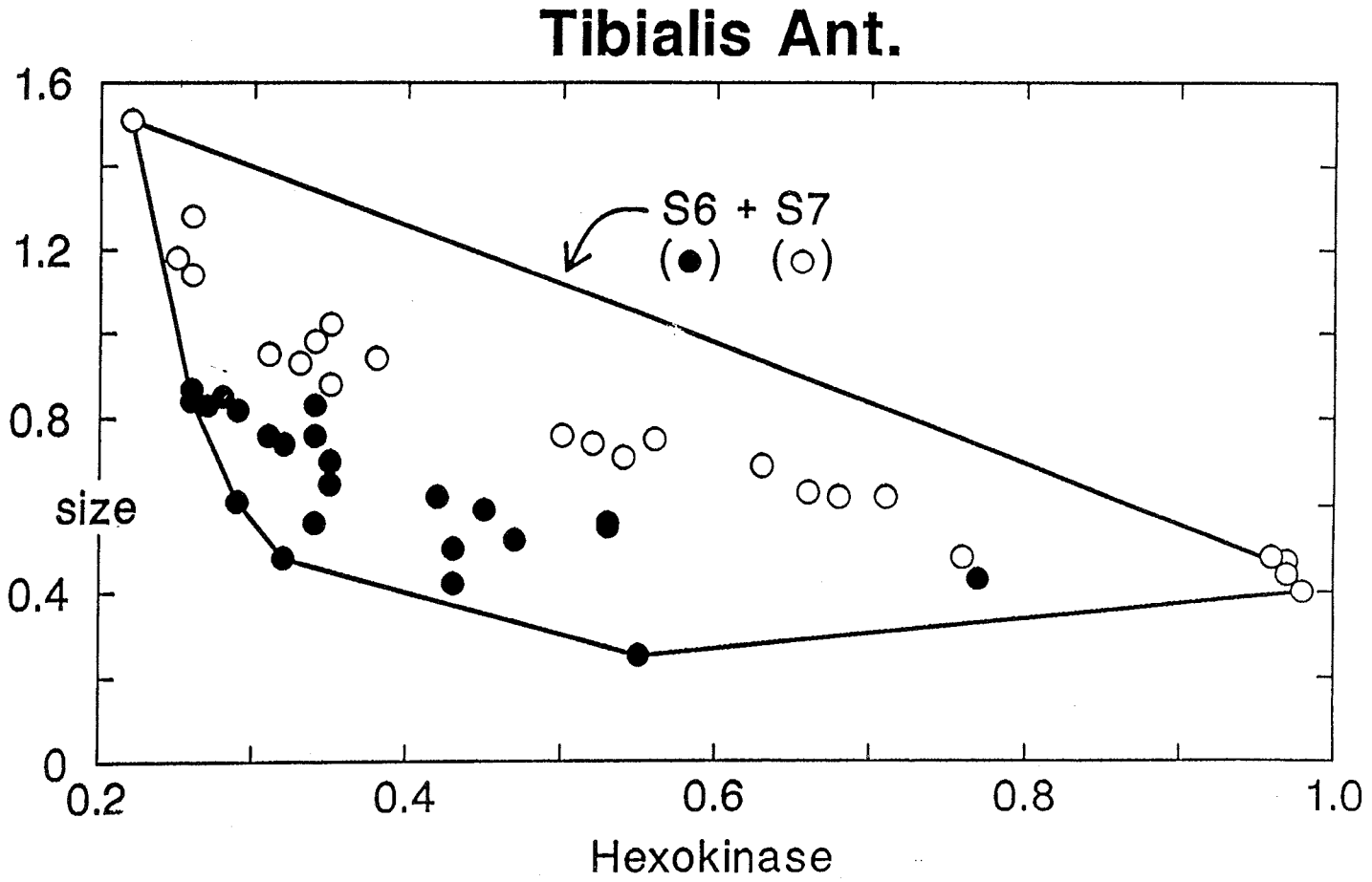

Figure 12. Fiber size (µg/mm) and hexokinase levels in the same individual TA, S6 and S7 fibers. Hexokinase activity is recorded as for the enzymes of figure 1.

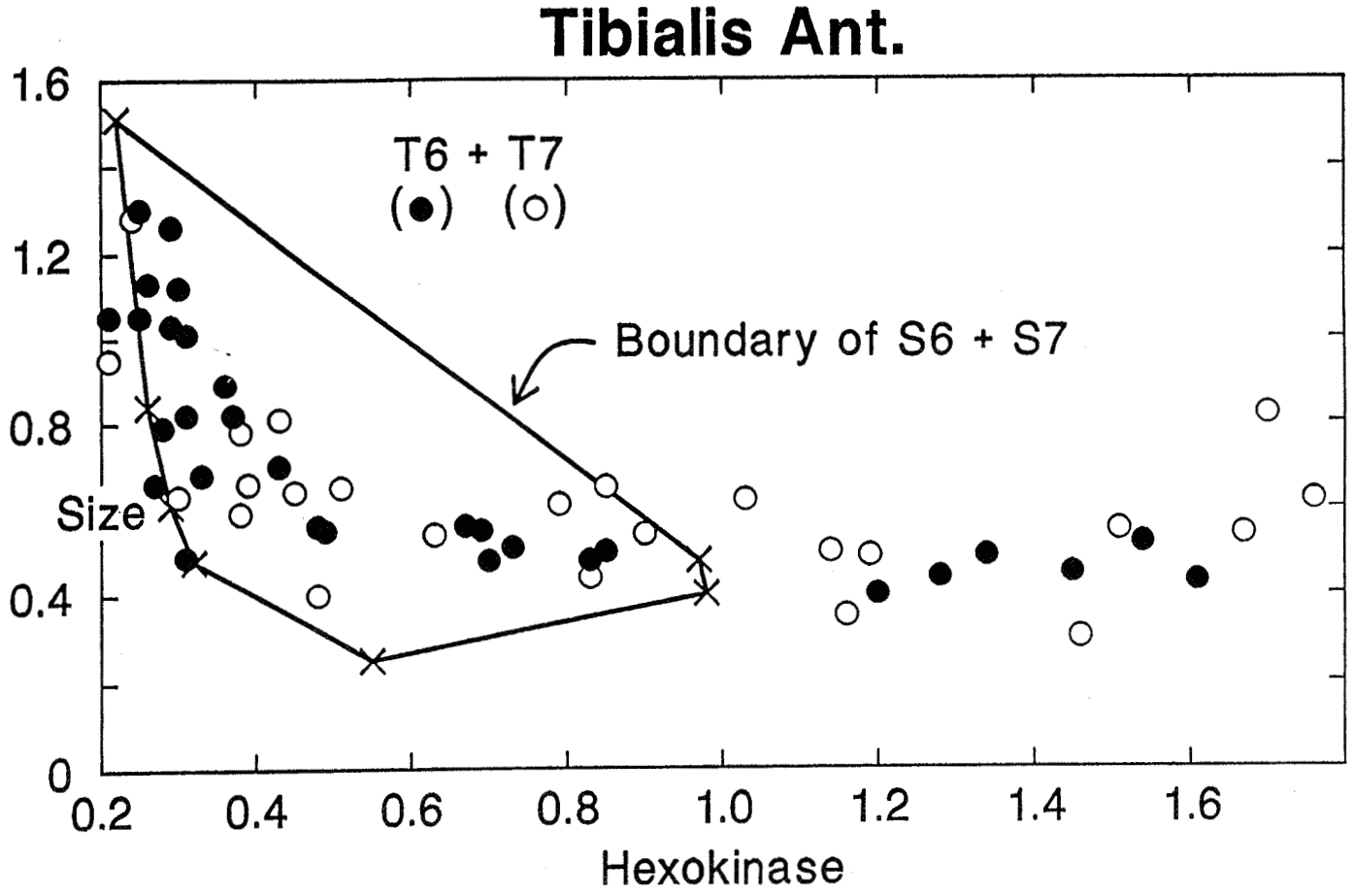

Figure 13. The same as figure 12 but for T6 and T7 fibers. The boundary for S6 + S7 is shown.

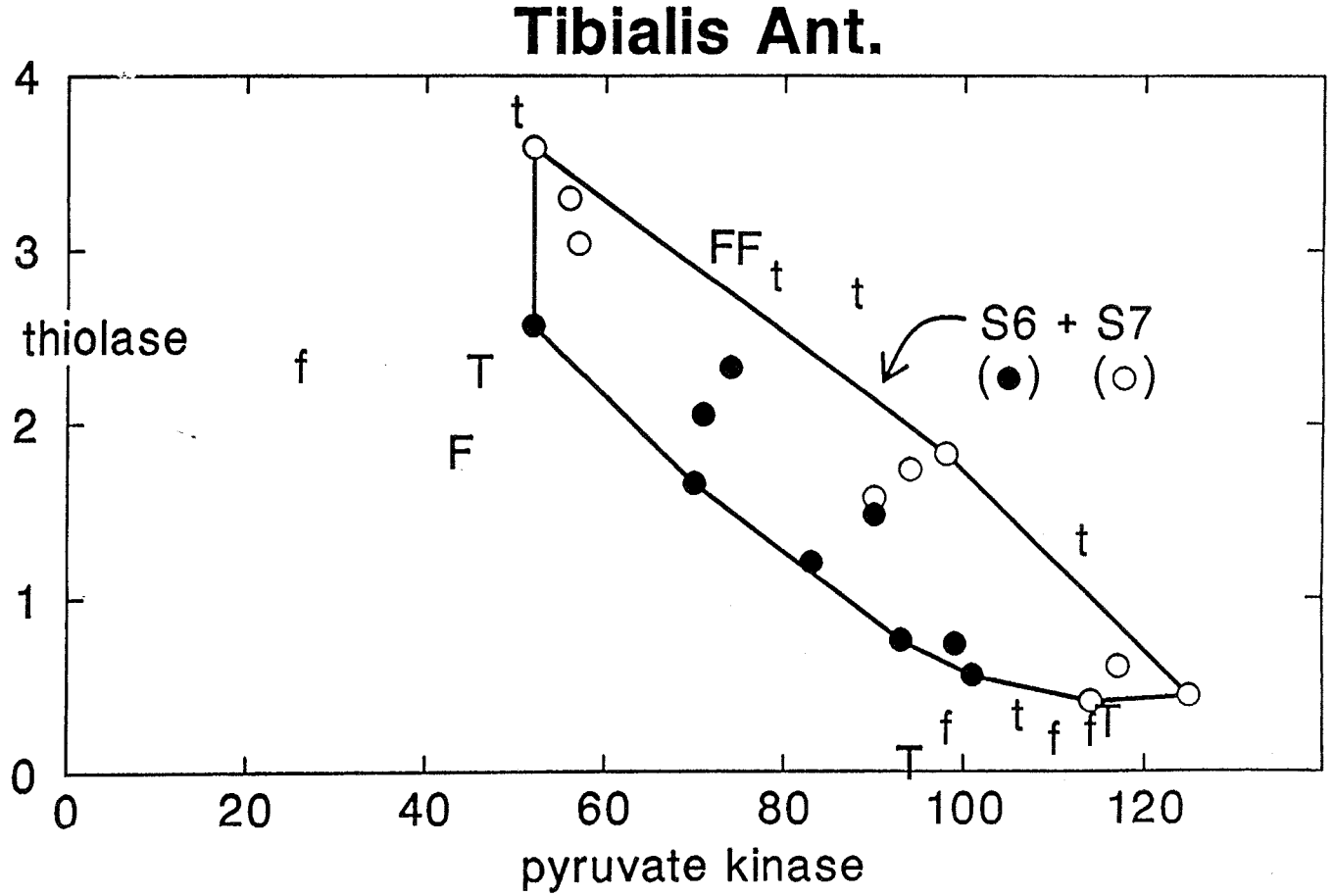

Figure 14. Thiolase (mitochondrial) levels in TA S6 and S7 individual fibers. Also shown are entries representing those individual fibers from the two flight and two tail suspension muscle that fall outside *the domain of the S6 + S7 fibers. These outside fibers are designated F and f respectively for those from F6 and F7 muscles, and T and t for those from T6 and T7 muscles. Activities are recorded as for figure 1.*

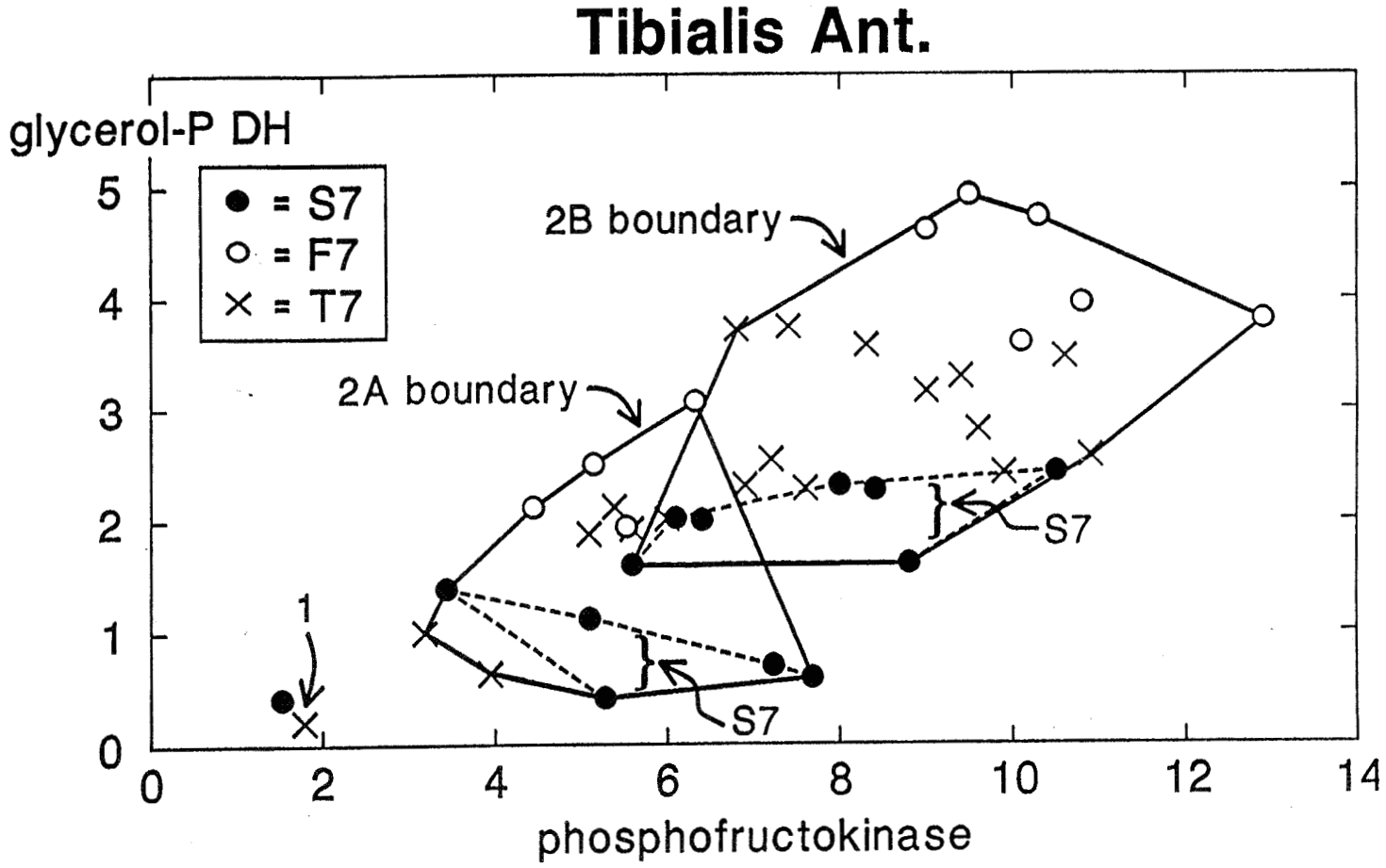

Figure 15. GOPDH and phosphofructokinase levels in individual TA fibers obtained from S7, F7 and T7 muscles and typed by myosin ATPase staining. Activities are recorded as in figure 1.

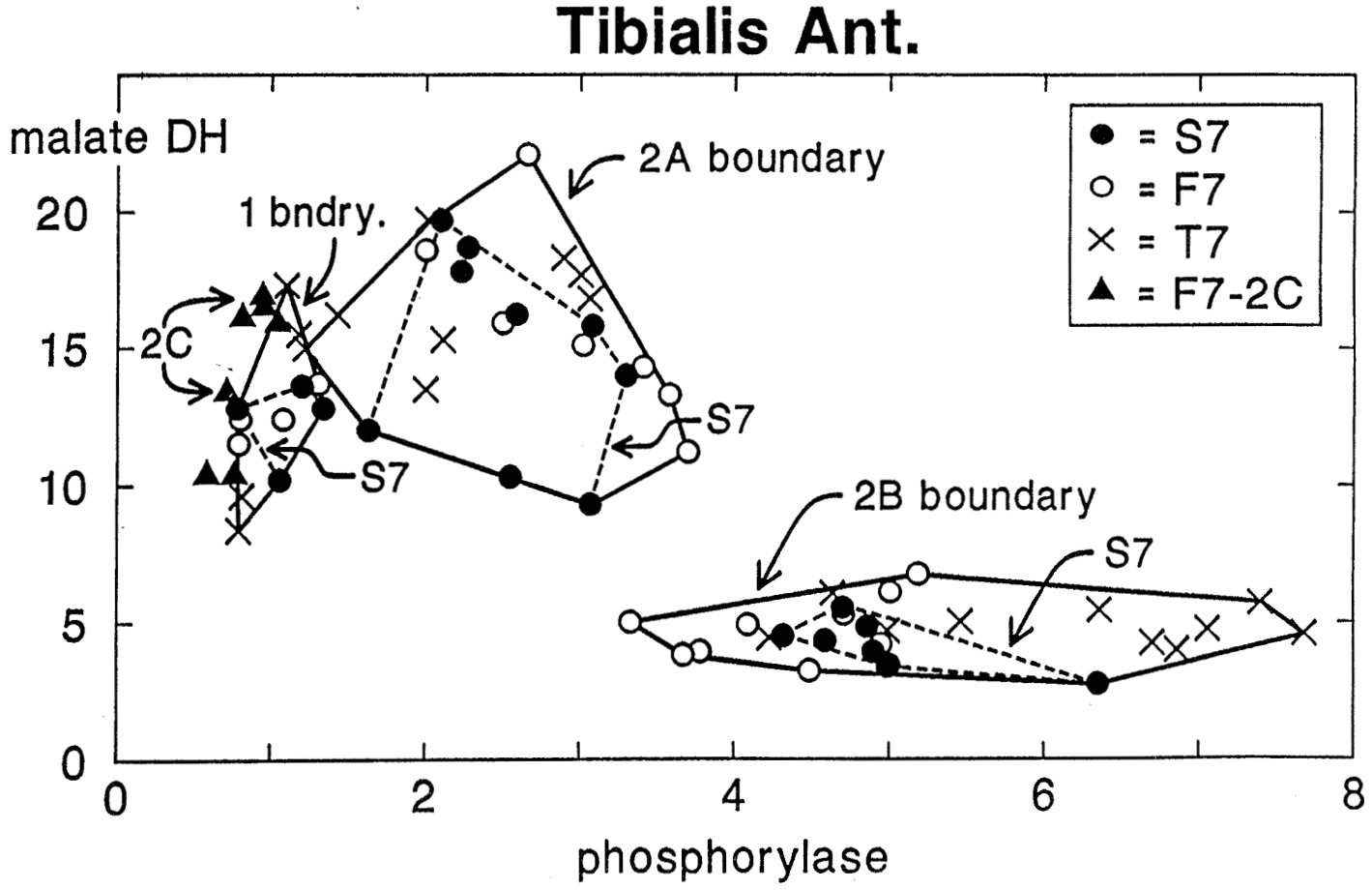

Figure 16. MDH and phosphorylase levels in individual TA fibers obtained from S7, F7, and T7 muscles and typed by myosin ATPase staining. Activities are recorded as in figure 1.

Page intentionally left blank

S8-51
57353

EXPERIMENT K-7-21

PART II: THE DISTRIBUTION OF SELECTED ENZYMES AND AMINO ACIDS IN THE HIPPOCAMPAL FORMATION.

O.H. Lowry, I. Krasnov, E.I. Ilyina-Kakueva, P.M. Nemeth, D.B. McDougal, Jr., R. Choksi, J.G. Carter, M.M.Y. Chi, J.K. Manchester and M.E. Pusateri

SUMMARY

Six key metabolic enzymes plus glutaminase and glutamate decarboxylase, as well as glutamate, aspartate and GABA, were measured in 11 regions of the hippocampal formation of synchronous, flight and tail suspension rats. Major differences were observed in the normal distribution patterns of each enzyme and amino acid, but no substantive effects of either microgravity or tail suspension on these patterns were clearly demonstrated.

METHODS

All of the assays were performed with samples dissected from 20 μm freeze dried coronal microtome sections. The size of the samples and preparation for assay varied with the substance to be measured. In the case of *aspartate* and *glutamate* samples from the 11 hippocampal areas, weighing 30-50 ng, were heated in 0.5 μl of NaOH to destroy tissue enzymes and NAD^+; 0.1 μl of this was used for glutamate and 0.4 μl for aspartate. In addition a larger sample (1-1.5 μg) from three larger subdivisions of the hippocampus from additional rats were assayed for aspartate alone.

For *GABA*, samples weighing about 200 ng were heated in 0.1 μl of dilute HCl to destroy tissue enzymes and NADPH, and then incubated with 0.06 μl of the specific reagent. Samples for glutamate decarboxylase (GAD) were of about the same size. These were added directly to the specific reagent and incubated for 2 hours to increase the proportion of GABA formed from glutamate relative to preformed GABA which constituted a tissue blank.

The six *metabolic enzymes* were measured in each case in a single 150-300 ng sample which was dispersed in 5 μl of medium similar to that used for multiple enzyme assays of the muscle samples, and which likewise allowed indefinite storage without loss at -70°C. Duplicate 0.2 μl aliquots (0.1 μl for pyruvate kinase) were then used for each separate enzyme assay.

Glutaminase, which did not tolerate storage in this special medium, was measured in individual samples and added directly to the specific reagent. For separate assays of the 11 hippocampal areas, samples weighing 10-25 ng were added to 2 μl of reagent. For the assay of larger hippocampal subdivisions, samples weighing about 600 ng were added to 10 μl of reagent.

All of the methods employed were based on the conversion of NAD^+ to NADPH, NADH to NAD^+, or NADPH to $NADP^+$. The amount of pyridine product formed varied from about 1×10^{-12} mole in the aspartate assays to about 200×10^{-12} mol in the pyruvate kinase assays. It was therefore in all cases necessary to increase the sensitivity 1,000 to 10,000-fold by enzymatic cycling.

RESULTS

Six Enzymes of Energy Metabolism

Hexokinase (Fig. 17) was most active in CA1 with a peak in stratum radiatum and levels almost as high in the CA1 molecular layer. Lowest levels were found in CA3 with intermediate hexokinase levels in fascia dentata. The lowest consistent activities were in the pyramidal layer of CA3. The exceptionally high level in stratum oriens of T6 should be checked with brains from other tail suspension animals.

Pyruvate kinase (Fig. 18) located near the other end of the glycolytic pathway, was also highest in radiatum of CA1, but levels in the other parts of CA1 were not especially high and lowest average levels were found in fascia dentata.

Citrate synthase (Fig. 19), responsible for the first step in the citrate cycle, was like hexokinase highest among subdivisions of CA1 and lowest in CA3. The peak level was, however, in the molecular layer instead of radiatum of CA1 with the molecular layer of fascia dentata a close second.

ß-hydroxyacyl CoA dehydrogenase (ßOAC) (Fig. 20), the catalyst for a key step in fatty acid oxidation, was in contrast to the three previous enzymes, present at by far the highest levels among layers of fascia dentata, with CA1 a poor second. Note the extreme contrast between the relative positions of this enzyme and the positions of hexokinase and pyruvate kinase in radiatum of CA1. In spite of this general contrast, the highest levels for both ßOAC and citrate synthase were found in the molecular layers.

Glucose-6-P dehydrogenase (G6PDH) (Fig. 21) and especially *aspartate aminotransferase* (Fig. 22) varied the least among the different regions. In the case of G6PDH, some attention should be given to the generally higher levels in many of the T6 regions.

In this regard, there are quite a few instances where enzyme activities of F8 or T6 deviate substantially from corresponding activities in S7. Note, however, that the range in most figures is only between 60% and 100%. Nevertheless, it may be possible and desirable to check on some of the largest deviations by analysis of samples from other S, F and T brains.

Glutaminase

This enzyme, associated with the role of glutamate as a transmitter, showed a wider range of activities than any of the above six purely metabolic enzymes (Fig. 23). Moreover, the distribution did not resemble that of any of these. Note that levels were on average at least as high in CA3 as in CA1, and that the levels were relatively high in stratum oriens of both CA3 and CA1 and in hylus of fascia dentata, all regions which were in general on the low end of the scale for the metabolic enzymes. Because glutaminase levels in T6 were consistently low in CA1 and CA3, this enzyme was measured in three larger samples from each of S8, S10, F8, F9, T6 and T9. These samples encompassed all the layers analyzed in Figs. 17-23 from CA1, CA3 and fascia dentata respectively (Fig. 24). Although it seems quite obvious that there are some substantial differences among the several brains, there is no sign of consistent differences attributable to flight or tail suspension. Note that in all three of these gross regions, levels are higher for S8 than S10 and higher for F9 than F8.

Glutamate and Aspartate

Both glutamate and aspartate varied over about a 30% range among the 12 subdivisions of the hippocampal formation analyzed (Fig. 25). There was a statistically significant correlation between

aspartate and glutamate of S7 ($r=0.605$, $P < 0.05$) but not between these two amino acids for F8. There was also a highly significant correlation between *glutamate* levels of S7 and F8 ($r=0.832$, $p < 0.01$) but not between *aspartate* levels of S7 and F8. Because of this and because aspartate appeared substantially higher in F8 than S7 for 3 portions of CA1, and lower in all but 1 portion of CA3, CA4, and fascia dentata (Fig. 9), aspartate concentrations were determined as in the case of glutaminase in 3 larger samples from each of S8, S10, F8, F9, T6, and T9. These samples were respectively comprised of all the segments represented in either the CA1, CA3 or fascia dentata zones of Fig. 25. The results (Fig. 26) show that aspartate is higher in S10 than S8 in each of the 3 zones, lower in F9 than F8 in each of the 3 zones, and higher in T9 than T6 in each of the 3 zones. Thus, consistent and substantial differences in aspartate concentrations do exist within the hippocampus of different rats. However, there is no significant difference on this score between synchronous and flight hippocampi or synchronous and tail suspension hippocampi.

Glutamate Decarboxylase (GAD) and GABA (Tables 5 and 6)

GAD was consistently highest in the molecular layers of CA1 and fascia dentata and pyramidal layers of CA1. Lowest levels were observed in stratum oriens and radiatum (Figs. 27, 28). This enzyme was also subject to wide variation; note especially the differences in levels between S7 and S9 in four of the subdivisions of CA3 and fascia dentata. This makes it difficult to come to any conclusion about possible effects of flight or tail suspension.

GABA data were somewhat more consistent (Figs 29, 30). Relatively high levels were also found in the pyramidal cell and molecular layers, and the concentrations in the granular layer of fascia dentata were among the highest. There was no sign of consistent effects of flight or tail suspension on the GABA levels.

TABLE 5

GLUTAMATE DECARBOXYLASE DISTRIBUTION AMONG ELEVEN AREAS OF THE HIPPOCAMPAL FORMATION

Area	S7	S9	F8	F10	T6	A11
CA1						
Oriens	14.5 (6) ± 1.8	17.8 (3) ± 0.9	18.4 (5) ± 2.8	16.5 (3) ± 2.5	21.3 (5) ± 1.8	17.7 ± 1.1
Pyramidalis	35.1 (6) ± 4.4	30.6 (4) ± 1.0	31.5 (4) ± 3.3	31.7 (3) ± 1.0	43.1 (6) ± 1.2	34.4 ± 2.3
Radiatum	21.3 (4) ± 1.0	17.4 (5) ± 0.8	21.7 (4) ± 1.4	20.7 (3) ± 1.0	18.5 (8) ± 0.8	19.9 ± 0.8
Molecularis	38.0 (7) ± 1.0	32.1 (3) ± 2.3	36.2 (3) ± 3.7	30.8 (3) ± 2.7	39.3 (7) ± 1.0	35.3 ± 1.6
CA3						
Oriens	25.1 (3) ± 2.4	21.0 (3) ± 3.1	34.4 (6) ± 4.1	17.5 (3) ± 0.5	27.5 (6) ± 4.4	25.1 ± 2.9
Pyramidalis	28.3 (2) ± 3.4	22.9 (3) ± 1.6	36.6 (5) ± 3.5	18.6 (3) ± 1.0	32.5 (5) ± 4.1	27.8 ± 3.2
Radiatum	33.4 (7) ± 2.1	16.9 (3) ± 0.3	19.4 (6) ± 1.6	16.4 (3) ± 0.6	24.8 (5) ± 0.9	22.2 ± 3.2
CA4						
Pyramidalis	23.6 (2) ± 0.8	21.0 (4) ± 1.3	27.1 (3) ± 1.0	27.2 (3) ± 1.6	21.0 (2) ± 3.8	24.0 ± 1.4
Fascia Dentata						
Molecularis	45.6 (8) ± 3.8	24.6 (3) ± 1.2	38.5 (4) ± 4.9	46.1 (4) ± 2.9	49.9 (7) ± 2.4	40.9 ± 4.5
Granularis	21.7 (3) ± 0.5	36.1 (4) ± 1.4	22.1 (3) ± 0.5	40.8 (2) ± 2.0	- -	30.2 ± 4.9
Hylus	28.0 (3) ± 2.0	22.1 (3) ± 2.0	24.6 (2) ± 3.0	26.4 (3) ± 2.2	23.5 (3) ± 0.5	24.9 ± 1.0

TABLE 6

GABA DISTRIBUTION AMONG ELEVEN AREAS
OF THE HIPPOCAMPAL FORMATION

Area	S7	S9	F8	F10	T6	All
CA1						
Oriens	6.0 (7) ± 0.2	8.3 (4) ± 0.3	13.5 (4) ± 0.6	8.4 (4) ± 0.6	7.2 (6) ± 0.8	8.7 ± 1.3
Pyramidalis	12.3 (9) ± 0.9	11.9 (6) ± 0.4	15.6 (3) ± 2.5	15.2 (3) ± 1.7	10.3 (6) ± 0.4	13.0 ± 1.0
Radiatum	10.0 (4) ± 0.3	8.8 (6) ± 0.2	10.3 (3) ± 1.0	9.0 (4) ± 0.2	10.1 (3) ± 0.4	9.6 ± 0.3
Molecularis	13.0 (7) ± 0.6	13.3 (5) ± 1.0	16.0 (5) ± 0.5	13.0 (4) ± 0.3	13.3 (5) ± 0.6	13.7 ± 0.5
CA3						
Oriens	8.3 (3) ± 1.9	14.7 (6) ± 1.5	11.8 (5) ± 1.1	15.0 (3) ± 0.3	10.5 (6) ± 0.9	12.4 ± 1.2
Pyramidalis	15.0 (5) ± 0.6	19.2 (5) ± 1.4	16.5 (4) ± 0.9	18.4 (2) ± 0.1	15.6 (5) ± 0.8	16.9 ± 0.8
Radiatum	14.7 (7) ± 0.4	15.0 (6) ± 0.5	12.0 (5) ± 1.0	12.2 (3) ± 0.6	14.7 (5) ± 0.4	13.8 ± 0.5
CA4						
Pyramidalis	14.8 (7) ± 0.8	15.1 (5) ± 1.1	13.9 (2) ± 0.1	14.8 (4) ± 0.6	16.8 (2) ± 0.1	15.0 ± 0.4
Fascia Dentata						
Molecularis	15.8 (7) ± 0.5	16.3 (5) ± 1.4	18.7 (6) ± 1.7	14.1 (3) ± 0.4	16.3 (3) ± 0.2	16.2 ± 0.7
Granularis	15.8 (4) ± 0.3	20.9 (4) ± 0.9	14.9 (4) ± 0.6	18.1 (4) ± 2.1	15.0 (4) ± 0.5	17.2 ± 1.1
Hylus	14.7 (3) ± 1.5	13.6 (8) ± 1.0	13.2 (3) ± 0.8	11.7 (3) ± 0.8	15.6 (2) ± 0.2	13.8 ± 0.6

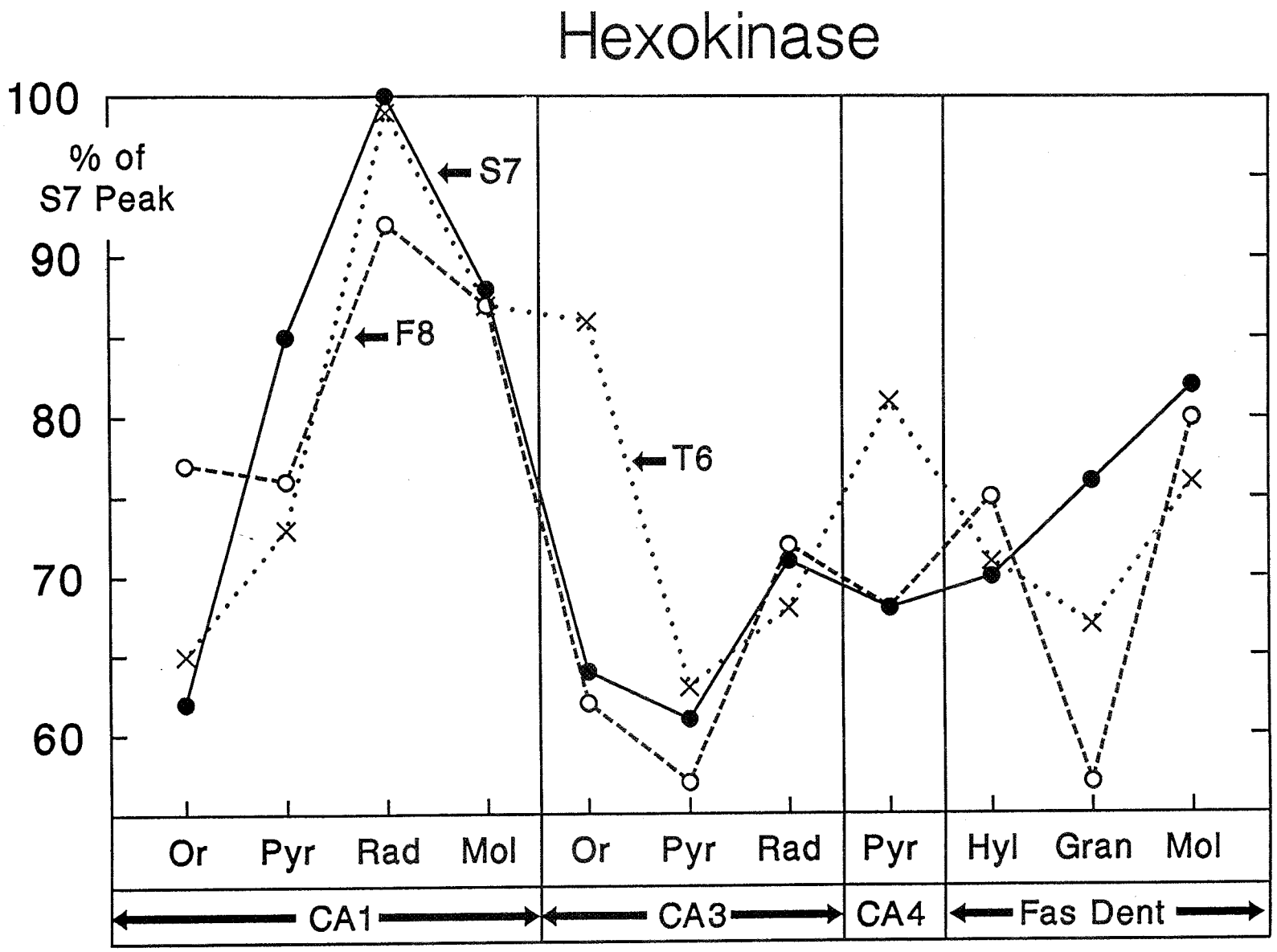

Figure 17. Hexokinase in hippocampal subdivisions of S7, F8 and T6. The peak activity in S7 was 8 mol kg^{-1} (dry) h^{-1} at $20^{o}C$. Abbreviations are: Or, Oriens; Pyr, pyramidalis; Rad, radiatum; Mol, molecularis; Gran, granularis; and Hyl, hylus.

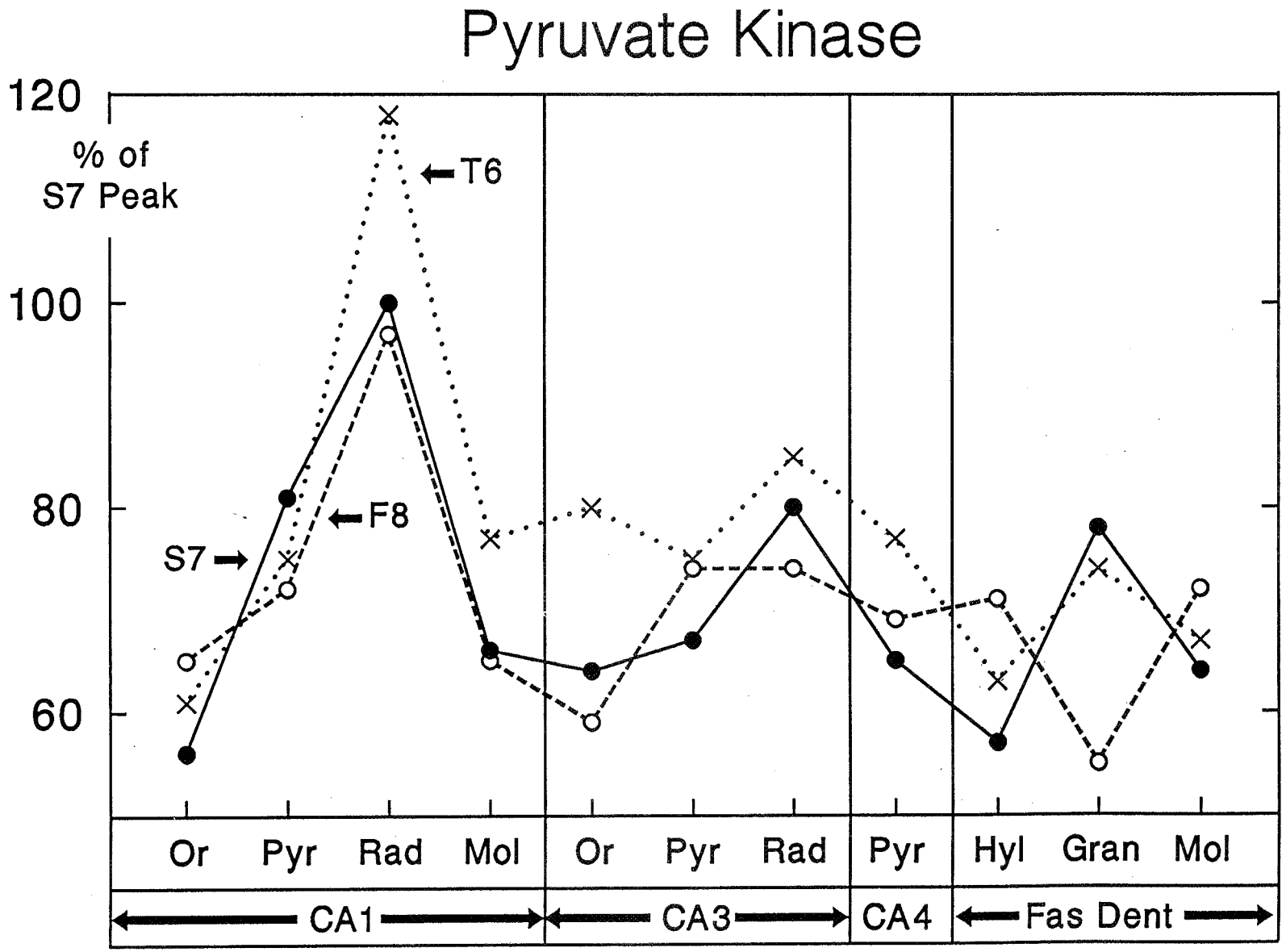

Figure 18. Pyruvate kinase in hippocampal subdivisions of S7, F8 and T6. The peak level in S7 was 74 mol kg^{-1} (dry) h^{-1} at 20°C. Abbreviations as for figure 17.

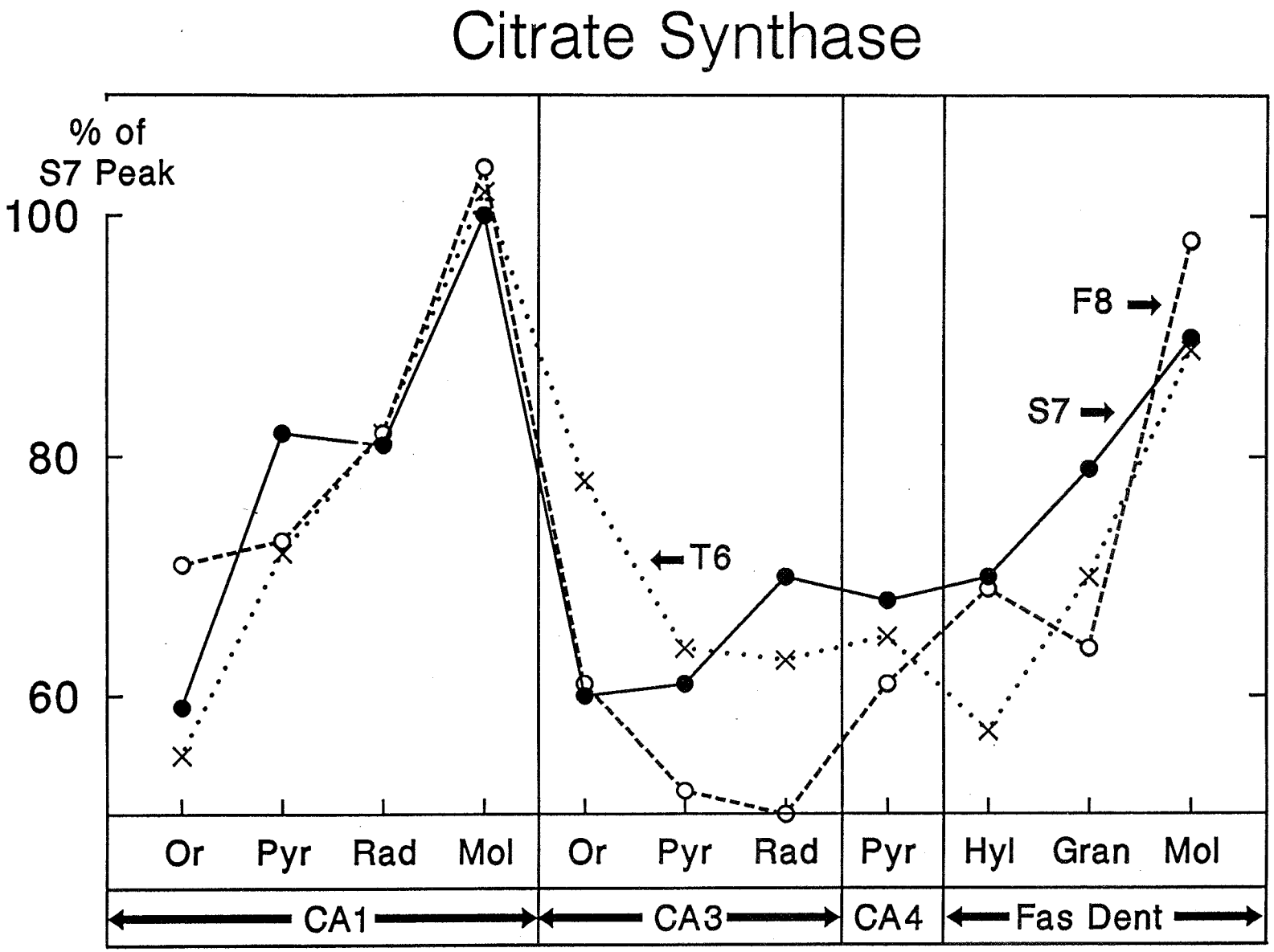

Figure 19. Citrate synthase in hippocampal subdivisions of S7, F8 and T6. The peak activity in S7 was 11 mol kg^{-1} (dry) h^{-1} at 20°C. Abbreviations as for figure 17.

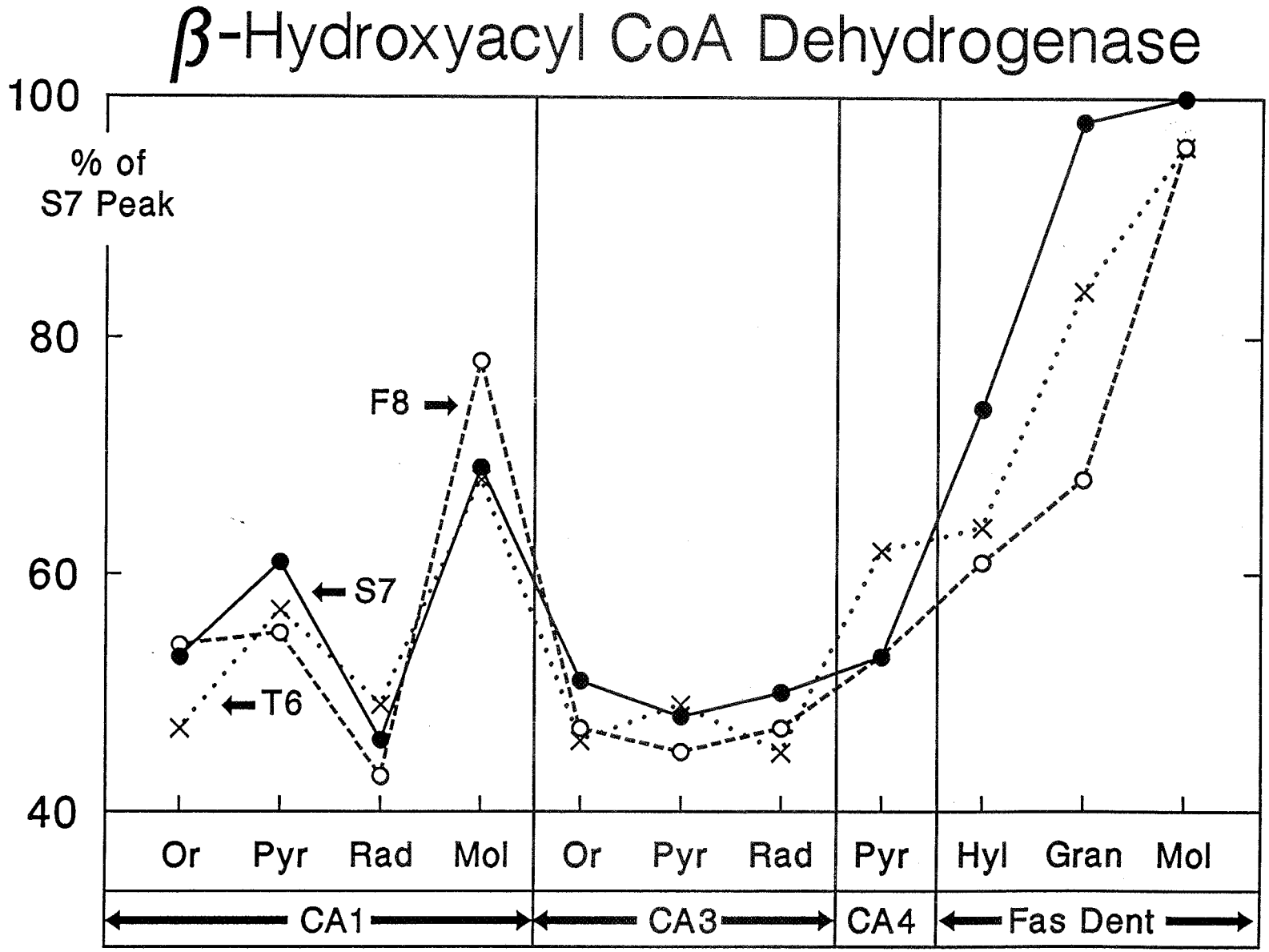

Figure 20. ß-hydroxyacyl CoA dehydrogenase in hippocampal subdivisions of S7, F8 and T6. The peak activity in S7 was 1.7 mol kg^{-1} (dry) h^{-1} at 20°C. Abbreviations as for figure 17.

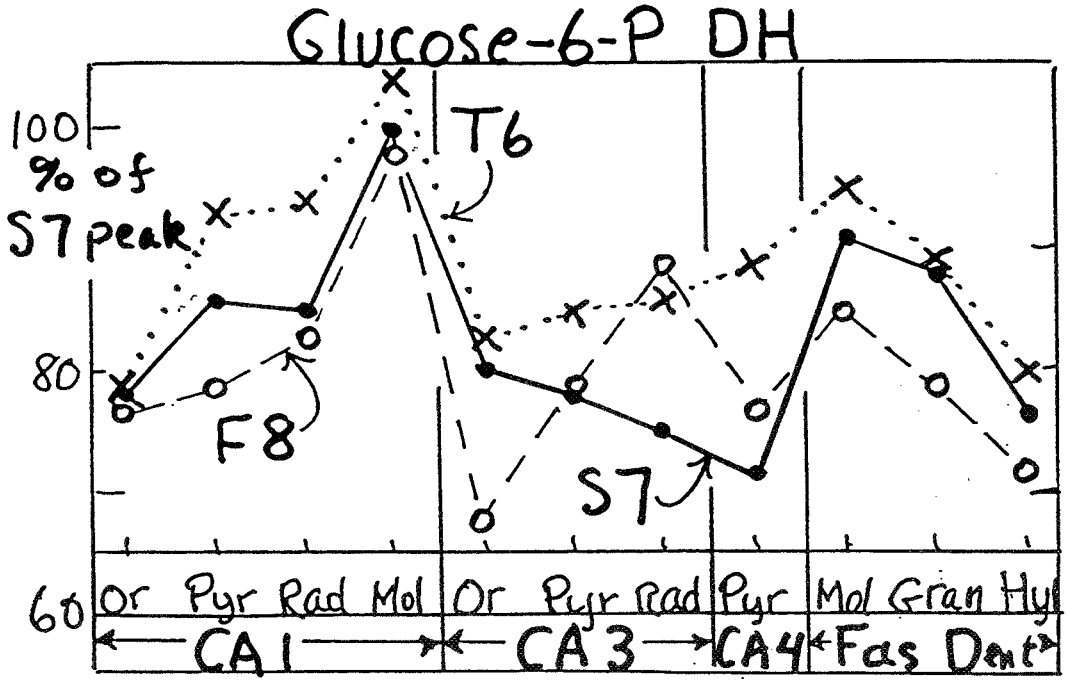

Figure 21. Glucose-6-phosphate dehydrogenase in hippocampal subdivisions of S7, F8 and T6. The peak activity in S7 was 0.36 mol kg^{-1} (dry) h^{-1} at 20°C. Abbreviations as for figure 17.

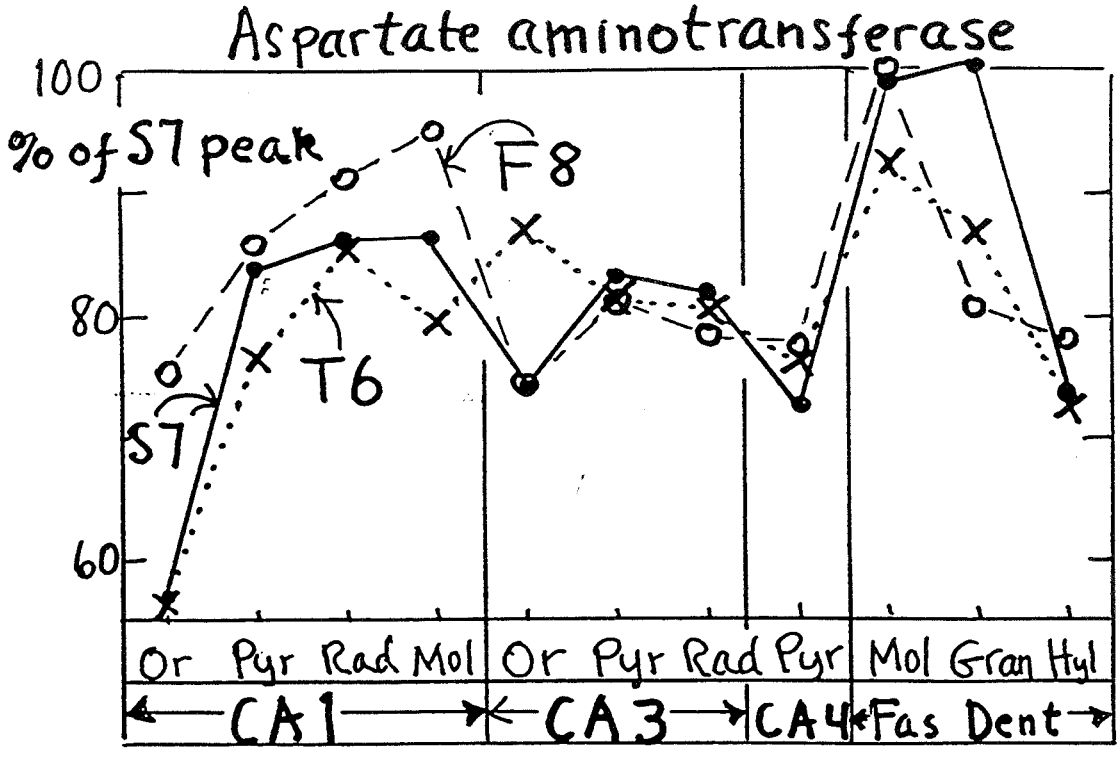

Figure 22. Aspartate aminotransferase in hippocampal subdivisions of S7, F8 and T6. The peak activity in S7 was 31 mol kg^{-1} (dry) h^{-1} at 20°C. Abbreviations as for figure 17.

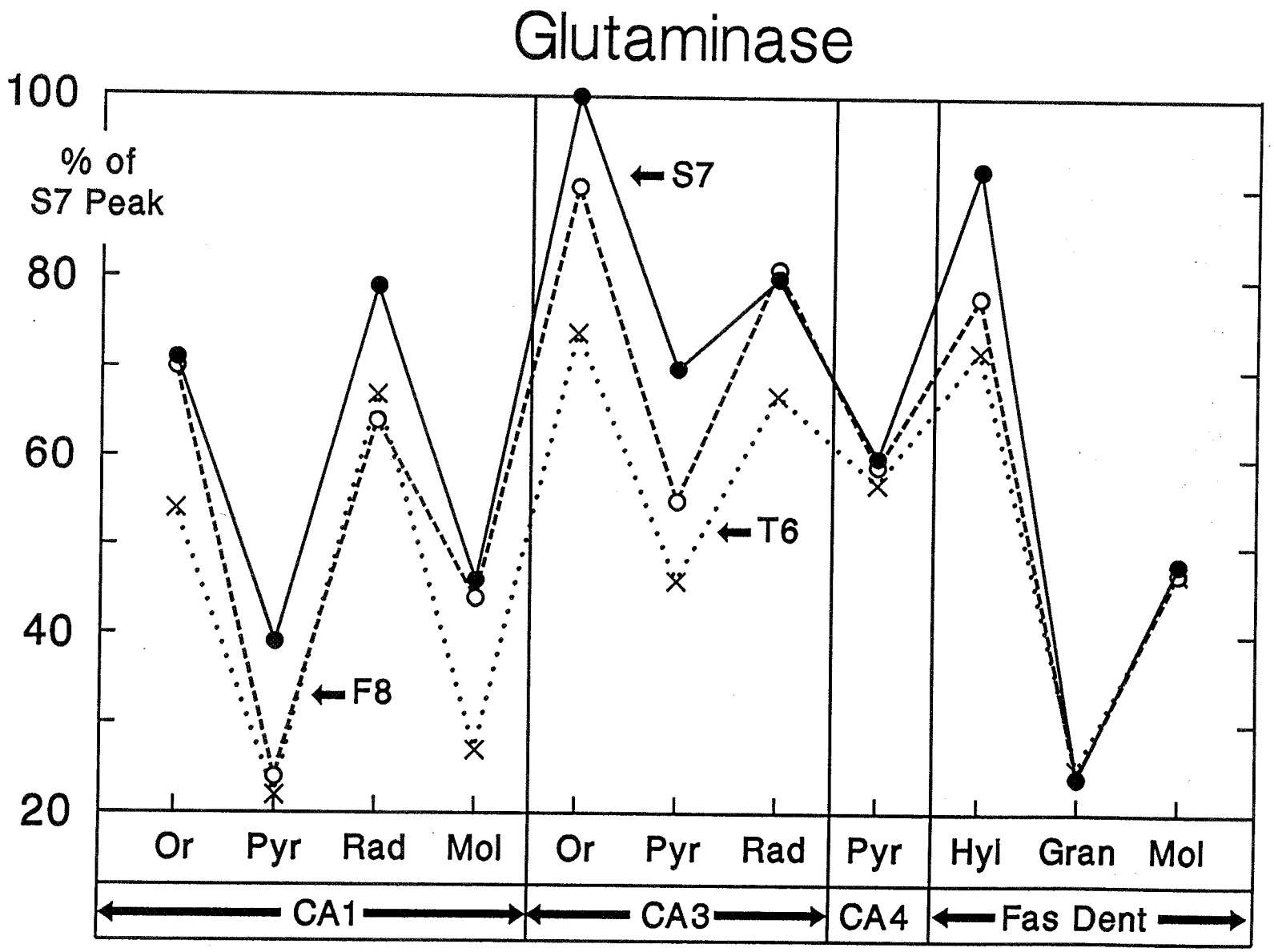

Figure 23. Glutaminase levels in hippocampal subdivisions of S7, F8 and T6. The peak level in S7 was 8.6 mol kg^{-1} (dry) h^{-1} at 20°C. Abbreviations as for figure 17, plus Lu, stratum lucidum.

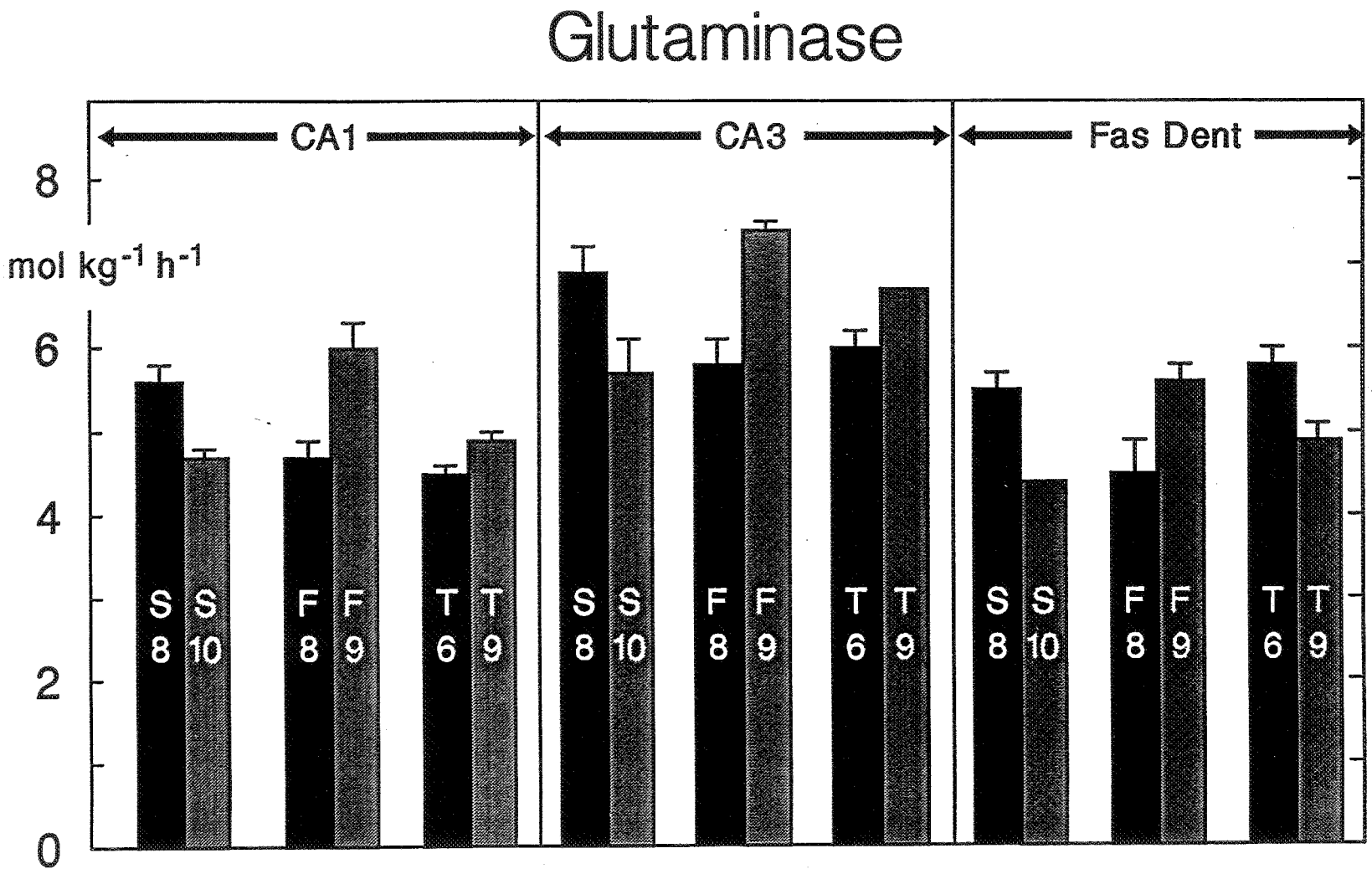

Figure 24. Bar graph of glutaminase levels in 3 major zones of hippocampus of S8, S10, F8, F9, T6 and T9. Standard errors are indicated.

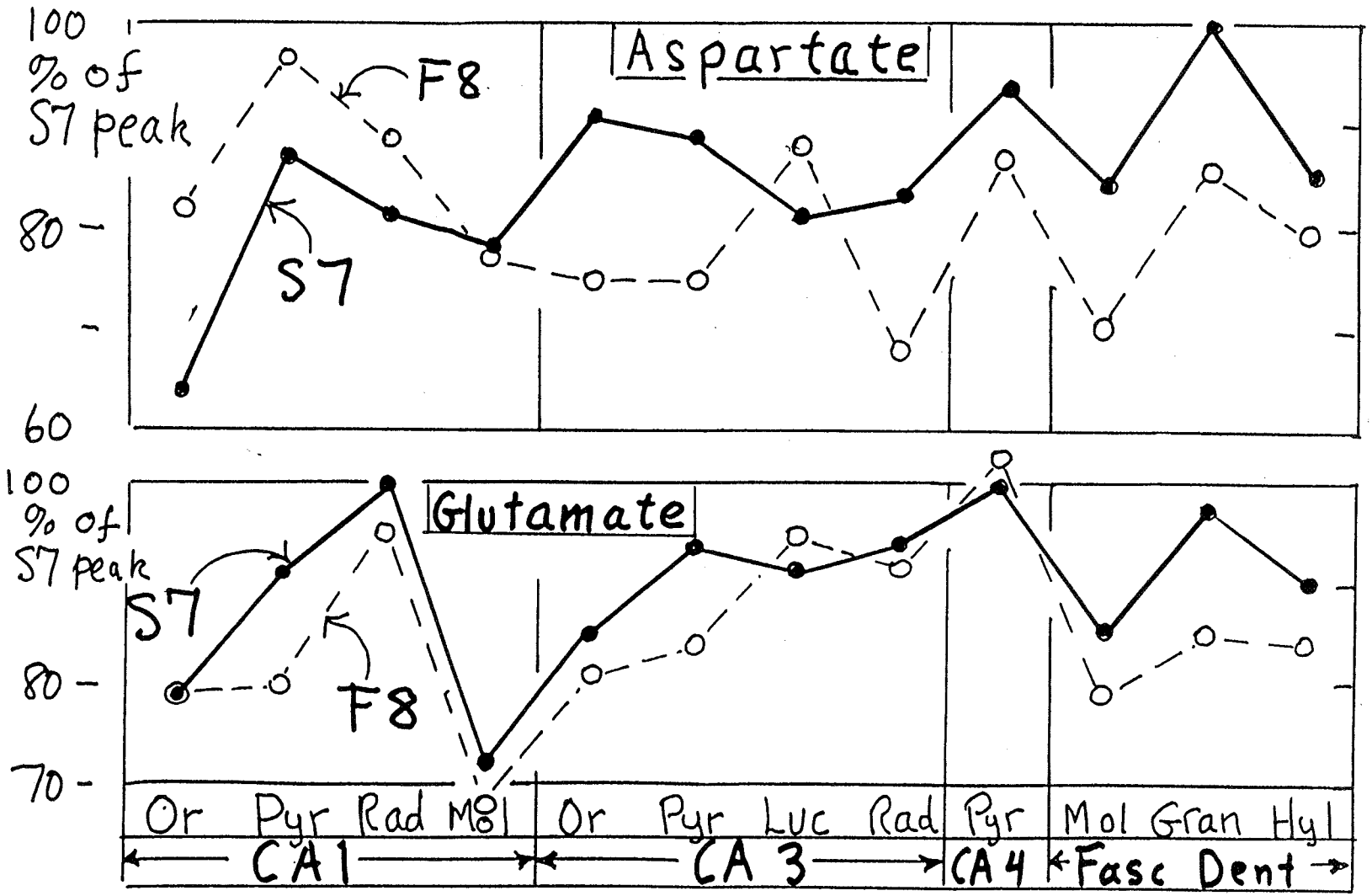

Figure 25. Aspartate and glutamate in hippocampal subdivisions of S7 and S8. The peak levels in S7 were 14.6 and 73 mmol kg^{-1} (dry), respectively.

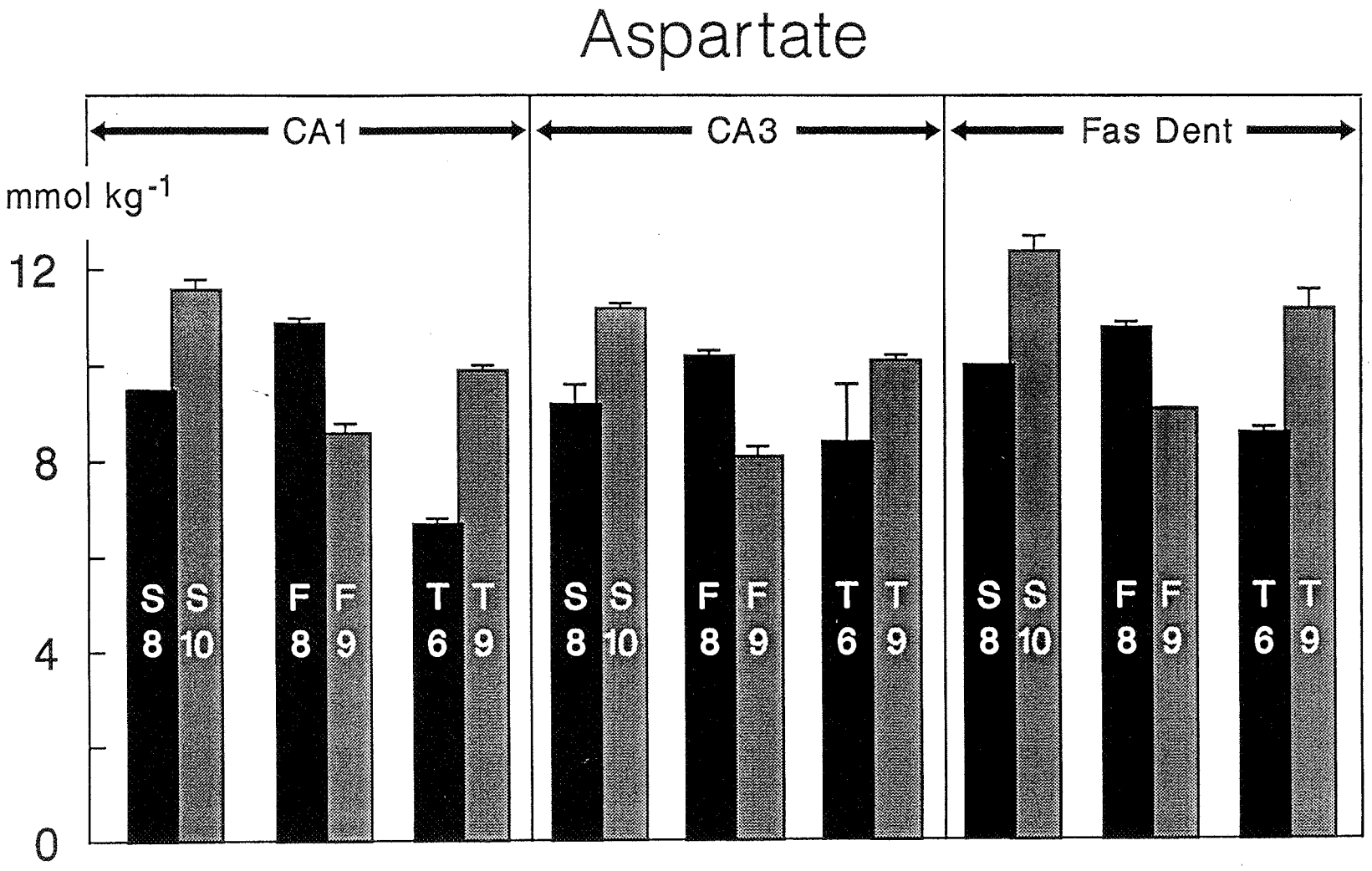

Figure 26. Bar graph of aspartate levels in 3 major hippocampal zones of S8, S10, F8, F9, T6 and T9.

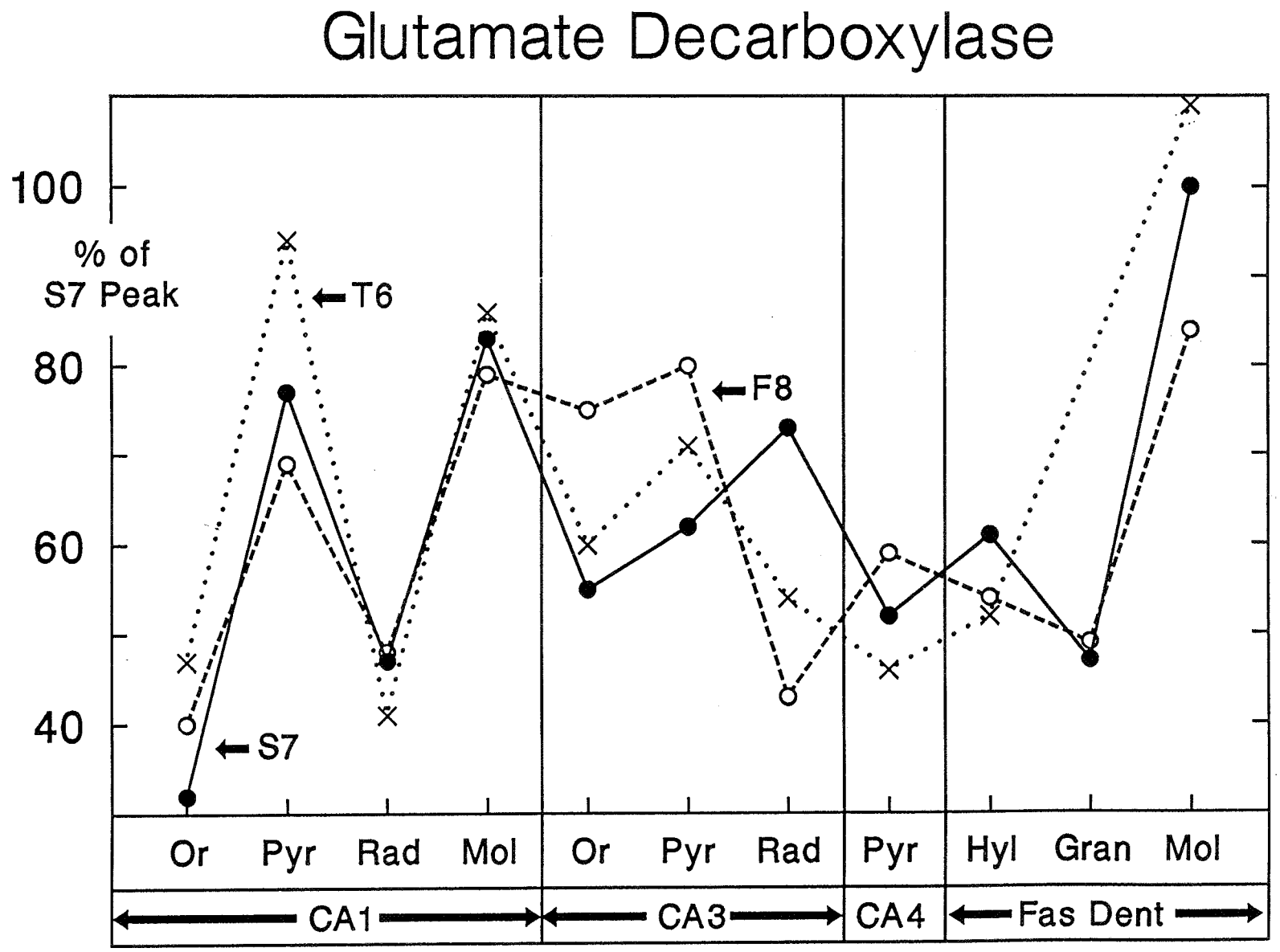

Figure 27. GAD levels in hippocampal subdivisions of S7, S9, F8, F10 and T6. The peak activity in S7 was 46 mmol kg^{-1} (dry) h^{-1} at 38°C.

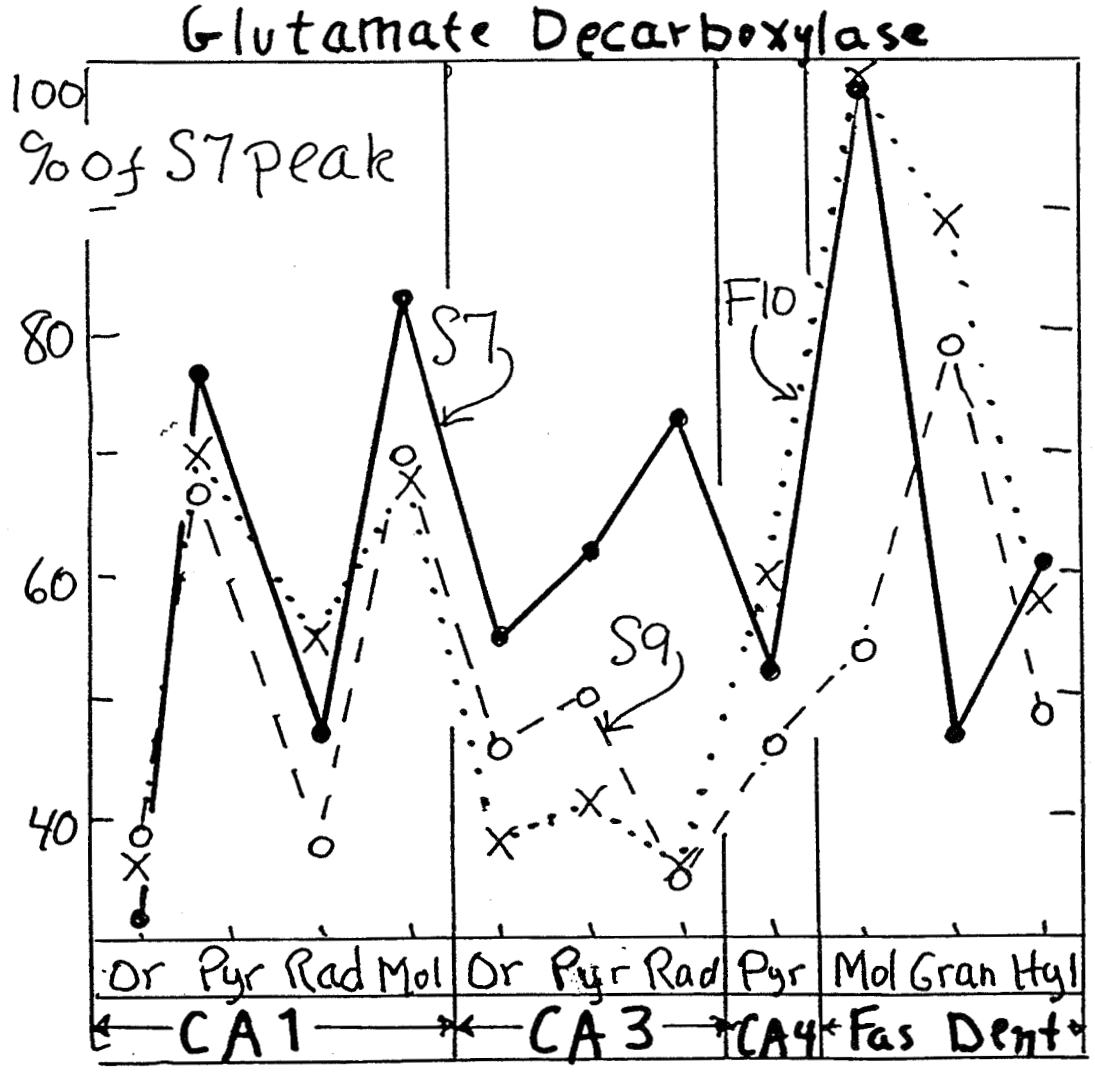

Figure 28. GAD levels in hippocampal subdivisions of S7, S9, F8, F10 and T6. The peak activity in S7 was 46 mmol kg^{-1} (dry) h^{-1} at 38°C.

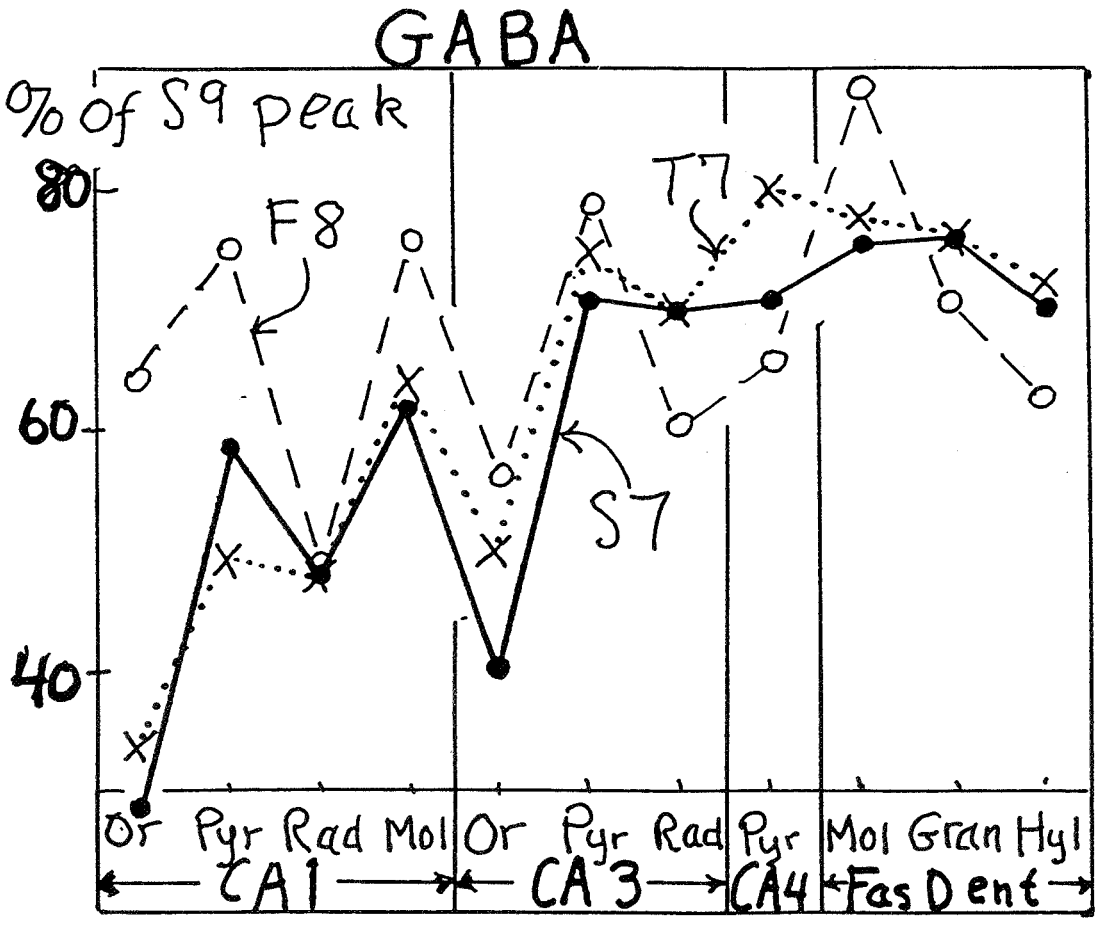

Figure 29. GABA levels in hippocampal subdivisions of S7, S9, F8, F10 and T6. The peak concentration in S9 was 21 mmol kg^{-1} (dry).

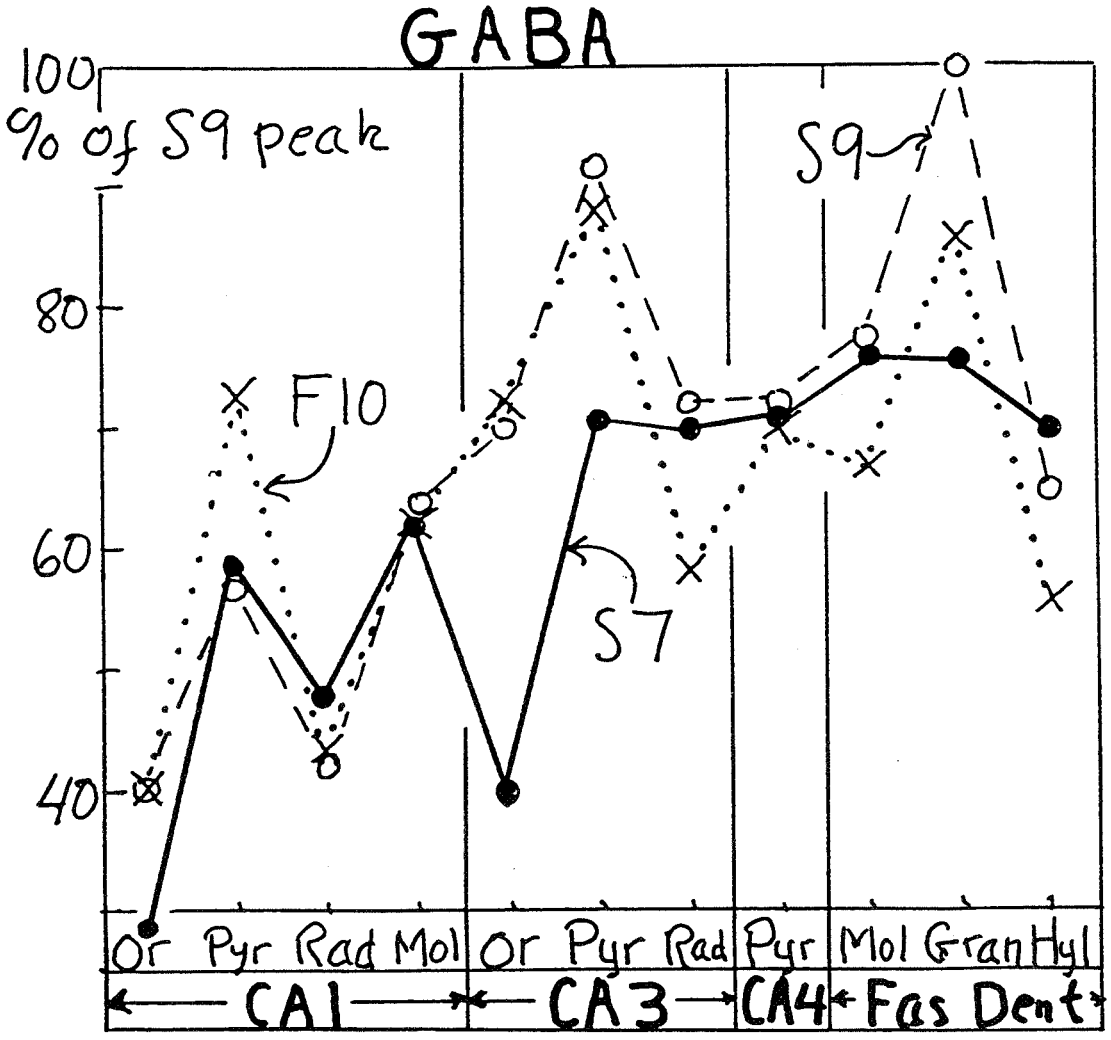

Figures 30. GABA levels in hippocampal subdivisions of S7, S9, F8, F10 and T6. The peak concentration in S9 was 21 mmol kg^{-1} (dry).

EXPERIMENT K-7-22

GROWTH HORMONE REGULATION SYNTHESIS AND SECRETION IN MICROGRAVITY

PART I: GROWTH HORMONE REGULATION SYNTHESIS AND SECRETION IN MICROGRAVITY

PART II: HYPOTHALAMIC GROWTH HORMONE-RELEASING FACTOR, SOMATOSTATIN IMMUNOREACTIVITY AND MESSENGER RNA LEVELS IN MICROGRAVITY

PART III: PLASMA HORMONE MEASUREMENTS

PART IV: MUSCLE HORMONE RECEPTORS (NOT AVAILABLE AT TIME OF PUBLICATION)

Principal Investigator:

R. Grindeland
NASA Ames Research Center
Moffett Field, CA

Co-Investigators:

W. Hymer
Pennsylvania State University
University Park, PA

C. Arias
P. Sawchenko
W. Vale
Salk Insitutue
La Jolla, CA

E. Grossman
I. Rudolph
NASA Ames Research Center
Moffett Field, CA

E.I. Ilyina-Kakueva
I.B. Krasnov
I. Popova
Insitute of Biomedical Problems
Moscown, USSR

I. Victorov
Brain Research Institute
USSR Ministry of Health

Page intentionally left blank

59-57
51354

EXPERIMENT K-7-22

PART I: GROWTH HORMONE REGULATION SYNTHESIS AND SECRETION IN MICROGRAVITY

W.C. Hymer, R. Grindeland, W. Vale, P. Sawchenko and E.I. Ilyina-Kakueva

INTRODUCTION

Changes in the musculoskeletal, immune, vascular and endocrine system of the rat occur as a result of short-term spaceflight (9). Since pituitary gland growth hormone (GH) plays a role in the control of these systems, and since the results of an earlier spaceflight mission (Spacelab 3, 1985) showed that GH cell function was compromised in a number of post-flight tests (12), we repeated and extended the 1985 experiment in two subsequent spaceflights: the 12.5 day mission of Cosmos 1887 (in 1987) and the 14 day mission of Cosmos 2044 (in 1989). The results of these later two flight experiments are the subject of this report. They document repeatable and significant changes in the GH cell system of the spaceflown rat in several post-flight tests.

METHODS AND MATERIALS

Details of the 1887 and 2044 missions, hereafter referred to as experiments 1 and 2, respectively, are described elsewhere (9,10). In each experiment, anterior pituitary glands from 5 flight (F) and 5 synchronous control rats (C) were removed aseptically and transported in individual teflon vials from the landing site to the laboratory in Moscow. Results of extensive pre-flight testing indicated that storage of intact pituitary glands for 24-26 hrs at room temperature in Spinners Minimum Essential Medium (SMEM) containing 0.1% bovine serum albumin, 25mM Hepes buffer (pH 7.4), 0.2% $NaHCO_3$, gentamycin sulfate (10 µg/ml), and penicillin (100 U/ml)/streptomycin (100 µg/ml) was optimal for subsequent preparation of cells with high viability (>90%) and good yield (~1.7×10^6) (data not shown). Each of these parameters is within the range of those reported for preparation of fresh cells from the rat pituitary (14). During transport of the glands in the above medium (22 ml/vial) the temperature was maintained between 23-24°C.

Cells were prepared from individual glands by trypsinization (7) and kept separate during culture tests to permit statistical analysis of the data. However, some tests required large numbers of cells, so samples from each gland within a group were pooled. The protocol for both flight experiments was similar except that in Exp. 2 an additional group of animals was subjected to tail suspension on Earth for 14 days in order to see how well the results from this approach (19) mimicked actual spaceflight. (Figure 1). In each experiment, 5 Wistar male rats/group were housed under conditions detailed in (9,10).

Specific Methods (individual glands)

Cell Preparation:

Cells were prepared by trypsinization, counted by hemocytometry and their viability determined as described previously (13).

Cell Culture:

Cells ($2.5x10^5$) - Exp. 1; $5x10^4$) - Exp. 2) were cultured in 250 µl of modified Eagle's medium (αMEM) containing 5% calf serum and antibiotics (24) or in chemically defined medium containing insulin, transferrin, selenium and other trace elements in MEM base (24) in 96-well plates for 3 days in a humidified atmosphere of 5% CO_2:95% air at 37°C. There were 3 or 4 wells of cells from each gland. After 3 days the media were saved, stored at -20°C and fresh media added for an additional 3 day culture.

Intracellular Hormone Extraction:

Cells were incubated overnight in 0.01N $NaHCO_3$ at 4°C, particulate material centrifuged (1000 xg, 30 min) and the supernatant fraction frozen for later hormone analyses. Greater than 90% of intracellular GH and prolactin (PRL) is extracted under these conditions (7).

Hormone Assays:

Concentrations of immunoreactive GH and PRL in culture media and extracts were determined by established enzyme immunoassays (5,6,23). The antisera for GH and PRL have been validated; their cross reactivities are <0.3% at the final dilutions used (1:80,000-GH; 1:40,000-PRL) (13). The tibial line bioassay of Greenspan (8) was used to measure concentrations of bioactive GH. These were 4 point assays, using a bovine GH (1.5 IU/mg) preparation as standard. These data are expressed in terms of rat GH (3.0 IU/mg). PRL bioassays used were either the NB-2 lymphoma cell division assay originally described by Tanaka et. al. (26) or the IL2 receptor assay of Mukherjee et. al. (21). Results of all these assays are expressed in terms of rat GH Standard (B-11) or PRL Standard (B-6) kindly provided by the National Institute of Diabetes and Digestive and Kidney Diseases (NIDDK) and the National Hormone and Pituitary Program (University of Maryland School of Medicine).

Morphology:

Immunocytochemistry for GH cells ($2.5x10^4$) attached to poly-l-lysine-coated coverslips was done using a diaminobenzidine procedure (13). These preparations were used for 1) determining GH cell percentages (Exp. 2 only) using a scoring method on coded samples by 6 investigators, and 2) determining the cytoplasmic area occupied by GH, a procedure which involved image analysis that uses a digitized color image of the stained cell to quantify both the area of the cell stained and the intensity of the stain. An OASYS optical analysis system (Lemont Scientific, State College, PA) was used to digitize the image and colorize according to intensities within the system's 256 gray levels (17) so that the area of GH-specific cytoplasmic staining could be quantitated. Care was taken to maintain constant light settings, condenser height, and aperture size in addition to normalizing variations in light using a light meter placed at the level of the camera.

Specific Methods (pooled cells)

Cell Implants:

In order to determine the amount of bioactive GH secreted from cells of flight animals after implantation into hypophysectomized rats, the hollow fiber method of Hymer et. al. was used (16). In this case, $2x10^5$) cells were loaded into 10 mm long XM 50 Amicon fibers (n=10/treatment group) and implanted into the lateral cerebral ventricles of 100 g male rats 7 days after pituitary gland removal. Ten days post-implantation, the tibia of the host animals

were prepared for staining and measurements of epiphyseal cartilage width taken with an ocular micrometer. Fiber placement was verified by visual inspection of brain slices. This implantation procedure was done only in Exp. 1.

Flow Cytometry:

Cells ($2x10^5$)) were fixed in suspension, their membranes permeabilized with 0.1% Triton X-100, incubated in GH or PRL antisera (1:10,000) overnight, followed by incubation in FITC-conjugated antisera, counterstained with propidium iodide and analyzed on an Epics flow cytometer (Model 753) exactly as described (13). Analysis included the determination of GH and PRL cell percentages (30,000 cells/trial), intensity of hormone fluorescence, size (forward angle light scatter, FALS) and cytoplasmic granularity (perpendicular light scatter, PLS).

Statistical Analysis:

When appropriate, data were analyzed by ANOVA and the Students t-test using $p<0.05$ as a significant difference.

RESULTS

Hormone Contents of Storage (Transport) Media

GH:

The concentrations of GH and PRL in the 30 hr. storage media of F, C, and tail suspended (TS) animal groups are shown in Table 1. These levels reflect hormone release from the glands into the media during tissue transportation. In Exp. 1 there was a significant increase in levels of immunoreactive GH (iGH) in F vials relative to the C group; in Exp. 2 levels of iGH were significantly decreased in the flight group. However, in the F groups of both experiments, there was a marked reduction in levels of biologically active GH (bGH) secreted into the medium. Transport media from glands of the TS animals was markedly elevated in iGH, but was again significantly lower in bGH content.

PRL:

Concentrations of PRL in the transport media, measured by immunoassay (iPRL), NB2 bioassay or IL-2R assay (bPRL) were usually similar between all treatment groups; however, transport media from the TS group usually had lower amounts of PRL (Table 1).

Characteristics of GH and PRL Cells:

The yield of cells from individual glands of most groups averaged $1.9x10^6$) with viabilities >90% (Table 2). The reason for lower yield and viability in the TS group is unknown. Relative to the GH cells in the C group, F GH cells were a) lower in frequency in Exp. 2 but not affected in Exp. 1; b) markedly and consistently increased (2 fold) in GH-specific immunofluorescence staining intensities; c) slightly larger, as evidenced by increased FALS signal; d) not different in PLS signal, and e) consistently and significantly different in the cytoplasmic area occupied by GH (Table 2). As with F cells, GH cells from the TS group were less frequent than those in the C group; however, in the other parameters they were more like C cells. An example of the increased GH-specific cytoplasmic staining intensity seen in F cells from Exp. 1 is shown in Fig. 2.

Relative to the PRL cells in the C group, F PRL cells were a) inconsistent in differences in their frequency distribution and PLS laser light scatter signals; b) somewhat larger (FALS),

and c) not different in staining intensities. PRL cells from the TS group again tended to be lower in responses than those in the F and C groups.

In both experiments the intracellular concentrations of iGH before or after culture tended to be similar between all treatment groups; however, the intracellular concentrations of bGH in the F group, both before and after the culture, were always significantly lower than the corresponding C group. This was also true for cells from the TS group.

Release of GH from F Cells Post-Flight:

In general, levels of iGH in media of the first 3 day and second 3 day cultures were not significantly different between treatment groups. The limited sensitivity of the tibial line bioassay precluded analysis of bGH in media of individual culture wells. However, the levels of bGH in pooled culture media from F or TS cells were so low that they were either below the assay sensitivity (Exp. 1) or were reduced by ~50% relative to those in the C media (Exp. 2).

The design of Exp. 1, but not Exp. 2, also allowed us to test the ability of the F cells to secrete bGH upon implantation into the cerebral ventricles of hypophysectomized rats. As seen in Table 1, GH secretion from post-flight F cells in this *in vivo* test was one-half of that produced by the C cell implants.

DISCUSSION

The first objective of experiments 1 (Cosmos 1887) and 2 (Cosmos 2044) was to determine whether our earlier findings on the SL-3 mission (12) were repeatable and statistically significant. A second objective was to determine whether the biological (B) and immunological (I) potencies of the GH and PRL molecules secreted from the flight cells during various post-flight trials were similar. The rationale for this objective is based on reports that the B/I activity ratio of hormone preparations are not necessarily one (4); therefore a marked change in the activity of one form as a result of spaceflight might help identify one hormonal mechanism underlying the cause of microgravity-induced osteopenia, muscle atrophy, suppression of the immune system, etc. A third objective of experiment 2 was to test the effects of tail suspension on the same parameters that we chose to test with the flight cells. Tail suspension is an established model for mimicked microgravity (19) but the fidelity of the mimic is not completely defined. Our previous preliminary studies indicated that secretion of iGH from cells of suspended rats was suppressed (28); the Cosmos 2044 mission offered us the unique opportunity to test the effects of tail suspension on the same functional and morphological parameters that we did on the flight cells so that the results could be compared directly with actual flight data.

In Figs. 3 and 4, a comparison of the post-flight secretory activities of GH and PRL cells with that of their ground-based counterparts is presented as ratios of F/C responses. It is interesting that in every spaceflight in which a GH bioassay measurement was made the F/C ratio was always <1 (7/7), and the magnitude of the suppression was usually on the order of 50-75%. On the other hand GH secretory responses measured by immunoassay were obviously inconsistent; about half of the time they were lower (4/8) than responses from the control groups. It is also interesting that the GH secretory responses patterns between the TS and flight cells in Exp. 2 are very similar (cf. Fig 3C vs. 3D). This similarity clearly establishes the utility of the tail suspension model as a means of mimicking spaceflight and this experimental approach can therefore be expected to aid considerably in the design of future spaceflight experiments.

The issue of the dichotomy between the activities of secreted bGH and iGH, initially reported in 1974 (4), is obviously important to understanding the mechanism(s) underlying these

microgravity-induced changes. Ongoing studies from our laboratories have established a) that a subpopulation of GH cells preferentially releases bGH *in vitro* and *in vivo*, (11) and b) that aggregate forms of the 22 K GH molecule have enhanced hormone biopotency (7). We hypothesize that exposure to microgravity could alter the secretory activity of a subpopulation of GH cells, perhaps mediated through changes in intracellular packaging of the hormone molecule. The Cosmos experiments offer three clues to unraveling mechanism(s) underlying the GH secretory defect. *First*, the cerebral ventricles of the hypophysectomized rat are rich in GRF, a peptide which normally regulates GH release from the somatotroph via cell surface receptors. The finding that F cells did not respond to ventricular GRF as well as the S cells (as evidenced by tibial line responses in the hypophysectomized host) argues that a receptor or post-receptor defect occurs in a GH cell subpopulation which does not recover under the conditions of Exp. 1. *Second*, cytoplasmic secretory GH granules are associated with a complex network of microtubules (22). An increase in the cytoplasmic area occupied by GH (and presumably secretory granules) in F cells (Table 2) could be interpreted to reflect "relaxation" of that network. *Third*, high molecular weight aggregates of GH are weakly immunoreactive; however, chemical reduction with mercaptoethanol enhances immunoreactivity several fold (7). The increased immunofluorescent staining intensity of F cells (Table 2) could reflect less S-S bridging between GH molecules; the consequence would be a loss in GH biopotency.

Most of the intracellular GH in the mammalian pituitary gland is stored in 0.3μm secretory granules as disulfide-linked aggregates of high molecular weight. These granules are capable of stimulating long bone growth when they are injected into hypophysectomized rats (2,15). If microgravity alters the packing density of the intragranular GH molecules, increased exposure of epitopes would result in increased cytoplasmic GH immunofluorescence and decreased biopotency of the hormone. In this regard, the repeatability of experiments 1 and 2 are striking and are considered significant. At the moment we have no explanation for the observation that comparable intracellular changes did not occur in the TS group in the face of changing biopotencies of secreted GH.

It is interesting that the post-flight secretory responses of the PRL cells paralleled those of the GH cells in the sense that the biological activity of secreted PRL was also suppressed as a result of flight or tail suspension while the immunologic assays gave spurious results (Fig. 4). While differing physiological conditions are known to affect the B/I activity ratio of secreted PRL (25), the molecular mechanisms involved are much less clearly defined. Since no major intracellular changes were found in the PRL cells after flight or tail suspension, we can only suggest that effects of microgravity on packaging and secretion within the PRL vs. GH cell are very different—yet its effect on one endpoint, *viz* activity of secreted bPRL (IL-2R), is obviously affected by flight or tail suspension.

As seen in Fig. 3, the times that elapsed between the landing of the vehicle after spaceflight and the preparation of pituitary cells was vastly different between the three missions. Other obvious differences in experimental conditions included animal strain, diet, housing, and spaceflight duration. However, in spite of these differences the results are remarkably similar (cf. Tables 1,2, Fig. 3 and (12)) and clearly establish the repeatability and statistical significance of the effects of microgravity on the pituitary GH cell system. Deconditioning of physiological systems in spaceflight is well documented (9); the time frame for readaptation of these systems on return to Earth's gravity is not. Our data show that the GH cells have not recovered in their ability to secrete bGH up to 2 weeks post-flight, the longest period studied thus far.

There is a growing awareness that the biological and immunological potencies of hormones and growth factors are not necessarily the same and that the physiological state of the organism can affect these activity ratios. Recent demonstrations of the importance of heat shock proteins in

processing molecules destined for export (3,1), and their activation by external environment (eg. heat, exercise, (18)), may provide an important clue for probing into the mechanism(s) underlying the changes in the GH cell system reported here. Equally plausible are microgravity driven changes in GRF receptors and/or microtubules in the GH cell. The limited opportunities for spaceflight experimentations are partially offset by the fidelity of some of the responses observed in the GH cells prepared from the tail suspended rat. Studies are underway to search for such mechanism(s) in this mimicked model of microgravity.

REFERENCES

1. Beckmann, R.P., L.A. Mizzen, and W.J. Welch. Interaction of HSP70 with Newly Synthesized Proteins: Implications for Protein Folding and Assembly. Science 248: 850-854, 1990.

2. Bell, J.A., D. Moffat, B.K. Vonderhaar, and D.W. Golde. Crystallization and Preliminary X-ray Characterization of Bovine Growth Hormone. J. Biol. Chem. 260: 8520-8525, 1985.

3. Deshaies, R. J., B.D. Koch, and R. Schekman. The Role of Stress Proteins in Membrane Biogenesis. TIBS 13: 384, 1988

4. Ellis, S. and R. Grindeland. Dichotomy Between Bioassayable and Immunoassayable Growth Hormone. In: Adv. In Human GH Research. Ed: S. Raiti. Washington, D.C., U.S. Govt. Printing Office: 409, 1974.

5. Ellis, S., R.E. Grindeland, J.M. Nuenke, and P. X. Callahan. Purification and Properties of Rat Prolactin. Endocrinology. 88: 886-895, 1968.

6. Farrington, M. and W.C. Hymer. Development of an Enzyme Immunoassay for Rat Growth Hormone. Life Science. 40: 2479-2488, 1987.

7. Farrington, M. and W.C. Hymer. Growth Hormone Aggregates in the Rat Adenohyophysis. Endocrinology. 126: 1630-1638, 1990.

8. Greenspan, F.S., C.H. Li, M.E. Simpson, and H.S. Evans. Bioassay of Hypophyseal Growth Hormone. Endocrinology. 45: 455-463, 1949.

9. Grindeland, R.E. Cosmos 1887: Science Overview. FASEB J. 4: 10-15, 1990.

10. Grindeland, R. E. Cosmos 2044: Mission Overview. (submitted).

11. Grindeland, R. and W. C. Hymer. Proc. Soc. Exp. Biol. Med. (submitted).

12. Grindeland, R.E., W.C. Hymer, M. Farrington, T. Fast, C. Hayes, K. Motter, L. Patil, and M. Vasques. Changes in Pituitary Growth Hormone Cells Prepared from Rats Flown on Spacelab 3. Am. J. Physiol. 252: R209-R215, 1987.

13. Hatfield, J.M. and W.C. Hymer. Flow Cytometric Analysis and Sorting of Live Male Rat Anterior Pituitary Cell Types by Forward Angle and Perpendicular Light Scatter. Endocrinology. 119: 2670-2682, 1986.

14. Hymer, W.C. and J. Hatfield. Purification of Cells from the Anterior Pituitary. In: Methods in Enzymology. Ed: Colowick and Kaplan. Academic Press, Vol 103, Part H, Ed. P. Conn: 257-287, 1983.

15. Hymer, W.C. and W. H. McShan. Isolation of Rat Pituitary Granules and the Study of their Biochemical Properties and Hormonal Activities. J. Cell Biol. 17: 67-86, 1963.

16. Hymer, W.C., D. Wilbur, R. Page, J.E. Hibbard, R. Kelsey, and J. Hatfield. Pituitary Hollow Fiber Units *In Vivo* and *In Vitro*. Neuroendocrinology. 32: 339-349, 1981.

17. Kendall, M. and W.C. Hymer. Cell Blotting: A New Method for Quantifying Hormone Release from Single Rat Pituitary Cells. Endocrinology. 121: 2260-2262, 1987.

18. Locke, M., E.G. Noble, and B.G. Atkinson. Exercising Mammals Synthesize Stress Proteins. Am. J. Physiol. 258: C723-C729, 1990.

19. Morey, E.R. Spaceflight and Bone Turnover: Correlation with a New Rat Model of Weightlessness. Bioscience. 29: 168-172, 1979.

20. Motter, K., M. Vasques, C. Hayes, M. Kendall, G. Tietjen, W.C. Hymer, and R. Grindeland. Effects of Microgravity on Rat Pituitary Growth Hormone (GH) Cell Function: Comparison of Results of the SL-3 Mission with Rat "Unloading" on Earth. Abstract for NASA Space Life Sciences Symposium, Washington, D. C., June 1987.

21. Mukherjee, P., A.M. Mastro, and W.C. Hymer. Prolactin Induction of Interleukin-2 Receptors on Rat Splenic Lymphocytes. Endocrinology. 126: 88-94, 1990.

22. Senda, T., J. Fujita, T. Ban, C. Zhong, K. Ishimura, K. Kanda, and K. Sobue. Ultrastructural and Immunocytochemical Studies on the Cytoskeleton in the Anterior Pituitary of Rats, with Special Regard to the Relationship Between Actin Filaments and Secretory Granules. Cell Tissue Res. 258: 25-30, 1989.

23. Signorella, A. and W.C. Hymer. Development of an Enzyme-Linked Immunoabsorbent Assay for Rat Prolactin. Anal. Biochem. 136: 372-381, 1984.

24. Signorella, A. and W.C. Hymer. Characterization of a Substance in Rat Serum which Modulates Prolactin Release *In Vitro* . Molecular and Cellular Endocrinology. 48: 1-10, 1986.

25. Subramaniam, M. and R. Gala. Do Prolactin Levels Measured by RIA Reflect Biologically Active Prolactin? J. Cell. Immunoassay. 9: 42, 1985.

26. Tanaka, T., R.P.C. Shiu, P.W. Gout, C.T. Beer, R.L. Noble, and H.G. Friesen. A New Sensitive and Specific Bioassay for Lactogenic Hormones: Measurement of Prolactin and Growth Hormone in Human Serum. Journal of Clinical Endocrinology and Metabolism. 51: 1058-1068, 1980.

TABLE 1

RELEASE OF GH AND PRL FROM PITUITARY CELLS OF RATS PREVIOUSLY FLOWN IN SPACE FOR 12.5 (EXP. 1) OR 14 (EXP. 2) DAYS

	Experiment 1 Cosmos 1887		Experiment 2 Cosmos 2044		
Parameter	Control	Flight	Control	Flight	Tail Suspended
GH					
Transport Media[1]					
iGH (ng/ml)	1550±190	1950±100*	160.2±10.6	127.5±9.2*	318.8±33.7**
bGH (μg/ml)	2.88 (2.76-2.99)	1.13*** (1.03-1.28)	2.73 (2.38-3.14)	0.58* (0.52-0.67)	0.60* (0.58-0.69)
Basal Secretion[2]					
iGH (ng/1000 GH cells)-3 day	57.2±4	62.2±5	25.29±3.31	26.81±3.84	36.8±4.0
iGH (ng/1000 GH cells)-6 day	142.9±7	73.0±10*	48.13±4.89	61.37±6.95	70.1±7.1*
bGH (μg/ml) - 3 + 6 day	2.34 (2.03-2.63)	0*	3.86 (3.42-4.35)	1.78* (1.63-1.94)	2.61* (2.43-2.76)
Implant Secretion[3]					
bGH (μg released)	2.2±0.3	1.0±0.1	ND	ND	ND
PRL					
Transport Media[1]					
iPRL (ng/ml)	307±45	351±63	145.4±16.2	113.6±12.4	56.1±7.3***
bPRL (NB2) (ng/ml)	122±26	188±17	203.5±56.4	172.7±23.5	75.0±9.9**
bPRL (IL-2R) (ng/ml)	ND	ND	320.3±38.5	203.0±41.3	191.5±26.4
Basal Secretion[2] (ng/1000 PRL cells)					
iPRL - 3 day	20.4±0.8	10.5±1.0*	27.9±1.9	24.3±2.4	35.1±7.8
iPRL - 6 day	29.1±3	16.2±0.2	53.9±4.1	41.8±4.3	79.9±16.2
bPRL (NB2) - 3 day	32.1±6	7.8±0.8	18.4±5.7	16.6±2.9	22.9±6.0
bPRL (NB2) - 6 day	47.7±13.9	12.7±2.5*	14.0±6.2	20.8±5	7.0±2.3
bPRL (IL-2R) - 3 day	ND	ND	12.8±1.1	6.3±0.2***	9.0±2.0**
bPRL (IL-2R) - 6 day	ND	ND	15.6±0.6	10.5±0.5***	5.5±0.5***

Footnotes to Table 1.

1. Transport media contains hormone released from intact pituitary glands during the 24-30 hrs. in transit from the landing site to the laboratory in Moscow.

2. Basal secretion represents hormone released into culture wells over two consecutive 3 day periods. Data are expressed on the basis of the number of GH or PRL cells seeded.

3. Implant secretion represents the amount of GH released from cells previously loaded into hollow fibers and implanted into the cerebral ventricle of hypophysectomized rats over a 15 day period. Tibial epiphyseal plate widths were compared to those in other hypophysectomized rats which had received bovine GH for 4 days in order to estimate concentrations of hormone secreted from implant. 95% confidence limits are shown in ( ).

iGH/PRL = immunoreactive growth hormone/prolactin
bGH/PRL = biologically active growth hormone/prolactin
bPRL (NB2) = prolactin activity detected by lymphoma cell bioassay (13)
bPRL (IL-2R) = prolactin activity detected by interleukin 2 receptor assay (14)
ND = assay not done
– indicates insufficent sample volume

Data Represent Averages ± Standard Error of Mean
*$p<0.05$
**$p<0.01$
***$p<0.001$ (relative to control)

TABLE 2

CHARACTERISTICS OF GH AND PRL CELLS PREPARED FROM PITUITARIES OF RATS PREVIOUSLY FLOWN IN SPACE FOR 12.5 (EXP. 1) OR 14 (EXP. 2) DAYS

	Experiment 1 Cosmos 1887		Experiment 2 Cosmos 2044		
Parameter	Control	Flight	Control	Flight	Tail Suspended
General					
Cell Yield	1.68±0.1	1.98±0.2	1.8±0.1	2.2±0.1*	1.67±0.08
Viability	90±0.9	93±0.7	94.2±0.6	92.3±0.9	83.8±1.3***
GH					
% (flow cytometry)	23	27	36	24	27.6
% (ICC)	ND	ND	26.3±2.8	20.2±2.9	16.1±2.0*
Fluorescence Intensity (marker index)	13.1	24.5	4.4	8	4.3
FALS	151	181	32	40	31
PLS	145	145	37	41	38
% Area Occupied by GH	37.1±4.7	49.9±4.1*	36.6±2.5	48.6±2.3*	34.1±1.5
Extracts					
Initial iGH (ng/1000 GH cells)	61±17	40±17	-	-	-
Initial bGH (μg/ml)	9.13	4.18*	2.11 (1.63-2.74)	0*	0*
Final iGH (ng/1000 GH cells)	22±2.0	8.6±0.8	18±2	22±3	18.3±2.3
Final bGH (μg/ml)	2.05	1.63*	3.31 (3.20-3.49)	0*	0*
PRL					
% (flow cytometry)	32	47	33.3	34.4	22.6
% (marker index)	5.1	4.1	5.7	4.7	3.7
FALS	24	40	12	21	10
PLS	64	92	25	21	21
Initial Intracellular PRL	0.24±0.02	0.22±0.05	-	-	-

Footnotes to Table 2.

Percentages of GH/PRL cells were determined by flow cytometry (30,000 cells counted/trial) or, in one case, by immunocytochemistry as well.

Intensity of cytoplasmic fluorescence hormone staining (see Fig. 2) were quantified by flow cytometry using the marker index method, which is based on fluorescence intensity converted to voltage.

The ratio of voltages of stained to unstained cells equals marker index.

FALS and PLS (forward angle light scatter and perpendicular light scatter, respectively) were determined by flow cytometry. Values represent peak channels of size (FALS) and cytoplasmic granularity (PLS), respectively (7).

Area of GH in cytoplasm of GH cells was determined by image analysis and intracellular hormone levels before and after culture determined on alkaline extracts of cells (see Materials and Methods).

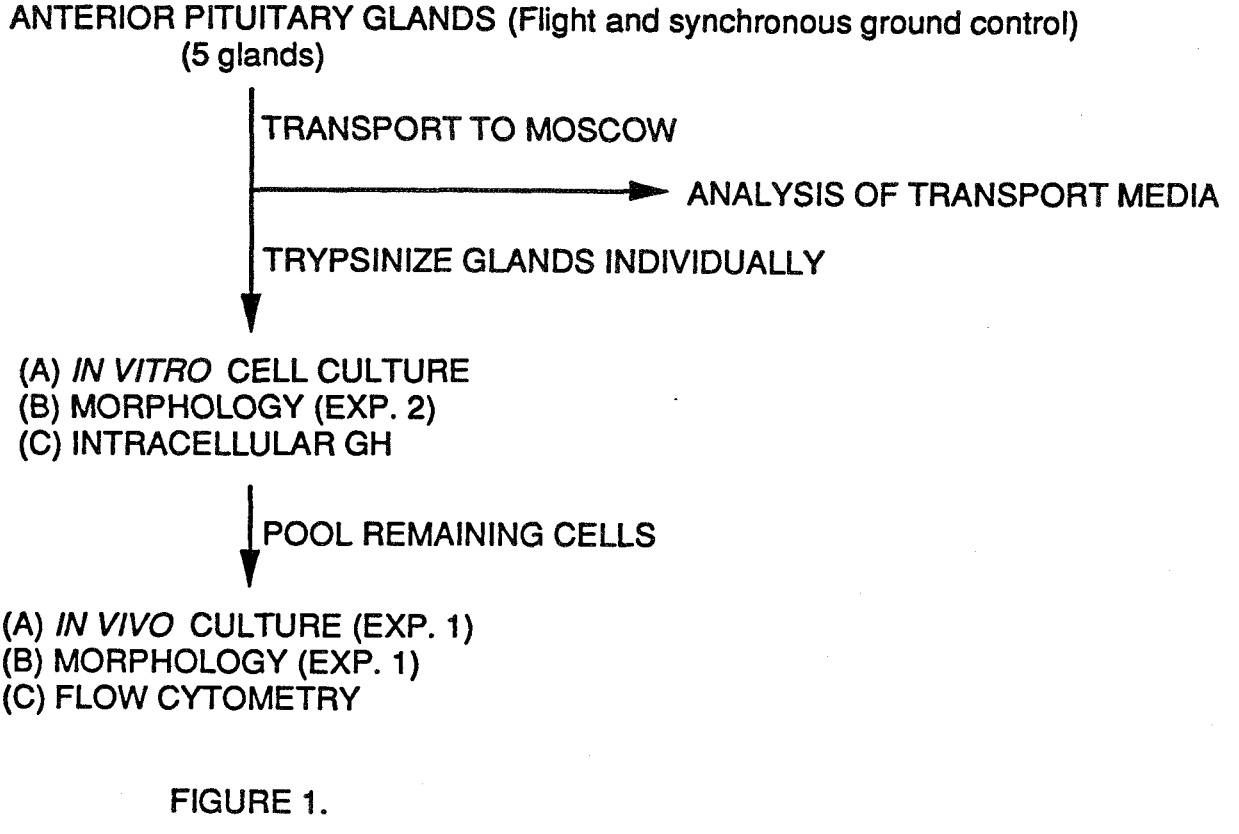

FIGURE 1.

Figure 1. Experimental protocol followed for Experiments 1 (Cosmos 1887) and 2 (Cosmos 2044). See Materials and Methods for specific assays.

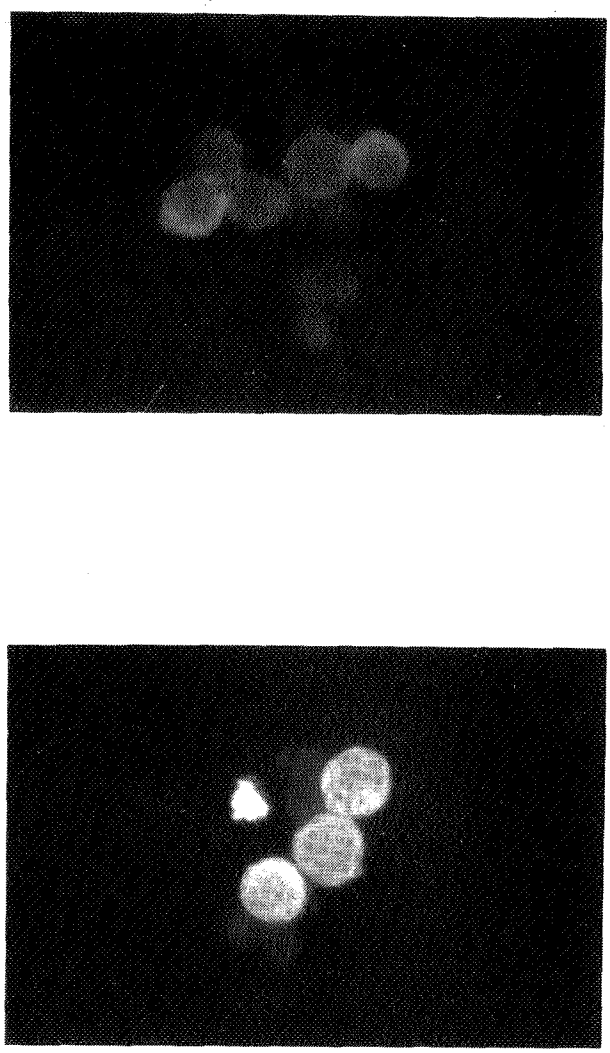

Figure 2. Photomicrographs of GH cells (yellow) from Exp. 1 stained by an immunofluorescence procedure (see Materials and Methods). Top: control; bottom: flight.

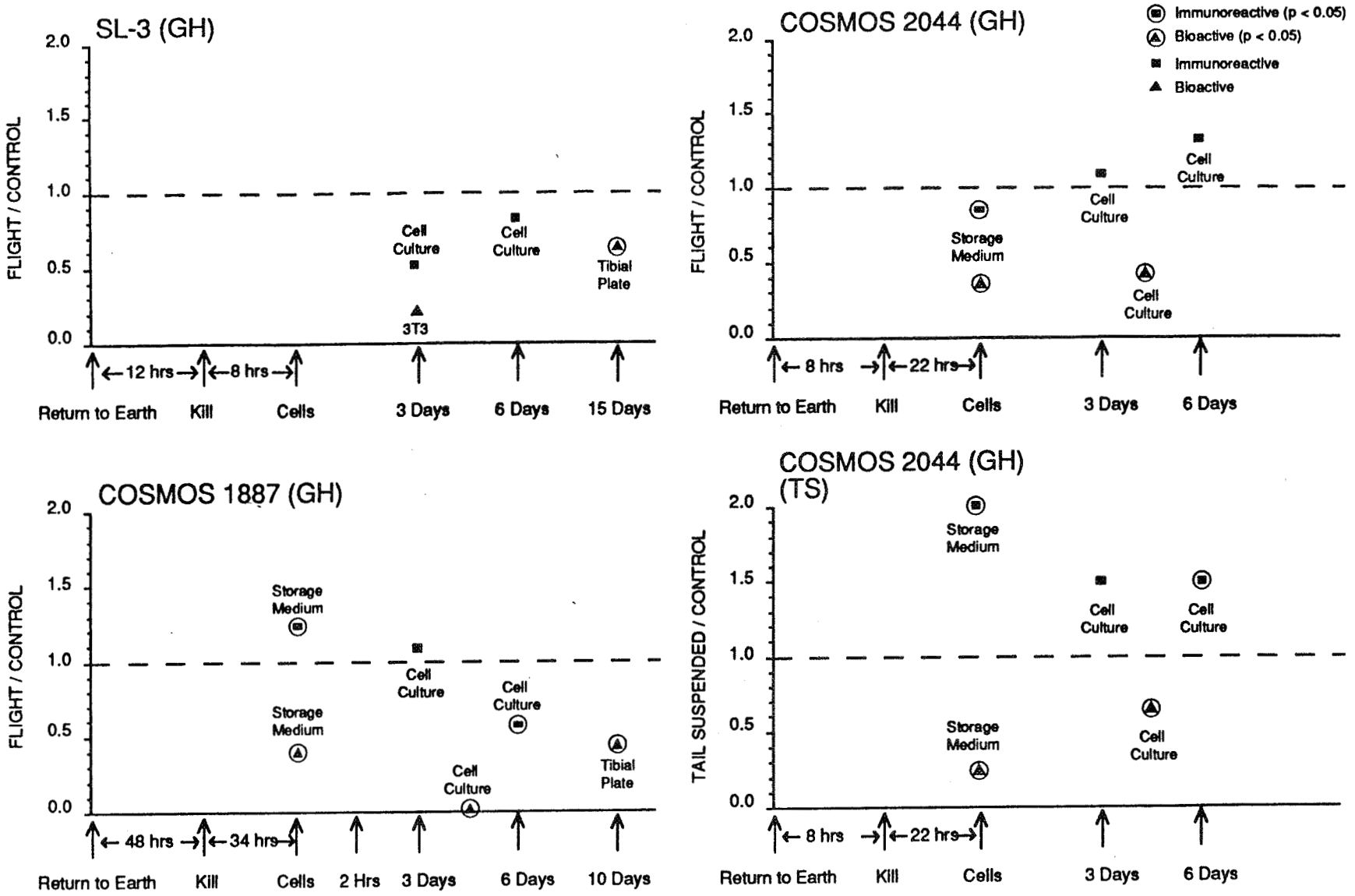

Figure 3. Comparison of post-flight secretory responses of GH cells from rats flown on the Spacelab 3 mission in 1985; Cosmos 1887 (Exp. 1); Cosmos 2044 (Exp. 2); and tail suspended animals (TS-Exp. 2) expressed as the ratios of experimental to control. Data for the SL-3 experiment previous published in (12); permission to use these data obtained from American J. Physiology.

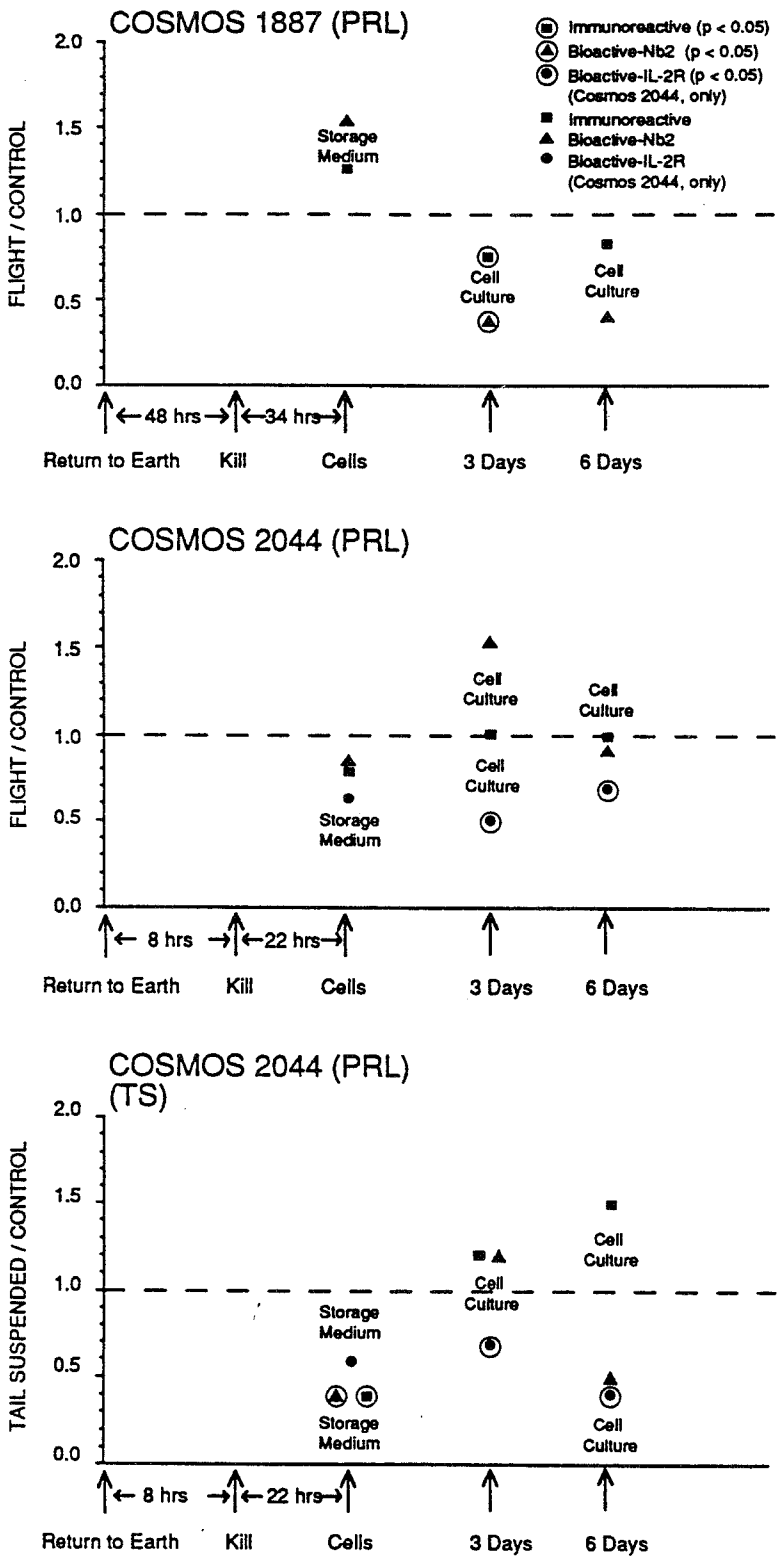

Figure 4. Comparison of post-flight secretory responses of PRL cells from rats flown on the Cosmos 1887 mission (Exp. 1); Cosmos 2044 mission (Exp. 2) and tail suspended animals (TS-Exp. 2) expressed as the ratio of experimental to control.

Page intentionally left blank

516-51
51355

EXPERIMENT K-7-22

PART II: HYPOTHALAMIC GROWTH HORMONE-RELEASING FACTOR, SOMATOSTATIN IMMUNOREACTIVITY, AND MESSENGER RNA LEVELS IN MICROGRAVITY

P.E. Sawchenko, C. Arias, I. Krasnov, R.E. Grindeland,and W. Vale

INTRODUCTION

Immunohistochemical analyses of hypothalamic hormones carried out on tissue from rats flown on an earlier flight (Cosmos 1887) suggested preferential effects on hypophysiotropic principles involved in the regulation of growth hormone secretion and synthesis. We found that staining in the median eminence for peptides that provide both stimulatory (growth hormone-releasing factor, or GRF) and inhibitory (somatostatin, SS) influences on growth hormone secretion were depressed in flight animals relative to synchronous controls, while staining for other neuroendocrine peptides, cortocotropin-releasing factor and arginine vasopressin, were similar in these two groups. While this suggests some selective impact of weightlessness on the two principal central nervous system regulators of growth hormone dynamics, the fact that both GRF- and SS-immunoreactivity (IR) appeared affected in the same direction is somewhat problematic, and makes tentative any intimation that effects on CNS control mechanisms may be etiologically significant contributors to the sequelae of reduced growth hormone secretion seen in prolonged space flight.

To provide an additional, and more penetrating, analysis we attempted in hypothalamic material harvested from animals flown on Cosmos 2044 to complement immunohistochemical analyses of GRF and SS staining with quantitative, *in situ* assessments of messenger RNAs encoding the precursors for both these hormones.

MATERIALS AND METHODS

Five flight, tail-suspended and synchronous control animals were decapitated, and their hypothalami removed, longitudinally bisected, and placed in neutral buffered 10% formalin at 4°C for 20 hr. They were then placed in 10% sucrose in 0.1M phosphate buffer for 24 hr, and transferred to a fresh sucrose solution in which they were stored for shipment. Upon receipt, the hypothalami were frozen in dry ice and five 1-in-5 series of 20 µm thick frozen sections were cut on a sliding microtome. Sections were rinsed (2 X 10 min) in 0.05M phosphate-buffered saline (PBS) and stored at -20° C in cryoprotectant (30% ethylene glycol, 15% sucrose in 0.05M phosphate buffer) until staining.

One series of sections was stained for with thionin for Nissl material, and used for reference. Two were prepared for immunohistochemical localization of somatostatin-28 and GRF; the remaining two series were prepared for hybridization histochemical localization of the mRNAs encoding the somatostatin and GRF precursors.

Immunohistochemistry

A conventional avidin-biotin-immunoperoxidase procedure was used for staining. The reagents were obtained in kit form from Vector Laboratories (Burlingame, CA), and the protocol is described in detail elsewhere (Gerfen and Sawchenko, 1985; Sawchenko et al., 1990). For GRF, a polyclonal antiserum raised in rabbits against synthetic rat GRF_{1-43} was used (serum G75 of Sawchenko et al., 1985); for SS, we employed an antiserum against SS-

28 (serum S309 of Benoit et al., 1982a and b; see also Sawchenko et al., 1988). Details of the characterization and specificities of the antisera may be found in these citations.

In Situ Hybridization

Techniques for cRNA probe synthesis, hybridization and autoradiographic localization of mRNA signal have been described previously (Simmons et al., 1989). Briefly, tissue was processed as described above, and then mounted onto poly-L-lysine-coated slides. These sections were then digested with 10 µg/ml of proteinase K for 30 min, at 37°C. Antisense prepro-GRF (ppGRF) probes were generated from a 400 base pair cDNA clone (prghrf-2; generously provided by K. Mayo, University of Chicago), which contains the entire coding region of rat ppGRF (Mayo et al., 1985). This cDNA was subcloned into the SP64 transcription vector (Promega Biotech), next to the SP6 promoter. The plasmid was linearized with Puv II, and labeled antisense probes were generated using SP6 RNA polymerase and ^{35}S-UTP. ppSS probes were generated from a construction (pSR-1) provided by Dr. M. Montminy (The Salk Institute; see Montminy et al., 1986) employing a 450 base pair cDNA encompassing the entire coding sequence and a portion of the 3' untranslated region of rat ppSS (Goodman et al., 1983). An Xba 1 - Sau 3A restriction fragment was subcloned into the Promega Biotech pSP65 expression vector. The plasmid was linearized with Sal 1, and antisense probes synthesized using SP6 polymerase and ^{35}S-UTP. All probes were used at concentrations of about 10^7 cpm/ml. Probes were applied to sections overnight at 56-58°C in a solution containing 50% formamide, 0.3 M NaCl, 10 mM Tris (pH 8.0), 1 mM EDTA, 0.05% tRNA, 10 mM dithiothreitol, 1x Denhardt's solution and 10% dextran sulfate, after which they were treated with 20 ug/ml of ribonuclease A for 30 min, at 37°C, and washed in 15 mM NaCl/1.5 mM sodium citrate, at 55-60°C. Sections were then dehydrated and exposed to X-ray films for 3-4 days. Sections were defatted in xylene, rinsed in absolute ethanol, air dried, coated with Kodak NTB-2 liquid autoradiographic emulsion, and exposed at 4°C, in the dark and desiccated, for 14 days. They were then developed with Kodak D-19 for 3.5 min at 14°C, rinsed briefly in distilled water, fixed with film strength Kodak rapid fixer for 2 min at 14°C, and washed in distilled water for at least one hour.

Quantification

Cell- and grain-counting procedures were used to compare the strengths of mRNA signals on autoradiographic material. For the GRF system, two cell groups were analyzed, the arcuate nucleus, which is acknowledged as the principal source for the delivery of GRF to the portal vasculature, and the region surrounding the ventromedial nucleus of the hypothalamus, which appears to give rise principally to intra-CNS pathways (Niimi et al., 1990; Sawchenko and Swanson, 1990). For SS, analysis was restricted to cells in the anterior periventricular nucleus, a majority of which project to the median eminence (Merchenthaler et al., 1989). For both peptide systems we first obtained estimates of the diameters of GRF- and SS-IR cells in the regions described above from previously prepared immunoperoxidase preparations. We then used a counting reticle that contained a grid which circumscribed these respective cell-sized areas and placed it over non- positively hybridized regions of the experimental material. Background grain densities were estimated from 20 cells per region per probe per rat. We adopted the arbitrary criterion of considering any accumulation of sliver grains within a cell sized area that was five times above background levels as representing a positively hybridized neuron. Counts were then made in each animal of the total number of cells positively hybridized for ppGRF in the arcuate and peri-ventromedial hypothalamic regions, and of those bearing positive signal for ppSS in the anterior periventricular nucleus from the levels of the rostral pole of the suprachiasmatic nucleus to the mammillary recess.

Estimates of grain density per cell were carried out by counting (at 1000 X magnification) the number of reduced silver grains overlying cell-sized areas than contained above-background

accumulations as defined above. A total 20 cells per animal (or 100 total per group) were sampled in each of the three areas (two for ppGRF and one for ppSS) chosen for analysis.

Controls

The limited amount of experimental tissue available for analysis precluded exhaustive control studies. To verify the effectiveness and specificity of the reagents controlled immunostaining and hybridization histochemistry was carried out on more conventionally fixed (transcardially perfused) tissue obtained from non-manipulated animals. In addition, immunostaining was carried out with antisera preadsorbed overnight with anti-GRF and SS-28 sera that had been preadsorbed (overnight at 4° C) with 30 μM concentrations of the respective synthetic immunogens. For both antisera, this procedure abolished all staining in the hypothalamus. For *in situ* hybridization, application of labeled sense-strand cRNA probes, generated from the same constructions used to produce anti-sense probes used for analysis, to sections of hypothalamus also failed to provide any suggestion of discrete cellular labeling.

RESULTS

Immunohistochemistry

Positive staining patterns, consistent with their consensus distributions (e.g., Johansson et al., 1982; Sawchenko et al., 1985; Sawchenko and Swanson, 1990), were seen for both GRF- and SS-28-IR in hypothalami of rats from each of the three groups. Fibers stained for both peptides were most prominent in the external (hypophysiotropic) zone of the median eminence (Fig. 1). Staining for both GRF and SS-28 in flight animals appeared consistently less prominent in flight animals, relative to synchronous controls; this effect in the flight animals was most marked for GRF. Tail-suspended rats showed GRF-IR staining patterns and intensities in the median eminence that were indistinguishable from controls, while median eminence SS-28 staining in suspended rats showed a tendency toward modest reduction, though this was evident in only three of five animals.

Extra-hypophysiotropic fibers stained for the two peptides showed tendencies toward between-group variation that were similar, though less marked, to those seen in the median eminence. SS-28-IR cell bodies were detected in the anterior periventricular nucleus of animals from all three groups; no consistent differences in the intensity of perikaryal staining were observed. Perikaryal staining for GRF, which normally requires pretreatment with colchicine, was not observed in any of the animals.

In Situ Hybridization

Attempts at hybridization histochemical localization of ppGRF and ppSS mRNAs proved surprisingly effective in immersion-fixed material. ppGRF mRNA signal was detected in all animals in each of the consensus sites of GRF peptide and ppGRF mRNA expression (Sawchenko and Swanson, 1990): the arcuate nucleus, the region encapsulating the ventromedial nucleus of the hypothalamus, and, least prominently, the paraventricular nucleus of the hypothalamus (Fig. 2). The former two areas were analyzed quantitatively. The most prominent effect seen in this material was a robust, 46%, decrease in the number of cells showing a positive GRF mRNA signal in the arcuate nucleus of the flight group, relative to synchronous controls ($p<0.001$, two-tailed t-statistic; see Fig. 3). The density of silver grains overlying positively hybridized cells in the arcuate nucleus was comparably reduced in flight animals ($p<0.001$; see Figs. 4 and 5). This effect on ppGRF mRNA was at least somewhat specific to the arcuate nucleus. Grain density per cell in the region around the ventromedial nucleus was significantly reduced ($p<0.05$), though not to the extent that it was in flight

animals. Moreover, the number of cells in the ventromedial region that displayed a positive hybridization signal was not significantly different than synchronous control values ($p>0.05$).

Tail-suspended rats did not differ significantly from synchronous controls in either measure of mRNA expression in either the arcuate or ventromedial regions, though values from this group tended, surprisingly, to be elevated.

Positive signal for ppSS mRNA was detected most prominently in the anterior periventricular nucleus (Fig. 6), though a number of non-hypophysiotropic sites of SS peptide and/or gene expression (Johansson et al., 1982; Fitzpatrick-McElligott, 1988), including the arcuate nucleus, were seen consistently. Analysis was restricted to the periventricular region, since current evidence suggests that the SS-expressing cells in the arcuate nucleus do not contribute to the hypophysiotropic projection (Merchenthaler et al., 1989). The suspended and flight groups tended to show modest reductions in both the number of positively hybridized cells and the grain density per cell in the anterior periventricular nucleus, though none of these values differed reliably from those of synchronous controls ($p's>0.05$).

DISCUSSION

The results provide a clear demonstration of differential effects of spaceflight on the hypothalamic peptides involved most directly and prominently in the regulation of pituitary growth hormone secretion. Further, the data are consistent with the notion that the disordered pituitary growth hormone secretion that has been described as a consequence of prolonged weightlessness (e.g., Grindeland et al. 1987) may have at least a partial central nervous system basis. Flight animals evinced a clear decrement in ppGRF mRNA levels in the arcuate nucleus, the acknowledged source for the delivery of GRF to the hypophyseal portal vasculature for the stimulatory control of growth hormone secretion. Staining for GRF peptide in the portal plexus was correspondingly reduced. The effect of flight on ppGRF mRNA levels was preferentially exerted on presumed hypophysiotropic neurons, as peri-ventromedial ppGRF expressing cells were less prominently affected. Moreover, no significant differences among the three groups in indices of ppSS mRNA levels were apparent.

The results complement and extend the immunohistochemical analyses carried out on tissue from rats flown of Cosmos 1887, which showed roughly comparable decrements in both SS- and GRF-IR in the median eminence of flight animals, relative to synchronous controls. In the present study, compatible effects were noted, though hypophysiotropic GRF-IR fibers were more severely depleted. Based on our experience with the Cosmos 1887 material, we were able to improve fixation and tissue handling procedures, and, consequently, the resolution that was evident in immunostained sections. We are thus inclined to view the present immunohistochemical results as being more representative.

In line with the immunostaining data, we found both indices of ppGRF mRNA levels in the arcuate nuclei of flight animals to be significantly reduced, relative to both synchronous control and hindlimb-suspended rats. Two basic factors argue for the specificity of this effect. First, ppSS mRNA levels were not significantly altered in flight animals. Second, while the intensity of the ppGRF mRNA signal was also reduced in the peri-ventromedial region, this effect was of a considerably lesser magnitude than that in the arcuate nucleus, and, in the absence of independent identification of hypophysiotropic neurons in our protocol, we cannot discount the possibility that the peri-ventromedial cell population defined here solely on the basis of topography, may have included some neurons that project to the median eminence.

The analysis included a group of animals subjected to hindlimb-suspension, a manipulation which has been shown to mimic the effects of weightlessness on growth hormone secretion. ppGRF levels in this group tended consistently, though non-significantly, to be *increased*

relative to synchronous control values. In addition, no consistent alterations in immunostaining for either SS or GRF were noted. The data are thus quite clear in indicating that the tail-suspension paradigm does not effectively model flight effects, at least insofar as the dynamics of central hypophysiotropic factors are concerned.

The reduction in the ppGRF mRNA signal in the arcuate nucleus, which has been shown by various means to comprise the principal source for the delivery of GRF peptide to the hypophyseal portal vasculature (Bloch et al., 1985; Niimi et al., 1990; Sawchenko and Swanson, 1990), may provide at least a partial basis for explaining the reduced growth hormone secretion seen as a consequence of prolonged spaceflight (Grindeland et al., 1987). While this effect on indices of ppGRF mRNA levels may be representative of an influence exerted at the level of ppGRF gene transcription, alternative explanations (e.g., effects on mRNA stability) cannot be discounted. Potential means by which weightlessness might effect such targeted alterations in mRNA levels are completely obscure, and could involve neural, hormonal and/or physical intermediaries.

REFERENCES

1. Abercrombie, M. Estimation of Nuclear Populations from Microtome Sections. Anat. Rec. 94:239-247, 1946.

2. Benoit, R., P. Bohlen, N. Ling, A. Briskin, F. Esch, P. Brazeau,S.-Y. Ying, and R. Guillemin. Presence of Somatostatin 28_{1-12} in Hypothalamus and Pancreas. Proc. Natl. Acad. Sci.USA. 79:917-921, 1982a.

3. Benoit, R., N. Ling, B. Alford, and R. Guillemin. Seven Peptides Derived from Prosomatostatin in Rat Brain. Biochem. Biophys. Res. Commun. 107:944-950, 1982b.

4. Fitzpatrick-McElligott, S., J.P. Card, M.E. Lewis, and F. Baldino,Jr. Neuronal Localization of Prosomatostatin mRNA in the Rat Brain with *In Situ* Hybridization Histochemistry. J. Comp. Neurol. 273:558-572, 1988.

5. Gerfen, C.R. and P.E. Sawchenko. An Anterograde Neuroanatomical Tracing Method that Shows the Detailed Morphology of Neurons, Their Axons and Terminals: Immunohistochemical Localization of an Anterogradely Transported Plant Lectin, *Phaseolus Vulgaris* -Leucoagglutinin(PHA-L). Brain Res. 290:219-238, 1984.

6. Goodman, R.H., D.C. Aron, and B.A. Roos. Rat Pre-Prosomatostatin. J. Biol. Chem. 258:5570-5573, 1893.

7. Grindeland, R., W.C. Hymer, M. Farrington, T. Fast, C. Hayes, K. Motter, L. Patil, and M. Vasques. Changes in Pituitary Growth Hormone Cells Prepared from Rats Flown of Spacelab 3. Am. J. Physiol. 252:R209-R215, 1987.

8. Johansson, O., T. Hökfelt, and R.P. Elde. Immunohistochemical Distribution of Somatostatin Immunoreactivity in the Central Nervous System of the Adult Rat. Neuroscience. 13:265-339, 1984.

9. Mayo K.E., G.M. Cerelli. M.G. Rosenfeld, and R.M. Evans. Characterization of cDNA and Genomic Clones Encoding the Precursor to Rat Hypothalamic Growth Hormone-Releasing Factor. Nature. 314:464-467, 1985.

10. Merchenthaler, I., C. Csontos, G. Setalo, P. Petrusz, and B.Flerko. Combined Retrograde Tracing and Immunocytochemical Identification of Luteinizing Hormone-Releasing Hormone- and Somatostatin-Containing Neurons Projecting to the Median Eminence of the Rat. Endocrinology. 125:2812-2821, 1989.

11. Montminy, M.R., M.J. Low, L. Tapaia-Arancibia, S. Reichlin, G.Mandel, and R.H. Goodman. Cyclic AMP Regulates Somatostatin mRNA Accumulation in Primary Diencephalic Cultures and in Transfected Fibroblast Cells. J. Neurosci. 6:1171-1176, 1986.

12. Niimi, M., J. Takahara, M. Sato, and K. Kawanishi. Immunohistochemical Identification of Galanin and Growth Hormone-Releasing Factor-Containing Neurons Projecting to the Median Eminence of the Rat. Neuroendocrinology. 51:572-579, 1990.

13. Sawchenko, P.E., R. Benoit, and M.R. Brown. Somatostatin 28-Immunoreactive Inputs to the Paraventricular Nucleus: Origin from Non-Aminergic Neurons in the Nucleus of the Solitary Tract. J. Chem. Neuroanat. 1:81-94, 1988.

14. Sawchenko, P.E., E.T. Cunningham, Jr., M.T. Mortrud, S.W. Pfeiffer, and C.R. Gerfen. *Phaseolus Vulgaris* Leucoagglutinin Anterograde Axonal Transport Technique. Meth. Neurosci. 3:247-260, 1990.

15. Simmons, D.M., J.L. Arriza, and L.W. Swanson. A Complete Protocol for *In Situ* Hybridization of Messenger RNAs in Brain and Other Tissues with Radio Labeled Single-Stranded RNA Probes. J. Histotechnology. 12:169-181, 1989.

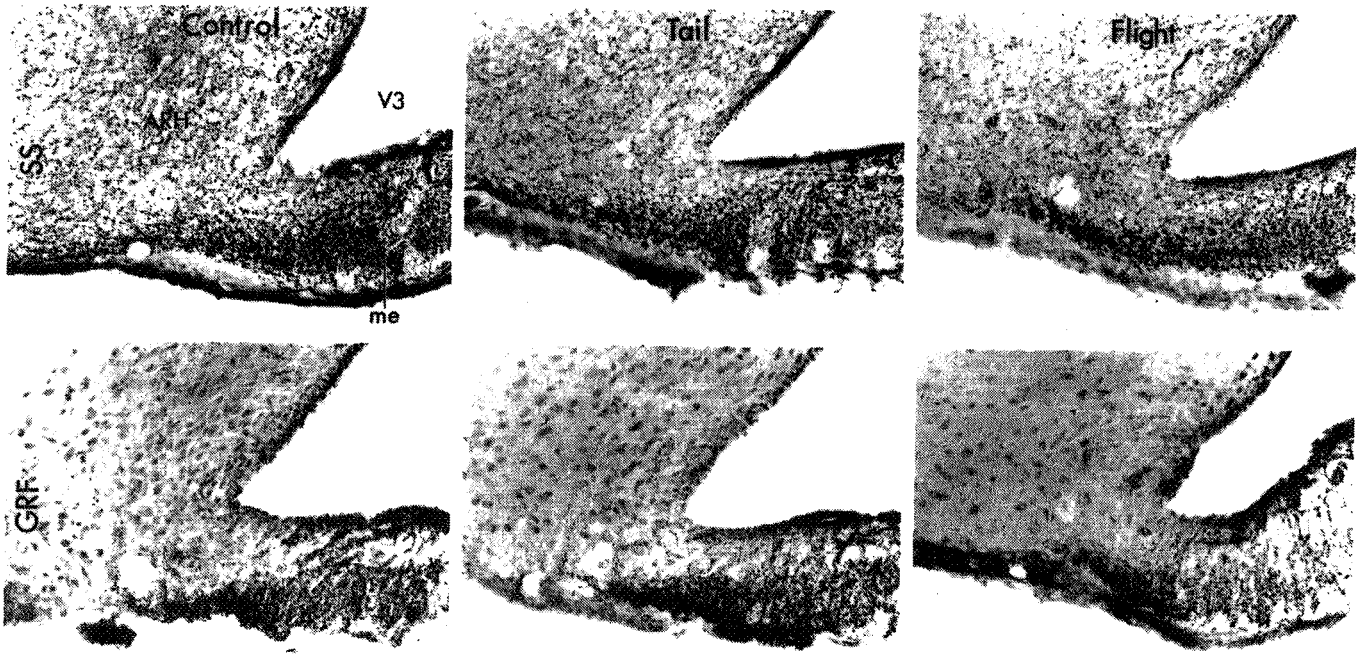

Figure 1. Somatostatin-28- (SS) and GRF-IR in the median eminence of synchronous control (Control), tail-suspended (Tail), and flight animals. Brightfield photomicrographs of avidin-biotin-immunoperoxidase-stained coronal sections showing varicosities stained for both hypophysiotropic peptides in the external lamina of the median eminence. The most marked effect observed was a marked reduction in GRF-IR, and a less pronounced depletion of SS-IR, in the portal plexuses among members of the flight group. All micrographs X 190.

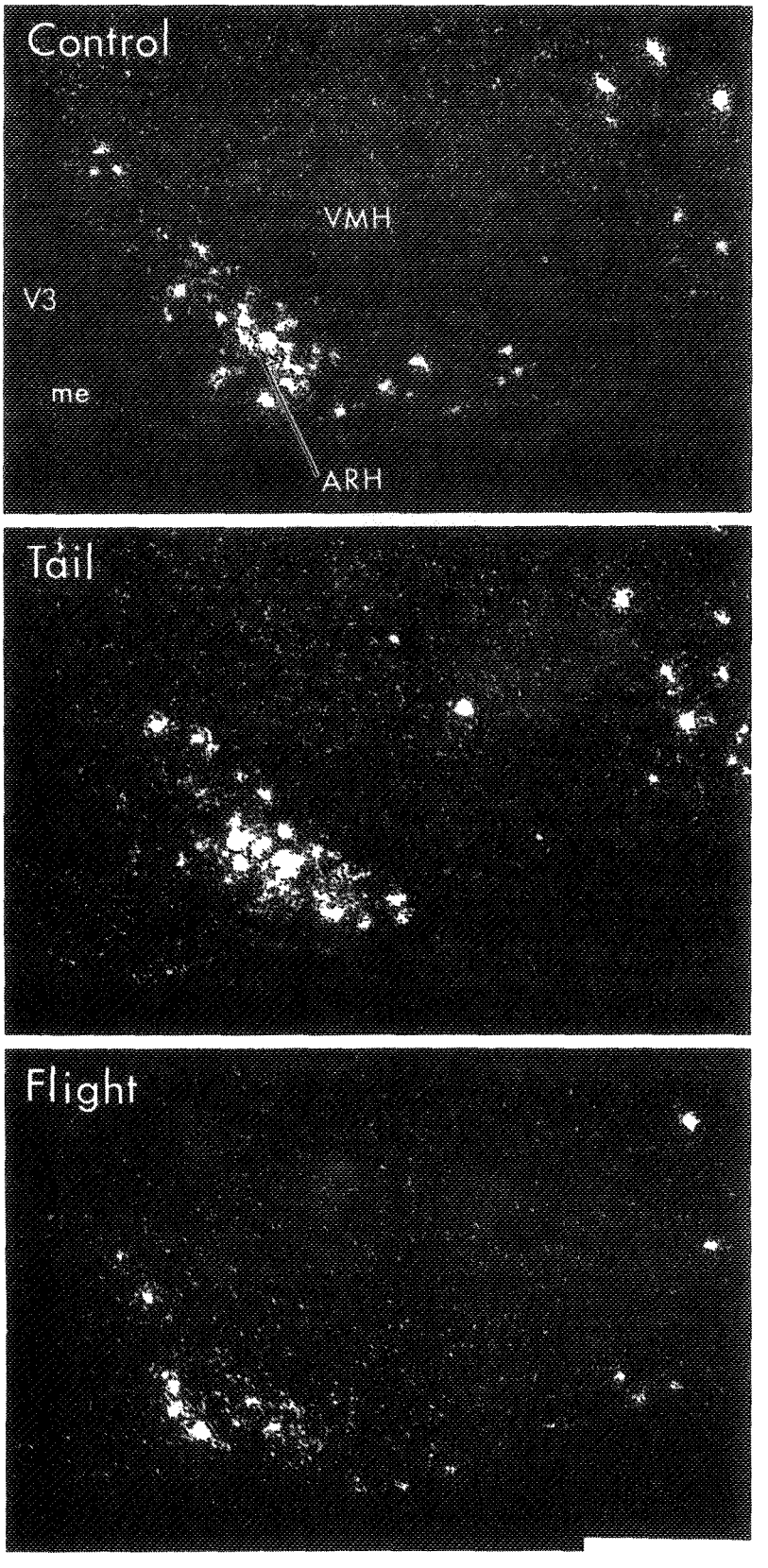

Figure 2. ppGRF mRNA localization in the medial basal hypothalamus. Darkfield photomicrographs of emulsion-dipped autoradiograms showing two major ppGRF-expressing cell groups in the hypothalamus: in the arcuate nucleus (ARH), and in the region encapsulating the ventromedial nucleus of the hypothalamus (VMH). Note in the arcuate nucleus of the flight group the reductions in the number of positively hybridized cells and in the intensity of the hybridization signal per cell, relative to both synchronous control (Control) and hindlimb-suspended (Tail) groups; ppGRF signal in the peri-ventromedial area of flight animals was less markedly affected. All micrographs X 75.

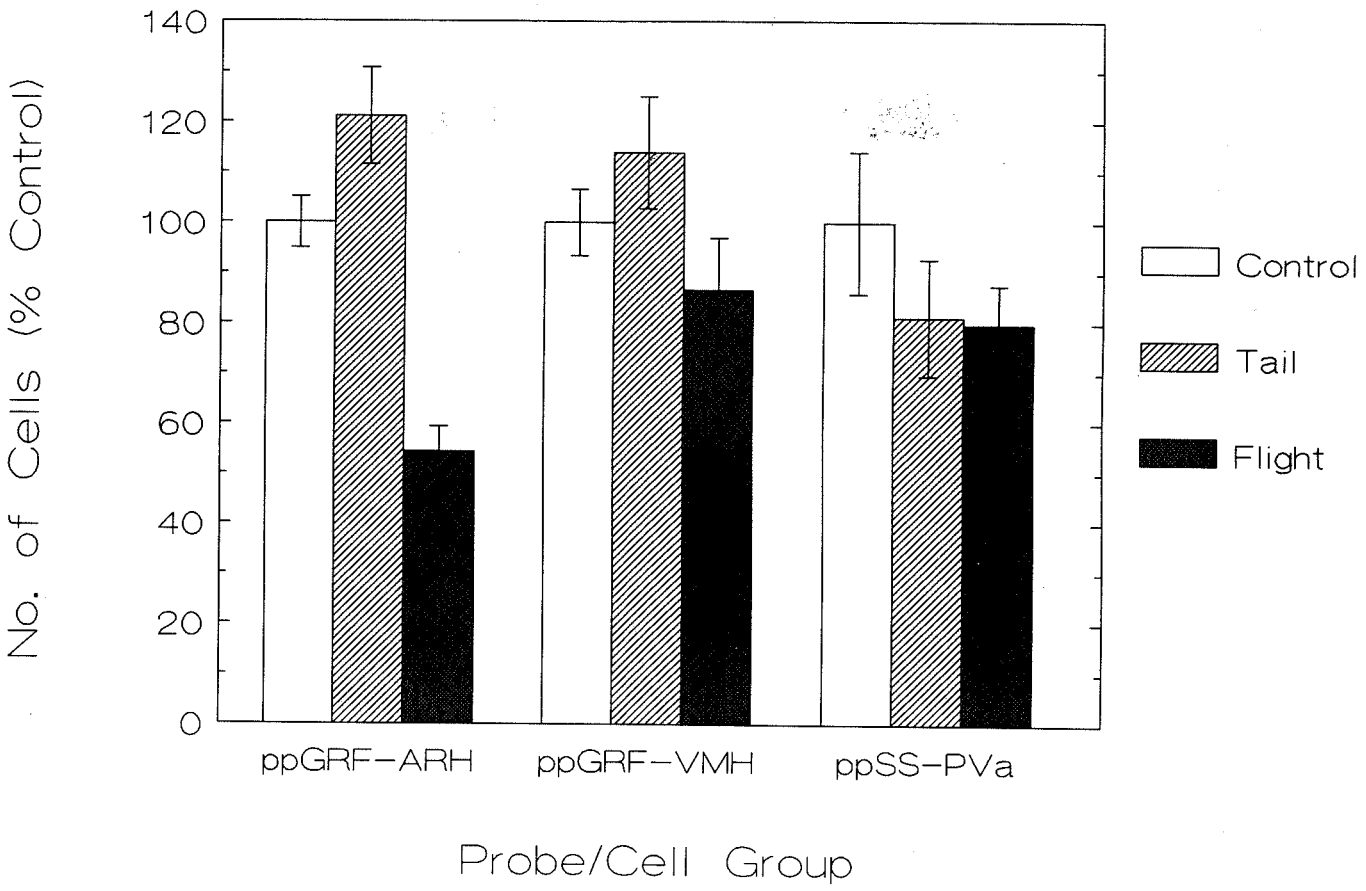

Figure 3. Mean (± SEM) number of cells showing a positive mRNA signal for ppGRF in the arcuate (ARH) and periventromedial (VMH) regions, and for ppSS in the anterior periventricular nucleus (PVa), in synchronous control (Control), tail-suspended (Tail) and flight groups. The only statistically reliable effect was a reduction in the number of ppGRF-hybridized cells in the arcuate nucleus of flight animals, relative to synchronous control values. n = 5 rats per group.

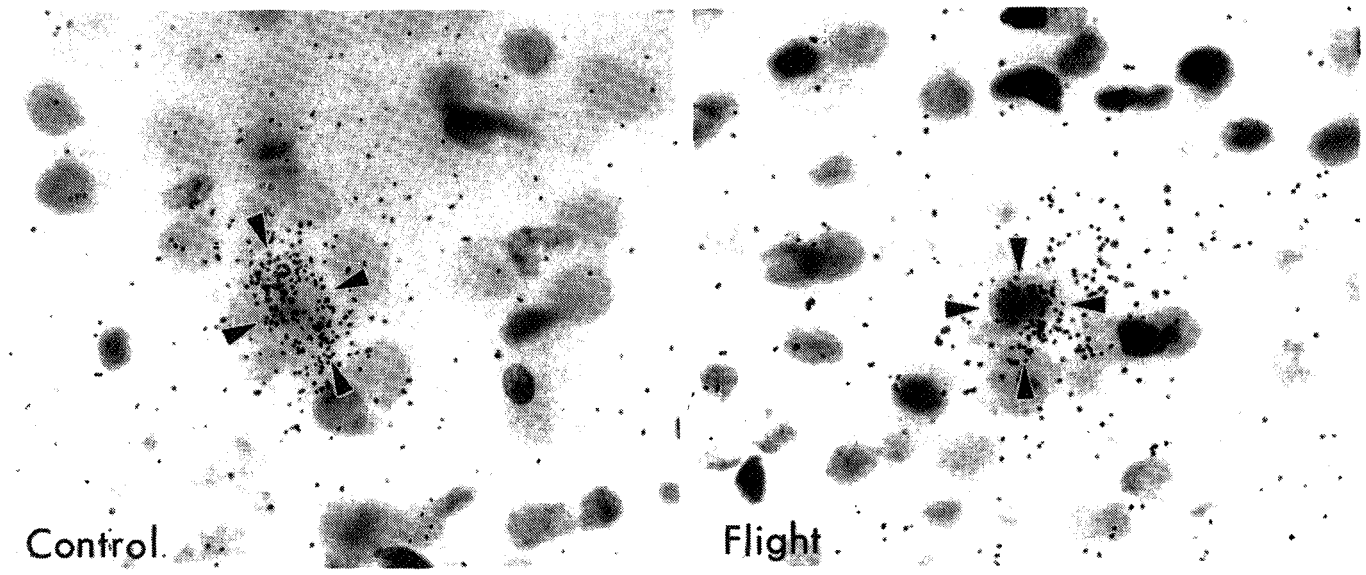

Figure 4. Brightfield photomicrograph to illustrate the difference in grain density indicative of ppGRF mRNA signal in the arcuate nuclei of control and flight animals. Arrowheads show clusters of sliver grains surrounding stained cell nuclei; note reduced grain density in the flight animal. Both micrographs X 750.

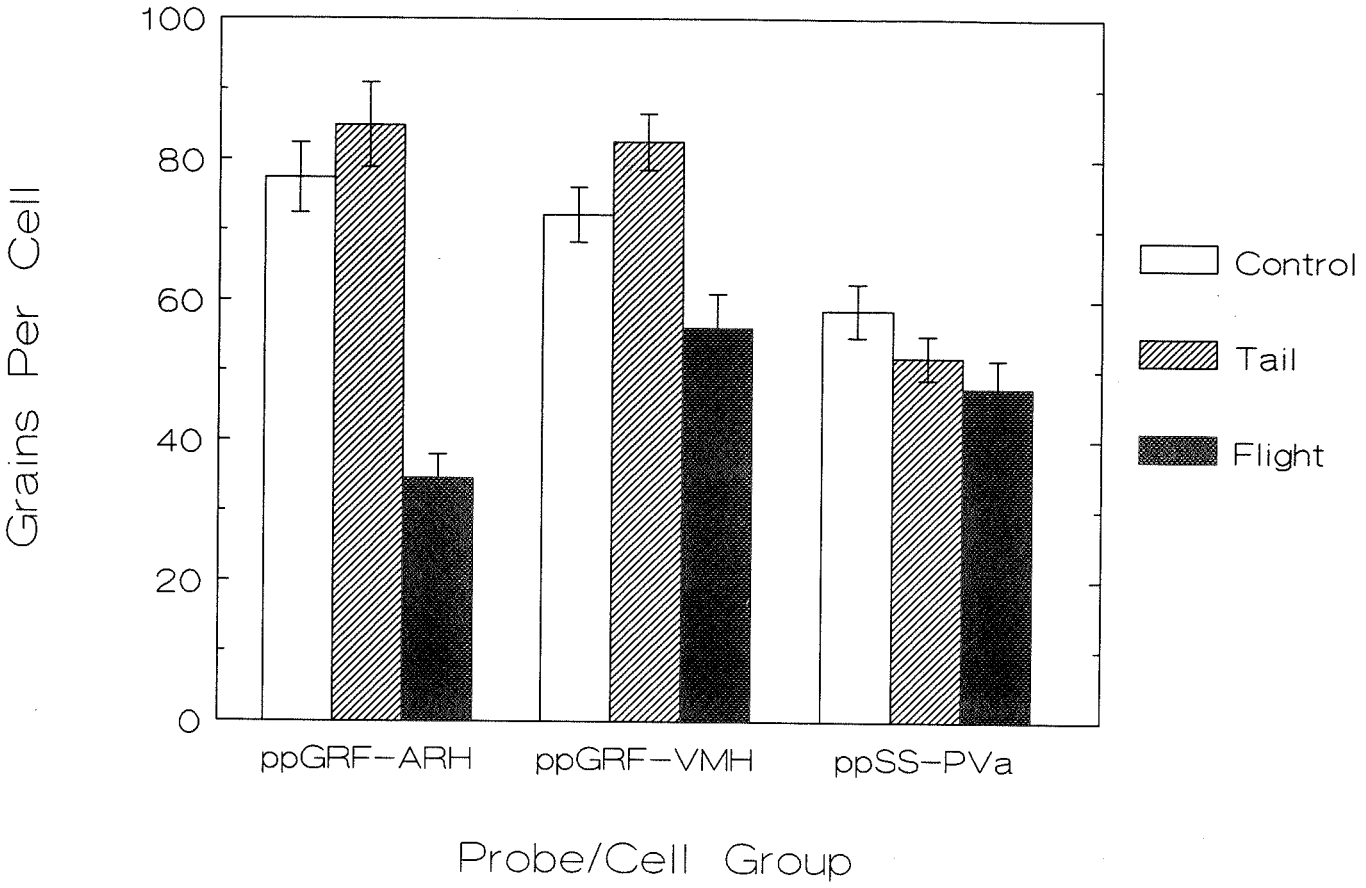

Figure 5. Mean (± SEM) number of silver grains per cell-sized area in material hybridized for ppGRF in the arcuate (ARH) and peri-ventromedial (VMH) regions, and for ppSS in the anterior periventricular nucleus (PVa), in synchronous control (Control), tail-suspended (Tail) and flight groups. Relative to control values, grain densities for ppGRF-hybridized cells were significantly reduced in the arcuate and ventromedial nuclei of flight animals. n = 5 rats (100 cells) per group.

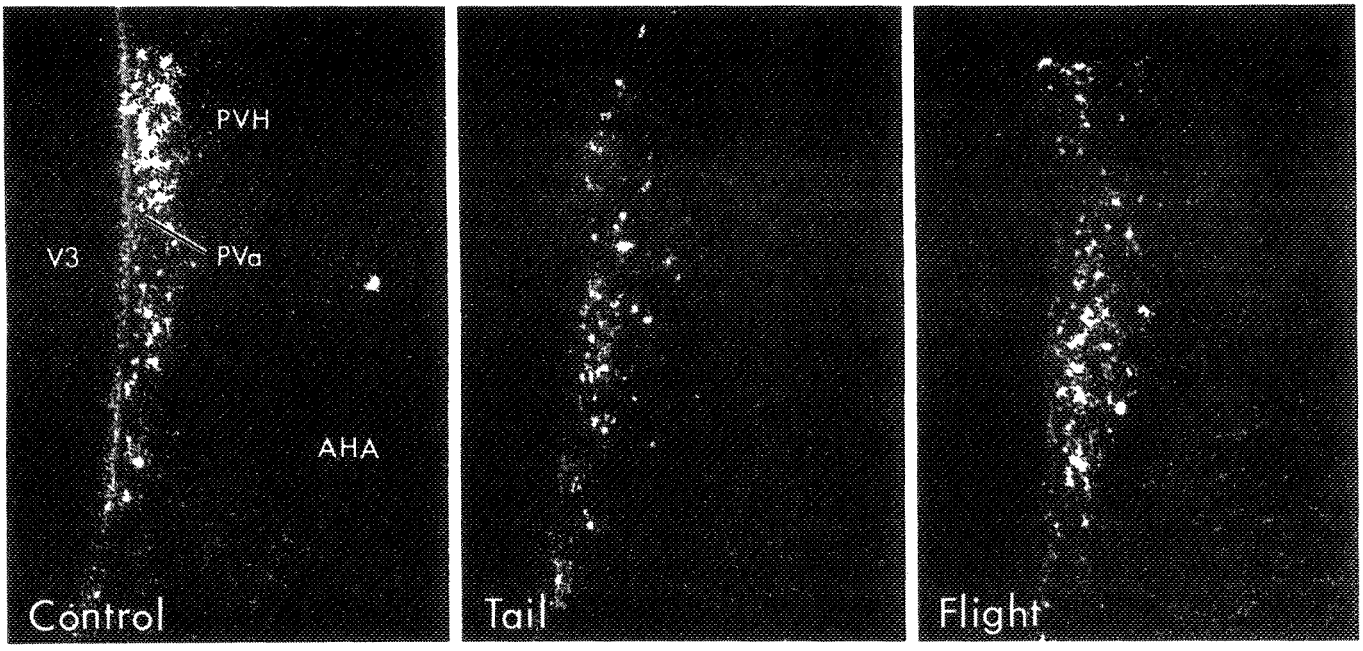

Figure 6. ppSS mRNA localization in the anterior periventricular nucleus of the hypothalamus (PVa). Darkfield photomicrographs of emulsion-dipped autoradiograms showing the major hypophysiotropic ppSS-expressing cell group, at the level of the paraventricular nucleus (PVH) in control, hindlimb-suspended (Tail) and flight groups. No significant between-group differences in cell number or grain density were evident. All micrographs X 75.

511-51
51356

EXPERIMENT K-7-22

PART III: PLASMA ANALYSIS HORMONE MEASUREMENTS

R.E. Grindeland, I.A. Popova, E. Grossman, and I. Rudolph

Plasma from space flight and tail suspended rats was analyzed for a number of constituents in order to evaluate their metabolic status and endocrine function. Plasma electrolytes, proteins, glucose, nitrogenous products of metabolism, and cholesterol were analyzed by Dr. A. H. Merrill and colleagues; these results are included in the final report on K-7-14. Dr. S. Arnaud has measured plasma hormones involved in regulation of calcium metabolism and included the data in her final report (K-7-01). The data presented here cover plasma hormone measurements.

Methods

Corticosterone, thyroxine, and testosterone were measured by radioimmunoassay using kits obtained from ICN Biomedicals, Inc., Costa Mesa, Ca. (corticosterone) and Diagnostic Products Corp; Los Angeles, Ca. (thyroxine, testosterone). Prolactin and growth hormone were measured by double antibody immunoassays using hormones and antisera prepared in house. The procedure was adapted from Schalch and Reichlin (Endocrinology 79; 275-280, 1966). Data were evaluated by analysis of variance.

Results

Plasma concentrations of corticosterone varied widely between groups, ranging from 3 μg/dl for Basal rats to 41 μg/dl for Flight animals. (Table 1). In spite of the high concentration in Flight rats the levels did not differ significantly ($p>0.05$) from those of the Synchronous group; Flight rat corticosterone was higher than for Basal, Vivarium and Suspended groups, however. Although suspended rats showed significant adrenal hypertrophy (Table 2) their corticosterone concentrations did not vary significantly from those of any group except Flight rats. Synchronous rats also showed adrenal hypertrophy and had higher corticosterone levels than Basal rats. (Table 1,2). The correlation between adrenal weights and corticosterone concentrations was not statistically significant.

Thyroxine levels in Flight rats were significantly lower than in Synchronous rats ($p<0.01$) and marginally lower than in Vivarium ($p<0.06$) and Suspended ($p<0.08$) rats, but not different from Basal values. (Table 3) Suspended rats showed marginally lower levels ($p<0.07$) than Synchronous rats but did not differ from Basal or Vivarium rat concentrations.

Testosterone titres were significantly lower in Flight rat plasma than in any other group except Suspended rats ($p<0.05$). (Table 4) Testosterone was also decreased significantly ($p<0.05$) in Suspended rats when compared to Basal, Vivarium, or Synchronous groups. One or more rats in all groups had hypotrophic testes, either bilaterally or unilaterally. Only Suspended rats had significantly smaller testes, however. Testicular levels of testosterone paralleled plasma concentrations of the hormone. (see Amann, K-7-16). Testes size, however, did not correlate with plasma testosterone concentrations.

Plasma immunoreactive growth hormone (IGH) concentrations were lower in Flight rats than Synchronous and Basal controls ($p<0.05$) but did not differ from Vivarium or Suspended rat values. (Table 6) Suspended rats also had lower IGH concentrations ($p<0.05$) than Basal and Synchronous rats, but not Vivarium or Flight animals.

Plasma prolactin levels also varied widely between and within groups. (Table 7). In the tail suspended rats only one animal had detectable levels of prolactin and for the Vivarium group only two rats, thus calculations of standard errors and statistical comparison was not possible. In contrast three Flight and three Basal rats had values in excess of 25 ng/ml. The limited plasma available precluded reassay of the samples. It is clear, however, that Flight and Basal groups had significantly greater levels of prolactin than Synchronous rats and apparently higher concentrations than Suspended or Vivarium animals.

Discussion

Corticosterone concentrations varied nearly 14 fold between groups with levels of 3 μg/dl in the Basal rats, a value similar to that found in our laboratory for gentled rats under quiescent conditions. In contrast the Flight rats had values of 41 μg/dl, a value similar to that found for highly stressed rats under earth laboratory conditions. Although the Flight rats had high levels of corticosterone they were not significantly different from Synchronous control. Corticosterone levels respond rapidly to stress, but one would presume that all rats were handled similarly at sacrifice, thereby obviating any handling effect. The fact that synchronous and suspended rats, with much larger adrenals, had lower levels of corticosterone further suggests that the elevated corticosterone titres of Flight rats is a response to post-flight conditions but perhaps synergized by flight experience. The hypertrophic glands of suspended rats also suggest that a sustained stress occurred over the period of suspension, but the equally hypertrophied adrenals of synchronous rats suggest that some subtle factor not related directly to suspension was responsible. Except for transitory, small increases in corticosterone rats suspended in our laboratory do not show increased concentrations of the hormone nor adrenal hypertrophy. Whether this difference is due to differences in rat strain, rat age, or other, less apparent causes remains unknown.

Thyroxine levels were significantly lower in Flight rats than in controls and were suggestively lower ($p<0.08$) than in Suspended rats. The cause of the decreased thyroxine levels is unknown; it appears not to be attributable to either dietary iodine insufficiency or to excessive metabolic demands. A deficit apparently occurs at the thyroid gland, pituitary, or hypothalamic levels. The low thyroid follicular epithelium found by Dr. Alexander Kaplansky in previous flights (personal communication) suggests that the deficit is in the pituitary gland or hypothalamus. The tail suspended rat does not mimic the flight rat in its thyroid physiology. Again, the reason is not apparent.

Testosterone concentrations were decreased in response to space flight and to tail suspension. The slight reduction in spermatagonia production (R. Amann, K-7-16) in Flight rats suggests that follicle stimulating hormone is not affected in Flight rats, whereas tail suspension significantly depressed testicular weights and sperm production. The fact that receptors for leuteinizing hormone were unchanged in Flight rats (Amann, K-7-16) indicates that either a post-receptor deficit exists in the testes or that leuteinizing hormone is not being secreted.

Plasma growth hormone concentrations measured by radioimmunoassay were lower in Flight rats than Synchronous but not Vivarium controls. This observation suggests that the slight differences-7ng/ml-between Flight and Synchronous rats are probably not important physiologically. However, growth hormone measured by biological assay in pituitary culture media was decreased substantially after flight or tail suspension.(R. Grindeland, K-7-22). In previous studies (Space Lab 3, Cosmos 1887) bioassayable but not immunoreactive growth hormone was decreased in response to microgravity exposure. The fact that suspended and Flight rats both show decreases in plasma bioassayable growth

hormone would argue that the decreased secretion is due to weightlessness and/or hyopdynamia and not to reentry stress.

Prolactin levels could not be accurately quantified because in some rats concentrations were either in excess or less than the standards used (0.8-25 ng/ml). Nonetheless, Basal and Flight rats had high levels and the Vivarium and Suspended rats low concentrations of the hormone. There was no apparent relationship between experimental conditions and plasma prolactin levels, and, accordingly, no explanation for the results observed. Clarification of this problem will require further study.

TABLE 1

COSMOS 2044 PLASMA CORTICOSTERONE LEVELS (AVERAGE OF 2 ASSAYS)
(ng/ml)

Rat#	Basal	Synchronous	Vivarium	Suspended	Flight
6	61.6	256.5	214.7	369.3	452.3
7	5.3	152.9	25.1	64.0	414.7
8	6.6	151.8	140.6	50.6	390.3
9	4.2	255.7	199.4	48.5	163.4
10	71.0	429.0	206.2	167.3	629.8
Mean:	29.7[a]	249.2[b]	157.2[a,b]	139.9[a]	410.1[b]
S.D.	33.6	113.1	79.4	137.4	166.8
S.E.	15.0	50.5	35.4	61.3	74.5

[a] Differs from Flight ($p<0.05$)
[b] Differs from Basal ($p<0.05$); no other significant differences

TABLE 2

COSMOS 2044 ADRENAL WEIGHTS (mg)

Rat #	Flight	Synchronous	Vivarium	Suspended
6	42	45	43	56
7	45	51	40	49
8	42	50	43	48
9	47	57	42	50
10	44	46	45	53
Mean:	43.8	49.7[b]	42.2	51.2[a]
S.E.	1.2	2.6	0.8	1.5

[a] Differs from flight and vivarium ($p<0.001$)

[b] Differs from vivarium ($p<0.01$); no other significant differences

TABLE 3

COSMOS 2044 PLASMA THYROXINE CONCENTRATIONS
(ng/ml)

Rat #	Basal	Vivarium	Suspended	Flight	Synchronous
6	38.4	73.0	116.8	64.8	142.7
7	26.9	87.0	56.8	84.5	155.8
8	57.0	93.3	83.4	55.8	87.3
9	39.9	78.6	98.3	42.4	103.1
10	136.5	139.4	86.7	70.3	123.3
Avg.	59.7[b]	94.3	88.4	63.6	122.4[a]
S.D.	44.2	26.4	22.0	15.8	28.0
S.E.	19.7	11.8	9.8	7.1	12.5

[a] Differs from Flight ($p<0.05$);
[b] Differs from Synchronous ($p<0.05$)

TABLE 4

COSMOS 2044 PLASMA TESTOSTERONE CONCENTRATIONS (ng/ml)

Rat #	Basal	Vivarium	Suspended	Flight	Synchronous
6	1.28	4.88	.88	.41	1.44
7	4.96	1.93	1.40	.28	2.64
8	.70	4.90	.22	.27	1.70
9	2.46	3.80	.03	.09	.79
10	5.68	1.98	.04	.32	3.00
Avg.	3.02[a,b]	3.50[a,b]	.51	.27	1.91[a,b]
S.D.	2.21	1.48	.61	.12	.90
S.E.	.99	.66	.27	.05	.40

Testis weights and testosterone concentrations do not correlate. (r= 0.44)

[a] Differs from Flight ($p<0.05$)
[b] Differs from Suspended ($p<0.05$)

TABLE 5

COSMOS 2044 TESTES WEIGHTS (g)

Rat #	Flight	Synchronous	Vivarium	Suspended
6	1.0	2.0	1.8	1.0
7	2.6	3.0	2.8	1.0
8	1.7	2.7	2.4	0.7
9	2.3	2.8	1.6	1.1
10	2.4	3.1	3.1	1.2
Mean:	1.98	2.69	2.34	1.0[a]
S.E.	0.35	0.22	0.32	0.08

[a] Differs from all other groups ($p<0.05$); no other significant differences.

TABLE 6

COSMOS 2044

PLASMA IMMUNOREACTIVE GROWTH HORMONE CONCENTRATIONS (ng/ml)

Rat #	Basal	Vivarium	Suspended	Flight	Synchronous
6	23.0	15.0	17.0	16.0	28.0
7	35.0	15.0	16.0	16.0	23.0
8	17.0	16.0	15.0	16.0	22.0
9	19.0	17.0	14.0	16.0	23.0
10	39.0	14.0	14.0	16.0	19.0
Mean:	26.5	15.30[a]	15.40[a]	15.80	22.9
S.D.	9.7	1.20	1.30	.35	3.2
S.E.	4.4	.53	.60	.16	1.4

[a] Differs from Basal and Synchronous ($p<0.05$); no other significant differences.

TABLE 7

COSMOS 2044 PLASMA PROLACTIN CONCENTRATIONS (ng/ml)

Rat #	Basal	Vivarium	Suspended	Flight	Synchronous
6	10.3	13.4	8.8	>25.0	2.0
7	7.7	NQ*	NQ*	>25.0	0.4
8	>25.0	NQ*	NQ*	>25.0	1.2
9	>25.0	NQ*	NQ*	0.2	0.9
10	>25.0	0.5	NQ*	1.9	3.0
Mean:	>18.6	2.8	1.7	15.4	1.5
S.E.	----	----	----	5.9	0.5

*Not quantifiable (below lowest standard)

51357

EXPERIMENT K-7-23

EFFECT OF SPACEFLIGHT ON LEVEL AND FUNCTION OF IMMUNE CELLS

PART I. IMMUNOLOGY STUDIES

PART II. PROLIFERATION AND CYTOKINES

Principal Investigator:

G. Sonnenfeld
University of Louisville
Louisville, KY

Co-Investigators:

A. Mandel
NASA Ames Research Center
Moffett Field, CA

P.V. Nash
A. Mastro
Dept. of Molecular and Cell Biology
Pennsylvania State University
University Park, PA

G.R. Taylor
NASA Johnson Space Center
Houston, TX

W.D. Berry
Dept. of Microbiology and Immunology
University of Louisville
Louisville, KY

I.V. Konstantinova
A.T. Lesnyak
Institute of Biomedical Problems
Moscow, USSR

B.B. Fuchs
A.L. Rakhmilevich
Institute of Human Morphology
Academy of Medical Sciences
Moscow, USSR

Page intentionally left blank

S12-51
51257

EXPERIMENT K-7-23

PART I: IMMUNOLOGY STUDIES

G. Sonnenfeld, A.D. Mandel, I.V. Konstantinova, W.D. Berry, G.R. Taylor, A.T. Lesnyak, B.B. Fuchs, and A.L. Rakhmilevich

SUMMARY

Two different experiments were carried out in this segment of the immunology protocol for samples received from rats flown on Cosmos 2044. Control groups included vivarium, synchronous and antiorthostatically suspended rats. In the first experiment, rat bone marrow cells were examined in Moscow for their response to recombinant murine colony stimulating factor-granulocyte/monocyte (CSF-GM). In the second experiment, rat spleen and bone marrow cells were stained in Moscow with a variety of antibodies directed against cell surface antigenic markers. These cells were preserved and shipped to the United States for analysis on a flow cytometer. The results of the studies indicated that bone marrow cells from flown and suspended rats showed a decreased response to CSF-GM as compared to bone marrow cells from control rats. Spleen cells from flown rats showed increased percentages of suppressor-cytotoxic-T and helper-T cells amongst the entire cell population. Bone marrow cells showed an increase in the percentage of helper-T cells in the myelogenous population and increased percentages of anti-asialo GM-1 bearing, interleukin-2 receptor bearing, pan-T and helper-T cells in the lymphocytic population. Cell populations from rats suspended antiorthostatically did not follow the same pattern of distribution of leukocytes as cell populations for flown rats. These results are similar, but not identical to, earlier results from Cosmos 1887, and confirm that space flight can have profound effects on immune system components and activities.

INTRODUCTION

Over the past several years, various alterations in immunological parameters have been reported after space flight (Barone and Caren, 1984; Cogoli, 1981 and 1984; Durnova *et al.*, 1978; Gould *et al.*, 1987a; Konstantinova *et al.*, 1985; Lesnyak and Tashputalov, 1981; Mandel and Balish, 1977; Sonnenfeld *et al*, 1990; Talas *et al.*, 1983 and 1984; Taylor *et al.*, 1983 and 1984. Similar changes have been observed after antiorthostatic suspension (Caren *et al.*, 1980; Gould and Sonnenfeld, 1987b; Rose *et al.*, 1984; Sonnenfeld, *et al..*, 1982). The changes have ranged from alterations in lymphoid organ size (Durnova *et al.*, 1976) to alterations in the production of interferons (Talas *et al.*, 1983 and 1984; Gould *et al.*, 1987a) to alterations in lymphocyte activation (Cogoli *et al.*, 1981 and 1984).

The purpose of the immunology studies flown on Cosmos 2044 was to continue our systematic attempt to define the range of immunological parameters affected by space flight. The experiments were designed to allow repetition and expansion of experiments carried out on the previous Cosmos 1887 flight. In addition, an antiorthostatic suspension study was included to allow direct comparison of the effects of space flight with the effects of suspension on immunological parameters, thereby testing the efficacy of suspension as a microgravity model.

Two different areas of immunological studies were chosen. The first involved a determination of the effects of space flight on the ability of cells to respond to colony

stimulating factor-granulocyte/monocyte (CSF-GM). CSF-GM is an important regulator of the differentiation of bone marrow cells of both the monocyte/macrophage and granulocyte lineages. An alteration in the ability of cells to respond to CSF-GM can result in altered immune function (Waheed and Shadduck, 1979).

The second set of studies involved a determination of the effect of space flight on the expression of cell surface markers of both spleen and bone marrow cells. These markers represent various immunologically important cell populations. An alteration in the percentage of cells can also result in an alteration of immunological function (Jackson and Warner, 1986). The markers that were tested included T-cell markers, B-cell markers, natural killer cell markers, and interleukin-2 receptors. The studies were carried out by staining the cell populations with fluorescein-labelled antibodies directed against the appropriate antigens. The stained cell populations were then analyzed utilizing a flow cytometer, and compared with stained cell populations from control rats for changes in percentages of cells expressing the markers.

MATERIALS AND METHODS

Ten male specific pathogen free rats of Czechoslovakia-Wistar origin (Institute of Endocrinology, Bratislava Czechoslovakia) were flown on the Cosmos 2044 Biosputnik flight for 14 days. Flight, housing, feeding and recovery conditions were as described in the Mission Description section of this technical report. Tissue from rats number 6-10 were used in our project. After sacrifice of the rats, bone marrow cells were extruded with a needle and syringe from the left femur of each rat using RPMI-1640 medium (MA Bioproducts, Walkersville, MD) supplemented with 10% fetal bovine serum, antibiotics glutamine and 2-mercaptoethanol. One-third of the spleen of each of five rats was dissociated into individual cells and placed into supplemented RPMI-1640 medium. All of the samples were placed into transporter vials, held at 4°C, and transported to Moscow. Samples reached the laboratory and analytical work began approximately 24 hr after removal of the tissue from the rats.

Synchronous control, vivarium control, and antiorthostatically tail-suspended rats were treated as described in the Mission Description section of this technical report. Tissues were removed and treated as described for the flight tissue. In addition, a normal rat was sacrificed and tissue harvested and analyzed to serve as an internal control for our assay procedures.

Upon arrival at the laboratory in Moscow, the cells were centrifuged and washed. Cells were washed in RPMI-1640 medium, and counted in a hemocytometer using trypan blue dye exclusion for determination of viability. For colony stimulating factor assays, 1 x 10^5 bone marrow cells were suspended in McCoy's 5a medium (MA Bioproducts, Walkersville MD) supplemented with 10% fetal bovine serum and antibiotics and containing 3% agar (Shadduck and Nagabhushanam, 1971). Included in the medium was 0.1 ml of 1,000 units of recombinant murine CSF-GM (a gift of Dr. Steven Gillis, Immunex Research and Development Corp, Seattle, WA). The CSF-GM was lot 620-028-5 and was of specific activity of at least 5 x 10^7 units/mg protein. Five replicate cultures were set up for each sample. The suspended cells were then placed in 35 mm tissue culture dishes and incubated in a 37°C incubator with 5% CO_2 (Shadduck and Nagabhushanam, 1971). After the appropriate incubation period (5 days), 10 microscope fields on each slide were evaluated for the number of colonies (aggregates of 50 cells or more) formed (Sonnenfeld, *et al.*, 1990).

For the cell surface antigenic markers, the following procedure was carried out (Jackson and Warner, 1986). One x 10^6 bone marrow or spleen cells were placed in a

microcentrifuge tube. The cells were resuspended in FTA buffer (BBL Microbiology Systems, Cockeysville, MD) with 0.1% sodium azide and 0.5% normal mouse serum to decrease background staining. The cells were centrifuged for 1.5 min at 1,000 x g, Supernatants were removed and cells resuspended. Five µl of the appropriate antibody was added to each cell suspension. All antibodies were obtained from Accurate Chemical and Scientific, Westbury, NY except for anti-asialo GM-1, which was obtained from Wako Fine Chemicals, Dallas, TX. The cells were allowed to incubate at 4°C for 25 min. The antibodies used were as follows:

1. Anti-Asialo GM-1 (anti-natural killer cell antigen)
2. OX-39 (anti-interleukin-2 receptor)
3. OX-1 (anti-pan leukocyte marker)
4. W3/25 (anti-helper T-cell)
5. OX-8 (anti-suppressor T-cell)
6. OX-12 (anti-rat lgG Fab')
7. W3/13 (anti-pan T-cell)
8. OX-4 (anti-polymorphic Ia)
9. Anti-Rabbit lgG
10. No Antibody Added.

All antibodies were fluorescein-tagged directly except for anti-asialo GM-1 and OX-39. For these two antibodies, the following indirect technique was carried out. Cells tagged with these antibodies were resuspended in 1 ml of FTA buffer and centrifuged for 1.5 m at 1,000 x g. The cells were resuspended in residual buffer and 5 µl of a second, fluorescein-conjugated antibody and 25 µl of fetal bovine serum were added. The second antibody for anti-asialo GM-1 was anti-rabbit IgG and for OX-39 was anti-mouse IgG. Incubation for these samples was at 4°C for 25 m.

At this point, the following procedure was carried out for all cells tagged with all of the antibodies. One ml of lysing solution (8.26 g ammonium chloride, 1.00 g potassium bicarbonate, 37 mg of tetrasodium EDTA, brought to 1 l with distilled water at pH 7.4) was added to each sample and the cells were allow to incubate at room temperature for 6 min to lyse erythrocytes. The cells were then centrifuged at 1,000 x g for 1.5 min, and then resuspended in 1 ml of FTA buffer. Cells were again centrifuged and fixed by resuspending in 0.5 ml of 1% paraformaldehyde. The cells were then placed at 4°C and transported to the United States.

In one experiment, 1 x 10^6 spleen cells were incubated with 120 units of recombinant murine interferon-gamma (a gift of Dr. Christine Czarniecki, Genentech, Inc., S. San Francisco, CA) for 24 h at 37°C in 5% CO_2. The interferon was lot 2271-68 of specific activity of 5.2 x 10^6 units/mg protein. This was done to determine if space flight affected the ability of interferon-g to enhance expression of Ia antigens. After the incubation period, the cells were harvested and stained with OX-4 as described above.

The cells were analyzed upon return to the United States for fluorescence, an indicator of presence of the antigen, using a FACSCAN flow cytometer (Becton-Dickinson Cytometry Systems, Mountain View, CA) with Consort 30 software. Lymphocytic and myelogenous regions were gated on three-part differentials using forward vs. side scatter plots. Negative gates were set using unstained samples for direct stains and second antibody as the negative control for indirect stains. Fluorescein isothiocyanate fluorescence greater than 530 nm was detected using the 488 nm line of an argon ion laser for excitation.

A Student's T test was carried out for statistical analysis of the CSF-GM data, and an ANOVA using transformed data was carried out for statistical analysis of the cell surface antigenic marker data. Alpha was set *a priori* at $P \leq 0.05$.

RESULTS

Effect of space flight and suspension on the response of bone marrow cells to CSF-GM

Bone marrow cells from flown rats have a reduced capacity to respond to CSF-GM compared to bone marrow cells from vivarium control rats (Table 1). Cells from synchronous control rats showed some degree of decreased responsiveness compared to cells from vivarium control rats; however, the reduction in responsiveness of cells from flight rats was greater than that of cells from synchronous control rats (Table 1). Cells from suspended rats also showed a pattern of reduced response to CSF-GM as did cells from flown rats (Table 1).

Effect of space flight on the percentage of cells expressing cell surface antigenic markers

For spleen cells, higher percentages of cells expressing helper T-cell antigenic markers (W3/25) and suppressor-cytotoxic T-cell antigenic markers were observed from flight animals (Table 2). These changes were beyond increases observed in synchronous controls compared to vivarium controls. There were some small, but statistically significant, differences in levels of unstained cells or anti-rabbit IgG stained cells after flight or synchronous control or suspension treatment. These small changes did not affect our results with other markers as these differences were subtracted (gated) from appropriate experimental values during the flow cytometric analysis (see Materials and Methods). Cells from suspended animals showed a pattern of staining different from that of cells from the flown rats (Table 2). No other changes in expression of antigenic surface markers were observed.

Spleen cells treated with interferon-gamma and then stained with OX-4 (anti-Ia) to determine if the interferon-gamma treatment could affect expression of Ia antigens after space flight were analyzed in the flow cytometer. The data were not interpretable because of a high level of non-specific background staining.

For bone marrow cells, lymphocytic and myelogenous cell populations were analyzed differentially as described in Materials and Methods. In the lymphoid cell population, increases in the percentages of cells expressing anti-asialo GM-1 markers, helper T-cell markers (W3/25), pan-T-cell markers (W3/13) and interleukin-2 receptors (OX-39) increased after flight compared to both synchronous and vivarium controls (Table 3). Cells from suspended animals produced a different pattern of markers compared to cells from flight animals (Table 3).

For the myelogenous population of bone marrow cells, the population of cells expressing the helper T-cell marker (W3/25) was increased compared to both synchronous and vivarium controls (Table 4). Cells from suspended animals produced a different pattern of markers compared to cells from flight animals (Table 4).

DISCUSSION

The results of the current study again show that space flight can profoundly affect immune responses. This supports several previous studies (Barone and Caren, 1984; Konstantinova *et al.*, 1985; Taylor *et al.*, 1983 and 1986) as well as our findings on the previous Cosmos 1887 flight (Sonnenfeld, *et al.*, 1990).

In the present series of experiments, the ability of bone marrow cells from animals exposed to space flight to respond to CSF-GM was severely compromised compared to vivarium controls. Cells from synchronous controls showed some inhibition of responsiveness to CSF-GM compared to cells from vivarium controls, but this decrease in responsiveness was not sufficient to account for the severe inhibition seen in cells from the flight animals. The cells from the synchronous control animals may have shown reduced responsiveness to CSF-GM because of stress factors induced by the synchronous treatment. This result is consistent with our studies carried out during the Cosmos 1887 flight, which showed that bone marrow cells from flight animals were compromised in their ability to respond to CSF-M (Sonnenfeld, *et al.*, 1990). It extends the previous finding to demonstrate that the response to a recombinant DNA-derived cytokine with broader biological activity affecting both monocyte and granulocyte cell populations in the bone marrow (CSF-GM) is also compromised by space flight.

The results of the leukocyte phenotyping experiments involving the determination of the percentage of cells stained by an antibody directed against cell surface antigenic markers also confirm earlier reports indicating that the distribution of these cell populations is altered by space flight (Konstantinova and Fuchs, 1988; Sonnenfeld *et al.*, 1990). In the current series of experiments spleen cells from flown rats showed increased percentages of helper-T and suppressor-cytotoxic-T cells. This is similar to results observed after the Cosmos 1887 flight (Sonnenfeld, *et al.*, 1990). The proportion of interleukin-2 receptor bearing cells did not increase after this flight, as they did after the Cosmos 1887 flight, indicating that differences in flight conditions could affect the nature and range of the immunological changes induced. In the Cosmos 1887 flight, the animals remained on the ground for two days prior to sacrifice and analysis of cell populations (Sonnenfeld, *et al.*, 1990).

The experiment to determine if incubation of spleen cells from flown animals with interferon-gamma would result in expected increases in expression of Ia antigens was not successfully carried out because of technical reasons. There was too much background fluorescence in all of the samples to allow accurate determination of fluorescence in any of the samples. This may have been due to disruption of cells during this particular assay procedure.

The results of the bone marrow staining with antibodies were also of interest. For this experiment, due to availability of additional bone marrow cells, we were able to stain the bone marrow cells with the full repertoire of antibodies. This was not possible after the Cosmos 1887 flight (Sonnenfeld, *et al.*, 1990). In the bone marrow myelogenous cell population, the percentage of cells expressing helper T-cell antigens was increased after flight, but the percentage of lg+ bearing cells was not increased as it was after the Cosmos 1887 flight. In the bone marrow lymphocytic cell population, the percentage of anti-asialo GM-1 bearing, interleukin-2 receptor bearing, pan-T, and helper T-cells was increased after flight. Although results were not identical with those observed after Cosmos 1887 (Sonnenfeld, *et al,* 1990), they were similar. The results of both flight studies suggest that immunological parameters are altered after space flight.

The use of a suspended rat control run in parallel with flight animals allowed a first-time direct comparison of the effects of flight and the effects of suspension on immunological parameters. It appeared that the effects of suspension and spaceflight were similar with regard to CSF-GM reactivity of bone marrow cells. There was, however, no agreement between space flight effects and suspension effects on the distribution of leukocyte subsets. This is consistent with our previous findings that suspension is useful for modeling effects of space flight of functional immune responses (Gould, *et al.*, 1987b; Rose,*et al,* 1984), but not adequate for modeling the effects of space flight on the distribution of cell populations (Berry, *et al.*, 1990).

SUMMARY AND CONCLUSIONS

The current study presents additional data to confirm that space flight affects certain parameters of the immune system. The current study has several advantages over our previous Cosmos 1887 study. There was no delay in sacrifice of the animals after return to earth, decreasing the possibility of re-adaptation to earth gravity playing a role in our results. In addition, our controls on the antibody staining of spleen and bone marrow cells were very clear and definitive for experiments carried out on this flight, adding confidence to the interpretation of our data. The availability of additional cells allowed for expansion of the CSF-GM and leukocyte phenotyping studies.

The experiment to determine if space flight affected the ability of interferon-gamma to enhance expression of Ia antigens did not produce useful data because of technical reasons. The handling and shipment of cells may have created an excess of background staining. We believe that this experiment is of fundamental importance to determine if space flight can affect the development of immune responses and the sensitization of a host to a foreign antigen. We are currently developing new technology that we believe will allow these experiments to be carried out for future flight opportunities.

The results of the suspension study are also of interest. The ability to carry out the same experiment in parallel using cells from flown and suspended animals is helping to determine the advantages and limitations of this model in simulating the effects of space flight on the immune response,

In any case, the results of the current study suggest and confirm that several profound alterations in parameters that play important roles in regulation of immune responses occur as a result of space flight. This is a result of interest that supports the previous studies, and the results suggest the effects of space flight on immune responses and resistance to infection should be an area of continued and expanded study.

ACKNOWLEDGEMENTS

The authors wish to thank Dr. A.S. Kaplansky and the Soviet Cosmos recovery and dissection teams. Without their heroic efforts, these studies could not have been carried out. In addition, we would like to thank Igor Krasnow, Galya Tverskaya, Marilyn Vasques, Richard Grindeland and James Connolly, without whose planning and support successful completion of these studies would have been impossible. We also express our gratitude to the Academician and staff of the Institute of Biomedical Problems, Academy of Sciences of the U.S.S.R., and the Institute of Human Morphology, Academy of Medical Sciences of the U.S.S.R. for their help and the use of their laboratories. This work could not have been accomplished without them. We would also like to thank Drs. John Oldfather and Sandy Helman of the Jewish Hospital of Louisville, KY, USA for their help with the flow cytometric analysis. This study was funded in part by NASA Grant NAG2-614 and the NASA Cosmos 1989 Parts Program.

REFERENCES

1. Barone, R.B. and L.D. Caren. The Immune System: Effects of Hypergravity and Hypogravity. Aviat. Space Environ. Med. Vol. 55: 1063-1068, 1984.

2. Berry, W.D., J.D. Murphy, G.R. Taylor and G. Sonnenfeld. The Relationship of Dihydroxyvitamin D to Cellular Immunity in Simulated Weightlessness. In preparation, 1990.

3. Caren, L.B., A.D. Mandel and J.A. Nunes. Effect of Simulated Weightlessness on the Immune System in Rats. Aviat. Space Environ. Med. Vol. 51: 251-256, 1980.

4. Cogoli, A. Hematological and Immunological Changes During Space Flight. Acta Astronautica Vol. 8: 995-1002, 1981.

5. Cogoli, A., P. Tschopp and P. Fuchs-Bislin. Cell Sensitivity to Gravity. Science. Vol. 225: 228-230, 1984.

6. Durnova, G.N., A.S. Kaplansky, and V.V. Portugalov. Effect of a 22-day Space Flight on Lymphoid Organs of Rats. Aviat. Space Environ. Med. Vol. 47: 588-591, 1976.

7. Gould, C.L., M. Lyte, J.A. Williams, A.D. Mandel, and G. Sonnenfeld, Inhibited Interferon-Gamma but Normal Interleukin-3 Production from Rats Flown on the Space Shuttle. Aviat.Space Environ. Med. Vol. 58: 983-986, 1987a.

8. Gould, C.L. and G. Sonnenfeld. Enhancement of Viral Pathogenesis in Mice Maintained in an Antiorthostatic Suspension Model - Coordination with Effects on Interferon Production. J.Biol. Regulators Homeostatic Agents. Vol. 1: 33-36, 1987b.

9. Jackson, A.L. and N.L. Warner. Preparation, Staining and Analysis by Flow Cytometry of Peripheral Blood Leukocytes. In: Manual of Clinical Laboratory Immunology, 3rd ed. Eds:N.K. Rose, H. Friedman, and J.L. Fahey. American Society for Microbiology, Washington, D.C.: 226-235, 1986.

10. Konstantinova, I.V., E.N. Antropova, M.P. Rykova, O.A. Guseva, A.T. Lesnyak, I.I.E. Vorotnikova, and E.F. Vasilyeva. Cell-Mediated and Humoral Immunity in Cosmonauts Exposed to Space Flight Factors. Vestnik, Akad, Med. Nauk CCCP, No. 8: 51-58, 1985.

11. Konstantinova, I.V. and B.B. Fuchs. The Immune System Under Extreme Condition: Space Immunology. Nauka, Moscow, 1988.

12. Lesnyak, A.T. and R.Y.U. Tashputalov. Effects of Space Flight on Leukocyte Transformation in Cosmonauts' Peripheral Blood. Komich. Biol. Vol. 1: 32-34, 1981.

13. Mandel, A.D. and E. Balish. Effect of Space Flight on Cell-Mediated Immunity. Aviat. Space Environ. Med. Vol. 48: 1051-1057, 1977.

14. Rose, A., J.M. Steffen, X.J. Musacchia, A.D. Mandel, and G. Sonnenfeld. Effect of Antiortho-static Suspension on Interferon-Alpha/Beta Production by the Mouse. Proc. Soc. Exp. Biol. Med. Vol. 177: 253-256, 1984.

15. Shadduck, R.K. and N.G. Nagabhushanam. Granulocyte Colony Stimulating Factor I. Response to Acute Granulocytopenia. Blood. Vol. 38: 14-22, 1971.

16. Sonnenfeld, G., E.R. Morey, J.A. Williams, and A.D. Mandel. Effect of a Simulated Weightlessness Model on the Production of Rat Interferon. J. Interferon Res. Vol. 2: 467-470, 1982.

17. Sonnenfeld, G., A.D. Mandel, I.V. Konstantinova, G.R. Taylor, W.D. Berry, S.R. Wellhausen, A.T. Lesnyak, and B.B. Fuchs. Effects of Space Flight on Levels and Activity of Immune Cells. Aviat. Space Environ. Med. Vol. 61: 648-653, 1990.

18. Talas, M., L. Baktai, I. Stoger, K. Nagy, L. Hiros, I. Konstantinova, M. Rykova, I. Mozgovaya, O. Guseva, and V. Kohzarinov. Results of Space Experiment Program "Interferon" I. Production of Interferon in Vitro by Human Leukocytes Aboard Space Laboratory Soylut-6 ("Interferon-I") and Influence of Space Flight on Lymphocyte Function of Cosmonauts ("Interferon-III"). Acta Microbiol. Hungarica. Vol. 30: 53-61, 1983.

19. Talas, M.,L. Baktai, I. Stoger, K. Nagy, L. Hiros, I. Konstantinova, M. Rykova, L. Mozgovaya, O. Guseva, and V. Kozharinov. Results of the Space Experiment Program "Interferon". Acta Astronautica. Vol. 11: 379-386, 1984.

20. Taylor, G.R. and J.R. Dardano. Human Cellular Immune Responsiveness Following Space Flight. Aviat. Space Environ. Med. Vol. 54, suppl. 1: 555-559, 1984.

21. Taylor, G.R., L.S. Neal, and J.R. Dardano. Immunological Analysis of U.S. Space Shuttle Crewmembers. Aviat. Space Environ. Med. Vol. 57: 213-217,1986.

22. Waheed, A. and R.K. Shadduck. Purification and Properties of L Cell Derived Colony Stim-ulating Factor. J. Lab. Clin. Med. Vol. 94: 180-194, 1979.

TABLE 1

EFFECT OF SPACE FLIGHT ON THE RESPONSE OF BONE MARROW CELLS TO CSF-GM

	Mean Number of Colonies (± Standard Error) in 10 Microscope Fields¶		
Flight	Synchronous	Vivarium	Suspension
1.3 ± 0.4*	7.4 ± 0.9*	24.0 ± 15.3	12.4 ± 3.6*

¶ Mean of 10 replicate cell cultures of each of 5 rats

* Statistically significant difference from vivarium control

TABLE 2

EFFECT OF SPACE FLIGHT ON THE PERCENTAGE OF SPLEEN CELLS EXPRESSING CELL SURFACE MARKERS

Antibody	Mean ± Standard Deviation of % of Cells Expressing Markers ¶			
	Flight	Synchronous	Vivarium	Suspension
No Antibody Added	2.7 ± 1.2*	1.1 ± 1.0	0.6 ± 1.4	1.0 ± 1.0
OX-1(pan-leukocyte)	95.6 ± 4.6*	96.5 ± 4.6	98.4 ± 0.9	98.4 ± 1.2
W3/13 (pan T-cell)	52.0 ±20.6	30.5 ± 5.8	41.0 ± 7.1	39.8 ± 8.2
W3/25 (helper T-cell)	71.6 ± 6.2*	44.1 ± 6.5	49.4 ± 3.4	56.2 ± 3.8
OX-8 (suppressor T-cell)	58.4 ±17.8*	39.3 ±10.9	45.8 ± 4.0	44.6 ± 5.4
OX-4 (la)	40.7 ± 7.2	36.1 ± 9.9	41.8 ± 2.1	64.2 ± 9.6*
OX-39 (interleukin-2 recep.)	28.5 ± 4.9	21.3 ± 2.6	19.8 ± 2.1	48.7 ± 9.6*
Anti-lgG Fab'	60.3 ± 7.6	51.9 ± 3.5	62.4 ± 5.7	65.9 ± 8.0
Anti-Asialo GM-1 (NK cell)	31.7 ± 4.7	34.7 ±12.5	18.9 ± 0.8	53.7 ±12.2
Anti-Rabbit lgG	0.8 ± 2.9*	0.4 ± 2.7*	1.9 ± 2.1	0.1 ± 1.4*

¶ Mean of five different rats

* Statistically significant difference from vivarium control

TABLE 3

EFFECT OF SPACE FLIGHT ON THE PERCENTAGE OF THE LYMPHOCYTIC POPULATION OF BONE MARROW CELLS EXPRESSING CELL SURFACE MARKERS

Antibody	Mean ± Standard Deviation of % of Cells Expressing Markers¶			
	Flight	Synchronous	Vivarium	Suspension
No Antibody Added	0.6 ± 1.0	1.7 ± 0.9*	0.5 ± 1.0	0.8 ± 1.3
OX-1 (pan-leukocyte)	75.0 ±13.3	80.2 ± 0.5	82.6 ± 0.8	82.3 ± 0.4
W3/13 (pan T-cell)	75.2 ± 5.8*	47.9 ±17.2*	26.8 ± 9.7	30.6 ± 1.4
W3/25 (helper T-cell)	72.0 ± 4.5*	36.3 ± 6.0	33.5 ±14.3	32.1 ± 1.5
OX-8 (suppressor T-cell)	54.8 ±16.3	57.0 ± 2.9	51.0 ±17.5	43.9 ±16.0
OX-4 (la)	48.1 ±17.8*	39.2 ± 8.1	27.6 ± 3.1	40.6 ± 3.7
OX-39 (interleukin-2 recep.)	36.8 ± 5.1*	25.1 ± 7.1	20.7 ± 7.2	27.7 ± 2.0
Anti-lgG Fab'	49.3 ±17.5	51.8 ±13.3	44.2 ± 2.6	68.1 ±12.3*
Anti-Asialo GM-1 (NK cell)	37.2 ± 2.9*	25.3 ± 9.1*	17.2 ± 5.0	29.8 ± 2.8*
Anti-Rabbit lgG	13.6 ± 1.9*	4.0 ± 2.8	5.4 ± 4.9	3.7 ± 2.7

¶ Mean of five different rats

* Statistically significant difference from vivarium control

TABLE 4

EFFECT OF SPACE FLIGHT ON THE PERCENTAGE OF THE MYELOGENOUS POPULATION OF BONE MARROW CELLS EXPRESSING CELL SURFACE MARKERS

Antibody	Mean ± Standard Deviation of % of Cells Expressing Marker ¶			
	Flight	Synchronous	Vivarium	Suspension
No Antibody Added	1.2 ± 1.0	1.6 ± 1.6	1.1 ± 1.4	0.9 ± 0.8
OX-1 (pan-leukocyte)	97.4 ± 2.5	97.4 ± 1.3	97.5 ± 2.1	98.3 ± 1.5
W3/13 (pan T-cell)	85.0 ±11.3*	78.4 ± 3.2	71.1 ± 1.6	77.1 ± 1.6
W3/25 (helper T-cell)	69.4 ±14.7*	31.4 ± 5.9	38.1 ±12.9	35.7 ± 7.9
OX-8 (suppressor T-cell)	23.8 ±13.0	16.6 ± 3.0	16.5 ± 5.7	22.3 ± 5.7
OX-4 (la)	31.6 ±12.8	22.0 ±13.5	6.2 ± 3.9	13.2 ± 4.8
OX-39 P (interleukin-2 recep)	67.2 ±23.7	55.6 ±12.1	62.5 ±13.0	46.3 ± 6.9
Anti-lgG Fab'	26.2 ±30.0	32.0 ±18.7	22.1 ± 9.1	54.3 ±19.6
Anti-Asialo GM1 (NK cell)	87.2 ± 6.2	75.0 ±10.6	71.8 ±10.4	58.6 ± 2.8
Anti-Rabbit lgG	3.0 ± 2.8	2.0 ± 3.5*	4.5 ± 2.9	0.7 ± 1.3*

¶ Mean of five different rats

* Statistically significant difference from vivarium control

S13-51

513658

EXPERIMENT K-7-23

PART II: PROLIFERATION AND CYTOKINES

P.V. Nash, I.V. Konstantinova, B.B. Fuchs, A.L. Rakhmilevich,
A.T. Lesnyak, and A.M. Mastro

SUMMARY

Lymphocytes from the superficial inguinal lymph nodes of rats flown on the Cosmos 2044 space mission were tested for proliferation in response to polyclonal activators. Cells were cultured with T or B cell mitogens, phorbol ester and calcium ionophore, or T cell mitogen and the lymphokines interleukin-1 (IL-1) or interleukin-2 (IL-2), and assayed for DNA synthesis by ^{3}H-thymidine incorporation. Lymphocytes also were incubated with concanavalin A (Con A), a T cell mitogen, and tested for IL-2 production. Mitogen-stimulated proliferation of lymphocytes from rats exposed to microgravity was not significantly different from synchronous or vivarium controls. Responses to Con A and IL-2, and Con A and IL-1 likewise were unaffected by space flight. Lymphocytes from all of these groups responded well to phorbol ester and calcium ionophore stimulation. Furthermore, lymph node cells (LNC) from control rats and rats flown on Cosmos 2044 produced similar amounts of IL-2. The results obtained using hindlimb suspended rats were notably different from those of flight and control animals. LNC from suspended rats generally had greater proliferative responses to T cell mitogens than did lymphocytes from other groups. Responsiveness to a B cell mitogen was not enhanced. Con A-stimulated LNC from hindlimb suspended rats also produced more IL-2 than did lymphocytes from the other groups. This difference was statistically significant at both IL-2 induction times tested.

INTRODUCTION

There is ample evidence from the study of human peripheral blood lymphocytes (PBL) following space flight that many astronauts have an impairment of mitogen-induced T cell proliferation. The depression in lymphocyte responsiveness observed following the Soyuz 6, 7 and 8 missions (1) has since been reported in astronauts in the Skylab (2), Salyut (3), and Space Shuttle (4,5) programs. Experiments using *in vitro* and *in vivo* simulations of microgravity also indicate there is a reduction in lymphocyte proliferation (6,7). There are, however, conflicting reports from some studies of human PBL (5,8,9) and rat splenocytes (10). Furthermore, there is no information about the effects of space flight on other lymphatic tissues.

Only a small portion of the total lymphocyte complement circulates in the blood. Thus, to accurately assess immunocompetence it is important to measure the activity of cells from regional lymphatic tissue as well. Our experiments using a rat hindlimb suspension model of weightlessness indicated that the effect of microgravity on LNC proliferative responses differs from the effect on PBL or splenocytes (7). The Cosmos 2044 biosatellite afforded us the first opportunity to study the effects of space flight on the proliferation of T and B cells from rat lymph nodes. Con A or phytohemagglutinin (PHA), mitogens which may stimulate different subpopulations of T lymphocytes, or lipopolysaccharide (LPS) and dextran sulfate (DxS), a B cell mitogen, were used to assess the ability of cells to proliferate. The experiments also were designed to investigate potential mechanisms involved in any observed T cell deficiency. LNC were stimulated with 12-O-tetradecanoylphorbol-13-acetate (TPA) and ionomycin, compounds that can bypass the

need for T cell receptor/ligand interactions, Con A and IL-1 to test for an accessory cell defect, or Con A and IL-2 to test for a deficiency in IL-2 production. Finally, lymphocytes were incubated with Con A to measure the ability of the cells to produce IL-2, a lymphokine necessary for T cell proliferation.

MATERIALS AND METHODS

Tissue Preparation

Ten 4-month old male Czechoslovakian Wistar rats (Institute of Experimental Endocrinology, Bratislava, Czechoslovakia) were flown for 13d 19h on the Cosmos 2044 biosatellite. Five of these rats (numbers 6-10) were used for this study, and 5 vivarium control, 5 synchronous control and 5 hindlimb suspended rats were assayed on subsequent days as described for the flight rats. Maintenance of animals, control groups, hindlimb suspension protocol, and flight and recovery conditions are described elsewhere. The superficial inguinal lymph nodes were removed with the surrounding fat pad and placed in RPMI 1640 medium (GIBCO, Grand Island, NY) supplemented with 2% fetal calf serum (FCS; Hyclone Laboratories Inc., Logan, UT) and kept at 4°C until arrival in Moscow, approximately 26h later. The lymph nodes were dissected from the fat, crushed, and the cells suspended in RPMI 1640 medium supplemented with 2mM L-glutamine, 2.5 x 10^{-5}M 2-mercaptoethanol (2-ME) and 50 ug/ml gentamycin sulfate (S-RPMI). Viability as determined by trypan blue exclusion was generally >90%, and LNC were resuspended at 1 x 10^6 cells/ml in S-RPMI with 6% FCS. There was insufficient tissue to do all of the assays for every rat. Tables 1 and 2 list the number of rats whose lymph nodes were tested for proliferation and IL-2 production, respectively.

Proliferation

Lymphocytes (0.2 ml/well) were cultured in triplicate wells of 96-well culture plates and incubated at 37°C in 5% CO_2/95% air for 2 or 3 days with medium (control wells) or an optimal concentration of mitogen. The compounds tested were Con A (ICN Biomedicals Inc., Lisle, IL; 1ug/ml for 3 days), PHA (Burroughs-Wellcome, Greenville, NC; 2.5 ug/ml for 2 days), LPS/DxS (Difco Laboratories, Detroit MI, Sigma Chemical Co., St. Louis, MO; 10/10 ug/ml for 3 days), TPA/ionomycin (Chemsyn, Lenexa, KS, Calbiochem, San Diego, CA; 10^{-7}M/7.5 x 10^{-7}M for 2 days), IL-2 alone (Boehringer-Mannheim, Indianapolis, IN; 100 U/ml for 3 days), Con A/IL-2 (1 ug/ml/100 U/ml for 3 days), and Con A/IL-1 (IL-1 from LAO Enterprises, Gaithersburg, MD; 1ug/ml/25 U/ml for 3 days). ^{3}H-thymidine (ICN Biomedicals Inc., Costa Mesa, CA; 6.7 Ci/mM) was added at 2 uCi/well after 30h of mitogen incubation for 2d cultures, and after 48h of stimulation for 3d cultures. Lymphocytes were harvested onto glass filter papers (LKB, Gaithersburg, MD) 18h after ^{3}H-thymidine addition using a Skatron harvester (Flow Laboratories Inc., McLean, VA), and transported to the U.S. for liquid scintillation counting (LKB, Gaithersburg, MD).

IL-2 Production

IL-2-containing culture media were produced by stimulating 1 x 10^5 cells/well in S-RPMI/6% FCS, with 1 ug/ml Con A. Cultures were incubated for 48h or 66h in 5% CO_2/95% air at 37°C. Control cultures were incubated in medium without Con A. Cells were centrifuged and the culture media collected and frozen (-20°C) for shipment to the U.S. Media then were thawed and assayed for IL-2 production using CTLL-2 cells, an IL-2-dependent line, and ^{3}H-thymidine incorporation (11). Recombinant human IL-2 (a

generous gift from Hoffman-LaRoche Inc., Nutley, NJ) was used for preparation of the standard curve.

Statistics

The data presented are the mean counts per minute (CPM) +/- the S.E.M. The stimulation index (SI) was calculated by dividing the average CPM of stimulated cultures by the average CPM of the appropriate control cultures (2d or 3d unstimulated cells) for each group. The degree of significance of differences between groups was determined by an analysis of variance test on untransformed IL-2 production data. Proliferation data were normalized by log transformation before analysis. Groups were judged to be significantly different from each other if $p \leq 0.05$.

RESULTS

Proliferation

Basal level uptake of ^{3}H-thymidine by unstimulated LNC was measured after 2d and 3d of incubation. Incorporation in all cultures from all groups of animals was slightly greater after 3d than after 2d of culture, but none of the groups was significantly different from the others at either time (Fig. 1). Addition of IL-2 to unstimulated cells from flight and synchronous controls resulted in a 15-fold increase in proliferation. There was a 10-fold increase in incorporation in vivarium controls and a 21-fold increase in cells of suspended rats when compared with unstimulated cultures (Fig. 1). IL-2-stimulated proliferation was greater in cells from suspended rats than in those of the flight group ($p=0.04$), but the differences between the other groups were not significant.

Lymphocytes from rats of all groups responded well to Con A stimulation. The largest response was seen in LNC from suspended rats (SI=206). LNC from flight rats had slightly lower responses (SI=166) to this mitogen than did the LNC from the suspended group, followed by those of the synchronous controls (SI=117) and the vivarium controls (SI=83) (Fig. 2). Proliferation in cultures from hindlimb suspended rats was significantly greater than that in the vivarium control group ($p=0.02$), but not greater than the synchronous controls ($p=0.06$) at the $p=0.05$ level. Con A responsiveness of LNC from flight rats was not significantly different from that of suspended rats cells. Addition of IL-2 or IL-1 to Con A-stimulated cells resulted in a small enhancement of Con A-induced proliferation (1.1-1.3-fold) in all groups except vivarium controls (Fig. 2), in which there was no change. IL-2-enhanced proliferation in LNC of suspended rats was significantly greater than in LNC of flight rats ($p=0.05$) and vivarium controls ($p<0.01$). Cultures of lymphocytes from flight rats also were greater than vivarium controls ($p=0.04$), as were synchronous controls ($p=0.05$). Stimulation with Con A and IL-1 was significantly greater in the suspended group than in vivarium controls ($p<0.01$), but not greater than flight ($p=0.07$) or synchronous control ($p=0.06$) groups at the $p=0.05$ level. LNC of flight rats were more responsive to Con A and IL-1 than vivarium controls ($p=0.05$), but not more than synchronous controls.

Stimulation with another T cell mitogen, PHA, was greatest in lymphocytes from flight (SI=279) and suspended rats (SI=260). Vivarium and synchronous controls had stimulation indices of 177 and 134, respectively (Fig. 3). ^{3}H-thymidine incorporation after PHA stimulation was significantly greater in LNC of suspended rats than in those of flight ($p=0.01$), synchronous control ($p=0.03$) and vivarium control ($p<0.01$) groups.

TPA and ionomycin were used to circumvent the requirement for interaction between mitogen and receptor. Again, proliferation was greatest in cells from flight (SI=536) and

suspended (SI=371) rats. The increase in proliferation for synchronous controls was 208-fold, while the vivarium control cultures proliferated 354 times more than background (Fig. 3). Statistical analysis of TPA/ionomycin-induced proliferation showed significantly greater stimulation in LNC from suspended rats than in synchronous ($p<0.01$) or vivarium ($p<0.01$) controls, but not than flight animals ($p=0.07$). Stimulation in flight cultures was greater than in synchronous controls ($p=0.03$).

Stimulation with LPS/DxS resulted in a 33-37-fold increase in proliferation in flight, synchronous control and vivarium control rats. Suspended rats had an SI of 42 (fig. 3). There were no significant differences between any of the experimental groups. The differences between groups in their responses to mitogens are summarized in Table 3.

IL2 Production

LNC from flight rats produced similar amounts of IL-2 after either 48h (22 U/ml) or 66h (26 U/ml) of Con A stimulation. The vivarium control group likewise showed no change in production between 48h (15 U/ml) and 66h of incubation (16 U/ml). Culture media from synchronous control and suspended rat lymphocytes on average contained more IL-2 after 66h of Con A stimulation than after 48h (Fig. 4). There were no significant differences between the flight group and the control groups in the amount of IL-2 produced at either induction time. However, at 48h of incubation, LNC from suspended rats produced more IL-2 than synchronous ($p<0.01$) or vivarium ($p<0.01$) controls, or flight rats ($p=0.02$); after 66h of stimulation, cultures from hindlimb suspended animals contained more IL-2 than synchronous controls ($p=0.02$) and vivarium controls ($p=0.01$). The average production by LNC of the suspended group also was greater than from cells of flight rats at 66h, but this was not statistically significant ($p=0.07$). The differences between groups in their ability to produce IL-2 are summarized in Table 4.

DISCUSSION

The proliferation of rat LNC stimulated with polyclonal T or B cell mitogens was unaffected by a 2 week space flight on Cosmos 2044. Responses to Con A, PHA and LPS/DxS were not statistically different between flight and control groups. This result was unexpected in view of the evidence that human PBL responses are suppressed following exposure to microgravity (1-5). There may be fundamental differences between human and rat lymphocyte responses to space flight, but more likely, the effects may vary depending on which lymphoid tissue is examined. A study of T and B cell reactivity using a hindlimb suspension model of weightlessness demonstrated tissue-specific differences in lymphocyte responsiveness. Proliferation of T lymphocytes from blood was significantly depressed, while splenocytes and LNC from posterior lymph nodes were not (7). The finding that lymphocytes in regional lymphatic tissue are not suppressed by microgravity is potentially important. The implication that a significant number of lymphocytes in the body may be fully responsive and that only the circulating T cells are particularly sensitive to microgravity may have significance for evaluating the immunocompetence of astronauts.

T cells from flight rats were more responsive to Con A and IL-2, and Con A and IL-1, than were the vivarium controls. However, proliferation of flight rat lymphocytes was not greater than synchronous controls, so the increase does not appear to be associated specifically with space flight. TPA/ionomycin responses in the flight group were greater than synchronous controls, but not than vivarium controls. These results indicate there may be a trend toward heightened responsiveness in flight rats, but this was not confirmed statistically.

The proliferative responses of LNC from suspended rats were greater than controls for Con A, PHA, Con A and IL-2, Con A and IL-1, and TPA/ionomycin stimulations. LNC from suspended rats also had greater responses than flight animals for some mitogens. The method of suspension in this study involved more restraint than is typically used with this model (12). Since restraint could affect the lymphocyte responses of suspended rats (13), it may not be useful to compare these animals with the flight group. However, a trend toward increased responsiveness to mitogens in both groups was noted.

Production of IL-2, another indicator of T cell competence, also was unaffected by space flight in this study. LNC from flight rats made this lymphokine in amounts similar to controls at both 48h and 66h of stimulation. Splenocytes from rats flown on Cosmos 1667 for 7d produced less IL-2 at 48h than did controls (14). The differing results in these two studies may reflect an adaptation to microgravity during the 2 week Cosmos 2044 flight, or a tissue-specific difference in responsiveness.

LNC from the suspended group produced more IL-2 than did lymphocytes from the other three groups. There was significantly more IL-2 in 48h and 66h culture media from suspended rats than in media from both control groups. There also was more IL-2 in supernatants from suspended rats than in flight cultures at 48h. Again, the significance of these findings is unclear because of the method of suspension, but both flight and suspended rat LNC produced more IL-2 on average than did the controls.

CONCLUSIONS

A 2 week space flight did not impair the responsiveness of rat inguinal LNC, as measured by mitogen-stimulated proliferation and IL-2 production. This result indicates that lymphocyte responses may be tissue-specific, since some studies have suggested that microgravity decreases PBL reactivity to T cell mitogens. An opportunity to measure proliferative responses in spleen, regional lymph nodes, and blood from each animal flown on future missions will help to answer this question. However, mission duration should be considered since the IL-2 results of this study and those of Konstantinova (14) indicate that adaptation may occur after a period of time.

The results of the hindlimb suspension model are less clear. These animals were studied in an attempt to validate the model. While a trend toward greater proliferation and IL-2 production in LNC from flight rats was observed in the suspended group, the responses of LNC from suspended animals were statistically different from the flight rats in some assays. The results from these suspended animals agree with our previous findings of no significant depression in mitogenic responsiveness in LNC of hindlimb suspended rats (7). However, we did not note an enhancement, as seen in this study. We hope to have another opportunity to make the comparison between the effects of simulated microgravity and space flight.

ACKNOWLEDGMENTS

We would like to thank Dr. A.S. Kaplansky and the team of scientists who dissected the tissues for this study. We gratefully acknowledge the staff of the Institute of Biomedical Problems and the Institute of Human Morphology, Academy of Medical Sciences of the U.S.S.R. for their assistance in carrying out this work and for the use of their laboratories. This study was funded in part by NASA grant NAG 2-599.

REFERENCES

1. Konstantinova, I.V., Ye.N. Antropova, V.I. Legen'kov and V.D. Zazhirey. Study of Reactivity of Blood Lymphoid Cells in Crew Members of the Soyuz-6, Soyuz-7, and Soyuz-8 Spaceships Before and After Flight. Space Biol. Aerosp. Med. 7:48-55, 1973.

2. Kimzey, S.L. Hematology and Immunology Studies. In: Biomedical Results from Skylab, NASA-SP 377. U.S. Government Printing Office, Washington, D.C. 249-282, 1977.

3. Konstantinova, I.V., Yu.G. Nefedov, A.V. Yeremin, V.I. Drozdova, A.S. Skryabin, O.A. Guseva, and N.N. Mukhina. Immunological Reactivity and Prediction of Allergic Complications in the Crew of the Second Expedition Salyut-4. Space Biol. Aerosp. Med. 12:16-21, 1978

4. Taylor, G.R. and J.R. Dardano. Human Cellular Immune Responsiveness Following Space Flight. Aviat. Space Environ. Med. 54(#1 suppl.):S-55-S-59, 1983.

5. Taylor, G.R., L.S. Neale, and J.R. Dardano. Immunological Analyses of U.S. Space Shuttle Crewmembers. Aviat. Space Environ. Med. 57:213-217, 1986.

6. Cogoli, A., M. Valluchi-Morf, M. Mueller, and W. Briegleb. Effect of Hypogravity on Human Lymphocyte Activation. Aviat. Space Environ. Med. 51:29-34, 1980.

7. Nash, P.V., B.A. Bour, and A.M. Mastro. Effect of Hindlimb Suspension Simulation of Microgravity on *In Vitro* Immunological Responses. Exp. Cell Res. (accepted for publication), 1991.

8. Fischer, C.L., J.C. Daniels, W.C. Levin, S.L. Kimzey, E.K. Cobb, and S.E. Ritzmann. Effects of the Space Flight Environment on Man's Immune System: II. Lymphocyte Counts and Reactivity. Aerospace Med. 43:1122-1125, 1972.

9. Cogoli, A., B. Bechler, O. Müller, and E. Hunzinger. Effect of Microgravity on Lymphocyte Activation. In: Biorack on Spacelab D1. Eds: N. Longdon and V. David. ESA Publications, Noordwijk, The Netherlands. 89-100, 1987.

10. Mandel, A.D. and E. Balish. Effect of Space Flight on Cell-Mediated Immunity. Aviat. Space Environ. Med. 48:1051-1057, 1977.

11. Gillis, S., M.M. Ferm, W. Ou, and K.A. Smith. T cell Growth Factor: Parameters of Production and a Quantitative Microassay for Activity. J. Immunol. 120:2027-2032, 1978.

12. Wronski, T.J. and E.R. Morey-Holton. Skeletal Response to Simulated Weightlessness: A Comparison of Suspension Techniques. Aviat. Space Environ. Med. 58:63-68, 1987.

13. Griffin, J.F.T. Stress and Immunity: A Unifying Concept. Vet. Immunol. Immunopathol. 20:263-312, 1989.

14. Konstantinova, I.V. Space Flights of Animals on COSMOS Biosatellites. In: The Immune System Under Extreme Conditions: Space Immunology. NASA-USSR Space Life Sciences Digest. 24:45-51, 1989.

TABLE 1

NUMBER OF RATS TESTED FOR LNC RESPONSES TO POLYCLONAL MITOGENS AND LYMPHOKINES

	No. of rats/group			
Mitogen	Flight	Synchronous	Vivarium	Suspended
^{3}H control (2d)	2	1	4	4
^{3}H control (3d)	4	4	5	5
IL-2	4	2	4	4
Con A	5	4	5	5
Con A + IL-2	5	3	4	5
Con A + IL-1	5	3	4	5
PHA	3	2	4	4
LPS/DxS	5	4	5	5
TPA/Ionomycin	5	3	4	5

TABLE 2

NUMBER OF RATS TESTED FOR LNC PRODUCTION OF IL-2

	No. of rats/group			
Time of Induction	Flight	Synchronous	Vivarium	Suspended
48 hours	3	4	5	5
66 hours	3	4	5	5

TABLE 3

SUMMARY OF THE SIGNIFICANT DIFFERENCES BETWEEN EXPERIMENTAL GROUPS IN PROLIFERATIVE RESPONSES OF LNC TO POLYCLONAL MITOGENS

Mitogen	Differences Between Groups	p value
Con A	SUSP>SYNC	0.06
	SUSP>VIV	0.02
PHA	SUSP>FLT	0.01
	SUSP>SYNC	0.03
	SUSP>VIV	<0.01
LPS/DxS	No significant differences	
Con A + IL-1	SUSP>FLT	0.07
	SUSP>SYNC	0.06
	SUSP>VIV	<0.01
	FLT>VIV	0.05
IL-2 alone	SUSP>FLT	0.04
Con A + IL-2	SUSP>FLT	0.05
	SUSP>VIV	<0.01
	SYNC>VIV	0.05
	FLT>VIV	0.04
TPA	SUSP>FLT	0.07
	SUSP>SYNC	<0.01
	SUSP>VIV	<0.01
	FLT>SYNC	0.03

TABLE 4

SUMMARY OF THE SIGNIFICANT DIFFERENCES BETWEEN EXPERIMENTAL GROUPS IN PRODUCTION OF IL-2 BY LNC

Time of Induction	Differences Between Groups	p value
48 hours	SUSP>SYNC	<0.01
	SUSP>VIV	<0.01
	SUSP>FLT	0.02
66 hours	SUSP>SYNC	0.02
	SUSP>VIV	0.01
	SUSP>FLT	0.07

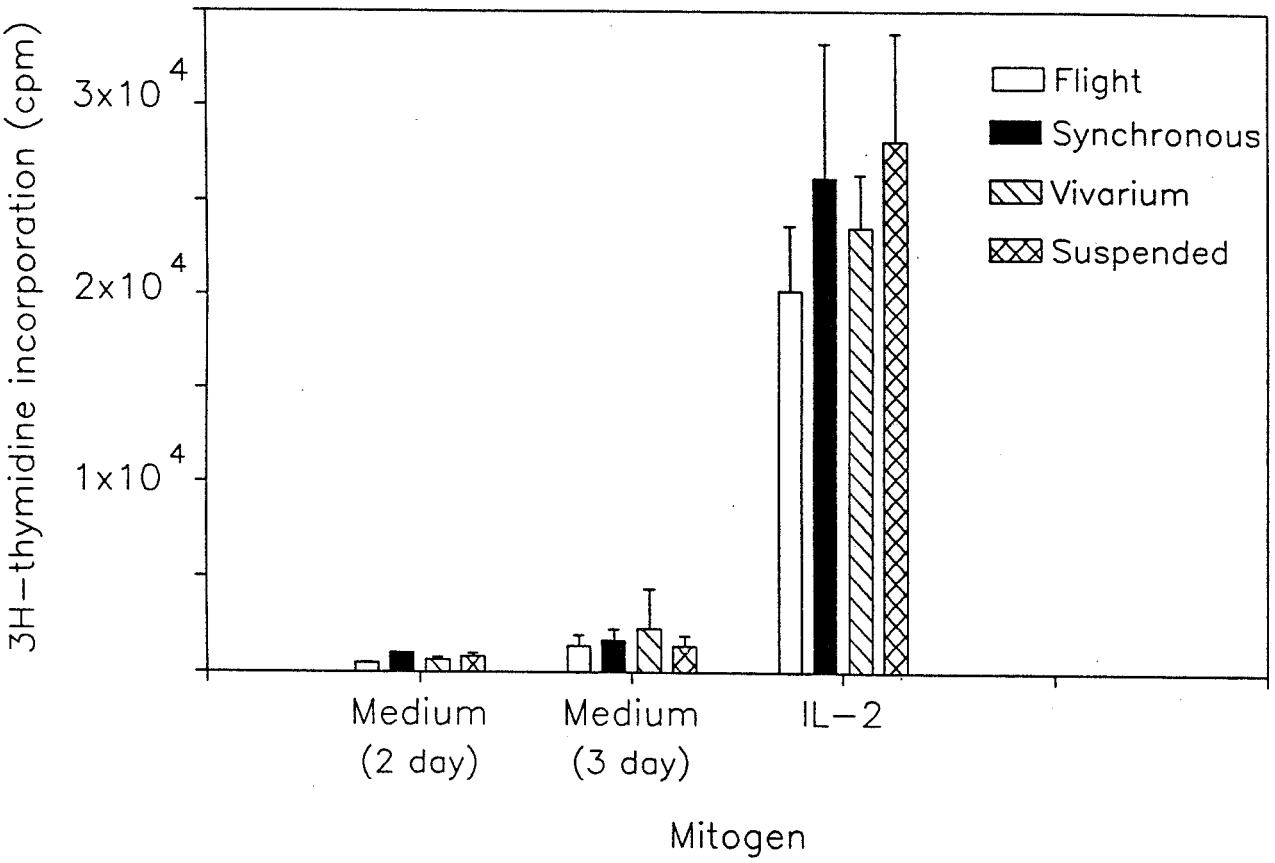

Figure 1. The effect of space flight on basal level of ^{3}H-thymidine uptake and on proliferation in response to exogenous IL-2 ^{3}H-thymidine incorporation by unstimulated cells was measured at 2d and 3d of incubation. The effect of IL-2 alone (100 U/ml) was tested after 3d of stimulation. Lymphocytes were cultured at 2 x 10^{5} /well in RPMI/6% FCS/2.5 x 10^{5} M 2-ME/50 ug/ml gentamycin sulfate. Cells were pulsed with 2 uCi/well ^{3}H-thymidine 18h before harvest.

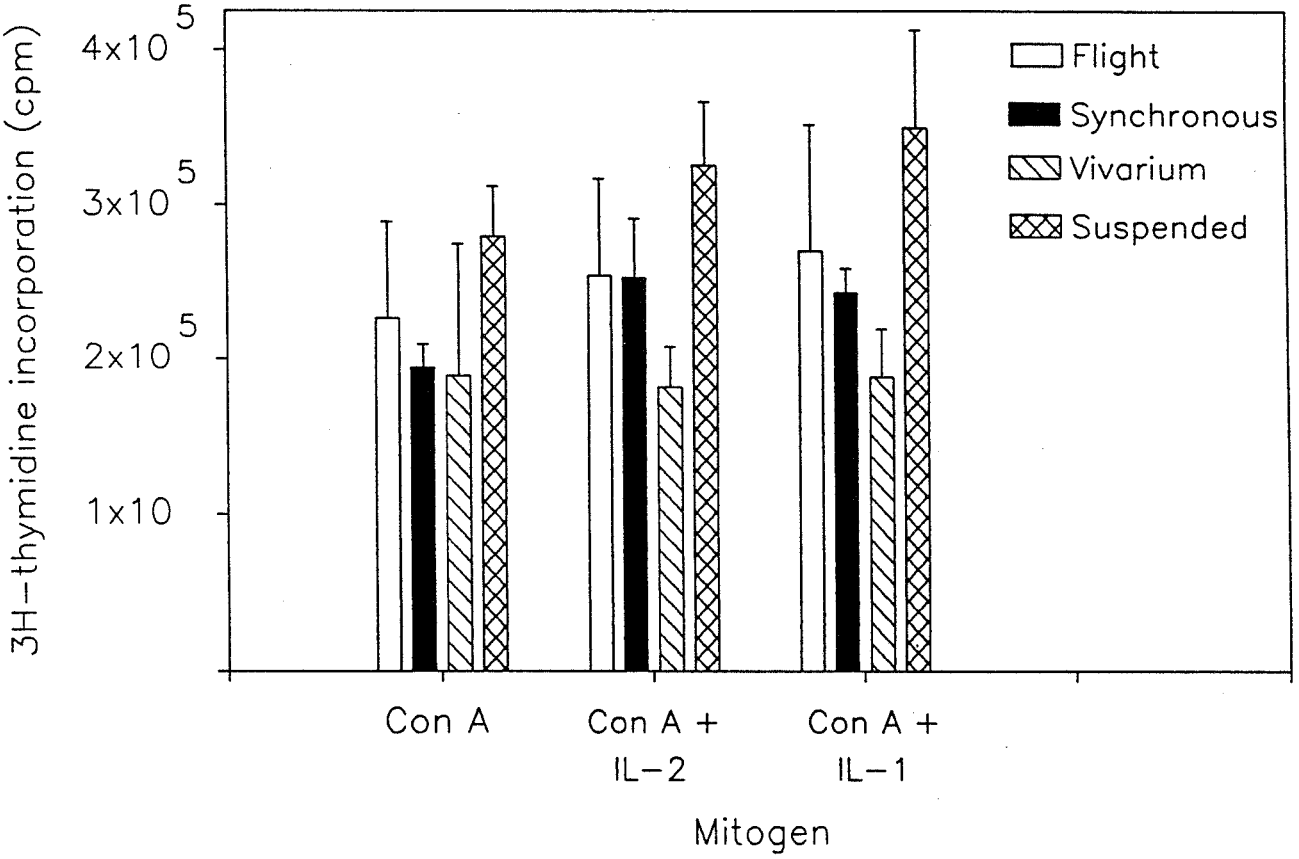

Figure 2. The effect of Con A, Con A + IL-2, and Con A + IL-1 on LNC from experimental rats. Lymphocytes were incubated 3d with 1 ug/ml Con A, 1 ug/ml Con A + IL-2 (100 U/ml), or 1 ug/ml Con A + IL-1 (25 U/ml). Cells were pulsed with ^{3}H-thymidine 18h before harvest.

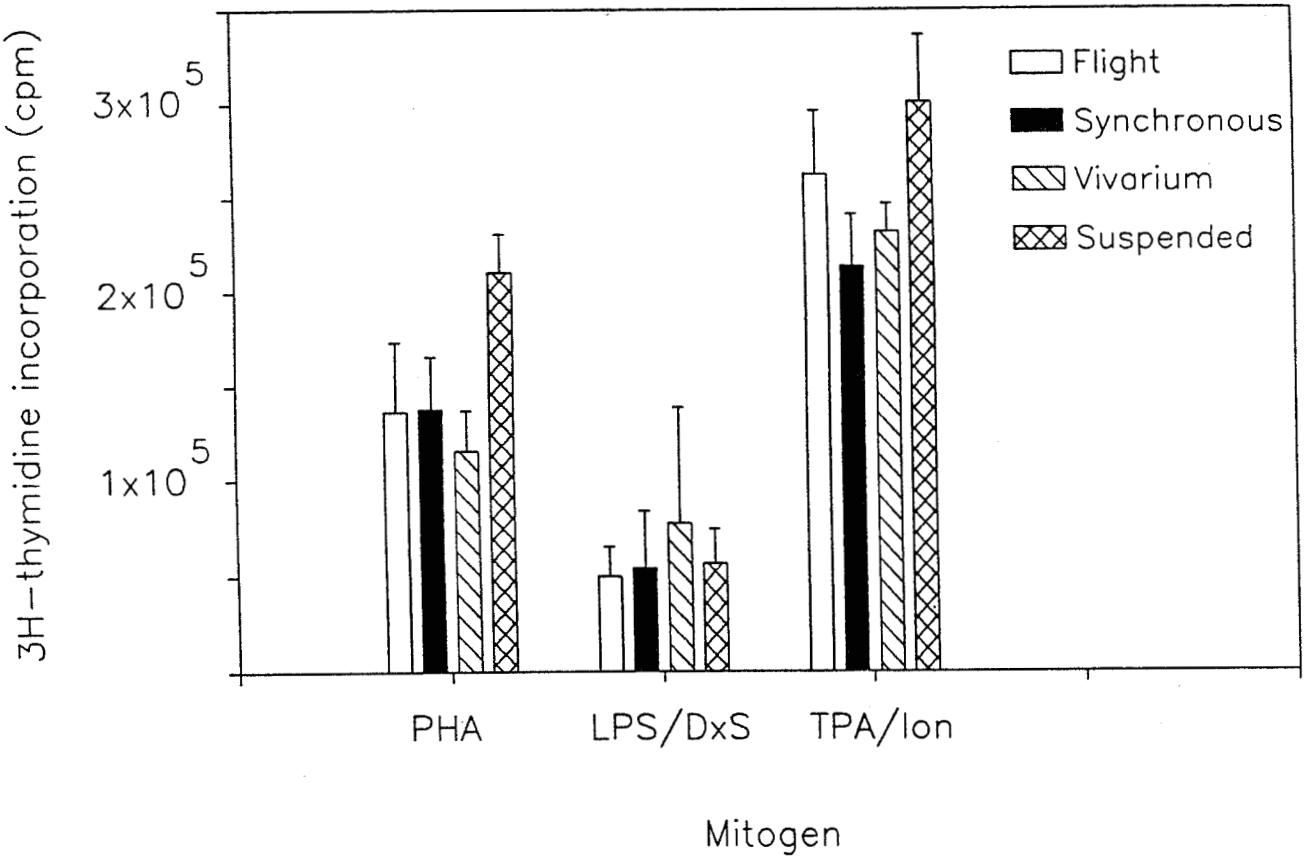

Figure 3. The effect of space flight on PHA, LPS/DxS, and TPA/ionomycin responses. Lymphocytes were stimulated with 2.5 ug/ml PHA for 2d, 10/10 ug/ml LPS/DxS for 3d, or 10^7 M TPA and 7.5 x 10^7 M ionomycin for 2d. Cells were pulsed with ^{3}H-thymidine 18h before harvest.

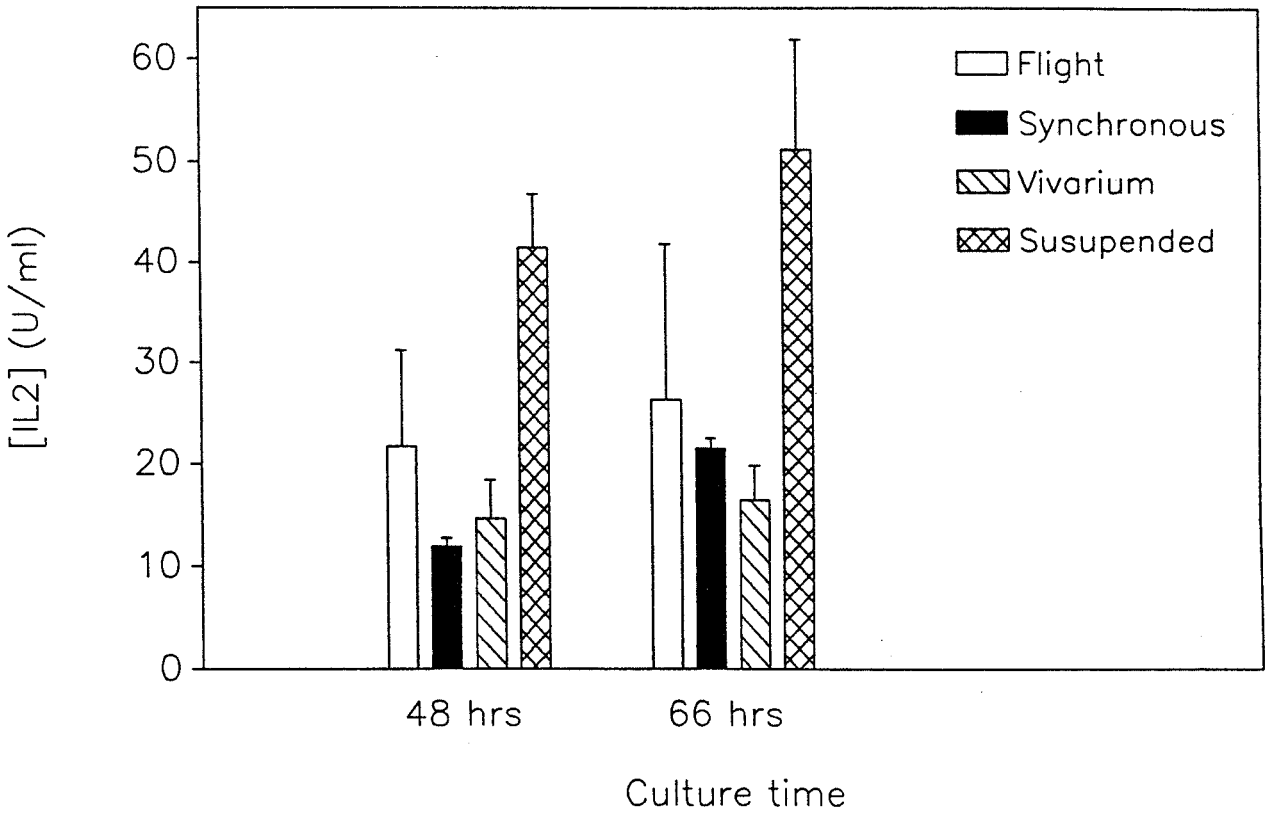

Figure 4. IL-2 production by Con A-stimulated rat LNC. Lymphocytes (1 x 10^5 /well in RPMI/6% FCS/2.5 x 10^5 M 2-ME) were incubated with 1 ug/ml Con A for 48h or 66h. Cells were centrifuged at the appropriate time and the supernatants collected and frozen. Culture media were thawed and assayed for IL-2 bioactivity using the CTLL-2 cell line.

Page intentionally left blank

SM-51
51359

EXPERIMENT K-7-28

LUNG MORPHOLOGY STUDY

Principal Investigator:

J.B. West
Department of Medicine
University of California at San Diego
La Jolla, CA

Co-Investigators:

A.R. Elliott
O. Mathieu-Costello
Department of Medicine
University of California at San Diego
La Jolla, CA

A. S. Kaplansky
Institute of Biomedical Problems
Moscow, USSR

Page intentionally left blank

EXPERIMENT K-7-28

LUNG MORPHOLOGY STUDY

A.R. Elliott, O. Mathieu-Costello, and J.B. West.

SUMMARY

There are no previous studies investigating the effect of microgravity exposure during spaceflight on lung tissue. We examined the ultrastructure of the left lungs of 5 Czechoslovakian Wistar rats flown on the 13 day, 19+ hr. Cosmos 2044 mission, and compared them to 5 vivarium and 5 synchronous controls at 1-g conditions, and 5 rats exposed to 14 days of tail-suspension. Within 10 minutes of sacrifice by decapitation, the lungs were removed and immersed in 3% glutaraldehyde in 0.1M phosphate buffer (total osmolarity of the fixative: 560 mOsm; pH = 7.4). The tissue stored at 5°C was transported to our laboratory where it was processed for light and electron microscopy.

No significant perivascular cuffing caused by interstitial edema was present in the tissue samples. Some of the flight, tail-suspended, and synchronous control rats showed alveolar edema, while vivarium controls did not. The pulmonary capillaries appeared to be more congested in the flight animals than in the other groups. This could be related to the increased hematocrit due to the microgravity exposure. In all 5 flight, 4 tail-suspended, and 3 synchronous rats, red blood cells (RBC) were present in the alveolar spaces. The RBC were either suspended free in the alveoli or observed lining the alveolar wall. The frequency of RBC lining the alveolar walls appeared greater in the dorsal (gravity non-dependent) than in ventral (gravity dependent) regions of the lung in these three animal groups. In 3 of the vivarium controls, a few RBC were found in the alveolar spaces. Intra-capillary fluid-filled vesicles were observed in the flight, tail-suspended and synchronous animals, but not in the vivarium controls. The formation of intra-capillary fluid-filled vesicles has been previously associated with pulmonary hypertension induced by high altitude exposure and mitral stenosis.

In conclusion, pulmonary hemorrhage and alveolar edema of unknown origin occurred to a greater extent in the flight, tail-suspended, and synchronous control animals, and in the dorsal regions of the lung when compared to the vivarium controls. The etiology of these changes, which are possibly due to an increase in pulmonary vascular pressure, requires further investigation.

INTRODUCTION

COSMOS 2044 has provided us the first opportunity to examine lung tissue in animals that were exposed to 14 days of space flight, as well as in rats exposed to 14 days of tail-suspension. We also examined the lungs of the synchronous control rats which were exposed to similar acceleration, vibration, and environmental temperature profiles as the flight animals, and vivarium control rats which were maintained at 1-g conditions.

Limited information is available regarding the effect of microgravity on the respiratory system. Several functional aspects of the respiratory system, such as alveolar ventilation, pulmonary blood flow, and respiratory mechanics have all been shown to be exquisitely sensitive to changes in gravity (West, 1977; Glaister, 1977). Microgravity exposure in man may cause a cephalad shift in body fluid. Pulmonary blood flow and alveolar ventilation becomes more uniform in microgravity (Stone, 1965; West, 1977; Michels, 1978). An increase in acceleration (as is experienced in the Soviet's Biosatellite during launch and re-entry phases)

accentuates the non-uniformity of pulmonary ventilation and blood flow (Glaister, 1977), as well as producing pulmonary interstital edema (Weidner et al., 1981). Thus, exposure to extreme gravitational forces, from 0-g (spaceflight) to 6-g (deceleration phase of re-entry) as occurred in both the flight and synchronous animals, may induce pathological changes in the lung related to abnormal lung fluid balance, altered pulmonary capillary hemodynamics, and possible pulmonary hypertension.

Though small animals such as rats are not expected to undergo a major cephalad fluid shifts during microgravity exposure as does man, tail-suspension rats do experience large cephalad shifts in body fluids (Deavers et al., 1980). The fluid shift due to tail-suspension may be similar to that seen in man during head-down tilt, head-out-of water immersion, and microgravity exposure (Arborelius et al., 1972; Blomqvist and Stone, 1985). In man exposed to these three experimental conditions, an increase in intrathoracic fluid and transient increase in pulmonary vascular pressures are seen (Arborelius et al, 1972; Katkov, 1983). Thus, the tail-suspension rat model gave us the opportunity to investigate the effects of increased intrathoracic fluid and pulmonary vascular pressure on lung ultrastructure.

This report summarizes our findings in the COSMOS 2044 flight, tail-suspended, synchronous and vivarium controls. Our data, which are preliminary, suggest that microgravity, cephalad fluid shift, and/or positive acceleration may have induced pathologic changes in the lung.

METHODS

The lungs from each of the five flight, tail suspension, synchronous, and vivarium animals were removed from the thoracic cavity within 10 minutes of decapitation. No precautionary measures were taken to ensure that aspiration of blood did not occur post-decapitation. The left lungs were immersed in glutaraldehyde (GA) fixative, (3% GA in 0.1M phosphate buffer total osmolarity of fixative: 560mOsm; pH = 7.4), and then transported to our laboratory at 5°C.

First, a 3-4 mm thick tissue slab was cut perpendicular to the cranio-caudal axis just across the most caudal aspect of the hilum. This tissue was embedded in paraffin. Sections (5-6 μm) were stained with hemotoxin-eosin stain and examined by light microscopy.

Samples for electron microscopy were then taken from the most ventral and dorsal aspects of the remaining lower lobe. A piece of lung tissue (approx. 2mm x 2mm x 4mm) was removed from each region and further divided into 1mm x 1mm x 2mm cubes. The tissue samples were rinsed overnight in 0.1M phosphate buffer adjusted to 350 mOsm with NaCl. They were post-fixed for 2 hours in 1% solution of osmium tetroxide in 0.125 M sodium cacodylate buffer adjusted to 350 mOsm with NaCl (total osmolarity: 400 mOsm, pH 7.4). They were dehydrated in increasing concentrations (70%-100%) of ethanol, rinsed in propylene oxide, and embedded in Araldite. One block was selected randomly from each site (dorsal/ventral). One micron sections were cut from each block using an LKB ultratome III. They were stained with 0.1% toluidine blue aqueous solution and examined by light microscopy. Ultrathin sections (50-70 nm) were contrasted with uranyl acetate and bismuth subnitrate (Riva, 1974) and examined with a Phillips 300 electron microscope.

All the paraffin embedded tissue was examined at magnifications of 1000X and 400X for evidence of perivascular cuffing of the large pulmonary vessels and gross changes in the dependent/non-dependent lung regions. The 1 μm sections were systematically examined at magnifications of 400X and 1000X (oil immersion) for peribronchial cuffing of smaller pulmonary vessels, presence of alveolar edema, and general appearance of the pulmonary capillaries and lung parenchyma. The ultrastructure of the blood-gas barrier (capillary endothelium layer, interstitium space and epithelium layer) was examined by electron microscopy.

RESULTS

The preliminary COSMOS-2044 report by V.I. Korolkov (from the Institute of Biomedical Problems,Moscow, USSR) during the NASA/Ames Preliminary Results Symposium at San Jose, CA, 1990, indicated that when the animals were first examined at the recovery site, they appeared active and in satisfactory condition. By the onset of dissection, 5 hrs post-recovery, they were inactive and had reddish fluid drops on the tips of their nose. These signs were attributed to the gravitational stress which developed after the transition from 0-g to Earth's gravity. The re-entry profile consisted of approximately 3-5 minutes of 6-g deceleration phase, followed by 10 milliseconds of approximately 50-g during impact, and finally a return to Earth's gravity.

A reddish nasal discharge was not reported to occur in either the tail-suspended or synchronous control rats. However, it has been described to occur during the first few days post tail-suspension in rats (COSMOS 2044 Investigator, Dr. Daniel Riley, Medical College of Wisconsin, Expt. #K-7-09; personal communication). This nasal discharge, which has not been systematically investigated, may be associated with the stress response which occurs during the first few days of tail suspension (Thomason and Booth, 1990).

Light Microscopic Examination

The degree of lung inflation was not uniform within the tissue samples. All lung slabs tended to be centrally collapsed, while the periphery was moderately to well inflated. This could be due to the immersion fixation process since lung inflation was not controlled. No obvious evidence of perivascular cuffing was observed in any group. Red blood cells (RBC) were seen in the lumen of major airways in all samples, with the least observed in the vivarium animals. RBC could be seen in the airspaces of the centrally collapsed regions of the sections, as well as the periphery.

The vivarium control animals showed no evidence of alveolar edema in either the dorsal or ventral aspects of the lung (Fig. 1a). This tissue showed a few RBC in the alveoli, and the pulmonary capillaries did not appear distended with RBC. No apparent dorsal/ventral gradient in the presence of RBC was detected in these control animals.

In the flight animals no evidence of perivascular cuffing was observed (Fig. 1b). Some evidence of alveolar edema was found in one out of five animals. It occurred in both the dorsal and ventral regions of the lung. A small number of RBC was observed in the alveoli of the flight tissue, except for one animal which showed a greater number RBC in the alveoli than the others. Overall, the dorsal sections generally showed more RBC in the airspaces than the ventral sections. RBC were seen in the alveoli (dorsal samples, 5 out of 5 animals; ventral, 4 out of 5). Densely packed RBC were found lining the alveoli (dorsal samples, 4 out of five; ventral, 2 out of 5). Finally, in 3 out of 5 animals, densely RBC packed pulmonary capillaries were observed in both the dorsal and ventral samples.

Tail-suspension in the rat is primarily used as a model for producing hind limb muscle atrophy and bone degeneration. It also can be used as a model for producing a cephalad fluid shift similar to that seen in humans exposed to microgravity, head-down tilt, and head-out of water immersion. Therefore, it was of particular interest to us for studying the effects of a cephalad fluid shift, and the associated possible increase in thoracic intravascular pressures on pulmonary ultrastructure. We found evidence of alveolar edema in both dorsal and ventral samples from 2 of the 5 animals. Four of the 5 tail-suspended animals also showed both RBC free in the alveolar space, as well as lining the alveoli (Fig. 1c). This generally occurred to a greater extent in the dorsal than the ventral samples. Capillary RBC congestion was not apparent in this group of animals.

In the synchronous control group, 2 animals showed evidence of alveolar edema in the dorsal region of the lung. RBC were seen the alveoli (dorsal/ventral samples) in 3 of the 5 animals (Fig. 1d). Capillaries appeared moderately distended with RBC in two of the synchronous control animals.

Electron Microscopic Examination

In the vivarium controls, the lung tissue appeared well preserved (Fig. 2a). The alveolar epithelium layer was smooth and intact with few cytoplasmic vesicles. The capillary endothelium appeared very thin on the alveolar side. This attenuation of the endothelial layer is commonly seen in rat pulmonary capillaries (Weibel, 1972). Several plasmalemmel vesicles were seen on the interstitial side of the capillary. The basement membrane appeared fused along the thin side of the blood-gas barrier. It separated into epithelial and endothelial basement membranes at the transition to the thick portion of the blood gas barrier. The interstitial fibrous and collagen network appeared free of any excess interstitial fluid. Occasionally macrophages were observed lining the alveoli and in the interstitium.

In flight, tail-suspension and synchronous animals, RBC were seen densely packed along the epithelial lining of the alveoli (Fig. 2b) or singly in the alveolar space. Alveolar edema was observed in these three groups, as well as fluid-filled protrusions into the pulmonary capillary (Fig. 2c). The vesicles appeared to be formed by the invagination of the endothelium. They contained some granular material which appeared "incapsulated" by the endothelial layer. We interpreted this granular material as edema fluid. Such vesicles were not seen in the vivarium control animals. Complete epithelial disruption, and edematous blebbing was observed in one tail-suspended rat (Fig. 2d)

An increase in the number of alveolar macrophages occurred in some animals. This occurred especially in one of the synchronous control rats where the macrophage population showed a large density of dark cytoplasmic lysosomes occlusions (Fig. 2c), suggesting an increase in the proteolytic activity of the cells.

DISCUSSION

The major finding of this study is the evidence of pulmonary hemorrhage of unknown origin, and the abnormality of pulmonary fluid balance in all three treatment groups: flight, tail-suspension and synchronous animals as compared to the vivarium controls.

Limitations and Technical Problems

An obvious limitation in this study is the immersion fixation of the lung. Understandably, optimal fixation of the lung tissue by vascular perfusion *in situ* could not be performed since it was incompatible with the collection of several other tissues. Immersion fixation provided us with an effective means of tissue preservation, but it did not allow us to control a uniform degree of lung inflation for a quantitative comparison of the blood-gas barrier thickness and/or the degree of perivascular cuffing between groups. In spite of this limitation, we were successfully able to qualitatively describe the ultrastructure of the lung parenchyma in each animal group.

A second limitation could be the fact that no precautionary measures (such as clamping the trachea immediately post decapitation) were taken to prevent possible aspiration of blood by the animal post-decapitation. Indeed, it clouds our interpretation of the etiology of the pulmonary hemorrhage seen in flight, tail-suspension and synchronous animals. However, we believe that the origin of the observed alveolar hemorrhage is not solely due to the aspiration of blood,

since the vivarium animals sacrificed in the exact same manner as the other animals showed far fewer RBC in the alveolar space.

Findings

Pulmonary hemorrhage has been shown to occur in response to a severe elevation in pulmonary vascular pressures during exposure to extreme high altitude (reduced ambient oxygen tension), severe chronic mitral stenosis disease, and in neurogenic pulmonary edema. In all these cases, extravasation of RBC outside the pulmonary capillary have been observed (Cottrell et al., 1967; Heath et al., 1973; Kay et al., 1973; Minnear et al., 1987; Bachofen et al., 1988). Very recently we systematically investigated the effect of increased capillary transmural vascular pressure on lung ultrastructure. We consistently found structural disruptions of the blood-gas barrier, with RBC squeezing into the interstitial and alveolar spaces at capillary transmural pressures greater than 52.5 cm water (Tsukimoto et al., 1990). It is possible that exposure to different gravitational forces, as occurs during tail-suspension, positive acceleration, and/or during the readaptation to Earth's gravity may induce a transient elevation in pulmonary vascular pressure and possible pulmonary hemorrhage.

Although conclusive characterization of the exact etiology of the pulmonary hemorrhage is not possible at this point, it is noteworthy that the appearance of RBC on the alveolar spaces occurred to a greater extent in the flight, tail-suspended and synchronous animals than in the vivarium controls. The slightly greater occurrence of hemorrhage on the dorsal regions could reflect a difference in the vulnerability of the capillaries in that region, in spite of the limited dorsal/ventral gravity dependent gradient expected to occur in such a small animal as the rat.

Other evidence that suggest that the flight, tail-suspended and synchronous rats may have been exposed to either chronic or transient pulmonary hypertension is the finding of disrupted epithelial layers of the blood gas barrier, and the presence of intra-capillary endothelial vesicles. Both these abnormalities have been associated with hemodynamically induced pulmonary edema. In the study by Tsukimoto et al. (1990), disruptions of the epithelial layer of the blood-gas barrier were consistently observed at capillary transmural pressures of 52.5 cm water and above. Minnear et al. (1981) also showed evidence of epithelial disruptions after animals were transiently exposed to severe pulmonary hypertension caused by experimentally induced neurogenic pulmonary edema. Strikingly similar vesicle formation has been observed in rats exposed to simulated high altitude conditions (Heath et al., 1973) and in humans with chronic mitral stenosis and pulmonary hypertension (Kay and Edwards, 1973). Intra-capillary vesicles have also been observed in permeability induced pulmonary edema. Toxic agents, such as monocrotaline, ammonium sulphate and alpha-naphthylthiourea, used to induce acute pulmonary edema in experimental animals were found to induce similar vesicle formation in the pulmonary capillary (Valdivia et al., 1967; Kay et al., 1969; Hayes et al., 1970; and Meyrick et al., 1972). These substances are believed to cause a permeability type of pulmonary edema, by inducing toxic changes in the endothelial and epithelial layers causing fluid to accumulate in the interstitial space on the thin side of the blood gas barrier, thus inducing separation and invagination of the endothelial layer forming edema filled vesicles. The flight, tail-suspension and synchronous animals which showed intra-capillary vesicles probably experienced pulmonary hypertensive episodes which could have induced a hemodynamic form of pulmonary edema.

Further studies are clearly needed to characterize the etiology of the structural changes observed in the lungs of the COSMOS 2044 rats. First of all, the effects of decapitation on lung ultrastructure must be clearly identified. Is the blood in the alveolar spaces due to aspiration of blood or is the blood coming from the pulmonary vasculature? Secondly, the effects of microgravity exposure on lung ultrastructure need to be further analysed in other groups of

rats, such as in the SLS-1 rodent experiments, as well as the systematic analysis of lungs by vascular perfusion in tail-suspended rats.

ACKNOWLEDGEMENTS

We would like to thank Dr. A.S. Kaplansky and the Soviet Cosmos recovery and dissection teams. Without their efforts, this study could not have been carried out. We are also very grateful to the NASA/Ames Science team for their support and planning of the tissue collection and transport to our laboratory. We are indebted to Ms. Carlita Durand, Dr. Xeng Xing Fu and Mr. Rick Logeman for the technical assistance. Supported by NASA grant NAG-2-616.

REFERENCES

1. Arborelius, M., U.I. Balldin, B. Lilja, and C.E.G. Lundgren. Hemodynamic Changes in Man During Immersion with the Head Above Water. Aerosp. Med. 43:592-598, 1972.

2. Bachofen, H., M. Bachofen, and E.R. Weibel. Ultrastructural Aspects of Pulmonary Edema. J. Thorac, Imag. 3(3):1-7, 1988.

3. Blomqvist, C.G. and H.L. Stone. Cardiovascular Adjustments to Gravitational Stress. In: Handbook of Physiology, Sect. 2: The Cardiovascular System. Vol. III, Eds: J.T. Shepard and F. M. Abboud. Bethesda, American Physiological Society: 1025-1063, 1985.

4. Cottrell, T.S., O.R. Levine, R.M. Senior, J. Wiener, D. Spiro, and A.P. Fishman. Electron Microscopic Alterations at the Alveolar Level in Pulmonary Edema. Circulat. Res. 21:783-797, 1967.

5. Deavers D.R., X.J. Musacchia, and G.A Meininger. Model for Antiorthostatic Hypokinesia: Head-Down Tilt Effects on Water and Salt Excretion. J. Appl. Physiol. 49(4):576-582, 1980.

6. Glaister, D.H. Effect of Acceleration. In: Regional Differences in the Lung. Ed: J.B. West. Academic Press, New York, 1977.

7. Hayes, J.A., and A. Shiga. Ultrastructural Changes in Pulmonary Oedema Produced Experimentally with Ammonium Sulphate. J. Pathology. 100:281, 1970.

8. Heath, D., H. Moosavi, and P. Smith. Ultrastructure of High Altitude Pulmonary Oedema. Thorax. 28:694-700, 1973.

9. Katkov, V.E., V.V. Chestukhin, E.M. Nikolayenko, V.V. Rumyantsev, and S.V. Gvozdev. Central Circulation of a Normal Man During 7-Day Head-Down Tilt and Decompression of Various Body Parts. Aviat. Space Environ. Med. 54(Suppl. 1):S24-S30, 1983.

10. Kay, J.M., P. Smith, and D. Heath. Electron Microscopy of *Crotalaria* Pulmonary Hypertension. Thorax. 24:639, 1969.

11. Kay, J.M. and F.R. Edwards. Ultrastructure of the Alveolar-Capillary Wall in Mitral Stenosis. J. Pathology. 111:239-245, 1973.

12. Meyrick, B., J. Miller, and L. Reid. Pulmonary Oedema Induced by ANTU, or by High or Low Oxygen Concentrations in the Rat: An Electron Microscopic Study. Br. J. Exp. Path. 53:347, 1972.

13. Michels, D.B. and J.B. West. Distribution of Pulmonary Ventilation/Perfusion During Short Periods of Weightlessness. J. Appl. Physiol. 45:987-998, 1978.

14. Minnear, F.L. and R.S. Connell. Increased Permeability of the Capillary-Alveolar Barriers in Neurogenic Pulmonary Edema (NPE). Microvasc. Res. 22:345-366, 1981.

15. Minnear, F.L., C. Kite, L.A. Hill, and V. Hoyte. Endothelial Injury and Pulmonary Congestion Characterize Neurogenic Pulmonary Edema in Rabbits. J. Appl. Physiol. 63(1):335-341, 1987.

16. Riva, A. A Simple and Rapid Staining Method for Enhancing the Contrast of Tissue Previously Treated with Uranyl Acetate. J. Microsc. (Paris). 19:105-108, 1974.

17. Stone, H.L., B.H. Warren, and H. Wagner. The Distribution of Pulmonary Blood Flow in Human Subjects During Zero-G. AGARD Conf. Proc. 2:129-148, 1965.

18. Thomason, D.B. and F.W. Booth. Atrophy of the Soleus Muscle by Hindlimb Unweighting. J. Appl. Physiol. 68(1):1-12, 1990.

19. Tsukimoto, K., O.Mathieu-Costello, R. Prediltto, A.R. Elliott, and J.B. West. Ultrastructural Appearances of Pulmonary Capillaries at High Transmural Pressures. J. Appl. Physiol. (in press), 1990.

20. Valdivia, E. R., J.J. Lalich, Y. Hayashi, and J. Sonnad. Alterations in Pulmonary Alveoli after a Single Injection of Monocrotaline. Archs. Path. 84:64, 1967.

21. West , J.B. Ed. Regional Differences in the Lung. Academic Press, New York, 1977.

22. Weibel, E.R. Morphometric Estimation of Pulmonary Diffusing Capacity V: Comparative Analysis of Mammalian Lungs. Resp. Physiol. 14:26, 1972.

23. Weidner W.J., L.F. Hoffman, and D.O. Defouw. Effect of Sustained Gz Acceleration on Lung Fluid Balance: An Ultrastructural Study. Physiologist. 24(6):S85-S86.

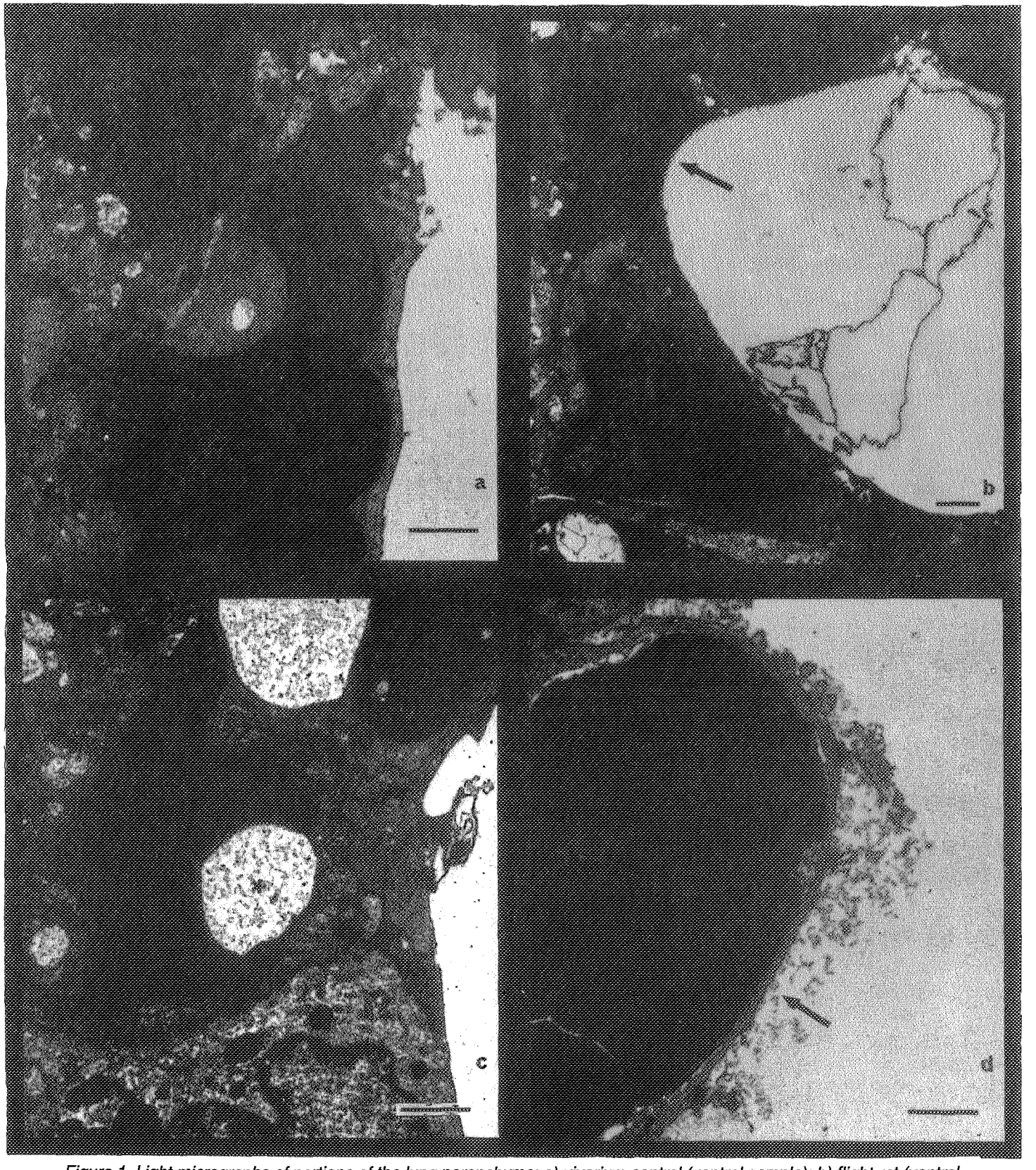

Figure 1. Light micrographs of portions of the lung parenchyma: a) vivarium control (ventral sample); b) flight rat (ventral sample) showing no RBC in the airway and no perivascular cuffing of the artery; c) tail-suspended rat (dorsal sample) showing RBC lining the alveoli (arrows); d) synchronous rat (dorsal sample showing RBC lining the alveoli (arrows) and free RBC in the alveoli (asterisk). Bar = 20 µm.

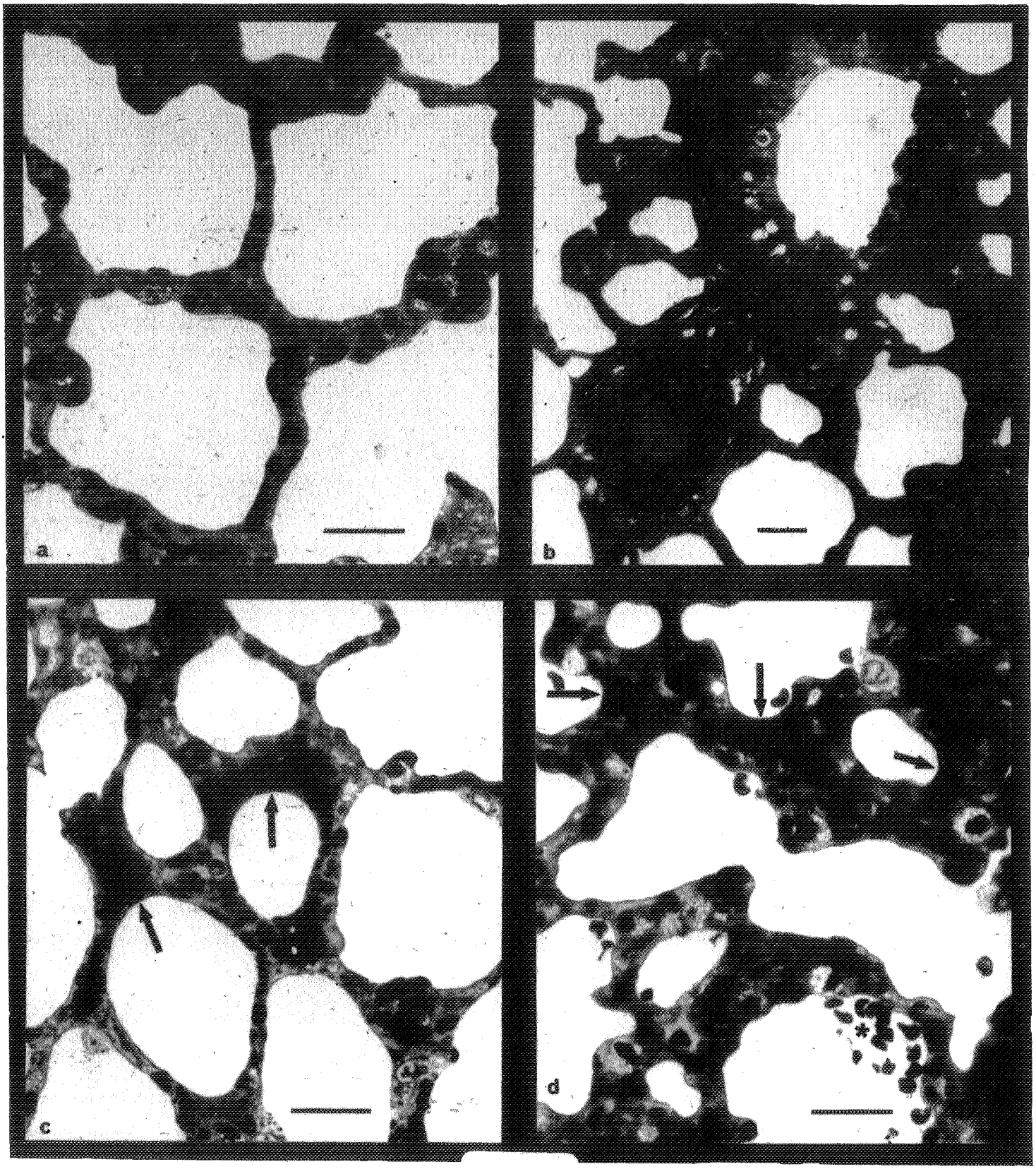

Figure 2. Electron micrographs showing the lung ultrastructure of portions of pulmonary capillaries and adjacent alveoli: a) vivarium control (dorsal sample); b) flight rat (dorsal sample) showing RBC lining an alveolus (arrow); c) synchronous animal (ventral sample) showing an intra-capillary vesicle (asterisk); d) tail-suspended rat (dorsal sample). Note the disruption of the epithelial layer of the blood-gas barrier (arrow). Bar = 1 μm.

Page intentionally left blank

515-51
51360

EXPERIMENT K-7-29

CONNECTIVE TISSUE STUDIES

I. RAT SKIN, NORMAL AND REPAIR

II. CHANGES IN MUSCLE SERINE PROTEASES, SERPINS AND MATRIX MOLECULES

III. RODENT TISSUE REPAIRS

Principal Investigator:

A.C. Vailas
University of Wisconsin
Madison, WI

Co-Investigators:

B. Festoff
University of Kansas
Kansas City, KS

R. Grindeland
NASA Ames
Moffett Field, CA

J.S.Rao
A.R. Rayford
B.R. Reddy
Veteran's Affairs
Medical Center
Kansas City, KS

V.K. Fritz
W. Stauber
West Virginia University
Morgantown, WV

V. Choy
B. Graf, M.D.
P. Griffith
S. Kolis
D. Martinez
R. Thielke
M. Ulm
R. Vanderby
University of Wisconsin

J. Sears
University of Iowa

R. Ashman
University of Texas

T.E. Burkovskaya
E.I. Ilyina-Kakueva
A.S. Kaplansky
Institute of Biomedical Problems
Moscow, USSR

Page intentionally left blank

EXPERIMENT K-7-29

PART I: RAT SKIN, NORMAL AND REPAIR

A.C. Vailas, R. Grindeland, R. Ashman, V. Choy, G. Durnova, B. Graf, P. Griffith, A.S. Kaplansky, S. Kolis, D. Martinez, J.S.Rao, A.R. Rayford, B.R. Reddy, J. Sears, R.Thielke, M. Ulm, R. Vanderby.

The skin repair studies started to be problematic for the following reasons: (1). It was very difficult to locate the wound and many lesions were not of the same dimensions. A considerable amount of time was devoted to the identification of the wound using polarized light. We understand that this experiment was added on to the overall project. Marking of the wound site and standard dimensions should be recommended for the next flight experiment. (2). The tissue was frozen, therefore thawing and fixation caused problems with some of the immunocytochemical staining for obtaining better special resolution with light microscopy image processing. Despite these problems, we were unable to detect any significant qualitative differences for the following wound markers:

1. Collagen Type III
2. Hematotoxylin and Eosin
3. Macrophage Factor XIII

All protein markers were isolated from rat sources and antibodies prepared and tested for cross reactivity with other molecules at the University of Wisconsin Hybridoma Facility.

However, rat skin from the non lesioned site "normal" showed interesting biochemical results. Skin was prepared for the following measurements: (1). DNA content. (2). Collagen content by hydroxyproline and (3). uronic acid content and estimation of ground substance. The results indicated there was a non-significant increase (10%) in the DNA concentration of skin from flight animals. However, the data expressed as a ratio DNA/Collagen estimates the cell or nuclear density that supports a given quantity of collagen showed a dramatic increase in the flight group (33%). This means flight conditions may have slowed down collagen secretion and/or increased cell proliferation in adult rat skin. Further biochemical tests are being done to determine the crosslinking of elastin which will enhance the insight to assessing changes in skin turnover.

NORMAL SKIN BIOCHEMICAL PROPERTIES

TABLE 1. Skin DNA, uronic acid and collagen concentration

	SYNCH	VIVAR	FLIGHT	T-SUSPENDED
DNA (μg/mg dry wt)	20.91 ± 1.6	20.88 ± 1.4	24.02 ± 1.5	22.30 ± 1.9
DNA/Collagen (μg/mg collagen)	604 ± 51.6	643 ± 42.0	801.4 ± 59.3 *	632.3 ± 48.2
Uronic Acid (μg/mg dry wt)	2.19 ± 0.17	2.23 ± 0.23	2.26 ± 0.21	1.85 ± 0.12
Uronic Acid/Collagen (ug/mg collagen)	85.72 ± 10.5	86.3 ± 9.1	98.3 ± 8.2	67.8 ± 2.8
Hydroxyproline (μg/mg dry wt)	44.32 ± 2.7	41.95 ± 3.2	38.59 ± 2.6	44.10 ± 1.7

*Flight group is significantly different than the Synch group ($p \leq 0.05$).
Values represent Means ± SE.

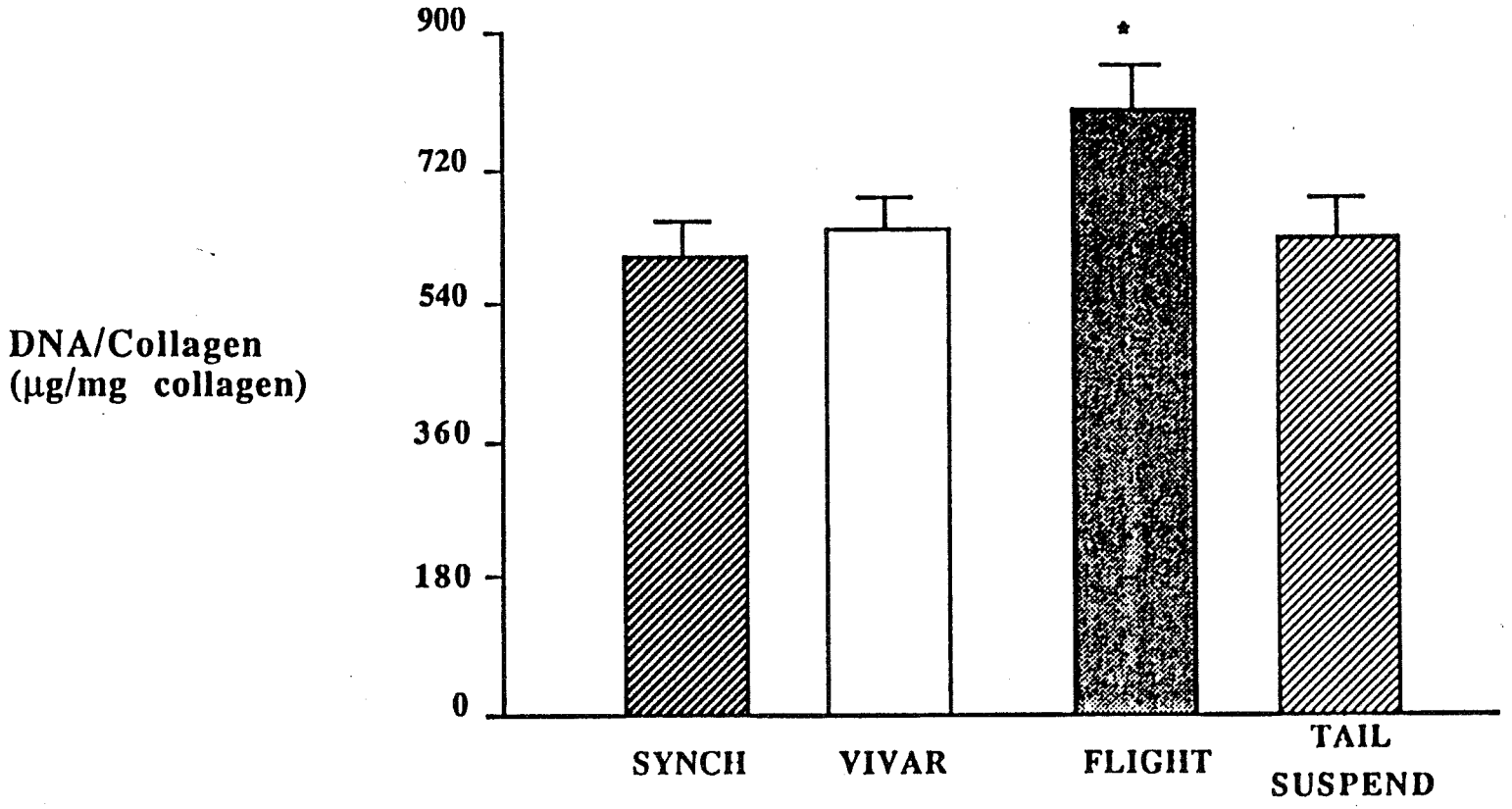

*Figure 1. Skin DNA/Collagen concentration (µg/mg collagen). *Flight group is significantly different from the Synch group ($p \leq 0.05$). Values represent Means ± SE.*

S16-51

51361

EXPERIMENT K-7-29

PART II: CHANGES IN MUSCLE SERINE PROTEASES, SERPINS AND MATRIX MOLECULES

B.W. Festoff, E.I. Ilyina-Kakueva, A.R. Rayford, T.E. Burkovskaya, B.R. Reddy, and J.S. Rao

INTRODUCTION

Muscle injury results in the infiltration of mononuclear cells leading to myofiber degeneration (Carlson, 1973). However, regeneration after muscle injury can proceed with subsequent re-establishment of functional fibers with equal or greater capability (Carlson, 1973; Allbrook; Mauro, 1979). Although a controversy existed as to the origin of the mononuclear cells in muscle, since macrophage precursor cells have been found in blood vessel walls following injury (Snow, 1977) many of these cells have been found by immuno-histochemical techniques to be myoblast in origin, known as "satellite" cells, which proliferate, fuse and form new myofibers (Mauro, 1961; Carlson, 1973; Bischoff, 1975; Mauro, 1979; Lipton and Schultz, 1979; Allbrook, 1981). It is known that macrophages produce several types of neutral extracellular proteases, including several serine proteases such as the plasminogen activators (PAs) and others capable of extracellular matrix (ECM) component degradation (Werb et al., 1980; Danø et al., 1985). More recent studies have shown that muscle satellite cells also produce and secrete these important enzymes (Festoff et al., 1982; Festoff et al., 1986; Hantaï et al., 1988; Hantaï et al., 1989; Hantaï et al., 1990; Festoff et al., 1990a). In intact muscle, the ECM resists deformation, but after injury it provides a scaffold for the regenerative process (Vracko, 1978; Sanes, 1986). In this situation, it is likely that protease-sensitive components are degraded breaking barrier connections, thus allowing myoblast proliferation and eventual fusion to form new myofibers (Gulati et al., 1981; Gulati et al., 1983a,b; Gulati, 1987; Hantaï and Festoff, 1987). After denervation, urokinase-like PA (uPA), and to a lesser extent, tissue-type PA (tPA), increases in skeletal muscle (Festoff et al., 1986; Hantaï et al., 1990).

More recent studies show that regulation of urkinase-like PA (uPA), the major extravascular PA, can occur at the levels of mRNA transcription, translation, intra-cellular or extra-cellular post-translational processing of the enzyme (Danõ et al., 1985) as well as by inhibition of fully-processed uPA by cellular proteinaceous inhibitors (Travis and Salvesen, 1983) and now termed serpins, serine protease inhibitors (Carrell and Boswell, 1987; Travis et al., 1990). One such serpin, protease nexin I (Baker et al, 1986; McGrogan et al., 1988), has been localized to the basement membrane of the neuromuscular junction (Hantaï et al., 1989; Festoff et al, 1990c) and is produced by muscle cells (Festoff et al., 1990b), Schwann cells (Meier et al., 1989) and CNS glia (Guenther et al, 1985; Monard, 1988), as well as by fibroblasts (Baker et al., 1986). Another inhibitor, PA inhibitor I (PAI-1) was originally isolated from endothelial cells (Van Mourik et al 1984; Loskutoff et al., 1986) but is also produced by a number of cell types (Loskutoff et al., 1986) including glial cells (Rao et al, 1990; Keohane et al., 1990). These and similar molecules are likely important regulators of uPA, tPA, thrombin and trypsin-like enzymes in the nervous system (Hantaï et al, 1988; Festoff, 1990; Sawaya, 1990).

In zero or micro-gravity, type I muscle fibers atrophy and lose predominance, especially in slow-twitch muscles (Riley et al., 1990; Benton et al., 1979). No increase in mononuclear cells has been observed, just as in simple denervation, where both types I and II fibers atrophy, again without infiltration of cells, but with clear satellite cell proliferation. However, ECM degradation takes place after denervation (Hantaï and Festoff, 1987) and if re-innervation is encouraged, functional recovery to near control levels may be achieved. No information is available concerning the ECM milieu, the

activation of serine proteases, their efficacy in degrading ECM components and the production of locally-derived natural protease inhibitors (serpins) in effecting surface proteolytic control. In addition, no studies are available concerning the activation of these enzymes in micro-or zero gravity or their response to muscle injury on the ground and what alterations, if any, occur in space. These studies were the basis for the experiments in Cosmos 2044.

MATERIALS AND METHODS

Materials

PNI was purified from human fibroblasts as described by Scott et al. (1985) or from 9L gliosarcoma cells (Rao et al.,1990). Plasminogen was prepared from fresh human plasma obtained from the Community Blood Center of Greater Kansas City (courtesy Dr. David Jenkins) and purified on lysine-agarose by the method of Deutsch and Mertz (1970). Tween-20, Triton X-100, and Coomassie Brilliant Blue-G were all from Sigma (St. Louis, Mo.). Hirudin was purchased from Calbiochem (La Jolla, CA). Sea-Kem agarose and Gelbond were from FMC Marine Colloids (Rockland, ME). The thrombin-specific synthetic peptide substrate, Tosyl-Gly-Pro-Arg-4-nitroanilide, was obtained from Boehringer Mannheim (Indianapolis, IN). S-2251 (H-D-Val-Leu-Lys-par-nitroanilide), tPA stimulator (fibrin monomer; Fm) and plasminogen-free human fibrinogen were from KABI VITRUM (Helena Diagnostics, Beaumont, TX). ^{125}-Iodine (13.9 mCi/μg) was obtained from Amersham Corp. (Arlington Hts, IL) and used according to manufacturer's instructions. Iodogen (diphenylglyocluril) was from Pierce Biochemicals (Rockford, IL). Aprotinin (Trasylol) was a gift of Dr. F. Schumann (AG Bayer, Wuppertal, FRG). Human α thrombin was a gift of Dr. John Fenton, II, Public Health Labs., Albany, NY. Human urokinase (uPA) and tPA, antibodies to uPA and tPA were purchased from American Diagnostica (New York,NY). Polyvinilidene difluoride (PVDF, 0.45 μm) membrane (Immobilon) was from Millipore Corp. (Bedford, MA). X-OMAT X-ray film as obtained from Kodak (Rochester, NY). Immulon-2 microtiter plates were obtained from Dynatech Laboratories (Chantilly, VA).

Methods

Preparation of Conditioned Media from 9L Cells.

Rat 9L gliosarcoma cells were grown in microcarrier cultures as described previously (Rao et al., 1990) as a source of purified PNI. The cells on beads were rinsed 3 times with serum-free medium and then left 24 hours in the same medium. Three liters of serum-free medium was collected after this time and centrifuged at 5,000 rpm to remove cellular debris. Concentration and heparin-agarose affinity chromatography to obtain PNI was as described (Scott et al., 1985; Festoff et al., 1990b). After concentration, aliquots of 0.2 ml were removed and flash-frozen in liquid N_2 and stored at -80°C until used.

Preparation of Muscle Extracts.

The muscle tissue was thawed, weighed, homogenized in Tris-buffer [(50 mM Tris-HCl, pH 7.6, 10 mM EDTA and 0.2% Triton X-100 either with 10 mM n-ethylmaleimide (NEM), 10 mM benzamidine, 25 mM phenylmethylsulfonyl fluoride (PMSF), and 5 mM epsilon aminocaproic acid)] or without protease inhibitors and centrifuged at 5, 000 g for 30 minutes. The pellet was dissolved in Tris buffer, aliquoted separately from the supernatant and stored at -80°C until used. The samples containing protease inhibitors were used to estimate the levels of serpins and those without inhibitors were used to estimate the levels of serine proteases.

Muscle Crush of Ground-Based Animals.

SASCO/Wistar rats (each weighing 300-500g) were anesthetized using a rodent cocktail containing ketamine-HCl (100 mg/ml), xylazine (20 mg/ml), and acepromazine (10mg/ml) at the dosage level of 0.5 ml/kg of animal weight, given sub-cutaneously. Prior to surgery, the legs were shaved and an incision was made through the skin to expose the gastrocnemius muscle of the animal. The muscle on the right leg was crushed by using a sterile hemostat and clamping it down for 30 seconds, while the muscle on the left leg served as a control (not crushed). The muscles and the skin were sutured using Ethicon 4-0 chromic gastrointestinal G-181H and Ethicon 4-0 Ethiflex tapercut 6975H sutures, respectively. Extraction of these crushed muscle samples was as for the experimental material from Cosmos 2044.

Amidolytic Assay of PA Activity.

To indirectly measure PA activity the activation of plasminogen to plasmin by muscle extracts was followed by determination of plasmin activity on the synthetic substrate S-2251 (Rånby et al., 1982; Weinberg et al., 1984). To 50 µl of either clonal muscle extracts (or purified diluted standard human uPA or tPA) were added 50 µl of S-2251 (150 µg/ml) with or without fm (130 µg/ml) and 50 µl of glu-plasminogen (45 µg/ml), all diluted in 0.1 M sodium phosphate, 10 mM EDTA, 0.01% NaN_3, 0.01% Triton X-100, pH 7.3. Incubation was performed at 37°C in flat-bottomed microtiter plates (Imulon II, Dynatech Laboratories, Inc., Alexandria, VA). The release of paranitroaniline from S-2251 was determined in each well by measuring the absorbance at 405 nm using a micro-ELISA autoreader (Titertek Multiscan, Flow Labs, Arlington, VA). Color development was linear for 6 hours after a 2 hour lag, or if expressed to the fourth power (Weinberg et al., 1984). Controls, including buffer alone and extracts without plasminogen, were performed in parallel wells. Generally, 2 or 3 replicate wells were included in each assays. Two separate assays for each rat and condition was done while duplicate wells were used for each point in the separate experiments. Our current results are expressed in absorbance units per mg protein after 4 hours incubation at 37°C.

Protease Inhibition by Muscle Extracts.

As a means of estimating serpin activity in the muscle extracts from rat in the various conditions several synthetic chromogenic assays were employed that are relatively specific for the target protease. In particular, for thrombin inhibition Chromozym TH is based on a synthetic peptide substrate, Tos-Gly-Phe-Arg-4-paranitroaniline, and was used according to previously published methods (Festoff et al., 1990). The residual thrombin activity after active-site titration of bovine thrombin with extracts or hirudin, the anti-thrombin from the medicinal leech, activity was measured by the change in absorbance at 405nm in an automated microtiter reader, Flow Multiscan, (Flow Labs, Arlington, VA) and compared with the uninhibited enzyme as 100% control.

Western Blot (Immunoblot) Analysis.

The muscle extract samples were electrophoresed overnight, by SDS-PAGE according to the method of Laemmli (1970) in 10% gels. Following electrophoresis, samples were transferred to nitrocellulose by Towbin et al (1979) or Immobilon membranes (PVDF) as described by Domingo and Marco (1989). The nitrocellulose or Immobilon-bound samples were sequentially probed with polyclonal antibodies to uPA, tPA, PNI and PAI-1 followed by second biotinylated IgG antibodies (1:1000 dilution), and streptavidin-biotinylated horseradish peroxidase (1:500 dilution). After the final wash the blots were stained with 2,4-chloronaphthol to develop color. Antibody to human PNI, uPA, tPA or PAI-1 were used. Antibodies to human PNI and PAI-1, uPA and tPA cross-react with homologous

polypeptides from several rat tissues (Monard, 1988; Loskutoff, 1989; Rao et al., 1989; Hantaï et al., 1989; Festoff et al, 1990).

Protease: Serpin Complex Formation.

Purified human α thrombin or uPA was iodinated using the Iodogen method as previously described (Scott et al., 1985; Festoff et al., 1990). Labeled protease was separated from free iodide on a Sephadex G-25 column. Complex formation was performed as described (Baker et al., 1986; Loskutoff et al., 1986; Rao et al., 1990) and followed by autoradiography for either uPA (or thrombin):serpin (either PNI or PAI-1) complexes. For complex formation, 50 μg of rat muscle extract protein was incubated with ^{125}I-labeled target protease (approximately 100,000 cpm/5 μg) for 20 minutes at 37°C. Duplicate incubations were performed at 100°C for an additional 5 minutes in the presence of SDS. The samples were then subjected to SDS-PAGE under non-reducing conditions in a standard 10% acrylamide gel (Laemmli, 1970). Quantification of specific complex activity involved excising the labeled band, counting in a gamma spectrometer (Packard AutoGamma) and relating the dpm to moles of complex formed (Scott et al., 1985; Festoff et al., 1990). Since one mole of protease is complexed with one mole of serpin, the specific serpin activity in a given extract was calculated.

Enzyme-Linked Immunosorbent Assay (ELISA).

PAs and serpin antigen in various rat muscle extracts were determined according to previously published methods (Rao et al., 1989; Festoff et al., 1990b; Rayford et al., submitted). In brief, aliquots of extracts, normalized for protein, or dilutions (6-100 ng) of purified uPA, tPA, PNI or PAI-1, were added to microtiter plates and incubated overnight at 4°C. Serpin concentration was determined using specific polyclonal rabbit anti-uPA, tPA, serpin antibodies at 1:1000 dilution, and an alkaline phosphatase-conjugated anti-rabbit goat IgG (1:1000 dilution). The phosphatase substrate used was para-nitrophenyl phosphate. The appearance of para-nitrophenol was used to quantitate the uPA, tPA and serpin concentration by monitoring absorbance at 405 nm in the Flow Multiscan.

Fibrin Zymography.

SDS-PAGE was performed according to Laemmli (1970) in 10% gels using pre-stained standards and was followed by fibrin-plate zymography according to the method of Granelli-Piperno and Reich (1978). Our modification consisted of binding the fibrinogen to Gelbond (FMC Bioproducts, Rockland, ME) before casting the fibrin gels (Hantaï et al., 1989; 1990). After SDS-PAGE and removal of SDS by washing the acrylamide gels in 2.5% Triton X-100 the gels were transferred onto the pre-cast fibrin plates, incubated in a moist atmosphere at 37°C for 24 hours and then stained with amido black (Granelli-Piperno and Reich, 1978; Festoff et al., 1986). Photography of the fibrin plates was performed with transillumination.

Other Assays.

Protein determination was estimated by the method of Bradford (1976) using Coomassie Brilliant Blue-G (Sigma Chemical Co., St. Louis, MO) as the color indicator.

Statistical analysis was performed using the two-tailed Student's t-test and chi square in the STATSPAC program.

RESULTS

Response of PAs to Ground-Based Injury in Muscle Extracts

For these biochemical measurements we were struck by the absence of "normative" data for muscle injury in the rat, either from the literature or from our own laboratory. We have considerable experience with denervation of mouse muscle and the kinetics of PA activation (Festoff et al., 1986; Hantaï et al., 1989; Hantaï et al., 1990). Our previous data also pointed to uPA as the predominant regulator of the pathophysiologic response to muscle injury and temporal studies after nerve crush showed that it was under tight neural (or non-injury) control (Hantaï et al., 1990). We needed to have similar chronologic data after muscle crush in the rat and, consequently, crushed the gastrocnemius of age-matched Wistar rats and made extracts from this muscle from 1-15 days after injury approximating the time after injury for the Czechoslovakian strain of Wistar rats used by our Soviet colleagues for Cosmos 2044. In Table 1 we show the uPA and tPA data for ground-based crush along this two-week time course along with the functional assay of plasminogen activation (S-2251 amidolysis). Previous data from mouse (Festoff et al., 1986) and rat (Festoff, unpublished) muscle indicate that all of the amidolysis of this substrate with muscle extracts is plasminogen-dependent. As can be seen the values for uPA increases along this time course to 10 days and then begins to decrease. Both functional activity and antigen content parallel each other over this period. On the other hand, tPA shows little variation over this same period of time.

These quantitative data were confirmed by qualitative evaluation using the less sensitive but more specific technique of fibrin zymography (Granelli-Piperno and Reich, 1978; Festoff et al., 1986). This allowed us to identify the Mr of the specific PA involved and also made possible the detection of complexes of protease and inhibitors (Saksela and Rifkin, 1988; Andreasen et al., 1990). As can be seen in Figure 1 muscle extracts from contralateral control muscles (Lanes 11, 12) show faint hydrolytic zones at 33 kDA and about 65 kDA. The lower Mr zone co-migrates with the low Mr sub-unit of two-chain uPA (tcuPA) as seen in Lane 15. The higher Mr zone, however, appears to migrate just behind high Mr (55 kDA) tcuPA and slightly ahead of single-chain (sctPA) at 65 kDA (lane 1). No definite higher Mr zones, suggestive of pre-formed complexes of protease and inhibitor, were found.

To further determine the identity of the 60-65 kDA fibrinolytic zone from zymography (Figure 1) we performed Western (immuno) blots of these ground-based muscle crush extracts.

PAs in Cosmos 2044 Muscle Extracts

Having obtained these data we felt more confident that we might be able to interpret data from the Cosmos 2044 mission when a single time point after 15 days was evaluated. In Table 2 we show the data for uPA and tPA, both antigen content and amidolytic activity, for the various conditions. Note that uPA increases in all situations above the low levels in basal animals' muscle with the exception of flight, and to a lesser degree, tail-suspension. In contrast, tPA values do not show significant differences amongst the various conditions.

Fibrin zymography was also performed, as we had for the Wistar rat muscle crush extracts. In contrast to ground-based crush samples, with this assay definite decreases in flight and also tail-suspension muscles were found compared to the synchronous and vivarium specimens (Figure 2). Little fibrinolysis was found in basal, uncrushed rat muscle, confirming previous studies with the mouse in support of the data for contralateral control muscle as (Figure 1). From these data we can conclude that zero gravity has a major effect on the 33 kDA sub-unit of rat muscle tcuPA. Such data are in accord with the S-2251 and ELISA studies.

Western blots of these muscle samples showed that synchronous and vivarium extracts were similar to the ground-based muscle crush experiments but that flight and tail- suspension showed fainter uPA bands. However, in addition, these muscle extracts now showed the appearance of 75-89 kDA immunoreactive bands not found in the basal or ground-based crush muscles. (Figure 2)

Serpins in Ground-Based and Cosmos 2044 Muscle Extracts

The Western blot experiments suggested that, in addition to decreases in uPA, there was an increase in PNI in muscle that was exposed to zero or micro-gravity after crush injury. Therefore, ELISA of PNI and PAI-1 was performed in these muscle extracts. The summary is shown in Table 3 where we see that although some increase in PNI is detected in flight, it is less so than in tail suspension, when compared to vivarium and synchronous crush controls. .

Complex Formation with Labeled Target Proteases

We used these techniques to quantify the moles of active serpin extractable from muscle after injury amongst the various experimental conditions. Iodinated α thrombin or uPA were utilized in the presence or absence of 1000 fold molar excess of non-labeled protease in order to detect complexes formed with serpin(s) in the extracts. In addition, the pre-exposure of muscle extract samples to 2 mM SDS was also used to activate latent PAI-1 (Loskutoff et al., 1986) or to inactivate PNI (Baker et al., 1986). Table 4 shows the moles of serpin detected under these conditions using this technique. As seen in the table, an increase in moles of PNI was detected in all situations where muscle crush was performed but that this was particularly increased in flight and synchronous samples when compared with basal. The table also shows an increase in moles of active PAI-1 occurred after muscle crush; in all cases PAI-1 was increased compared with basal extracts.

DISCUSSION

The basement membrane of adult skeletal muscle plays other important roles in muscle regeneration following injury (Anglister and McMahan, 1984; Sanes, 1986). It has been suggested that macromolecules within the synaptic region of the basement membrane influence the aggregation of acetylcholoine receptors (Sanes, 1986). One such molecule, called agrin, has been isolated and characterized (Nitkin et al., 1987). Very recently, agrin has been shown to possess protease inhibitory activity suggesting inhibition of normally-present proteases results in the more differentiated, and regenerative state, of acetylcholine receptor aggregation. The basement membrane has also been implicated in the plasticity of neuromuscular connections, i.e., synapse elimination, that occurs during postnatal development (Hantaï et al., 1989). The acceleration of synaptic turnover may result from increased neutral protease activity by degrading basement membrane proteins at the site of the synapses (Hantaï et al., 1988). It has been further suggested that such a process could play a role in the pathogenesis of amyotrophic lateral sclerosis (Festoff, 1980), and in neuromuscular regeneration (Festoff and Hantaï, 1987; Hantaï et al., 1988). Some of the major structural components of the ECM, unique to the basement membrane, are laminin, type IV collagen and a heparan sulfate proteoglycan (HSPG). Little is known about the turnover rate of these specific components nor the enzymes involved in their turnover in normal, developing or injured muscle. In a previous study, Hantaï and Festoff (1987) demonstrated that locally released plasminogen activators (PAs) act on these basement membrane components via activation of plasminogen. Plasmin is not only the final, major protease in fibrinolysis, it is a primary enzyme in ECM degradation both directly as well as by activating the metalloprotease procollagenase to active collagenase (Werb et al., 1980). When fresh frozen muscle sections were exposed to various proteases, it was found that fibronectin was the most sensitive ECM component to protease digestion, followed by type IV collagen and then laminin. Of the serine proteases studied, trypsin was the most active but was not selective, since it digested the

sarcoplasmic components as well as the basement membrane. However, urokinase, in the presence of plasminogen previously exposed to the treated tissue section, digested the matrix antigens of the basement membrane (Hantaï and Festoff, 1987). The presumed mechanism of this effect is by local activation of plasminogen to plasmin, due to increased release of PAs from injured muscle. In this regard, PAs were 8-10 times higher after 10 days of denervation of the mouse sternomastoid or soleus muscle at the same time when the selective sensitivity to digestion of some antigens as noted above were evident (Festoff et al., 1986).

These studies were initiated because it was not known whether the various processes involved in muscle regeneration could take place at zero or micro-gravity as on earth. As mentioned above, we had very little information regarding the molecules in question, the serine proteases and their serpin inhibitors, in either ground-based or flight response to muscle injury by crush. Our impression was that uPA is a rapid response molecule to muscle injury after crush, as it is after nerve injury (Festoff et al., 1986; Hantaï et al., 1990). Like nerve crush and axotomy the muscle uPA increases rapidly after crush, peaks at about 5-8 days and then decreases approaching the levels of controls by 2 weeks or so after injury (Figure 1). These qualitative results were confirmed by a sensitive amidolytic assay (Table 2).

Armed with this information we were prepared to analyze the influence of flight, and a ground-based model of micro-gravity (tail suspension), at a single time point after injury, the 15 days of flight or its simulation. Therefore, it was of interest to discover that of all the conditions analyzed for uPA activity, as well as for content (by ELISA) and for active moles of serpin complex activity, in general, correlated reproducibly, and significantly, the flight specimens were the lowest (Table 2-4).

We were also interested in determining the response of cellular serpins to the effects of space flight after injury. As discussed, we chose to measure the serpins, PNI and PAI-1, using several confirmatory tests for content and activity. ELISA for both serpins indicated that crush injury itself increased the amount of active plus complexed serpin and that this was greater, but barely significantly, in the flight after crush samples (Table 3). In addition, although only two experiments were performed due to scarcity of sample, complex formation with ^{125}I-uPA disclosed an increase in moles of functional PNI and PAI-1 in all crushed samples, somewhat higher in flight and tail suspension samples (Table 4).

From these data we can summarize the effects of flight on the injury response modifiers, urokinase and the serpins PNI and PAI-1. Any kind of muscle injury, but dramatically with crush, there is a rapid activation of the plasminogen activator, uPA. uPA, as shown previously, is under tight neural control (Festoff et al., 1986; Hantaï et al., 1990) but muscle crush over-rides any neural influence and allows the rapid expression of this activity. In other experiments, mRNA for uPA increases in denervation of muscle, but only at 5 days after nerve injury, well behind the dramatic increase in amidolytic activity (Hantaï et al. 1990b). This correlates with other work with transgenic mice in which the human uPA gene has been inserted (Botteri et al., 1990). In these elegant experiments, good correlation of uPA mRNA expression and endogenous uPA activity was found in kidney, which had the highest uPA activity. However, in adult innervated muscle, where uPA activity is barely detectable, uPA mRNA expression was second only to the kidney. This suggests that uPA message in kidney is in "ready-reserve" awaiting some type of injury for rapid activation.

Such a suggestion fits our current data with muscle crush, and our previous data with denervation. We (Beach et al., 1982; Festoff and Hantaï, 1987; Hantaï et al., 1988), and others (Gulati et al. 1983; Gulati, 1987) have proposed that neutral, extracellular proteases are essential to degrade components of the old basement membrane/ECM in order to allow for a basement membrane to scaffold for orderly regeneration (Vracko and Benditt, 1978) to take place. This differs, somewhat from the concept that

the entire basement membrane and its components is long-lived and remains after injury for regeneration and re-innervation of muscle (see Sanes, 1988). We may speculate that some interference with activation of this "ready-reserve" of uPA mRNA after injury characterizes zero gravity. These exciting results should now allow a more complete evaluation of gene regulation of proteases and serpins in the neuromuscular system in actual and simulated space flight and the regenerative response of organisms in these situations to injury. Evaluation of the hormonal regulation, shown by substantial data to also be dysregulated in zero gravity, of these activators (Danõ et al., 1985) and the serpins (Andreasen et al., 1990) will be essential.

ACKNOWLEDGEMENTS

The authors wish to acknowledge the following: the expert assistance of Dr. A.S. Kaplansky and the Soviet Cosmos recovery and dissection teams, without whose remarkable efforts this work could not have been accomplished; the advice and encouragement of Dr. Richard Grindeland throughout this enterprise, and Jim Connolly, Marilyn Vasques and other members of NASA-Ames Life Sciences Division for their expert planning and organization, both for the mission and for the Preliminary Results meeting; and, finally, Richiro Suzuki, Robbie Hickman and, especially, Marnie Van Becelaere for untiring energy in the Neurobiology Research Lab in support of this venture. This study was funded from NASA Cosmos 2044 Program.

REFERENCES

1. Allbrook, D. Skeletal Muscle Regeneration. Muscle & Nerve. 4:234-245, 1981.

2. Andreasen, P.A., B. Georg, L.R. Lund,A. Riccio,and S.N. Stacey. Plasminogen Activator Inhibitors: Hormonally Regulated Serpins. Molec. Cell. Endocrinol. 68:1-19, 1990.

3. Anglister, L. and U.J. McMahan. Ciba Foundation Symposium 108. 163-178, 1984.

4. Baker, J.B., D.J. Knauer, and D.D. Cunningham. Protease Nexins: Secreted Protease Inhibitors that Regulate Protease Action at and near the Cell Surface. In: The Receptors. Ed: Conn, P.M. Academic Press, New York. 153-172, 1986.

5. Beach, R.L., W.J. Hendricks, W. Burton, and B.W. Festoff. Extracellular Matrix Synthesis by Skeletal Muscle Cells in Culture: Proteins and Effect of Enzyme Degradation. J. Biol. Chem. 257:11437-11442, 1982.

6. Benton, E.V., D.D. Petersen, A.M. Marenny, and V.I. Popov. HZE Particle Radiation Studies Aboard Kosmos 782. Health Phys. 35:643-648, 1979.

7. Bischoff, R. Regeneration of Single Skeletal Muscle Fibers *In Vitro*. Anat. Rec. 182:215-236, 1975.

8. Botteri, F.M., H. Van der Putten, B. Rajput, K. Ballmer-Hofer, and Y. Nagamine, Y. In: Serine Protease and Their Serpin Inhibitors in the Nervous System: Regulation in Development and Malignant and Degenerative Diseases. Ed: Festoff, B.W. Plenum, New York. 1990.

10. Bradford, M.M. A rapid and Sensitive Method for the Quantitation of Microgram Quantities of Protein Utilizing the Principle of Protein Dye Binding. J. Anal. Biochem. 225:619-627, 1976.

11. Campion, D. R. The Muscle Satellite Cell: A Review. Int. Rev. Cytol. 87:225-251, 1984.

12. Carlson, B.M. The Regeneration of Skeletal Muscle: A Review. Am J. Anat. 137:119-150, 1973.

13. Carrell R., and J. Travis. α_1-Antitrypsin and the Serpins: Variation and Countervariation. Trends Biochem. Sci. 10:20-24, 1985.

14. Carrell, R.W. and D.R. Boswell. Serpins: The Superfamily of Plasma Serine Protease Inhibitors. In: Protease Inhibitors. Eds: Barrett A. and G. Salvesen . Elsevier, Amsterdam. 403-420, 1987.

15. Danõ, K., P.A. Andreasen, J. Grøndahl-Hansen, P. Kristensen, L.S. Nielsen, and L. Skriver. Plasminogen Activators, Tissue Degradation and Cancer. Adv. Cancer Res. 44:139-266, 1985.

16. Denny-Brown, D. The Influence of Tension and Innervation on the Regeneration of Skeletal Muscle. J. Neuropathol. Exp. Neurol. 10:94-95, 1951.

17. Deutsch, D.G. and E.T. Mertz. Plasminogen: Purification from Human Plasma by Affinity Chromatography. Science. 170:1095-1096, 1970.

18. Domingo A. and R. Marco. Visualization Under Ultraviolet Light Enhances 100-Fold the Sensitivity of Peroxidase Stained Blots. Anal.Biochem. 182:176-181, 1989.

19. Festoff, B.W.: Neuromuscular Junction Macromolecules in the Pathogenesis of Amyotrophic Lateral Sclerosis. Med. Hypotheses. 6:121-131, 1980.

20. Festoff, B.W. In: Serine Proteases and Their Serpin Inhibitors in the Nervous System: Regulation in Development and Malignant and Degenerative Diseases. Plenum, New York. 356, 1990.

21. Festoff, B.W. and D. Hantaï. Plasminogen Activators and Inhibitors: Specific Roles in Neuromuscular Regeneration. Progr. Brain Res. 71:423-431, 1987.

22. Festoff, B.W., M.R. Patterson, and K. Romstedt. Plasminogen Activator: the Major Secreted Neutral Protease of Cultured Muscle Cells. J. Cell. Physiol. 110:190-195, 1982.

23. Festoff, B.W., D. Hantaï, J. Soria, A. Thomaidis, and C. Soria. Plasminogen Activator in Mammalian Skeletal Muscle: Characterization of Effects of Denervation on Urokinase-Like and Tissue Activators. J. Cell Biol. 103:1415-1421, 1986.

24. Festoff, B.W., J.S. Rao, and D. Hantaï. Plasminogen Activators and Their Inhibitors in the Neuromuscular System: I. Developmental Regulation of Isoforms During *In Vitro* Myogenesis in Two Cell Lines. J. Cell. Physiol. 144:649-659, 1990a.

25. Festoff, B.W., D. Hantaï, and J.S. Rao. Plasminogen Activators and Inhibitors in the Neuromuscular System: II. Serpins and Serpin: Protease Complex Receptors Increase During *In Vitro* Myogenesis. J. Cell. Physiol. 144:660-668, 1990b.

26. Festoff, B.W., D. Hantaï, and J.S. Rao. Plasminogen Activators and Inhibitors in the Neuromuscular System: III. Protease Nexin I, a Neurite-Outgrowth Promoting Serine Protease

Inhibitor (Serpin), Synthesized by Muscle Co-Localizes with Acetylcholine Receptors at Neuromuscular Synapses. J. Cell. Physiol. (in press), 1990c.

27. Granelli-Piperno, A. and E. Reich. A Study of Protease and Protease-Inhibitor Complexes in Biological Fluids. J. Exp. Med. 148:223-224, 1978.

28. Guenther, J., H. Nick, and D. Monard. A Glia-Derived Neurite-Promoting Factor with Protease Inhibitory Activity. EMBO J. 4:1963-1966, 1985.

29. Gulati, A.K. The Effect of X-Irradiation on Skeletal Muscle Regeneration in the Adult Rat. J. Neurol. Sci. 78:111-120, 1987.

30. Gulati, A.K., A.H. Reddi, and A.A. Zalewski, A.A. Changes in the Extracellular Matrix Components, Fibronectin and Laminin, During Immune Rejection of Skeletal Muscle. Anat. Rec. 209:21-27, 1981.

31. Gulati, A.H., A.H. Reddi, and A.A. Zalewski. Changes in the Basement Membrane Zone Components During Skeletal Muscle Fiber Degeneration and Regeneration. J. Cell Biol. 97:957-962, 1983a.

32. Gulati, A.H., A.A. Zalewski, and A.H. Reddi. An Immunofluorescence Study of the Distribution of Fibronectin and Laminin During Limb Regeneration in the Adult Newt. Dev. Biol. 96:355-365, 1983b.

33. Hantaï, D. and B.W. Festoff. Degradation of Muscle Basement Membrane Zone Antigens by Locally-Generated Plasmin. Exp. Neurol. 95:44-55, 1987.

34. Hantaï, D., J.S. Rao, and B.W. Festoff. Serine Proteases and Serpins: Their Possible Roles in the Motor System. Revue Neurologique. 144:680-687, 1988.

35. Hantaï, D., J.S. Rao, C. Kahler, and B.W. Festoff. Decrease in Plasminogen Activator Correlates with Synapse Elimination During Neonatal Development of Mouse Skeletal Muscle. Proc. Natl. Acad. Sci. USA. 86:362-366, 1989.

36. Hantaï, D., C.B. Kahler, J.S. Rao, and B.W. Festoff. Rapid Neural Regulation of Muscle Urokinase-Like Plasminogen Activator as Defined by Nerve Crush. Proc. Natl. Acad. Sci. USA. 87:2926-2930, 1990.

37. Hantaï, D., R. Suzuki, J.S. Rao, and B.W. Festoff. Regulation of uPA mRNA in Mouse Sciatic Innervated Muscle. Neurosci. Abstr. (in press), 1990.

38. Heimer, G.V. and C.E.D. Taylor. Improved Mountant for Immunofluorescence Preparations. J. Clin. Pathol. 27: 254-256, 1974.

39. Kao K. and P.A. Klein. A Monoclonal Antibody-Based Enzyme-Linked Immunosorbent Assay for Quantitation of Plasma Thrombospondin. Amer. J Clin. Path. 86:317-323, 1986.

40. Keohane, M.E., S.W. Hall, S.R. VanDenberg, and S.L. Gonias. Secretion of 12¡ α2-Macroglobulin, α2-Antiplasmin, and Plasminogen Activator Inhibitor-1 by Glioblastoma Multiforme in Primary Organ Culture. J. Neurosurg. 73:234-241, 1990.

41. Laemmli, U.K. Cleavage of Structural Proteins During the Assembly of the Head of Bacteriophage. Nature (London). 227:680-85, 1970.

42. Lipton, B.H. and E. Schultz. Developmental Fate of Skeletal Muscle Satellite Cells. Science. 205:1292-1294, 1979.

43. Loskutoff, D.J., M. Sawdey, and J. Mimuro. Type 1 Plasminogen Activator Inhibitor. Progr. Haemost. Thromb. 9:87-115, 1989.

44. Mauro, A. Satellite Cell of Skeletal Muscle Fibers. J. Biophys. Biochem. Cytol. 9:493-495, 1961.

45. Mauro, A. Muscle Regeneration. Raven, New York. 1979.

46. McGrogan, M.P., J. Kennedy, M.P. Li, C. Hsu, R.W. Scott, C. Simonsen, and J.B. Baker. Molecular Cloning and Expression of Two Forms of Human Protease Nexin I. Biotechnology. 6:172-177, 1988.

47. Meier, R., P. Spreyer, R. Ortmann, et al. Induction of Glia-derived Nexin After Lesion of a Peripheral Nerve. Nature. 342:548-550, 1989.

48. Monard, D. Cell Derived Proteases and Protease Inhibitors as Regulators of Neurite Growth. Trends Neurosci. 11:541-544, 1988.

49. Nitkin, R.M., M.A. Smith, C. Magill, J.R. Fallon, Y.M.M. Yao, B.G. Wallace, and U.J. McMahan. Identification of Agrin, a Synaptic Organizing Protein from Torpedo Electric Organ. J. Cell Biol. 105:2471-2478, 1987.

50. Rånby, M., B. Norman, and P. Wallén. A Sensitive Assay for Tissue Plasminogen Activator. Thromb. Res. 27:743-748, 1982.

51. Rao, J.S., C. Kahler, and B.W. Festoff. Inhibition of Extracellular Matrix Degradation by Protease Nexin I in Cultured Muscle Cells. Muscle and Nerve. 12:640-646, 1989

52. Rao, J.S., J.B. Baker, R.A. Morantz, B. Kimler, R. Evans, and B.W. Festoff. Serpin Inhibitors of Urokinase and Thrombin in Normal Rat Brain and the 9L Brain Tumor: Evidence for Elevated Expression of PNI-Like Inhibitor and a Novel SDS-Activated Tumor Antithrombin. Cancer Res. 50:5039-5044, 1990.

53. Riley, D.A., E.I. Ilyina-Kakeuva, S. Ellis, J.L.W. Bain, G.R. Slocum, and F.R. Sedlak. Skeletal Muscle Fiber, Nerve and Blood Vessel Break-Down in Space-Flown Rats. FASEB J. 4:84-91, 1990.

54. Sanes, J.R. The Extracellular Matrix. In: Myology. Eds: Engel, A.G and B.Q. Banker. McGraw-Hill, New York. 155-175, 1986.

55. Saksela, O. and D.B. Rifkin. Cell-Associated Plasminogen Activation: Regulation and Physiological Functions. Annu. Rev. Cell. Biol. 4:93-126, 1988.

56. Sawaya, R. In: Fibrinolysis and the Central Nervous System. Handley & Belfus, New York. 340 pp., 1990.

57. Scott R.W., B.L. Bergman, A. Bajpai, R.T. Hersh, H. Rodriguez, B.N. Jones, S. Watts , and J.B. Baker. Protease Nexin: Properties and a Modified Purification Procedure. J. Biol. Chem. 260:7029-7034, 1985.

58. Snow, M.H. Myogenic Cell Formation in Regenerating Rat Muscle Injured by Mincing: II. An Autoradiographic Study. Anat. Rec. 188:201-218, 1977.

59. Towbin, H., T. Staehlin, and J. Gordon. Electrophoretic transfer of Proteins from Polyacrylamide Gels to Nitrocellulose Sheets: Procedure and Some Applications. Proc. Natl. Acad. Sci. USA. 76:4350, 1979.

60. Travis J., and G.S. Salvesen. Human Plasma Proteinase Inhibitors. Ann. Rev. Biochem. 52:655-709, 1983.

61. Travis, J., A. Guzdek, J. Potempa, and W. Watorek. Serpins: Structure and Mechanism of Action. Biol. Chem. Hoppeseyler. 371(S):3-11, 1990.

62. Van Mourik, J.A., D.A. Lawrence, and D.J. Loskutoff. Purification of an Inhibitor of Plasminogen Activator (Antiactivator) Synthesized by Endothelial Cells. J. Biol. Chem. 259:14914-14921, 1984.

63. Vracko, R. and E.P. Benditt. Basal Lamina: The Scaffold for Orderly Cell Replacement, Observations on Regeneration of Injured Skeletal Muscle Fibers and Capillaries. J. Cell Biol. 55:406-419, 1972.

64. Weinberg, J.B., M.M. Hobbs, and S.V. Pizzo. Microassay for the Photometric Quantitation of Cell-Associated Plasminogen Activator Using a Chromogenic Tripeptide Substrate. J. Immunol. Methods. 75:289-294, 1984.

65. Werb, Z., M.J. Banda, and P.A. Jones. Degradation of Connective Tissue Matrices by Macrophages: III. Morphological and Biochemical Studies on Extracellular, Pericellular and Intracellular Events in Matrix Proteolysis by Macrophages in Culture. J. Exp. Med. 152:1537-1553, 1980.

TABLE 1

AMIDOLYTIC ACTIVITY OF uPA IN NORMAL AND MUSCLE CRUSH SAMPLES

Animal Description		U/mg of Protein (Mean ± SEM)	% Control
Control		4.8 ± 0.219	100.00
After Crush	Day 1	6.8 ± 0.308	141.67
	Day 2	8.0 ± 0.154	166.67
	Day 5	7.2 ± 0.043	156.00
	Day 7	4.6 ± 0.132	95.83
	Day 10	4.7 ± 0.154	97.92
	Day 15	5.5 ± 0.374	114.58

Amidolytic assay s2251 is described in Methods section.

TABLE 2

AMIDOLYTIC ACTIVITY OF uPA IN VARIOUS MUSCLE EXTRACTS

Animal Description	U/mg of Protein (Mean ± SEM)	% Basal	P
Basal (Orange)	1.340 ± 0.321	100.00	-
Tail Suspension (Blue)	1.490 ± 0.230	82.65	0.01
Vivarium (Green)	0.947 ± 0.049	83.41	0.01
Synchronous (Yellow)	1.120 ± 0.019	71.19	0.01
Flight (Red)	0.768 ± 0.130	56.41	0.001

Amidolytic activity of uPA in various muscle extracts is described in Methods section. Comparisons were made for all conditions with basal, as uncrushed samples.

Acronym Key for Tables and Figures: ECM, extracellular matrix; PNI, protease nexin I ; PNII, protease nexin II; PA, plasminogen activator; uPA, urokinase-like PA; tPA, tissue-type PA; scuPA, single-chain uPA; tcuPA, two chain uPA; PAI-1, plasminogen activator inhibitor-1; ELISA, enzyme-linked immunosorbent assay; FITC, fluorescein isothiocyanate; BSA, bovine serum albumin, PBS, phosphate buffered saline; NEM, n-ethylmaleimide; PMSF, phenylmethylsulfonyl fluoride

TABLE 3

ELISA FOR PNI (μG/MG PROTEIN) AND PAI - 1 (NG/MG PROTEIN) IN MUSCLE

Animal Description	PNI	PAI
Basal (Orange)	1.340 ± 0.321	9.321 ± 1.397
Tail Suspension (Blue)	1.490 ± 0.230	12.020 ± 1.820
Vivarium (Green)	0.947 ± 0.049	10.060 ± 0.954
Synchronous (Yellow)	1.120 ± 0.019	7.130 ± 1.750
Flight (Red)	0.768 ± 0.130	5.970 ± 0.418

ELISA's for PNI and PAI - 1 are described in Methods section.

TABLE 4

SPECIFIC ACTIVITIES (CPM/μMOLE) OF PNI AND PAI - 1 COMPLEXES WITH LABELED UROKINASE IN VARIOUS MUSCLE EXTRACTS

Animal Description	PNI	PAI
Basal (Orange)	22.87 ± 0.99	11.31 ± 1.06
Tail Suspension (Blue)	33.28 ± 2.87	21.69 ± 4.80
Vivarium (Green)	30.82 ± 1.53	20.53 ± 6.40
Synchronous (Yellow)	36.54 ± 2.96	18.35 ± 2.66
Flight (Red)	39.21 ± 3.61	15.40 ± 5.13

Average of two samples.

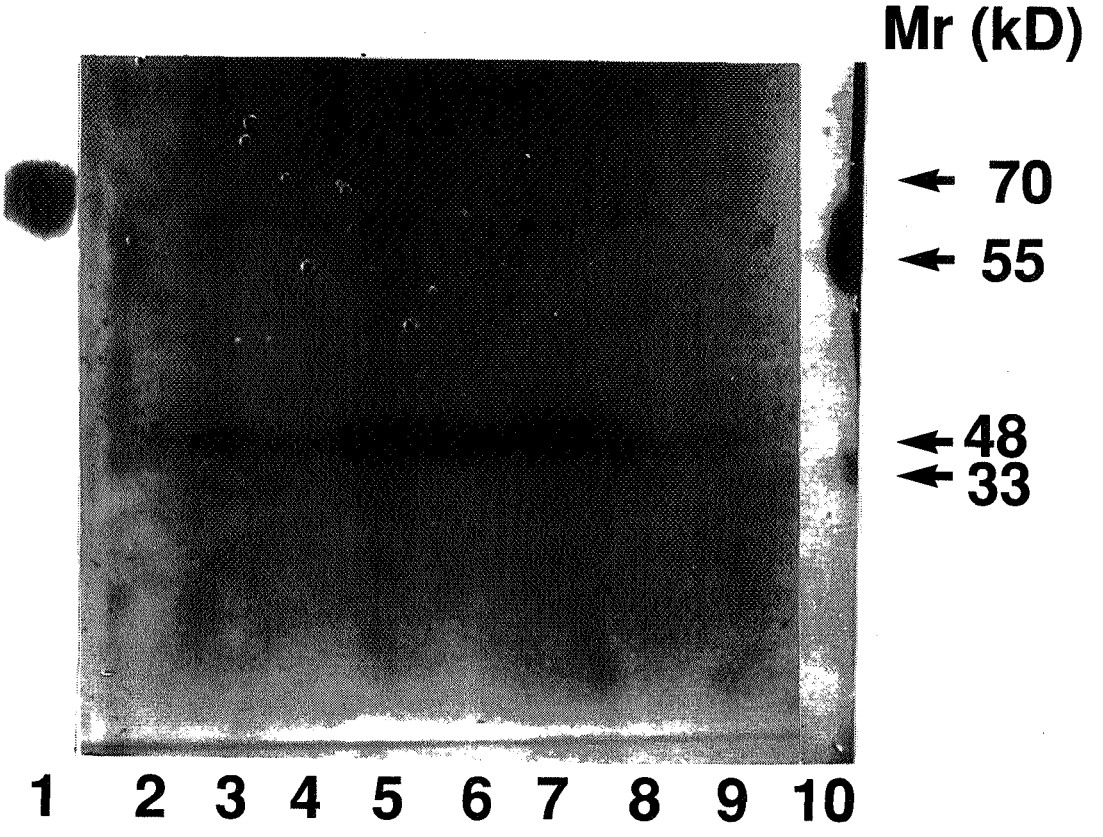

Figure 1. Fibrin zymogram of ground-based muscle crush time course. Fibrin zymography performed as in Methods. Lanes are: 1, human tPA standard; 2, rat muscle extract 15 days after muscle crush; 3, muscle extract after 10 days; 4, after 7 days; 5, after 5 days; 6, after 2 days; 7, after 1 day; 8 and 9, control muscle extracts; 10, standard human uPA.

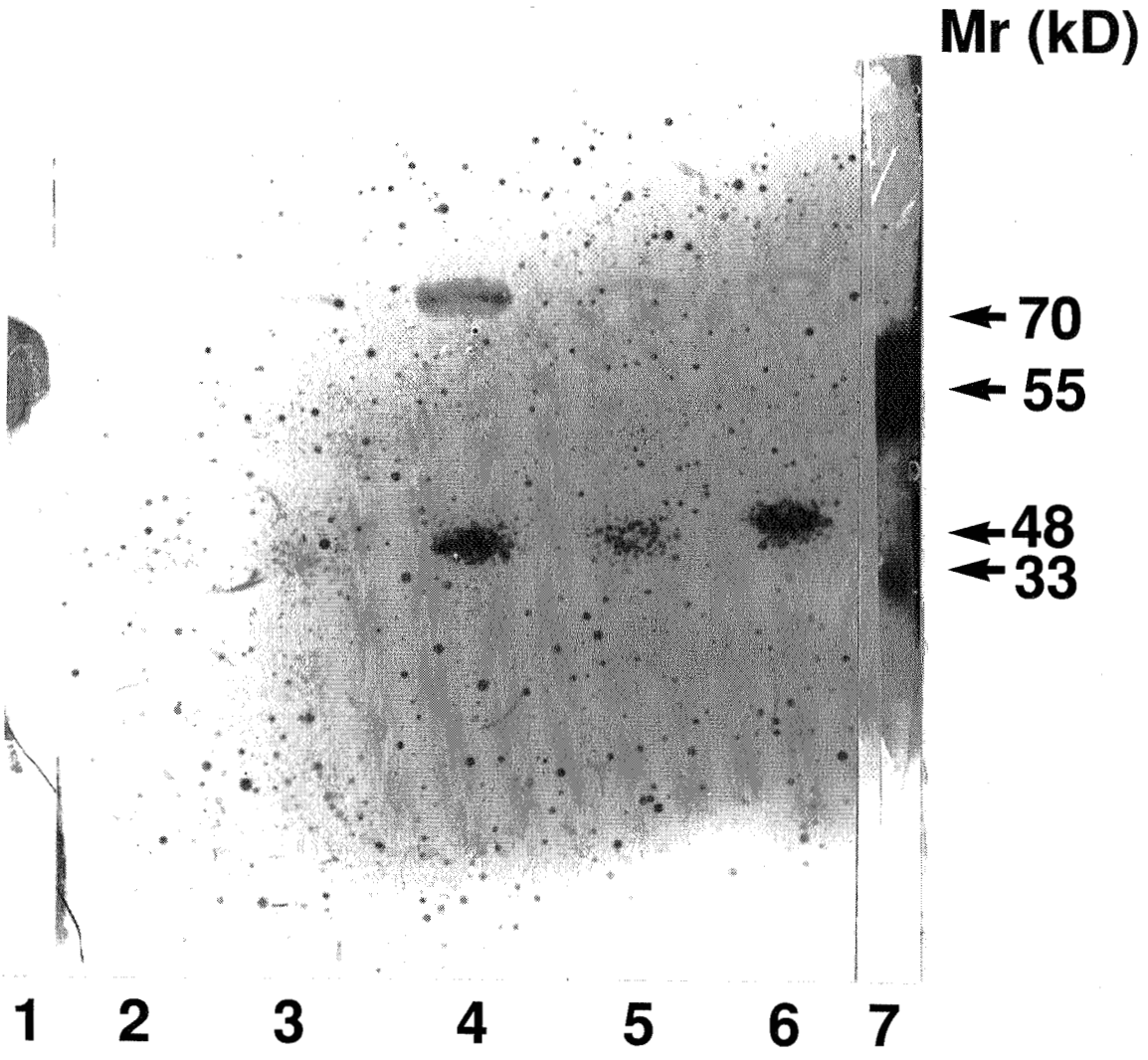

Figure 2. Fibrin zymogram of COSMOS 2044 muscle extracts. Fibrin zymography performed as in Methods. Lanes are: 1, human tPA; 2, basal; 3, synchronous; 4, vivarium; 5, flight; 6, tail suspension and 7, human uPA.

S17-51
51362

EXPERIMENT K-7-29

PART III: RODENT TISSUE REPAIR: SKELETAL MUSCLE

W.T. Stauber, V.K. Fritz, T.E.Burkovskaya, and E.I. Ilyina-Kakueva .

SUMMARY

Myofiber injury-repair was studied in the rat gastrocnemius following a crush injury to the lower leg prior to flight in order to understand if the regenerative responses of muscles are altered by the lack of gravitational forces during Cosmos 2044 flight. After 14 days of flight, the gastrocnemius muscle was removed from the 5 injured flight rodents and various Earth-based treatment groups for comparison. The Earth-based animals consisted of three groups of five rats with injured muscles from a simulated, tail-suspended and vivarium as well as an uninjured basal group. The gastrocnemius muscle from each was evaluated by histochemical and immunohistochemical techniques to document myofiber, vascular and connective tissue alterations following injury.

In general the repair process was somewhat similar in all injured muscle samples with regard to extracellular matrix organization and myofiber regeneration. Small and large myofibers were present within a newly organized extracellular matrix indicative of myogenesis and muscle regeneration. In the tail-suspended animals, a more complete repair was observed with no enlarged area of non-muscle cells or matrix material visible. In contrast, the muscle samples from the flight animals were less well differentiated with more macrophages and blood vessels in the repair region but small myofibers and proteoglycans, nevertheless, were in their usual configuration. Thus, myofiber repair did vary in muscles from the different groups, but for the most part, resulted in functional muscle tissue.

INTRODUCTION

The skeletal muscle atrophy seen in actual or simulated weightlessness (18) appears to be due to a combination of local and systemic factors - muscle tension and exogenous growth factors. These same factors play a role in the normal repair of injured skeletal muscle as seen following contusion or mechanical strains which are common as industrial injuries. As man begins to undertake construction of space and moon stations, it is to be expected that injuries will occur as a result of the deceleration of objects which have been moved or are moving. It is precisely this deceleration by muscular tissues that has been under investigation in our laboratory (6,16). These include the study of the repair of muscle and connective tissues surrounding the myofibers (fascia).

A muscle contusion is a common household, occupational and athletic injury and will most likely result from construction work in zero G environments as well. Under most conditions studied, the injured muscle recovers completely without any impairment. Still, little is known about the role muscle tensions and/or gravitational forces play in wound healing and fascial repair. Is the atrophic muscle found in animals at zero G a special risk for fibrosis or incomplete repair? Alternatively, does the lack of gravity have a beneficial effect on muscle repair and regeneration? Spaceflight presents a unique opportunity to investigate the biology of skeletal muscle repair in the absence of normal muscular tensions but under normal neural activation with a direct benefit to understanding future problems of man working in space. If gravitational forces are necessary for optimal connective tissue organization and muscle repair, then muscle injuries at zero G might require a special type of rehabilitation to prevent muscle fibrosis and/or movement dysfunction.

The purpose of this study was to describe the repair of muscles in rats which have been subjected to a crush injury prior to the Cosmos 2044 flight and compare them to a variety of Earth-based rats injured

and subjected to different environments (e.g. 1-G, tail-suspended, vivarium) to document if connective tissue and myofiber repair were different at zero gravity.

MATERIALS AND METHODS

Muscles from the injured spaceflight (F) rats were compared with those of four earth-based groups: basal (B) control rats killed near time of launch; synchronous (S) control rats injured and maintained like flight rats; vivarium (V) control rats which were injured and kept under normal laboratory conditions; and tail-suspended (T) rats which were injured and maintained in a head down tail-suspended position known to simulate the effects of weightlessness (18).

Ten male pathogen free rats of Czechoslovakian-Wister origin (Bratislava, Czechoslovakia) were flown on the Cosmos 2044 Biosputnik for 14 days. Five of these animals were subjected to a crush injury to their hind-limb including the gastrocnemius muscle three days prior to flight. Flight, housing, feeding, and recovery conditions were as described in the Mission Description of this report. Upon landing, the gastrocnemius muscles were dissected free by the Soviet dissection team headed by Dr. A.S. Kaplansky, a portion of the gastrocnemius muscle was removed by the Soviets for their study and the remainder frozen. Similar samples were provided for the other groups (B, S, T, V). All the frozen muscles were sent to NASA -Ames with the aid of Dr. R. Grindeland who was responsible for their safe arrival and reshipment to West Virginia University in good condition in spite of an earthquake. Upon arrival the frozen muscle samples (5 from each group) were unpacked, photographed, and divided longitudinally into two equal parts: 1) one half was sent to Dr. B. Festoff; 2) the other half was was sectioned for analysis and was used for the experiments reported herein.

In all cases, the muscle tissues were sectioned at -20° C in a an International CTI cryostat (Needham Heights, MA) at a thickness of 4 μm, collected on alcohol cleaned glass slides, and allowed to air dry. The slides were stored in airtight containers at -20° C until use. The gastrocnemius muscles from the four earth-based groups of rats generally sectioned well. The muscle samples from the flight animals had a more delicate nature and sections were more difficult to obtain and study.

Macrophages were localized in muscle sections from all groups using an α–naphthyl acetate esterase kit (Sigma, St. Louis, MO) according to manufacturers instructions. The slides were observed by light microscopy and photographed.

Blood vessels and capillaries in the muscle sections (13) were visualized using a histochemical procedure for the localization of dipeptidyl peptidase IV (12). This peptidase is localized by a simultaneous coupling technique using fast blue BB for the detection of the 4-methoxy-2-naphthylamine from a dipeptide substrate (Enzyme Systems Products, Dublin,Ca). An incubation mixture was prepared containing 0.1 M phosphate buffer, pH 7.4, 20 mg/ml gly-pro-4-methoxy-2-naphthylamine and 20 mg/ml fast blue BB salt. The slides of sectioned muscle were incubated for 45 min at room temperature, rinsed in tap water, and counterstrained with Harris hematoxylin for 5 minutes. The slides were mounted with 50% glycine/50% PBS, pH 7.4 and observed under the light microscope.

Localization of proteinases, proteins, and proteoglycans were performed by indirect immunohistochemical techniques using fluorescein- labeled second antibodies. Antiserum to rat chymase was prepared by conventional methods of immunization in rabbits by Dahlmann et al. (5). The antiserum was provided as affinity-purified immunoglobulin (IgG) fractions from Affigel 15 (Biorad, Richmond, CA). Antisera to rat fibrinogen, albumin, and fibronectin were obtained commercially (Organon Teknika-Cappel, Malvern, PA). Briefly, the immunohistochemical staining procedure for fibrinogen, albumin, fibronectin , and chymase included washing the slides three times for 5 min with filter sterile 0.01 M sodium phosphate in 0.15 M NaCl, pH 7.4 (PBS). 50 μl of the appropriate dilution of antiserum was applied to each slide. The slides were incubated at room

temperature for 30 min in a moist chamber to prevent evaporation. The antisera were diluted to approximately 1 mg/ml protein as determined by protein assay [13] using albumin as a standard. Following incubation, all slides were washed five min in PBS. Finally, 50 ul of fluorescein-labeled goat $F(ab')_2$ anti-rabbit IgG at a 1:20 dilution was added to all experimental and control slides. After another 30 min incubation and a final wash for five min in PBS, glass coverslips were applied over the tissue sections with 50% glycerine-50% PBS containing 1 mg/ml p-phenylenediamine (Sigma, St. Louis, MO) and viewed on a Leitz Orthoplan fluorescence microscope (15). The localization of the plasma proteins was used to evaluate vascular permeability and cellular membrane integrity.

The presence or absence of specific proteoglycans has been useful in identification of muscle injury (where chondroitin 6-proteoglycan disappears) and regeneration (where embryonic forms of proteoglycans reappear in the extracellular matrix). Monoclonal antibodies directed against proteoglycans digested with chondroitinase ABC were provided by Dr. Bruce Caterson. Antigen isolation, monoclonal antibody production and characterization have been completely described previously (2,4). Digestion of the tissue with chondroitinase ABC results in a proteoglycan fragment of small oligosaccharide stubs with at least one characteristic unsaturated disaccharide (0,4 or 6 sulfated) of the chondroitin sulfate isomer and the linkage region attached to the proteoglycan core protein (3). These antibodies were specific for chondroitin-4-sulfate (4/8/2B6), chondroitin-6-sulfate (5/6/3B3) and unsulfated chondroitin (5/6/1B5) proteoglycans.

Localization of specific proteoglycans was performed using a modification of the previously described technique (1). The slides were washed for five min with 0.05 Tris/HCl, 0.05 M NaCl, pH 8.0 and predigested with 0.05 units/ml Chondroitinase ABC (Sigma, St. Louis, MO) diluted in the same buffer for 45 min at room temperature in a moist chamber. After a 10 minute wash in PBS, 50 ul of diluted specific monoclonal antiserum was added to each slide and incubated for 30 min. Following incubation, all slides were washed again in PBS followed by the application of fluorescein-labeled goat $F(ab')_2$ antimouse IgG (TAGO, Burlingame, CA) at a 1:20 dilution. After another 30 min incubation the slides were washed with PBS and glass coverslips applied as described above. The slides were viewed on the fluorescence microscope.

The controls for the fluorescent immunohistochemical experiments included tissue sections either incubated with normal rabbit serum instead of specific antibody or culture media instead of monoclonal antibody followed by fluorescien-labeled antiserum. Controls for the monoclonal antisera to proteoglycans included fresh frozen sections of rat ear as positive controls treated in the same manner as the normal and injured muscle tissue. Each monoclonal antibody to proteoglycans was localized in the cartilaginous portion of the rat ear. The specificity of the monoclonal antibodies was tested by excluding the chondroitinase ABC digestion prior to monoclonal antibody application followed by fluorescein-labeled second antibody. Another group received only Chondroitinase ABC, diluted mouse serum and fluorescein-conjugated second antibody. Normal and injured muscle sections incubated with monoclonal antibodies to proteoglycans without prior chondroitinase ABC digestion or vice vers were devoid of any specific fluorescent localization.

Fluorescein-conjugated Concanavalin (Con A) (Vector Laboratories, Burlingame, CA) was used to localize non-specific glycoproteins rich in mannose residues such as found in the pericellular basement membrane of the basal lamina (8) and to outline the intact myofibers. Fluorescein-labeled Con A at a 1:200 dilution in PBS, was applied directly to slides of flight, tail-suspended, vivarium, basal, and simulated muscles after an initial wash for 5 min in PBS. Following a second wash in PBS, coverslips were applied and the samples photographed after viewing under the microscope.

RESULTS

Gross examination of the frozen muscle samples revealed a very small ecchymotic area for two of the five muscle from the flight group but not in any of the other muscles. Upon dividing the muscles, a white band could be seen in both halves of the muscle indicative of the injured area. It appeared that all

animals except the basal controls were injured and in most instances the injured site was large enough to be seen by the naked eye.

Microscopic observation confirmed the injury site which in most cases was quite large. This area included loosely organized connective tissue, small myofibers, enlarged interstitial spaces, and macrophage infiltration. With the exception of the tail-suspended (T) group, these general features were quite similar in most injured animals with a few unique features which will be discussed in detail below.

Myofibers were distinguished from supporting cells and the extracellular matrix by the binding of the lectin , Concanavalin A (Con A). Since Con A binds to mannose-rich components associated with extracellular matrix and related constituents, it was never found inside myofibers. In the injured muscles the injury site could be identified as a large Con A positive area (Figure 1) with little or no myofibers present. However, such an area could not be found in the muscles from the tail-suspended animals and, of course, the uninjured basal group. In the muscles from the basal group, the fiber sizes were relatively uniform with a small area of extracellular matrix surrounding each myofiber. Following injury, the presence of a variety of myofiber sizes was noted in all samples except the tail-suspended where uniformly small and large myofibers existed in separate but adjacent areas (Figure 1).

In the flight, simulated, and vivarium groups, many non-muscle cells were located in the area surrounding myofibers and included macrophages, mast cells, and fibroblasts. Macrophages were identified by the presence of an esterase using histochemical staining techniques (Figure 2). The macrophages were observed in larger numbers than in the basal (uninjured) group at the injury site in all samples, except the tail-suspended group, where their numbers approximated those seen in the basal group. Interestingly an increased number of macrophages were not only found at the injury site in the flight group but also throughout the entire section including uninjured areas. This was an unexpected finding.

Mast cells were identified by employing antisera to rat chymase. The number of mast cells present was greater in the flight and simulated groups, and to a lesser extent in the tail-suspended group. Mast cells were seen in clusters as well as individual cells-often found near blood vessels and nerves in the perimysium. There was scant evidence of mast cell degranulation, but when present, it was greater in the flight, simulated, and vivarium groups but not in the tail-suspended or basal groups.

Localization of multicatalytic protease (MCP) (Figure 3) revealed an increased number of enlarged nuclei present in the flight (F), simulated (S) and vivarium (V) groups. Whereas only a few enlarged nuclei were observed in the tail-suspended (T) and none in the basal (B) group. In addition to myofibers, the MCP positive cells included fibroblasts, myoblasts and satellite cells. The enhanced localization of MCP in the injured muscles was consistent with a on-going process of tissue repair.

Capillaries were visualized using dipeptidyl peptidase IV localization which revealed an increased number of small blood vessels found in the flight group. These blood vessels were most pronounced in the area of repair.

Evidence of increased vascular permeability was observed using specific antisera for plasma constituents: fibronectin, fibrinogen and albumin. These plasma proteins were localized throughout the enlarged interstitial spaces in the injury site. Albumin was generally diffusely localized throughout the interstitial spaces. Fibronectin (Figure 4) and fibrinogen demonstrated very similar distribution patterns with a diffuse uneven fluorescence apparent at the repair site while a more intense fluorescence was observed on portions of some small myofibers.

Chondroitin-6-sulfate proteoglycan was localized around myofibers, blood vessels, and nerves. Overall fluorescence was closely associated with myofibers and vessels with very little localization

found among the smaller non-muscle cells in the injury site (Figure 5). Groups of small myofibers were clustered together with very intense staining in the flight rats whereas the simulated and vivarium rats had a more random distribution of fiber sizes. The tail-suspended and the basal control samples were quite similar except for smaller fibers in the suspended muscle. No extracellular matrix staining was observed in muscle sections incubated with this monoclonal antibody or any of the others whenever predigestion with chondroitinase ABC was excluded.

Chondroitin 4-sulfate proteoglycan was localized unevenly around fibers and diffusely filling in the enlarged extracellular space in the injured area (Figure 6). Localization was increased around presumptive regenerating fibers which were clustered in groups in the flight animals. Chondroitin-4-sulfate proteoglycan was also found in the perimysium.

Monoclonal antibodies to unsulfated chondroitin proteoglycan stained the myofibers from the flight animals brightly and were useful for identifying very small myofibers not seen in the Earth-based groups of muscles (Figure 7). In addition, the distribution of the staining was more pronounced in the enlarged extracellular space in all of the Earth-based controls except those of tail-suspended and basal groups. In the latter samples, this proteoglycan was observed faintly outlining the fibers and small blood vessels.

DISCUSSION

Skeletal muscle injury is generally followed by a series of processes that result in some form of repair to the damaged tissue. These processes include inflammation, satellite cell activation, myogenesis, fibroblast proliferation, and connective tissue reorganization. The magnitude of the injury and the degree of disruption of the vascular supply alter the time course for repair, overall involvement of the various cell populations, and the final outcome of the repair of a functional muscle. The repair can vary from complete restoration of an essentially normal muscle (6,16) to a muscle with extensive fibrosis (11) and restricted motion (e.g. contracture).

In order to study the regenerative potential of injured skeletal muscles subjected to zero gravity, a crush injury was produced by squeezing one of the lower legs of a rat with forceps. This type of injury is known to result in a large area of trauma and extensive damage to muscle. In general, crush injuries have been reported to be complex in nature including crushed myofibers, disrupted fascia, and ruptured blood vessels with evidence of bleeding and hematoma formation. Using histochemical techniques, indicators of inflammation, cell infiltration, and connective tissue reorganization were monitored in animals which were injured and flown aboard the Cosmos 2044 satellite for 14 days. These rats waited 3 days after the injury before flight and thus some degree of healing had already begun before zero gravity conditions were experienced.

When comparing flight, simulated, and vivarium groups subjected to identical conditions, the gross differences among the injured groups at first appeared minimal, except that two of the flight rats had evidence of a fresh hematoma on the surface of the muscle perhaps indicating that a small injury occurred upon reentry or during reambulation. The area of the muscle form the experimental crush injury could be easily localized and characterized by an enlarged interstitial space containing plasma constituents and extracellular matrix materials typical of muscle repair after other types of injury (17). Surprisingly, in the tail-suspended group, no area of injury could be found. Instead, a large area of small myofibers was present adjacent to normal sized fibers. It is possible that the immobilization had actually enhanced the healing process so that the tail-suspended muscles were further along in the repair process (i.e. suspension improved muscle healing). Other possibilities certainly exist because the crush injuries might not have been identical. In humans, immobilization can help certain healing processes such as torn muscles. So the difference between flight and tail-suspended muscles needs further clarification - especially since the rodent hindlimb unweighting is a popular Earth-based model to study microgravity-induced muscle atrophy.

Some other group specific observations were unique only to the flight animals. These included increased vascularity of the injured area, increased numbers of macrophages both at the injury site and throughout the entire muscle sample, and variations in the content and distribution of certain proteoglycans and plasma constituents. It is possible that these subtle variations indicate that muscle might be more subject to scarring under zero gravity as increased vascularity is a well known characteristic of granulation tissue and not of muscle regeneration. Unfortunately, the final stages of healing were not available to allow a definitive statement to be made.

Evidence of a slow repair process in all of the crush injured muscles except the tail-suspended group was supported by the content and distribution of extracellular matrix components. In mature muscle as illustrated by the basal animals, proteoglycans reside as a thin band around myofibers; however, following injury, proliferation of matrix material occurs similar to that seen during embryogenesis and development. An early disorganized appearance of the matrix with a loss of chondroitin-6-sulfate proteoglycan (an indication of degeneration) immediately follows crushing with subsequent fluid accumulation leading eventually to digestion by hydrolytic enzymes. In all the injured muscles in the present study, chondroitin-6-sulfate proteoglycan was present surrounding both small and large myofibers indicating that continued destruction of extracellular matrix by invading phagocytes, characteristic of a chronic inflammatory state, was not ongoing. This concept was further supported by limited mast cell degranulation in the same muscle samples.

Unsulfated chondroitin proteoglycan was observed in the injury area after more than two weeks post-injury. Since unsulfated chondroitin proteoglycan is synthesized by prefusion myoblasts, continued myoblast or satellite cell activity was still on-going in all the injured muscles except the tail-suspended ones. In contrast, chondroitin-4- and-6-sulfated proteoglycans are synthesized by post-fusion cells (9). The brightly stained small fibers adjacent to the injury site were enriched in these proteoglycans similar to that of myofibers observed during muscle development. Thus, myofiber development and regeneration were present in all muscle samples even after more than two weeks following injury.

Fibronectin requires special consideration because two types of fibronectin are present and can not be differentiated by present immunohistochemical techniques (7,10). Fibronectin is a normal constituent of plasma and follows the expected route of albumin and other blood constituents when vascular damage is sustained. A separate tissue fibronectin is also present and resides as a thin band along with the proteoglycans around each myofiber - part of the extracellular matrix. Fibronectin, fibrinogen, and chondroitin-6-sulfate proteoglycan appeared around small presumptive, regenerating fibers perhaps providing a specialized matrix for cell growth and differentiation.

In summary, muscle tissue repair seems to continue the same pattern of processes begun during the initial healing on Earth, even when gravity was removed. However, two of the differences in the muscle samples from the flight animals should be explored further. These are: 1) an increase in vascularity on the repair site; 2) an increase in the number of macrophages throughout the entire muscle from the flight rodent. Taken together, these findings might indicate the development of granulation tissue at the repair site of the flight animals. If this granulation tissue developed into scar tissue instead of functional myofibers, then a less than optimal repair of injured muscle would be expected. Alternatively, these differences might indicate that muscle regeneration was only slowed do to the variation in growth factors such as growth hormone and insulin. These and many other hormones are known to influence muscle growth and tissue repair in general. These same hormones have been shown to be influenced by exposure to zero G even during short duration flights. Still, without adequate understanding of the significance of these slight differences, further comment cannot be made concerning the possibility that any movement dysfunction might result from muscle injuries which occur in space.

ACKNOWLEDGEMENTS

The authors wish to thank the Soviet Cosmos recovery and dissection teams organized by Dr. A.S. Kaplansky for their splendid work in tissue removal and fixation; Dr. R. Grindeland, NASA-Ames, for transportation and distribution of the muscle samples; Dr. B. Caterson, University of North Carolina, Chapel Hill, NC, for a liberal supply of monoclonal antibodies to unsulfated chondroitin, chondroitin 4- and chondroitin 6-sulfated proteoglycans; Ms. A. Soltis for her technical assistance. This work was supported in part by funds from NASA grant NAG2-590 and Comptex, Inc. to W.T.S.

REFERENCES

1. Bertolotto, A., L. Palmucci, A. Gagliano, T. Mongini, and G. . Immunohistochemical Localization of Chondroitin Sulfate in Normal and Pathological Human Muscle. J. Neurol. Sci. 73:233-244, 1986.

2. Caterson, B., J.R. Baker, J.E. Christner, J.F. Kearney, and R.L. Stroher. The Characterization of Clonal Antibodies Directed Against Bovine Nasal Cartilage Proteoglycan and Link Protein. In: Monoclonal Antibodies and T-Cell Hybridomas. Eds: G.J. Hammerling, B. Hammerling, and J.F. Kearney. Elsevier/North-Holland, New York. 259-268, 1981.

3. Caterson, B., T. Calabro, and A. Hampton. Monoclonal Antibodies as Probes for Elucidating Proteoglycan Structure and Funtion. In: Biology of Proteoglycans. Eds: T.N. Wight and R.P. Mecham. Academic, New York. 1-26, 1987.

4. Caterson, B., J.E. Christner, J.R. Baker, and J.R. Couchman. Production and Characterization of Monoclonal Antibodies Directed Against Connective Tissue Proteoglycans. Fed. Proc. 44:386-393, 1985.

5. Dahlmann, B., L. Kuehn, M. Rutschmann, and H. Reinauer. Purification and Characterization of a Multcatalytic High-Molecular-Mass Proteinase from Rat Skeletal Muscle. Biochem. J. 228:161-170, 1985.

6. Fritz, V.K. and W.T. Stauber. Characterization of Muscles Injured by Forced Lengthening: II. Proteoglycans. Med. Sci. Sports Ex. 20:354-361, 1988.

7. Gulati, A.K., A.H. Reddi, and A.A. Zalewski. Distribution of Fibronectin in Normal and Rgenerating Skeletal Muscle. Anat. Rec. 204:175-183, 1982.

8. Gulati, A.K., A.H. Reddi, and A.A. Zalewski. Changes in the Basement Membrane Zone Components During Skeletal Muscle Fiber Degeneration and Regeneration. J. Cell Biol. 97:957-962, 1983.

9. Hutchison, C.J. and R. Yasin. Developmental Changes in Sulphation of Chondroitin Sulphate Proteoglycan During Myogenesis of Human Muscle Çultures. Dev. Biol. 115:78-83, 1986.

10. Kleinman, H.K., R.J. Klebe, and G.R. Martin. Role of Collagenous Matrices in the Adhesion and Growth of Cells. J. Cell Biol. 88:473-485, 1981.

11. Lehto, M., M. Jarvinen, and O. Nelimarkka. Scar Formation After Skeletal Muscle Injury: A Histological and Autoradiographical Study in Rats. Arch. Orthop. Trauma Surg. 104:366-370, 1986.

12. Lojda, Z. Studies on Dipeptidyl (Amino) Peptidase IV (Glycyl-Proline Naphthylamidase). II. Blood Vessels. Histochemistry 59: 153-166, 1979.

13. Mrazkova, O., M. Grim, and B.M. Carlson. Enzymatic Heterogeneity of the Capillary Bed of Rat Skeletal Muscles. Amer. J. Anat. 177: 141-148, 1986.

14. Stauber, W., V. Fritz, B. Dahlmann, F. Gauthier, H. Kirschke, and R. Ulrich. Fluorescence Methods for Localizing Proteinases and Proteinase Inhibitors in Skeletal Muscle. Histochem. J. 17:787-796, 1985.

15. Stauber, W.T., V.K. Fritz, B. Dahlmann, and H. Reinauer. Immunofluorescent Localization of an Alkaline Proteinase in Skeletal Muscles from Diabetic Rats. Basic Appl. Histochem. 30:147-152, 1986.

16. Stauber, W.T., V.K. Fritz, D. W. Vogelbach, and B. Dahlmann. Characterization of Muscles Injured by Forced Lengthening. I. Cellular Infiltrates. Med. Sci. Sports Ex. 20:345-353, 1988.

17. Stauber, W.T., V.K. Fritz, and B. Dahlmann. Extracellular Matrix Changes Following Blunt Trauma to Rat Skeletal Muscles. Exp. Mole. Pathol. 52: 69-86, 1990.

18. Thomason, D.B. and F.W. Booth. Atrophy of the Soleus Muscle by Hindlimb Unweighting. J. Appl. Physiol. 68: 1-12, 1990.

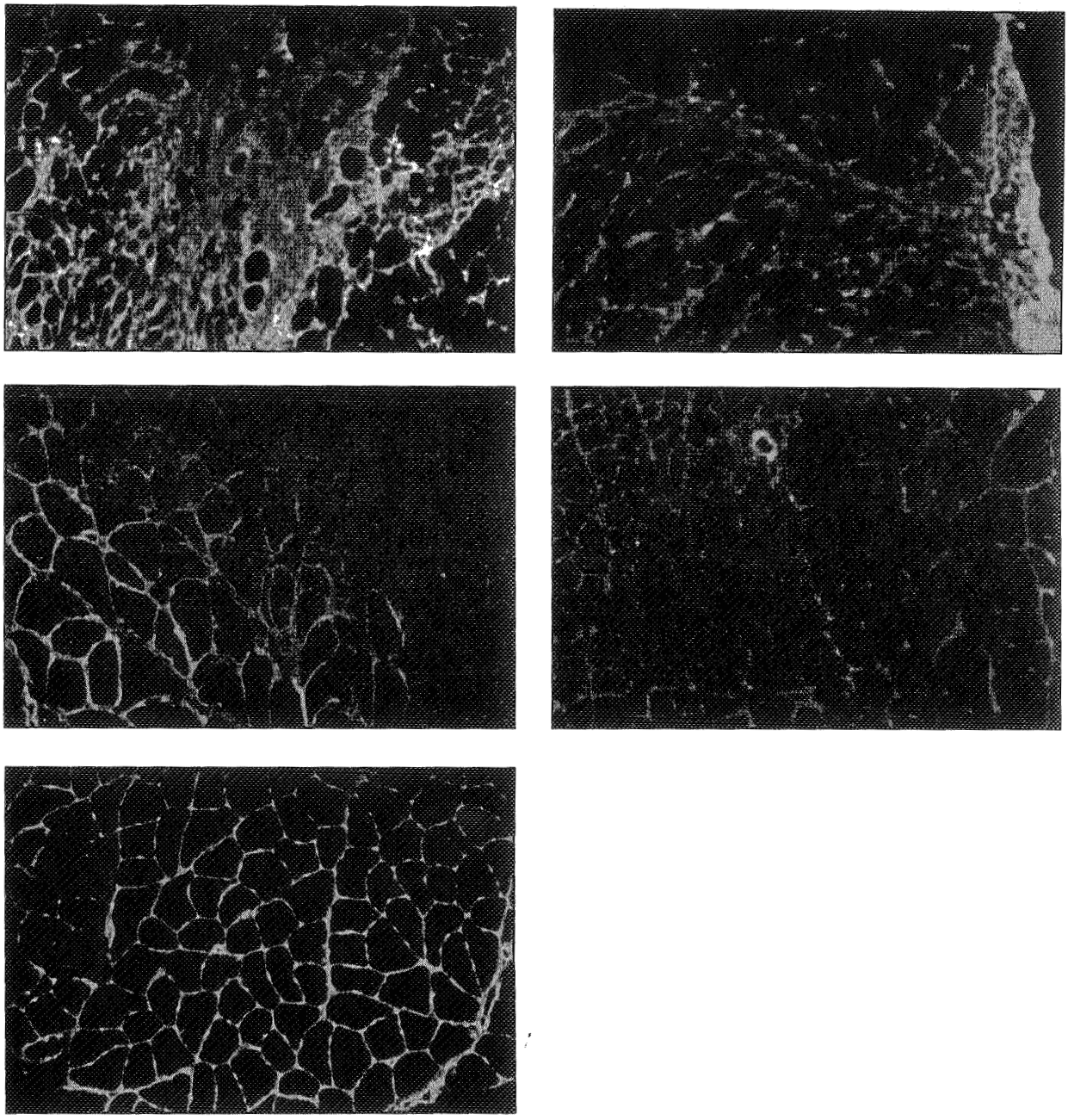

Figure 1. Histochemical localization of Con A in injured and uninjured rat gastocnemius muscles. A: Flight, B: Simulated, C: Vivarium, D: Tail-suspended, E: Basal (uninjured). Original magnification, 40 X.

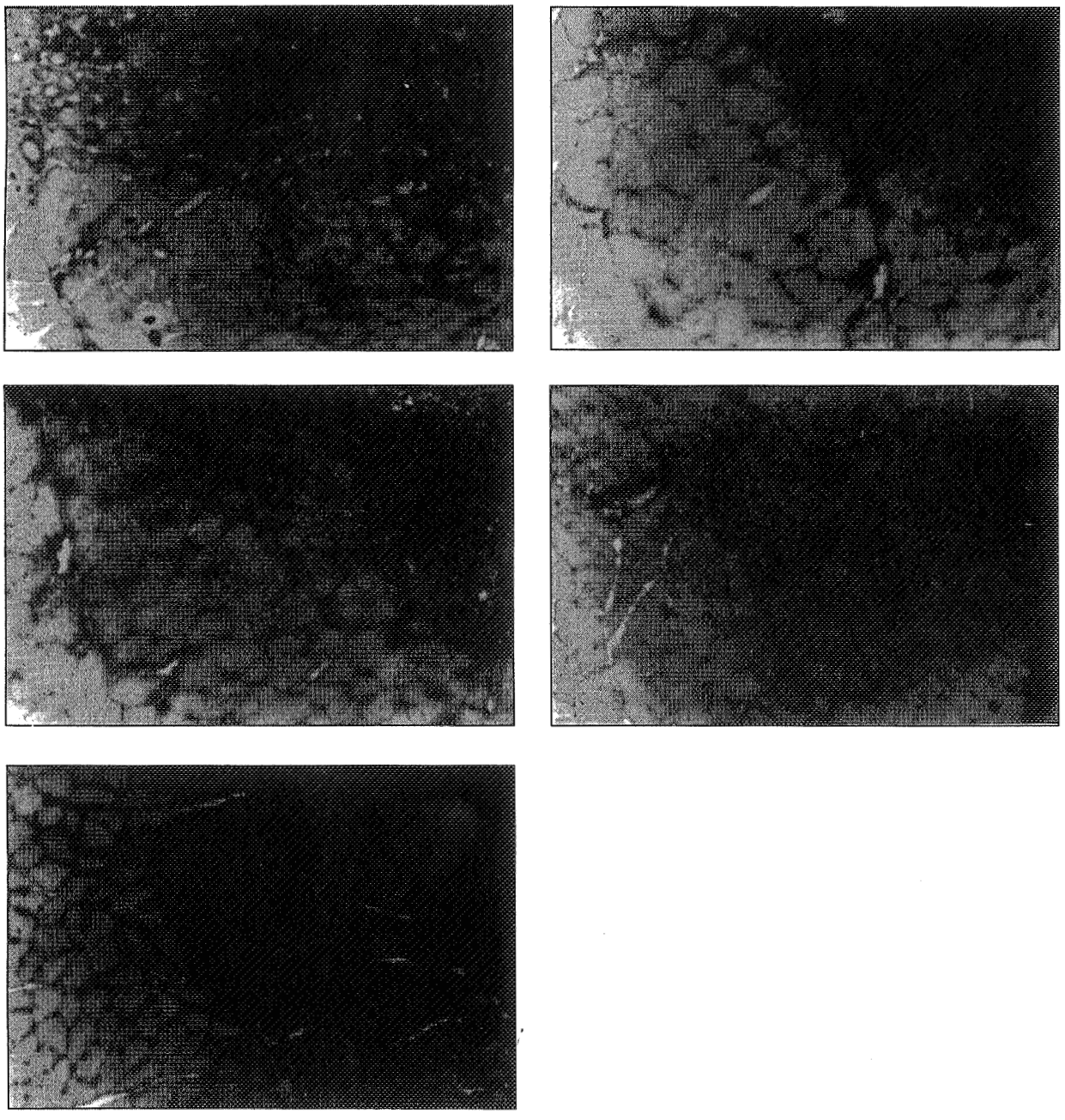

Figure 2. Esterase staining for macrophages in injured and uninjured rat gastrocnemius muscles. A: Flight, B: Simulated, C: Vivarium, D: Tail-suspended, E: Basal (uninjured). Original magnification, 40 X.

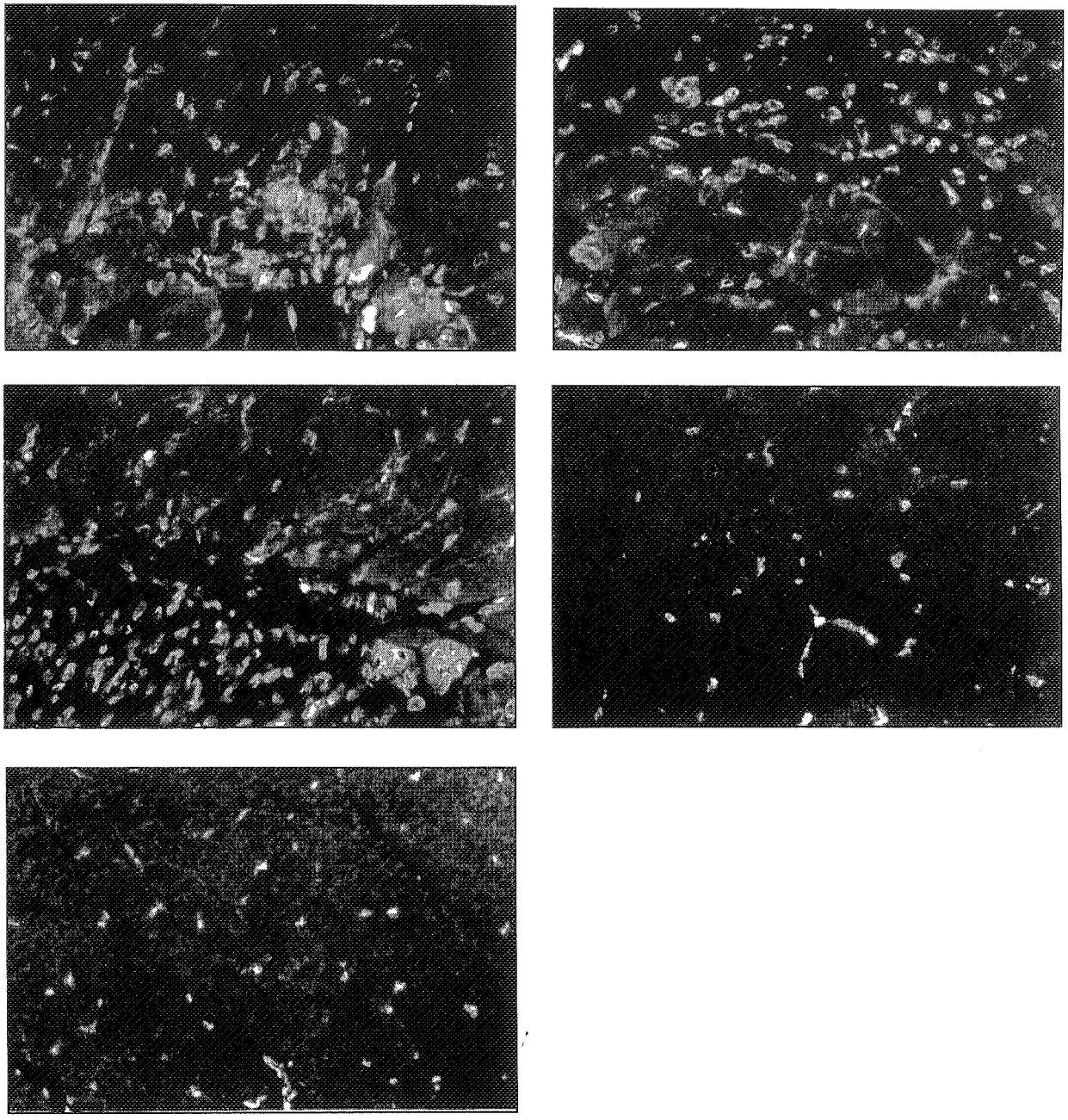

Figure 3. Immunohistochemical localization of multicatalytic proteinase in injured and uninjured rat gastrocnemius muscles. A: Flight, B: Simulated, C: Vivarium, D: Tail-suspended, E: Basal (uninjured). Original magnification, 100 X.

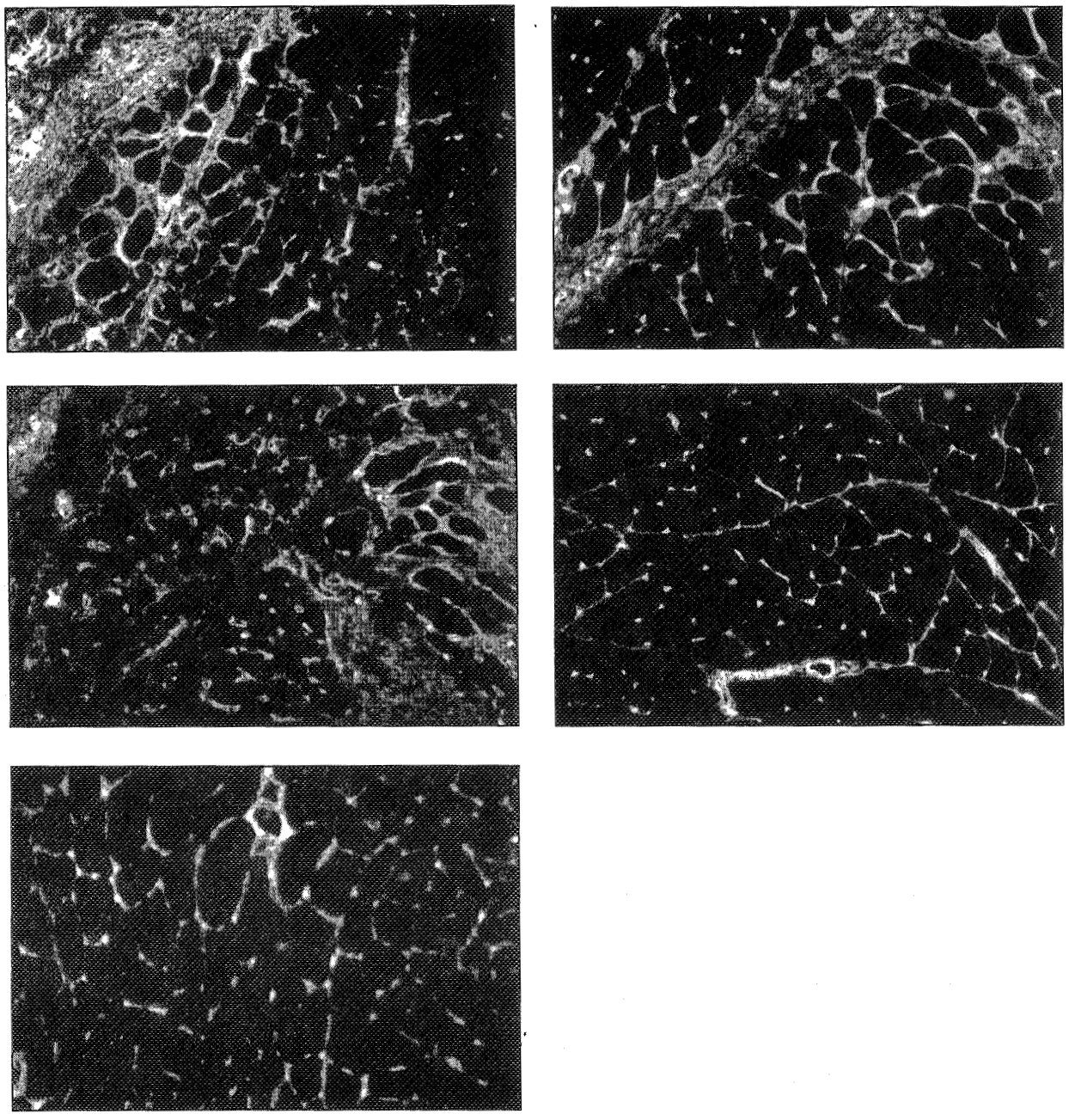

Figure 4. Immunohistochemical localization of fibronectin in injured and uninjured rat gastrocnemius muscles. In injured muscle. A: Flight, B: Simulated, C: Vivarium, D: Tail-suspended, E: Basal (uninjured). Original magnification, 40 X.

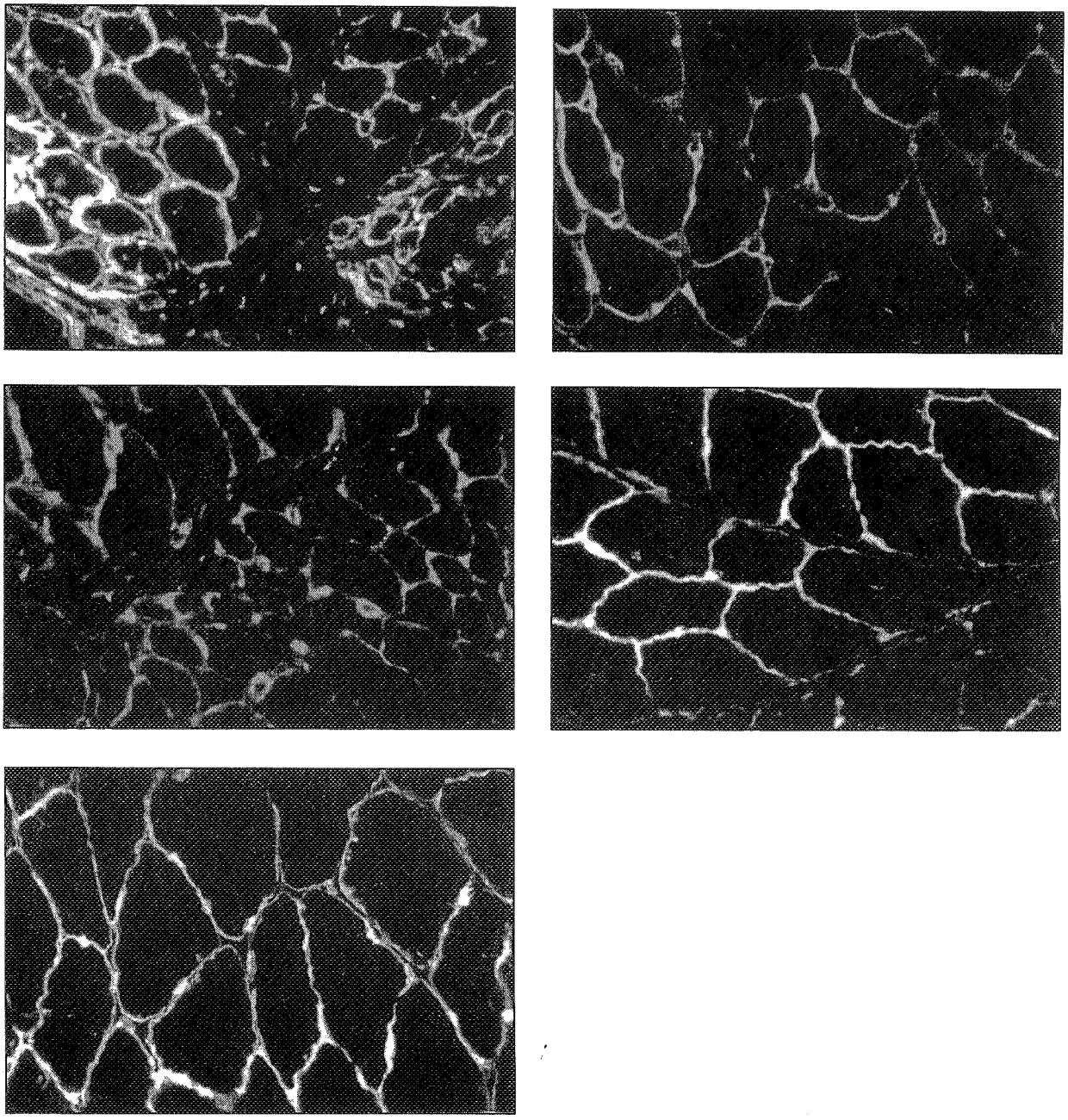

Figure 5. Immunohistochemical localization of chondroitin-6-sulfate proteoglycan in injured and uninjured rat gastrocnemius muscles. A: Flight, B: Simulated, C: Vivarium, D: Tail-suspended, E: Basal (uninjured). Original magnification, 100 X.

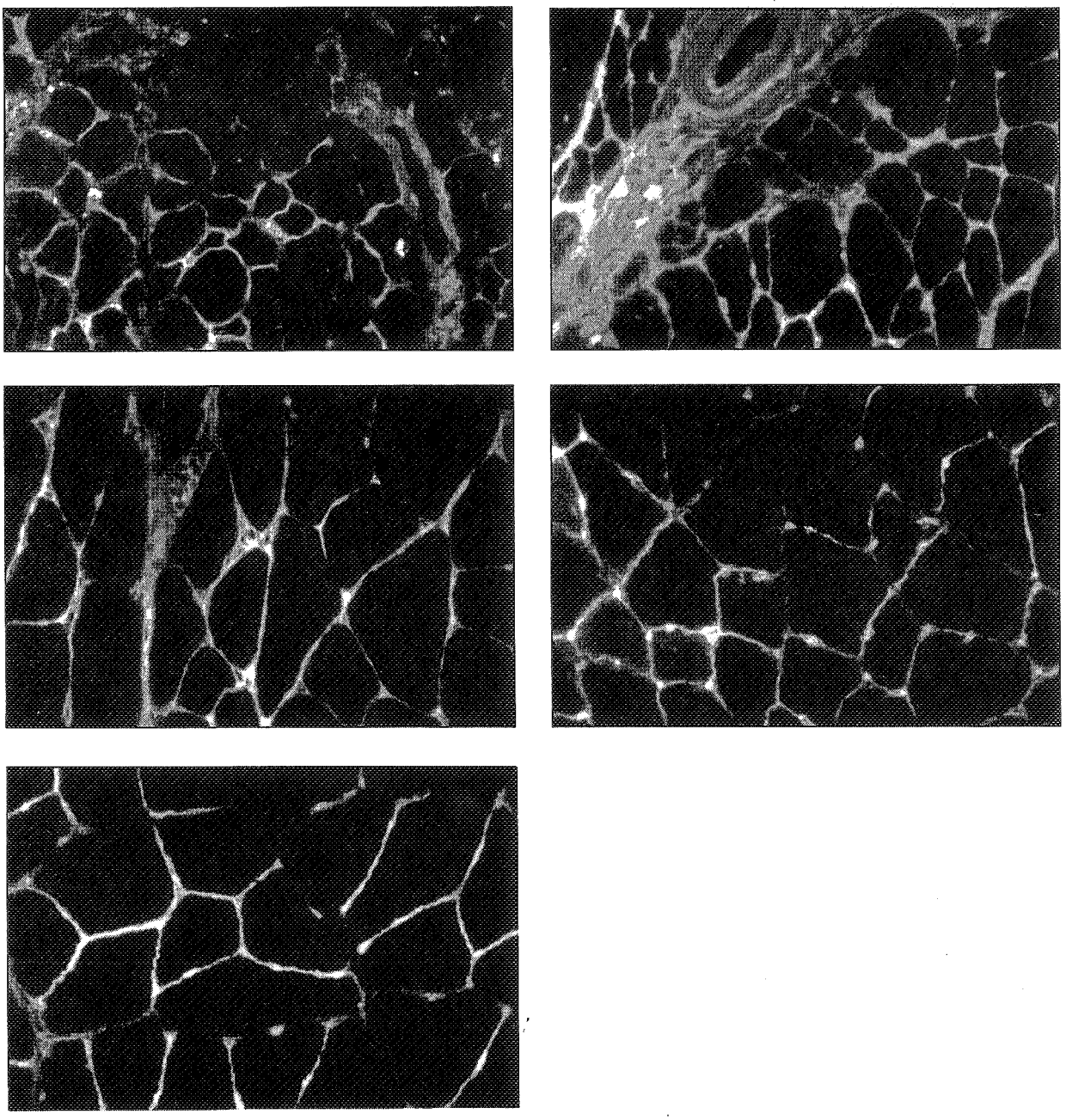

Figure 6. Immunohistochemical localization of chondroitin-4-sulfated proteoglycan in injured and uninjured rat gastrocnemius muscles. A: Flight, B: Simulated, C: Vivarium, D: Tail-suspended, E: Basal (uninjured). Original magnification, 100 X.

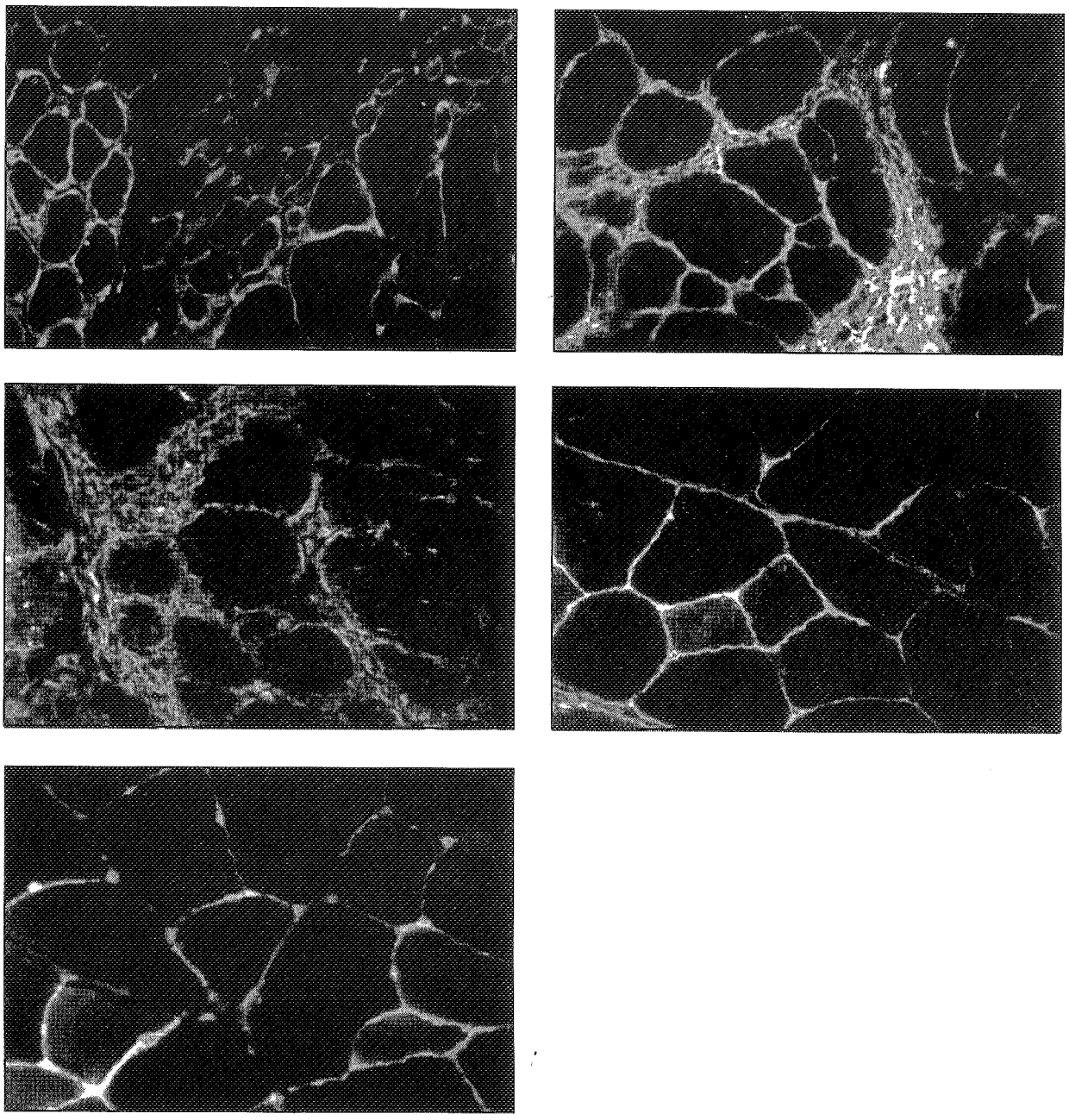

Figure 7. Immunohistochemical localization of unsulfated proteoglycan in injured and uninjured rat gastrocnemius muscles. A: Flight, B: Simulated, C: Vivarium, D: Tail-suspended, E: Basal (uninjured). Original magnification, 100 X.

Page intentionally left blank

Omit
this
page

III. SCIENCE REPORTS

B. COMPARISON OF THE PHYSIOLOGY OF THE SPACEFLIGHT AND THE HINDLIMB SUSPENDED RAT

Page intentionally left blank

SB-51
51363

COMPARISON OF THE PHYSIOLOGY OF THE SPACEFLIGHT AND HINDLIMB SUSPENDED RAT

Investigators:

F.W. Booth
Department of Physiology
University of Texas
Houston, TX

R.E. Grindeland
NASA-Ames Research Center
Moffett Field, CA

Page intentionally left blank

COMPARISON OF THE PHYSIOLOGY OF THE SPACEFLIGHT AND HINDLIMB SUSPENDED RAT

F.W. Booth and R.E. Grindeland

INTRODUCTION

The suspended rat has been used extensively as a simulation of the spaceflight animal (33). In suspension hindlimbs are unloaded from the acceleration of gravity, much as they are in spaceflight. Comparisons of data from spaceflight (microgravity) and suspended (one gravity) rats have suggested that suspension may be an appropriate model, but no direct comparisons had been made between the spaceflight and suspended rat. The Cosmos 2044 mission afforded the first opportunity to directly compare the effects of hindlimb suspension (HS) and spaceflight (SF) on a broad range of physiological and histological parameters.

In the Cosmos 2044 studies, spaceflight, suspended and control rats of the same strain, sex and age were fed the same diet and kept under similar lighting regimens and temperature. Tissues were harvested and processed by the same laboratory staff and the same tissue preservation procedures used; tissue analyses were done by the same investigators. The similarities in animals and conditions permitted rigorous comparison of microgravity and suspension effects of the various physiological systems.

Availability of a high fidelity simulation of microgravity has immense value for Earth-based physiological studies and, alternatively, for spaceflight investigations. Access to the space environment is rare and expensive, and animal manipulations in space are limited and often difficult. The HS rat provides an opportunity to identify "microgravity-induced" changes and to investigate underlying mechanisms or the effects of countermeasures before pursuing these studies in space. Suspension studies enable investigators to focus flight studies and to materially increase the science yield from space. As space physiology evolves from descriptive studies to investigations of underlying mechanisms and to countermeasures, the HS rat becomes increasingly important in defining space experiments.

For those physiological changes which are adequately mimicked by the HS rat, HS also produces a means for separating microgravity effects from those of spaceflight in which the effects of launch and reentry g-forces may confound those of weightlessness. This distinction is especially important for those physiological systems, such as neural and endocrine, which may change very rapidly in response to a g-force, but also may be of significance to skeletal muscle and other systems. The delay between spacecraft return to earth and tissue collection may also obfuscate microgravity induced changes.

Two major attributes of a suitable Earth model of microgravity is, first, that longer duration studies can be done than will be available in the near future in space, and secondly, that larger numbers of animals can be studied. While many of the physiological responses to microgravity have been identified in the spaceflights, to date the maximum duration of animal flights has been 22 days. Thus, the time course of changes (e.g. muscle atrophy) during extended spaceflights is unknown. Whether skeletal muscles, for example, continue to atrophy, reaches a new, lower steady state, or if the changes actually begin to reverse, is not known. The HS rat provides a means of doing such extended studies. Limitations on the number of animals that can be flown in space compared to 1-g studies, further enhance the value of the HS rat.

In the present study the hindlimb suspension system of Morey (1) was used. It is recognized, however, that other suspension models, such as those of Mussachia (2) and Tipton (3) are in use, and that the different suspension systems may simulate, for a given physiological system, more or less faithfully to the spaceflight rat, than the HS used here.

In the synopsis of spaceflight and HS effects which follows, it will be obvious that for some physiological parameters HS is an excellent simulation and for others (e.g. liver histology and metabolism, hypothalamic pituitary regulatory factors) it is not. At least two phenomena, and perhaps a third, are instrumental in effecting the observed changes in spaceflight physiology. Clearly, unloading of support and locomotor systems is the major contributor to the loss of bone and skeletal muscle. In the flight rat the entire body is unweighted whereas the forelimbs, back, and head of the headdown HS rat are not. Secondly, fluid shifts in the spaceflight animal are probably limited in comparison to those of an astronaut in space or to the headdown HS rat. Thus, physiological changes resulting from fluid shifts may differ in flight and HS animals. Lastly, in the HS rat a transitory, but marked, reduction in muscle electrical activity (EMG) occurs. Whether this is also true in the SF animal is unknown, but this aberration suggests that sensory (proprioceptive) input is also reduced, yielding HS and SF rats, which are in part sensory deprived.

Comparisons of spaceflight and suspension effects on physiology also need to be tempered by data suggesting that while similar changes occur in SF and HS, they occur more quickly in the SF rat, as exemplified by the greater reduction in concentrations of hypothalamic factors which regulate growth hormone secretion. The reverse, that is a slower change, may occur in testes weight of the SF rat. These differences will be alluded to in discussions of specific systems.

The synopsis which follows is based on reviews of Cosmos 2044 publications and a working group session held at NASA-Ames Research Center in March, 1990, and chaired by Dr. F.W. Booth. The comparisons apply rigorously only to the Cosmos 2044, 14 day mission, using the rats and conditions described above. Data from other suspension studies or spaceflights are included only in amplification on present results.

SKELETON

Biomechanical properties, morphology and chemistry were similar for the SF, HS and control (C) groups (4). Histologically SF, HS and C rats were essentially the same except for periosteal and subperiosteal vascular inclusions, which were found in SF rats only (5). The rats in this study were appreciably older than in previous flights, suggesting that the lower rate of bone turnover in older rats requires a longer microgravity exposure to show the changes seen previously (4, 5, 6). The SF rats showed smaller tibial epiphyseal proliferative zones, which were not found in the HS rats (7). In young rats HS suppresses bone formation, but less than in SF. Intervertebral discs were reduced in size in the SF but not HS rats; proteoglycans leached out of the discs in both groups, but the loss was greater in the SF group (8).

SKELETAL MUSCLE

Histological studies of one predominantly slow twitch muscle, the adductor longus (AL), revealed similar decreases in fiber cross-sectional areas (CSA) for SF and HS and similar degrees of atrophy between fiber types (slow, oxidative, fast oxidative glycolytic, and fast glycolytic) (9). Interestingly, AL weight was reduced in HS, but not SF; apparently due to the edema in SF muscles. It is likely that edema occurs rapidly in slow muscle upon return to one-gravity. SF animals also showed reduction in mitochondria, presence of

thrombi, and a tripling in the number of eccentric contraction lesions compared to the HS rats. In the vastus medialis (VM) region of mixed fibers, SF rats showed atrophy of Types I and II fibers but atrophy of only Type I in the HS animals (10). In the area of homogenous fiber type in the VM only the SF rats showed atrophy. Lactic dehydrogenase was in greater concentrations in SF than HS rats, where as citrate synthase was similar for the two groups. Total RNA in the VM was reduced 41% in SF and 35% in HS. As with the AL, the soleus (Sol) showed a larger wet weight decrease in HS rats, but similar decrease in dry weight, suggesting that edema accounted for the wet weight difference (11-13). Fiber CSA was reduced, but the reductions were bigger in Type I than Type II fibers for both SF and HS. The Sol showed reduced succinic dehydrogenase in Type I fibers of SF and Type II fibers of HS rats. Surprisingly, HS animals showed an increase in the percentage of fast twitch fibers but SF rats did not as measured by myosin adenosinetriphosphatase activity. By immunohistochemistry for b-myosin heavy chain, 14% of the oxidative fibers expressed this protein in SF Sol and 9% in HS Sol (11, 12) compared to % in controls. Metabolic changes as determined by Sol single fiber analysis for pyruvate kinase, hexokinase, 3-ketoacid-CoA transferase, glycerol phosphate dehydrogenase, and phosphofructokinase were similar qualitatively and, for the most part, quantitatively in SF and HS rats (13). The tibialis anterior, which did not atrophy, showed similar increases in hexokinase in HS and SF; both experimental groups also showed marginal increases in phosphofructokinase, but no other changes in the enzymes studied (13). The vastus intermedius (VI) revealed comparable decreases in a-actin m RNA after SF and HS, but cytochrome-C mRNA decreased 36% in SF rats and increased 42% in HS animals (14). Repair of injured muscle was markedly retarded and disorganized in SF but not HS rats (15). Tendon collagen, proteoglycan and collagen cross-links decreased similarly in SF and HS rats (4).

HEART

Cardiac muscle fibers showed losses of CSA in papillary and ventricular muscles in SF rats, and smaller decreases in HS rats (16). Cyclic AMP regulatory subunit II was reduced in cardiac muscle particulate cell factors of SF but not of HS animals (17).

NEURAL

Ventral horn cells of the rostral part of the lumbar enlargement showed no changes in cell (soma) or nucleus size in either experimental group, but succinic dehydrogenase increased in SF neurons and decreased in HS rat neurons (18).

PULMONARY

Red blood cell numbers in pulmonary capillaries of SF and HS rats compared well (J. West, unpublished observation).

KIDNEY

Kidney weights were unchanged by HS but increased 20% in SF (A. Kaplansky, unpublished observation).

LIVER

Livers of SF rats had nearly ten times as much glycogen as HS rat livers, and significantly fewer Kuppfer cells (20, 21). SF rat livers contained less cholesterol and markedly less sphingolipids than control or HS rats. Serine palmitoyltransferase was elevated in HS rats relative to SF animals but tryptophan oxygenase was about twice as high in SF rats. The other enzymes involved in lipid, amino acid, or mixed functions

which were measured either did not respond to actual or simulated microgravity or showed similar changes by the two experimental groups.

INTESTINE

Mucosal cells of SF and HS rats were unaffected histologically as was mitotic rate by either SF or HS (21).

PLASMA

Glucose was raised in SF and HS rats and triglycerides decreased (22, I.A. Popova, personal communication). All other constituents measured were either unaffected by SF and/or HS, or changed in opposite directions. Interestingly, creatinine and blood urea nitrogen were both increased after SF and decreased after HS. The hematocrit increased less after suspension than after SF.

IMMUNE FUNCTION

The SF and HS rats show a good correlation of immune functional changes, but various subpopulations of immunogenic cells were increased or decreased by exposure to microgravity, but not by suspension (23, 24, 25).

RED BLOOD CELLS

Suspended, flight, and control rats had comparable numbers of erythroid cells in their bone marrow. Plasma erythropoetin levels were reduced in HS and SF animals. Flight rat cells showed a marked increase in colony forming activity after flight which was not shown by HS rat cells (26).

ENDOCRINE AND REPRODUCTIVE FUNCTION

Testes weights were markedly decreased by HS but only marginally by SF (27, A. Kaplansky, personal communication). However, the much greater reduction in testosterone in SF rats suggests that with longer duration flights testes weights would also be significantly decreased (19, 27). Recent experiments in our laboratory revealed a progressive decrease in testosterone with increased lengths of HS (C.M. Tipton and R.E. Grindeland, unpublished observations). Hypothalamic concentrations of somatostatin (SRIH) and growth hormone releasing factors (GRF) and mRNAs for these peptides were significantly decreased in SF rats; HS animals showed only a marginal decrease in SRIH and no changes in its mRNA, suggesting that longer suspension might yield results comparable to those of spaceflight (28). Growth hormone secretion measured by biological assay was similarly suppressed in SF and HS rats (29). Immunoreactive growth hormone was unchanged from controls in either group. Posterior pituitary content of vassopressin and oxytocin was significantly reduced only by SF (30). Atrial natriuretic factor was also diminished in cardiac tissues after SF (31). Thyroid hormones (thyroxine, triiodothyronine) were lower in SF and HS rats than in controls (19). Prolactin in plasma was unchanged, whereas corticosterone showed huge elevations in SF, HS and control rats from the usual laboratory values, apparently a reflection of animal handling immediately prior to blood collection (19). Only HS rats had hypertrophied adrenal glands. Calcitonin was decreased and parathyroid hormone increased similarly in HS and in SF rats (32).

SUMMARY

In general the HS rat appears to be a useful simulation of many organ systems in the spaceflight animal. This model is considered as good a predictor of spaceflight physiological changes as any currently available, Earth-based model, including human bedrest. Judicious use of this model on Earth can be expected to optimize the science yields from the infrequent animal experiments in space.

ACKNOWLEDGMENT

The authors are indebted to the Cosmos 2044 investigators for use of their data and for their views on physiology in space and in the suspended rat.

REFERENCES

1. Morey, E.R. Spaceflight and Bone Turnover: Correlation With a New Rat Model of Weightlessness. *Biosciences.* 29:168-172, 1979.

2. Musacchia, X.J., D.R. Davis, J.A. Meininger, and T.P. Davis. A Model for Hypokinesia: Effects on Muscle Atrophy in the Rat. *Journal of Applied Physiology.* Volume 48: 479-486, 1980.

3. Stump, C.S., J.M. Overton, and C.M. Tipton. Influence of Single Hindlimb Support During Simulated Weightlessness in the Rat. *Journal of Applied Physiology.* Volume 68: 627-634, 1990.

4. Vailas, A.C., R. Vanderby, D.A. Martinez, et al. Adaptations of Young Adult Rats Cortical Bone to 14 Days of Spaceflight. *Journal of Applied Physiology:* Supplement. Volume 73 (No. 2): 4-9, 1992.

5. Doty, S.B., E.R. Morey-Holton, G.N. Durnova, et al. Morphological Studies of Bone and Tendon. *Journal of Applied Physiology:* Supplement. Volume 73 (No. 2): 10-13, 1992.

6. Garetto, L.P., E.R. Morey, G.N. Durnova, et al. Preosteoblast Production in Cosmos 2044 Rats: Short-Term Recovery of Osteogenic Potential. *Journal of Applied Physiology:* Supplement. Volume 73 (No. 2): 14-18, 1992.

7. Montufar-Solis, D., P.J. Duke, and G. Durnova. Spaceflight and Age Affect Tibial Epiphyseal Growth Plate Physiology. *Journal of Applied Physiology:* Supplement. Volume 73 (No. 2): 19-25, 1992.

8. Perdrini-Mille, A., J.A. Maynard, G.N. Durnova et al. Effects of Microgravity on the Composition of the Intervertebral Disk. *Journal of Applied Physiology:* Supplement. Volume 73 (No. 2): 26-32, 1992.

9. Riley, D.A., S. Ellis, C.S. Giometti et al. Muscle Sarcomere Lesions and Thrombosis After Spaceflight and Suspension Unloading. *Journal of Applied Physiology:* Supplement. Volume 73 (No. 2): 33-43, 1992.

10. Musacchia, X.J., J.M. Steffen, R.D. Fell et al. Skeletal Muscle Atrophy in Response to 14 Days of Weightlessness: Vastus Medialis. *Journal of Applied Physiology:* Supplement. Volume 73 (No. 2): 44-50, 1992.

11. Ohira, Y. B. Jiang, R.R. Roy et al. Rat Soleus Muscle Fiber Responses to 14 Days of Spaceflight and Hindlimb Suspension. *Journal of Applied Physiology:* Supplement. Volume 73 (No. 2): 51-57, 1992.

12. Jiang, B. Y. Ohira, R.R. Roy et al. Adaptation of Fibers in Fast-Twitch Muscles of Rats to Spaceflight and Hindlimb Suspension. *Journal of Applied Physiology:* Supplement. Volume 73 (No. 2): 58-65, 1992.

13. Chi, M.M.-Y., R. Choksi, P. Nemeth et al. Effects of Microgravity and Tail Suspension on Enzymes of Individual Soleus and Tibialis Anterior Fibers. *Journal of Applied Physiology:* Supplement. Volume 73 (No. 2): 66-73, 1992.

14. Thomason, D.B., P.R. Morrison, V. Oganov et al. Altered Actin and Myosin Expression in Muscle During Exposure to Microgravity. *Journal of Applied Physiology:* Supplement. Volume 73 (No. 2): 90-93, 1992.

15. Stauber, W.T. V.K. Fritz, T.E. Burkovskaya et al. Effect of Spaceflight on the Extracellular Matrix of Skeletal Muscle After a Crush Injury. *Journal of Applied Physiology:* Supplement. Volume 73 (No. 2): 74-81, 1992.

16. Goldstein, M.A., R.J. Edwards, and J.P. Schroeter. Cardiac Morphology After Conditions of Microgravity During Cosmos 2044. *Journal of Applied Physiology:* Supplement. Volume 73 (No. 2): 94-100, 1992.

17. Mednieks, M.I., I. Popova, and R.E Grindeland. Photoaffinity Labeling of Regulatory Subunits of Protein Kinase A in Cardiac Cell Fraction of Rats. *Journal of Applied Physiology:* Supplement. Volume 73 (No. 2): 101-106, 1992.

18. Jiang, B., R.R. Roy, I.V. Polyakov et al. Ventral Horn Cell Responses to Spaceflight and Hindlimb Suspension. *Journal of Applied Physiology:* Supplement. Volume 73 (No. 2): 107-111, 1992.

19. Merrill, A.H., E. Wang, R.E. Mullins et al. Analyses of Plasma for Metabolic and Hormonal Changes in Rats Flown Aboard Cosmos 2044. *Journal of Applied Physiology:* Supplement. Volume 73 (No. 2): 132-135, 1992.

20. Racine, R.N. and S.M. Cormier. Effect of Spaceflight on Rat Hepatocytes: A Morphometric Study. *Journal of Applied Physiology:* Supplement. Volume 73 (No. 2): 136-141, 1992.

21. Sawyer, H.R., C.L. Moeller, R.W. Phillips et al. Proliferation of Jejunal Mucosal Cells in Rats Flown in Space. *Journal of Applied Physiology:* Supplement. Volume 73 (No. 2): 148-150, 1992.

22. Merrill, A.H., E. Wang, R. LaRocque et al. Differences in Glycogen, Lipids, and Enzymes in Livers from Rats Flown on Cosmos 2044. *Journal of Applied Physiology:* Supplement. Volume 73 (No. 2): 142-147, 1992.

23. Nash, P.V., I.V. Konstantinova, B.B. Fuchs et al. Effect of Spaceflight on Lymphocyte Proliferation and Interleukin-2 Production. *Journal of Applied Physiology:* Supplement. Volume 73 (No. 2): 186-190, 1992.

24. Sonnenfeld, G. , A.D. Mandel, I.V. Konstantinova et al. Spaceflight Alters Immune Cell Function and Distribution. *Journal of Applied Physiology:* Supplement. Volume 73 (No. 2): 191-195, 1992.

25. Rykova, M.P., G. Sonnenfeld, A.T. Lesnyak et al. Effect of Spaceflight on Natural Killer Cell Activity. *Journal of Applied Physiology:* Supplement. Volume 73 (No. 2): 196-200, 1992.

26. Lange, R.D., T.B. Driscoll, L.A. Gibson et al. Hematology Studies in Rats Flown on the Soviet Biosatellite Cosmos 2044. Cosmos 2044 Biosatellite Mission Description and U.S. Final Reports of Monkey and Rat Experiments. NASA TM (Experiment K-7-15, this volume).

27. Amann, R.P., D.R. Deaver, B.R. Zirkin et al. Effects of Microgravity or Simulated Launch on Testicular Function in Rats. *Journal of Applied Physiology:* Supplement. Volume 73 (No. 2): 174-185, 1992.

28. Sawchenko, P.E., C. Arias, I. Krasnov et al. Effects of Spaceflight on Hypothalamic Peptide Systems Controlling Pituitary Growth Hormone Dynamics. *Journal of Applied Physiology:* Supplement. Volume 73 (No. 2): 158-165, 1992.

29. Hymer, W.C., R. Grindeland, I. Krasnov et al. Effects of Spaceflight on Rat Pituitary Cell Function. *Journal of Applied Physiology:* Supplement. Volume 73 (No. 2): 151-157, 1992.

30. Keil, L., J. Evans, R. Grindeland et al. Pituitary Oxytocin and Vasopressin Content of Rats Flown on Cosmos 2044. *Journal of Applied Physiology:* Supplement. Volume 73 (No. 2): 166-168, 1992.

31. Keil, L., J. Evans, R. Grindeland, and I. Popova. Natriuretic Peptide Content of Atria from Rats Exposed to 14 Days of Spaceflight. Cosmos 2044 Biosatellite Mission Description and U.S. Final Reports of Monkey and Rat Experiments. NASA TM (Experiment K-7-12, this volume).

32. Arnaud, S.B. , P. Fung, I.A. Popova et al. Circulating Parathyroid Hormone and Calcitonin in Rats After Spaceflight. *Journal of Applied Physiology:* Supplement. Volume 73 (No. 2): 169-173, 1992.

33. Thomason, D.B. and F.W. Booth. Atrophy of the Soleus by Hindlimb Unweighting. *Journal of Applied Physiology:* 68: 1-12, 1990.

Page intentionally left blank

III. SCIENCE REPORTS

C. PRIMATE STUDIES

Page intentionally left blank

59-51
51364

EXPERIMENT K-7-30

EFFECTS OF SPACEFLIGHT IN THE COSMOS BIOSATELLITE 2044 ON THE VESTIBULAR-OCULAR REFLEX (VOR) OF RHESUS MONKEYS

Principal Investigator:

B. Cohen
Departments of Neurology and Physiology and Biophysics
Mount Sinai School of Medicine
New York, NY

Co-Investigators:

N. Cohen
D. Helwig
D. Solomon
Departments of Neurology and Physiology and Biophysics
Mount Sinai School of Medicine
New York, NY

I. Kozlovskaya
M. Sirota
S. Yakushin
Institute of Biomedical Problems
Moscow, USSR

T. Raphan
Department of Computer and Information Sciences
Brooklyn College
Brooklyn, NY

Page intentionally left blank

EXPERIMENT K-7-30

EFFECTS OF SPACEFLIGHT IN THE COSMOS BIOSATELLITE 2044 ON THE VESTIBULAR-OCULAR REFLEX (VOR) OF RHESUS MONKEYS

B. Cohen, N. Cohen, D. Helwig, I. Kozlovskaya, T. Raphan, M. Sirota, D. Solomon, and S. Yakushin

SUMMARY

1. The VOR of two rhesus monkeys was studied before and after 14 days of spaceflight to determine effects of microgravity on the VOR. Horizontal, vertical and roll eye movements were recorded in these and six other monkeys implanted with scleral search coils. Animals were rotated about a vertical axis to determine the gain of the horizontal, vertical and roll VOR. They were rotated about axes tilted from the vertical (off-vertical axis rotation, OVAR) to determine steady state gains and effects of gravity on modulations in eye position and eye velocity. They were also tested for tilt dumping of post-rotatory nystagmus.

2. The gain of the horizontal VOR was close to unity when animals were tested 15 and 18 hours after flight. VOR gain values were similar to those registered before flight. If the gain of the horizontal VOR changes in microgravity, it must revert to normal soon after landing.

3. Steady state velocities of nystagmus induced by off-vertical axis rotation (OVAR) were unchanged by adaptation to microgravity, and the phase of the modulations was similar before and after flight. However, modulations in horizontal eye velocity had more variation after landing and were on mean about 50% larger for angles of tilt of the axis of rotation between 50 and 90^0/s after flight. This difference was similar in both animals and was significant.

4. A striking finding was that tilt dumping was lost in the one animal tested for this function. This loss persisted for several days after return. This is reminiscent of the loss of response to pitch while rotating in the M-131 experiments of Skylab, and must be studied in detail in future spaceflights.

5. Thus, two major findings emerged from these studies: 1. After spaceflight the modulation of horizontal eye velocity was larger during OVAR, and 2. One animal lost its ability to tilt-dump its nystagmus. Both findings are consistent with the postulate that adaptation to microgravity causes alterations in the way that otolith information is processed in the central nervous system. The experiments lay the groundwork for studying the vertical and roll VOR before and after future space flights, as well as for studying modulations in vertical and roll eye position during OVAR and tilt dumping.

INTRODUCTION:

The goal of these experiments was to study the effects of adaptation to microgravity on the various components of the vestibulo-ocular reflex (VOR) of two rhesus monkeys who flew in the COSMOS 2044 Mission. The theoretical basis for the experiments will be considered briefly.

The VOR of the monkeys has been simulated by a model that has received extensive experimental and theoretical verification (Raphan et al. 1977, 1979, 1981, 1983, 1991; Cohen et al. 1977, 1983, 1987; Raphan and Cohen 1986, 1988; Dai et al. 1991). One portion of the VOR causes rapid changes in eye velocity. It has been labeled the 'fast' or 'direct' pathway, and it is largely responsible for producing the compensatory eye movements that counter head movements over a range of from 0.1 to 5-8 Hz. It encompasses the 'three-neuron' VOR and other similar oligosynaptic reflexes arcs that extend from the semicircular canals through synapses in the vestibular nuclei to the oculomotor motor nuclei. This portion of the VOR was tested by rotating animals around a vertical axis at various angular velocities in darkness with accelerations and decelerations in excess of $200^0/s^2$, and determining peak slow phase eye velocities generated by this stimulus.

A second, slow component of the VOR, labelled, 'velocity storage', has more sluggish characteristics. It also receives input from the semicircular canals, and projects back onto the vestibulo-ocular pathway, causing slower changes in eye velocity. It has been modeled as a leaky integrator that prolongs the nystagmus produced by constant velocity rotation well beyond the time constant of the activity from the semicircular canals (Raphan et al. 1979). Because its falling time constant is substantially longer than that of the input from the semicircular canals, it is primarily responsible for the dominant time constant of the VOR in the unhabituated state. Thus, the dominant time constant of the VOR is a measure of velocity storage.

Velocity storage is responsible for a variety of ocular compensatory responses (Raphan and Cohen 1985). It produces the slow component of optokinetic nystagmus (OKN) and optokinetic after-nystagmus (OKAN) (Cohen et al. 1977). The yaw axis component of OKN and OKAN is oriented around gravity, and if yaw OKN is induced in an animal tilted with regard to gravity, the axis of the ensuing OKAN tends to become spatially vertical (Raphan et al. 1986, 1988; Dai et al. 1991). This demonstrates that velocity storage has a three-dimensional structure, oriented around gravity (Raphan and Cohen 1986, 1988; Raphan and Sturm 1991; Dai et al. 1991). Velocity storage is also responsible for the bias or steady state component of nystagmus produced by rotation in darkness about axes tilted from the vertical (off-vertical axis rotation, OVAR) (Raphan et al. 1981; Cohen et al. 1983), as well as for the nystagmus produced by pitching while rotating (Raphan et al. 1983) and for the nystagmus generated in darkness during circular locomotion (Solomon and Cohen 1987).

The input to the central nervous system during OVAR comes both from the semicircular canals and the otolith organs. Thus, OVAR offers unique possibilities for testing the rapid and slow components of the VOR as well as changes in eye position produced by the otolith organs. The canals transduce head acceleration at the onset and end of rotation, converting angular acceleration into a signal related to head velocity (Steinhausen, 1931; Goldberg and Fernandez 1971). The otolith organs sense the continuous change in head position with regard to gravity and produce a series of sinusoidal changes in firing rate in otolith afferents, from which the nervous system extracts an estimate of head velocity about the tilted axes (Guedry, 1965; Benson and Bodin, 1966; Young and Henn, 1975; Raphan

et al. 1981; Cohen et al. 1983; Raphan and Schnabolk 1988). This estimate is utilized to activate the velocity storage integrator to generate steady state eye velocities and continuous nystagmus with slow phases in the compensatory direction. The signal arising in the otolith organs is also used in direct otolith-ocular pathways to produce compensatory changes in eye position as the head changes its position with regard to gravity.To analyze OVAR we measured the rising time constant of the nystagmus, the steady state component and the changes in phase and gain of modulations in eye velocity and in eye position as a function of head position with regard to gravity.

Finally, in preliminary experiments in one animal we also measured the ability of the animal to discharge post-rotatory nystagmus and velocity storage when it is tilted with regard to gravity (Benson 1974; Raphan et al. 1981). This function is dependent on processing of otolith information through the nodulus (Waespe et al. 1985), and has not been studied in space experiments before.

METHODS

Experiments were performed on eight juvenile rhesus monkeys (Macaca mulatta) who had been implanted under anesthesia and sterile surgical conditions with head bolts for head fixation, and with two scleral search coils on one eye to measure horizontal, vertical and roll eye position (Robinson 1963). Details of the surgery are given elsewhere (Fuchs and Robinson 1966; Judge et al. 1980; Cohen et al. 1987). During experiments animals sat in a primate chair with their heads fixed to a plastic frame, 12.5 cm on a side, that held the field coils. The eye with the scleral search coils was centered in the field coils.

Eye movements were induced by rotating the animals or the visual surround in an apparatus constructed by Neurokinetics, Inc. of Pittsburgh. The rotator was portable and was transported to the Soviet Union for this series of experiments. It consisted of a belt-driven, servo-controlled gimbal on which a primate chair was mounted. The chair could be manually rotated ±90 to position the animals for rotation in yaw, pitch or roll about the gimbal axis. A three axis optokinetic stimulator was mounted on the gimbal to provide relative motion of the visual surround. The gimbal and optokinetic stimulator were under computer control. Accelerations and decelerations of the gimbal at the onset and end of rotation were symmetrical and were approximately $200^0/s^2$ over the range of stimuli that were used (30 to 180^0/s. The gimbal was mounted in a 120 cm diameter stationary dome that served as the screen for the optokinetic stimulus. The dome and gimbal were mounted on an 'A' frame and could be positioned $\pm 90^0$ from the upright.

Vestibular testing was done in darkness. To elicit the rapid component of the VOR the gimbal axis was set vertical, and the animals were rotated in yaw, pitch and roll. To induce OVAR per-rotatory nystagmus was induced in darkness by rotation about a vertical axis. When the slow phase velocity had declined to zero, the gimbal axis was rapidly positioned to angles of 5 to 90^0 from the vertical, and the monkeys were rotated about the tilted axis in yaw. Tilt dumping was elicited by rotating the animals in yaw in darkness. When the per-rotatory nystagmus had died away, the yaw rotation was stopped, inducing post-rotatory nystagmus. Ten seconds after post-rotatory nystagmus had begun, the animals were tilted to the side in roll.

To calibrate the eye movements the monkeys were rotated at 30^0/s while the optokinetic stimulus counter-rotated at the same velocity, producing an earth-stationary visual surround. Under this condition, the gain of the VOR was assumed to be close to unity. A

typical calibration record is shown in Fig. 1A, and the sequence for eliciting OVAR nystagmus in Fig. 1B.

Voltages associated with eye position and with the position and velocity of the various axes were displayed on a chart recorder and an oscilloscope and recorded on FM magnetic tape for later analysis. Data were analyzed on a 386 PC computer, using the DAOS operating system (Mycon Technology). Eye position voltages were sampled at 625H2. Saccades were identified and slow phases were differentiated. From these, peak and steady state gains were obtained, as well as the falling time constant of the velocity declines, and averages of eye velocity re head velocity with regard to gravity.

RESULTS

General Description

Two of the 8 monkeys that were tested (M782 and M2483) flew for 14 days in the COSMOS 2044 Biosatellite. The animals landed at approximately 6:00 AM on 9/29/89 (Moscow time). After recovery they were transported back to Moscow, seated in their flight chairs. When they arrived at about 7:30 PM on the same day, they appeared healthy and were normally active. Testing of the VOR began at 9:00 PM for the first animal (M782), approximately 15 hours after landing. The second animal (M2483) was tested 3 hours later, about 18 hours after landing. Testing was also done on the day after landing (Day 2) and two days later (Day 4).

VOR: Gains

Fig. 2A,B shows horizontal eye movements of M2483 obtained in the preflight testing in response to short steps of velocity. The velocities are marked above the differentiated eye velocity traces. Also shown in Fig. 2B is a post-rotatory step response of this animal. The mean VOR gains and standard deviations of all 8 flight candidates, obtained in preflight testing, is shown in Fig. 3. The horizontal VOR gains were close to unity up to 120^0/s, and fell slightly for stimulus velocities of 150 and 180^0/s (Fig. 3A). Preflight and postflight data from the two flight monkeys are shown in Figs. 3B and 3C. The preflight and postflight data for M782 (Fig. 3B) and for M2483 (Fig. 3C) lay close to the group means shown in Fig. 3A, and were not different from each other. The pre- and postflight (Day 1) data for M2483 are shown in Table 1. They were not different at each stimulus velocity. Findings were similar for M782. The conclusion is that if there were changes in the horizontal VOR of the flight monkeys, these changes had disappeared by the time they were tested 15 and 18 hours after landing.

OVAR: Steady State Gains

Typical data obtained from M2483 in preflight testing is shown in Fig. 1B. Note the modulations in horizontal eye velocity and in roll eye position dependent on gravity. At the conclusion of the response the animal was stopped in light, suppressing its post-rotatory nystagmus. This accounts for the abrupt return of eye velocity to zero when rotation ended.

Steady state gains of eye velocity as a function of tilt angle for the seven monkeys (M2483 excluded) are shown in Fig. 4A. Individual data from M782 (Fig. 4C) lay close to the group means, and were not different for the pre- and post-flight data. M2483 habituated faster during OVAR than any of the other monkeys in the group, and therefore, its steady state levels were lower than the other monkeys (Fig. 4D). When the preflight data of M2483 was added to the group means, it increased the standard deviations and decreased

the means slightly (Fig. 4B). There was no difference in the pre and postflight steady state levels in either M782 (Fig. 4 C,E) or in M2483 (Fig. 4D,F), however. These values can be assessed in Table 2, which shows the mean preflight steady state velocities of OVAR induced by stimulation at 60^0/s at 50^0 of tilt of the axis of rotation (first column). The second column shows the phases of the modulations in slow phase velocities for the preflight and postflight data. Again there was no difference. Similarly the phases of the roll pre- and postflight modulations (fourth column) were not changed after spaceflight. (There were no preflight vertical recordings, and the data in the third column are added for future information).

From these measurements we conclude that the steady state gains of OVAR, which depend on the time constant of the velocity storage mechanism and the phase relations of the modulations in eye velocity were similar before and after flight.

OVAR: Phases and Amplitude of Modulation

As shown in Fig. 1B there is modulation in yaw or horizontal eye position and in slow phase eye velocity as the head rotates with regard to gravity. This modulation also occurs for vertical and roll eye position. Of interest was the finding that the modulation in the amplitude of the postflight horizontal slow phase velocity, as a function of head position re gravity was larger and more variable after than before flight for tilts of the axis of rotation between 40 and 90 degree of tilt (Fig. 5 A,B). The preflight modulations were somewhat larger in M2483 (Fig. 5A) than in M782 (Fig. 5B). However in both animals the curve had a similar shape, tending to saturate at a lower tilt angle after flight, and generally reaching somewhat higher velocities. There was also increase variance in results after flight.

Thus, although the steady state velocities were the same, the modulations in horizontal eye velocity were more variable and were increased after flight.

Tilt Dumping

When animals are tilted during post-rotatory nystagmus, eye velocity declines rapidly (See Benson, 1974 for review). An example from preflight recordings in M782 is shown in Fig. 6C (upward arrow). About one second after the animal was tilted 50^0 in roll, the nystagmus slow phase velocity dropped quickly to zero. After flight, surprisingly, there was little or no response to tilt of the animal during post-rotatory nystagmus. Three examples from the day of landing from the same animal are shown in Fig. 6A,B. In each the animal was tilted 50^0 suddenly during the post-rotatory nystagmus, but there was no apparent effect of the tilt on the time course of the nystagmus. In fact, in examples 1 and 2, the nystagmus appeared to be augmented. (These trials can be compared to velocity steps during per-rotatory nystagmus where the time constants fell unperturbed. Findings were similar on the day after landing in this monkey. Tilt dumping was not tested in M2483 because its time constant had habituated by the end of preflight testing, and it was deemed too short to adequately show these effects.

DISCUSSION

Both negative and positive findings have emerged from this study. It seems clear that if the horizontal VOR is altered in spaceflight, it adapts quickly on landing. This is in contrast to the findings of Kozlovskaya and coworkers (1989) who showed that the active VOR, elicited by head turning was enhanced during and after space flight. It is possible that the active component of the direct or rapid VOR is enhanced. This should be tested in future

flights by comparing the active and passive VOR. Unfortunately, the vertical VOR could not be tested before flight, only afterward. Measurements of vertical gain indicated that they were close to unity on the day of landing, but these findings are preliminary and need further study. Recording of the roll VOR was hampered by an inability to calibrate the gain of the roll coil between the pre- and postflight testing. This difficulty should be obviated by the use of another version of the roll coil (Hess, 1990).

Also unchanged were the time constant of the slow component of the VOR, i.e., of velocity storage. Consistent with this, the steady state component of OVAR was also unaltered by adaptation by microgravity when tested on landing. Lackner and DiZio (1988) have demonstrated that the time constant of per- and post-rotatory nystagmus becomes shorter in parabolic spaceflight. Whether this occurs in longer space flights is not known, but if there is a change in the VOR time constant, it must readapt quickly on landing.

The first major positive finding was that there is increased modulation in horizontal eye velocity during OVAR after flight. This suggests that otolith-ocular pathways are more sensitive to input from the otolith organs when animals return from space flight and adaptation to microgravity. The direct otolith-ocular pathways are also manifest in roll and vertical eye movements, and this must be studied in greater detail in the next flight. Factors that cause an increase in modulation in eye position are probably related to the gain of the direct otolith-ocular pathways (Baker and Berthoz, 1974).

One caveat should be noted. Habituation also causes a decrease in the velocity storage or steady state component, and an increase in the eye position modulation. Therefore, it is important to separate the present effects from those of habituation. The finding that the steady state gains of OVAR were similar suggests that habituation was not responsible for the present findings, but this must be verified in future missions. Also to be studied is the increased variability in the peak to peak modulation after spaceflight. The system may be trying to achieve stability, by going through stages whereby there is an increase and then a subsequent decrease in gain after flight.

The second positive finding was a loss of tilt dumping in one animal that was tested. This recalls one of the most striking findings of early vestibular investigations on Skylab (M-131), i.e., a loss of susceptibility of astronauts to head pitching while rotating (Graybiel et al. 1977). This immunity persisted into the postflight period for at least three days.

If the loss of tilt dumping is verified, it means that central circuits that sense head position with regard to gravity and establish spatial orientation function differently after adaptation to microgravity. These circuits depend on the integrity of the nodulus, and the ability to tilt-dump is lost after nodulo-uvulectomy (Waespe et al. 1985). The ability of the velocity storage mechanism to home on the spatial vertical by sensing gravity is lost after nodulo-uvulectomy (Cohen and Dai, unpublished data). This implies that circuitry in the nodulus is affected by adaptation to microgravity. This would not be surprising, given the heavy input of the otolith organs to the nodulus, and the potential involvement of the nodulus in producing motion sickness. Further work needs to be done to establish this finding in future spaceflights.

REFERENCES

1. Baker, R., A. Berthoz. Organization of Vestibular Nystagmus in Oblique Oculomotor System. J. Neurophysiol. 37: 195-217, 1974.

2. Benson A.J. Modification of the Response to Angular Accelerations by Linear Accelerations. In: Kornhuber H (ed) Handbook of Sensory Physiology, Vol VI/2. Springer Berlin, pp 281-320, 1974.

3. Benson A.J., M.A.Bodin. Interaction of Linear and Angular Accelerations on Vestibular Receptors in Man. Aerosp Med 37: 144-154, 1966.

4. Cohen B., V. Matsuo, T. Raphan. Quantitative Analysis of the Velocity Characteristics of Optokinetic Nystagmus and Optokinetic After-Nystagmus. J Physiol, 270: 321-344, 1977.

5. Cohen B., J. I. Suzuki, T. Raphan. (Role of the Otolith Organs in Generation of Horizontal Nystagmus: Effects of Selective Labyrinthine Lesions. Brain Res, 276: 159-164, 1983.

6. Cohen B., D. Helwig, T. Raphan. Baclofen and Velocity Storage: a Model of the Effects of Drug on the Vestibulo-Ocular Reflex in the Rhesus Monkey. J Physiol, 393: 703-725, 1987.

7. Dai M., T. Raphan, D. Sturm, B. Cohen. Characterization of the Three Dimensional Structure of Velocity Storage in the Monkey. Soc Neurosci Abstr 16: 735, 1990.

8. Fuchs A.F., D.A. Robinson. A Method for Measuring Horizontal and Vertical Eye Movement Chronically in the Monkey. J Applied Physiol 21: 1068-1070, 1966.

9. Goldberg J. M., C. Fernandez Physiology of the Peripheral Neurons Innervating Semicircular Canal of the Squirrel Monkey. I. Resting Discharge and Response to Constant Angular Accelerations. J Neurophysiol 34: 635-660, 1971.

10. Graybiel, A., E.R. Miller, J.L. Homick . Experiment M-131: Human Vestibular Function. In R.S. Johnston and L.F. Dietlein (eds) Biomedical Results from Skylab. Section II. Washington, DC: US Government Printing Office 1977 (NASA SP-377), 1977.

11. Guedry F.E. Orientation of the Rotation Axis Relative to Gravity: Its Influence on Nystagmus and the Sense of Rotation. Acta Otolaryngol (Stockh) 60: 30-48, 1965.

12. Hess B.J.M. Dual-Search Coil for Measuring 3-dimensional Eye Movements in Experimental Animals. Vision Res 30: 597-602, 1990.

13. Judge S.J., B.J. Richmond , F.C. Chu. Implantation of Magnetic Search Coils for Measurement of Eye Position: an Improved Method. Vision Res 20: 535-538, 1980.

14. Kozlovskaya, I.B. E.A. Ilyin, M.G. Sirota, V.I. Korolokov, B.M. Babayev, I.N. Beloozerova, and S.B. Yakushin . Studies of Space Adaptation Syndrome in Experiments on Primates Performed on Board of Soviet Biosatellite ""Cosmos-1887". The Physiologist 32: Suppl. S455-S48, 1989.

15. Lackner J., P. DiZio. Gravitational Effects of Nystagmus and on Perception of Orientation. Ann NY Acad Sci 545: 93-104, 1988.

16. Raphan T., V. Matsuo, B. Cohen. Velocity Storage in the Vestibulo-Ocular Reflex arc (VOR). Exp Brain Res, 35: 229-248, 1979.

17. Raphan T., B. Cohen , V. Henn. Effects of Gravity on Rotatory Nystagmus in Monkeys. Annals of the New York Academy of Sciences, 374: 44-55, 1981.

18. Raphan T., B. Cohen. Velocity Storage and the Ocular Response to Multidimensional Vestibular Stimuli. In: A.Berthoz, G.Melvill Jones (eds.): Adaptive Mechanisms in Gaze Control. Reviews in Oculomotor Research, Vol 1, Elsevier Science Publishers, Amsterdam, pp 123-143, 1985.

19. Raphan T., B. Cohen. Multidimensional Organization of the Vestibulo-Ocular Reflex (VOR). In: E. L. Keller & D. S. Zee (eds.), Adaptive Processes in Visual and Oculomotor Systems (pp. 285-292), New York: Pergamon Press, 1986.

20. Raphan T., B. Cohen. Organizational Principles of Velocity Storage in Three Dimensions. The Effect of Gravity on Cross Coupling of Optokinetic After-Nystagmus. Ann NY Acad Sci 545: 74-92, 1988.

21. Raphan T., B.Cohen, Matsuo V. A Velocity-Storage Mechanism Responsible for Optokinetic Nystagmus (OKN), Optokinetic After-Nystagmus (OKAN) and Vestibular Nystagmus. In: R Baker & A Berthoz, (eds) Control of Gaze by Brain Stem Neurons; Development in Neuroscience, Vol. 1. Elsevier/North-Holland Biomedical Press, Amsterdam pp 37-47, 1977.

22. Raphan T., C. Schnabolk. Modeling Slow Phase Generation During Off-Vertical axis rotation. Ann NY Acad Sci 545: 29-50, 1988.

23. Raphan T., B. Cohen. Organizational Principles of Velocity Storage in Three Dimensions: The Effect of Gravity on Cross Coupling of Optokinetic After-Nystagmus. Ann NY Acad Sci 545: 74-92, 1988.

24. Raphan T., D. Sturm. Modelling Spatio-Temporal Organization of Velocity Storage in the Vestibulo-Ocular Reflex. J Neurophysiol. (submitted), 1991.

25. Robinson D. A. A Method of Measuring Eye Movement Using a Scleral Search Coil in a Magnetic Field. IEEE Trans Biomed Eng 10: 137-145, 1963.

26. Solomon D., B. Cohen. Head and Eye Movements During Circular Locomotion. Soc. Neurosci. Abstr. 13: 1225, 1987

27. Steinhausen. Uber den Nachweis der Bewegung der Cupula in der Intakten Bogengangsampulle des Labyrinths bei der Naturlichen Roatorischen und Calorischen Reizung. Pfleugers Arch Ges Physiol 228: 322-328, 1931.

28. Young L.R., V. Henn. Nystagmus Produced by Pitch and Yaw Rotation of Monkeys about Non-Vertical axes. Fortschr Zool 23: 235-246, 1975.

29. Waespe W., B. Cohen, T. Raphan. Role of the Flocculus and Paraflocculus in Optokinetic Nystagmus and Visual-Vestibular Interactions: Effects of Lesions. Exp Brain Res 50: 9-33, 1983.

30. Waespe W, B. Cohen , T. Raphan. Dynamic Modification of the Vestibulo- Ocular Reflex by the Nodulus and Uvula. Science, 228: 199-202, 1985.

TABLE 1

HORIZONTAL VOR GAINS
MONKEY 2483

VELOCITY	PREFLIGHT GAIN (^{0}/s)		POSTFLIGHT GAIN (deg/s)	
30^0/s	28.9 ±2.1	(n=16)	30.9 ±3.2	(n= 8)
60^0/s	59.4 ±2.2	(n=13)	57.6 ±2.4	(n=10)
90^0/s	89.5 ±6.7	(n= 8)	88.0 ±2.8	(n= 7)
120^0/s	117.5 ±1.8	(n=12)	117.0 ±3.7	(n= 4)
150^0/s	144.8 ±1.3	(n= 4)	145.5	(n= 2)
180^0/s	170.9	(n= 2)	169.4 ±10.9	(n= 4)

TABLE 2

OVAR
STEADY STATE GAINS & PHASES

	HORIZONTAL VEL		VERTICAL POS	ROLL POS
	MEAN VEL (deg/s)	PHASE (deg)	PHASE (deg)	PHASE (deg)
2483 LT PREFLIGHT	16 ± 2 n=7	224 ± 10 n=6		259 ± 6 n=7
2483 LT POSTFLIGHT	16 ± 2 n=5	223 ± 14 n=6	348 ± 9 n=4	268 ± 3 n=7
2483 RT PREFLIGHT	33 ± 4 n=5	214 ± 11 n=9		80 ± 11 n=8
2483 RT POSTFLIGHT	30 ± 3 n=6	199 ± 15 n=6	316 ± 114 n=8	80 ± 11 n=8
		MONKEY 782		
782 LT PREFLIGHT	42 ± 3 n=5	252 ± 8 n=5	272 ± 7 n=8	
782 LT POSTFLIGHT	48 ± 4 n=7	232 ± 13 n=7	361 ± 14 n=5	279 ± 9 n=10
782 RT PREFLIGHT	49 ± 4 n=9	221 ± 88 n=8		105 ± 3 n=3
782 RT POSTFLIGHT	48 ± 5 n=7	221 ± 20 n=8	47 ± 21 n=8	80 ± 19 n=7

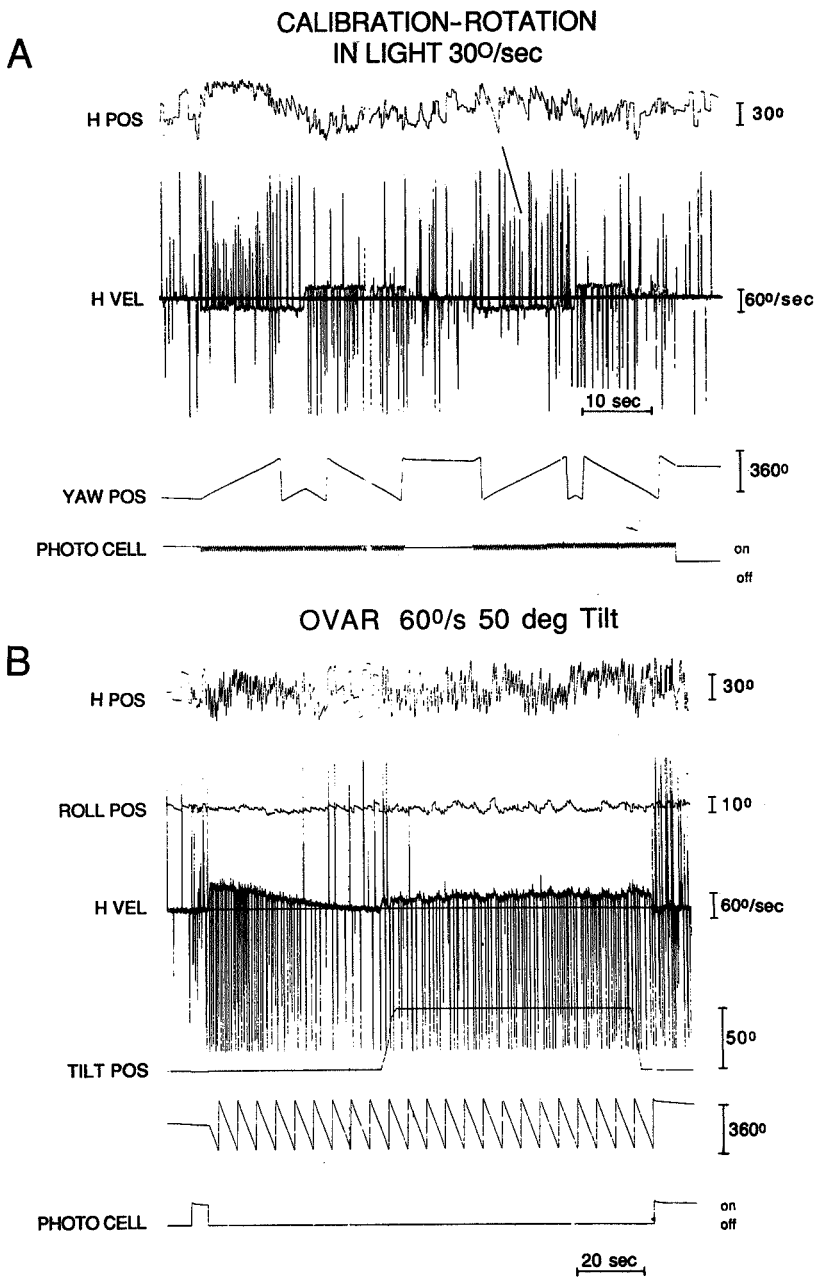

Figure 1. A. Horizontal eye position (H Pos, top trace) and horizontal eye velocity (H Vel, second trace) in response to yaw rotation about a vertical axis (Yaw Pos, third trace). Yaw position was recorded with a potentiometer that reset every 360°. Hence, the 'sawtooth' nature of the recording. The bottom trace shows the status of the light, recorded with a photocell. Note the stable steady state velocities induced by rotation in light in an earth-stationary surround at 30°/s. The diagonal line below the center of the H Pos trace shows the slope of the eye movement during the slow phases, and was used to calibrate the H Pos recording.

B. Rotation at 60°/s about a vertical and tilted axis. The animal was in darkness during stimulation. It was first rotated at 60°/s about a vertical axis, inducing per-rotatory nystagmus whose slow phase velocity declined steadily to zero. As shown in the Tilt Position recording (Tilt Pos, fourth trace), the axis of rotation was tilted 50° during the continuous rotation, inducing nystagmus. Note the modulations in slow phase velocity (H Vel) and in roll eye position (Roll Pos, second trace) during the OVAR. At the end of rotation the animal was tilted back to the upright and the lights were turned on to expose an earth stationary surround.

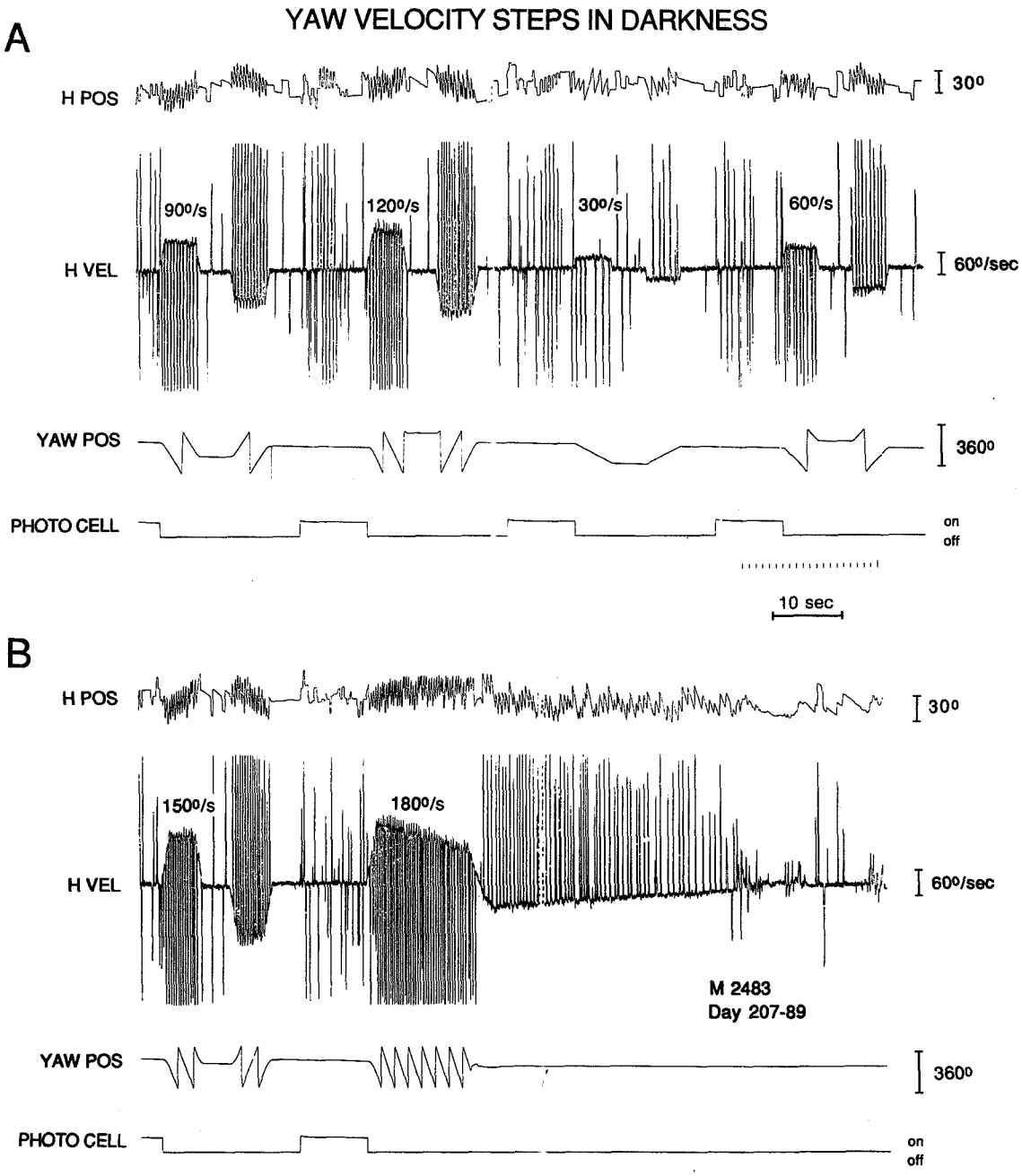

Figure 2. Recording scheme as in figure 1A. The animal (M2483) was in darkness during stimulation. It was rotated for 5 sec to the left and then to the right at velocities of 90°, 120°, 30°, 60°, and 150°/s. Nystagmus was induced at each of these velocities. Between each set of tests the lights were briefly turned on to 'dump' any nystagmus that was present after the stimulus had ceased. In the middle of B a longer stimulus of 180°/s was given, causing a decline in per-rotatory nystagmus. At cessation of rotation a typical period of post-rotatory nystagmus followed.

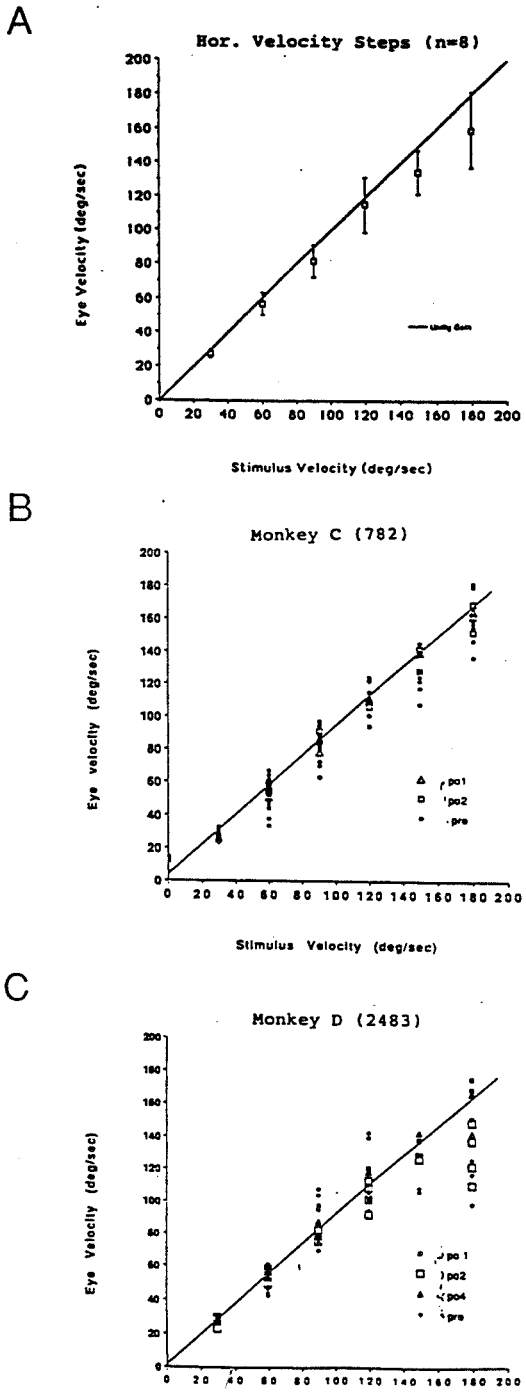

Figure 3. A. Means and 2 SD's for preflight VOR gains for the 8 monkeys studied in this series. The gains were close to unity (solid line) for stimulus velocities up to 120°/s.

B. Preflight (pre) and postflight recordings of M782, taken on the day of landing (PO1) and the following day (PO2).

C. Preflight (pre) and postflight recordings of M2483, taken on the day of landing (PO1), the following day (PO2) and two days later (PO4). Note that the preflight and postflight VOR gains were close to unity for both monkeys up to 120°/s.

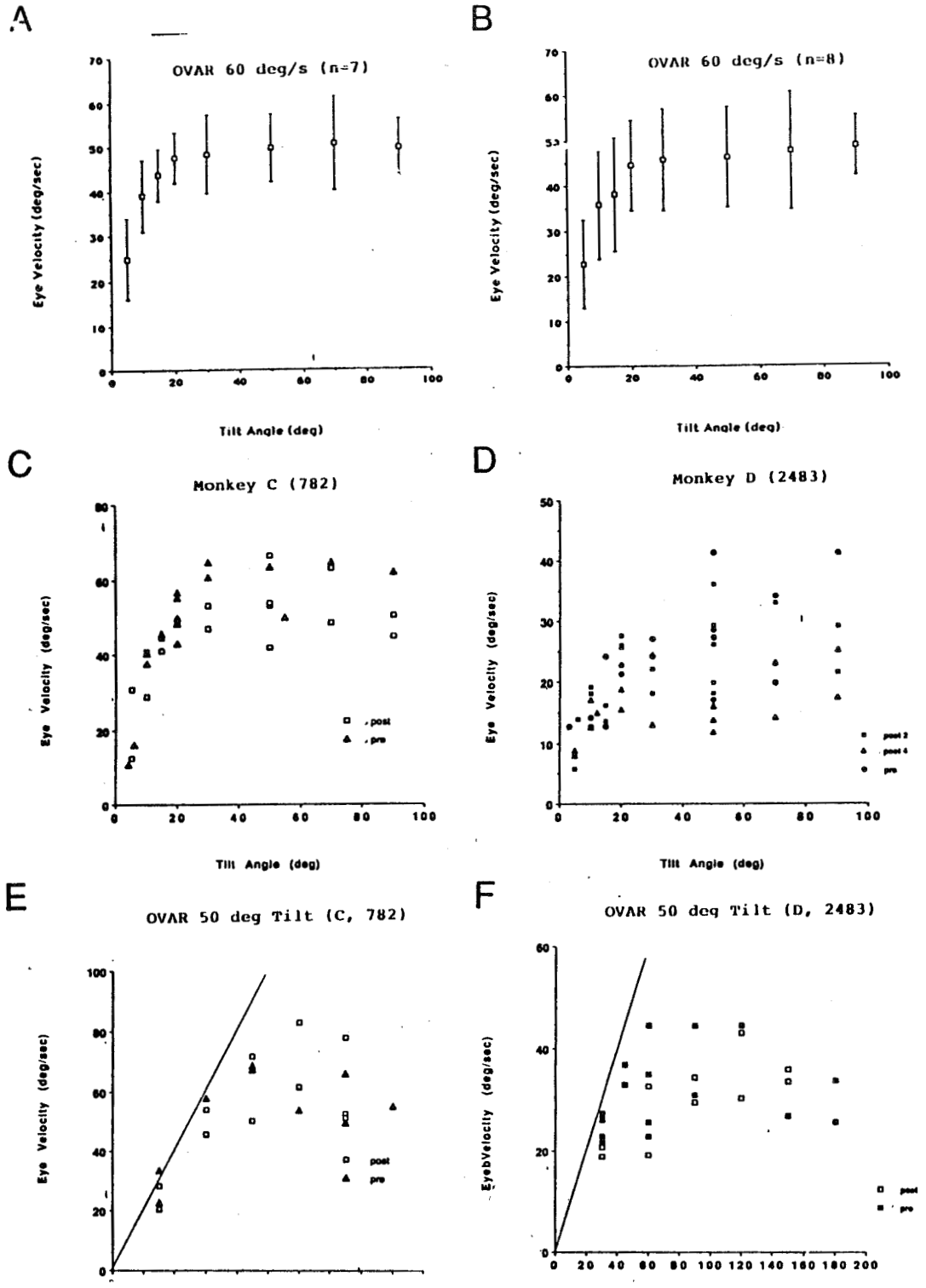

Figure 4. Analysis of steady state horizontal slow phase velocities during OVAR induced by rotation at 60°/s for various angles of tilt of the axis of rotation (A-D) and for various velocities of rotation at 50° tilt of the axis of rotation (E,F). Mean values and 2 SD's from the 7 monkeys, excluding M2483, are shown in A and for the entire group are shown in B. Individual values for M782 before and after flight are shown in C & E, and for M2483 in D & F. The steady state values for M2483 on post 4 were lower than either the preflight or the postflight 2 data. (This animal habituated much more rapidly than the other 7 animals.)

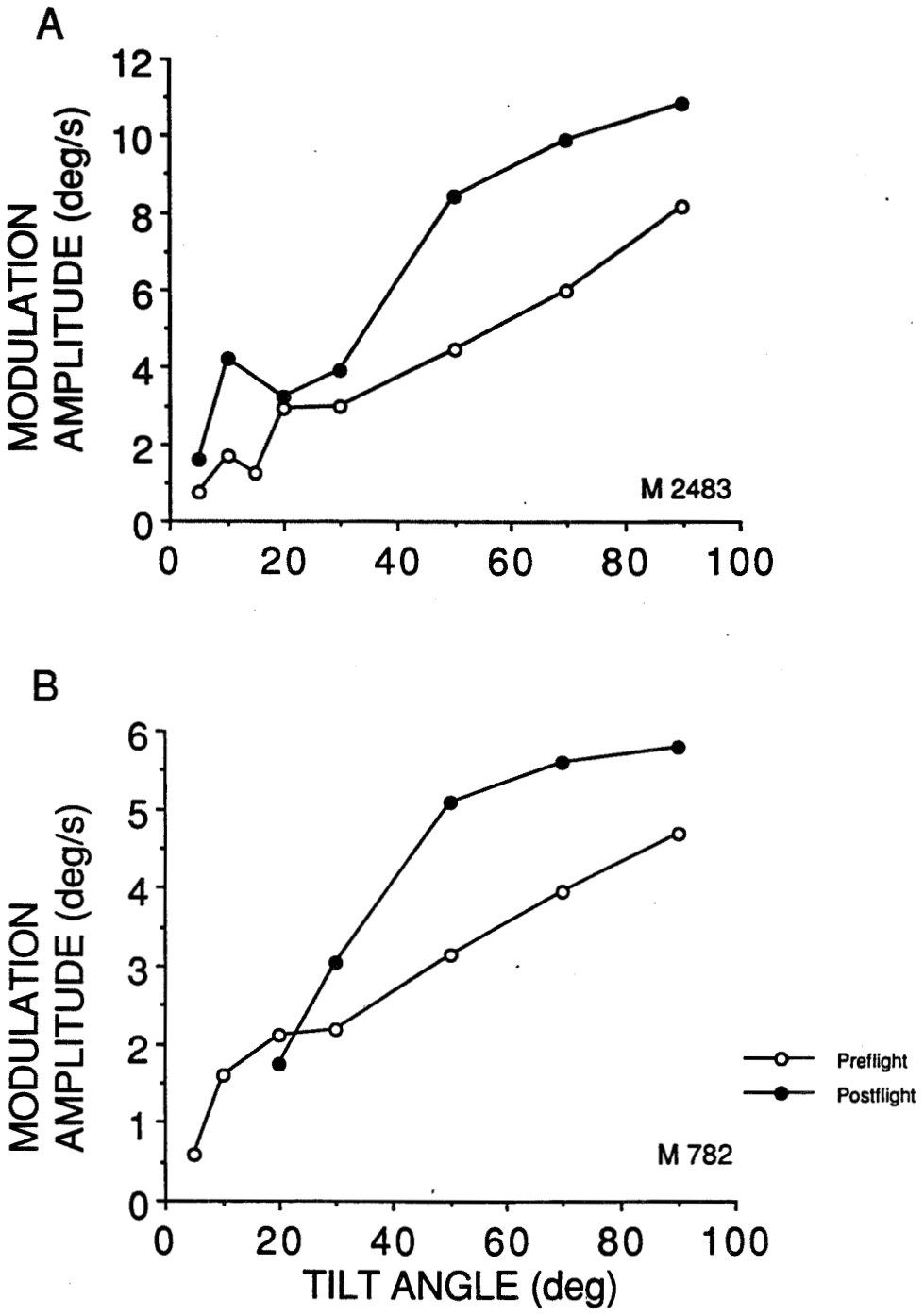

Figure 5. Mean values of the modulation in amplitude of horizontal slow phase velocity before (preflight) and after (postflight) adaptation to microgravity. There was also an increase in scatter of the values after flight. Mean values were about 50 % above the preflight values for tilt angles of 50-90°/s. The shape of the curves was also somewhat different, there being a relatively linear increase in modulation with tilt angle before flight. After flight the curve tended to saturate at lower angles of tilt.

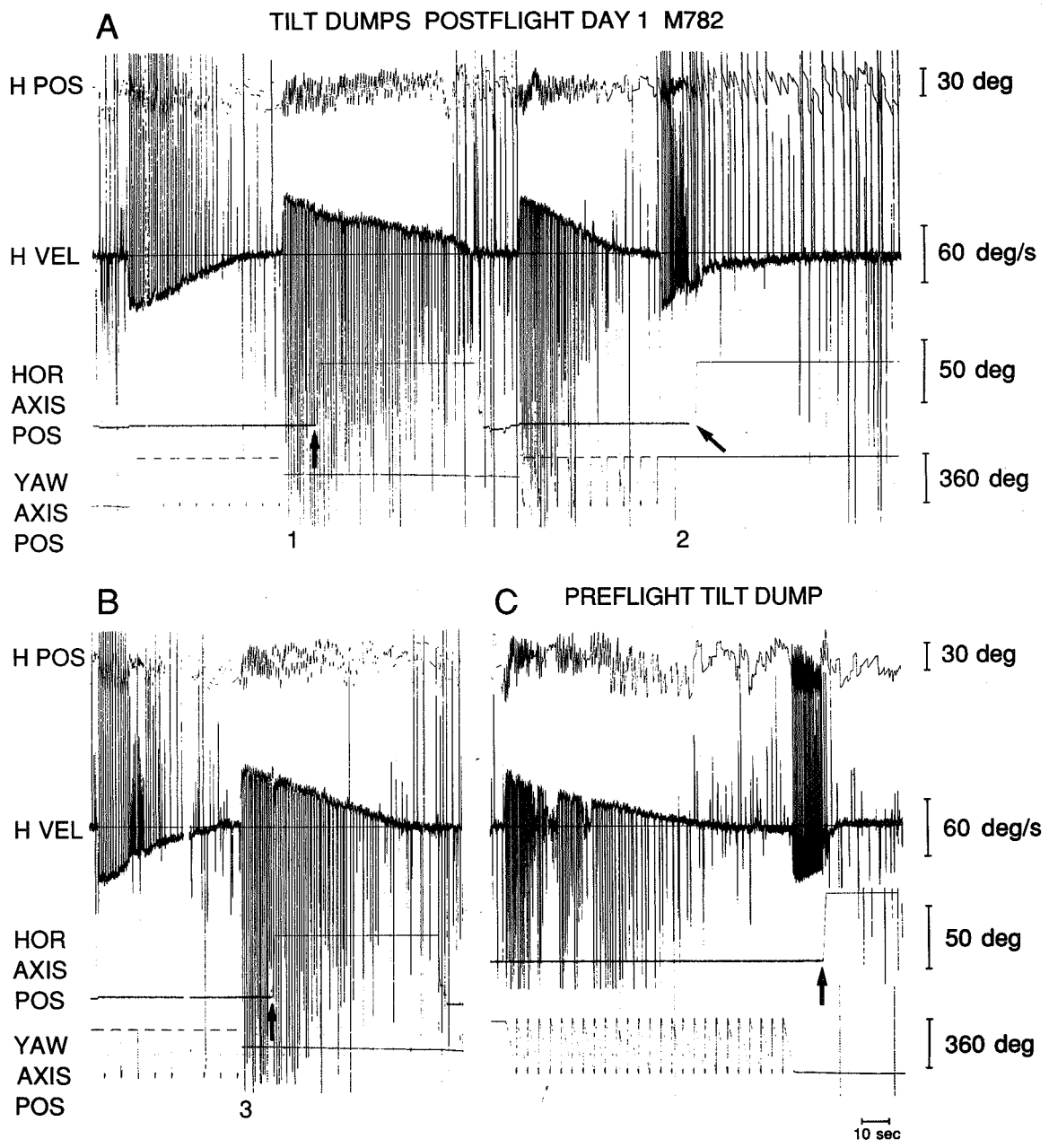

Figure 6. Eye movement recordings of tilt dumps postflight (1,2,3 of A,B) and preflight (C) in M782. The animal was in darkness throughout the experiment. In each set the animal was rotated about a vertical axis, inducing per-rotatory nystagmus, which declined to zero. Rotation then ceased, and 10 s later the gimbal axis and the animal was tilted 50°. Preflight lower right, C) this caused a prompt decline in slow phase velocity. Postflight (A,B) there was essentially no 'dumping' effect of the tilt on the time course of the slow phase velocity. In fact, in 1 and 2 the tilt caused an increase in slow phase velocity. The time course of the decline in post-rotatory nystagmus after tilting can be compared to the time course of the decline in per-rotatory nystagmus in the same direction in other trials. The data were taken on the day of landing.

52-51
51365

EXPERIMENT K-7-31

STUDIES OF VESTIBULAR PRIMARY AFFERENTS AND EYE MOVEMENTS IN NORMAL, HYPERGRAVITY AND HYPOGRAVITY - AXON COSMOS FLIGHT 2044

Principal Investigator:

M.J. Correia
Departments of Otolaryngology,
Physiology & Biophysics
The University of Texas Medical Branch
Galveston, TX

Co - Investigators:

A. A. Perachio
Departments of Otolaryngology,
Physiology & Biophysics
The University of Texas Medical Branch
Galveston, TX

J. D. Dickman
Department of Surgery (Otolaryngology)
The University of Mississippi Medical School
Jackson, MS

I. Kozlovskaya
M. Sirota
S. Yakushin
I.N. Beloozerova
Institute of Biomedical Problems
Moscow, USSR

Page intentionally left blank

EXPERIMENT K-7-31

STUDIES OF VESTIBULAR PRIMARY AFFERENTS AND EYE MOVEMENTS IN NORMAL, HYPERGRAVITY AND HYPOGRAVITY - AXON COSMOS FLIGHT 2044

M.J. Correia, A.A. Perachio and J.D. Dickman

INTRODUCTION

In recent years, studies have been carried out to investigate the effects of microgravity on the monkey horizontal vestibulo-ocular reflex and the underlying neural substrates. Horizontal eye and head movement recordings and multi-unit recordings from the vestibular nerve, medial vestibular nucleus, and the cerebellar flocculus (Gazenko et al., 1987, Sirota et al.; 1987, 1988, Kozlovskaya et al., 1981, 1983, 1985, 1989) have been made during space flight in five rhesus monkeys on Cosmos missions 1514, 1667 and 1887. These horizontal eye movements and neural recordings were made during active horizontal eye and head movements required to achieve gaze fixation on targets presented in front of the monkeys (Bizzi, 1979). Previously, it has been shown (Bizzi, 1971; Morasso et al., 1973) that this gaze fixation task is achieved, on earth, by monkeys, exclusively through the use of the vestibulo-ocular reflex.

For all Cosmos flights, it has been reported that head movement amplitude and velocity decrease relative to pre-flight values by about 30% as early as 2 hours following lift-off and by about 50% after 5-7 days. This hypometria of head movements is more than offset by a hypermetria of eye movements, where generally the amplitudes of gaze fixation saccades increase during flight, reach a maximum at about 6 days into the flight and level off but remain above pre-flight values. These relations are summarized, for example, by the observation that K_{vor} (the ratio of eye velocity to head velocity) values for the monkeys on flights 1667 and 1887 generally increased to a maximal value on the fifth or sixth day of flight and remained elevated relative to the pre-flight level for the remainder of the flight.

Chronic multi-unit and sometimes single unit recordings were also made from the vestibular nerve, the medial vestibular nucleus and the flocculus during the entire Cosmos flight 1887. The peak integrated neural output was determined on each day of flight for a 50 ms interval during the gaze fixation task. The most prominent changes during flight occurred in two recordings from the flocculus, since in both recordings, the integrated neural output from the first to the eighth day was three times that of pre-flight during the gaze fixation task. Less consistent changes were noted in the integrated neural activity from the vestibular nerve and vestibular nuclei. Generally, the integrated neural activity from two recordings from the vestibular nerve increased during the first four days of flight and by the end of the flight, the neural activity from one nerve recording was 400% above the pre-flight value but the other nerve recording was about 25% of the pre-flight value. When compared to pre-flight values, the integrated neural output from each of the four of the vestibular nuclei recordings was higher at two days into the flight. However, by the tenth day, two of the recordings had decreased to below pre-flight values.

We were interested in determining if the task of making numerous coordinated active horizontal eye and head movements during 14 days of microgravity modified the response of vestibular primary afferents to controlled passive rotations. We were unable to place a multi-axis rotator in the spacecraft but we assumed that if we could test these afferents

immediately post-flight we could obtain information about the dynamic response properties of the horizontal semicircular canals before they recalibrated to the terrestrial gravitational environment. In conjunction with Cosmos flight 2044, we tested individual vestibular primary afferents in control and flight monkeys before, on the first day and on subsequent days after flight (see schedule in Table 8). We report here evidence, albiet based on a small sample of afferents, that on post-flight day 1, the average gain of the step response of 6 horizontal semicircular canal afferents, that were thoroughly tested, was nearly twice and statistically significantly greater than a sample of 20 horizontal semicircular canal afferents studied during pre-flight (flight and control monkeys) and post-flight tests. Also, the mean time constant of decay of the afferent response was roughly 1/2 on the first post-flight day. In three other units, the average (±SEM) response to sinusoidal rotation (f=0.2051) was 0.65±0.12 compared to 0.56±0.1 (n=26) for pre-flight and post-flight control tests. Finally, the average sum of sine response gain for 3 different afferents was greater at each of six frequencies across the entire bandwidth 0.03 - 1.8 Hz when compared to 10 afferents tested during pre-flight and control tests. Preliminary results have been presented elsewhere. (Correia et al., 1990 a,b,c).

METHODS

Pre-flight Studies

Eleven rhesus (Macaca mulatta) monkeys weighing from 3.4 to 4.2 kg were instrumented for pre-flight testing. The instrumentation, relevant to the results reported herein, included circular head restraint rings (Sirota et al., 1988), indwelling corneo-retinal potential electrodes and microelectrode support platforms. The head restraint rings were chronically fixed to the animals' heads and the plane of the ring was in the stereotaxic horizontal head plane. The corneo-retinal potential electrodes (after the method of Bond and Ho, 1970) were chronically secured in small holes drilled in the bone near the outer canthi and above and below one eye. Since space inside the rings was also occupied by electrodes of other investigators, we made a 8mm wide aluminum bridge that extended across the diameter of the ring and had its long axis centered at approximately stereotaxic anterior - posterior (A-P) zero (the inter- aural line). This bridge defined our recording territory. The bridge had inset in it, two delrin rectangular pieces that could be slid 2 mm in the anterior-posterior direction. Drilled in the delrin inserts was a matrix of 25 holes (5 rows X 5 columns); each hole was .020 inch in diameter. With each monkey deeply anesthetized and in a stereotaxic apparatus, the aluminum bridge was fastened to the head restraint ring and the delrin inserts were positioned so that the center row was colinear with A-P - 0; the most medial hole was at lateral - 9 (L-9) and the most lateral hole was at L-13. The bridge was positioned about 1 cm above the skull and care was taken to make sure that the top planes of delrin inserts, and the ring were coplanar with the stereotaxic horizontal plane. Also while the animals were deeply anesthetized, they were inverted, the top plane of the head restraint ring was placed on an x-ray film plate and x-rays were made through the skull in the horizontal head plane After experimentation with x-ray parameters, x-rays (final x-ray parameters - 1.2 MAS @52 kV @ a distance of 161 cm) were obtained in which the holes in the delrin inserts were superimposed on the internal auditory meatus of the temporal bone. Therefore, start values for the A-P and M-L coordinates of the vestibular nerve could be obtained from the x-rays.

Single unit electrophysiological studies were carried out to obtain the stereotaxic location of the vestibular nerve and obtain pre-flight data. Stainless steel guide tubes (26 guage) containing tungsten microelectrodes (0.005" diameter blanks) insulated with (0.002-0.003") Epoxylite were lowered through the holes in the delrin inserts into the brain and through the tentorium. The microelectrodes were further advanced through the flocculus into the vestibular nerve using a hydralic microdrive. The microelectrodes had tip

impedances of 5-20 MΩ measured at 1 KHz. The single unit action potentials were amplified by standard techniques. The system amplification was 1000 X and the bandpass was 300 - 10 KHz. Corneo-retinal potentials corresponding to horizontal and vertical eye movements were amplified by a dual channel amplifier with a gain of 2000 X and a bandpass of DC - 200Hz. The amplifier automatically reset the baseline when it drifted beyond a preset value. The action potential train, eye movements, and stimulus reference signals from the rotator (see below) were taped using a Teac model 510C - 14 channel tape recorder. In parallel, data was analyzed on line using a computer system consisting of a CED (Cambridge Electronic Design) 1401 interface, a PC/XT (10 M Hz) and a suite of computer programs (UT) written especially for these studies. These programs controlled the two motors (yaw-30 ft/lb and pitch-80 ft/lb) of the multi-axis rotator, acquired eye movement and action potential signals, stored them in files and produced standard cycle (C), post-stimulus time (PST) and interspike interval (ISI) histograms. The rotation protocols (specified in terms of a kinematics based acceleration nomenclature, Hixson et al., 1966 - see figures in Figure 10 generated by the computer, used during the pre-flight studies that produced data reported herein and listed in order of presentation are: (A complete listing of all pre-flight and post-flight protocols are listed in Tables 4-7) 1) *static testing* with the animal in the standard position (A_y = -20 deg) for 60 s; 2) *single sinusoids* (four cycles of yaw sinusoidal oscillation ±20,30,40,60 °/s peak amplitude and a frequency of 0.2051 Hz; 3) *sum of sinusoids* (3 cycles of a sum of sinusiodal yaw oscillation consisting of the following frequencies each having a peak amplitude of 30°/s - 0.0293, 0.0879, 0.2051, 0.3809, 0.9083, and 1.7873 Hz); 4) *trapezoids* (two alternating trapezoids $\alpha_z = \pm 12$ °/s^2 for 10 s followed by constant velocity for 60 sec. 5) *pulses* (2 alternating yaw (ω_z) pulses ±60 °/s in amplitude and 30 s in duration separated by zero velocity for 60 sec); and 6) *static pitch* (two alternating pitch trapezoids of steady state duration of 60 s and steady state amplitude of ±20°). All yaw rotations were made with each animal's head in the standard position (horizontal semicircular canals in the earth's horizontal plane). This was achieved securing the monkey's head to the monkey holder in a 20 ° pitch down position (Blanks et al., 1985). All pitch rotations were made about the monkey's inter-aural axis and 0° tilt was defined as that position when the monkey was in the standard position (A_y = -20°). Also, prior to beginning the rotation sequence for each neural unit, 60 s of spontaneous discharge was gathered. Neural recordings were typically made in a dimly lit room. During eye movement recordings, the animals were covered with a light tight bag and alerted only by loud sounds. We built a multi-axis rotator (Fig. 1) to provide the passive rotations described above. It consisted of a monkey carrier (C) on an axis that could be yawed and fixed at 90° intervals about 360°. That axis was attached to a a positioning (P) axis that could be rotated and locked at 10° intervals over a range of ± 90°. Thus the animal could be pre-yawed, pre-pitched or pre-rolled ± 90° relative to the inner (I) gimbal that contained a motorized (30 ft/lb DC torque motor) axis of rotation. All the above gimbals were attached to an outer (O) motorized (80 ft/lb DC torque motor) gimbal. The motors could be operated independently in velocity or position servo feedback mode (Neurokinetics Inc.). A schematic drawing of the multi-axis rotator is shown below.

In-flight studies

One indwelling multi-unit microelectrode was implanted in the vestibular nerve of flight monkey 2483. A guide tube was fabricated with wings made of wire mesh. The guide tube was cemented to the bridge that was attached to the head ring. The microelectrode was lowered through the guide tube into the vestibular nerve and then cemented to the guide tube. Five candidate flight monkeys were implanted and monkey 2483 flew. Based on preliminary analysis of the recordings, the microelectrode remained in the

nerve during 13 days of the flight. On the 14th day of the flight, the microelectrode moved into the cerebellum. This conclusion is based on the observation of entrainment of the neural response to eye movements rather than to head movements. Large movement artifacts occurred throughout the taped record. Because of these artifacts, since the pre- and post-flight data analysis was labor intensive and since single unit discrimination will be difficult, data analysis has been delayed beyond the presentation of this report. Recording from an array of electrodes in the vestibular nerve and the vestibular nucleus will be one of the priority items during the 1992 flight.

Post-flight studies

The rotation protocols for both the single unit experiments and the eye movement experiments were abbreviated for the post-flight studies since the recording time was set at 4 hrs./animal. Lists of the protocols are specified in Tables 4-7 and the pre-and post-flight protocols can be compared. The sequence of the single unit experiment protocols was also altered for the post-flight experiments. The sequence was as follows: 1) Spontaneous discharge, 2) sinusoidal oscillation; 3) velocity pulses, 4) sum of sinusoids and 5) tilt sensitivity. The order of the velocity pulses and the sum of sinusoids was reversed for the pre-flight and post-flight tests.

The post-flight sequence of testing animals on a daily basis was as follows: 1) Flight animals 2483 and 782 were tested on post-flight days 1, 2, 4, and 5. Control animals were tested on post-flight days 6, 7, and 8.

RESULTS

Fig. 2 presents representative horizontal canal afferent pulse responses for pre- (Left) and post-flight (Right) tests on monkey 782. The top panel of each figure is the rate gyro output (ω_Z) and the bottom panel is a post-stimulus time histogram. Comparison of the two figures reveals that: 1) The peak excitatory and inhibitory response is almost 2 times on post-flight day 1 when compared to the pre-flight response and 2) the rate of decay from the peak during constant velocity rotation is much shorter on post-flight day 1.

A single component exponential function was fit to pulse responses of a number of the afferents. The form of the function was $y(t) = \text{gain}\{\exp[-(x(t)-x_0(t))/\tau]\}+DC$, where gain is the best-fit amplitude minus DC divided by stimulus amplitude{(Spikes/s) - DC(Spikes/s)}/(60)(°/s), x_0 is the amplitude value at t_0, τ is the time constant of decay and DC is asymptotic value. Best-fit values for the two afferents in Fig. 2 are shown as legends. It can be noted that the gain (gain =1.05) of the afferent in Fig. 2 (Right) is greatly increased over the gain (gain =0.34) of the afferent shown in Fig. 2 (Left). Moreover, the time constant of decay following the peak response (Right), is much shorter (τ =1.96 s) than for the afferent illustrated on left of Fig. 2 (τ=6.03 s). This result for two afferents of one of the flight monkeys is supported by data from 5 additional horizontal afferents recorded on post-flight day 1. A comparison of mean gain and mean time constant for 6 horizontal afferents recorded on post-flight day 1 compared to mean gain and mean time constant for 20 afferents recorded from the flight animals during pre-flight tests and from non-flight animals recorded during control tests is presented in Fig 3.

The mean (±SEM) excitatory gain during post flight recordings was 0.83 (±0.11); the inhibitory gain was 0.85 (±0.10). The mean (±SEM) excitatory time constant was 3.29 (±0.51); the mean inhibitory time constant was 3.49 (±0.55). Three of four of these values are statistically significantly different ($p< 0.01$, one way ANOVA), from

pre-flight and control test pulse rotation tests where the mean (±SEM) excitatory gain was 0.49 (±0.04) and the inhibitory gain was 0.39 (±0.03). The mean (±SEM) excitatory time constant was 6.01 (±0.51); the mean inhibitory time constant was 4.79 (±0.55). The elevated gain noted for the pulse responses during first post-flight day were also noted for the sinusoidal and sum of sinusoidal stimulation. Fig. 4 presents representative cycle histograms illustrating that the gain was elevated in one afferent tested on post-flight day 1 compared to a pre-flight response.

The mean gain (±SEM) and phase (±SEM) of afferent responses from a sample of neurons during pre-flight and post-flight studies, during single sine oscillation at 0.2051 Hz, was 0.56 (±0.14, n = 26) and 14.8 (±6.7, n = 26) as compared to post-flight day 1 values of 1.02 (±0.24, n = 7) and 23.8 (±4.1, n = 7). Four of the units that comprised the post-flight sample were not part of the sample obtained for pulse responses during post-flight day 1.

Pre- and post-flight responses to a sum of sinusoidal stimuli during pre-flight and control tests is illustrated for two typical afferents in Fig.5.

Fig. 6 presents Bode plots for the average (±SEM) of a sample of afferents tested during pre-flight/control studies, during post-flight day 1, and during post-flight days 4 & 5. It can be seen that the post-flight day 1 mean gain is elevated above the pre-flight/control levels at all frequencies and the phase is advanced across all frequencies. Also, it can be noticed that the gain slope is greater for post-flight day 1 when compared to pre-flight/control gain values. These latter two conditions indicate that neural adaptation, modeled as a fractional exponent in the transfer function of the response, is greater for the post-flight day 1 response (see transfer function with best fit parameters in figure caption). On post-flight days 4-5, the gain is still above the pre-flight/control levels but it is less than that measured on post-flight day 1. Plus or minus one SEM for the phase angles overlap for each frequency except the lowest.

The frequency independent gain terms in the figure caption of Fig. 6 do not reflect the magnitude of the gain changes at each frequency between tests during pre-flight and during post-flight days 1 and 4-5. These values are presented in Table 1.

As can be noted from Fig. 6 and Table 1, the gain values obtained from the sum of sines test remained elevated during post-flight days 4 and 5. A comparison of the results from the other tests during each of the post-flight days is presented in Table 2.

From Table 2, it appears that the mean inter-spike interval and the coefficient of variation (CV) of the spontaneous firing rate did not change following flight. With the exception of the gain for the single sine test on post-flight day 2, the mean gain for sine and pulse responses (like the sum of sines test - Table 1) remained elevated during the first 5 post-flight test days.

In other species, gerbil and pigeon, we (Perachio and Correia, 1983, Anastasio et al., 1985) have reported that some (50-60%) horizontal canal afferents demonstrate a pitch tilt sensitivity. During static pitch down, some horizontal canal afferents, particularly those that fire irregularly, increase their mean firing rate by more than 10% when compared to no pitch (standard position); during pitch up these same afferents decrease their firing rate by more than 10%. Pre-flight and post-flight tests of tilt sensitivity and representative traces are presented in Fig. 7.

A summary of the results from the tilt sensitivity test for a sample of horizontal canal afferents is presented in Table 3.

It can be noted that the 'DC' bias of the response during constant velocity rotation for both flight monkeys is greater on post-flight day 1 than on post-flight day 9. This was quantified by scoring the average slow phase velocity over the interval 20-89 s. The ratio of this total for post-flight day 1 over post-flight day 9 for slow phase velocity left and slow phase velocity right was 4.5 and 3.9 for monkey 2483 and 1.7 and 1.2 for monkey 782.

Eye movements were recorded to provide controls for the single unit studies. If changes occurred in the afferent responses, we wanted to know if the same changes occurred in the eye movement responses. Two of the eye movement tests produced interesting results. Pre-flight results have been analyzed and are being tabulated. But if it is assumed that the animals had recalibrated during the first eight days post -flight, comparisons can be made between responses on post-flight day 1 and post-flight day 9. Comparisons between responses to two of the post-flight eye movement tests (see complete list in the Tables 4-7) on post-flight day 1 and post-flight day 9 for the two flight monkeys are presented in the next two figures. Fig. 8 compares responses during horizontal axis rotation on post-flight day 1 and post-flight day 9.

Fig. 9 compares the horizontal slow phase eye velocity for the flight monkeys on post-flight day 1 and post-flight day 9 during yaw ($\omega_Z = 60°/s$) step rotations with the animal's head in the standard position (horizontal semicircular canals coplaner with the earth's horizontal plane). This condition is presented in the left figure. The responses shown in the right figure were obtained with the animal pitched down 45 ° from the standard position.

Fig. 9 shows that while there is no difference between the gain and time constant of decay of the slow phase eye velocity in the right figure, the gain and the time constant of decay is greater and lengthened for the pitch down condition.

DISCUSSION

The mean firing rate and CV for the horizontal canal afferents obtained during pre-flight/control studies was 92 spikes/s and 0.14 (Table 2), respectively. These values compare well to average values of 98 (Miles and Braitmann, 1980), 106 (Keller, 1976; n = 33) 105 spikes/s (Louie and Kimm, 1976; n = 43) and 102 spikes/s (Buttner and Waespe, 1981, n = 32) also obtained for horizontal canal afferents in the alert rhesus monkey. The range of CVs in the present study fall within the range determined by previous investigators. Louie and Kimm (1976) divided their sample of CVs into three groups: regularly firing (CV between zero and 0.13); irregularly firing (CV greater than 0.35) and intermediately firing (CV between 0.13 and 0.35). The distribution of CVs [mean (±SEM)= 0.14 (±0.02)] in the present study, like those of Louie an Kimm (1976) and Buttner Waespe (1981), was skewed toward the regularly firing neurons. A new result from the present study is that during post-flight testing following 14 days of microgravity, the mean firing rate varies only 4 spikes/s and the CV changes 0.05. Neither of these changes are reflected by a systematic trend (see Table 2).

Pulse responses

Buttner and Waespe (1981) found in 5 alert rhesus monkeys, in response to pulse stimuli, that the mean (±SEM) excitatory time constant for 26 horizontal canal afferents was 5.9 (±0.11)s; the inhibitory time constant was 5.1 (±0.16)s. The excitatory sensitivity (spikes/s/o/s) was 0.57 (±0.06) for irregular neurons and 0.38(±0.05) for regular

neurons. The excitatory sensitivity [0.41±(0.04)] was higher than the inhibitory sensitivity [0.35±(0.04)] for the total sample of neurons.

The excitatory and inhibitory sensitivity for the preflight/control sample (n = 20) of neurons in the present study was 0.47±0.06 and 0.40±0.05, respectively. These results are almost the same as the results of Buttner and Waespe (1981).

During post-flight days 1, 2, and 4-5 the excitatory sensitivity was 1.7, 1.6 and 2.1 times that of the preflight/control values and the inhibitory sensitivity was 2.1, 1.6 and 2.1 times that of the preflight/control values respectively. As indicated in Fig. 3, the increased gains that we noted for post-flight day 1 (compared to the pre-flight/control data) were statistically significantly ($p<0.01$, ANOVA). These results suggest that activities during 14 days of microgravity result in an increased gain during the first post-flight day and probably for at least for 5 days following return to earth.

The shortening of the decay to the step response during the post flight days is less dramatic than the gain changes but the reduction is 42% for the excitatory time constant and 34% for the inhibitory time constant. This reduction persists during the first five post-flight days. The parameters of the fit (Fig. 6 caption) of the transfer function to the average response to the sum of sines during the first post flight-day indicate that the so-called cupula time constant τ_L is slightly reduced (11%) but the *majority* of the reduction seen during the post-flight tests is probably due to across frequency neural adaptation (Thorson and Biederman-Thorsen, 1974). Greater across frequency neural adaptation during the post-flight tests is indicated by the greater gain slope and phase advance seen for the Bode plot values (Fig. 6) and the greater value of the parameter k (see Fig. 6 caption).

Single sines

The mean (±SEM) gain and phase for the pre-flight/control afferent (n=26) response to a single sine stimulus (f=0.2 Hz, ω_Z=60°/s) was 0.56 (±0.14) and 14.8 (±6.7). Miles And Braitmann (1980), studied 121 horizontal canal afferents in alert rhesus monkeys. They oscillated the monkeys at 0.2 Hz, ±20°. They found the mean gain to be 0.63 spikes/s//s and the mean phase to be an advance re velocity of 17.0 degrees.

On post-flight day 1 the mean gain was 1.02 (±0.24). Only 21% of the horizontal canal afferents studied by Miles and Braitmann (1980) had gains this high or higher (see Miles and Braitmann, 1980, Fig. 4, p. 1431). On post-flight day 2 the gain level dropped to 0.48 but rebounded to 0.83 on post-flight days 4-5. The phase angles on post-flight days 1-5 did not change (Table 2) but were phase advanced by about 10 degrees.

Sum of sines

The pre-flight sum of sine horizontal canal afferent data extend, for the first time, sine wave analysis to low frequencies for the alert rhesus monkey. Previously, the lowest frequency tested was 0.1 Hz. Transfer function fits to all frequencies for the pre-flight/control horizontal canal afferent data produced an estimate of the cupula time constant, τ_L = 9.6. This value is larger than the time constants calculated by pulse analysis, but as pointed out above and elsewhere (Correia et al., 1978) those cupula time constants derived from pulse analysis may be contaminated by neural adaptation which also is operative over the low frequency ranges. The Bode plot presented in Fig. 6. also suggests that neural adaptation is operative over the entire bandwidth 0.03 Hz to 1.78 Hz. This is indicated by a monotonically increasing gain and a phase advance in the mid range

(0.2 Hz) frequencies. In this respect, neural adaptation in the alert rhesus monkey is like birds (Landolt and Correia, 1980, Correia et al., 1981) and rodents (Schneider and Anderson, 1976) and unlike the anesthetized squirrel monkey (Fernandez and Goldberg, 1971).

Compared to pre-flight and control values, the gain at all frequencies during post-flight day 1 was increased (Table 1). The slope of the gain curve was also increased. The phase angle at each frequency was phase advanced. On post-flight days 4 & 5 the gain was reduced from post-flight day 1 but is greater than the pre-flight/control values (Table 1). These results support the pulse and single sine data and further suggest that 14 days of activities during microgravity cause the gain to increase in the horizontal semicircular canals.

Tilt sensitivity

Table 3 presents the results of the tilt sensitivity test for the pre-flight/control group and for afferents tested on post-flight days 1 &2. Previously, we (Perachio and Correia, 1983) found that 17/30 or 57% of the horizontal canal afferents we tested in the gerbil showed a change in firing rate (re the firing rate in the standard position) of greater than 10% when we pitched (Ay =±10°) them ±10°. From Table 2 it can be seen that on average during pre-flight/control tests 14 afferents did not show a change of 10% or more for ±20° tilt. One of 14 afferents showed a change of greater than 10% for tilt up re standard position and one afferent showed a change of more than 10% for tilt down re standard position. During post-flight day 1, the percent change was 1% for the two afferents tested. From these data it appears that in the alert rhesus monkey horizontal canal afferents do not demonstrate tilt sensitivity normally. Increase in tilt sensitivity following 14 days of activity in microgravity is less clear. Two regular afferents tested on post-flight day 1 showed no tilt sensitivity but two afferents tested on post-flight day 2 did show tilt sensitivity and the mean difference was 18% for tilt up and 16% for tilt down. A larger sample of irregularly firing afferents is needed to draw strong conclusions about the tilt sensitivity of horizontal canal afferents in normal animals and in animals following activity in microgravity.

Thus the major findings that we report are an increased gain and increased neural adaptation in the horizontal semicircular canals following active horizontal head movements during 14 days of microgravity. The gain changes and adaptation changes appear to be *primarily neural*, i.e., not associated with the cupula-endolymph system since the cupula time constant, τ_L, does not change but about 10%. However, it should be noted that the operator reflecting cupula velocity at high frequencies of rotation, τ_V, does change by about 30%.

Eye movement responses

Pre-flight eye movement responses have been scored but not completely tabulated. However, all post-flight data has been scored and tabulated. To see if activities of microgravity affected horizontal eye movement we have compared responses on post-flight day 1 with post -flight day 9 on the assumption that by day 9 the responses should have recalibrated to pre-flight values. Figs. 8-9 show the only positive findings we have observed. From Fig. 8 it appears that for both flight monkeys, during constant velocity horizontal axis rotation, that the constant level of slow phase eye velocity was greater during post-flight day 1 when compared to post-flight day 9.

The graph on the left of Fig. 9 presents an important result. There is no change in the peak slow phase velocity or the decay during pulse testing during the post flight days when the animal is yawed about earth vertical. Thus the eye movement response is accurate during passive rotation even though the semicircular canal afferent output shows increased gain and increased neural adaptation. However when the animal is pitched 45 ° down (A_y = -65°) the peak velocity is decreased and the time constant of decay is shortened on post-flight day 9. This latter result must be interpreted with caution since the results on day 1 are the same as for the no pitch condition. The reduced response during day 9 could result from habituation due to repeated testing.

Interpretation

The responses from the horizontal canal afferents suggest that the vestibular end-organ remains normal during and following the activities related to 14 days in microgravity. However, it appears that the gain and neural adaptation increase. The first question that must be asked is why does the gain and neural adaptation change and the second question that must be asked is how does the gain and neural adaptation change. It seems that during the early phases of flight (see introduction), the animals demonstrate head movement hypometria and eye movement hypermetria. The former behavior may be a strategy to reduce vestibular stimulation and decrease disorientation and space motion sickness; the latter strategy permits the animals to make correct gaze eye movements with reduced head movements and obtain (nourishment) throughout flight. If the gain of the semicircular canals changed, so that for a reduced head velocity, the eyes moved more than before flight then the above facts could be reconciled. It is extremely important to measure head velocity *directly* during the 1992 flight. The vestibular efferent system is about the only candidate as a feedback mechanism that can change and maintain the gain changes in the horizontal semicircular canal primary afferent response that we observed during the 5 days post-flight testing. Future ground based studies can be conducted to test this speculation. It is also interesting that even though the gain was increased from the vestibular primary afferents the eye movement response to passive yaw rotation was accurate (see Fig. 9). This implies that the increased gain and increased adaptation from the afferents is compensated for in the central nervous system. One of the goals of our experiments on the 1992 Cosmos flight is to study eye movement related neurons in the medial vestibular nucleus to see if their response changes following exposure to activities in microgravity.

The results detailed in this progress report are important for two reasons. First, this is the first report, to our knowledge, indicating that the vestibular end organ can change its output due to activities (many active horizontal head movements) in an unusual vestibular environment (microgravity) and second, if the speculation above is correct, we may have a start on understanding the neural basis for the space adaptation syndrome.

SUMMARY

1. Fourteen days of active head movements in microgravity appear to modify the gain and neural adaptation properties of the horizontal semicircular canals in the rhesus monkey. This is the first demonstration of adaptive plasticity in the sensory receptor. Reversing prisms, for example, do not modify the gain of the primary afferent response. Pulse yaw rotation, sinusoidal rotation, and sum of sinusoidal rotation testing during the first day following recovery revealed that the gain of a sample of afferents was significantly greater than the gain derived from afferent responses obtained during pre-flight and control monkey testing. There was no strong evidence

of tilt sensitivity in the sample of afferents that we tested either during the pre-flight or control tests or during the first day post-flight. Two irregular afferents tested on post-flight day 2 showed changes with tilt but the responses were not systematic. The spontaneous discharge did not change following flight. Mean firing rate and coefficient of variation remained constant during the post flight tests and was near the value measured during pre flight tests. The change in gain of horizontal canal afferents might be adaptive. The animals were required to look at a target for food. This required active head and eye movements. Active head movements have been shown to be hypometric and eye movements have been shown to be hypermetric during the first few days of past Cosmos flights (see introduction). It might be that the increased gain in the horizontal semicircular canals permit accurate target acquisition during hypometric head movements by driving the eyes to greater angles for smaller angles of head movement. The mechanism by which the semicircular canals recalibrate (increase their gain) is unknown. The efferent vestibular system is a logical candidate.

2. Horizontal nystagmus during rotation about an earth vertical axis with the horizontal semicircular canals in the plane of rotation produced the same response during post-flight day 1 and post-flight day 9. But when the head was pitched down 45° the nystagmus slow phase velocity was *greater* and the duration was about *twice* during post-flight day 1. Apparently, this response involving the interaction of the horizontal and vertical semicircular canals and the otoliths did not recalibrate during post-flight day 1.

3. The 'DC' bias of the slow phase velocity of the horizontal nystagmus during constant velocity horizontal axis rotation was roughly 4 times for one flight monkey and roughly 2 times for the other on post-flight day 1 compared to post-flight day 9. These results suggest that the otolith mediated response during constant velocity rotation also did not recalibrate on post-flight day 1.

ACKNOWLEDGMENTS

The principal and co - investigators gratefully acknowledge the splendid support and selflessness provided by their cherished colleagues from the Institute of Biomedical Problems, the Animal Care Facility where the pre-flight and post-flight studies were conducted and the following individuals from NASA and UTMB: Stuart Abrams, Ph.D., Rod Ballard, Ph.D., Terry Behrends, Glenda Bowne, John Brassard, Geoffrey Bush, Joe Byers, James Connolly, Ed Coleman, Pat Daly, Sam Dotson, Beth Faulkner, Judy Hall, Charles Hightower, Julia Hilliard, Ph.D., Ike King, Daniel Lang, Ph.D., Bill Little Luann Marchi, Douglas Obeck, DVM, Keith Ramsey, M.D., Al Reinarz, M.D., Milliard Reschke Ph.D., Tom Rice, III, Barbara Rose, Fred Schuster, Claudia Starr, Sid Steffens, Ray Stinson, Ph.D., Roger Stone, David Stoner, Cheryl Welch, C.L. Williams (deceased), This work was supported, in part, by a grant (NAG-2-446) from NASA.

REFERENCES

1. Anastasio, T.J., M.J.Correia, and A.A.Perachio. Spontaneous and Driven Responses of Semicircular Canal Primary Afferents in the Unanesthetized Pigeon. J. Neurophysiol. 54: (2) 335-347; 1985.

2. E. Bizzi. Strategies of eye-head coordination. Prog. Brain Res. 50: 795-803; 1979.

3. E. Bizzi, R.E. Kalil, and V.Tagliasco. Eye-head Coordination in Monkeys. Evidence for Centrally Patterned Organization. Science 173: 452-454; 1971.

4. R.H.I. Blanks, I.S. Curthoys, M.L. Bennett, and C.H. Markham,. Planar relationships of the Semicircular Canals in Rhesus and Squirrel Monkeys. Brain Res. 340: 315-324; 1985.

5. Bond, H.W. and P.Ho. Solid Miniature Silver-Silver Chloride Electrodes for Chronic Implantation. Electroenceph. Clin. Neurophysiol. 28: 206-208; 1970.

6. Buttner, U. and W.Waespe. Vestibular Nerve Activity in the Alert Monkey During Vestibular and Optokinetic Nystagmus. Exp. Brain Res. 41: 310-315; 1981.

7. Correia, M.J., J.P. Landolt, M.D. Ni, A.R. Eden, and J.L. Rae. A Species Comparison of Linear and Nonlinear Transfer Characteristics of Primary Afferents Innervating the Semicircular Canal. IN: The Vestibular System: Function and Morphology 280-316; 1981.

8. Correia, M.J.,, A.A. Perachio, J.D. Dickman, I.B. Kozlovskaya, M.G. Sirota, S.B. Yakushin, and I.N. Beloozerova. Semicircular Canal and Otolith Mediated Eye Movement and Primary Afferent Responses in Rhesus Monkeys Before and After 14 Days of Orbital Flight On-Board Cosmos 2044, Barany Soc. Abs; 87, 1990a.

9. Correia, M.J.,, A.A. Perachio, J.D. Dickman, I.B. Kozlovskaya, M.G. Sirota, S.B. Yakushin, and I.N. Beloozerova. Vestibular Primary Afferent and Vestibulo-ocular Changes in Rhesus Monkey Following 14 Days of Microgravity, Neurosci. Abs., 735, 1990b.

10. Correia, M.J.,, A.A. Perachio, J.D. Dickman, I.B. Kozlovskaya, M.G. Sirota, S.B. Yakushin, and I.N. Beloozerova. The Effects of 14 Days of Microgravity on Post-Flight Semicircular Canal Primary Afferent Responses, IUPS Abs., 1990c.

11. Dichgans, J., E. Bizzi, P. Morasso, and V.Tagliasco. The Role of Vestibular and Neck Afferents During Eye-Head Coordination in the Monkey. Brain Res. 71: 225-232; 1974.

12. Dichgans, J., E . Bizzi, P. Morasso, and V.Tagliasco. Mechanisms Underlying Recovery of Eye-Head Coordination Following Bilateral Labyrinthectomy in Monkey. Exp. Brain Res. 18: 548-562; 1973.

13. Fernandez, C. and J.M. Goldberg. Physiology of Peripheral Neurons Innervating Semicircular Canals of the Squirrel Monkey. II. Response to Sinusoidal Stimulation and Dynamics of Peripheral Vestibular System. J. Neurophysiol. 34: (4) 661-675; 1971.

14. Gazenko, O.G., A.I. Grigoriev, and I.B. Kozlovskaya. Mechanisms of Acute and Chronic Effects of Microgravity. Physiologist 39: (1); 1987.

15. Goldberg, J.M. and C. Fernandez. Physiology of Peripheral Neurons Innervating Semicircular Canals of the Squirrel Monkey. I. Resting Discharge and Response to Constant Angular Accelerations. J. Neurophysiol. 34: (4) 635-660; 1971.

16. Goldberg, J.M. and C. Fernandez. Physiology of Peripheral Neurons Innervating Semicircular Canals of the Squirrel Monkey. III. Variations Among Units in Their Discharge Properties. J. Neurophysiol. 34: (4) 676-684; 1971.

17. Hixson, W. C., J.I. Niven, and M.J. Correia. Kinematics Nomenclature for Physiological Accelerations with Special Reference to Vestibular Applications. NASA Monograph 14; 1966.

18. Keller, E.L. Behavior of Horizontal Semicircular Canal Afferents in Alert Monkey During Vestibular and Optokinetic Stimulation. Exp. Brain Res. 24: 459-471; 1976.

19. Kisberger, S.G. and T.A. Pavelko. Vestibular Signals Carried by Pathways Subserving Plasticity of the Vestibulo-Ocular Reflex in Monkeys. J. Neurosci. 6: (2) 346-354; 1986.

20. Kozlovskaya, I.B., V.A. Barmin, V. Yu. Kreidich, and A.A. Repin. The Effects of Real and Simulated Microgravity on Vestibulo-Oculomotor Interaction. Physiologist 28: (6); 1985.

21. Kozlovskaya, I.B., I.F.Aslanova, V.A. Barmin, L.S. Grigorieva, G.I. Gevlich, A.V. Kirenskaya, and M.G. Sirota. The Nature and Characteristics of a Gravitational Ataxia. Physiologist 26: (6); 1983.

22. Kozlovskaya, I.B., Yu. V. Kreidich, V.S. Oganov, and O.P.Koserenko. Pathophysiology of Motor Functions in Prolonged Manned Space Flights. Acta Astronautica 8: (9-10) 1059-1072; 1981.

23. Kozlovskaya, I.B., E.A. Ilyin, M.G. Sirota, V.I. Korolkov, B.M. Babayev, I.N. Beloozerova, and S.B.Yakushin. Studies of Space Adaptation Syndrome in Experiments on Primates Performed on Board of Soviet Biosatellite "Cosmos-1887". Physiologist 32: (1); 1989.

24. Landolt, J.P. and M.J. Correia. Neurodynamic Response Analysis of Anterior Semicircular Canal Afferents in the Pigeon. J. Neurophysiol. 43: 1746; 1980.

25. Lisberger, S.G. and T.A. Pavelko. Vestibular Signals Carried by Pathways Subserving Plasticity of the Vestibulo-Ocular Reflex in Monkeys. J. Neurosci. 6: (2) 346-354; 1986.

26. Louie, A.W. and J. Kimm. The Response of 8th Nerve Fibers to Horizontal Sinusoidal Oscillation in the Alert Monkey. Exp. Brain Res. 24: 447-457; 1976.

27. Morasso, P., E. Bizzi, and J. Dichgans. Adjustment of Saccade Characteristics During Head Movements. Exp. Brain Res. 16: 492-500; 1973.

28. Miles, F.A. and D.J. Braitman. Long-Term Adaptive Changes in Primate Vestibulo-Ocular Reflex. II. Electrophysiological Observations on Semicircular Canal Primary Afferents. J. Neurophysiol. 43: (5) 1426-1436; 1980.

29. Miles, F.A. and B.B. Eighmy. Long-term Adaptive Changes in Primate Vestibulo-Ocular reflex. I. Behavioral Observations. J. Neurophysiol. 43: (5) 1406-1425; 1980.

30. Miles, F.A. and Braitman, D.J. Long-Term Adaptive Changes in Primate Vestibulo-Ocular reflex. II. Electrophysiological Observation on Semicircular Canal Primary Afferents. J. Neurophysiol. 43: (5) 1426-1436; 1980.

31. Miles, F.A., J.H. Fuller, D.J. Braitman, and B.M. Dow. Long-Term Adaptive Changes in Primate Vestibulo-Ocular Reflex. III. Electrophysiological Observations in Flocculus of Normal Monkeys. J. Neurophysiol. 43: (5) 1437-1476; 1980.

32. Miles, F.A., D.J. Braitman, and B.M. Dow. Long-Term Adaptive Changes in Primate Vestibulo-Ocular Reflex. IV. Electrophysiological Observation in Flocculus of Adapted Monkeys. J. Neurophysiol. 43: (5) 1477-1493; 1980.

33. Perachio, A.A. and M.J. Correia. Responses of Semicircular Canal and Otolith Afferents to Small Angle Static Head Tilts in the Gerbil. Brain Res. 280: 287-298; 1983.

34. Schneider, L.W. and D.J. Anderson, Transfer Characteristics of First and Second Order Lateral Canal Vestibular Neurons in Gerbil. Brain Res. 112: 61; 1976.

35. Sirota, M.G., B.M. Babaev, I.N. Beloozerova, A.N. Nyrova, S.B. Yakushin, and I.B. Kozlovskaya. Neuronal Activity of Nucleus Vestibularis During Coordinated Movement of Eyes and Head in Microgravitation. Physiologist 31: (1); 1988.

36. Sirota, M.G., B.M. Babayev, I.B. Beloozerova, A.N. Nyrova, S.B Yakushin, I.B. Kozlovskaya. Characteristics of Vestibular Reactions to Canal and Otolith Stimulation at an Early stage of Exposure to Microgravity. Physiologist 30: (1); 1987

37. Thorson, J. and M. Biderman-Thorson. Distributed Relaxation Processes in Sensory Adaptation: Spatial Non-uniformity in Receptors Can Explain Curious Dynamic Logarithmic Statistics of Adaptation. Science 183,161-172,1974.

TABLE 1

Mean gain (g) and phase (ϕ) for horizontal canal afferent responses to sum of sinusoidal yaw rotation. Gain units are spikes/s per °/s and phase angles are in units of degrees; positive phase values indicate phase lead re velocity. Mean, SEM and number of afferents tested are presented for pre-flight/control, post-flight day 1 tests and post-flight days 4-5 tests. The results presented for post-flight days 1, 4 and 5 were obtained from the two flight monkeys 782 & 2483.

Frequency (Hz)	0.0293		0.0879		0.2051		0.3809		0.9083		1.7873	
Gain(g); Ph.(ϕ)	g	ϕ	g	ϕ	g	ϕ	g	ϕ	g	ϕ	g	ϕ
Pre./Contrls.												
Mean	0.34	44.5	0.44	28.0	0.51	18.4	0.58	19.2	0.66	21.7	0.79	28.5
SEM	0.04	4.46	0.05	3.58	0.06	3.00	0.08	3.87	0.10	3.45	0.14	4.56
Afferents	10	10	10	10	10	10	10	10	10	10	10	10
Po. Flt. Day 1.												
Mean	0.51	54.3	0.76	33.2	0.97	27.7	1.11	26.9	1.42	30.9	1.73	41.7
SEM	0.06	1.96	0.11	5.85	0.14	6.79	0.23	9.88	0.37	10.1	0.51	11.2
Afferents	3	3	3	3	3	3	3	3	3	3	3	3
Po. Flt.Days 4-5												
Mean	0.35	53.8	0.60	28.7	0.69	29.0	0.84	26.1	1.02	31.0	1.26	38.5
SEM	0.10	13.1	0.26	12.9	0.28	7.81	0.40	7.13	0.51	7.63	0.63	7.97
Afferents	3	3	3	3	3	3	3	3	3	3	3	3

TABLE 2

A summary of the tests and statistics for pre-flight and for certain post flight days. All data are for horizontal semicircular canal primary afferents. The results presented for post-flight days 1, 2, 4, and 5 were obtained from the two flight monkeys. Frequency of firing is presented in parentheses and in the column summarizing the results from tests during post-flight day 2, the frequency of firing and CV values that are presented in brackets represent the mean values after the removal of one discrepant value.

Statistics and tests	Pre- and post-flight controls		Post-flight day 1		Post-flight day 2		Post-flight days 4-5	
Spontaneous firing (ISI, ms)								
MEAN (freq, I/s)	10.83 (92)		10.48 (95)		12.35 (81) [93]		10.99 (91)	
SEM	2.01		0.90		1.58		1.56	
# Afferents	29		7		4		6	
CV								
Mean	0.14		0.09		0.15 [0.14]		0.11	
SEM	0.02		0.02		0.07		0.04	
# Afferents	29		7		4		6	
Single sine (0.2051 Hz, 60°/s)								
GAIN								
Mean	0.56		1.02		0.48		0.83	
SEM	0.14		0.24		0.06		0.05	
# Afferents	26		7		3		4	
PHASE								
Mean	14.8		23.8		25.9		26.8	
SEM	6.7		4.1		4.3		5.0	
# Afferents	26		7		3		4	
Step (2 pulses, 60°/s)								
GAIN	Fac.	Inh.	Fac.	Inh.	Fac.	Inh.	Fac.	Inh.
Mean	0.47	0.40	0.78	0.83	0.77	0.64	0.97	0.84
SEM	0.06	0.05	0.15	0.12	0.01	0.04	0.32	0.30
# Afferents	20		6		2		3	
TIME CONSTANT	Fac.	Inh.	Fac.	Inh.	Fac.	Inh.	Fac.	Inh.
Mean	6.11	5.18	3.57	3.43	5.23	4.47	4.12	3.81
SEM	0.50	0.76	0.63	0.62	3.80	1.16	0.79	0.41
# Afferents	20		6		2		3	

TABLE 3

Mean interspike interval, standard deviation and coefficient of variation for horizontal canal afferents tested during pre-flight and control studies, during post-flight day 1 and post-flight day 2 .

Segment	20° up		Std. Pos.		20° Dwn.		Std. Pos.	
Measures	ISI	CV	ISI	CV	ISI	CV	ISI	CV
Pre./Conts.								
Mean	11.0	0.22	11.2	0.26	12.3	0.27	11.6	0.25
SEM	1.19	0.06	1.19	0.07	1.93	0.09	1.13	0.06
Afferents	14	14	14	14	14	14	14	14
Po. Flt. Day 1.								
Mean	9.95	0.17	9.81	0.17	9.92	0.17	9.54	0.17
SEM	1.86	0.07	1.97	0.07	1.93	0.07	1.67	0.07
Afferents	2	2	2	2	2	2	2	2
Po. Fl. Day 2								
Mean	25.9	0.68	31.4	0.75	26.4	0.7	-	-
SEM	0.88	0.07	0.6	0.08	2.29	0.06	-	-
Afferents	2	2	2	2	2	2	-	-

TABLE 4

PRE-FLIGHT VESTIBULAR PRIMARY AFFERENT (VPA) TEST PROTOCOLS	
Horizontal Ampullary Afferents	Vertical Ampullary Afferents
1. Spontaneous Rate - standard position (static; duration 60s)	1. Spontaneous rate (same as #1)
2. Pulse - standard position (2 alternating pulses - yaw amplitude - ±60°/s; duration -30s; profile - positive velocity step ($+\omega_Z$)-constant velocity-return to zero velocity-negative velocity step ($-\omega_Z$)	2. Pulse - left ear down (same as #2, but change yaw to pitch)
3. Trapezoid - standard position (2 alternating trapezoids - yaw acceleration ± 12°/s^2; profile - ramp accel. duration 10s; constant velocity 60s, ramp decel. duration 10 s, rotator stationary 60 s (repeat but with reversed signs)	3. Single Sine - left ear down (same as #2, but change yaw to pitch)
4. Single Sine - standard position (4 cycles, 0.2051 Hz; yaw amplitudes ±20,40 and 60°/s. Cosine bell ramp up and ramp down; bell duration 10 s)	4. Sum of Sines - left ear down (same as #2, but change - 60°/s to 40–/s)
5. Sum of Sines - standard position (3 cycles, 6 freq. (in Hz) 0.0293, 0.0879, 0.2051, 0.3809, 0.9083, 1.7873; yaw amplitude ±30 °/s. Cosine bell ramp up and ramp down; bell duration 10 s)	5. Single Sine - standard position (4 cycles, pitch amplitude -±20°, 0.0879 Hz)
6. Tilt Test - (2 alternating trapezoids - protocol - standard position 10s, tilting duration 5 s, pitch up amplitude 20°-duration - 60s, return to standard position-60s, pitch down amplitude 20°-duration - 60s)	6. Sum of Sines - standard position (3 cycles, pitch ±20°, 4 freq. 0.0293, 0.0879, 0.2051, 0.3809)
OVAR 1 (rotatory axis tilted 30° off - Earth vertical; 2 alternating pulses; yaw amplitude ±10°/s, duration 36s)	
OVAR 2 (rotatory axis tilted 30°off - Earth vertical, monkey tilted 15° relative to rotatory axis, 2 alternating pulses - yaw amplitude ±10°/s, duration 36s)	
METHODS	
Action potentials measured using etched tungsten wire insulated with Epoxylite. Electrode impedance 5-10 MΩ. Amplification (x100) using Grass P-15 amplifier (x10) followed by WPI DRAM amplifier (x100). System bandpass 300-10k Hz.	

TABLE 5

PRE-FLIGHT ELECTRO-OCULOGRAM (EOG) TEST PROTOCOL

1. HOKN - standard position (2 alternating pulses - yaw amplitude ±45°/s; duration 60s)
2. VOKN - left ear down (2 alternating pulses pitch amplitude ±45°/s; duration 60s)
3. HVOR SINGLE SINE - standard position (4 cycles, 0.2051 Hz; yaw amplitudes±60°/s, 40°/s and 20°/s)
4. HVOR SUM OF SINES - standard position (3 cycles, 6 freq. (in Hz) .0293, 0.879, .2051, 0.3809, .9083, 1.7873; amplitude ±30°/s)
5. HVOR TRAPEZOIDS - standard position (2 alternating trapezoids - yaw acceleration ±12°/s^2; - duration 10s)
6. HVOR STEPS - standard position (2 alternating pulses - yaw amplitude ±60°/s; duration 60s)
7. VVOR SINGLE SINE - left ear down (same as #3)
8. VVOR SUM OF SINES - left ear down (same as #4)
9. VVOR TRAPEZOIDS - left ear down (same as #5)
10. VVOR STEPS - left ear down (2 alternating pulses - pitch amplitude ± 60°/s duration 60s)
11. HVOR HAR (2 alternating pulses - yaw amplitude ±60°/s; duration 90s)
12. HOKN - standard position (same as #1)
13. VOKN - standard position (same as #2)

TABLE 6

POST-FLIGHT VESTIBULAR PRIMARY AFFERENT (VPA) TEST PROTOCOLS	
Horizontal Ampullary Afferents	Vertical Ampullary Afferents
1. Spontaneous Rate - standard position (static; duration 30s	1. Spontaneous rate (same as #1)
2. Pulse - standard position (2 alternating pulses - yaw amplitude - ±60°/s; duration -30s separated by 15 s at zero vel.)	2. Step - left ear down (same as #2, but change yaw to pitch)
3. Single Sine - standard position (4 cycles, 0.2051 Hz; yaw amplitude ±60°/s. Cosine bell ramp up and ramp down bell duration 10 s)	3. Single Sine - left ear down (same as #2, but change yaw to pitch)
4. Sum of Sines - standard position (3 cycles, 6 freq. (in Hz) 0.0293, 0.0879, 0.2051, 0.3809, 0.9083, 1.7873; yaw amplitude ±30 °/s. Cosine bell ramp up and ramp down; bell duration 10 s)	4. Sum of Sines - left ear down (same as #2, but change ±60°/s to 40°/s)
5. Tilt Test - (2 alternating trapezoids - protocol - standard position 10s, tilting duration 5 s, pitch up amplitude 20°-duration - 30s, return to standard position-30s, pitch down amplitude 20°-duration - 30s)	5. Single Sine - standard position (4 cycles, pitch amplitude ±20°, 0.0879 Hz)
	6. Sum of Sines - standard position (3 cycles, pitch ±20°, 4 freq. 0.0293, 0.0879, 0.2051, 0.3809)
1. OVAR 1 (rotatory axis tilted 30° off Earth vertical; 2 alternating pulses; yaw amplitude ±10°/s, duration 36s)	
2. OVAR 2 (rotatory axis tilted 30° off Earth vertical, monkey tilted 15°relative to rotatory axis, 2 alternating pulses - yaw amplitude ±10°/s-, duration 36s)	
METHODS	
Same as listed in Table 4	

TABLE 7

POST-FLIGHT ELECTRO-OCULOGRAM (EOG) TEST PROTOCOL

1. HOKN - standard position (2 alternating pulses - yaw amplitude ±45°/s; duration 60s)
2. VOKN - left ear down (2 alternating pulses - pitch amplitude ±45°/s; duration 60s)
3. Spontaneous Nystagmus - standard position (static; duration 30s)
4. HVOR STEPS - standard position (2 alternating pulses - yaw amplitude ±60°/s; duration 60s)
5. HVOR STEPS +45° nose up (same as #4)
6. HVOR STEPS -45° nose down (same as #4)
7. HVOR SUM OF SINES -standard position (3 cycles, 6 freq. (in Hz) .0293, .0879, .2051, .3809, .9083, 1.7873; amplitude $^{\pm}$30 °/s)
8. HVOR HAR (2 alternating pulses - yaw amplitude ±60°/s; duration 90s)
9. Positional Nystagmus - right ear down position (static; duration 30s)
10. Positional Nystagmus - left ear down position (static; duration 30s)
11. VVOR STEPS - left ear down (2 alternating pulses - pitch amplitude ±60°/s; duration 60s)
12. VVOR SUM OF SINES - left ear down (same as #7, but pitch amplitude attenuated 10dB)
13. HOKN - standard position (same as #1)
14. VOKN - left ear down (same as #2)

METHODS
Same as listed in Table 4

TABLE 8

POST FLIGHT STUDIES
Detailed Testing Schedule
9/29/89 - 10/7/89

_ Animals landing reported to be 6:00 A.M. 9/29/89

_ 1st test at 8:30 P.M. (14.5 hr. post landing)

_ Monkey *2483* (tested 8:30 P.M. - 11:35 P.M., 9/29/89) Day 1

_ Monkey *782* (tested 12:52 A.M. - 3:46 A.M., 9/30/89) Day 1

_ Monkey *782* (tested 5:29 P.M. - 9:30 P.M., 9/30/89) Day 2

_ Monkey *2483* (tested 9:41 P.M. - 12:41 A.M., 9/30/89) Day 2

_ Monkey *2483* (tested 3:15 P.M. - 6:30 P.M., 10/2/89) Day 4

_ Monkey *782* (tested 7:06 P.M. - 10:30 P.M., 10/2/89) Day 4

_ Monkey *782* (tested 11:23 A.M. - 2:30 P.M., 10/3/89) Day 5

_ Monkey *2483* (tested 2:50 P.M. - 5:50 P.M, 10/3/89) Day 5

_ Monkey 2592 (10/4/89) Day 6

_ Monkey 774 (10/4/89) Day 6

_ Monkey 774 (10/5/89) Day 7

_ Monkey 2592 (10/5/89) Day 7

_ Monkey 774 (10/5/89) Day 7

_ Monkey 774 (10/6/89) Day 8

_ Monkey *2483* (10/7/89) Day 9

_ Monkey *782* (10/7/89) Day 9

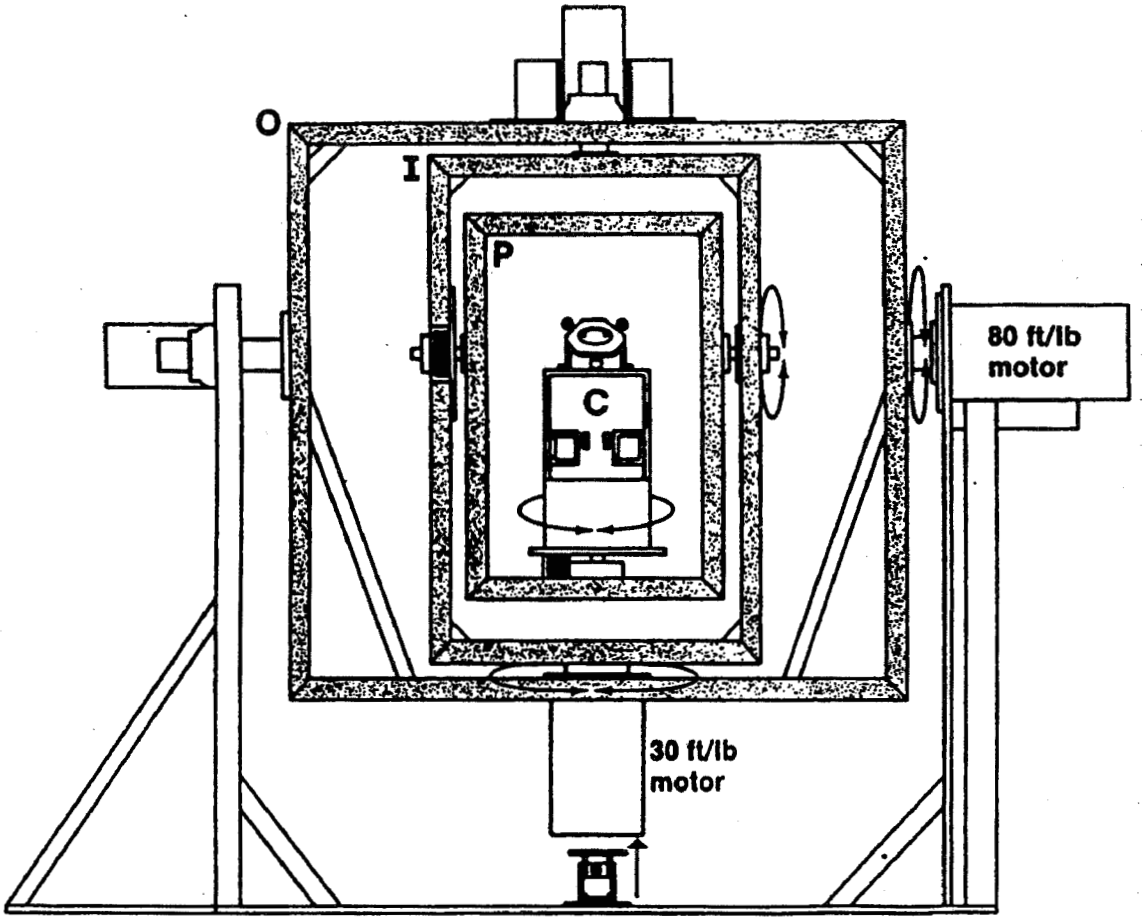

Figure 1. A schematic drawing of the multi-axis rotator. (O) outer gimbal, (I) inner gimbal, (P) positioning axis, (C) animal carrier.

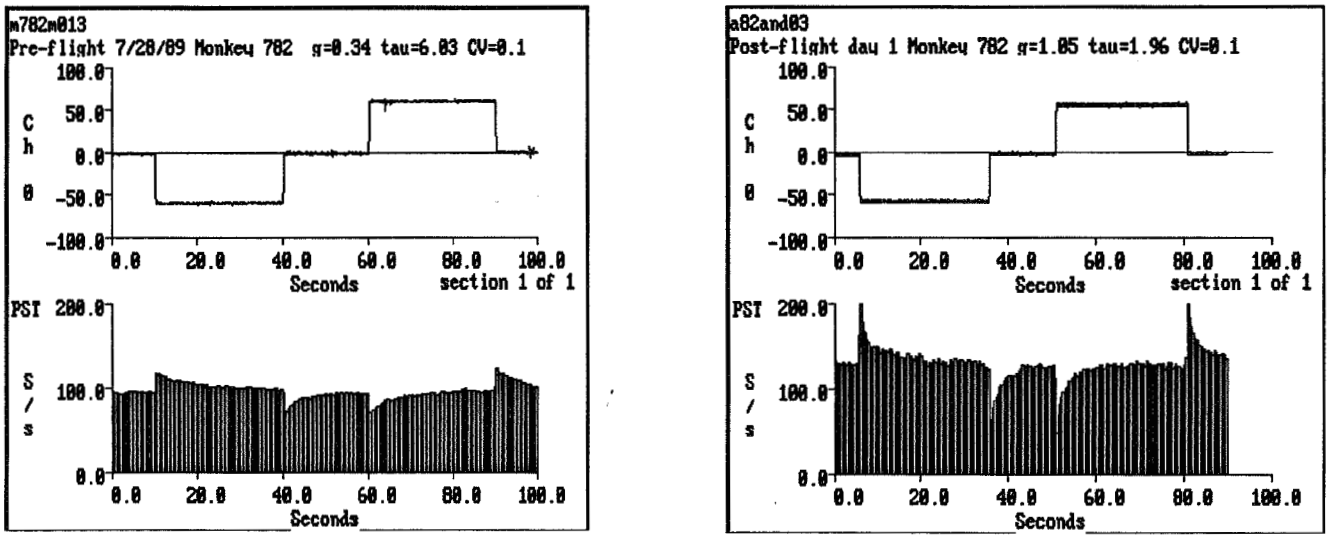

Figure 2. (Left) A post stimulus time histogram of the binned response of a horizontal semicircular canal afferent of one of the flight monkeys recorded during pre-flight pulse rotation tests. The top panel is the rate gyro signal and the bottom panel is the post stimulus time histogram. (Right) A post stimulus time histogram of the binned response of a horizontal semicircular canal afferent of the same flight monkey (as in the figure on the left) recorded during post-flight tests.

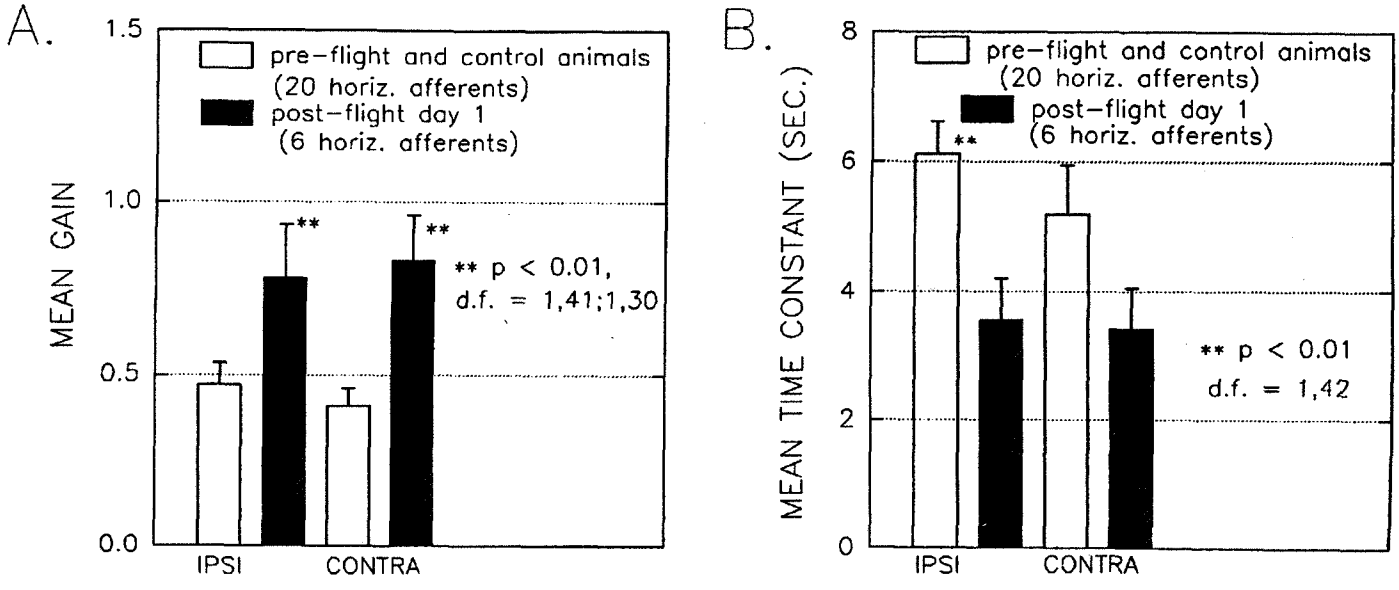

Figure 3. Bar graphs illustrating the difference between gain (A) and time constants (B) for horizontal primary afferents' responses to pulse yaw rotations.

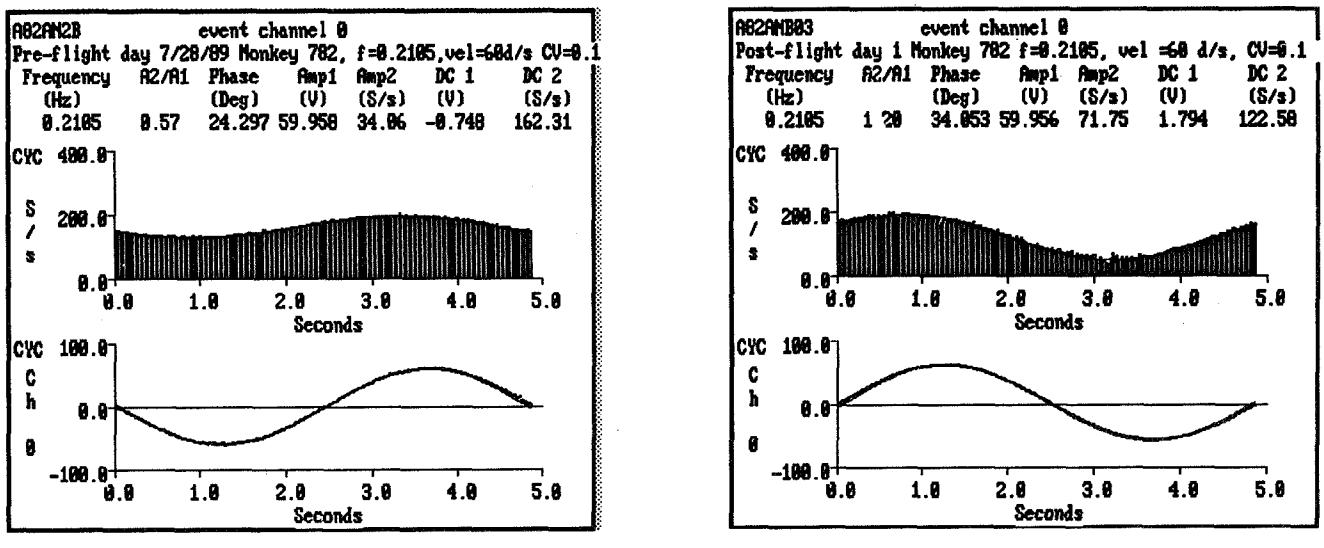

Figure 4. (Left) - Representative response of a horizontal canal afferent from Monkey 782 during pre-flight tests. Top panel is cycle histogram formed from responses to 4 cycles of stimulation at f=0.2051 Hz, $w_Z = \pm 60°/s$. Bottom panel is a rate gyro trace. Gain and phase values (presented at top of graph) were derived by fitting a sine wave through the digitized data points of the rate gyro (velocity) signal and through the value of each bin of the cycle histogram. Gain = peak amplitude of the response curve/peak amplitude of stimulus curve. Phase = difference between peak of the stimulus curve - the peak of the response curve. Phase is given in degrees and is defined so that a positive phase angle indicates a phase lead of the binned histogram fit re the velocity signal. (Right) - Representative response of a horizontal canal afferent from Monkey 782 during post-flight tests.

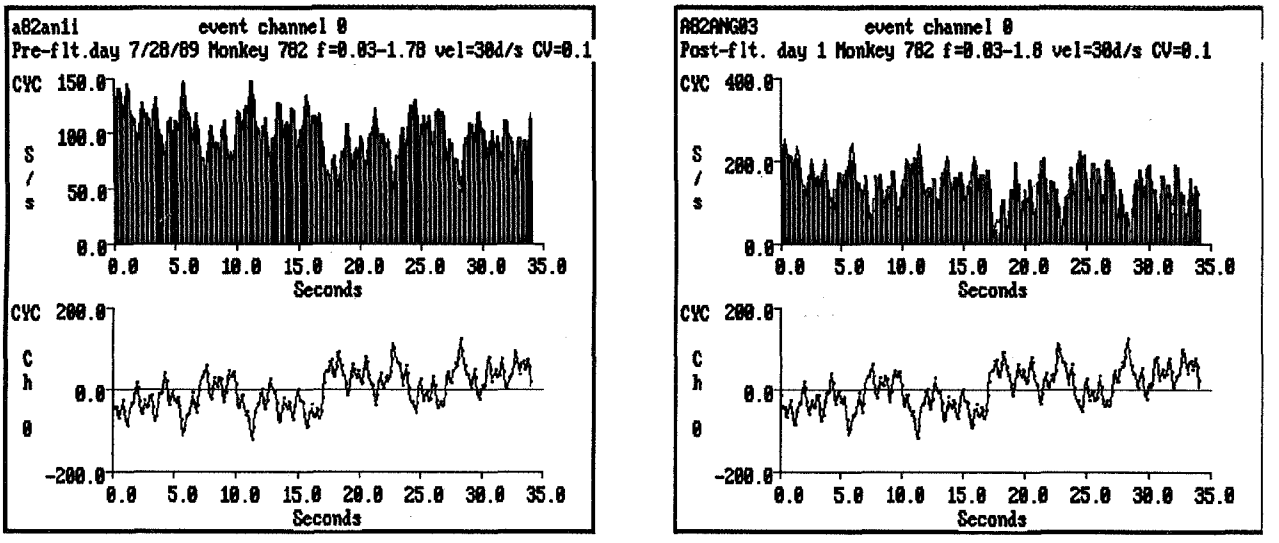

Figure 5. Two representative afferent responses during pre- and post-flight tests. Stimulation consisted of a sum of 6 sinusoids ranging from 0.0293 to 1.78 Hz. The amplitude of each component was 30°/s. Curves were fit through the stimulus and response traces and gain and phase were calculated as for single sines. (Left)- Top panel - cycle histogram (3 cycles of sum of sines presentations). Bottom panel - rate gyro trace. This panel represents a response from an afferent during pre-flight testing. (Right) - The response from an afferent tested on post flight day 1. Note that the cycle histogram scale in this figure is different than the figure on the left.

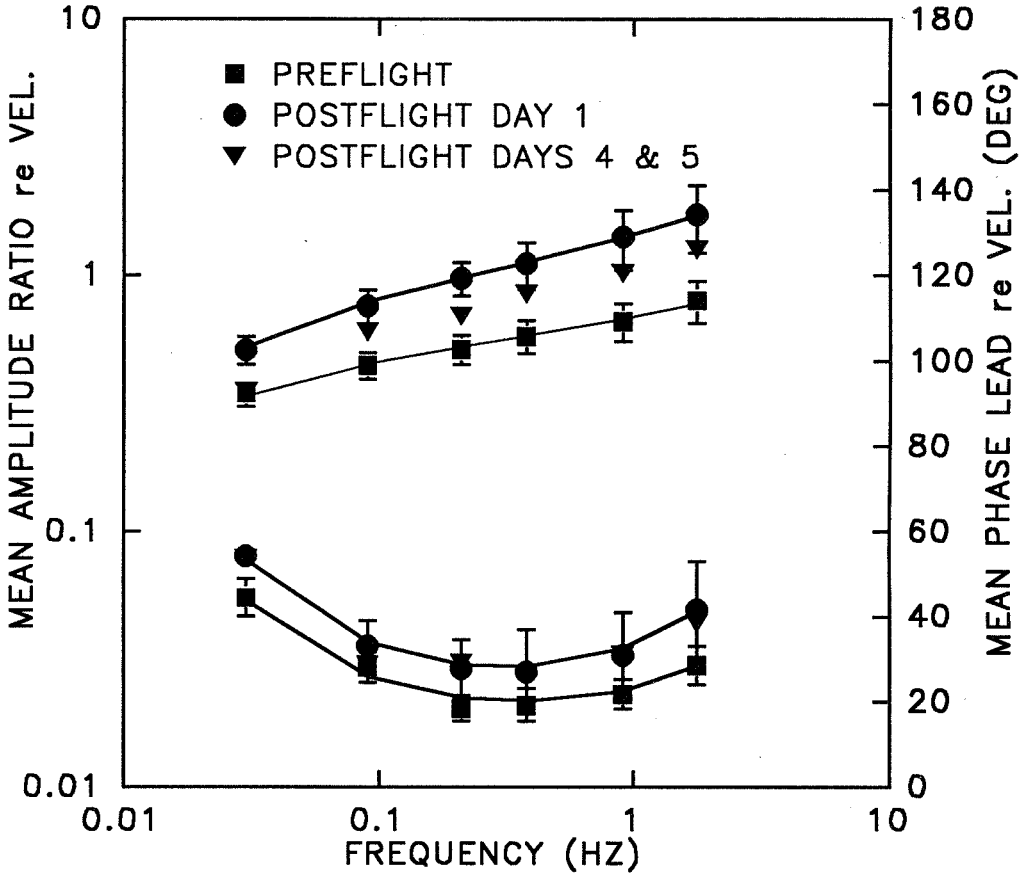

Figure 6. A plot of the mean (±SEM) gain and phase for 10 horizontal canal afferents tested during pre-flight studies and during control studies; 3 horizontal canal afferents tested on post-flight day 1 and 3 horizontal canal afferents tested on post-flight days 4-5. All afferents tested on post-flight days were from flight monkeys. The solid lines are an evaluation of the transfer function of the form :

$$H(s) = G(s)^{k+1} \frac{\tau_V s+1}{\tau_L s+1}$$

The parameter G is frequency independent gain; k is a fractional operator, that represents neural adaptation; tV is a zero that represents cupula velocity and tL is a pole that represents the cupula time constant. The best fit values for these parameters were found to be: Pre-flight and controls - G = 4.89, k = 1.16, t_V = 0.02, t_L = 9.64; Post-flight day 1 - G = 7.82, k = 1.23, t_V = 0.03, t_L = 8.51.

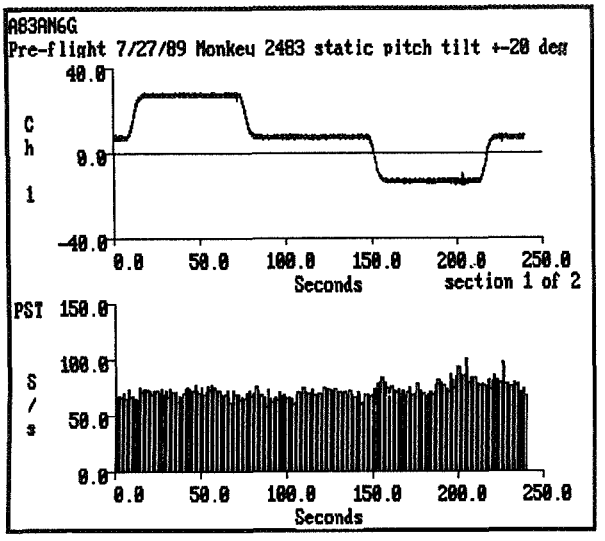

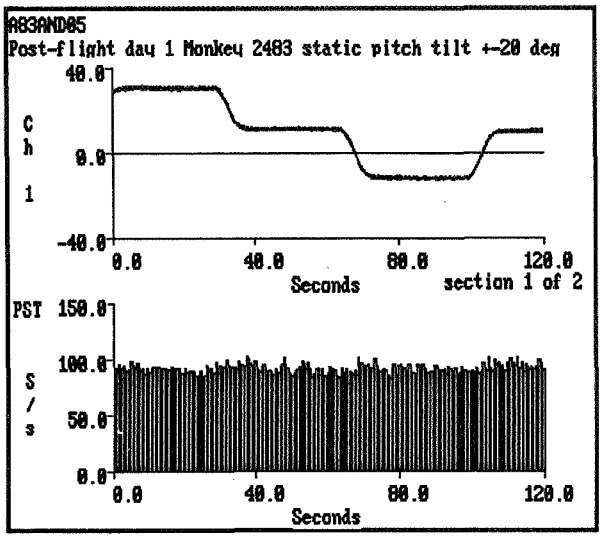

Figure 7. Responses from flight monkey 2483 during pre- (Left) and post- (Right) flight tilt sensitivity tests. The top trace in each figure represents tilt. The bottom trace in each figure is a post stimulus time histogram. The tilt sequence was tilt up 20°, standard position, tilt down 20°, standard position. Interspike interval histograms were formed from the action potential trains during the last 20 sec of each segment and the mean interspike interval and coefficient of variation was calculated. During the standard position segment, the mean ISI and CV for the afferent illustrated in figure 7 (Left) were 10.39 and 0.37 and for the afferent illustrated on the right were 11.78 and 0.25.

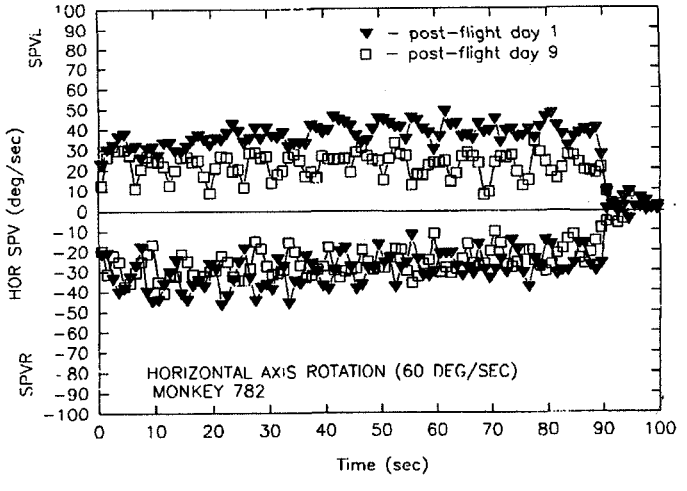

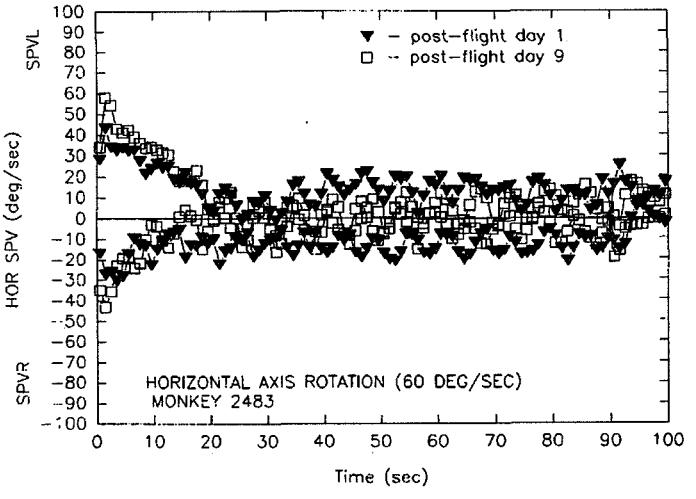

Figure 8. Horizontal axis rotation for both flight monkeys; monkey 782 in left graph and 2483 in the right graph. Slow phase eye velocity is compared during 90 sec. of rotation for tests on post-flight day 1 (inverted filled triangles) and post-flight day 9 (open squares).

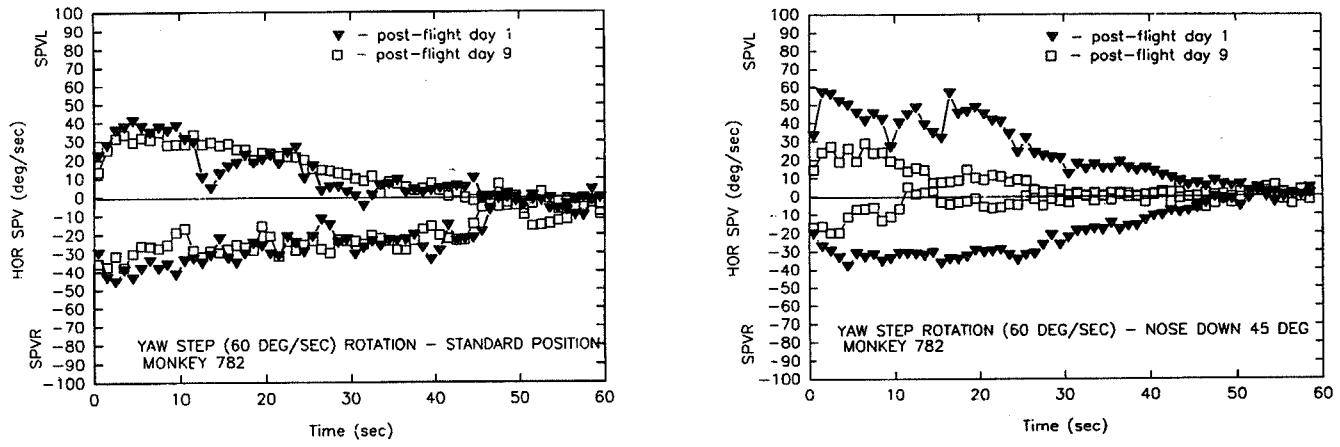

Figure 9. Horizontal slow phase eye velocity measured in flight monkey (782) on post-flight day 1 and post-flight day 9 with his head in the standard position (left panel) and with his head pitched 45° down relative to the plane of rotation (right panel).

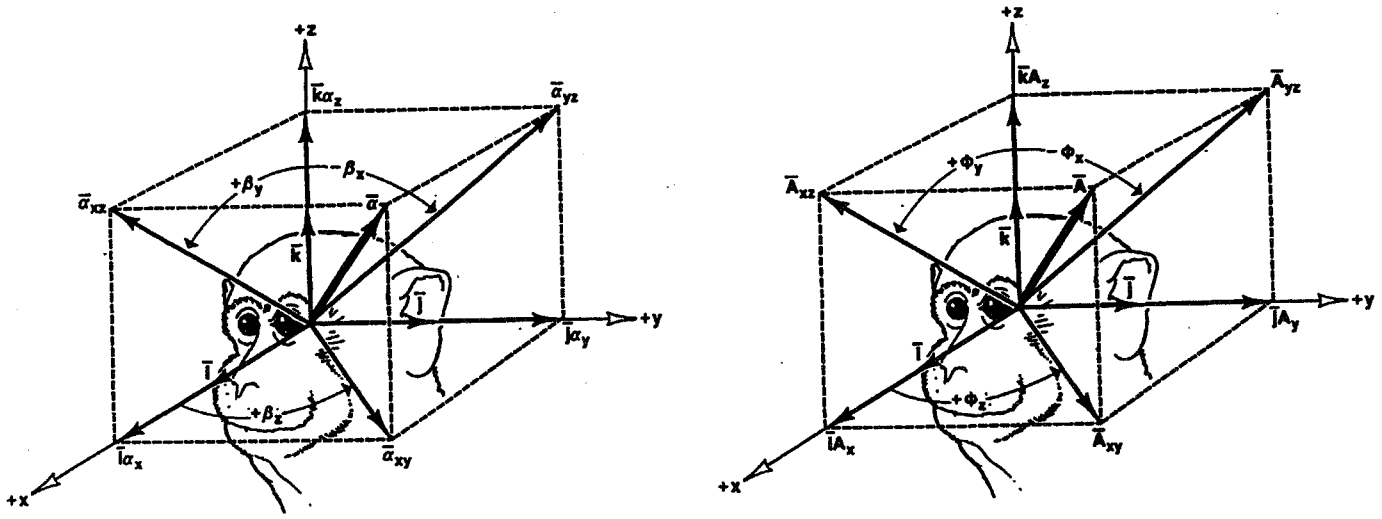

Figure 10. A head based coordinate reference system and vectors representing a kinematics acceleration nomenclature. The figure on the left shows angular accelération (a) vectors and the figure on the right shows linear acceleration (A) vectors. Vectors representing the mathematical derivatives or integrals (e.g. angular velocity; w) can be substituted for the acceleraton vectors.

Page intentionally left blank

S21-51
51366

EXPERIMENT K-7-33

FUNCTIONAL NEUROMUSCULAR ADAPTATION TO SPACEFLIGHT

Principal Investigator:

V. R. Edgerton
University of California
Los Angeles, CA

Co-Investigators:

S. Bodine-Fowler
J. A. Hodgson
R. R. Roy
University of California
Los Angeles, CA

I.B. Kozlovskaya
Institute of Biomedical Problems
Moscow, USSR

Page intentionally left blank

EXPERIMENT K-7-33

FUNCTIONAL NEUROMUSCULAR ADAPTATION TO SPACEFLIGHT

V. R. Edgerton, S. Bodine-Fowler, J.A. Hodgson, I.B. Kozlovskaya and R.R. Roy

The following data were collected from two Rhesus monkeys (782 and 2483) that were flown aboard a 14-day biosatellite mission (COSMOS 2044). The proposed study was designed to determine the effects of the absence of weight support on flexor and extensor muscles of the hindlimb. These effects were assessed morphologically and biochemically from muscle biopsies taken from a slow extensor, the soleus; a fast extensor, the medial gastrocnemius; and a fast flexor, the tibialis anterior. A second objective of this study was to determine the relative importance of activity (as determined by intramuscular electromyography, and force (as determined by joint torque) on the adaptation of muscle.

ELECTROMYOGRAPHIC RECORDINGS

Electromyographic Analysis

Pre- and postflight electromyograms (EMGs) were analyzed using amplitude histograms, scatterplots and joint probability density distributions of rectified, smoothed electromyograms (EMGs). Of the two flight animals (782 and 2483), only animal 782 provided a complete data set from all three implanted muscles (soleus, medial gastrocnemius and tibialis anterior). The soleus and medial gastrocnemius EMGs on the remaining flight animal and two control animals appeared defective in the postflight recording.

Activity of the tibialis anterior muscles appeared to be unchanged after flight. In monkey 782, the amplitude of soleus EMG was reduced after spaceflight and medial gastrocnemius EMG amplitude was elevated after spaceflight. Two weeks after flight the medial gastrocnemius amplitude had declined to normal values but recovery of soleus was incomplete. Figure 1 shows joint probability density distributions of soleus and medial gastrocnemius amplitudes preflight and on several days following the flight. The preflight distribution shows high probabilities along the soleus axis and along an approximate diagonal. Three days after recovery (Fig 1, 10-2), the distribution had moved away from the soleus axis, soleus amplitudes were lower and there was a greater probability of higher medial gastrocnemius amplitudes than in the preflight tests. Eight days after recovery (Fig 1, 10-7) the distribution had moved closer to the soleus axis although the soleus amplitudes were still low. Ten days after recovery (Fig 1, 10-9) most of the high probabilities once more lay along the soleus axis but the soleus amplitude had still not returned to preflight values. The amplitude of the medial gastrocnemius EMG appears to decline throughout the sequence of measurements taken after flight. Figure 2 illustrates the relationship between soleus and tibialis anterior activity. The distributions reflect the diminished amplitude of soleus after flight and the unchanged amplitude of tibialis anterior. Figure 3 shows similar distributions for the tibialis anterior and medial gastrocnemius.

Interpretation of results

The small number of animals studied after spaceflight preclude drawing any major conclusions for the present. The tibialis anterior muscle activities in both animals appeared to be unchanged after spaceflight. There were, however noticeable changes in the utilization of the soleus and medial gastrocnemius muscles which, if confirmed may have important consequences both in our understanding of basic motor mechanisms and on the ability to perform accurate movements during spaceflight or on return to a gravitational field. In the one animal where soleus and medial gastrocnemius EMG electrodes were still intact after flight, there appeared to have been a change in the recruitment patterns of the two muscles after spaceflight which took more than two weeks to return to normal values. Following spaceflight, the soleus muscle appeared to be used somewhat less than normal whereas the medial gastrocnemius muscle exhibited increased activity, possibly to compensate for the lower activity in soleus. The joint probability distribution shows that the two muscles are still coordinated in a similar manner but that the relative contribution of the two muscles has changed. One cause of a redistribution of activity between soleus and medial gastrocnemius may be the reduction of activity in Vestibulospinal pathways arising from otolith organs. This pathway normally excites motoneurons innervating the slow motor units of extensor muscles and any reduction in its activity may result in lower activities in slow motor units which predominate in the soleus muscle. It is possible that in a two week flight the nervous system readjusts patterns of muscle recruitment to compensate for lower soleus activity and that this takes some time to return to normal after flight.

MUSCLE BIOPSIES

Methods

Preflight muscle biopsies were taken from the soleus (SOL), medial gastrocnemius (MG) and tibialis anterior (TA) muscles of 11 flight candidate monkeys in June, 1989. Postflight biopsies were taken from those same muscles in the 2 flight monkeys (2483, 782) and 5 control monkeys (2471, 839, 2442, 543 and 2587) in which preflight biopsies had been taken. The postflight biopsies were taken on September 30, 1989 at approximately 3 pm (~ 39 hours after landing).

Muscle biopsies were taken from 2 independent sites with a Bergstrom needle with an outer diameter of 3mm. The biopsies weighed approximately 8-14 mg. For each of the biopsies, mean fiber cross-sectional area and succinate dehydrogenase (SDH) activity have been measured. The activity of SDH was determined in 10μm sections in a medium containing 100 mM phosphate buffer (pH=7.6), 0.15 M sodium azide, 0.30 M 1-methoxy-phenazine methylsulfate, 1.5 mM nitroblue tetrazolium, 5 mM EDTA-disodium salt and 58 mM succinate. The sections were analyzed using an image processing system.

Interpretation of Results

The results for the SOL, MG and TA are given in Tables 1-3. In the SOL and MG of both flight monkeys, the mean cross-sectional area of fibers taken from postflight biopsies were significantly larger than fibers from preflight biopsies. This growth in fiber size paralleled the growth observed in control monkeys of the same age and size (Figures 4 and 5). Muscle fibers in the postflight biopsies of the TA, however, were significantly smaller than preflight biopsies (Figure 6). Figure 7-9 show the distribution of fiber sizes in the pre and postflight biopsies if the SOL, MG and TA of flight monkey 782. Note the shift towards larger sizes in the SOL and MG and a shift towards smaller sizes in the TA.

The data from the control monkeys appears to suggest that the TA, a flexor muscle, may be maturing faster than the SOL and MG, which are extensor muscles. Further studies are needed to evaluate the growth and maturation of flexor and extensor hindlimb muscles in the Rhesus.

The mean SDH activity of the muscle fibers from pre and postflight biopsies were not significantly different in the SOL. Although the postflight values are not significantly different from the preflight values, they are significantly different from the postflight values in the controls (Table 1 and Figure 10). The mean SDH activity was decreased in the postflight biopsies from the MG and TA (Table 2-3, Figures 11-12).

The apparent differences in the response of the SOL, MG and TA in rats versus Rhesus monkeys to space flight may be related to the manner in which the animals are restrained and/or the possibility that the monkeys are doing some exercise with their unrestrained foot. These data emphasize the importance of defining the effects of several variables inherent in the flight protocol which can affect the morphological and biochemical responses of muscle. Definition of the impact of these variables will significantly contribute to our understanding of the etiology of muscle adaptation to spaceflight.

The questions which need to be addressed in ground base studies are:

1. What is the rate growth and maturation in flexors and extensors, are they similar? Does the training protocol affect the normal growth rate?
2. What are the effects of different periods of semi-restraint in the primate chair?
3. Is the effect of semi-restraint the same at 0 and 1 G?
4. Are the levels and kinds of adaptations to spaceflight similar in fast and slow flexor and extensor muscles

TABLE 1

SOLEUS
FIBER CROSS-SECTIONAL AREA (μm^2)

MONKEY	GROUP	n	MEAN	SEM
782	pre	52	1767	90
	post	37	3175	187
2483	pre	119	1993	54
	post	91	3464	122
2471	pre			
	post	41	3866	170
839	pre	54	2608	141
	post	24	3448	121
2442	pre	45	3510	156
	post	31	5420	312
2587	pre	23	2996	212
	post	21	3270	214

SOLEUS
SDH ACTIVITY (optical density/min)

MONKEY	GROUP	n	MEAN	SEM
782	pre	52	.0274	.0011
	post	37	.0278	.0018
2483	pre			
	post	37	.0281	.001
2471	pre			
	post	41	.0515	.0014
839	pre	54	.0192	.0012
	post	24	.0285	.0009
2442	pre	45	.0323	.0018
	post	31	.0475	.0019
2587	pre	23	.0453	.0015
	post	21	.0386	.0013

MONKEYS 782 AND 2483 WERE FLIGHT MONKEYS AND MONKEYS 2471, 839, 2442 AND 2587 WERE FLIGHT CANDIDATES THAT SERVED AS CONTROLS. VALUES ARE FOR PRE AND POST FLIGHT.

TABLE 2

MEDIAL GASTROCNEMIUS
FIBER CROSS-SECTIONAL AREA (μm^2)

MONKEY	GROUP	n	MEAN	SEM
782	pre	91	2799	139
	post	58	4427	247
2483	pre	64	2348	117
	post	55	3751	267
2471	pre	30	3721	229
	post			
839	pre	43	3336	141
	post	41	5135	249
2442	pre	42	2826	143
	post	32	3740	260
2587	pre	55	3881	249
	post	21	4282	524

MEDIAL GASTROCNEMIUS
SDH ACTIVITY (optical density/min)

MONKEY	GROUP	n	MEAN	SEM
782	pre	91	.0229	.0008
	post	58	.0200	.001
2483	pre	55	.0275	.0022
	post	33	.0131	.0007
2471	pre	30	.0141	.0017
	post			
839	pre	43	.0128	.0006
	post	41	.0179	.0019
2442	pre	42	.0383	.0028
	post	32	.0483	.0038
2587	pre	55	.0284	.0016
	post	21	.0413	.0045

TABLE 3

TIBIALIS ANTERIOR
FIBER CROSS-SECTIONAL AREA (μm^2)

MONKEY	GROUP	n	MEAN	SEM
782	pre	49	4850	370
	post	62	3857	296
2483	pre			
	post	55	3751	267
2471	pre	36	4631	339
	post	50	4653	305
839	pre	44	2582	117
	post	49	2840	115
2442	pre	14	4113	247
	post			
2587	pre	24	2982	219
	post	18	4643	520

TIBIALIS ANTERIOR
SDH ACTIVITY (optical density/min)

MONKEY	GROUP	n	MEAN	SEM
782	pre	49	.0391	.0025
	post	62	.0281	.0022
2483	pre			
	post	50	.0118	.0016
2471	pre	36	.0427	.0045
	post	50	.0234	.0017
839	pre	44	.0109	.0013
	post	49	.0164	.0009
2442	pre	14	.0185	.0029
	post			
2587	pre	24	.0456	.0020
	post	18	.0220	.0037

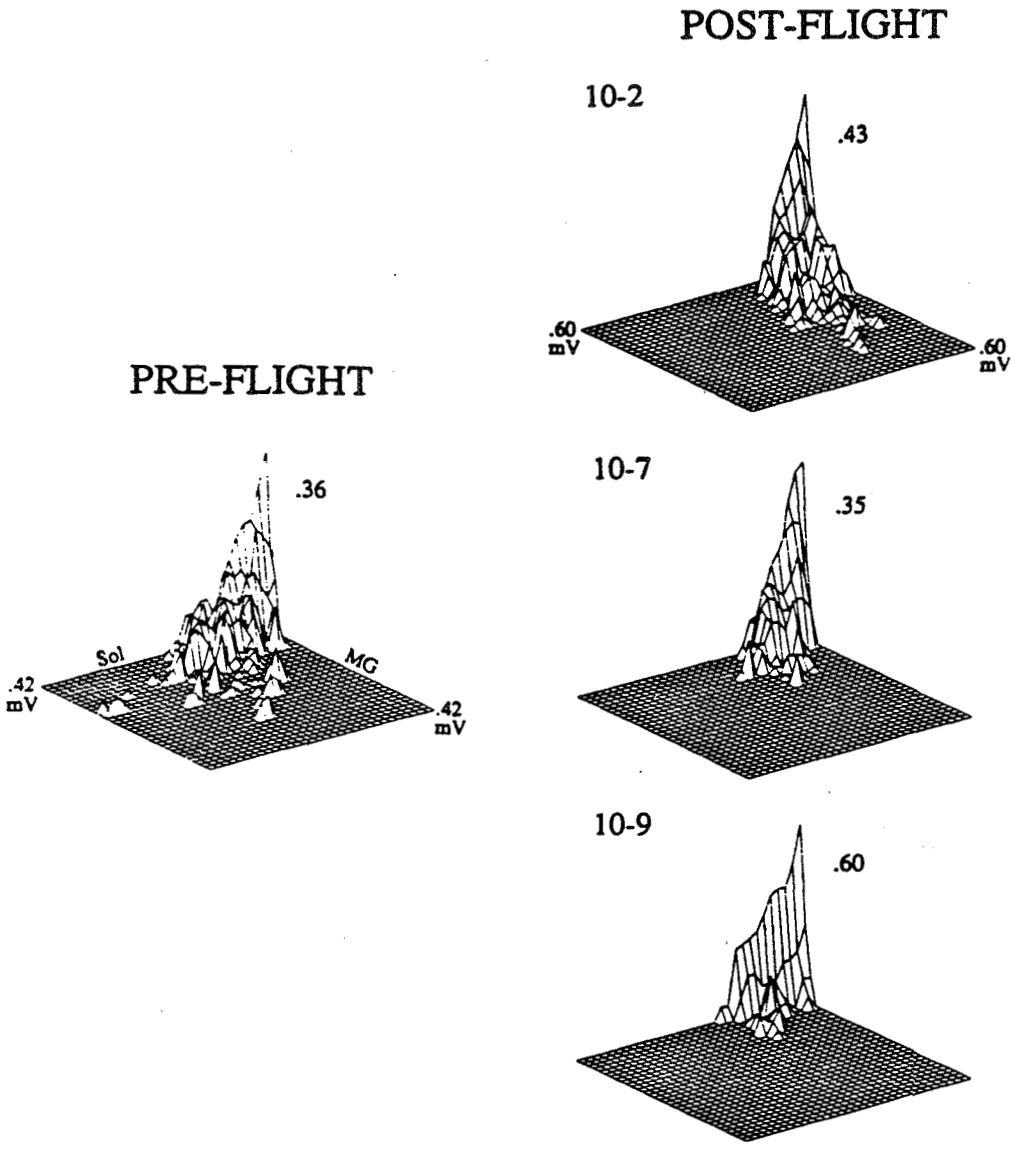

Figure 1. Joint probability density distributions of soleus (Sol) and medial gastrocnemius (MG) EMG amplitudes. The vertical axis of each distribution is on a logarithmic scale and the decimal number to the right of each distribution is the probability of the peak. All distributions are shown looking towards the origin which is obscured by data. Each distribution was generated using three consecutive trials and totalling 20,000 data points. Post flight dates are indicated in the top left hand corner of each distribution. Recovery was on 9-29.

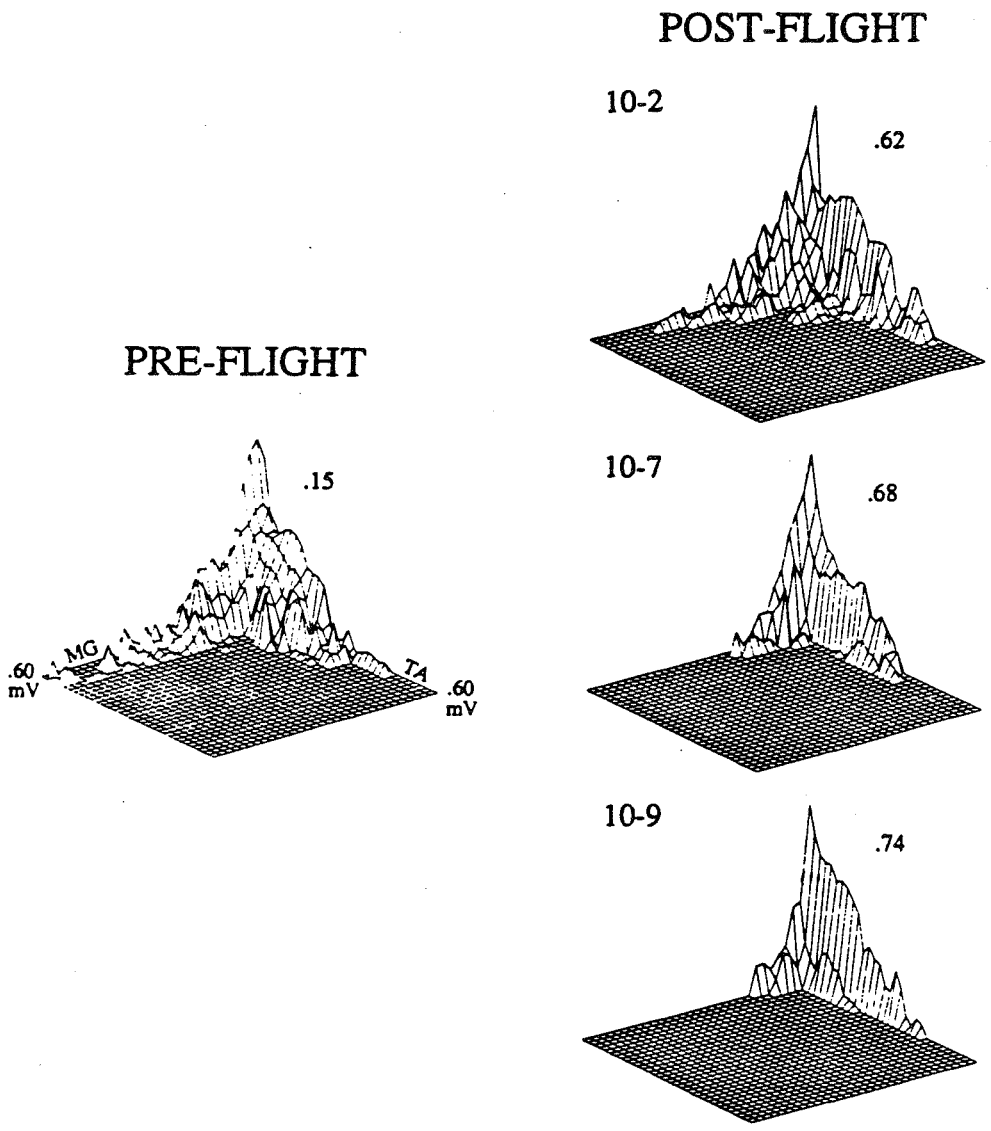

Figure 2. Joint probability density distributions of tibialis anterior (TA) and medial gastrocnemius (MG) EMG amplitudes. The arrangement is the same as for figure 1.

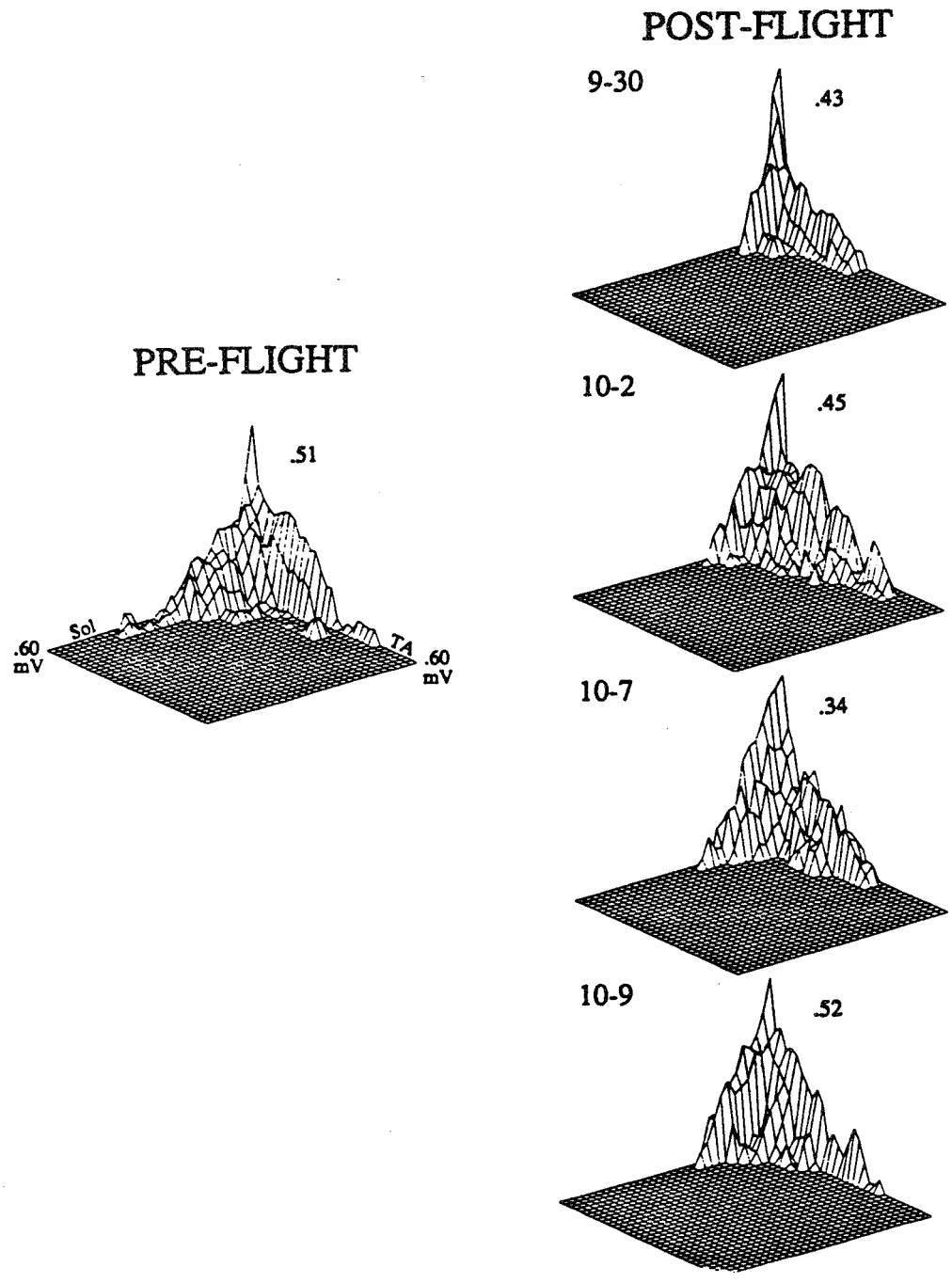

Figure 3. Joint probability density distributions of soleus anterior (Sol) and tibialis (TA) EMG amplitudes. The arrangement is the same as for figure 1.

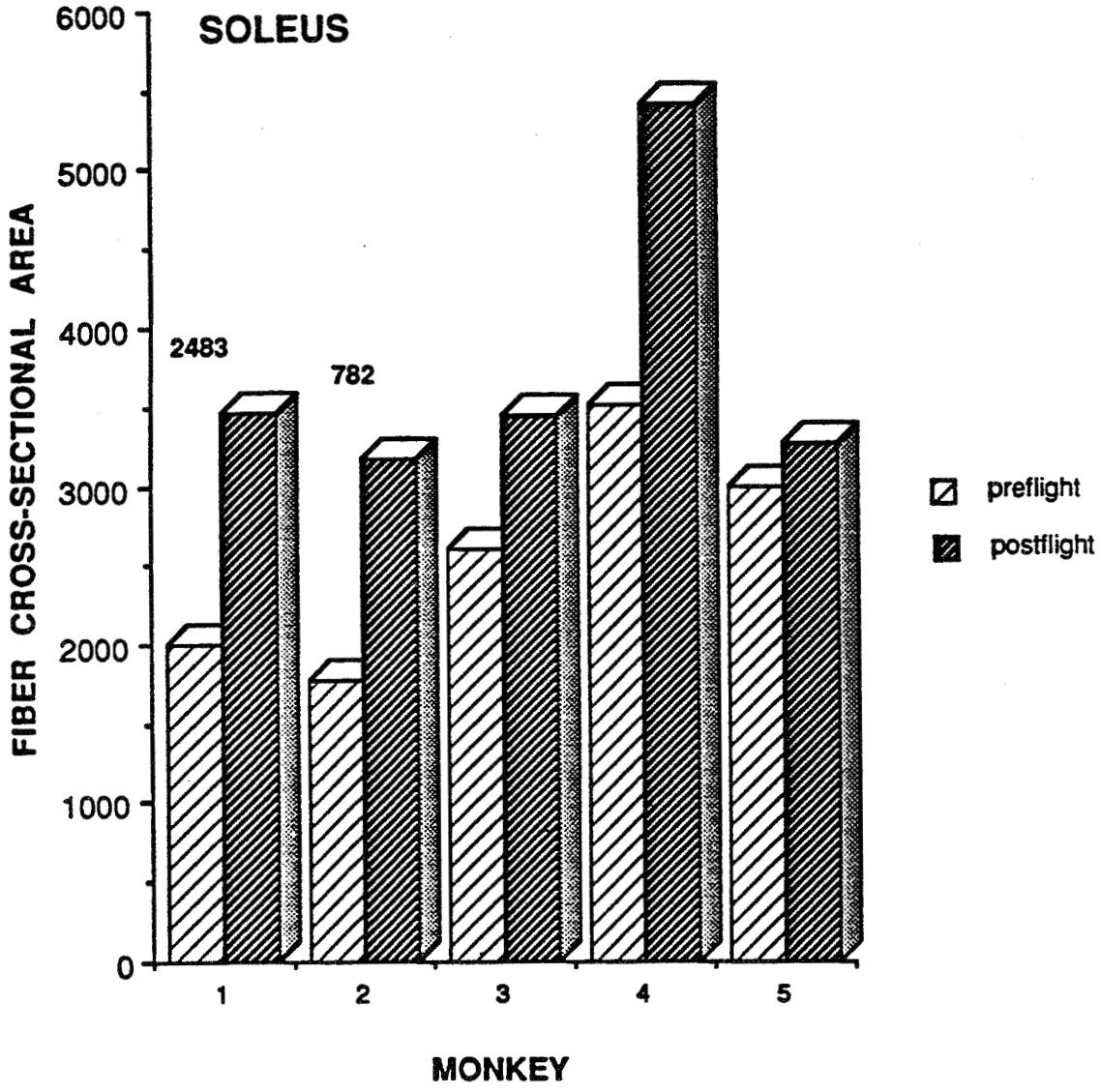

Figure 4. Mean fiber cross-sectional area for pre- and post- flight biopsies. Monkey 2483 and 782 were flight monkeys. Monkey 3, 4, and 5 correspond to monkey 839, 2442 and 2587 respectively.

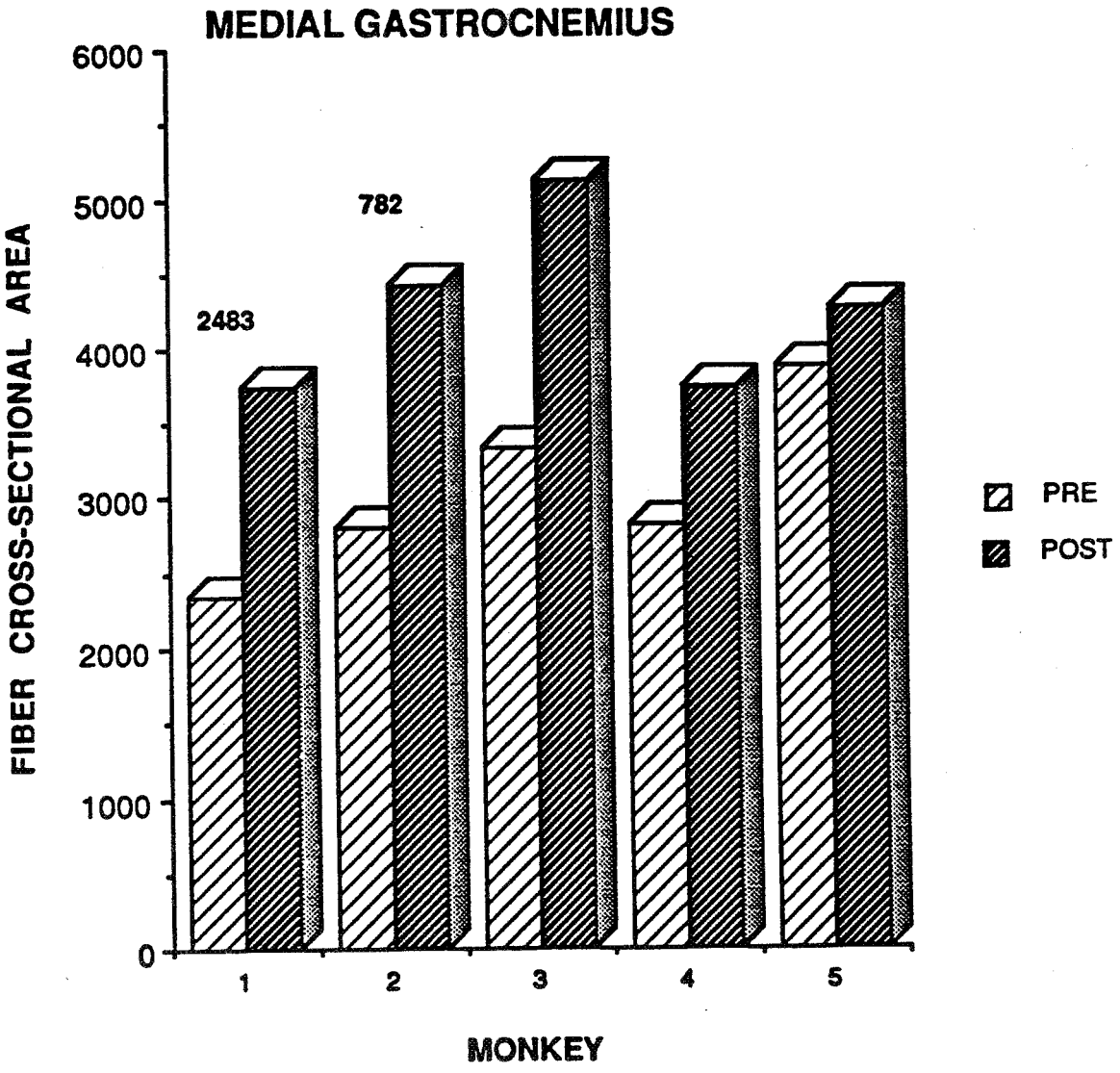

Figure 5. Mean fiber cross-sectional area for pre- and post- flight biopsies. Monkey 2483 and 782 were flight monkeys. Monkey 3, 4 and 5 correspond to monkey 839, 2442 and 2587, respectively.

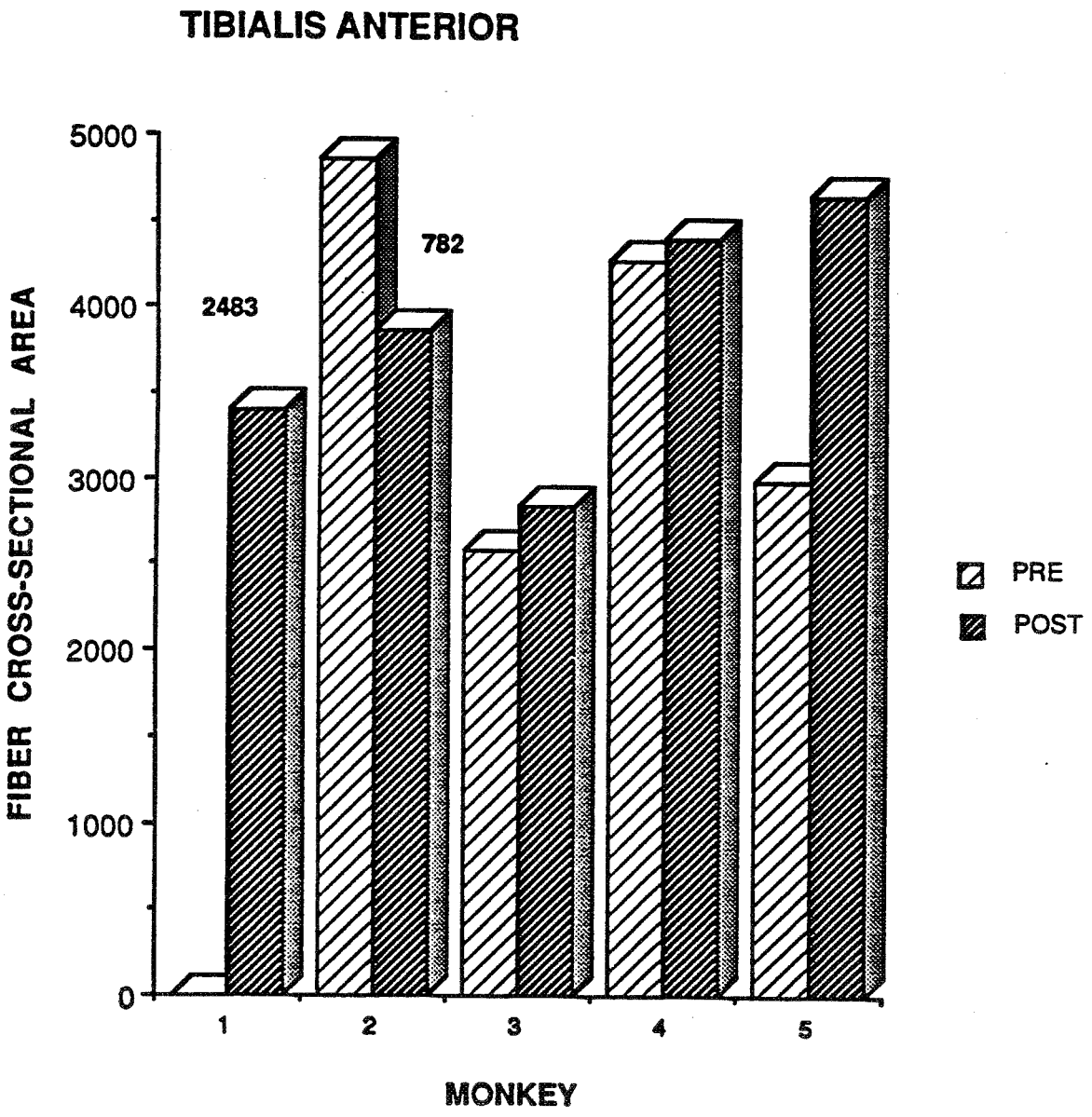

Figure 6. Mean fiber cross-sectional area for pre- and post- flight biopsies. Monkey 2483 and 782 were flight monkeys. Monkey 3, 4 and 5 corresponds to monkey 839, 2471 and 2587, respectively.

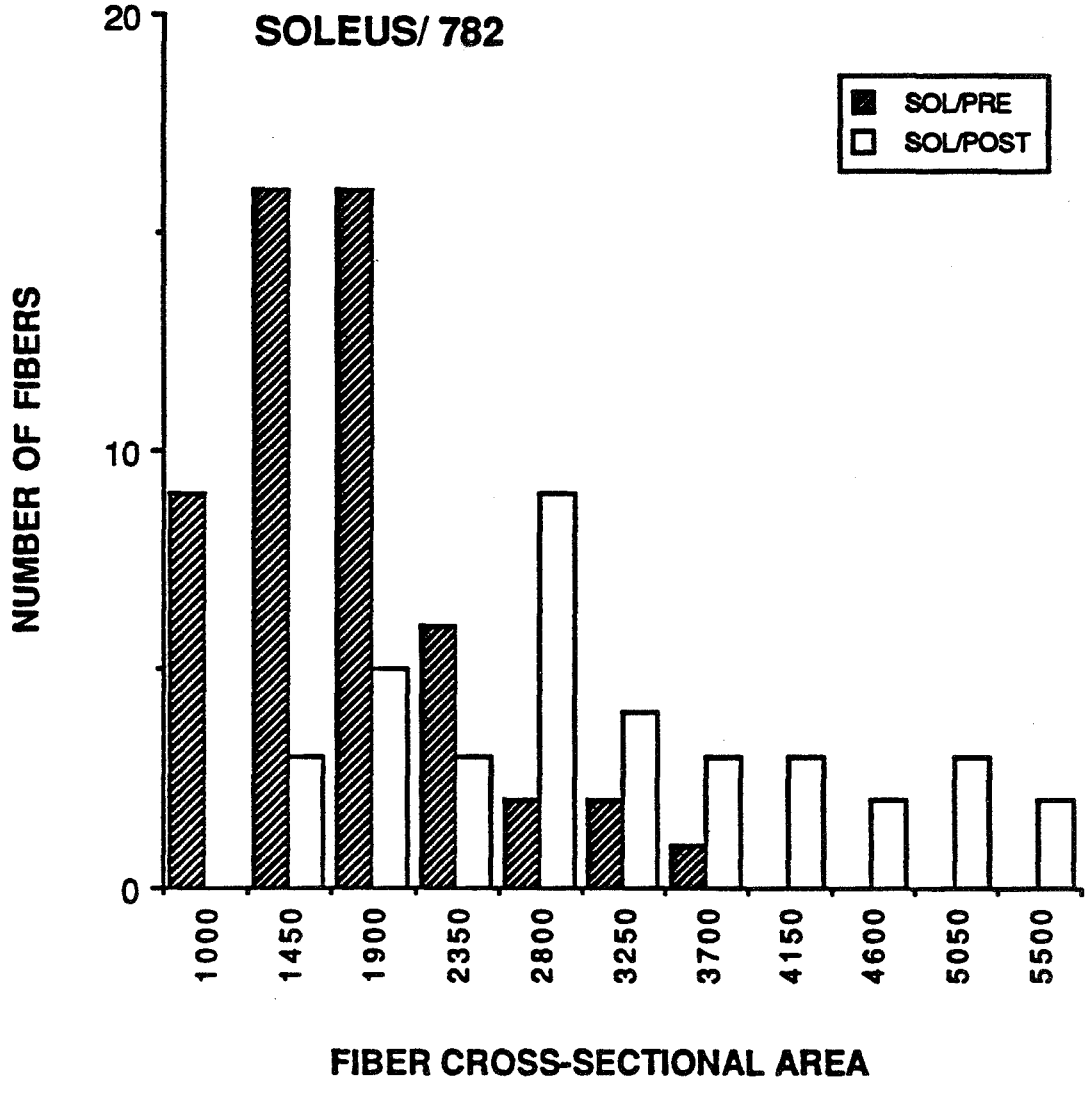

Figure 7. Distribution of fiber areas for pre- and post- flight biopsies in the soleus of flight monkey 782.

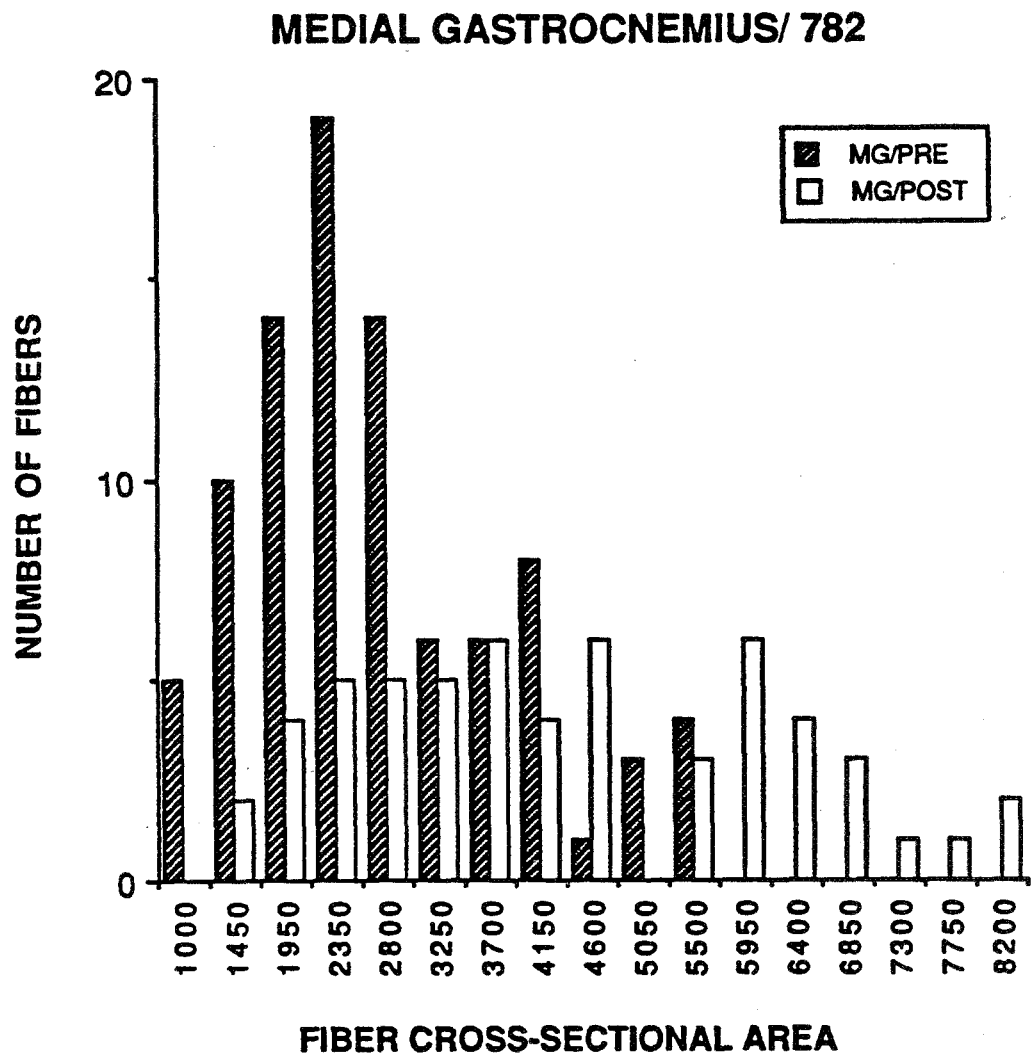

Figure 8. Distribution of fiber areas for pre- and post- flight biopsies in the medial gastrocnemius of flight monkey 782.

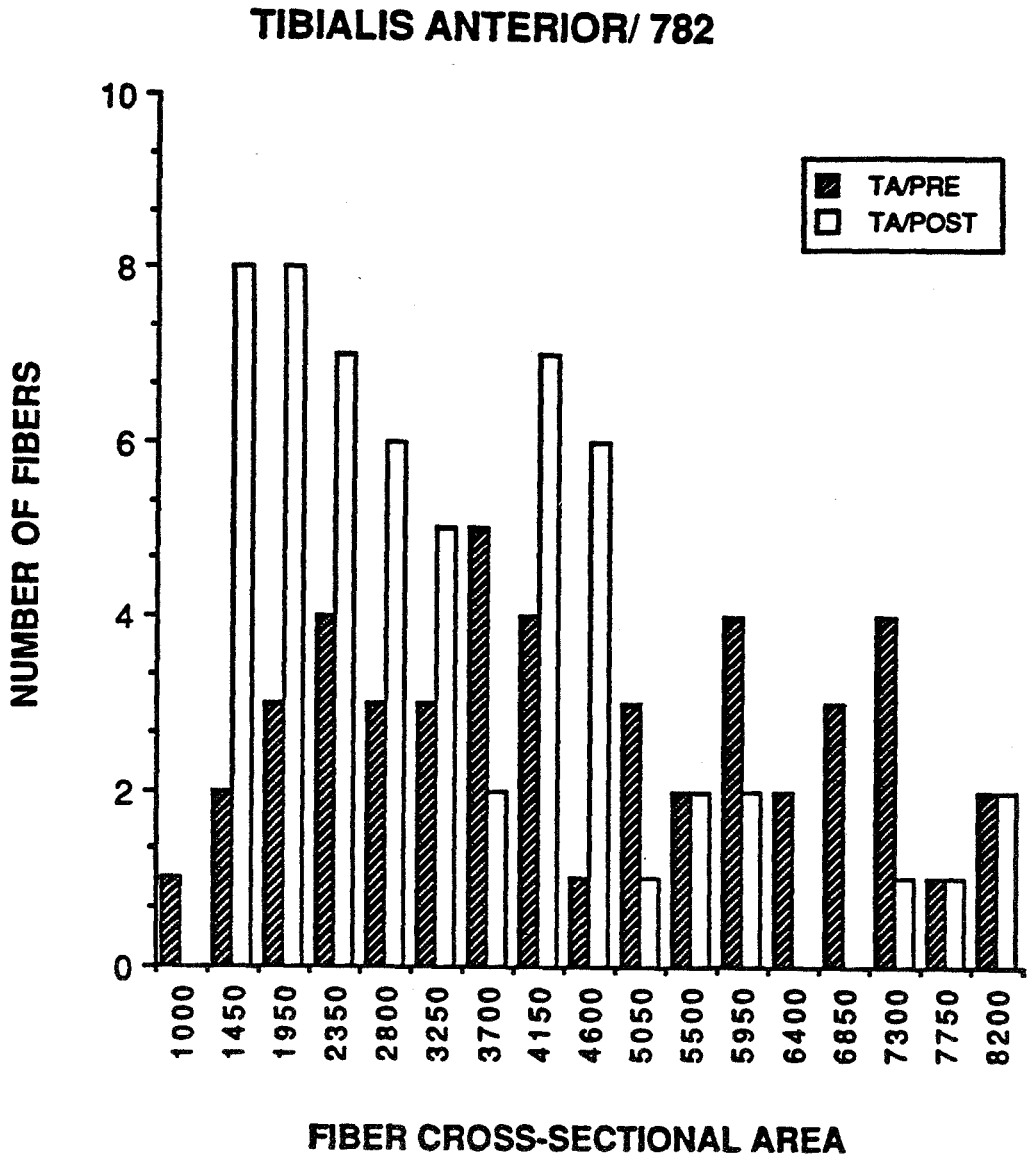

Figure 9. Distribution of fiber areas for pre- and post- flight biopsies in the tibialis anterior of flight monkey 782.

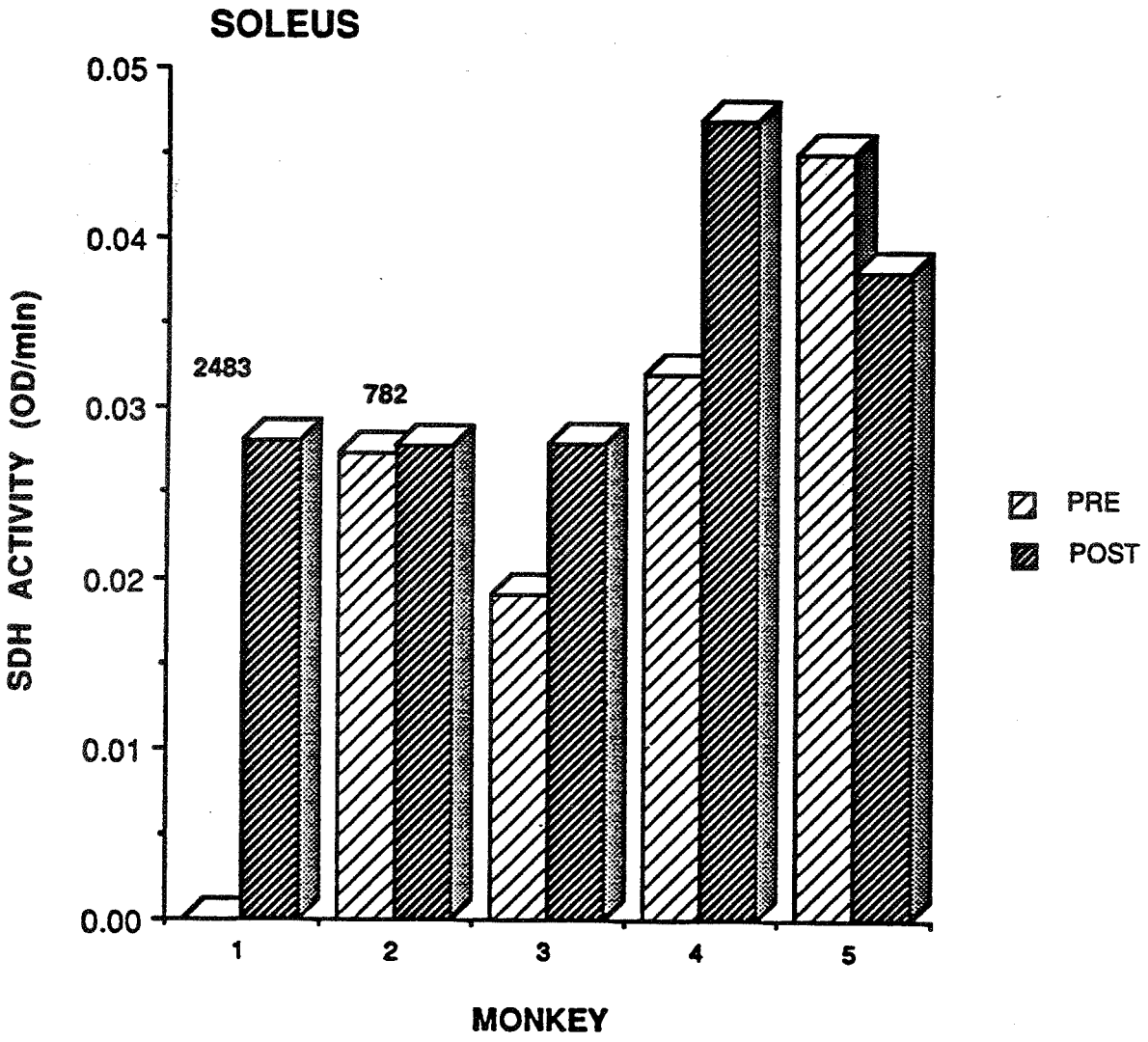

Figure 10. Mean SDH activity for pre- and post- flight biopsies. Monkey 2483 and 782 were flight monkeys. Monkey 3, 4 and 5 correspond to monkey 839, 2442 and 2587, respectively.

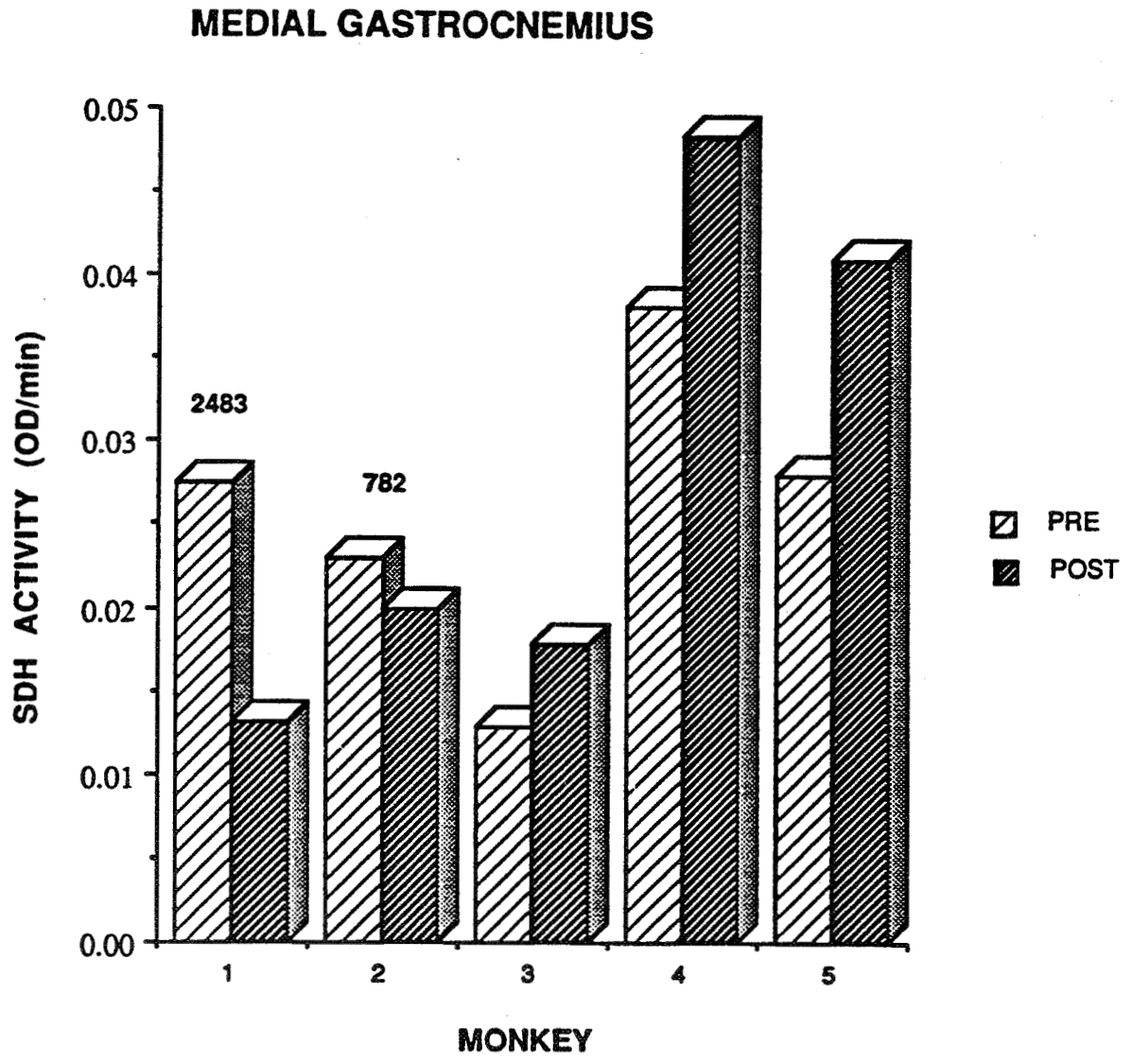

Figure 11. Mean SDH activity for pre and post flight biopsies. Monkey 2483 and 782 were flight monkeys. Monkey 3, 4, and 5 correspond to monkey 839, 2442, and 2587, respectively.

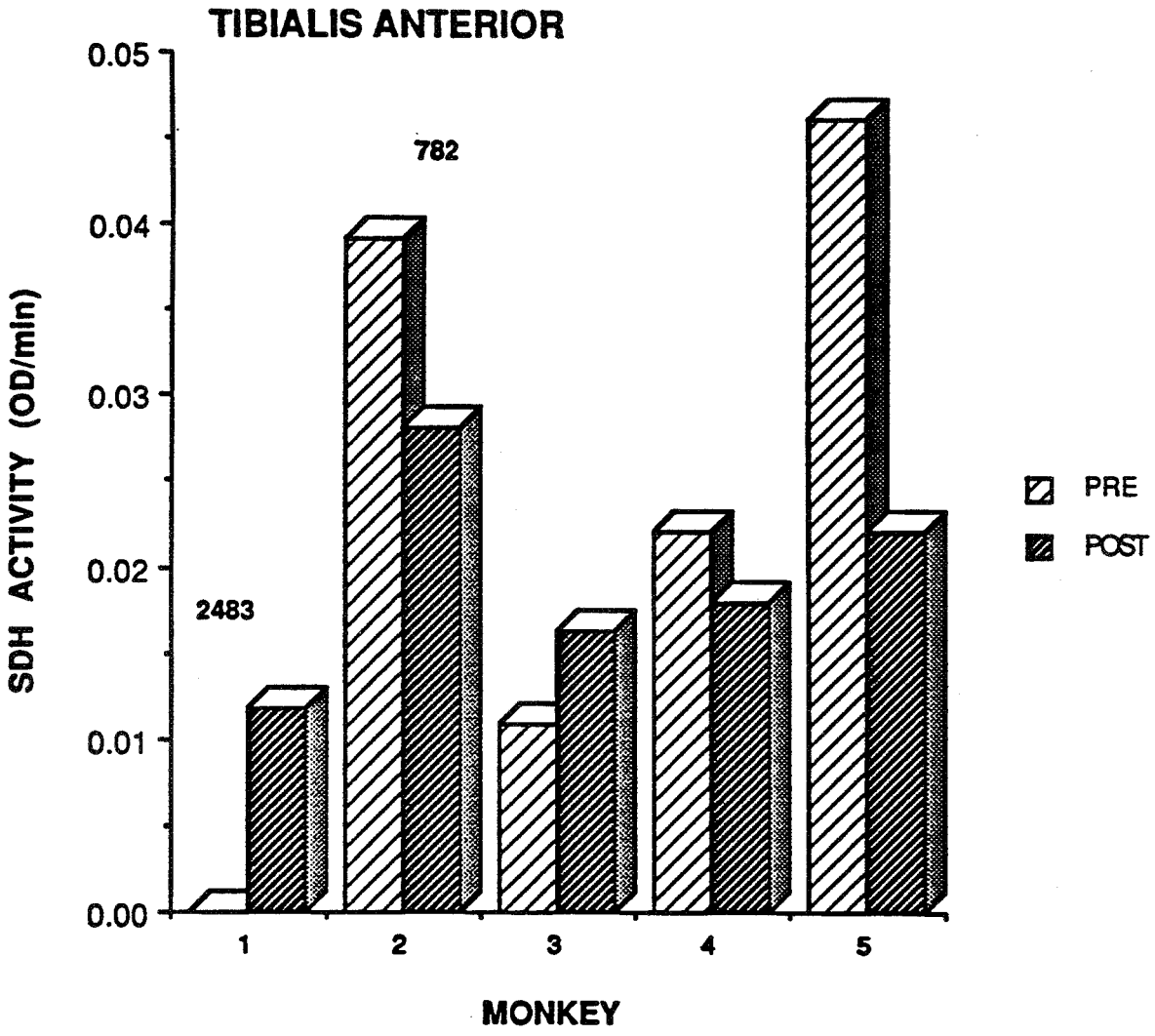

Figure 12. Mean SDH activity for pre and post flight biopsies. Monkey 2483 and 782 were flight monkeys. Monkey 3, 4, and 5 correspond to monkey 839, 2471 and 2487, respectively.

52-51
51367

EXPERIMENT K-7-35

CIRCADIAN RHYTHMS AND TEMPERATURE REGULATION DURING SPACEFLIGHT

PART I: CIRCADIAN RHYTHMS AND TEMPERATURE REGULATION

PART II: METABOLISM

Principal Investigator:

C. A. Fuller
Department of Animal Physiology
University of California
Davis, CA

Co-Investigators:

T.M. Hoban-Higgins
D.W. Griffin
Department of Animal Physiology
University of California
Davis, CA

A. M. Alpatov
M. A. Dotsenko
V. Ya. Klimovitsky
V I. Korolkov
Institute of Biomedical Problems
Academy of Medical Sciences of the USSR
Moscow, USSR

T. P.Stein
Department of Surgery
University of Medicine and Dentistry of New Jersey
Camden, NJ

Page intentionally left blank

EXPERIMENT K-7-35

PART I: BIOLOGICAL RHYTHMS AND TEMPERATURE REGULATION

C.A. Fuller, A. M. Alpatov, T.M. Hoban-Higgins, V.Y. Klimovitsky

INTRODUCTION

Mammals have developed the ability to adapt to most variations encountered in their everyday environment. For example, homeotherms have developed the ability to maintain the internal cellular environment at a relatively constant temperature. Also, in order to compensate for temporal variations in the terrestrial environment, the circadian timing system has evolved. However, throughout the evolution of life on earth, living organisms have been exposed to the influence of an unvarying level of earth's gravity. As a result changes in gravity produce adaptive responses which are not completely understood. In particular, spaceflight has pronounced effects on various physiological and behavioral systems. Such systems include body temperature regulation and circadian rhythms.

Numerous physiological changes occur during exposure of animals to increased acceleration fields produced via centrifugation (cf. Smith, 1975, for review). Typically these responses are triphasic (Oyama, 1971) in that an initial response is followed by a recovery period and then acclimation. One aspect of the response of primates (Fuller, 1984a), rats (Fuller, et al., 1977b; Oyama, et al., 1971; Schertel et al., 1980) and dogs (Oyama, 1975) to increased acceleration fields (hyperdynamic environments) is a substantial decline in colonic temperature. In rats, this initial decrease occurs immediately, reaching a minimum within 2 hours. The recovery period, however, can take up to several days. During this recovery period the circadian rhythm in body temperature remains markedly depressed (Oyama, 1975).

The initial decrease in colonic temperature observed in rats is accompanied by an increased heat loss (Fuller et al., 1977b). Decreases in oxygen consumption (heat production) have also been observed in rats (Oyama & Chan, 1973). These changes in heat production and loss were determined not to be thermoregulatory responses elicited by changes in temperature at the sites of temperature reception. This was determined by comparison of the skin (tail), hypothalamic and spinal cord temperatures. These anatomic locations are the site of receptors which, in the rat, serve as inputs for the neural control of core temperature (Fuller et al., 1975; 1977a). All sites showed depression similar to that seen in core temperature (Fuller et al., 1977b). The increased heat loss found to occur during the fall in body temperature would not have been predicted on the basis of thermoreceptor inputs to a normally functioning controller.

During the recovery phase of the temperature response, there is a marked deficit in the ability of rats to maintain body temperature during acute cold exposures (Fuller et al., 1977b; Giachino et al., 1979; Horowitz et al., 1979). The cause of this thermoregulatory impairment is not clear. It may be the result of changes in any of several factors including: 1) central and/or peripheral thermosensitivity, 2) the ability to gain or lose heat, or 3) integrative ability of the central neural controller for thermoregulation.

Little data has been collected on the effects of altered acceleration fields upon thermoregulation in primates. The Bioflights in the late 1950's provided the first temperature data from a primate in microgravity (Graybiel et al., 1959). Although many problems existed in interpretation of data (i.e., axillary instead of core temperature, short flight duration, highly stressed animals, etc.), there was a suggestion of a general decline in body temperature during the flights. More recently

(Fuller, 1984a), the regulation of body temperature of squirrel monkeys has been shown to be influenced by hyperdynamic environments. A time of day responsiveness to exposure to these increased acceleration fields has also been identified. During the animals' active phase (day) the body temperature falls almost 2°C during exposure to 2 G, while during its rest phase (night) the body temperature is unaffected.

The earliest record of primate temperature data during spaceflight is that of Biosatellite III (Hahn et al., 1971). Although this animal was compromised, three applicable observations are apparent from the data: 1) there was a depression in body temperature during the flight, 2) the circadian rhythm of body temperature persisted but was "free-running" and not entrained to the ambient light-dark cycle and 3) there were substantial changes in the sleep-wake behavior, including shifts in the phase-angle relationship to the LD cycle (with synchrony to 24-hr maintained) and fragmentation of the sleep-wake cycle (Hanley & Adey, 1971; Hoshizaki et al., 1971). The loss of synchronization of the temperature rhythm, while the sleep rhythm remained synchronized, suggests that the altered gravitational field had a selective effect on the circadian timekeeping system. These data are consistent with our current understanding of the mammalian circadian timekeeping system. The circadian clock regulating the temperature rhythm is different from the clock regulating behaviors such as drinking and rest-activity (Fuller et al., 1981). Some of the recent Soviet COSMOS monkeys also showed a decrease in body temperature of 0.50-0.75°C, with a suggestion of altered phase-control of the temperature rhythms.

This program has examined the influence of microgravity on temperature regulation and circadian timekeeping systems in Rhesus monkeys. Animals flown on the Soviet Biosatellite, COSMOS 2044, were exposed to 14 days of microgravity while constantly monitoring the circadian patterns temperature regulation, heart rate and activity. This experiment has extended our previous observations from COSMOS 1514, as well as providing insights into the physiological mechanisms that produce these changes.

METHODS

Four Rhesus monkeys, weighing 3.5 to 4.0 kg, were used in three experimental paradigms to study the effects of microgravity on circadian rhythms and temperature regulation. Two animals were studied in a 14 day baseline control experiment verifying all procedures and collecting baseline data prior to the flight of the Biosatellite. Two additional animals were flown for 14 days on the Biosatellite and subsequently studied in a postflight control experiment which began 45 days after the flight. In all conditions, the animals were housed in a 24 hour light-dark cycle (LD16:8). The primates were fed 250 gram meals twice each day (10:00-12:00 and 18:00-20:00). The atmosphere inflight was maintained at approximately sea level partial pressures and barometric pressure. The animals were extensively trained to sit in a chair-like restraint device for the duration of the tests.

Measured parameters for each animal included: heart rate, motor activity, axillary temperature, head skin temperature, thigh skin temperature, axillary skin temperature, ambient temperature at the upper portion of the chair and ambient temperature at the lower portion of the chair. Data were collected at 5 minute intervals and stored on a battery operated data logger (Vitalog, modified by L & M Electronics).

The heart rate was derived from the Soviet EKG signal by a US supplied R-wave detector (L & M Electronics). The axillary temperature measurements were taken from the output signals of a Soviet biotelemetry transmitter implanted in the axilla of each animal. The activity measurements were derived from a piezoelectric transducer (L & M Electronics) attached to a harness over the animals chest. The rest of the temperatures were measured via thermistors (YSI series 400 probes). The head skin temperature was attached to the temple of the animals. The thigh and ankle skin temperature sensors were glued to the animals skin in those locations. To provide strain

relief, the sensors were then taped in place. The ambient temperatures were measured at the top and bottom of the restraint system.

After each experiment the data were transferred to a microcomputer for analysis and storage. The analysis of the data included the examination of the raw data files, plus a phase analysis in which a sine wave was fitted with a least squares technique to the data to compute circadian phase, amplitude and 24 hour mean. Waveform analysis was performed by repetitive waveform reduction. Period analysis was performed by the periodogram technique.

RESULTS

It was clear from the results of all three of the experimental sets (baseline, flight, postflight controls) that circadian rhythms in all 8 variables persisted in the subjects. Figure 1 shows the data from each of these variables on one of the two monkeys flown on COSMOS 2044. In this figure, the data record begins on day one just prior to midnight. The animal was launched on the morning of day 3 (arrow) and recovered early in the morning on the last day of the record (arrow). Although there is some variability in the signal to noise ratio across the variables, circadian rhythms can be seen in each parameter. As can be seen, there was an increase in ambient temperature during the last three days of the flight. To avoid any confounding influence this increase may have had, data from these days were not used in determining the average values of the monitored values. Thus, the averages were computed from the first full flight day (flight day 2) to flight day 11. The summary of the responses of each animal is described individually by variable below.

Heart Rate

Figure 2 is a plot of the average heart rate circadian phase, amplitude and 24 hour mean for each animal in the three experimental conditions. The two baseline animals had an average phase of approximately 17.0 hours, an average amplitude of approximately 12 beats per minute (bpm) in the circadian rhythms with an average 24 hour mean of approximately 135 bpm. Subject M82 had an average phase of 19.6 hours inflight and 18.7 hours during the postflight control. Inflight the circadian amplitude was decreased to 18.3 bpm compared to 27.8 bpm during the control period. The 24 hour mean during the control run in M82 was 119.6 bpm; during the flight experiment the 24 hour mean was 127.6 bpm. Subject M83, on the other hand, had a postflight control phase of 19.6 hours in contrast to a phase advance of the circadian rhythm in heart rate to 13.7 hours during the flight. The amplitude of the circadian rhythm was 9 bpm during the flight and 5.5 bpm during the postflight control. The 24 hour mean was 126.0 bpm inflight and 140.1 bpm postflight.

Figure 3 shows an example of the daily trend analysis of the heart rate data from subject M82 flight data. As can be seen from day 5-15 the phase was relatively stable at approximately 20.0 hours. The amplitude of the circadian rhythm in heart rate was somewhat more variable and, except for days 5 and 6 where a reduction in amplitude occurred, the amplitude was approximately 20 bpm. The 24 hour mean showed relative stability over the duration of the flight except for the initial reduction after installation of the chair. Figure 4 shows the average 24 hour waveform pattern of M82 heart rate rhythm over the flight. The phase angle zero corresponds to the time of lights on. Finally, Figure 5 plots the average circadian period of M82 in the postflight control and flight experiments. The period of the heart rate rhythm of M82 was 24.25 hours in both the flight and postflight control experiments. M83 evidenced both a 24.0 and 24.25 hour period inflight, but only a 24.0 period in the postflight control.

Activity

The average phase of the activity rhythm of the two baseline control animals was 17.0 hours, as shown in Figure 6. The amplitude of the circadian rhythm was more variable, but averaged 95

counts/5 minutes and had an average 24 hour mean of 204 counts/5 minutes. Subject M82 showed an inflight pattern similar to the baseline animals with a circadian phase of 19.0 hours an amplitude of 68.9 counts/5 minutes and a 24 hour mean of 228.0 counts/5 minutes. Postflight, this animal showed a similar phase (19.2 hours) and an increase in both circadian amplitude (119.7 counts/5 minutes) and 24 hour mean (246.4 counts/5 minutes). Inflight, subject M83 showed an average activity phase of 19.6 hours, an amplitude of 100.9 counts/5 minutes and a 24 hour mean of 343.6 counts/5 minutes. However, during postflight control, subject M83 showed a significant reduction in motor activity. This could be accounted for by a change in sensor sensitivity, especially as this animal evidenced an increased average heart rate at the same time. The average postflight control phase was 15.8 hours with an amplitude of 3.1 counts/5 minutes and a 24 hour mean of 3.2 counts/minute. The circadian period of the activity rhythm for M82 was 24.0 hours inflight and 24.25 hours during the postflight control. M83 showed a 24.0 hour period in both the flight and postflight experiments.

Axillary Temperature

In both the baseline and flight experimental conditions the circadian phase of the axillary temperature rhythm was approximately 19.0 hours; the amplitude of the rhythms averaged 0.5 - 0.7°C, as shown in Figure 7. The mean axillary temperature of the baseline control animal for which we have a record was 38°C. In comparison, subject M82 had an inflight axillary temperature of 37.5°C and a postflight control axillary temperature of 37.8°C. The inflight axillary temperature of M83 registered 37.8°C on average, and 35.8°C postflight. Both M82 and M83 showed an inflight average circadian period greater than 24 hours, approximately 24.25 hours for each animal. The low frequency of data collection during postflight control (at 60 and 120 minute intervals) does not allow an accurate assessment of amplitude, phase or period.

Head Skin Temperature

The average phase of the circadian rhythm of head skin temperature was 17.4 hours in the two baseline control animals, as shown in Figure 8. The circadian amplitude was 0.55 and the 24 hour mean was 35.2°C. Inflight, M82 showed an average phase of 18.0 hours, a circadian amplitude of 0.7° and a 24 hour mean of 33.9°C. In the postflight control this animal showed a phase delay to 19.9 hours, a decreased circadian amplitude (0.4°C) and an increased 24 hour mean (34.9°C). In M83 the flight circadian phase was 18.8 hours compared to 18.2 hours in the postflight control. M83 also showed a decreased amplitude (0.9°C vs, 0.5°C) and an increased mean (34.7°C vs. 35.4°C) during the postflight control. M82 had a 24.25 hour period inflight and a 24.0 hour period postflight while M83 evidenced a 24.0 hour period inflight and both a 24.0 and 24.25 hour period postflight.

Thigh Skin Temperature

The baseline control animals had an average circadian phase of 18.2 hours, an amplitude of 1.1°C and a 24 hour mean of 34.7°C, as shown in Figure 9. Subject M82 showed a 19.5 hour phase inflight with an 19.3 hour phase in the postflight control. The inflight amplitude of 1.8°C was reduced to 1.6°C in the postflight experiment. The mean of the temperature was 32.6°C during the flight and increased to 33.4°C during the postflight experiment. The phase of subject M83 was 15.7 hours inflight and 17.4 hours postflight. In contrast to M83, M82's amplitude of 0.6°C increased to 0.8°C postflight. The inflight 24 hour mean of 30.9°C increased to 34.2°C postflight. The thigh skin temperature from M82 showed an average period of 23.75 and 24.0 hours inflight. This increased to 24.25-24.5 hours postflight. In contrast, M83 evidenced a 24.0 period inflight and a 23.75 hour periodicity postflight.

Ankle Skin Temperature

The two baseline control animals showed an average circadian phase of 21.0 hours for the ankle skin temperature rhythm with an amplitude of 1.5°C on average and a 24 hour mean of 28.9°C, as shown in Figure 10. Subject M82 showed a circadian phase of 21.9 hours inflight and 20.2 hours in the postflight control. The rhythm amplitude was 2.0°C inflight and 2.8°C postflight with a 24 hour mean of 30.4°C inflight which decreased to 28.6°C postflight. M83 had a delayed phase of 5.3 hours inflight with a 24.9 hour phase postflight. The inflight amplitude of 1.6°C increased to 1.7°C postflight, as did the 24 hour mean (30.0°C vs. 32.0°C). The period of the ankle skin temperature rhythm was for M82: 23.75 hours inflight, 24.25 hours postflight and for M83: 24.25 hours inflight and 24.0 hours postflight.

Ambient Temperature

Ambient temperature was measured both at the upper and lower portions of the animal cage. In the baseline experiment the mean temperature for both animals was 24.2°C. In the flight experiment the average upper temperature was 26.6°C for both animals; the average lower temperature was 26.8°C for M82 and 26.0°C for M83. In the postflight control the average upper temperature was 24.7°C for M82 and 25.4°C for M83; the average lower temperatures were 24.8°C for M82 and 24.2°C for M83. The differences in ambient temperature between the upper and lower measurements were not consistent and ranged from 0°C to 1.8°C. Figure 11 shows a plot of the average daily postflight temperature of M82 as well as the difference between the upper and lower temperatures.

DISCUSSION

These data indicate that the microgravity environment has a significant influence on both temperature regulation and the circadian timing system. In general, there is a tendency for a reduction in skin temperatures, an possible reduction in metabolism and concomitant reduction in deep body temperature. The circadian timing system appears to be more labile in the microgravity environment, even in the presence of a 24 hour light-dark cycle. Activity-related rhythms appear to be maintained with a 24 hour period, while thermoregulatory rhythms are more variable in their periodic responses and tend to show a greater variability in phase.

Temperature Regulation

The general trend of reduced skin temperature suggests a vasoconstriction and an active conservation mechanism. This is in concert with a reduced heart rate and activity level which combined with reduced food intake of the animals during the flight suggests a lower metabolism. Combined with the reduction in axillary temperature, these data continue to suggest that the thermoregulatory system is operating at a lowered level while the organism is in a microgravity environment.

However, there are variations between the animals and further experimental data will be required to more completely understand these responses. A more stable, reliable and appropriate marker of central core temperature will be required to fully identify the thermoregulatory responses to microgravity.

Circadian Timing System

Several previous observations of different organisms suggest that the circadian timing system is composed of two or more central pacemakers. The limited data sets that are available from spaceflight experiments suggest that these pacemakers show differential responses to the microgravity environment.

The pacemaker involved in regulating the timing of variables such as heart rate and motor activity consistently evidence appropriate 24 hour rhythms in the presence of a 24 hour light-dark cycle. Various reports have suggested the possibility of a phase angle shift but not a change in period. In contrast, the pacemaker that is involved with the circadian regulation of parameters such as body temperature does not show such stability. Frequent reports have indicated that temperature rhythms. in the microgravity environment, even in the presence of a light-dark cycle have non-24 hour or significantly altered 24 hour rhythms. While such robust changes were not observed in this flight, there were deviations from the 24 hour patterns in some of the temperature variables.

53-57
51368

EXPERIMENT K-7-35

PART II: METABOLISM

C.A. Fuller, M.A. Dotsenko, V. I. Korolkov, D.W. Griffin and T.P. Stein

INTRODUCTION

Few measurements of metabolism have been made in altered gravitational fields. The work of Oyama and Chan (1973) suggests that a reduction in metabolism occurs during an acute exposure to a hyperdynamic environment. The observed fall in body temperature during spaceflight, such as discussed in Section I, could in part be explained by an alteration in metabolism. Further, the depression of the skin temperatures suggests a heat conservation mechanism was activated for the duration of the flight. Whether these two factors (reduced body and skin temperatures) indicates an alteration in metabolism or a decrease in the thermoregulatory set point cannot as yet be determined.

A priori, one would expect an organism's energy requirements at 0 G to be less in space because of the absence of the work necessary to oppose gravity (Rambaut et al., 1977). However, data collected during the Skylab missions suggest that human energy expenditure may be increased during space flight (Leonard, 1983; Rambaut et al., 1977). The astronauts lost weight throughout the flight with most of the weight being lost early in the flight.

Energy expenditure can be regarded as the sum of two components; the basal metabolic rate and the energy costs of activity. Weight loss is usually associated with an energy deficit. A negative energy balance exists when energy intake is less that energy utilization. The deficit is made up by tissue catabolism (principally fat, but also some protein). By analyzing food and water intake, urine and fecal output, and changes in body weight, the Skylab investigators reached the unexpected conclusion that energy expenditure during spaceflight was about 5% greater than at 1 G (Leonard, 1983; Rambaut et al., 1977).

Conversely, two recent COSMOS flights (1514 and 1667) examined the daily food intake of rhesus monkeys during spaceflight. All four monkeys exhibited a decrease in food intake during spaceflight (5 to 7 days) relative to the amount consumed before flight (Sulzman et al., 1986; Gazenko & Ilyin, 1987). Similarly, two squirrel monkeys flown on Spacelab 3 showed decreased food intake (Fuller, 1985). It is not certain, however, what role space adaptation syndrome played in depression of appetite on these flights.

Possible explanations for the human metabolic responses are an increased workload during spaceflight (Leonard, 1983), or as Rambaut and co-workers (1977) suggested, a progressive decrease in metabolic efficiency. It is likely to be very difficult to distinguish between these two possibilities in man because the activity component may be different during spaceflight than it is on the ground. The problem is to measure energy expenditure with efficient precision during spaceflight in a non-invasive manner which will not interfere with other investigations or take any time. The doubly labeled water (DLW) method meets these criteria.

The doubly labelled water ($^2H_2{}^{18}O$) method for measuring energy expenditure is simple, non-invasive and highly accurate. The method was originally described by Lifson in 1955 and applied to man by Schoeller in 1982 (Lifson & McClintock, 1966; Schoeller & Webb, 1982). If $^2H_2{}^{18}O$ is given orally, it mixes with the body water in about 3 hours (Schoeller & van Santen, 1982; Schoeller, 1983). The two isotopes then leave the body at different rates. ^2H leaves as water, mainly in the urine, whereas ^{18}O leaves both as water and exhaled CO_2. Thus the turnover rate of

isotopic hydrogen and oxygen labeled water differ, and that difference is proportional to the rate of CO_2 production.

The method has been validated in man, normal animals, and in animals in metabolically perturbed states and animals in the grossly non-steady state such as a complete fast (Coward & Prentice, 1985; Klein et al., 1984; Schoeller & van Santen, 1982; Schoeller & Webb, 1982; Stein et al., 1987). It has been used to measure the energy cost of the flight of birds as well as of free ranging wild animals (for review, see Nagy, 1982). Thus, the method has been shown to be widely applicable. The principal sources of error with the method are analytical errors and non-steady state sampling of body fluids (Jones et al., 1988; Nagy, 1982; Schoeller & Taylor, 1988; Stein et al., 1987).

The DLW method is the only method available for continuously measuring energy expenditure during spaceflight given the severely restricted conditions in the spaceflight environment. Therefore, this study focuses on the development and use of this procedure on nonhuman primates during spaceflight.

Energy expenditure and total body water was determined in two Rhesus monkeys by the doubly labeled water ($^2H_2{}^{18}0$) method. Three determinations were made. Monkey B (#2483) was studied twice, during the flight of COSMOS 2044 and during a follow-up ground control study a month later. A second monkey was studied on the ground only (Monkey D, #782).

METHODS

A. Procedure

Two monkeys were studied, with one monkey (#2483) being studied twice, once during the flight of COSMOS 2044 and once postflight. The second monkey (#782) was a ground control.

The urine collection protocol is outlined in Figure 12. The same protocol was used for the inflight and two ground control studies. The first sample is the preflight baseline specimen. Samples 2, 3, and 4 (3,6,9 hr post DLW) are the post-dosing urines for determination of TBW by extrapolation. Samples 5 and 6 (Preflight) are dual purpose samples. They should be about 3 hours apart and are for: i) completion of the TBW extrapolation and ii) the first of the two points for calculation of the ^{18}O and ^2H loss rates. They are essentially duplicates. Samples 7 and 8 (Postflight) are also dual function points. They are the second point of the two points for the two pair determinations of the ^{18}O and ^2H loss rates and secondly, the baseline for the second dosing with ^{18}O to determine body water postflight. They are essentially duplicates. Samples 9, 10 and 11 (3,6,9 hr post DLW) are the post-second dose of isotope urines to be used for the poststudy TBW determination by extrapolation back to t = 0 (isotope dosing time).

17.0 g of 99.1% ^{18}O labeled water (Isotec Inc., Miamisburg, OH, batch #NS0894) was added to 4.32 g of 99.9% Deuterium oxide (ICONS Inc., Summit, NJ, batch #2084-2919) to give a mixture with the final composition listed in Table 1. In the subsequent paragraphs this is referred to the stock DLW or water.

A baseline urine was collected (sample #1) and then the animals dosed with $^2H_2{}^{18}0$ as indicated in Table 2 (1.25 g/kg of the stock DLW). The DLW was mixed with apple juice and administered orally.

Serial urines were then collected at three hourly intervals for the next 10-15 hours. Approximately 17 days later, at the end of the study period, two postflight/poststudy urines were collected. The

animals were then redosed with DLW (0.2 g/kg) and three serial urines collected at three hourly intervals later.

B. Calculation

(1) Isotope distribution spaces and the total body water (TBW).

The ^{18}O and ^{2}H isotope distribution spaces (IDS, in grams) were calculated from equation (1):

$$IDS = (d*APED_D*18.02*f)/(MW_D*(100*0.00208*D_D)) \quad (1)$$

d = dose (grams)
$APED_D$ = Atom Percent Excess = enrichments of the dose relative to the predose enrichment (D units)
f = fractionation effect (1.047 for CO_2)
MW_D = the molecular weight of the dose water
D_D = enrichments of the urine relative to the predose enrichment (D units)

For this study we assumed that the isotope distribution space is equal to the TBW. In man, the total body water (TBW) is assumed to be equal to the ^{18}O isotope distribution space divided by 1.01.

(2) Energy expenditure.

The rate of isotope loss from the body was calculated from equation 2:

$$k_O \text{ or } k_H = (\ln Dpre - \ln Dpost)/t \quad (2)$$

Dpre and Dpost = differences in isotopic enrichments of the sample and the pre-dosing background for ^{18}O or ^{2}H on pre- and postflight respectively.

k_O = fractional $H_2{}^{18}O$ turnover rates
k_H = fractional $^{2}H_2O$ turnover rates

The rate of CO_2 production was calculated from the equation of Schoeller, equation 3 (Schoeller et al, 1983):

$$rCO_2 = 0.481\ N(1.01k_O - 1.04k_H) - 0.0258N(k_O - k_H) \quad (3)$$

rCO_2 = rate of CO_2 production (mol/day)
N = total body water (moles).

The Weir equation (equation 4) was used to convert the rate of CO_2 production into energy expenditure values.

$$EE = 3.941\ VO_2 + 1.106\ VCO_2 - 2.17U \quad (4)$$
$$rCO_2 = VCO_2/22.4 \quad (5)$$
$$RQ = VCO_2/VO_2 \quad (6)$$

RESULTS

The actual isotopic enrichments found are tabulated in Tables 3, 4 and 5. Note that all delta values are relative to standard mean ocean water (SMOW).

DISCUSSION

A. Monkey B' (#2483) flight study 9/12/89 to 9/29/89

The data base in this study demonstrates the viability of this technique as an inflight measure of metabolism. Sample B'1 shows that the monkey had received a previous dose of isotopes. Day one (9/12/89, samples B'2-B'7) shows the expected enrichment pattern, a pre-equilibrium period and then by about 6 hours after body water has equilibriated with isotope, a steady decline in isotopic enrichment. Extrapolation of these points back to t = 0 gives ^{18}O = 646D.

The TBW value of 2.986 liters is also reasonable. It corresponds to 77.76% of body weight (4.20 kg). It is possible that this animal was in a dehydrated state when the measurements were made since a subsequent study on this animal was done October 31, 1989 (B") and the animal weighed 3.84 kg. Correlation with other TBW studies or clinical parameters (PCV, TP, BUN, Osm) would be useful in clarifying this observation.

Energy Expenditure Calculation

As predicted by the protocol, any one of points B'3, B'4, B'5 and B'6 can be used as the "first point" in a two pair calculation for calculating the isotope loss rates. The second data point is given by sample B'7. B'7 is a reasonable value, however, the duplicate B'8 sample for verification was not available. Again, the energy expenditure value of 266 kcal/monkey/d or 69.3 kcal/kg/d appears physiological.

Postflight TBW Analysis

Sample B'9 seems problematical. It appears to be unenriched, i.e., the sample is the same as the background. Accordingly, this sample was not considered in the data analysis. Further, not enough data points were available to obtain a reliable estimate of the postflight TBW. In future studies we need to increase the postflight DLW doses to enhance the reliability of this analysis.

Summary

The data demonstrate that the inflight protocol works, but the accuracy of the data could be greatly enhanced by collecting more urine samples. Specifically, two more urine samples collected at 15 and 18 hours after the initial dose and two more on return before redosing with ^{18}O would be recommended. Because the re-determination of body water postflight is of a lower priority, consideration should be given to dropping these urines in favor of collecting two more urine samples postflight approximately 3 hours apart.

B. Monkey B" (#2483) postflight study 10/31/89 to 11/19/89.

First TBW Study

Data points B"2 to B"4 are reasonable, with B"3 and B"4 suggesting that an equilibrium has been reached. Another point would have confirmed the extrapolation back to t = 0. In theory this should have been B"5. However, B"5 (^{18}O = 524.6) is so different from B"3 (^{18}O = 726.9) and B"4 (^{18}O = 722.1) that it cannot be correct. Since the ^{2}H values show the same anomalous pattern (B"3 ^{2}H = 2069; B"4 ^{2}H = 2006; B"5 ^{2}H = 1559) it must be concluded that there is a problem with the actual sample. Thus, the TBW (2.246 liters) value is best regarded as an estimate.

Energy Expenditure

Again, of the two "post" data points, only one (B"7) was available. However, this sample seems anomalous as the ^{2}H value is too high compared to the ^{18}O value. It may have been collected just after giving the second ^{18}O dose, rather than before. This would explain the anomalously high enrichment. Again, sample B"8, had it been available, might have helped resolve this problem.

Post TBW Determination

As described above, the crucial baseline points B"7 (questionable) and B"8 (missing) are not available. Samples B"9, B"10, B"11 looks fine, but with an uncertain baseline little can be done with them.

C. Monkey D' (#782) ground control 10/31/89 to 10/19/89

First TBW Study

As with data point B"5, data point D'5 seems to be much too dilute. Thus, the enrichments of D'3 ($^{18}O = 649$) and D'4 ($^{18}O = 664$), which are about 3 hours apart are reasonable. However, 3 hours later the D'5 enrichment had dropped to $^{18}O = 494$. Since the ^{2}H values show the same trend, it suggests a sample problem and not an analytical problem.

Energy Expenditure & Post TBW Determination

As with B"7, D'7 looks questionable and there is no D'8 (back-up) available. According to the protocol, following the collection of D'7, the animals were redosed with ^{18}O, (0.2 g/kg) and samples collected post-dose (D'9, D'10, D'11). D'9 to D'11 looks right, and D'7 (Table 5), is so similar that it is suggestive of a post-second ^{18}O dose sample. This may be possible for D'7 since the absence of a D'8 sample precludes both the calculation of energy expenditure rate and the second TBW determination.

CONCLUSIONS AND RECOMMENDATIONS

The successful inflight data from Monkey #2483 (B' samples) show that the DLW protocol is very workable. Furthermore, the results suggest that four changes be made on future flights to ensure the accuracy of the data set.

1. Following isotope dosing preflight, urine samples should be collected every 3 hours for the first 15 hours.

2. If the flight is delayed for a few days two additional urine samples should be collected as close to flight as feasible. Large volumes of fluid intake should be avoided at this time. If fluid intake records are available, they should become part of the data set.

3. Postflight serial urine samples should be collected at 3 hour intervals for 12 hours.

4. The postflight ^{18}O dosing should be discontinued or increased and delayed several hours.

III: ACKNOWLEDGEMENTS

We would like to thank our Soviet colleagues for their involvement and support of this project especially Drs.. E. A. Ilyin, A. Trushenekov, Y. Evstratov, M. Kaplansky, V. Magedov, and B. Perepech, at the Institute of Biomedical Problems. In the U. S., the role that Jim Connolly played as Project Manager was key to the successful U. S. participation in the flight. We also wish to acknowledge the participation of other individuals at Ames Research Center, especially: Mike Skidmore, Rod Ballard, Mike Souza and Dick Grindeland, support personnel Richard Mains and Edward Luzzi; the staff at the University of California, Davis: Wendy Lipman, Ina Green, Dr. Dave Griffin, Dr. Tana Hoban, Ed Robinson, Randy Gamage and Tom Morgan; and at the University of Medicine and Dentistry of New Jersey, Maria Leskiw, were essential in developing the equipment, procedures and tests necessary for this project. This work was supported by NASA Grant NAG2-587.

IV: REFERENCES

1. Coward W.A. and A.M.Prentice. Am. J. Clin. Nutr. 41:659-661, 1985.

2. Fuller, C. A. Aviat. Space. Environ. Med. 55:226-330, 1984a.

3. Fuller, C. A. Presented at IUPS Gravitational Physiology, 1984b.

4. Fuller, C. A. Physiologist 28: S201-202, 1985..

5. Fuller, C. A., J. M. Horowitz, and B.A. Horwitz. J. Appl. Physiol. 42:154-158, 1977a..

6. Fuller, C. A., B.A. Horwitz, and J.M. Horowitz. 1977b. J. Appl. Physiol. 42:74-79, 1977b.

7. Fuller, C. A., Horwitz, B. A., and Horowitz, J. M., 1975. Am. J. Physiol. 228:1519-1524.

8. Fuller, C. A., J. Tremor, J.P. Connolly, and B.A. Williams. Physiologist. 24:S111-112, 1981.

9. Gazenko, O. G., and E. A. Ilyin. The Physiologist 30(1):S31-S35, 1987.

10. Giacchino, J., J. M. Horowitz, and B. A. Horwitz. J. Appl. Physiol. 46:1049-1053, 1979.

11. Graybiel, A., R.H. Holmes, D.E. Beischer, G.E. Champlin, G.P. Pedigo, C. Hixson, T. R. A.Davis, N.L. Barr, W. G. Kistler, J. E. Niven, E. Wilbarger, D. E. Stullken, W.D. Augerson, R Clarke, J. H. Berrian, Aerospace Med. 30:871-931, 1959.

12. Hahn, P. M., T. Hoshizaki, and W.R. Adey.. Aerospace Med. 42:295-304, 1971.

13. Hanley, J., and W. R. Adey. Aerospace. Med. 42:204-313, 1971.

14. Hayashi, Y. and S. Endo. Sleep. 5(3):277-283, 1982.

15. Horowitz, J. M., E.R. Schertel, and B.A.Horwitz. The Physiologist. 22:S57-S58,1979.

16. Hoshizaki, T., R. Durham, and W.R. Adey. Aerosp. Med. 42:288-295, 1971.

17. Ingram, D. K., E. D. London, and M. A. Reynolds. Neurobiology of Aging 3:287-297, 1982.

18. Jones, P.J.,A.L. Winthrop, and D.A. Schoeller. Am. J. Clin. Nutr. 47: 799-804, 1988.

19. Klein, K. E., and H. M. Wegmann. In: Sleep, Wakefulness and Circadian Rhythms, vol. 105, A. N. Nicholson, ed., NATO Advisory Group for Aerospace Research and Development [Neuilly sur Seine, France] 10.1-10.25, 1979.

20. Klein, P. D., W. P. T. James, W. W. Wong, C.S. Irving, P.R. Murgatroyd, M. Carbrera, H. M. Dallosso, E.R. Klein,and B.L. Nichols. 1Human Nutrition: Clinical Nutrition. 38C:95-106, 1984.

21. Leonard, J. I.Am. J. Clin. Nutr. 38: 667-679, 1983.

22. Lifson, N.and R. McClintock. J. Theor. Biol. 12:46-74, 1966.

23. Nagy, K. Am. J. Physiol 238: R466-R473, 1982.

24. Novick, W. M., M. Nusbaum and T. P. Stein. Surgery. 103:99-105, 1988.

25. Oyama, J. In: Regulatory Biology: Depressed Metabolic States. NASA TM-X-69354: 27-51, 1971.

26. Oyama, J. COSPAR Life Scis. Space Res. XIII. P. H. A. Sneath, eds. Akademik-Verlag (Berlin): 2-17, 1975.

27. Oyama, J., and L. Chan, Fed. Proc. 32:392, 1973.

28. Oyama, J., W.T. Platt, and V.B. Holland. Am. J. Physiol. 221:1271-1277, 1971.

29. Parmeggiani, P. L., L. F. Agnati, G. Zamboni, and T. Cianci. EEG and Clin. Neurophysiol. 38:589-596, 1975..

30. Rambaut, P. C., C.S. Leach, and J.I. Leonard. Am. J. Physiol. 233:R208-R212, 1977.

31. Schertel, E. R., J.M. Horowitz, and B.A. Horwitz. J. Appl. Physiol. 49:663-668, 1980.

32. Schoeller, D. A., and E. van Santen.1982. J Appl Physiol 63:955-959, 1982.

33. Schoeller, D. A., and P. Webb. Am. J. Clin. Nutr. 40:153-58, 1982.

34. Schoeller, D. A. Am. J. Clin. Nutr. 38:905-919, 1983.

35. Schoeller, D. A., and P.B. Taylor. Hum. Nutr. Clin. Nutr. 41: 215-223, 1988.

36. Schoeller, D. A., E. Ravussin, Y. Schutz, K. J. Acheson, P. J. Baertschi and E. Jequier. Am. J. Physiol. 250:Rl823-R830, 1986.

37. Schoeller, D. A., R. F. Kushner and P. J. H. Jones.. Am. J. Clin. Nutr. 44:291-298, 1986.

38. Shipley, R. A., and R. E. Clark. Tracer Methods for in vivo Kinetics. Academic Press [New York], 1972.

39. Schoeller, D. A., W. Dietz, E. van Santen and P. D. Klein. Am. J. Clin. Nutr. 35:591-594, 1982.

40. Smith, A. H. In: Foundations of Space Biology and Medicine. M. Calvin and O. Gazenko, eds. NASA (Washington, , DC): 125-172, 1975.

41. Stein, T.P., R.W. Hoyt, M. O'Toole, R.G. Settle, and W.D.B. Hiller. Am. J. Clin. Nutr. 45:534-539, 1987.

42. Sulzman, F. M., C.A. Fuller, M.C. Moore-Ede, V. Klimovitsky, V. Magedov, and A.M. Alpatov,. In: Final Reports of U.S. Monkeys and Rat Experiments Flown on the Soviet Satellite COSMOS 1514, eds. R.C. Mains and W.W. Gomersall, NASA [Moffett Field]: 71, 1987.

43. Weir, J.B. deB.J. Physiol. (London) 109:1-9, 1949.

TABLE 1

ISOTOPIC ENRICHMENT OF LABELED WATER MIXTURE

$^{18}0$ enrichment	77.71 %
^{2}H enrichment	21.74%

TABLE 2

ISOTOPE DOSES

Monkey #	Study	Dose of DLW (g)
B' (2483)	Preflight	5.142
B' (2483)	Postflight	0.757
B" (2483)	Preground control	4.704
B" (2483)	Postground control	0.724
D' (782)	Preground control	5.151
D' (782)	Postground control	0.596

TABLE 3

ISOTOPIC ENRICHMENTS FOR FLIGHT STUDY

MONKEY B' (#2483)

Sample #	D ^{18}O	APE ^{18}O	D ^{2}H	APE ^{2}H
B'1	42.20	0.0148	150.34	0.0030
B'2	536.56	0.1165	1636.03	0.0253
B'3	592.42	0.1280	1792.98	0.0276
B'4	614.61	0.1325	1871.94	0.0288
B'5	605.40	0.1306	1861.86	0.0287
B'6	588.57	0.1272	1809.16	0.0279
B'7	24.01	0.0111	121.24	0.0026
B'9	-0.47	0.0061	-49.74	0.0000
B'10	192.78	0.0458	614.50	0.0100
B'11	175.55	0.0423	567.23	0.0093

TABLE 4

ISOTOPIC ENRICHMENTS FOR POSTFLIGHT GROUND CONTROL STUDY

MONKEY B" (#2483)

Sample #	D ^{18}O	APE ^{18}O	D ^{2}H	APE ^{2}H
B"1	-4.15	0.0053	-48.01	0.0000
B"2	778.92	0.1662	2189.52	0.0336
B"3	726.91	0.1556	2068.98	0.0318
B"4	722.10	0.1546	2005.82	0.0308
B"5	524.55	0.1140	1558.95	0.0241
B"7	142.07	0.0354	422.09	0.0071
B"9	213.15	0.0500	693.32	0.0112
B"10	192.29	0.0453	616.81	0.0100
B"11	201.35	0.0476	659.31	0.0106

TABLE 5

ISOTOPIC ENRICHMENTS FOR GROUND CONTROL STUDY

MONKEY D' (#782)

Sample #	D $^{18}0$	APE $^{18}0$	D ^{2}H	APE ^{2}H
D'1	-3.97	0.0054	-40.68	0.0002
D'2	631.89	0.1360	1831.97	0.0275
D'3	648.97	0.396	1858.06	0.0286
D'4	664.35	0.1427	1914.85	0.0295
D'5	494.01	0.1077	1467.96	0.0228
D'7	202.91	0.0479	469.00	0.0078
D'9	222.62	0.0520	749.89	0.0120
D'10	224.69	0.0524	575.27	0.0094
D'11	220.77	0.0516	754.00	0.0121

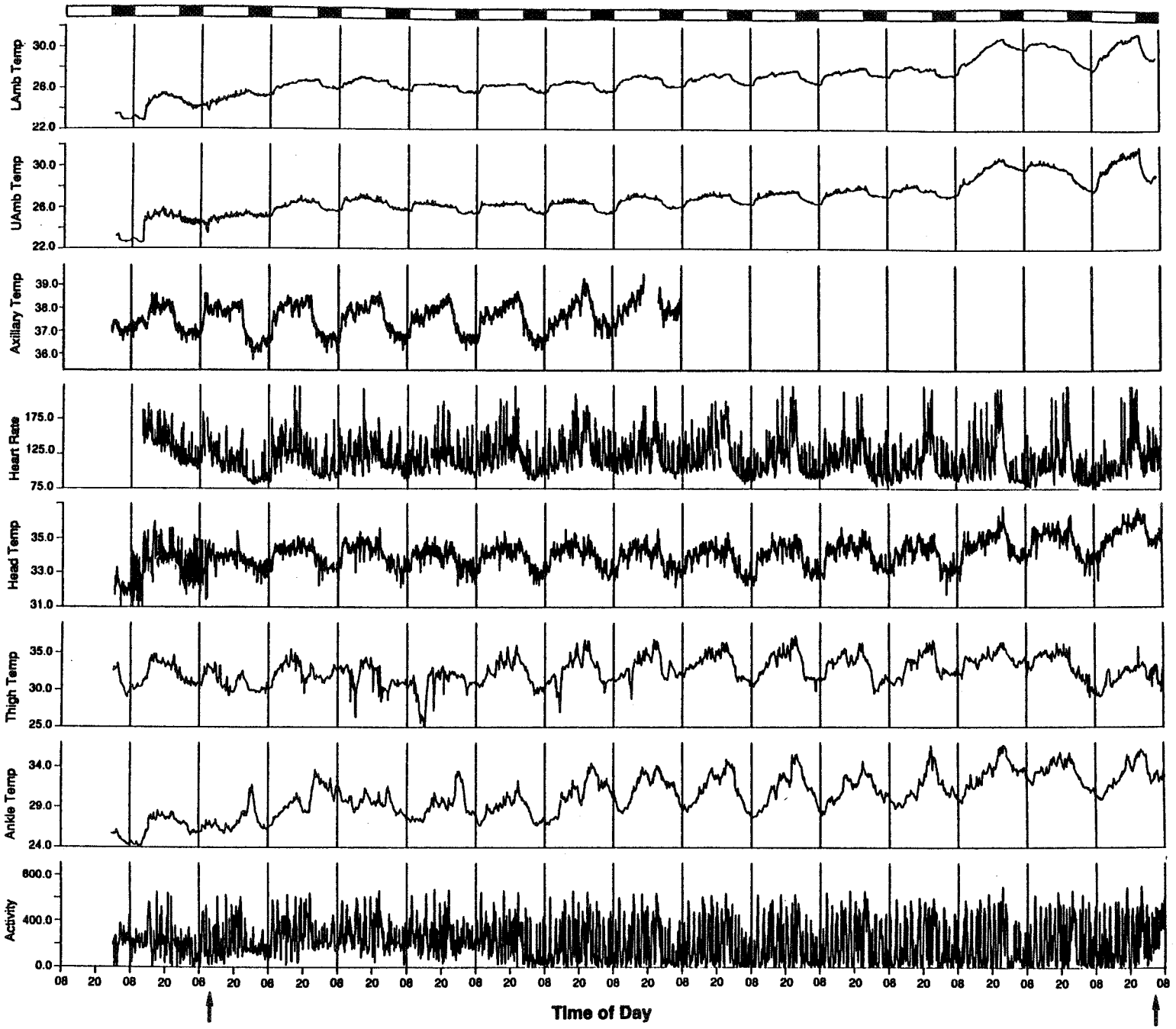

Figure 1. Data from one of the two monkeys flown on COSMOS 2044. Data record begins on day one just prior to midnight. Arrows indicate launch and recovery.

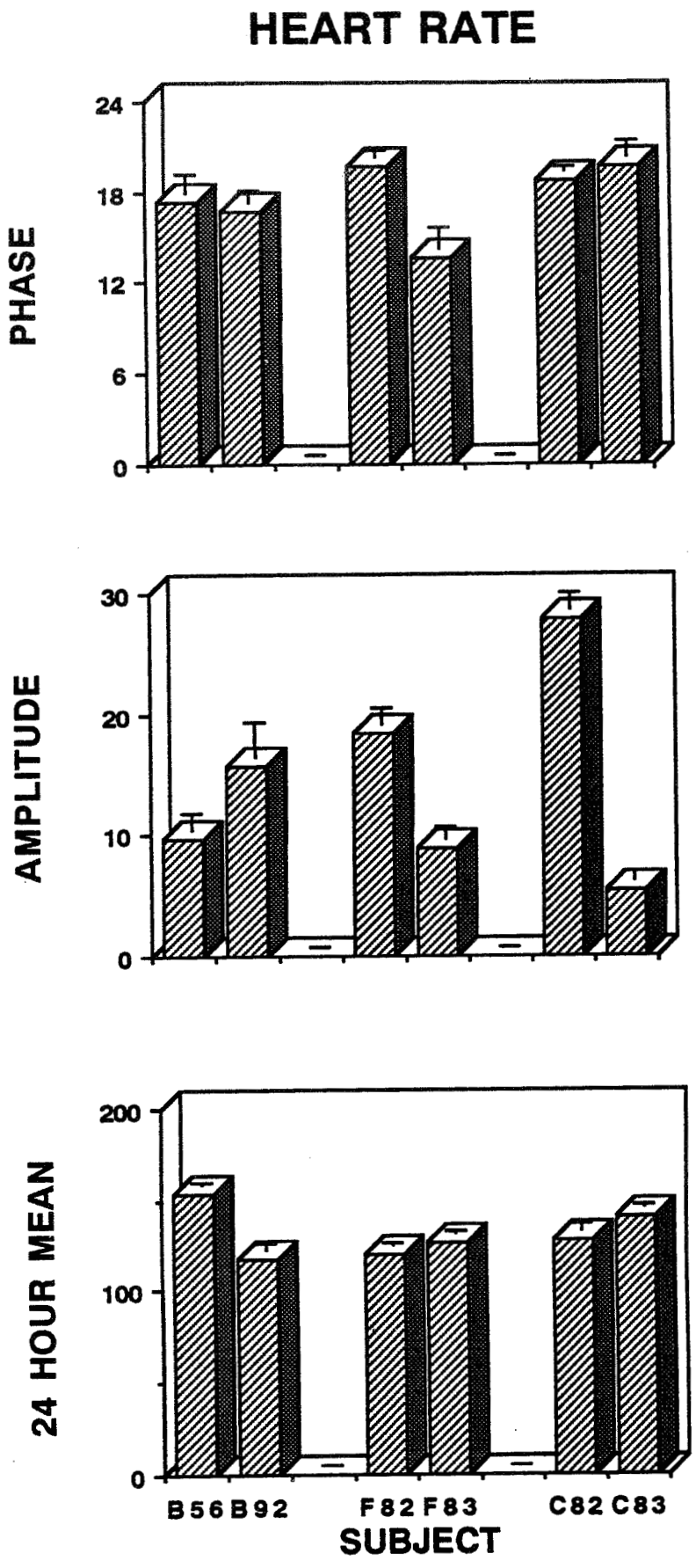

Figure 2. Plot of the average heart rate circadian phase (hours), amplitude (beats/min), and 24 hour mean (beats/min) for each animal in the three experimental conditions.

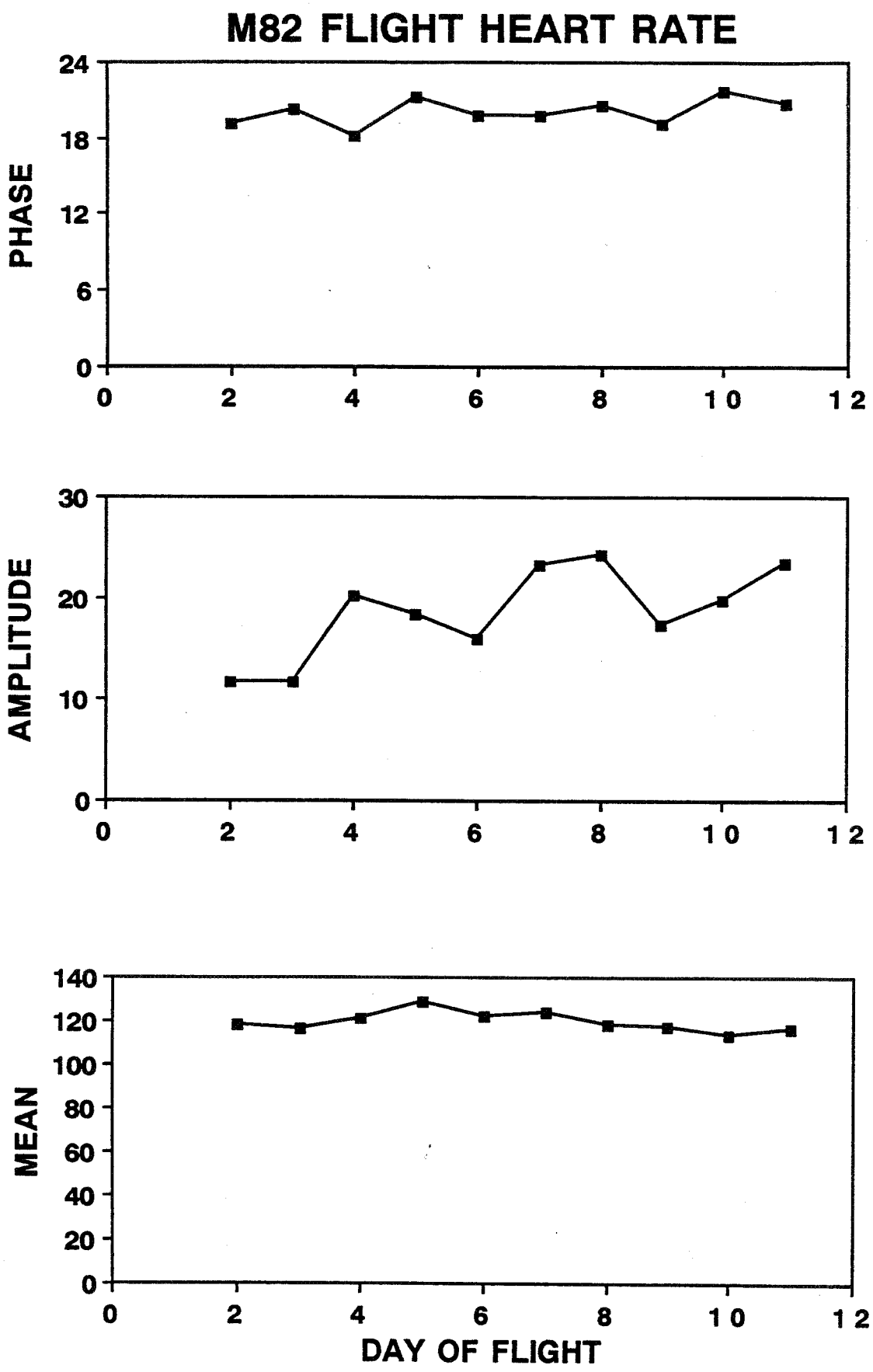

Figure 3. An example of the daily trend analysis of the heart rate data from subject M82 flight data.

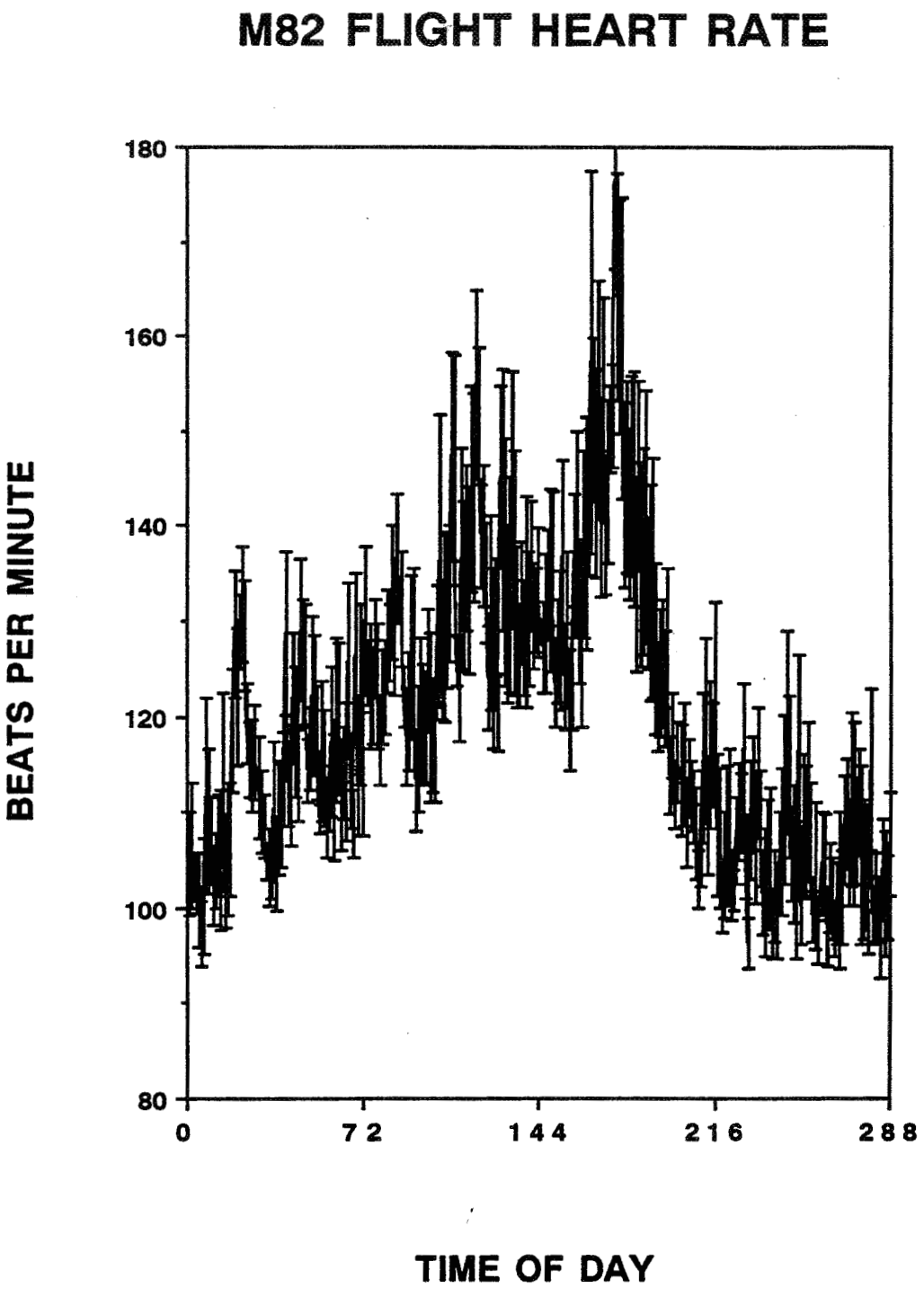

Figure 4. Average 24 hour waveform pattern of M82 heart rate rhythm over the flight. Phase angle zero corresponds to the time of lights on.

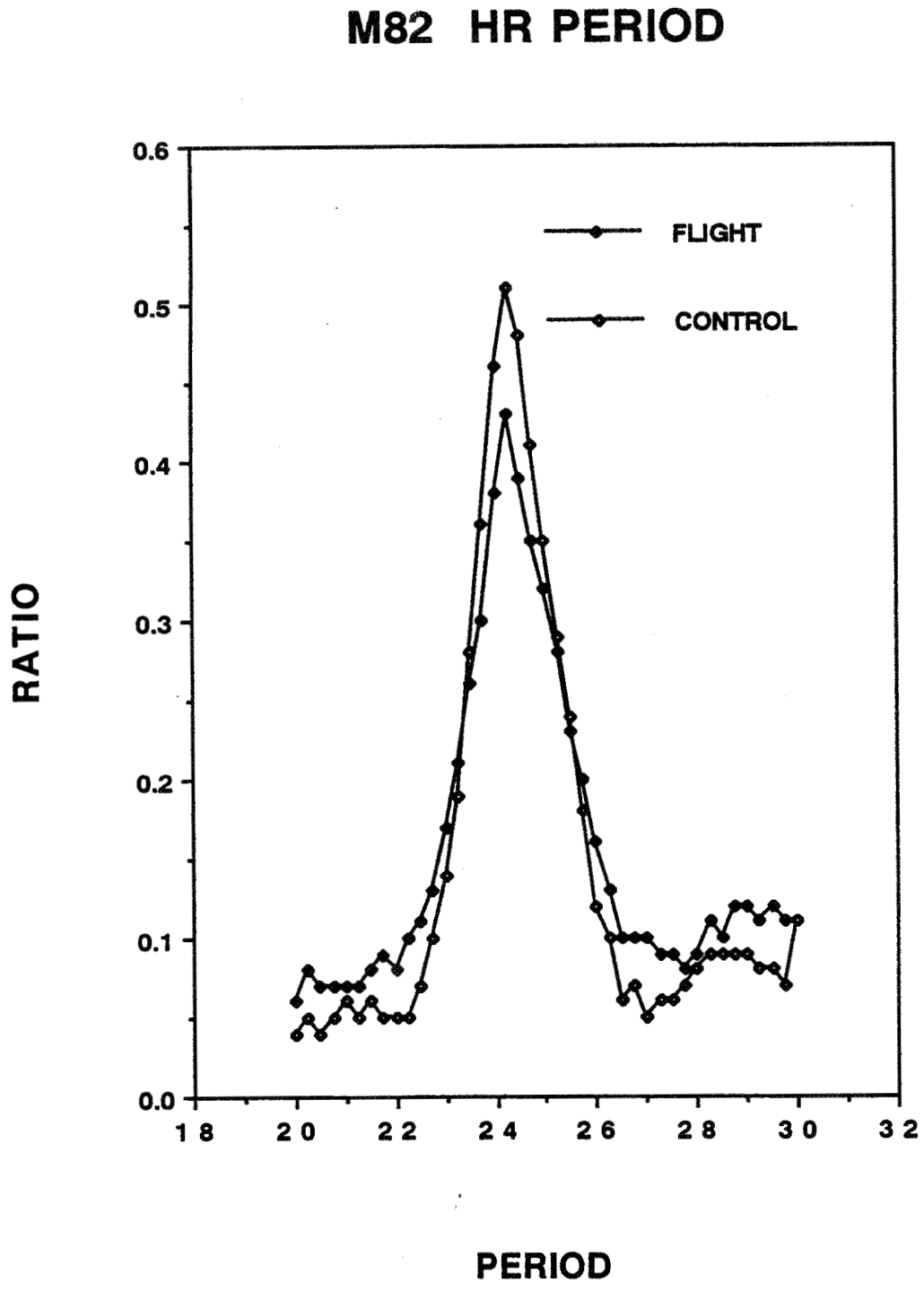

Figure 5. Plot the average circadian period of M82 in the postflight control and flight experiments.

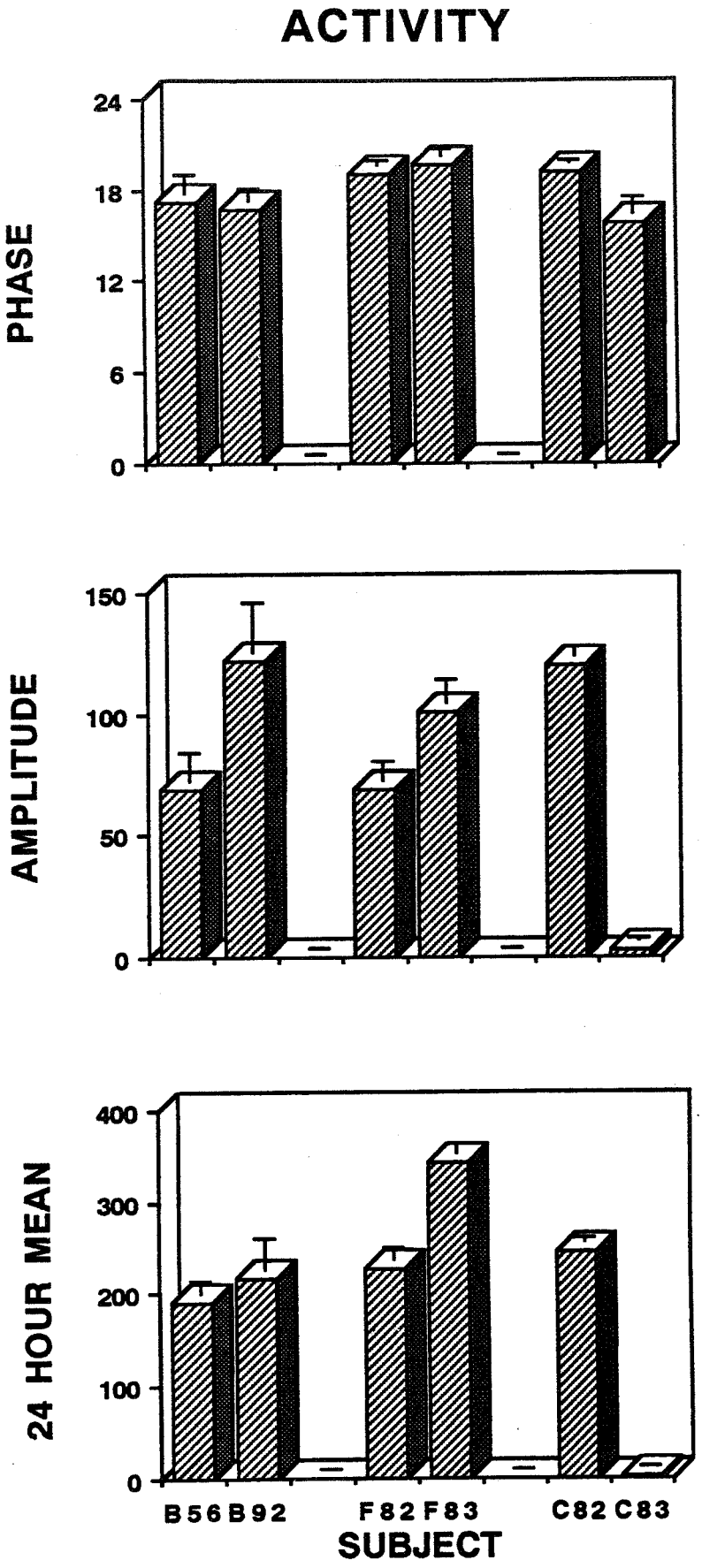

Figure 6. Average phase, amplitude, and 24 hour mean of the activity rhythm of the two baseline control animals.

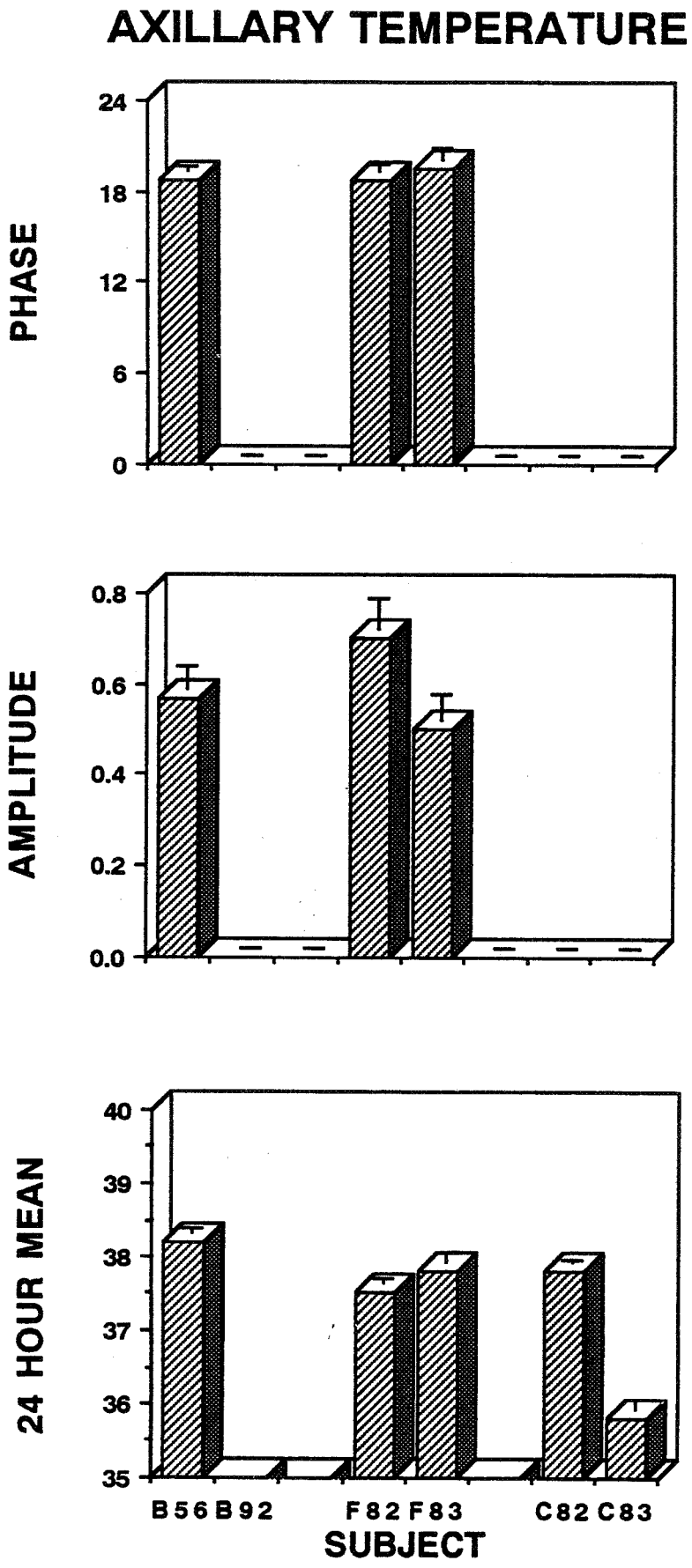

Figure 7. Average phase, amplitude, and 24 hour mean of the axillary temperature of the two baseline control animals.

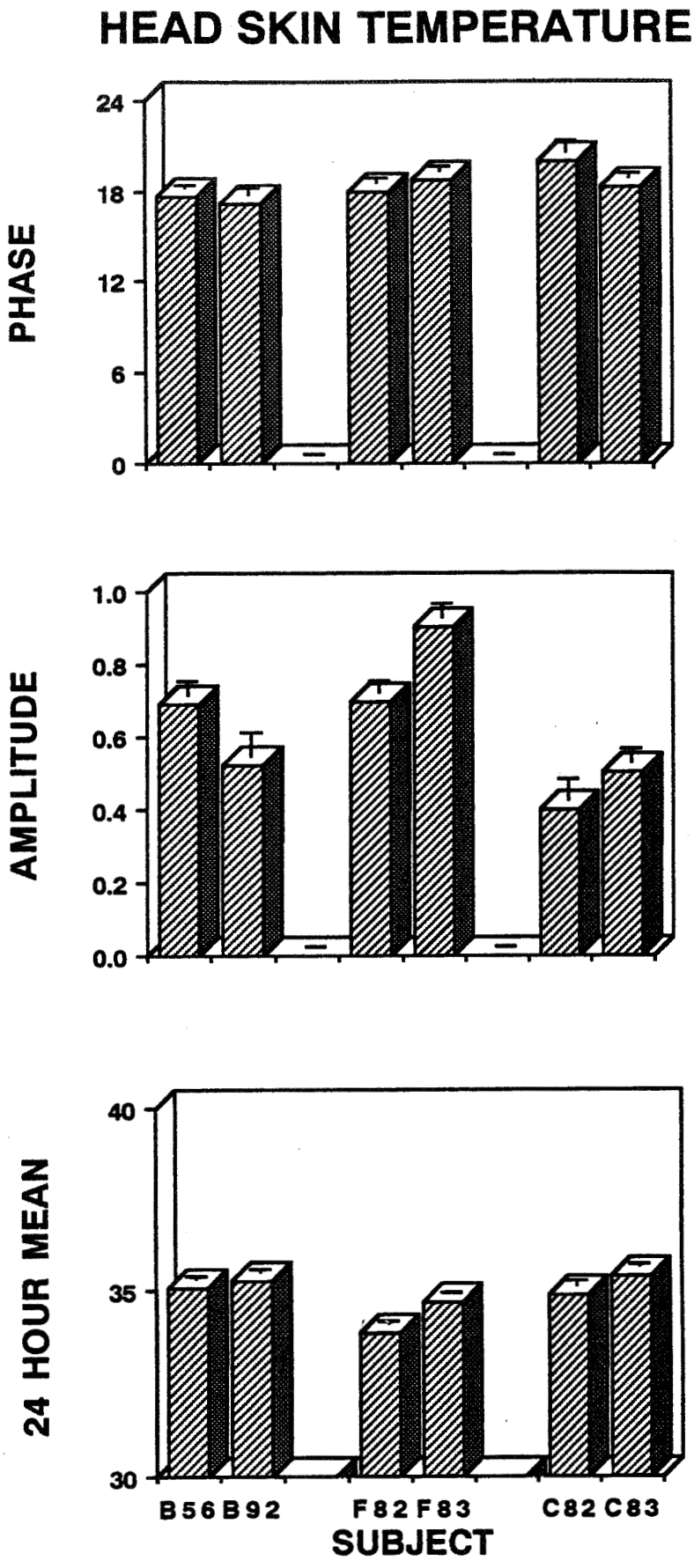

Figure 8. Average phase, amplitude, and 24 hour mean of the head skin temperature of the two baseline control animals.

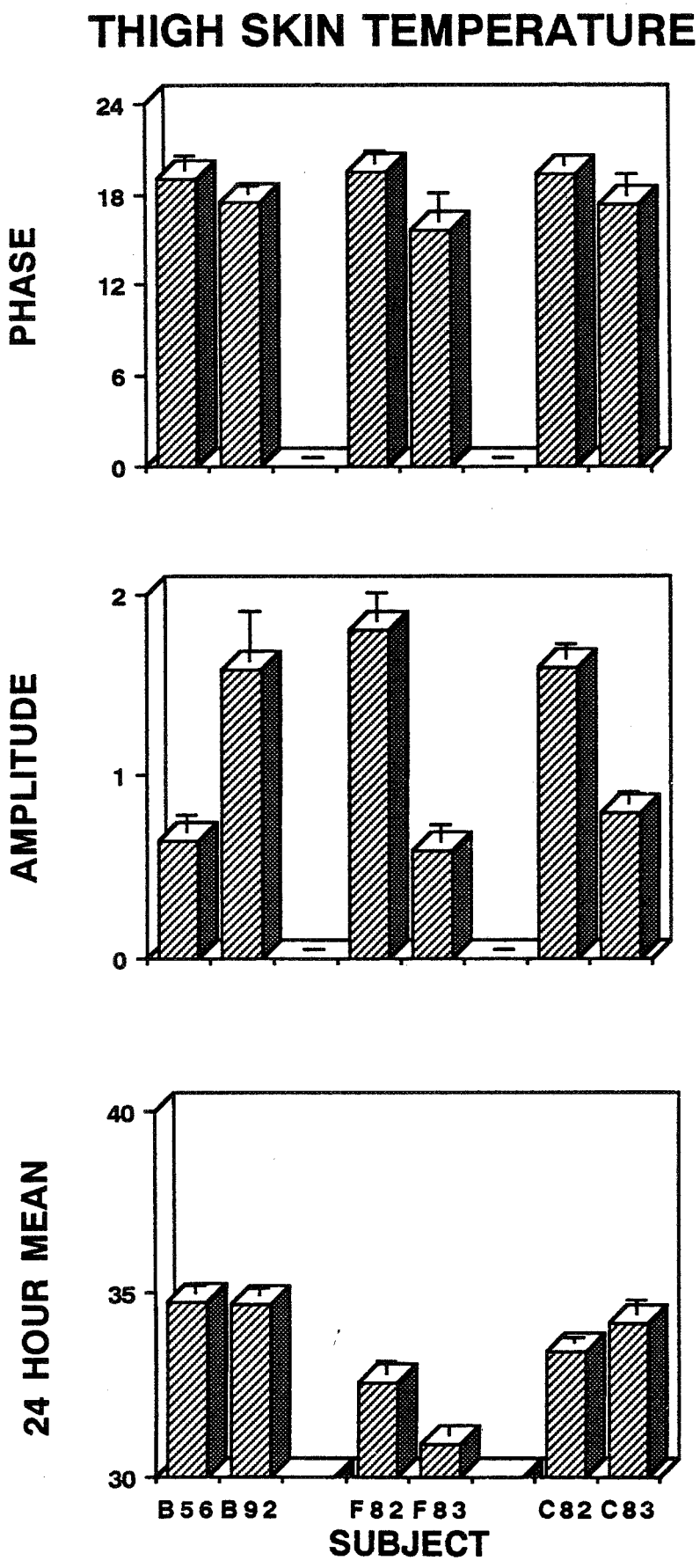

Figure 9. Average phase, amplitude, and 24 hour mean of the thigh skin temperature of the two baseline control animals.

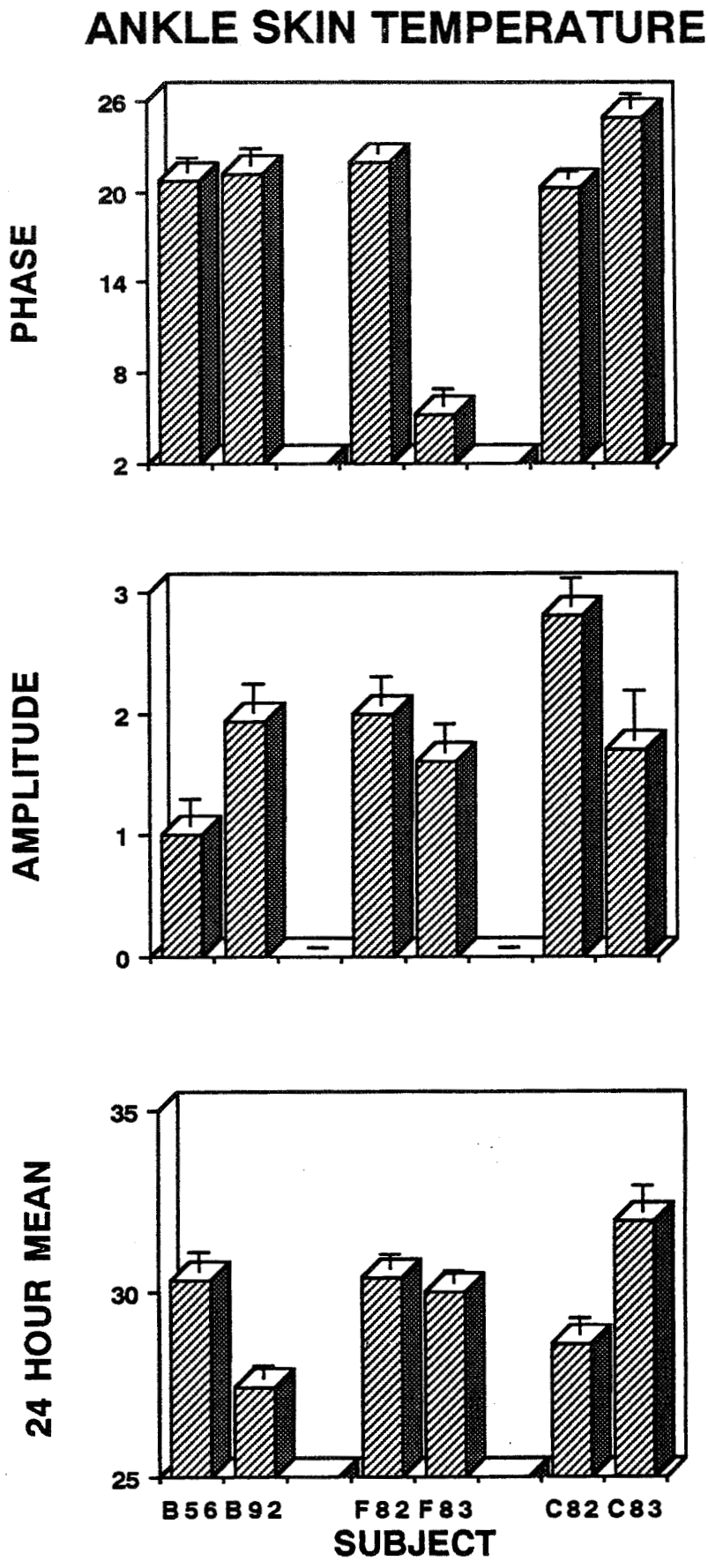

Figure 10. Average phase, amplitude, and 24 hour mean of the ankle skin temperature of the two baseline control animals.

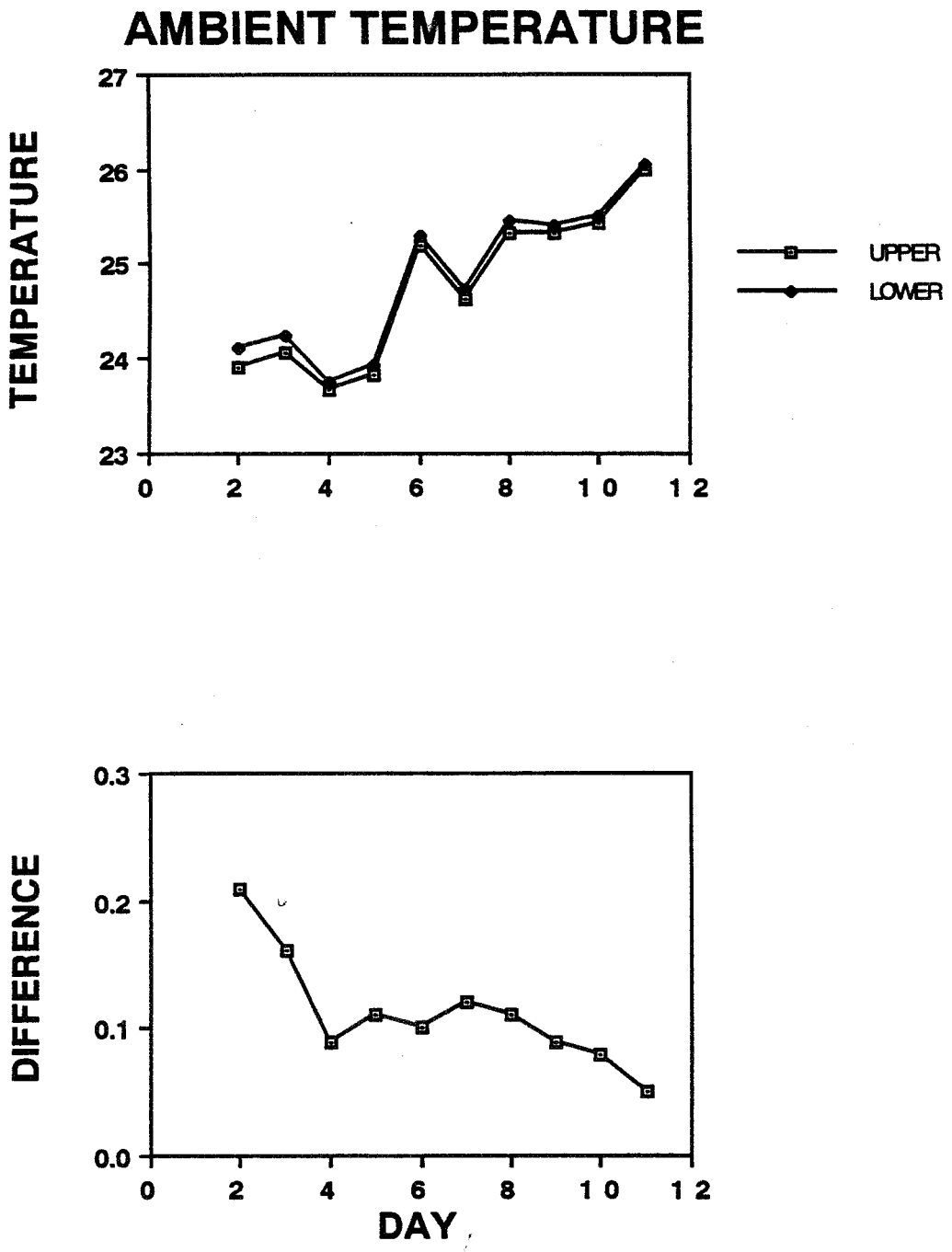

Figure 11. Daily postflight ambient temperature of the animal cage for M82 and difference between upper and lower temperatures.

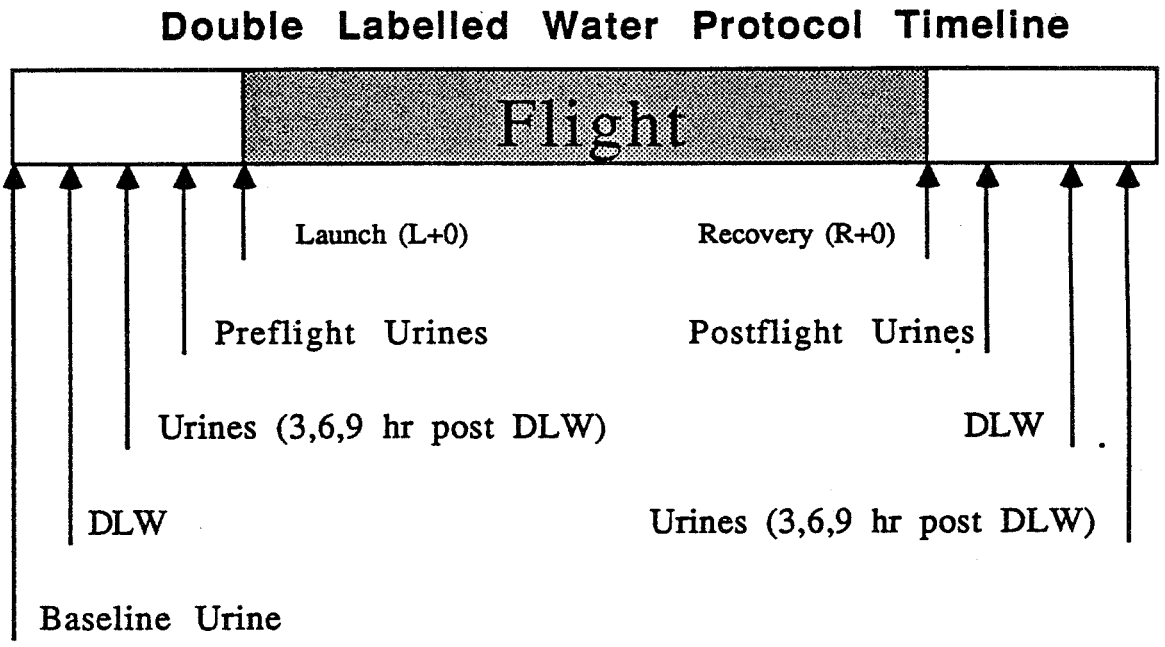

Figure 12. Urine collection protocol, used for inflight and two ground control studies.

Page intentionally left blank

III. SCIENCE REPORTS

D. RADIATION STUDIES

Page intentionally left blank

54-51
51369

EXPERIMENT K-7-41

RADIATION EXPERIMENTS ON COSMOS 2044

Principal Investigator:

E. V. Benton
Physics Research Laboratory
University of San Francisco
San Francisco, CA

Co-Investigators:

A. L. Frank
E. R. Benton
Physics Research Laboratory
University of San Francisco
San Francisco, CA

V. E. Dudkin
E.E. Kovalev
A. M. Marenny
Institute of Biomedical Problems
Moscow, USSR

Page intentionally left blank

EXPERIMENT K-7-41

RADIATION EXPERIMENTS ON COSMOS 2044: PARTS A, B, C, D, E

E.V. Benton, E.R. Benton, A.L. Frank, V.E. Dudkin and A.M. Marenny

ABSTRACT

The Cosmos 2044 biosatellite mission offered the opportunity for radiation measurements under conditions which are seldom available (an inclination of 82.3° and altitude of 294 x 216 km). Measurements were made on the outside of the spacecraft under near-zero shielding conditions. Also, this mission was the first in which active temperature recorders (the ATR-4) were flown to record the temperature profiles of detector stacks. Measurements made on this mission provide a comparison and test for modeling of depth doses and LET spectra for orbital parameters previously unavailable. Tissue absorbed doses from 3480 rad (252 rad/d) down to 0.115 rad (8.33 mrad/d) were measured at different depths (0.0146 and 3.20 g/cm^2, respectively) with averaged TLD readings. The LET spectra yielded maximum and minimum values of integral flux of 27.3 x 10^{-4} and 3.05 x 10^{-4} cm^{-2}s^{-1}sr^{-4} of dose rate of 7.01 and 1.20 mrad/d, and of dose equivalent rate of 53.8 and 11.6 mrem/d, for LET$_{\infty}$•$H_20 \geq 4$ keV/μm. Neutron measurements yielded 0.018 mrem/d in the thermal region, 0.25 mrem/d in the resonance region and 3.3 mrem/d in the high energy region. The TLD depth dose and LET spectra have been compared with calculations from the modeling codes. The agreement is good but some further refinements are in order. In comparing measurements on Cosmos 2044 with those from previous Cosmos missions (orbital inclinations of 62.8°) there is a greater spread (maximum to minimum) in depth doses and an increased contribution from GCRs, and higher LET particles, in the heavy particle fluxes.

INTRODUCTION

The Cosmos 2044 mission was the latest of five Soviet biosatellite missions in which the University of San Francisco has participated. The previous missions were Cosmos Nos. 782, 936, 1129 and 1887 /Peterson et al., 1978; Benton et al., 1978a, 1978b, 1981, 1988; Kovalev et al., 1981/. Previous work which applies to radiation measurements in space also covers a wide range of U.S. space flights, including the Gemini, Apollo, Skylab, Apollo-Soyuz and Space Shuttle missions /Benton et al., 1977a, 1977b; Benton and Henke, 1983; Benton, 1984; Benton et al, 1985; Benton, 1986; Benton and Parnell, 1987/.

The Cosmos biosatellites have been host to a wide variety of space biology and radiation experiments performed by international research groups. Radiation dosimetry and spectrometry experiments are typically included for the purpose of providing radiation measurements specific to the mission and to implement long-range goals of mapping radiation intensities in near-earth orbit and of providing measured comparisons for the radiation modeling codes. The Cosmos missions also offer the opportunity to intercompare measurements with other research groups and in this way compare measurements of certain quantities (i.e. dose, LET) using different techniques.

The Cosmos 2044 biosatellite mission took place between September 15 and 29, 1989, for a duration of 13.8 days. The orbit was elliptical, with minimum and maximum altitudes of 216 km and 294 km, respectively, and an inclination of 82.3° The selection of international experiments on the flight included K-7-41 from the University of San Francisco. This experiment was composed of five parts (A through E) for the purpose of measuring (A) depth dose distribution in thermoluminescent detector (TLD) stacks under very low shielding, (B) LET spectra of HZE particles under low shielding, with stacks composed of plastic nuclear track detectors (PNTD) and emulsions, (C) high energy neutron and proton fluxes with ^{59}Co activation foils, (D) high energy

neutron fluxes with ^{232}Th fission foils and (E) thermal and resonance neutron fluxes with ^{6}LiF foils. The measurements will be used to determine radiation levels for the special orbital parameters of this mission and will be compared with calculations from radiation modelling codes.

EXPERIMENTS

The five parts of the experiment K-7-41 are discussed individually below.

Part A

The objective of this experiment was to measure the depth dose under very thin shielding on the outside of the spacecraft and to determine what fraction of the dose was due to low energy electrons versus heavy charged particles. This required that the shielding of the outermost detectors be no more than a few mg/cm^2 and that the detectors themselves also be very thin (because of the short ranges of the particles). The maximum depth in the TLD stacks was 3.2 g/cm^2. Although computer codes exist for calculating doses encountered in LEO both from protons and electrons, there have been only a few instances where a direct comparison (under very thin shielding) has been possible between experiment and theoretical prediction. The orbit of Cosmos 2044 will allow the codes to be compared for parameters quite different from any for previous flights.

The TLD stacks were placed in cylindrical holders (Fig. 1) which were then arrayed in plates attached to the outside of the spacecraft. Three TLD stacks were placed in each of four mounting plates (B9-1, -2, -3, -4) for a total of twelve flight stacks. The TLDs and all other detectors mounted on the outside of the spacecraft were held in "clam-shell" style containers which were closed before re-entry to prevent heating of the detectors in the atmosphere. Some detectors and two containers are shown in Fig. 2.

Each stack was composed of both thin (0.02395 g/cm^2 thickness) and thick (0.2322 g/cm^2 thickness) TLD-700 extruded chips. Thin TLDs were used to a depth of 0.5175 g/cm^2 and thick TLDs at greater depths. A double window of 7.5 μm thick Kapton polyimide films, both aluminized to an optical density of 3, held the TLDs in place and shielded them from sun and space. In the depth-dose results, the mass density of the Kapton (0.00213 g/cm^2) has been converted to an equivalent mass density of ^{7}LiF (0.00266 g/cm^2) on the basis of low energy proton ranges.

Part B

The objective here was to measure the low energy, heavy particle (excluding electrons) LET spectra under very low shielding (outside the spacecraft) and as a function of depth. Although there have been some previous measurements of LET spectra under such conditions, the orbital dependence and the effects of solar cycle on the low energy charged particle component are still not well understood. The very high inclination orbit of Cosmos 2044 (82.3^0)will provide a test of radiation models in the polar regions, which has not been possible before.

The hardware consisted of two hermetically sealed flight units containing PNTD and nuclear emulsion stacks and with aluminized Kapton double-windows, as in Part A. The PNTD stacks were 3 cm in diameter and included sets of CR-39 and Cronar polyester detectors. The emulsion stacks were enclosed in thin stainless steel cylinders of the same diameters. The physical configurations of the units and stacks are shown in Figs. 3 and 4. The flight units were placed outside the spacecraft with F1 being in Plate B9-2 and F2 in Plate B9-1.

In addition to the radiation detector stacks, these units also held temperature sensors for the ATR-4 Ambient Temperature Recorder which has been developed by NASA for spacecraft use (NASA, 1989). This system allows a time-temperature profile to be determined for each sensor included on the mission (up to eight sensors). This is an important consideration for flight materials, such as some of the radiation detectors, which are heat sensitive.

Part C

Here the intent was to obtain some information on the neutron energy spectra. The detectors were located both on the outside and inside of the spacecraft.

The outside experiment consisted of two flight units containing ^{59}Co activation foils and PNTD films. An aluminum frame with aluminized Kapton double-windows was placed above the detectors but the sides of the units were open to vacuum. The PNTDs used were Cronar polyester. The purpose of the PNTDs in this experiment was for an intercomparison between those open to vacuum and those hermetically sealed. Due to space limitations, CR-39 was not included. The configuration of the units is shown in Fig. 5. The flight placement of the detectors was F1 in Plate B9-4 and F2 in Plate B9-3.

The inside detector consisted of a single ^{59}Co activation foil. In conjunction with the activation foil was a stack of nuclear emulsions to provide a comparison with the emulsions exposed on the outside of the spacecraft in Part B. The selection of available isotopes with suitable activation cross sections and decay product half-lives for spaceflights of a few days places severe limitations on this method. Cross sections exist for the measurement of both low energy (thermal plus resonance) and high energy (>10 MeV) neutrons, with some proton contribution, with the activations forming ^{60}Co and ^{58}Co. However, readout requires a very sensitive, low background spectrometer.

Part D

The goal of this part was to measure high energy (>1 MeV) neutron fluxes and dose equivalent rates averaged over the mission duration. The detectors were fission foils of ^{232}Th in conjunction with solid state nuclear track detectors (SSNTDs) of muscovite mica. There were two flight units (F1 and F2) and each unit was composed of four ^{232}Th foils with mica (1.27 cm in diameter) in an aluminum and Lexan polycarbonate holder (see Fig. 6). The arrangement of the foils was mica/^{232}Th /mica and lead discs of 0.5 mm thickness were placed to each side for reduction of radiation from the ^{232}Th foils. The flight units were mounted on the outside of the spacecraft, with F1 in Plate B9-8 and F2 in Plate B9-7.

Part E

The goal here was to measure the thermal (<0.2 eV) and resonance (0.2 eV <E_n <1 MeV) neutron fluxes and dose equivalent rates averaged over the mission duration. The detectors were layers of ^{6}LiF (TLD-600) in conjunction with CR-39 PNTDs. There were two flight units and each unit was composed of two ^{6}LiF layers with CR-39 (1.27 x 1.27 cm) in an aluminum and Lexan polycarbonate holder (see Fig. 7). The arrangement of the components was CR-39/^{6}LiF/CR-39 with Gd foil of 0.0025 cm thickness around one of the two detectors. The Gd foil absorbs thermal neutrons and allows a separation of thermal and resonance neutrons. The flight units were mounted on the outside of the spacecraft, with F1 in Plate B9-5 and F2 in Plate B9-6.

Processing and Readout of Detectors

a). Temperature Profile and Environmental Conditions During the Cosmos 2044 Mission

The exposed Cosmos 2044 detectors were returned to this laboratory on 12 October 1989, or thirteen days after satellite re-entry. The condition of the flight units appeared generally good, with the possible exception of the sealed PNTD/emulsion stack units (Part B) where the outer Kapton windows were found to be easily flexed. This was due to tiny perforations, apparently from micrometeorite impacts, causing the windows to lose their vacuum seals. It was subsequently determined that the inner windows were not perforated and that the flight units retained their air during the mission. This is important to the response of the PNTDs where a deficiency of oxygen results in faded or unformed latent particle tracks.

Temperature Measurement

During the mission, the temperature profiles were measured by two ATR-4 Ambient Temperature Recorders (NASA, 1989). Each of these devices had four temperature sensors which were distributed over plates containing flight dosimeters (Plates B9-2 and B9-6 in the KHA-1 clamshell container and Plates B9-1 and B9-7 in the KHA-3 container). The two aluminum canisters used in the K-7-41B experiment each had a sensor embedded in the side and sealed with a high-temperature conducting epoxy. The sensors were accurate to +/- 0.5^{o}C over the temperature range from -40^{o} to +60^{o}C. Temperature readings were taken from each sensor at intervals of 3.75 min.

In Fig. 8 is the temperature record of the sensor in the K-7-41B F1 canister. Aside from some brief temperature spikes the variation was between 3^{o} and 36^{o}C with an average of about 22^{o}C. Based on environmental studies of the PNTDs and TLDs, no measureable effect on detector response would be expected from this temperature profile. The closure of the clamshell containers about a day before landing, as the spacecraft began moving into the outer atmosphere, is obvious from the drop in temperature.

In Fig. 9 is the temperature record of the sensor in the B F2 canister. The temperature profile is similar to, but about 5^{o}C less than, the profile for F1 up to the last day. As the spacecraft began moving into the upper atmosphere prior to landing, the clamshell container (KHA-3) did not close. Where the F1 sensor temperature decreased, that of F2 increased to above 50^{o}C and then spiked to above 60^{o}C during the landing. Based on environmental studies for a more extended period of time, these temperatures could have affected the PNTD response, but because of the brevity of the conditions there was no measurable effect. The PNTDs from F1 and F2 were intercompared after the processing.

After disassembly of the flight units, the detectors were processed and read out as follows:

b). TLD Readout

The TLDs (TLD-700) were read out on Harshaw Model 2000 and 4000 Readers. In each case glow peak integrated current was measured between 120^{o} and 250^{o}C. In addition, the glow peak curves were recorded up to 325^{o}C with the Model 4000 Reader. Flight, background and standard exposures were read out together for both the thin and thick TLDs. Standard exposures of 1 rad from a ^{137}Cs source were employed and TLD calibrations extending up to 10^{4} rad were used to correct for the supralinear high dose response of the least shielded TLDs (Fig. 10). All flight TLD readings were then corrected for background and converted to tissue rad doses.

c). PNTD Processing and Readout

The CR-39 PNTDs were processed in 6.25*N* NaOH solution at 50°C for 7 days. The bulk etch, *B* (thickness removed from a single surface), was measured for each film. Pairs of detectors were reassembled in their flight orientations and the two inner, adjacent surfaces were scanned under an optical microscope. This enabled the particles to be separated into short range (SR): matching tracks appearing on only the two interior surfaces, and long range, galactic cosmic rays (GCR): matching tracks appearing on all four surfaces of the pair of films. The SR particles include short-range secondary particles from target nuclei within the plastic and stopping primary galactic and trapped particles. All protons are registered as SR particles because of their short registration range in CR-39. The GCR particles include both primary GCRs and the long-range secondaries which are mainly the projectile fragments of GCRs. The major and minor axes of the elliptical surface openings of tracks were measured. The axial measurements, together with the *B* of the samples and the calibrated LET response function of the CR-39 material, were then used to generate particle LET spectra.

d). Nuclear Photographic Emulsions

The nuclear emulsions (Fuji types 6B and 7B) have been processed by standard techniques and are being read out at Marshall Space Flight Center, Huntsville.

e). ^{59}Co Activation Foils
Immediately after arrival, the ^{59}Co foils were transferred to Dr. A. Smith of Lawrence Berkeley Laboratory (LBL) to be read out at a highly shielded site with high efficiency Ge(Li) detectors. The data analysis and background studies for these measurements are still in progress.

f). ^{232}Th/Mica Detectors

The muscovite mica discs from these detectors were processed for 2 hr at 21°C in 50% HF acid. They had been processed for 5 hr under the same conditions pre-flight to develop the fossil fission tracks to large size. The flight tracks on the discs were then counted under an optical microscope. Backgrounds were counted using the backs of the flight discs. Detector calibrations based on fission cross sections for neutrons and protons and assumed spectral distributions for neutrons and protons were used to convert track densities into neutron fluences (see Benton et al., 1978a). Dose equivalents were determined using Quality Factors (QF) of 10.

g)^{6}LiF /CR-39 Detectors

The CR-39 films from these detectors were processed in 6.25 *N* NaOH solution at 70°C for 5 hr. Track densities were counted on the surfaces both adjacent to and opposite to the ^{6}LiF layers in order to determine net alpha particle track densities from the ^{6}Li(n,α) T reaction. The ground control detectors were used to measure the non-flight alpha particle backgrounds. Since there were CR-39 films on both the space and spacecraft sides of the ^{6}LiF layers, the average track densities on the two films yielded a measure of 4π neutron incidence.

In each flight unit, one detector was covered with 0.0025 cm-thick Gd foil and one was not. The thermal neutron absorbance of the Gd gives an effective low energy cutoff of 0.2 eV for the covered detectors. By subtraction the measured track densities were separated into those due to neutrons below and above 0.2 eV.

The flight background track densities, counted on the backs of the CR-39 detectors, were quite large and also depth dependent. Since the front and back of the detectors were at different depths, it was necessary to interpolate between only two measured points to obtain the appropriate

backgrounds. Consequently, the measurement accuracy is somewhat less than implied by the associated standard deviations which were calculated from counting statistics. In addition, the neutron spectra assumed in the calibrations are the completely thermalized distribution below the Gd cutoff and a 1/E distribution above. Deviations of the flight spectra from these assumptions will also contribute to measurement error.

RESULTS

Part A

The average depth dose rates for the three TLD stacks in each of the four flight plates are plotted in Figs. 11, 12, 13 and 14. The measurements show more than a 4 order-of-magnitude decrease in dose rate down to 3 g/cm^2 depth. The average plate dose rates are given in Table 1. The total flight doses for the twelve TLD stacks are given in Tables 2a, -b, -c and -d. It can be seen that there are shielding differences for the various stacks. As an example, three individual TLD stack distributions for Plate No. B9-3 are shown in Fig. 15. Stack No. 1 dose rates are clearly less than Stacks Nos. 3 and 9. There are substantial variations at the tops of the stacks, as seen in Tables 2a--2d (2040 rad for No. 2 up to 4480 rad for No. 9) while stacks Nos. 1, 5 and 10 have smaller doses at the maximum depths than do the others.

Part B

The CR-39 PNTDs have been given the standard processing for 7 days in 6.25 *N* NaOH solution at 50^{0}C. Adjacent pairs from the flight stacks were reassembled, scanned and measured with a microscope and electronic micrometer. The particle tracks were separated into galactic cosmic rays (GCR), which traversed all four surfaces of the CR-39 pair, and short range (SR), which traversed only the two inner surfaces or the two inner surfaces plus one outer surface of the pair. The GCRs are mainly galactic cosmic rays or their projectile fragments where $Z \geq 2$. Anomalous particles may also contribute to the four-surface tracks. The SR tracks are mainly short range secondary particles or primary protons near their stopping points. The short registration range of protons in CR-39 makes four-surface proton tracks very low-probability events. GCR stopping particles of $Z \geq 2$ can contribute to SR tracks, but this also has a low probability.

Five sets of integral LET spectra (Total, GCR and SR) from the PNTD stack in the F1 canister are given in Figures 16--20. Four sets of spectra from the F2 canister are given in Figures 21--24. The minimum to maximum shielding is covered in each PNTD stack. The minimum shielding is greater for F1 because the least shielded CR-39 layer was damaged on one surface by the high electron dose encountered. An extra layer of thin plastic protected the least shielded CR-39 layer in F2.

The decrease in total flux with increasing shielding thickness is obvious in both F1 and F2. However, the least shielded PNTD in F1 has a greater integral flux than that in F2 (factor of 1.7) despite being more heavily shielded. This demonstrates a directional dependence of incoming radiation with F1 (Plate B9-2 in Container KHA-1) being in better alignment with the direction of maximum flux than F2 (Plate B9-1 in Container KHA-3).

The integral measurements are given numerically in Tables 3a and 3b. The differences between F1 and F2 are seen to be greatest at small shielding thicknesses. A comparison of fluxes, dose rates and dose equivalent rates reveals that average particle LET increases with shielding thickness (dose rate/flux and dose equivalent rate/dose rate increase as average LET increases). This agrees with previous measurements on Cosmos 1887. The fraction of total flux due to SR particles decreases with shielding thickness, although this is irregular in F2. The above two observances are

consistent with a more rapid filtering out of low energy protons than of higher Z particles with increasing shielding.

The nuclear emulsions which were a part of the detector stacks are still undergoing analysis and will be reported at a later time.

Part C

The ^{59}Co activation foils have been read out. Background studies and data analysis are still in progress. The results will be reported at a later time.

Part D

The measurement results from the ^{232}Th/mica fission foil detectors are given in Table 4. Each flight detector included eight mica discs (0.5 in diameter). The statistical standard deviations of the measurements were computed from the scatter of the eight counted track densities. There is a 15% difference between the neutron fluxes for the two flight units but this difference is within the limits of accuracy of the track counting statistics. The average dose equivalent rate of high energy neutrons for the mission was 3.3 mrem/d.

Part E

The results of the ^{6}LiF/CR-39 thermal and resonance neutron measurements are given in Table 5. An obvious feature is the much smaller resonance neutron dose in detector F1 as compared to F2. The CR-39 detectors both above (space side) and below (spacecraft side) the ^{6}LiF layer confirmed the difference. Most of the tracks measured in F2 were on the space side of the ^{6}LiF layer. The space side CR-39 yielded a track density 2.7 times higher than the spacecraft side CR-39. This could imply a large epithermal neutron flux, incident from the space side of detector F2, which was not present in detector F1. However, as mentioned in the Readout section, the background subtraction from the detectors contained an element of uncertainty. It is possible that the experimental uncertainty in the resonance neutron results is larger than expected. Because of the method of subtraction in the data reduction, the thermal neutron results are much less affected than the resonance results.

SUMMARY AND DISCUSSION

The results from Cosmos 2044 are compared with previous Cosmos measurements in Table 6. It is seen in the TLD results that in the total absorbed dose rates for tissue found outside the spacecraft there is a greater spread on Cosmos 2044 when compared to Cosmos 1887. The maximum dose rate (minimum shielding) is greater and the minimum dose rate (maximum shielding) is less. This indicates that the higher inclination, lower altitude orbit of 2044 must have encountered greater trapped electron fluxes but smaller trapped proton fluxes than 1887. The smaller trapped proton fluxes can be explained in that the lower altitude Cosmos 2044 orbit passed beneath the higher flux region in the South Atlantic Anomaly (SAA). The greater trapped electron fluxes are due to the extension of the electron belt horns to lower altitudes at the higher latitudes. The large uncertainties seen in the maximum and minimum dose rates on Cosmos 2044 are due to the spread in the three measurements of the TLD stacks in Plate No. B9-4.

The PNTD measurements on Cosmos 2044 are directly comparable with those of Cosmos 1887 outside the spacecraft. It can be seen that while the maximum flux on 2044 is 0.80 times as high as on 1887, the dose equivalent rate is 1.75 times higher. The average LET, and also particle Z, were greater on Cosmos 2044. This is consistent with the higher inclination, lower altitude orbit and the resulting greater relative contribution from GCRs.

The thermal and resonance neutron fluxes and dose equivalent rates were less than previously measured, but on Cosmos 2044 the measurements were on the outside of the spacecraft, while previous measurements were inside. Their comparability is therefore questionable.

The high energy neutrons have about half the flux and dose rate measured on Cosmos 936 and 1129; however, this comparison is also between detectors outside and inside the spacecraft.

In Figure 25, a measured depth dose profile in TLD-700 is compared with calculated depth doses for trapped electrons and protons behind plane aluminum shields for the Cosmos 2044 orbit at solar maximum /Watts, 1990/. This demonstrates that for shielding thicknesses up to 1 g/cm^2 trapped electrons contribute most of the dose. The model electron spectrum appears deficient at very low energies and somewhat harder than that measured. The trapped proton dose rate drops to about 0.001 rad/d at 3 g/cm^2 , where the electron dose is a very small fraction of the total. This is a factor of 8 lower than the measurements. GCRs dominate total doses under thicker shielding for the Cosmos 2044 orbit, so this general result is expected.

In Figures 26 and 27, measured LET spectra under 0.0935 g/cm^2 are plotted with some recent calculations made with the NRL CREME code. In Figure 26, an SR spectrum is compared with calculations which omit GCRs with Z >2. Most of the contributions to short-range tracks are included in these calculations. The fit below 100 MeV-cm^2 /g (10 keV/ μm) begins to diverge, but, as discussed above, the experimental measurements can also diverge in this LET region due to directional effects. The calculations are averaged over angle of incidence.

In Figure 27, the total flux spectrum is compared with calculations which include the GCRs through Z=28 (the contribution from particles with Z>28 is insignificant). The measured spectrum falls somewhat below the spectrum for the nearest calculated shielding (0.1 g/cm^2). It should be noted that there is some loss from the measured spectrum due to loss of very short tracks in etching of the PNTDs. However, the agreement between measurements and calculations may be off by a factor of 2 because of basic difficulties in modeling the orbital radiation environment.

REFERENCES

1. Benton, E.V., D.D. Peterson, J.V. Bailey, and T.A. Parnell.. High-LET exposure of Skylab Astronauts, Hlth. Phys. 32, 15-20, 1977a.

2. Benton, E.V., R.P. Henke, and D.D. Peterson.. Plastic Nuclear Track Detector Measurements of High-LET Particle Radiation on Apollo, Skylab, and ASTP Space Missions, Nucl. Track Det. 1, 27-32, 1977b.

3. Benton, E.V., R.M. Cassou, A.L. Frank, R.P.Henke and D.D.Peterson. Experiment K206: Space Radiation Dosimetry on Board Cosmos 936--U.S. portion of Experiment K206, in: Final Reports of U.S. Experiments Flown on the Soviet Satellite Cosmos 936 (Rosenzweig, S.N. and Souza, K.A., eds.) NASA TM 78526, 1978a.

4. Benton, E.V., D.D. Peterson, A.M. Marenny, and V.I. Popov. HZE Particle Radiation Studies Aboard Cosmos 782, Hlth. Phys. 35, 643-648, 1978b.

5. Benton, E.V., R.P. Henke, A.L. Frank, C.S. Johnson, R.M. Cassou, M.T.Tran, and E. Etter. Experiment K309: Space Radiation Dosimetry Aboard Cosmos 1129: U.S. Portion of Experiment, in: Final Reports of U.S. Plant and Radiation Experiments Flown on the Soviet Satellite Cosmos 1129 (Heinrich, M.R. and Souza, K.A., eds.), NASA TM 81288, 1981.

6. Benton, E.V. and R.P. Henke. Radiation Exposures During Spaceflight and Their Measurement, Adv. Space Res. 3, No. 8, 171-185, 1983.

7. Benton, E.V. Summary of Current Radiation Dosimetry Results on Manned Spacecraft, Adv. Space Res. 4, 153-160, 1984.

8. Benton, E.V., A.L. Frank, T.A. Parnell, J.W. Watts, Jr. and J.C. Gregory. Radiation Environment of Spacelab-1, American Inst. of Aeronautics and Astronautics Conference, AIAA Shuttle Environment and Operations II, Houston, TX, Nov. 13--15, 1984.

9. Benton, E.V., Summary of Radiation Dosimetry Results on U.S. and Soviet Manned Spacecraft, Adv. Space Res., 6, No. 11, 315-328, 1986.

10. Benton, E.V. and T.A. Parnell. Space Radiation Dosimetry on U.S. and Soviet Manned Missions, in: Terrestrial Space Radiation and its Biological Effects, P.E. McCormack, C.E. Swenberg and H. Buecker, eds., NATO ASI Series A, Life Sciences 154, N.Y.: Plenum Press, pp. 729-794, 1988.

11. Benton, E.V, A.L. Frank, E.R. Benton, V.E. Dudkin, and A.M. Marenny. Radiation Experiments on Cosmos 1887, University of San Francisco, USF-TR-74, 1988.

12. Dobson, P.N., Jr. and A.A. Midkiff. Explanation of Supralinearity in Thermoluminescence of LiF in Terms of the Interacting Track Model, Hlth. Phys. 18, 571-573, 1970.

13. Gorbics, S.G., F.H. Attix, and K. Kerris. Thermoluminescent Dosimeters for High-Dose Applications, Hlth. Phys. 25, 499-506, 1973.

14. Kovalev, E.E., E.V. Benton, and A.M. Marenny. Measurement of LET Spectra Aboard Cosmos 936 Biological Satellite, Rad. Prot. J. 1, 169-173,1981.

15. NASA-Space Life Sciences Payloads Office (1989), ATR-4 Ambient Temperature Recorder, Doc. No. A7SP-8801-D1, Ames Research Center, Moffet Field, Ca., 1989

16. Peterson, D.D., E.V. Benton, and M.Tran. K103: HZE Particle Dosimetry, in: Final Reports of U.S. Experiments Flown on the Soviet Satellite Cosmos 782,(Rosenzweig, S.N. and Souza, K.A., eds.), NASA TM 78525, 1978.

17. Watts, J.W., Jr. 1990), Marshall Space Flight Center, Huntsville, Alabama, private communication, 1988, 1990.

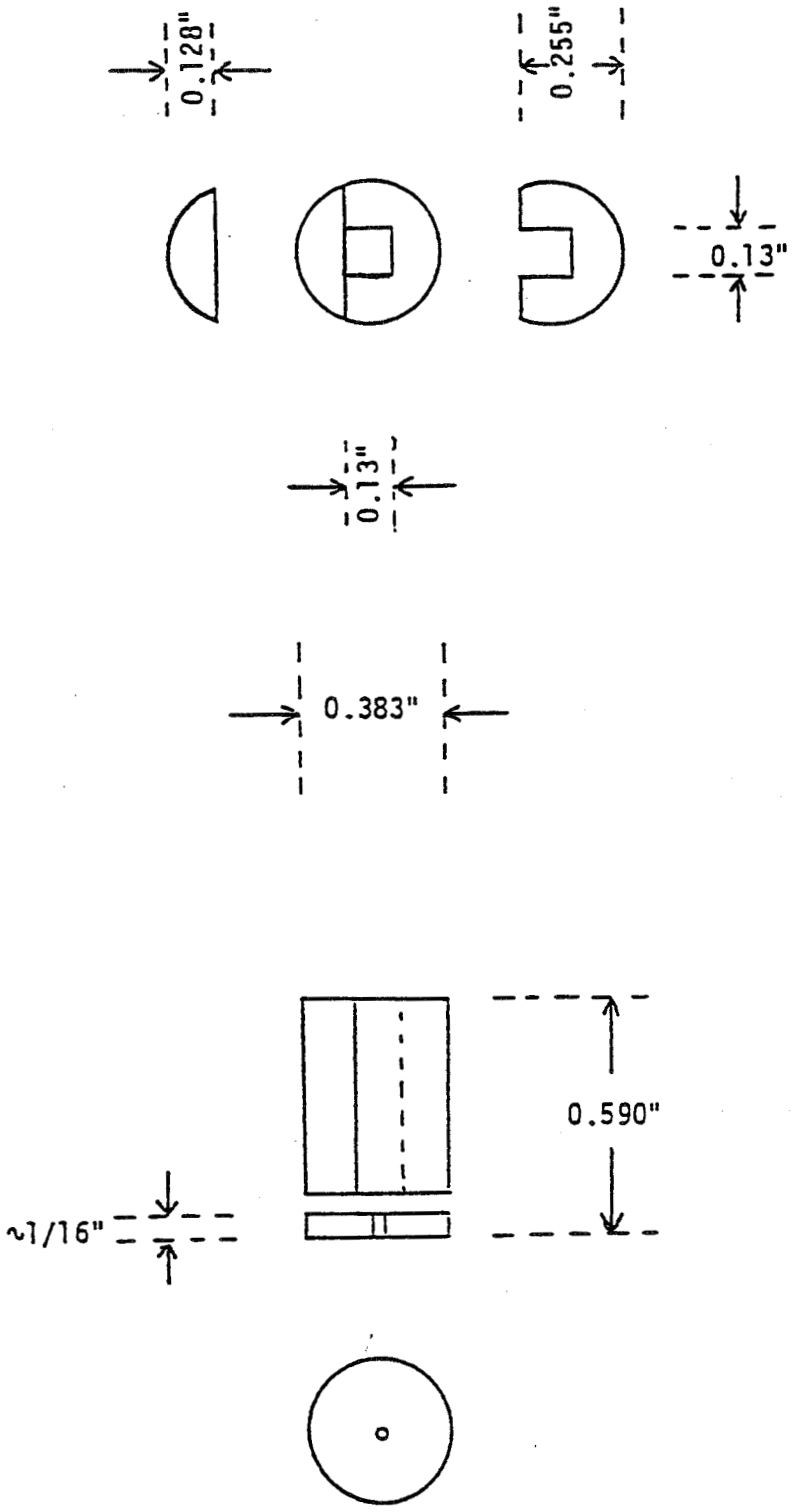

Figure 1. Sketch of a TLD stack holder made of acrylate. Three stacks were placed in each of four plates (Plate No. B9-1, -2, -3, -4) for a total of twelve flight stacks (outside the spacecraft). A double window of aluminized Kapton polyimide (total thickness: 15 μm) separated the stacks from space.

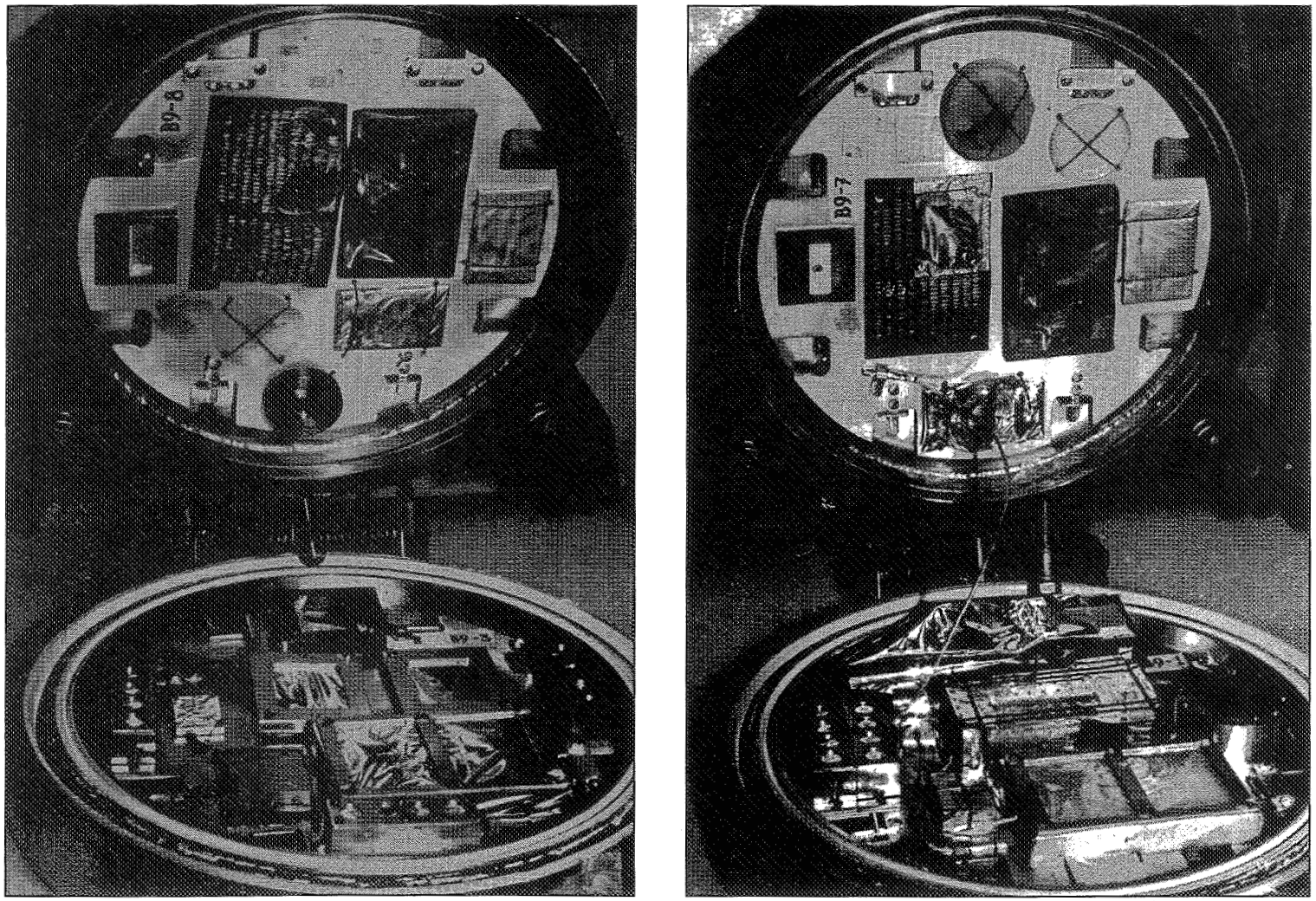

Figure 2. Photograph of Cosmos 2044 "Clam-Shell" type containers for mission dosimeters. The containers were mounted on the outside of the Spacecraft.

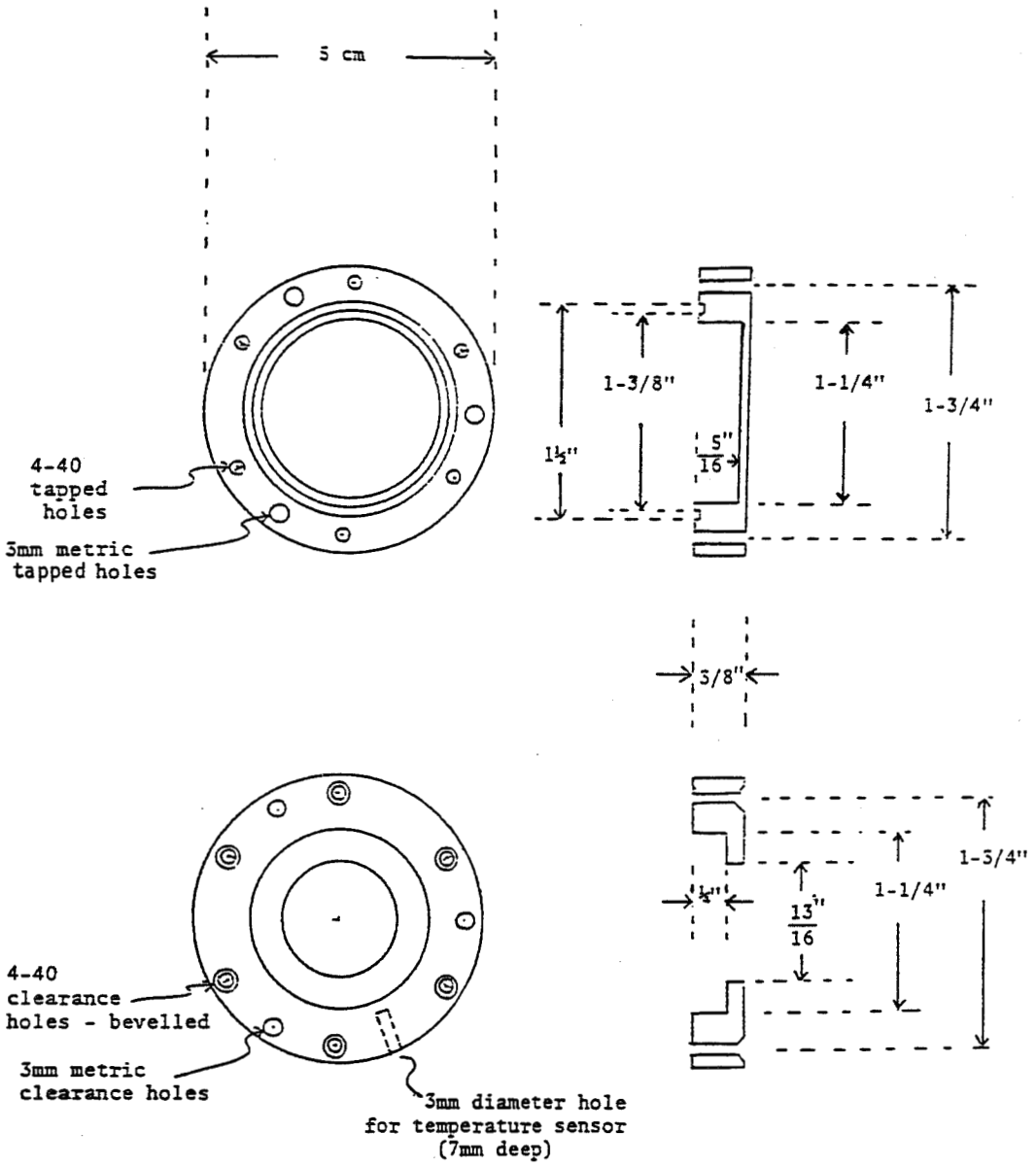

Figure 3. Sketch of an aluminum container with O-ring seal for the plastic and emulsion stacks. There were two flight units, F1 and F2 (outside the spacecraft). A double window of aluminized Kapton polymide (total thickness: 15μm) separated the stacks from space.

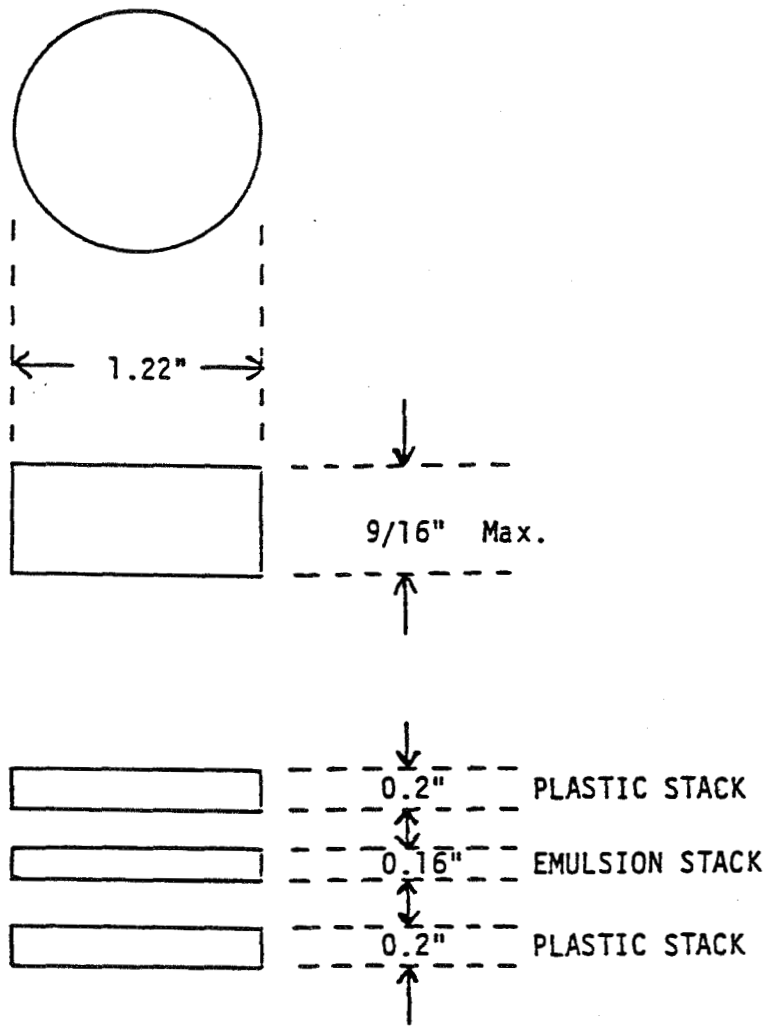

Figure 4. Sketch of the plastic and emulsion stacks.

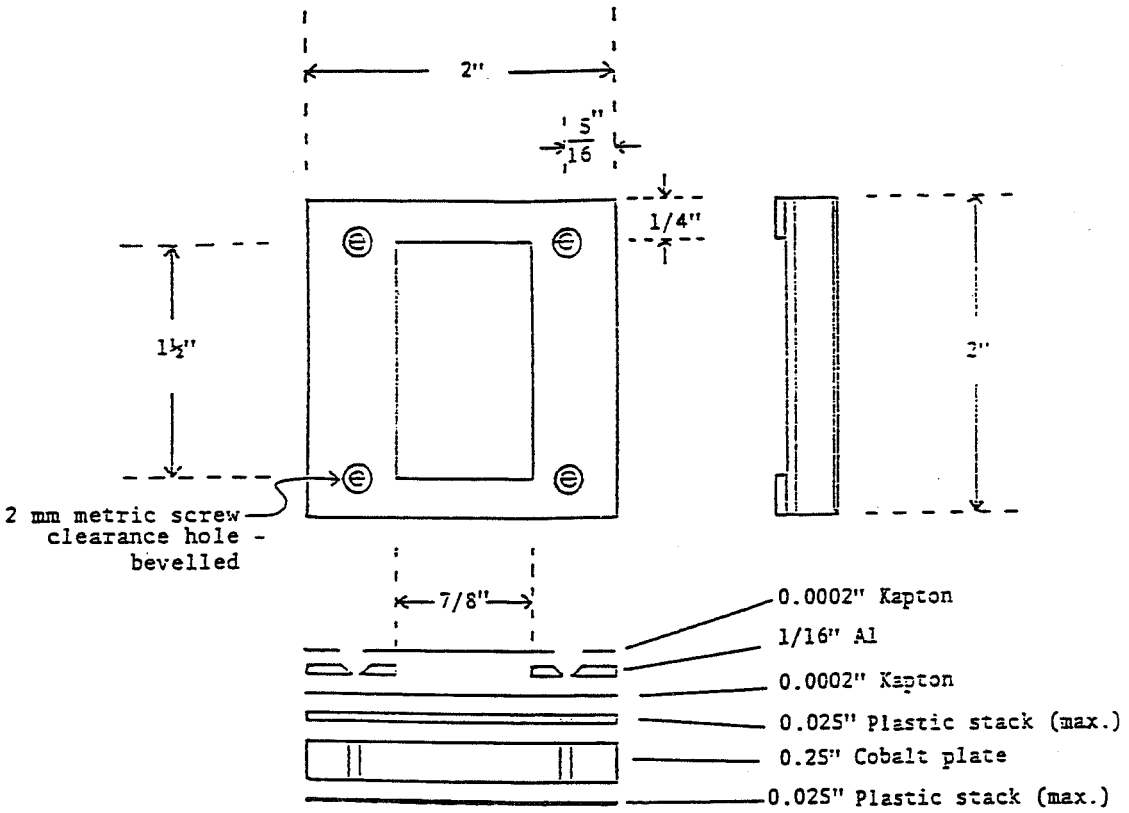

Figure 5. Sketch of ^{59}Co activation foil detector units, two of which were placed outside the spacecraft. A third activation foil with an emulsion stack was placed inside the spacecraft.

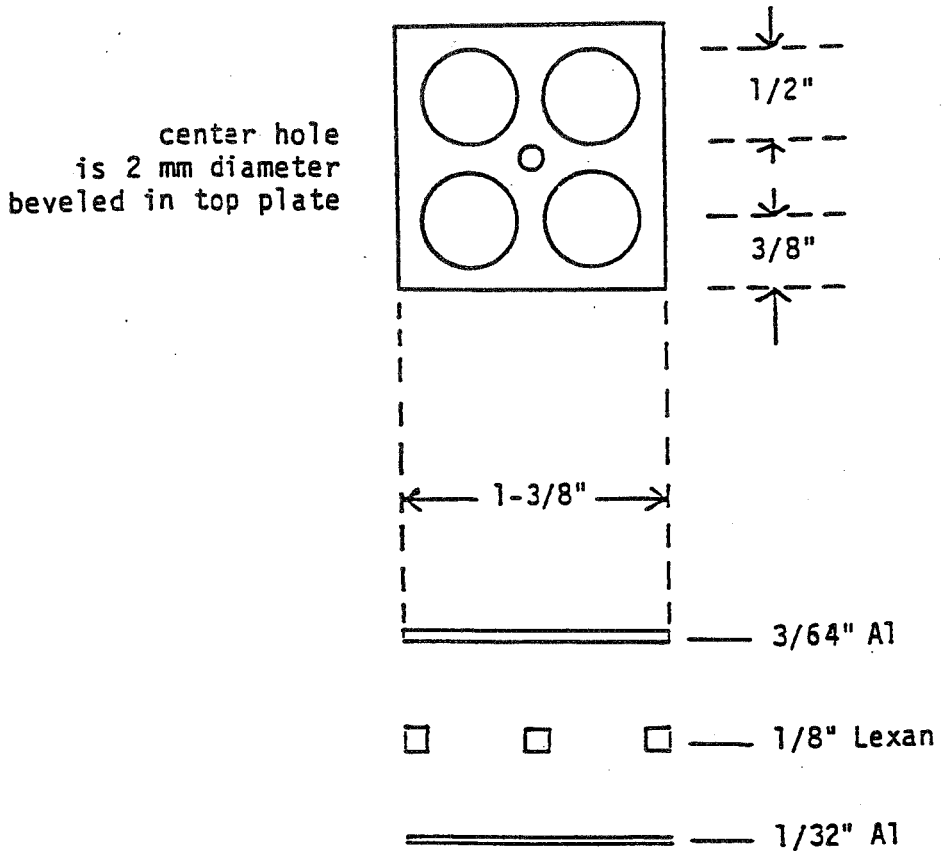

Figure 6. Sketch of the ^{232}Th fission foil detector holder. Two units, F1 and F2, were placed outside the spacecraft.

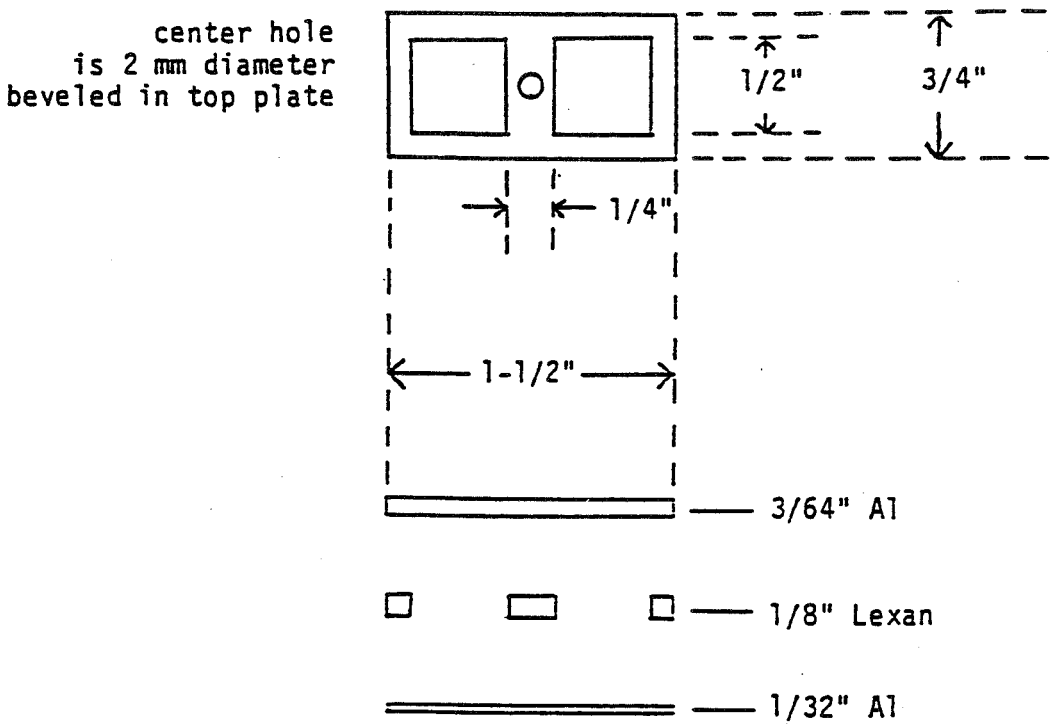

Figure 7. Sketch of the ^{6}LiF/CR-39 neutron detector holders. Each unit contained one unshielded detector and one shielded by 25 μm-thick Gd foil. Two units (F1 and F2) were placed outside the spacecraft.

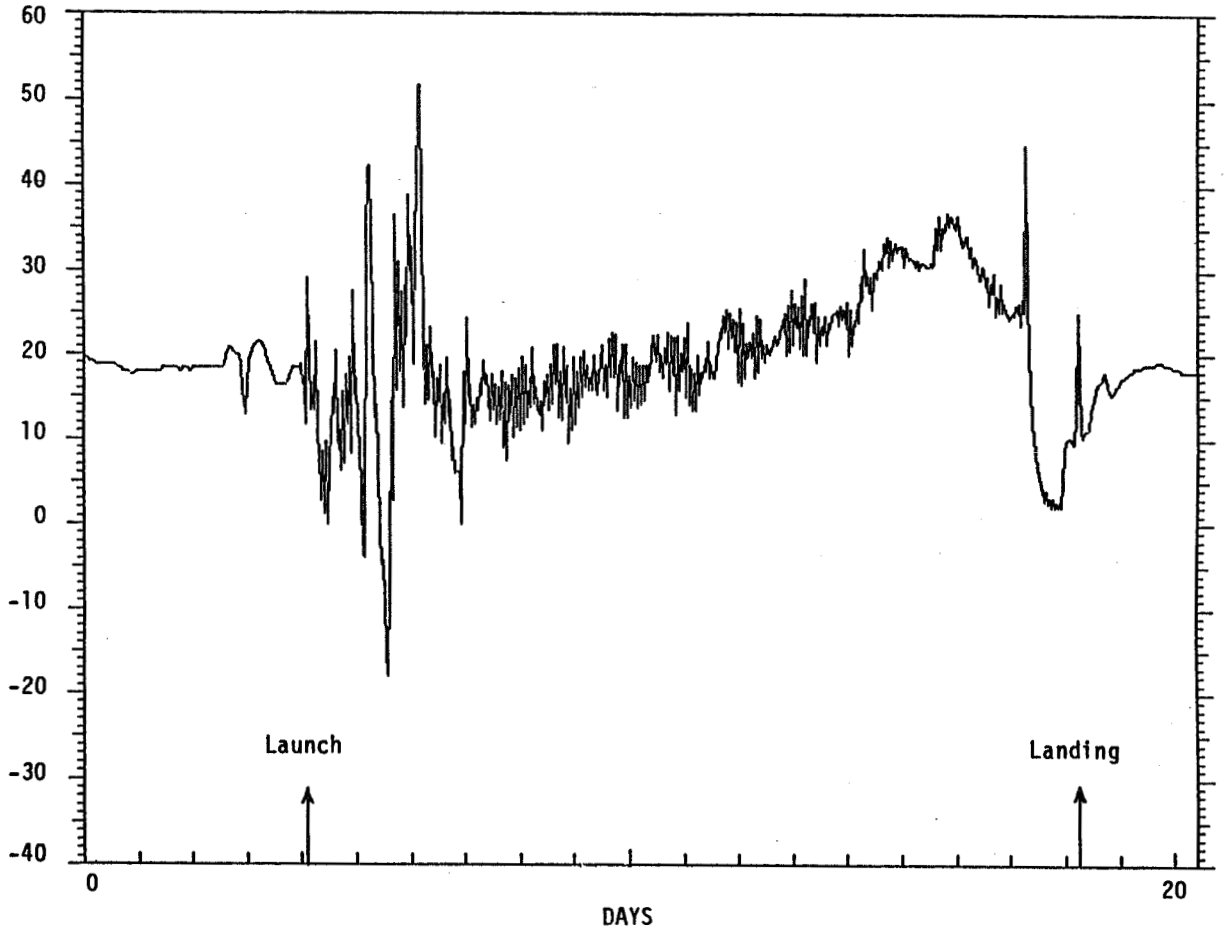

Figure 8. Record of ATR-4 temperature probe embedded in F1 cannister. (Plate B9-2; Container KHA-1).

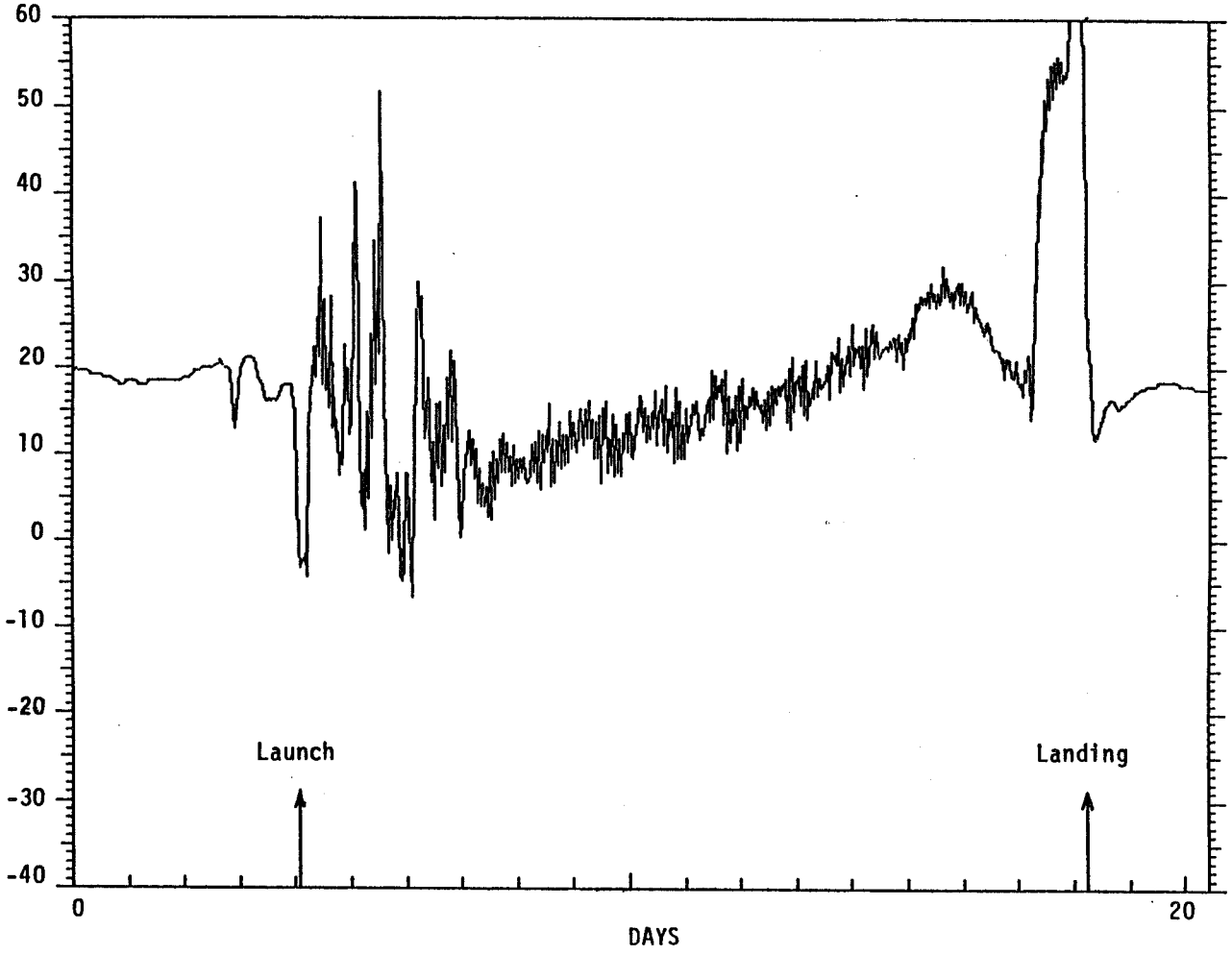

Figure 9. Record of ATR-4 temperature probe embedded in F2 cannister (Plate B9-1; Container KHA-3).

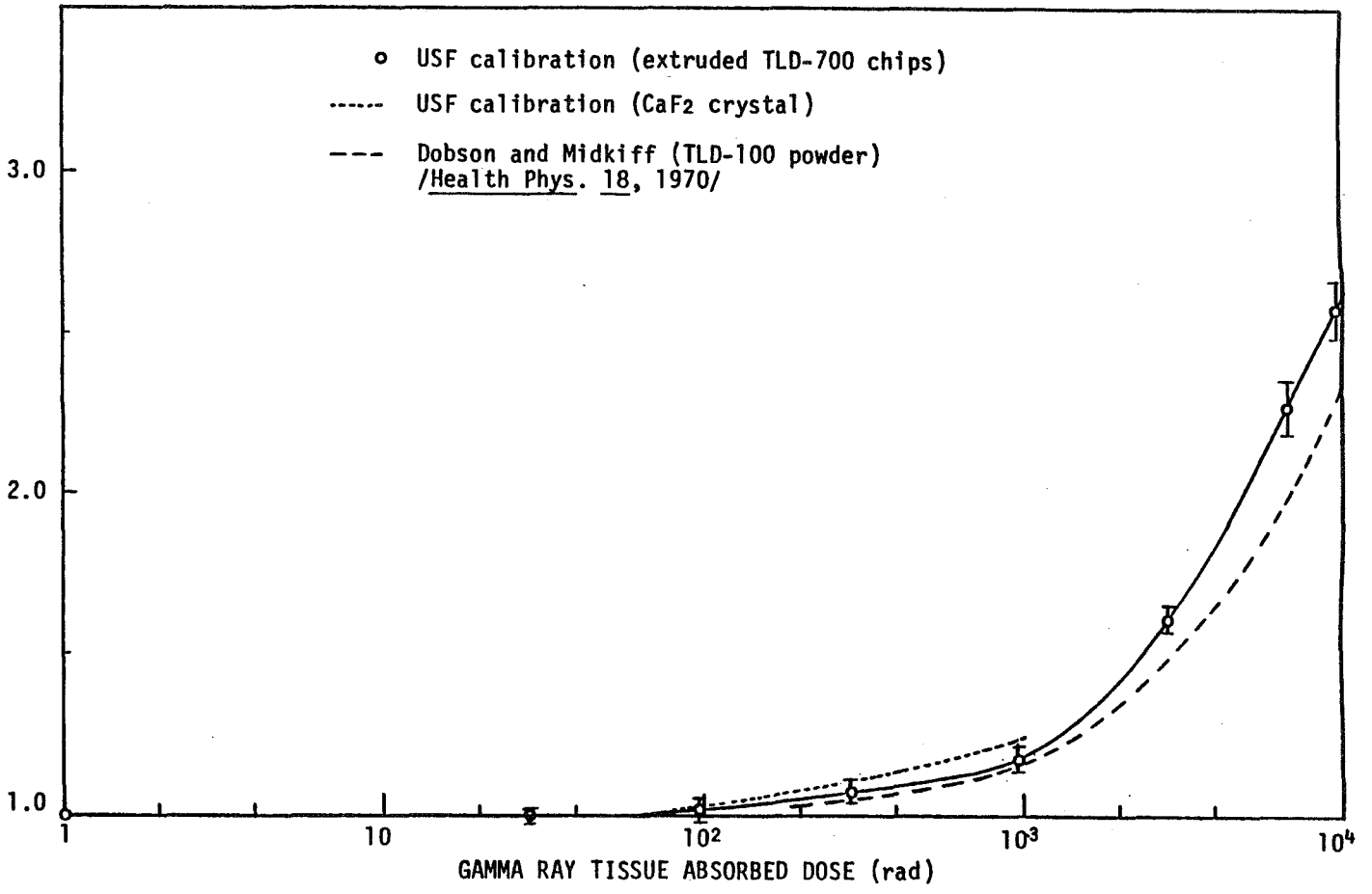

Figure 10. TLD calibration showing the high-dose supralinearity found in TLD-700 extruded chips. The data from Dobson and Midkiff /1970/ (TLD-100 powder) was typical of LiF supra-linearity reported.

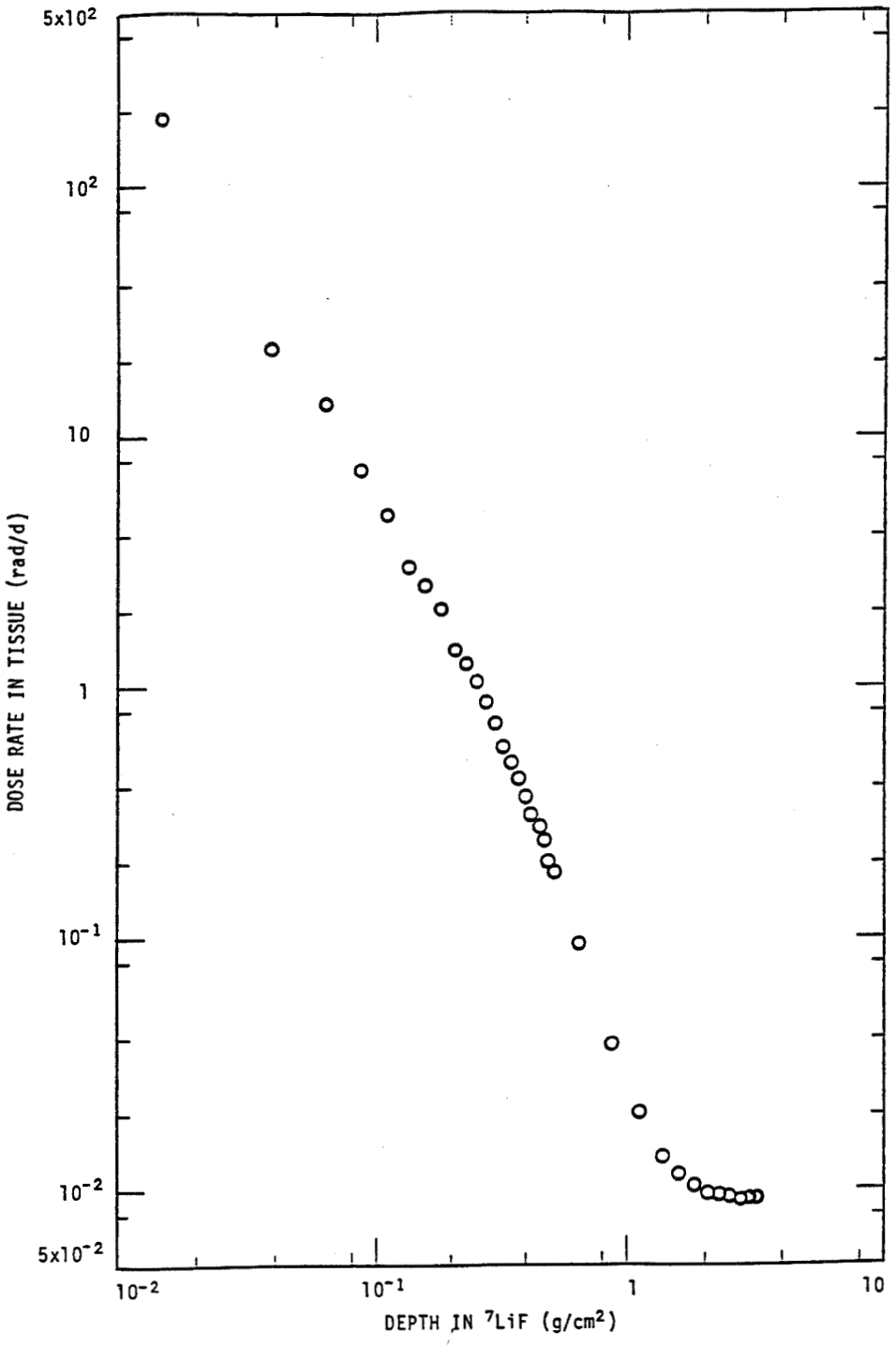

Figure 11. Average dose rates in Plate No. B9-1 (TLD stacks Nos 4, 8, 12).

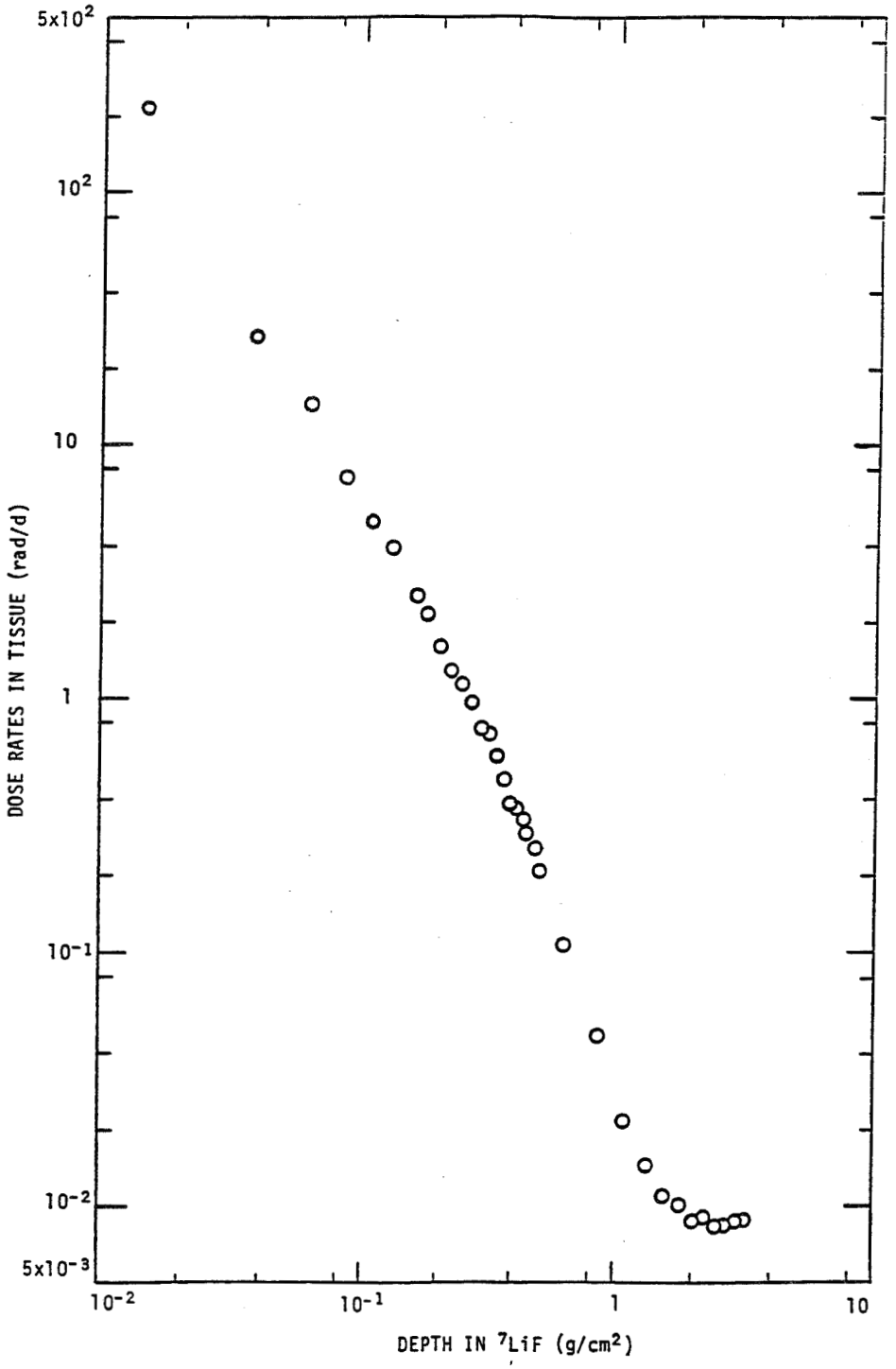

Figure 12. Average dose rates in Plate No. B9-2 (TLD stacks Nos. 2, 6, 10).

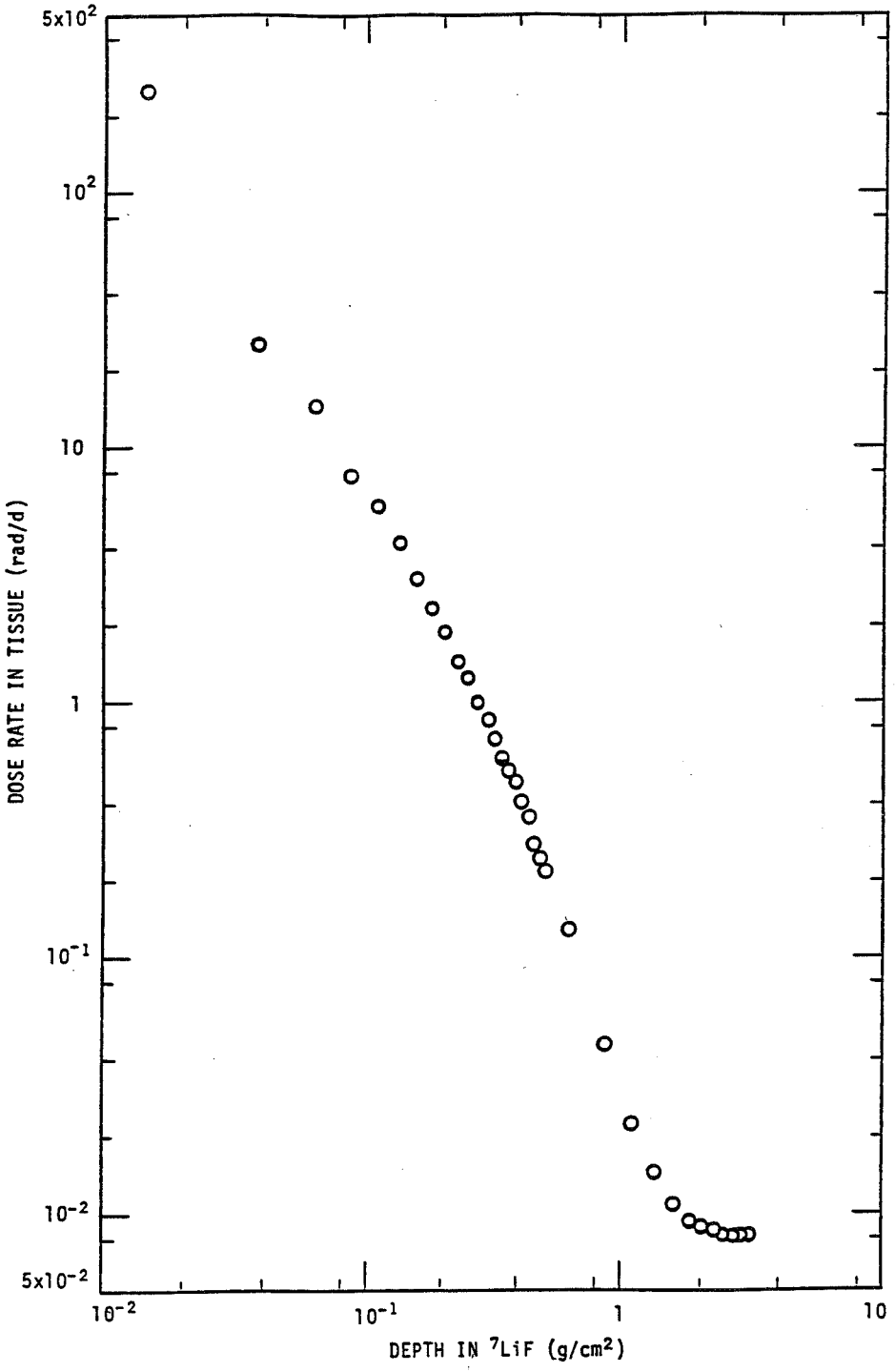

Figure 13. Average dose rates in Plate No. (-3 (TLD stacks Nos. 1, 3, 9).

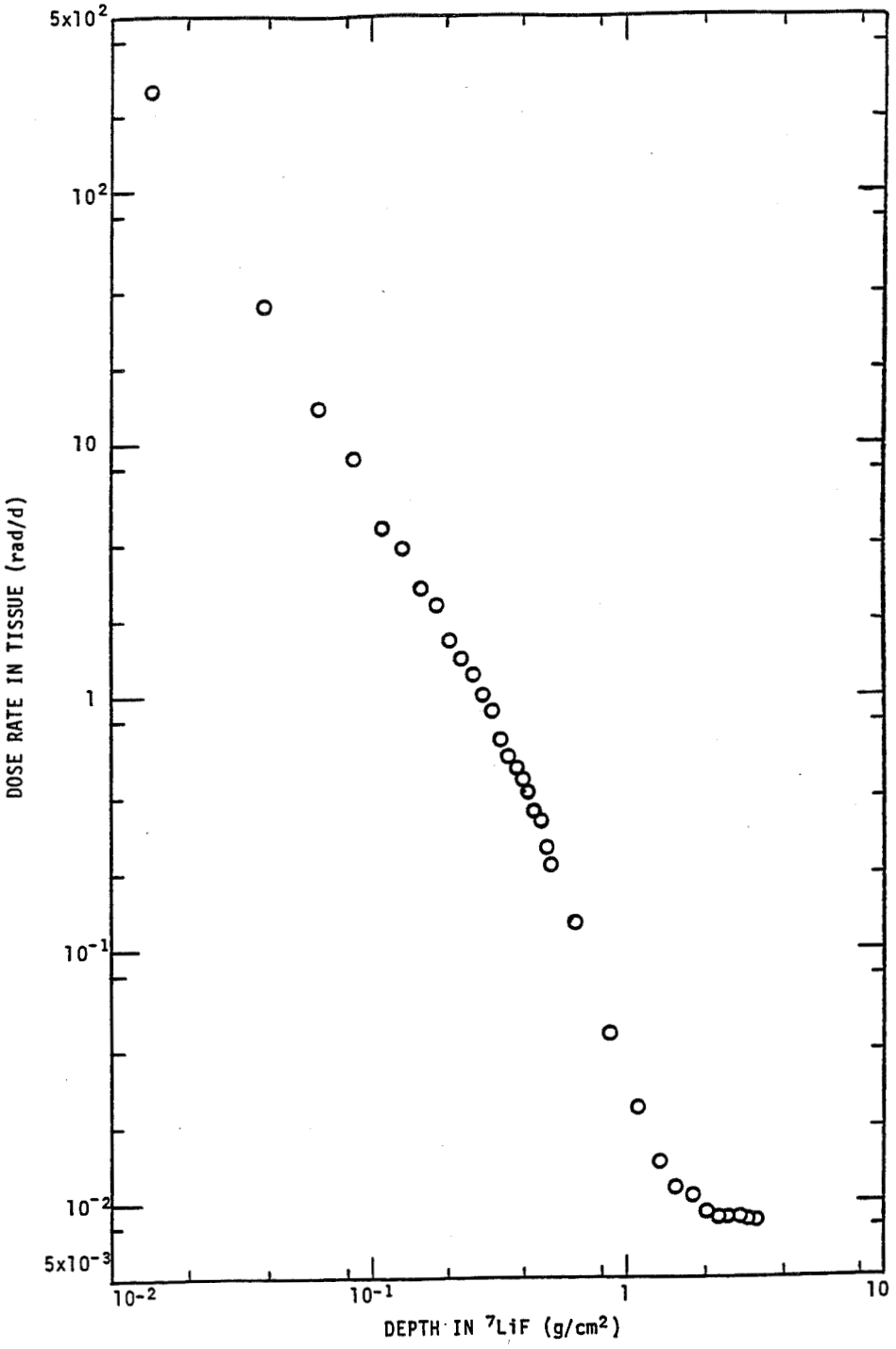

Figure 14. Average dose rates in Plate No. B(-4 (TLD stacks Nos. 5, 7, 11).

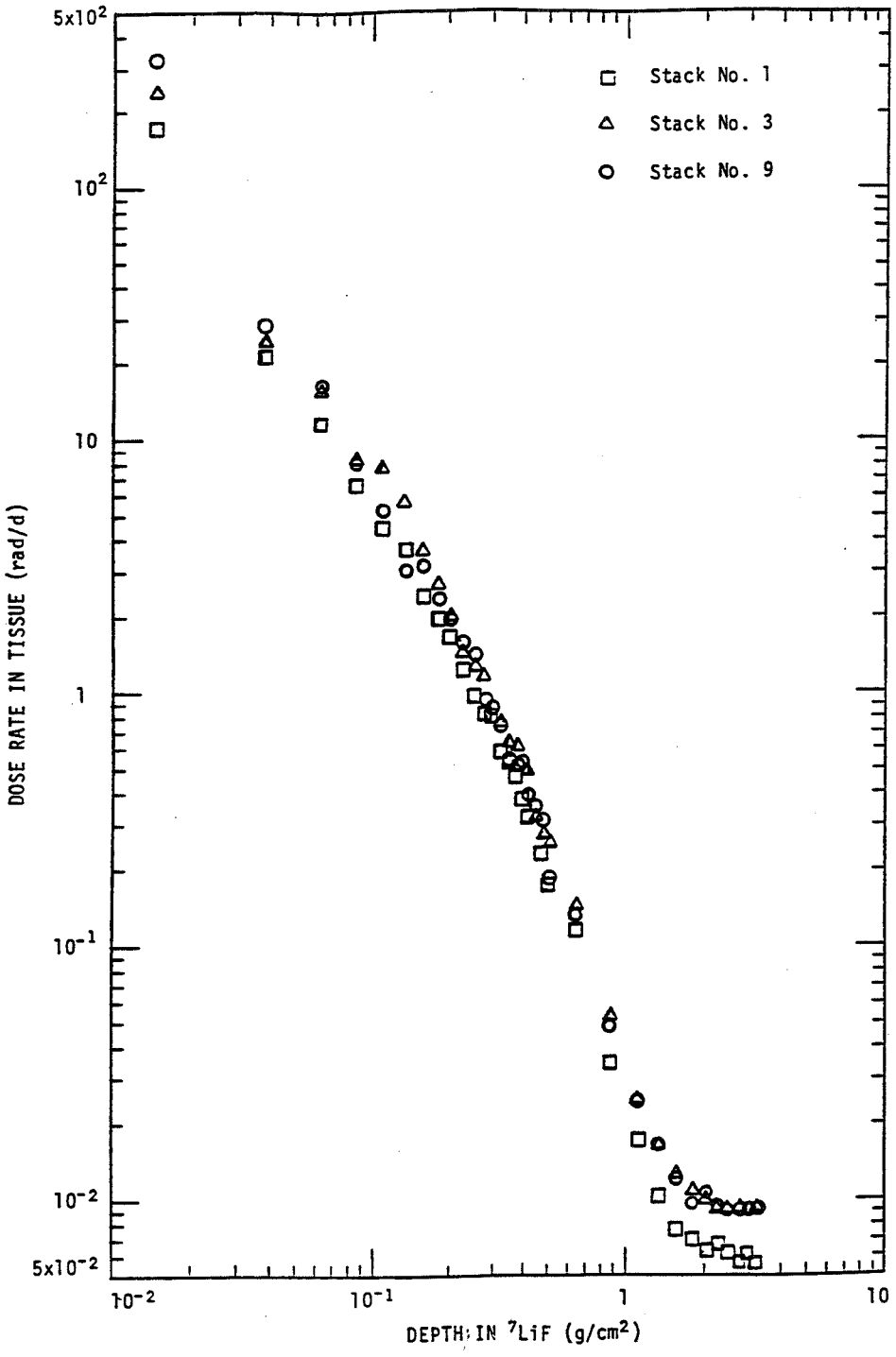

Figure 15. Dose rates for the three TLD stacks in Plate B9-3.

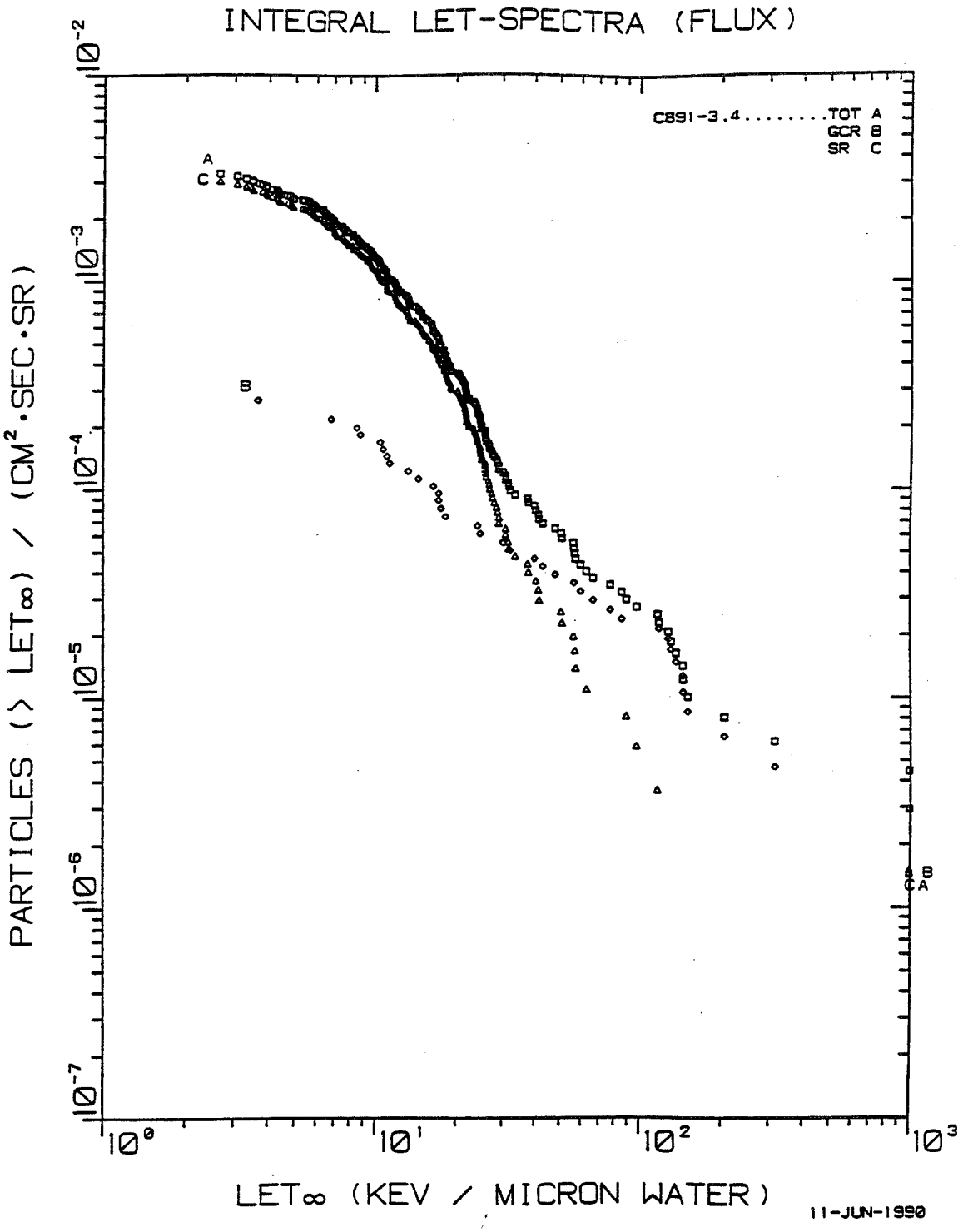

Figure 16. Integral LET flux spectra for PNTD stack F1 (outside the spacecraft). The minimum shielding was 0.164 g/cm^2 plastic.

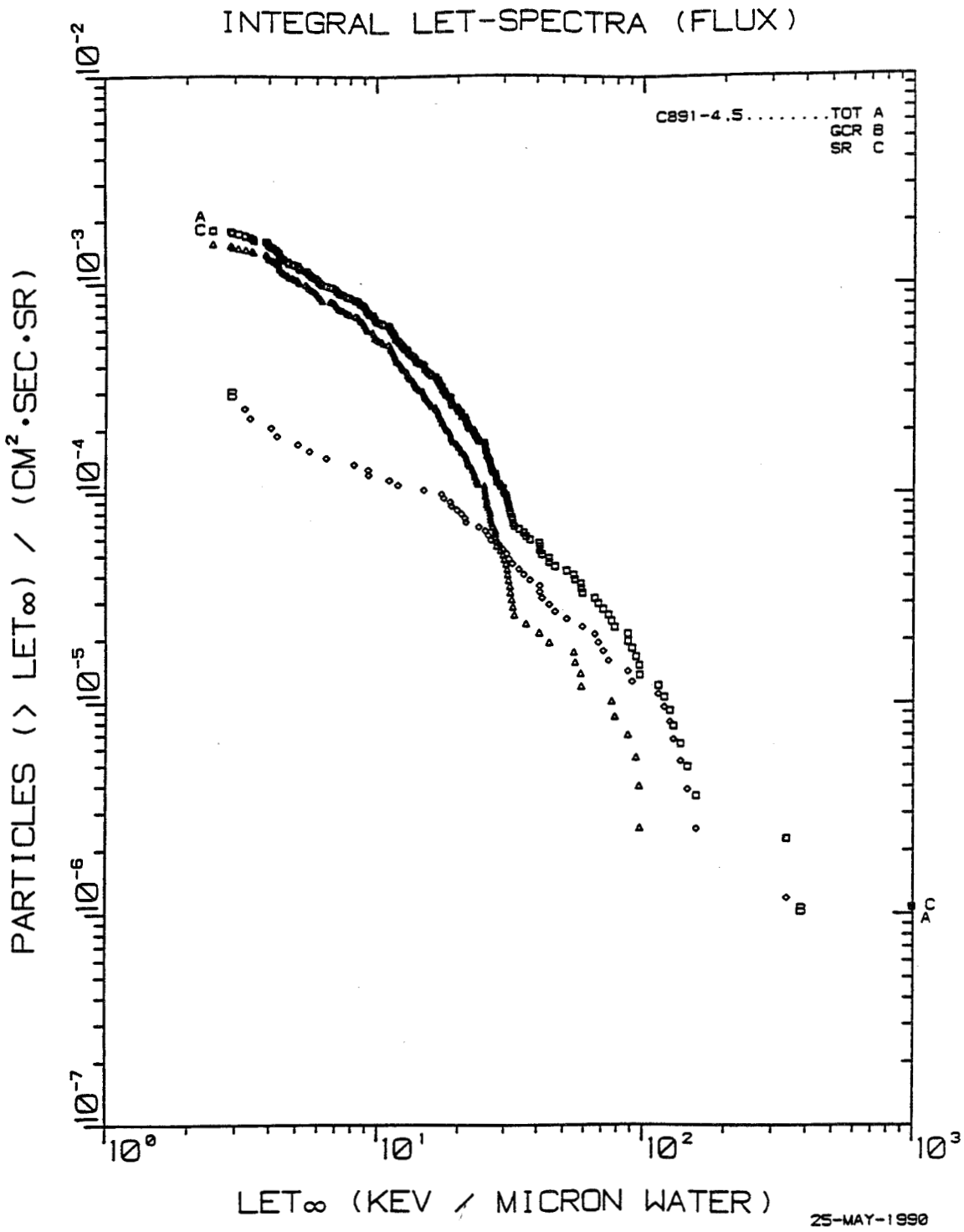

Figure 17. Integral LET flux spectra for PNTD stack F1 (outside the spacecraft). The minimum shielding was 0.239 g/cm^2 plastic.

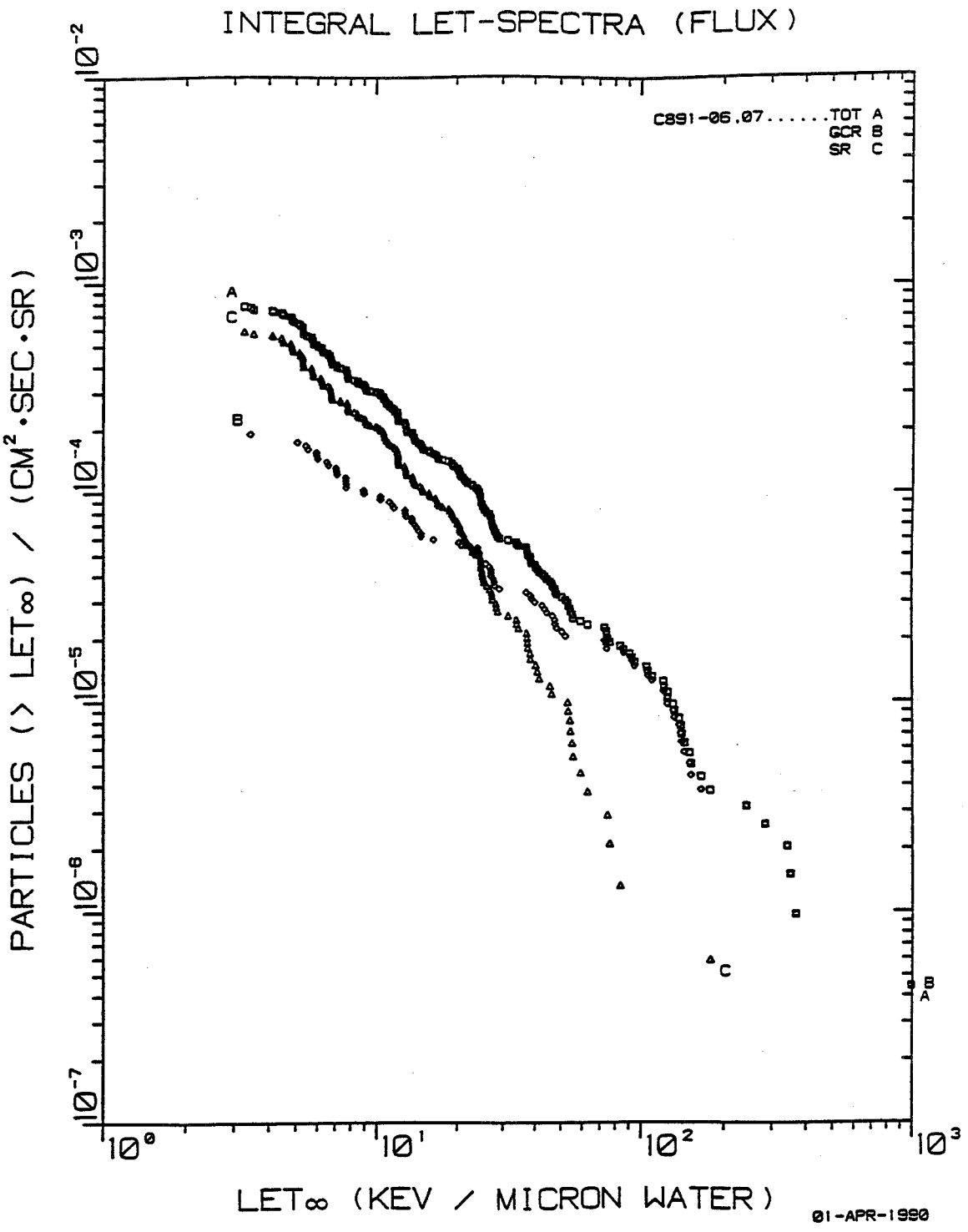

Figure 18. Integral LET flux spectra for PNTD stack F1 (outside the spacecraft). The minimum shielding was 0.397 g/cm^2 plastic.

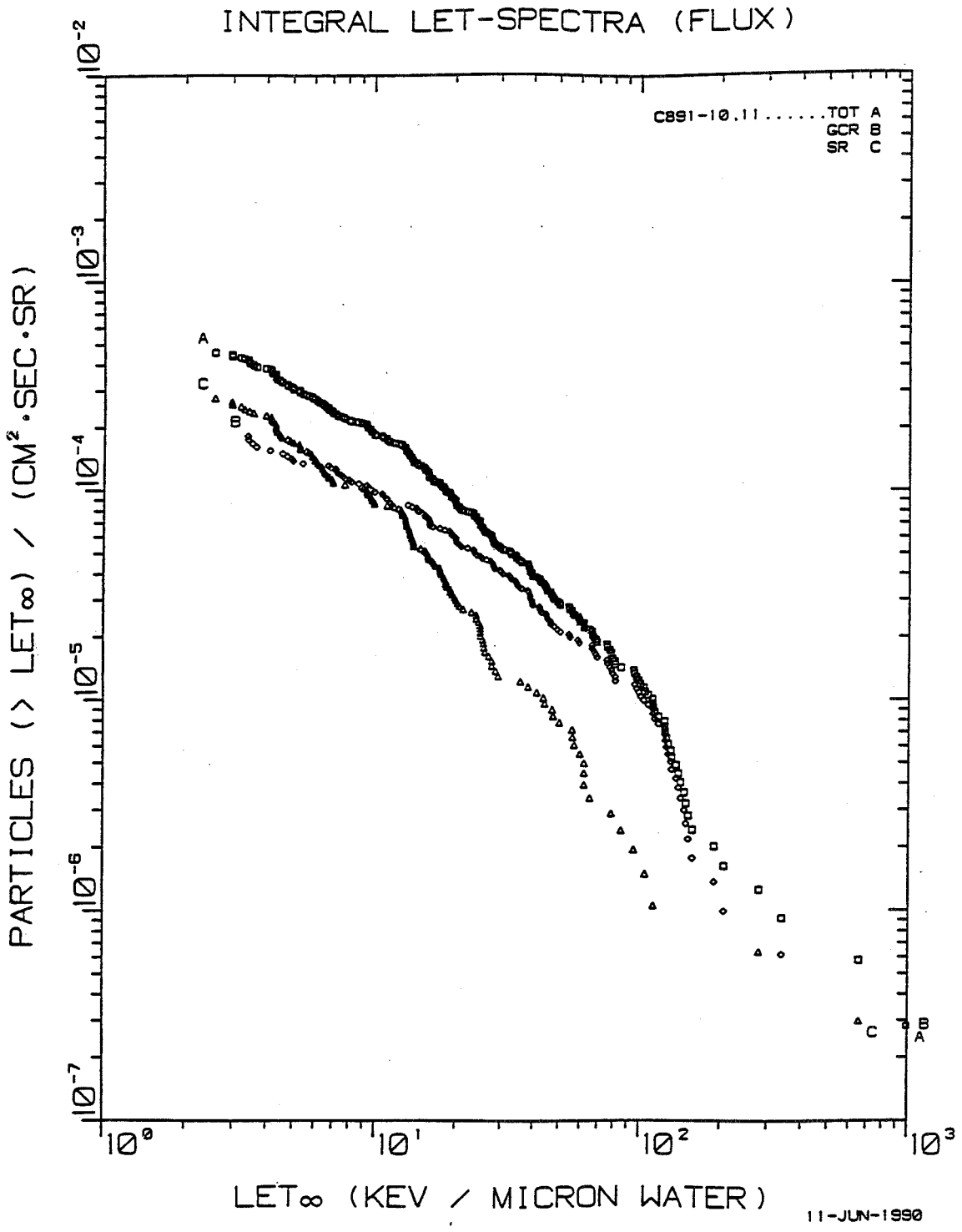

Figure 19. Integral LET flux spectra for PNTD stack F1 (outside the spacecraft). The minimum shielding was 1.47 g/cm^2 plastic, stainless steel and nuclear emulsion.

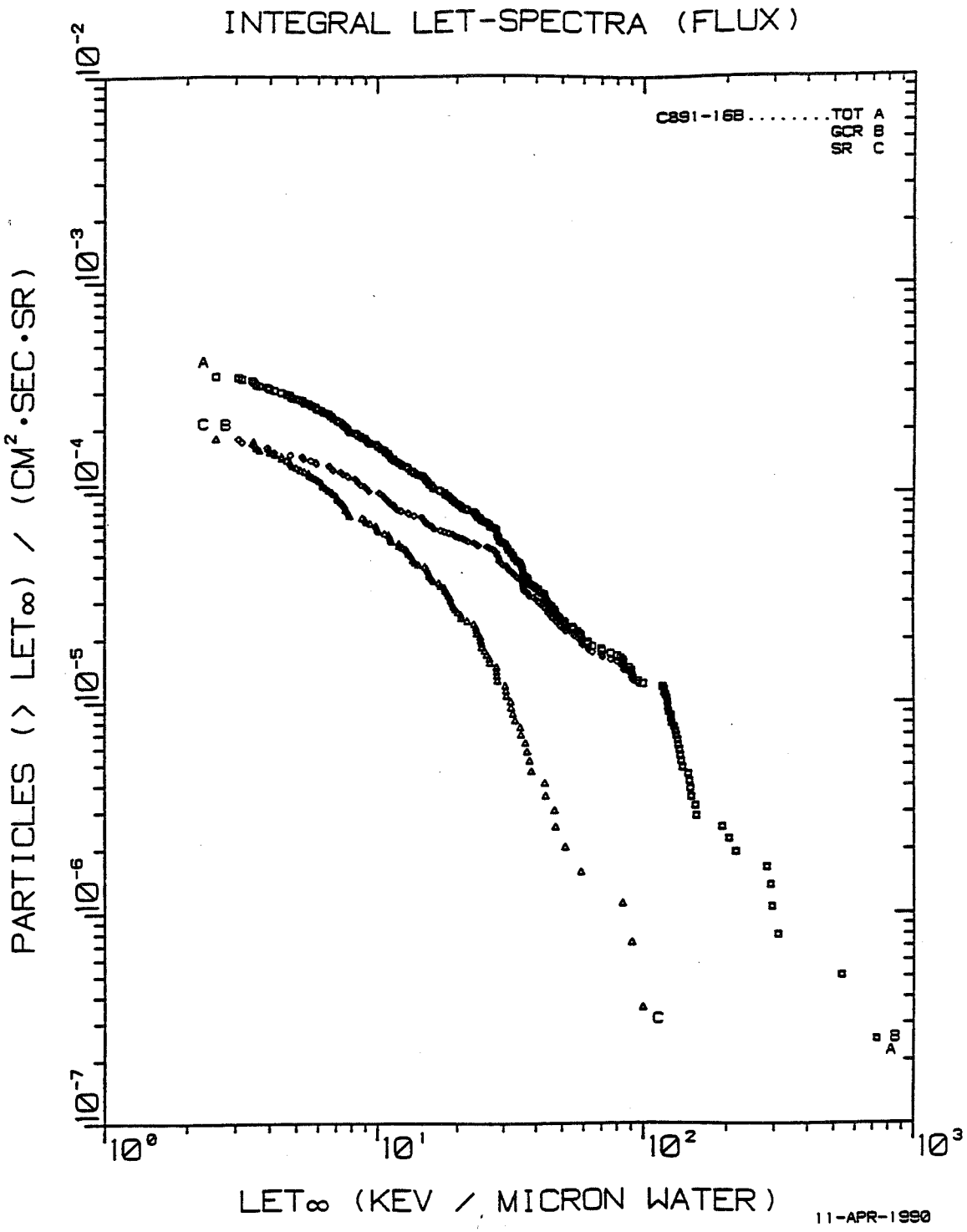

Figure 20. Integral LET flux spectra for PNTD stack F1 (outside the spacecraft). The minimum shielding was 1.95 g/cm^2 plastic, stainless steel and nuclear emulsion.

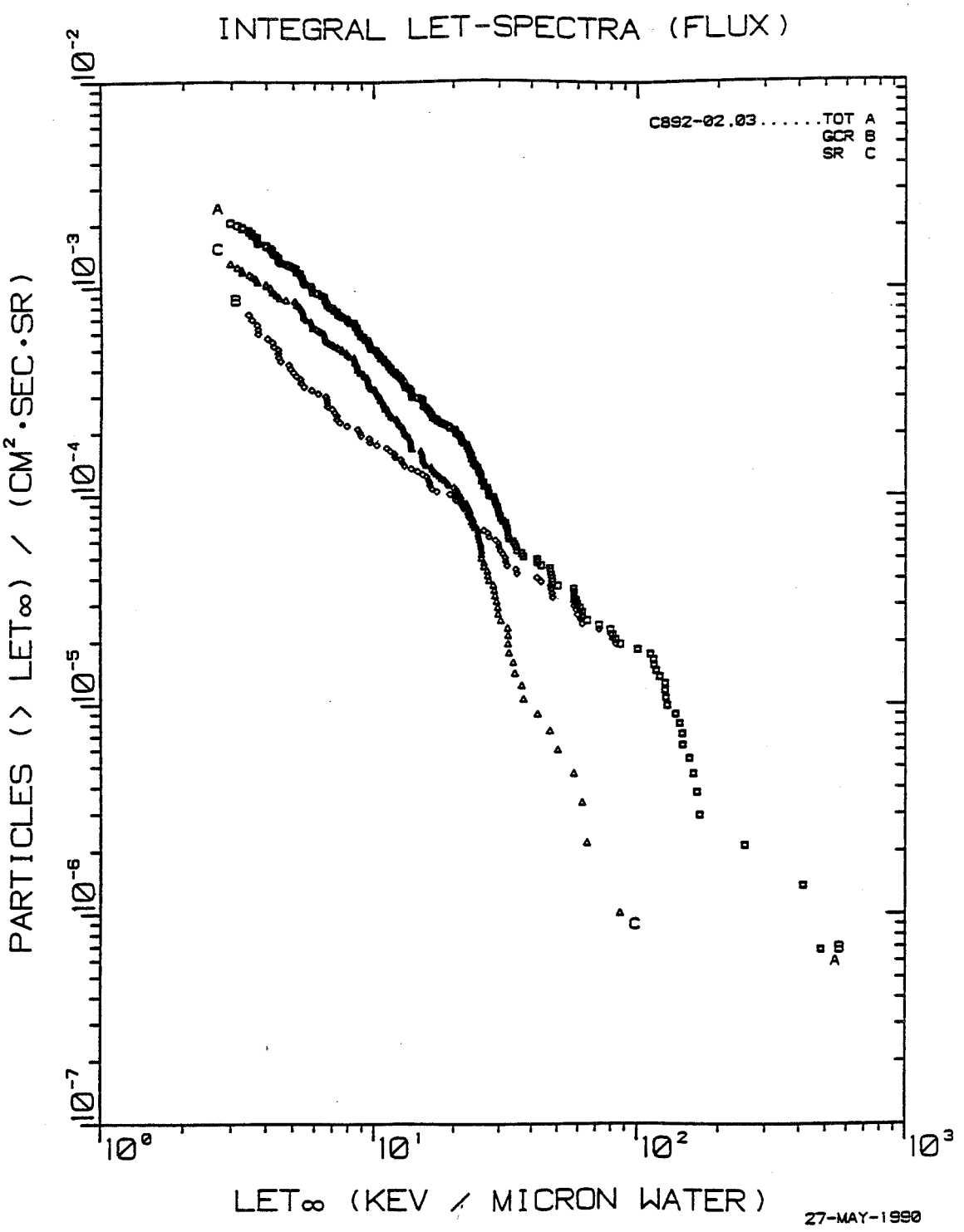

Figure 21. Integral LET flux spectra for PNTD stack F2 (outside the spacecraft). The minimum shielding was 0.0935 g/cm^2 plastic.

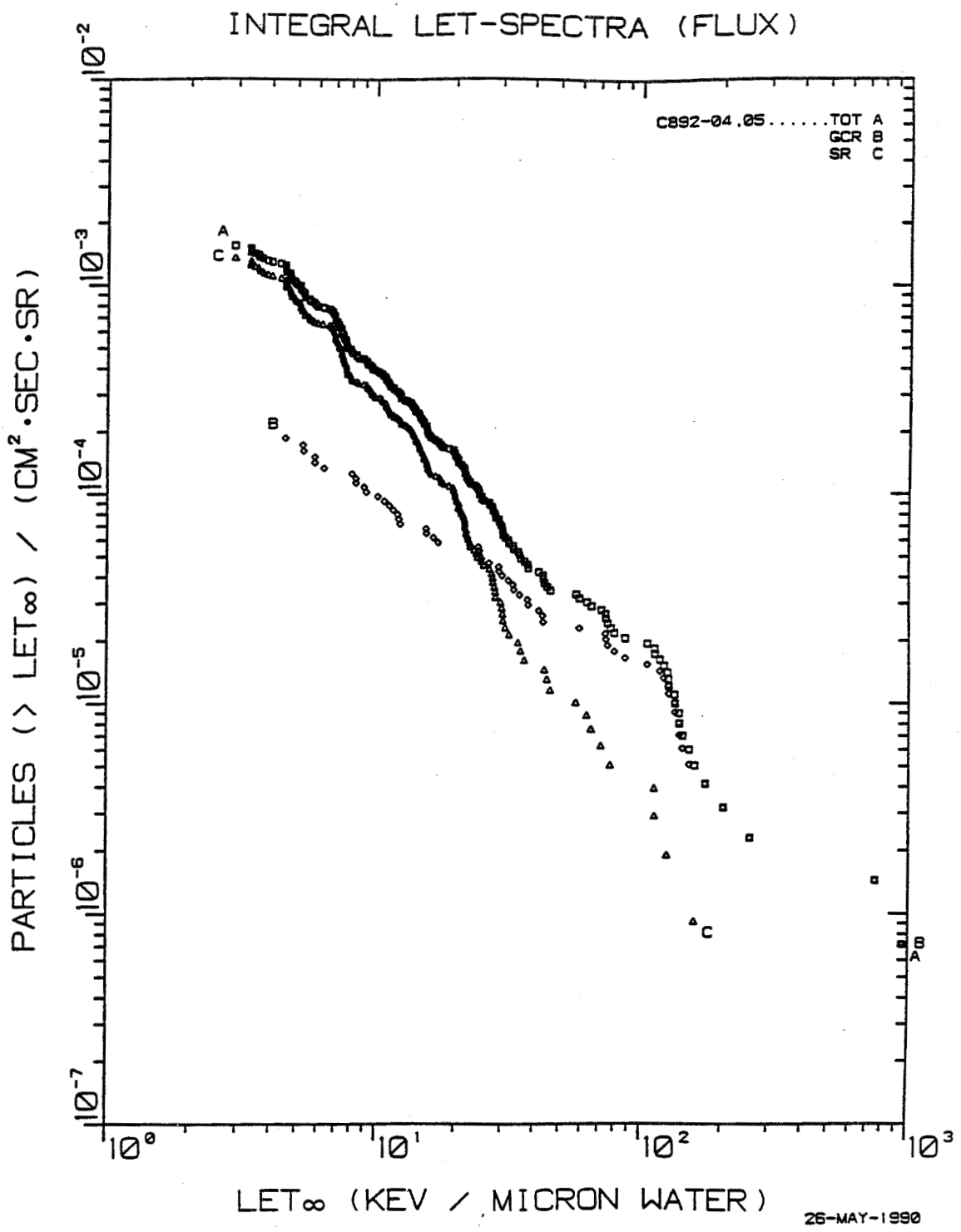

Figure 22. Integral LET flux spectra for PNTD stack F2 (outside the spacecraft). The minimum shielding was 0.250 g/cm^2 plastic.

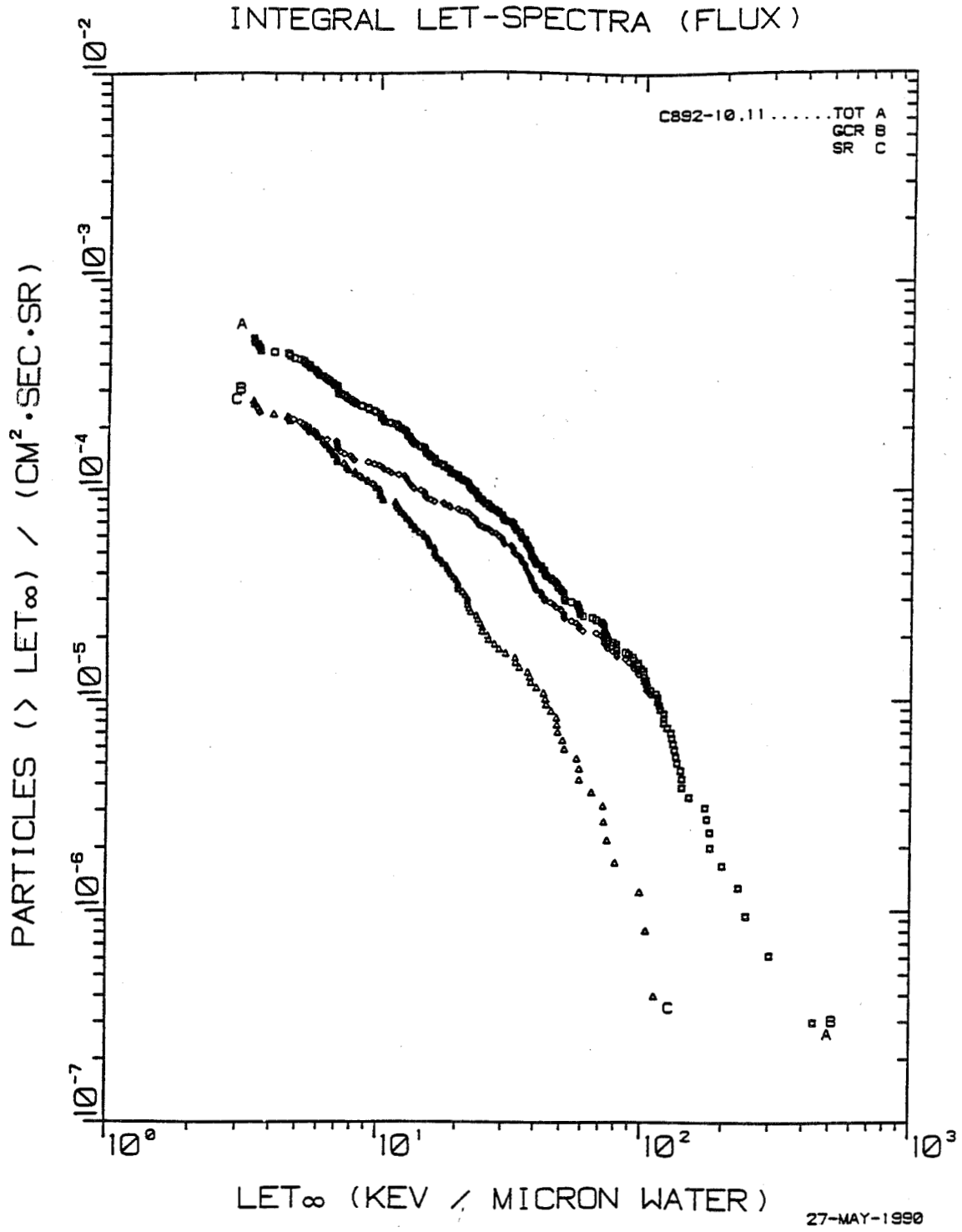

Figure 23. Integral LET flux spectra for PNTD stack F2 (outside the spacecraft). The minimum shielding was 1.9 g/cm^2 plastic, stainless steel and nuclear emulsion.

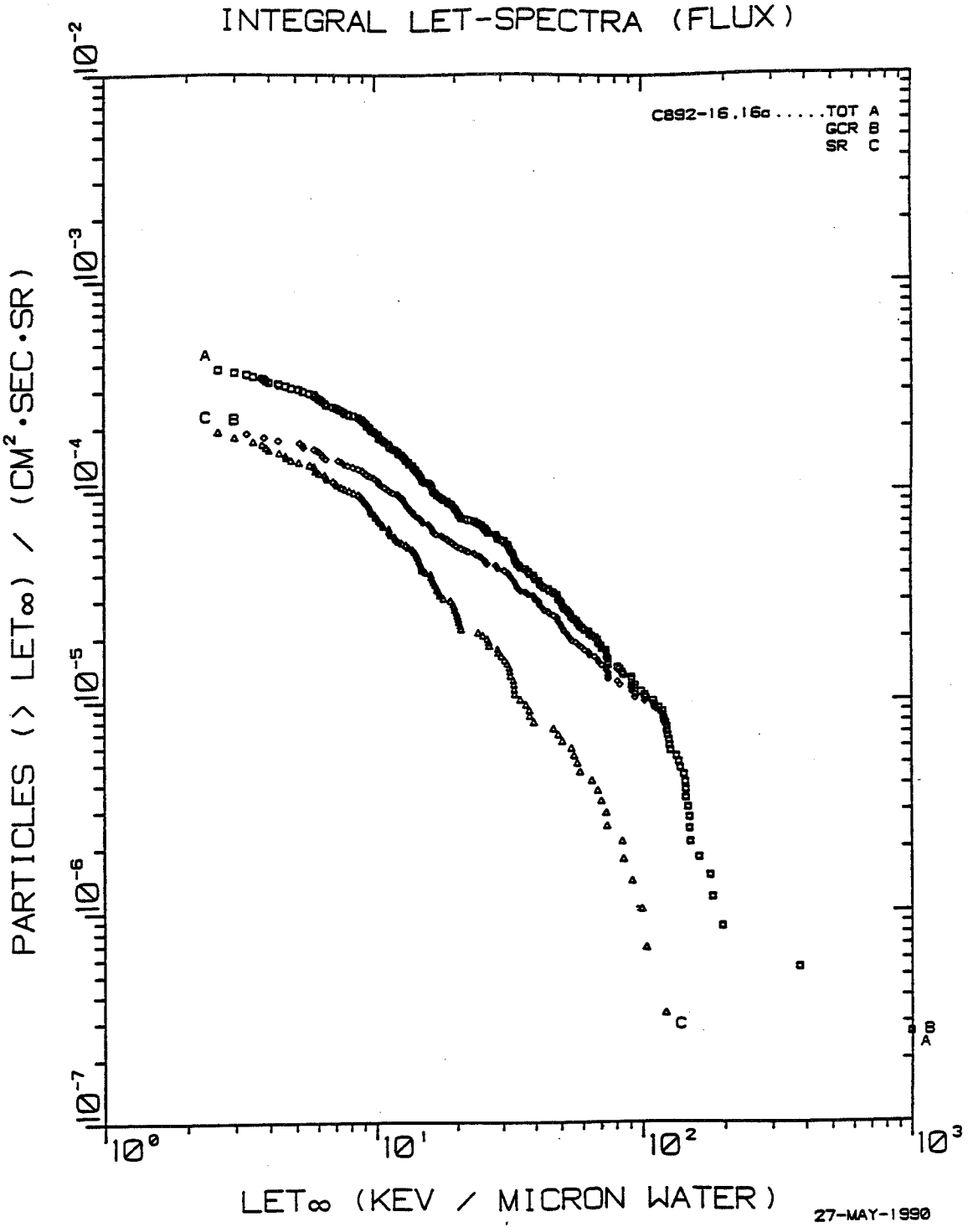

Figure 24. Integral LET flux spectra for PNTD stack F2 (outside the spacecraft). The minimum shielding was 1.97 g/cm^2 plastic, stainless steel and nuclear emulsion.

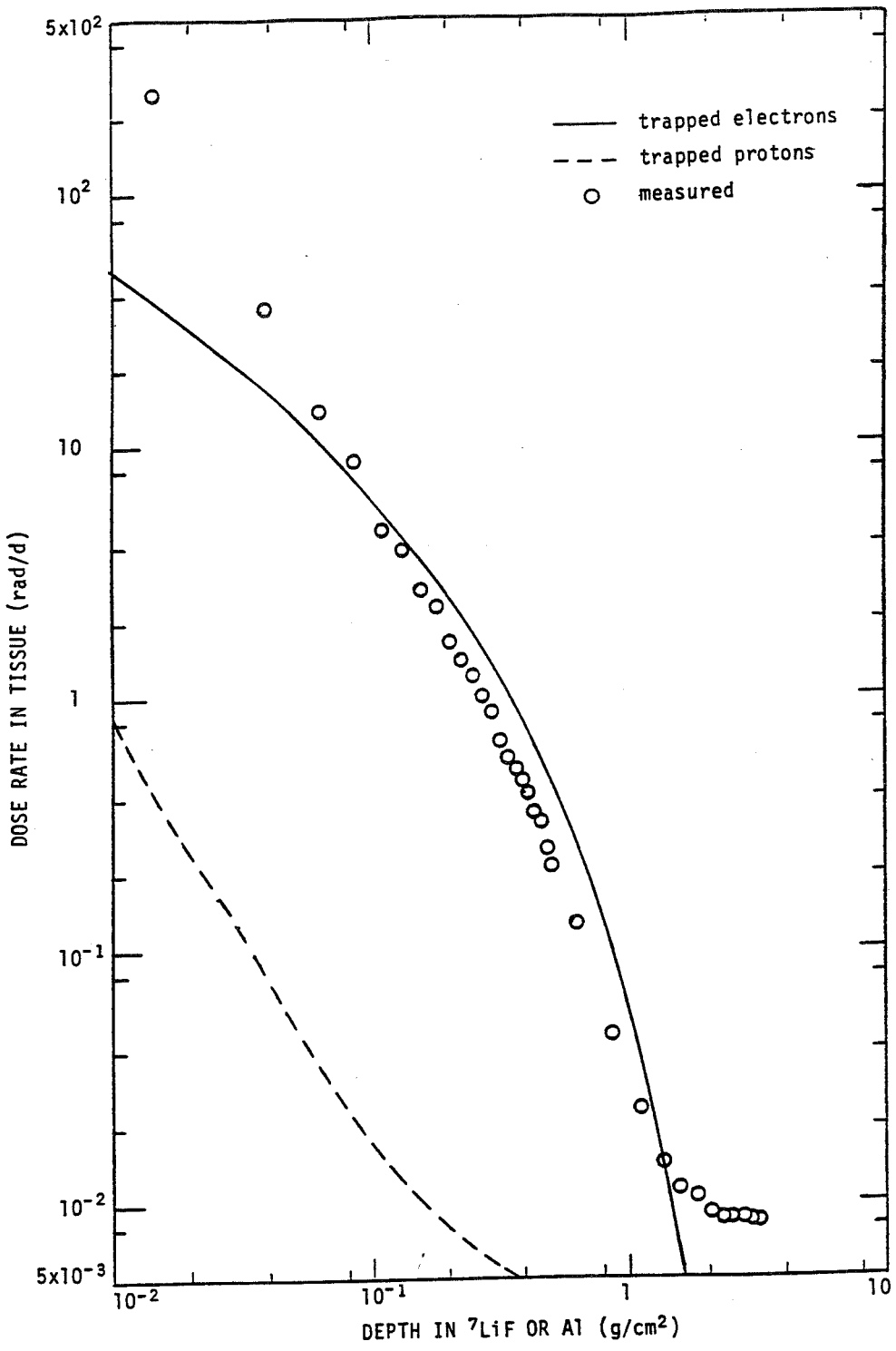

Figure 25. Comparison of the average TLD dose rates in Plate No. B(-4 with the calculated depth dose rates of trapped electrons and protons for tissue behind aluminum planer shields /Warra, 1990/. The calculations were for the Cosmos 2044 orbit at solar maximum.

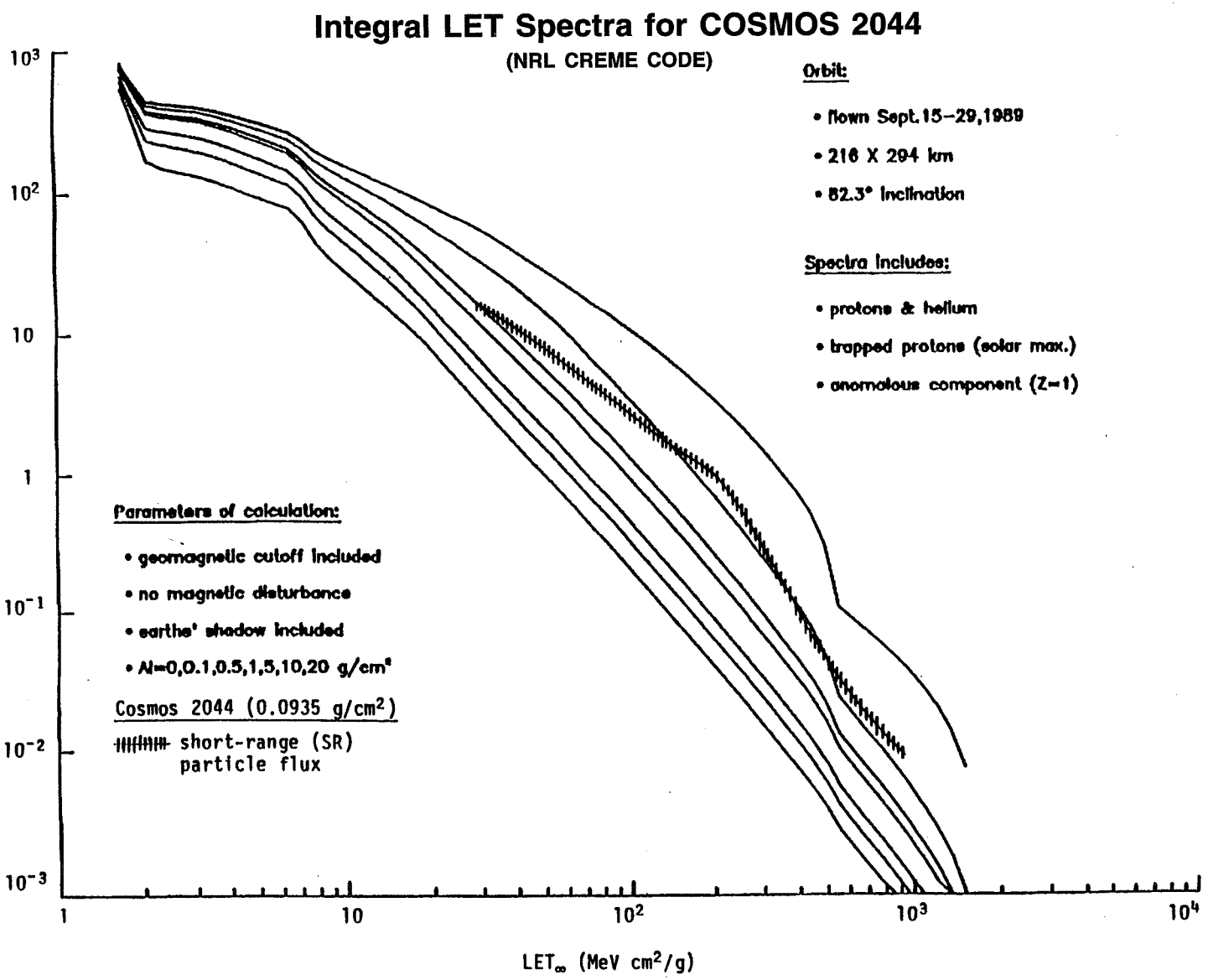

Figure 26. Comparison of a measured Cosmos 2044 SR Total flux spectrum (in H_2O) with the calculated spectra (in Si) of John Watts /1990/ for A1 shielding of 0-20 g/cm^2 and for Cosmos 2044 orbit.

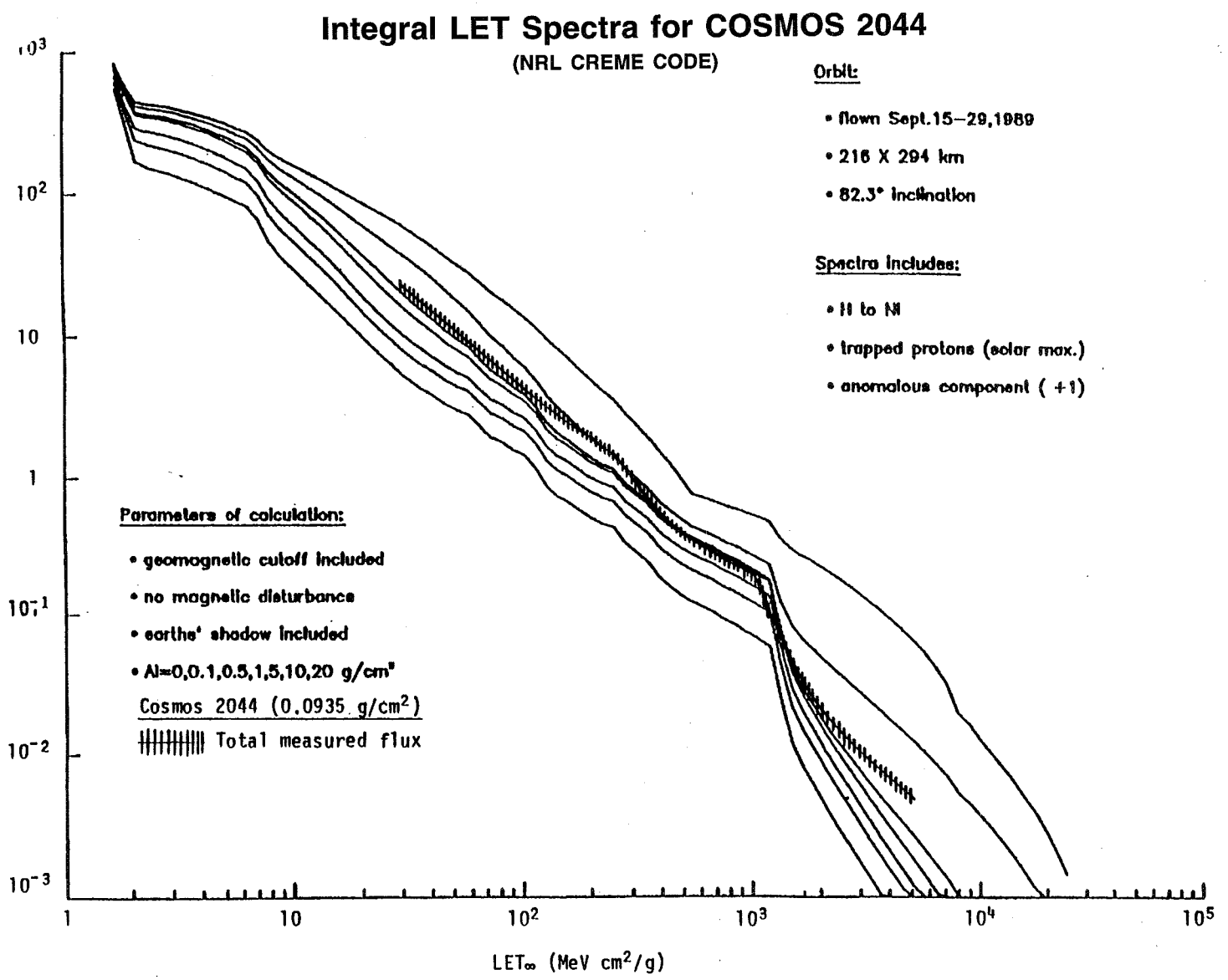

Figure 27. Comparison of a measured Cosmos 2044 SR Total flux spectrum (in H_20) with the calculated spectra (in Si) of John Watts /1990/ for A1 shielding of 0-20 g/cm^2 and for Cosmos 2044 orbit.

REPORT DOCUMENTATION PAGE

Form Approved
OMB No. 0704-0188

Public reporting burden for this collection of information is estimated to average 1 hour per response, including the time for reviewing instructions, searching existing data sources, gathering and maintaining the data needed, and completing and reviewing the collection of information. Send comments regarding this burden estimate or any other aspect of this collection of information, including suggestions for reducing this burden, to Washington Headquarters Services, Directorate for information Operations and Reports, 1215 Jefferson Davis Highway, Suite 1204, Arlington, VA 22202-4302, and to the Office of Management and Budget, Paperwork Reduction Project (0704-0188), Washington, DC 20503.

1. AGENCY USE ONLY *(Leave blank)*	2. REPORT DATE	3. REPORT TYPE AND DATES COVERED
	September 1994	Technical Memorandum

4. TITLE AND SUBTITLE
Final Reports of the U.S. Experiments Flown on the Soviet Biosatellite Cosmos 2044 *Volume II: Experiments K-7-16 – K-7-41*

5. FUNDING NUMBERS
199-08-12

6. AUTHOR(S)
James P. Connolly, Richard E. Grindeland, and Rodney W. Ballard, Eds.

7. PERFORMING ORGANIZATION NAME(S) AND ADDRESS(ES)
Ames Research Center
Moffett Field, CA 94035-1000

8. PERFORMING ORGANIZATION REPORT NUMBER
A-94031

9. SPONSORING/MONITORING AGENCY NAME(S) AND ADDRESS(ES)
National Aeronautics and Space Administration
Washington, DC 20546-0001

10. SPONSORING/MONITORING AGENCY REPORT NUMBER
NASA TM-108802

11. SUPPLEMENTARY NOTES
Point of Contact: James P. Connolly, Ames Research Center, MS 200-1, Moffett Field, CA 94035-1000; (415) 604-6483
Note: Technical Memorandum 108802 consists of 2 volumes.

12a. DISTRIBUTION/AVAILABILITY STATEMENT
Unclassified — Unlimited
Subject Category 55

12b. DISTRIBUTION CODE

13. ABSTRACT ***(Maximum 200 words)***

Cosmos 2044 was launched on September 15, 1989, containing radiation dosimetry experiments and a biological payload including two young male rhesus monkeys, ten adult male Wistar rats, insects, amphibians, protozoa, cell cultures, worms, plants and fish. The biosatellite was launched from the Plesetsk Cosmodrome in the Soviet Union for a mission duration of 14 days, as planned. The major research objectives were: 1). Study adaptive response mechanisms of mammals during flight; 2). Study physiological mechanisms underlying vestibular, motor system and brain function in primates during early and later adaptation phases; 3). Study the tissue regeneration processes of mammals; 4). Study the development of single-celled organisms, cell cultures and embryos in microgravity; 5). Study radiation characteristics during the mission and investigate doses, fluxes and spectra of cosmic radiation for various types of shielding. American and Soviet specialists jointly conducted 29 experiments on this mission including extensive preflight and postflight studies with rhesus monkeys, and tissue processing and cell culturing postflight. Biosamples and data were subsequently transferred to the United States. The U.S. responsibilities for this flight included development of flight and ground-based hardware, the preparation of rat tissue sample procedures, the verification testing of hardware and experiment procedures, and the postflight analysis of biospecimens and data for the joint experiments. The U.S. investigations included four primate experiments, 24 rat experiments, and one radiation dosimetry experiment. Three scientists investigated tissue repair during flight for a subgroup of rats injured preflight by surgical intervention. A description of the Cosmos 2044 mission is presented in this report including preflight, on-orbit and postflight activities. The flight and ground-based bioinstrumentation which was developed by the U.S. and U.S.S.R. is also described, along with the associated preflight testing of the U.S. hardware.

14. SUBJECT TERMS	15. NUMBER OF PAGES
Cosmos, Biosatellite	442
	16. PRICE CODE: A23

17. SECURITY CLASSIFICATION OF REPORT	18. SECURITY CLASSIFICATION OF THIS PAGE	19. SECURITY CLASSIFICATION OF ABSTRACT	20. LIMITATION OF ABSTRACT
Unclassified	Unclassified		